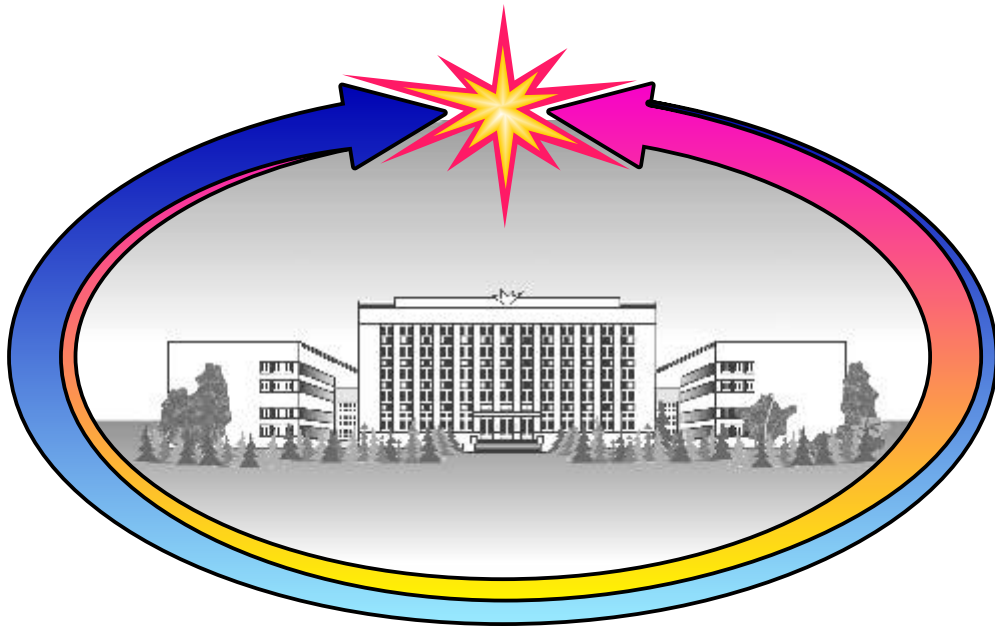


Russian Academy of Sciences
Siberian Branch

BUDKER INSTITUTE OF NUCLEAR PHYSICS



ANNUAL REPORT 2011

NOVOSIBIRSK 2012

Contents

Introduction	7
1. Particle physics	11
1.1 CMD-3	13
1.2 The SND detector.....	15
1.2.1 Detector performance and experiments at VEPP-2000	15
1.2.2 The first results of the experiments	15
1.3 Detector KEDR	18
1.3.1 Modernization of the KEDR detector for experiments in high energy region	18
1.3.2 Beam test of FARICH prototype	18
1.3.3 Extracted electron beam.....	18
1.3.4 Works with FARICH.....	19
1.4 Results of work of KEDR detector at the VEPP-4M collider in 2011.....	20
1.4.1 Search for narrow resonances.....	20
1.4.2 Measurement of the $\phi(3770)$ -meson parameters.....	20
1.4.3 Measurement of the $\phi(2S)$ -meson parameters.....	21
1.4.4 Measurement of the τ -lepton mass	22
1.4.5 Conclusion	23
1.5 Detectors for HEP	24
1.6 X-ray detectors	24
1.7 Other works	24
1.8 Microstructure gaseous detectors	24
1.8.1 Two-phase cryogen avalanche detectors (CRADs) on the basis of thick gas electron multipliers (THGEMs)	24
1.8.2 Investigation into infrared (IR) scintillations in gaseous and liquid Ar at cryogenic temperatures.....	26
1.8.3 Modernization of the system for scattered electrons in the KEDR experiment	27
1.8.4 Participation in collaborations	27
1.9 Experiment Belle	28
1.9.1 Main results	28
1.9.2 Data analysis of the Belle experiment	28
1.9.3 Detector upgrade	31
1.10 BABAR experiment	33
1.11 Participation in the ATLAS experiment at the Large Hadron Collider (LHC)	34
2. Electro – and photonuclear physics	37
2.1 Experiments with internal targets	39
3. Theoretical physics	41
3.1 Strong interaction	43
3.2 CP nonconservation	45
3.3 Quantum electrodynamics	45
3.4 Gravity	46
3.5 Astrophysics	47
3.6 Nonlinear dynamics and chaos, quantum	47
4. Plasma physics and controlled thermonuclear fusion	49
4.1 Experiments on the gas-dynamic trap (GDT) facility	51
4.1.1 Effect of ambipolar electric fields on longitudinal plasma losses in the gas-dynamic trap..	51
4.1.2 Results of first experiments on plasma heating with electron beam on the GDT facility....	56
4.1.3 Development of the system for ECR heating of plasma in the gas-dynamic trap (GDT) ...	58
4.2 GOL-3 facility.....	63
4.2.1 General description and operation regimes of GOL-3.....	63
4.2.2 Measurements of fast localized fluctuations in plasma density	64
4.2.3 Studies of a sub-THz plasma radiation	64

4.2.4 Investigation of azimuthal rotation of plasma	65
4.2.5 The interferometer based on CO ₂ laser	66
4.2.6 Neutral Particle Analyzer	67
4.2.7 Compact neutron detector with digital n-γ discrimination	68
4.2.8 Development of methods for modeling diode systems with plasma electrodes	69
4.2.9 Transportation of an intense submillisecond electron beam in a magnetic field of mirror Configuration	69
4.2.10 Summary	70
4.3 Plasma theory	71
4.3.1 Nonneutral plasmas	71
4.3.2 Plasma surface interaction theory	71
4.3.3 Theory of plasma wakefield acceleration	71
4.4 Beam injectors of hydrogen atoms and ions	72
4.4.1 Beam Injectors of Hydrogen Atoms.....	72
4.4.2 Development of powerful continuous injector of beam of fast hydrogen atoms	72
5. Electron-Positron Colliders.....	73
5.1 Work of vepp-2000 with round beams	75
5.2 VEPP-4 accelerator complex	80
5.2.1 Allocation of operation time	80
5.2.2 High-Energy Physics	80
5.2.3 Operation of VEPP-4 at energy $E = 3.5 \div 4$ GeV	81
5.2.4 DEUTERON experiment on VEPP-3	81
5.2.5 Extracted beam on VEPP-4M	82
5.2.6 Summer maintenance works on the VEPP-4 complex	82
5.3 Injection complex	83
5.4 Linear induction accelerator LIA-2	84
5.5 Electron beam welding	84
5.6 Production of quadrupole lenses for NSLS-II	85
5.7 Electron cooling system	87
5.8 Accelerator mass spectrometer	88
5.9 Ion beam lifetime in the presence of electrons in its orbit	88
5.10 Vacuum systems	89
5.10.1 Secondary emission and electron clouds	89
5.10.2 Examination of the effectiveness of supersonic washing of aluminum chambers	90
5.10.3 Vacuum system of the NSLS-II booster	91
5.10.4 Bellows units for the XFEL accelerator structure	92
5.11 Works on the electron-positron factories and beam physics	92
5.12 Magnets for the KEK Super-B	93
5.13 NSLS-II booster	93
5.13.1 Design	94
5.13.2 Magnetic system	94
5.13.3 Vacuum system	95
5.13.4 Diagnostics	96
5.13.5 Assembly of the modules of the booster ring at the BINP site	97
5.13.6 Power Supplies	97
5.13.7 Injection-extraction system	98
5.13.8 Control system	100
6. Synchrotron Radiation Sources and Free Electron Lasers	103
6.1 Introduction	105
6.2 Work on SR from VEPP-3.....	105
6.2.1 Station “Explosion (Extreme states of matter)”	105
6.2.2 Station “LIGA-technology and X-ray lithography”.....	107
6.2.3 Stations “Anomalous Scattering” and “Precision Diffractometry”	107
6.2.4 Station “X-ray fluorescence elemental analysis”	109
6.2.5 Station “Diffractometry with hard X-rays”	115
6.2.6 Station “X-ray microscopy and tomography”	117

6.2.7 Station "Diffraction movie"	119
6.2.8 Station "EXAFS spectroscopy"	121
6.3 Work on sr beams from VEPP-4M	122
6.3.1 Development of methodological support for the metrological station "Cosmos"	127
6.4 Work with beams of terahertz radiation	127
6.4.1 Novosibirsk terahertz free electron laser	128
6.4.2 Examples of experiments with THz radiation beams	128
6.4.3 Third stage of Novosibirsk FEL	128
6.4.4 Results of 2011 and plans for 2012	131
6.5 Design and development of specialized generators of SR	133
6.6 Conferences, meetings, and seminars	134
7. Radiophysics and electronics	137
7.1 Power supplies for electrophysical installations	139
7.1.1 Stabilized current sources	139
7.2 HV sources of stabilized DC voltage	140
7.2.1 High-voltage sources for atom injectors for diagnostics and heating of plasma in plasma installations	140
7.2.2 High-voltage power supplies for electron accelerating tubes	141
7.2.3 Switch-mode power supplies for electromagnets of accelerator complexes	141
7.3 Development of measurement systems and automation of physical experiments	141
7.4 Research related to modeling and solution to electrostatic and electrodynamic problems of accelerator physics	144
7.5 Equipment of the accelerating stations of the collider complex NICA	144
7.5.1 Cavities of RF system 2 (the 24th harmonic), NICA	146
7.5.2 Cavity of RF system 3 (the 72nd harmonic), NICA	147
7.5.3 Water-cooling system	149
7.5.4 Multipactor discharge	149
7.5.5 Suppression of multipactor discharge	149
7.5.6 Cavity design	149
7.6 RF injector of the microtron-recuperator	149
7.7 Development of RF system for high-power continuous injector of beams of fast hydrogen atoms ...	150
7.8 New 174 MHz RF system for the storage ring of the electron-positron booster (BEP)	151
7.9 Passive single-mode cavity for 816 MHz	151
7.10 Assembly and testing of the rf generator for the federal state unitary enterprise "Russian Federal Nuclear Center-VNIIEF" (Sarov)	152
7.11 Further development of RF system of the VEPP-4 storage ring	152
7.12 Upgrading the RF system of the microtron for the FEL	152
8. Powerful Electron Accelerators and Beam Technologies	153
8.1 Development of the model range and improve of operating characteristic of ELV accelerators	155
8.1.1 Stand based on industrial ELV-6 accelerator with extraction of focused electron beam into air	158
8.1.2 Nanoconstructions for medicine	158
8.2 ILU accelerators and their applications	160
8.2.1 Accelerator supplies	160
8.2.2 Modernization of the ILU machines	160
8.2.3 New technologies development	160
9. Physics for medicine	161
9.1 Status of BNCT project	163
9.2 X-ray detectors for medicine and security	164
9.2.1 Medical Radiography	164
9.2.2 X-ray inspection system (XIS) "Sibscan" for screening of people	164
Bibliography	165

List of publications	165
Preprints	203
Authorial papers	211
Participation in conferences	212
List of Collaboration Agreements	214
Research Personnel	217
Members of Russian Academy of Science	217
Director board	217
Scientific council	217
Specialized sections of scientific council	218
Research staff and publications	221

INTRODUCTION

The Institute of Nuclear Physics of the USSR Academy of Sciences was established in accordance with the decision of the Council of Ministers in May 1958 on the basis of the Laboratory of new acceleration methods of the Institute of Atomic Energy. Academician A.N. Skrinsky has been the Director of the Institute since 1977.

BINP with the personnel of about 2,800 is now the largest academic institution of Russia. The research staff of 420 includes 12 full members and corresponding members of the Russian Academy of Sciences, 60 doctors of science, and 170 candidates of science. BINP has a large-scale pilot production department with the personnel of about 1,000 people and high-class technical and technological equipment.

The Institute is actively engaged in the education of scientific and technical staff of high qualification. BINP is the base for seven subdepartments (about 200 students) of the Physics Department of Novosibirsk State University (NSU) and the Physics and Technology Department of Novosibirsk State Technical University (NSTU).

BINP is one of the world's leading centers in the areas of high energy physics, accelerator physics, plasma physics, and controlled fusion. The Institute has conducted large-scale experiments in elementary particle physics on electron-positron colliders and a unique complex of open plasma traps and developed up-to-date accelerators, intense sources of synchrotron radiation, and free electron lasers. In most areas of its activity, BINP is the only research institution in Russia.

Below are listed some of BINP major achievements in science and technology.

In the field of elementary particle physics and nuclear physics:

pioneering works on the development of the colliding-beam method (currently, the basic method in the high energy physics):

- first experiments on electron-electron interaction (simultaneously with the Princeton and Stanford works) (1965);

- world's first experiments in electron-positron interaction (1967);

- world's first observation of the process of double bremsstrahlung (1967);

pioneering works on the two-photon physics (1970);

study of the characteristics of vector mesons on installations with colliding electron-positron beams VEPP-2, VEPP-2M, and VEPP-4 (1967);

discovery of multiple hadron production in electron-positron annihilation (1970);

precise measurement of the hadronic vacuum polarization contribution to the value of muon anomalous magnetic moment for one of the most sensitive tests of the

Standard Model, in collaboration with Brookhaven National Laboratory (1984 - 2005);

development of the method of resonance depolarization for high-precision measurement of masses of elementary particles; attaining a record-high precision in the measurement of the mass of K -, ρ -, ω -, ϕ -, ψ -, and ν -mesons (1975 - 2004);

discovery of parity violation in atomic transitions and confirmation of the unified theory of electroweak interactions (1978);

development of a method for experimentation on superfine internal targets in storage rings (since 1967) and study of the electromagnetic structure of deuteron in polarization experiments (since 1984);

development of a method for production of intense fluxes of labeled gamma rays of high energy using inverse Compton scattering (1980 - 1982); experimental observation of photon splitting in the Coulomb field of nucleus (1997);

development of new methods for detection of charged and neutral particles of high energy, creation of unique detectors for colliding beams (OLYA, CMD-1, MD-1, CMD-2, CMD-3, ND, SND, and KEDR) (since 1974);

and development of X-ray detectors for medical purposes and creation on their basis of a low-dose digital X-ray installation with ultra-low level of irradiation to patient and X-ray inspection system for screening people "Sibscan" (since 1981).

In the field of theoretical physics:

development of the resonance theory of dynamical chaos and pseudochaos in the classical and quantum mechanics (since 1959);

the first calculation of charge renormalization in Yang-Mills theory (1969);

development of the QCD sum rule technique (1979 - 1984);

prediction of large enhancement of the parity violation effects in neutron resonances in heavy nuclei (1980 - 1985);

development of the theory of hard exclusive reactions in QCD (1977-1984);

development of the operator approach to quantum electrodynamics in external fields (1974 -1976);

development of quantum electrodynamics in periodic structures, including the laser wavelength (1972-1997);

development of the theory of radiation effects during the passage of charged particles and high-energy photons through single oriented crystals (since 1978);

derivation of the evolution equation in QCD for parton distribution by energy (the BFKL equation) (1975-1997);

prediction of the coherence effect in emission of gluons in QCD and study of its influence on hadron distributions (1981-1982).

In the field of accelerator physics and technology:

years of successful experience in the creation of storage rings and colliders;

invention, development and experimental verification of the method of "electron cooling" for beams of heavy particles (the method is currently in use at laboratories around the world); equipping complexes for acceleration of heavy ions in Germany and China and at CERN with effective "coolers" (1965-2005);

invention and development of new types of high-power RF generators (gyrocon, relativistic klystron, and Magnicon) (since 1967);

suggestion of the method of linear electron-positron colliding beams for production of ultra-high energies (1968) and representation of a physically self-consistent project (1978);

development of components for large-field pulsed magnetic optics (X lenses and lithium lenses), which are currently used at numerous laboratories (since 1962);

invention and experimental verification of the charge-exchange injection method, which is currently used on all large proton accelerators (1960-1964);

theoretical and experimental studies of creation of polarized beams and spin dynamics in accelerators and colliders, conceptual design and development of high-spin rotators and "Siberian snakes" for a number of accelerator facilities (1966-1995);

theoretical and experimental studies of stochastic instability and collision effects, which limit the luminosity of colliding beams (since 1966);

development of the physical concept of next-generation electron-positron colliders with very high luminosity, the so-called electron-positron factories (since 1987);

suggestion and development of the method of ionization cooling of muons for muon colliders and neutrino factories (1969 -1981 - 2002);

development and creation of high-power low-energy electron accelerators for a variety of technology applications, including environmental protection (accelerators ELV-12 with a power of 500 kW and an energy of 1 MeV and ILU-10 with a power of up to 50 kW and an energy of 5 MeV (since 1963);

suggestion and implementation of the scheme of high-efficiency energy recovery linac for free-electron lasers (1979 - 2003).

In the field of plasma physics and fusion:

invention (1954) and creation (1959) of a "classic" open magnetic trap (magnetic bottle) for hot plasma confinement;

invention and development of new schemes of open traps: with a few plugs, with a rotating plasma, ambipolar, and gas-dynamic; experimental implementation of multi-plug confinement of a plasma with sub-fusion parameters on the GOL-3 facility; experimental implementation of stabilization of MHD instabilities in an axially-symmetric gas-dynamic trap on the GDT facility (since 1971);

discovery of collisionless shock waves in plasma (1961);

development of the method of plasma heating with relativistic electron beams (since 1971);

development of high-intensity surface-plasma sources of negative ions, which became widespread throughout the world (1969-1981);

proposal and development of the concept of a high-power fusion neutron source on the basis of an open trap, for materials science (since 1987);

theoretical prediction of the Langmuir collapse (1972) and experimental observation of strong Langmuir turbulence and collapse of Langmuir waves in a magnetic field (1989-1997); and

creation of a series of unique high-power high-precision sources of hydrogen atoms for study of high-temperature plasma for a number of large installations (since 1997).

In the field of synchrotron radiation and free electron lasers:

use of synchrotron radiation of the BINP storage rings for various scientific and technological objectives and creation of the Siberian International Center for Synchrotron Radiation on the basis of the storage rings of VEPP-2M, VEPP-3, and VEPP-4 (since 1973);

theoretical and experimental studies of particle emission in periodic structures (undulators, wigglers, and crystals) (since 1972);

development and creation of specialized sources of synchrotron radiation (since 1983);

development and creation of one- and two-coordinate detectors for experiments with synchrotron radiation (since 1975);

invention and development of the optical klystron (1977); generation of coherent radiation in the infrared to the ultraviolet spectral region (since 1980);

designing and development of a high-power free electron laser (for photochemical research and technological applications, as well as energy transfer from the Earth to a satellite) based on the most promising scheme with a microtron-recuperator; attaining high-power (400 W) laser radiation in the terahertz range (since 1987);

creation of a series of high-field superconducting magnetic devices for SR sources and electron storage devices (wigglers and bending magnets with a field of up to 10 T and solenoids with a field of up to 13 T) (since 1996).

BINP application-oriented works are entirely based on the results of basic research of the Institute and focused in the following main areas:

high-power industrial electron accelerators used for polymer modification; treatment of industrial and domestic waste; production of nanopowders of pure metals, silica, and oxides, carbides and nitrides of metals;

radiation processing of food; sterilization of medical equipment, disposable instruments, etc.; and other technological applications;

low-dose digital radiographic installations of scanning type for medical and security systems, with ultra-low exposure of patient to radiation;

development of nuclear medicine facilities for proton, ion, and boron-neutron-capture therapy of malignant tumors;

electron beam welders;

and radiographic equipment for defense-oriented research.

Over the past 20 years, BINP has actively supported basic and applied research with funds received from contract works. The Institute has developed, manufactured, and supplied to consumers in Europe, Asia, and North and South America (20 countries), as well as to Russia, a wide range of high-tech products for tens of millions of dollars annually. So-earned money was used for the completion and commissioning of the accelerator complex VEPP-4M with the unique KEDR detector; designing and construction of up-to-date large and unique installations: the electron-positron collider VEPP-2000, the free electron laser, and the new injection system for existing and future installations of BINP. Throughout the post-Soviet period, these funds have supported the continuous operation of BINP facilities and related infrastructure.

The Institute is known for its long-term international cooperation with most major foreign and international centers. A striking example of this cooperation is the participation of BINP in the largest international project of modernity - the Large Hadron Collider at the European Center for Nuclear Research (Geneva). BINP designed, manufactured, and delivered to CERN unique high-tech equipment for an amount of over 100 million Swiss francs. Another examples of international cooperation includes the projects of B-factories in the U.S. and Japan, synchrotron radiation source PETRA-III, X-ray free electron laser (DESY, Hamburg), heavy-ion accelerator complex (GSI, Darmstadt), etc.

BINP has played a key role in several major Russian projects, including the Center for Synchrotron Radiation Research "Kurchatov Institute", Synchrotron Radiation Source TSC in Zelenograd, a neutron source for the JINR in Dubna, and radiographic equipment for defense-oriented research for the Federal State Unitary Enterprise "Russian Federal Nuclear Center -VNIITF" in Snezhinsk.

The Institute has strongly influenced the innovation economy of the country. A striking example is the development in conjunction with the ICG SB RAS and the company "Siberian Center for Pharmacology and Biotechnology" of a unique technology of electron-beam immobilization of biomolecules on an inert carrier. The technology is now used for mass production of the world's first oral thrombolytic "Trombovazim".

The Institute is deeply integrated into the work of RAS and SB RAS, exercising implementation of 22 projects under the program of the Presidium and Branches of the RAS; 16 interdisciplinary integration projects; 8 joint projects of SB RAS with regional RAS institutes, the National Academies of Sciences of Ukraine, Belarus and People's Republic of China; 2 custom projects of SB RAS (as a co-executor); 7 state contracts under the Federal Program "Research and development on priority directions of scientific-technological complex of Russia for the years 2007 - 2013"; 20 Government contracts under the Federal Program "Research and educational personnel of the innovation Russia" for the years 2009 - 2013; and over 50 RFBR projects.

Every year the Institute members present about 200 reports at Russian and international conferences, publish about 500 articles in leading Russian and foreign scientific journals, and issue monographs and training aids. According to materials published in the review "Bibliometric indicators of the Russian Science and Russian Academy of Sciences" (*Herald of the Russian Academy of Sciences*, June 2009, Volume 79, № 6), the number of references to works by BINP members in 1997-2007 in the reputable international database ESI is 28, 267. According to the survey, this is the highest result among all the institutions of the Russian Academy of Sciences. 4 members of the Institute have got the special award of Elsevier Publishing as the most cited authors in the natural sciences in the former USSR territory.

The BINP Scientific Council found the following works to be the best in 2011:

In the field of particle physics and fundamental interactions:

1) In the experiment Belle (KEK, Japan), resonance states with exotic quark structure were first discovered in the decays of $\gamma(5S)$.

2) In experiments with the KEDR detector on VEPP-4M, parameters of $\psi(2S)$ and $\psi(3770)$ mesons were measured with the world's best accuracy and the most sensitive limit on the cross section for narrow resonance production in the energy range $2E = 1.85 \div 3.1$ GeV was determined.

3) In the experiment with the SND detector on the electron-positron collider VEPP-2000, the cross section for the $e^+e^- \rightarrow \omega\pi^0 \rightarrow \pi^0\pi^0\gamma$ process was measured with a record accuracy.

4) The proof of the multi-Regge form of QCD amplitudes at high energies was completed in the approximation next to the leading logarithmic one.

In the field of plasma physics:

1) On the GOL-3 facility, generation of intense radiation at the second harmonic of plasma frequency, which lies in the terahertz range, was registered at

collective interaction of high-power relativistic beam with plasma.

2) For the first time in the world, a source of negative hydrogen ions with a steady-state beam current of 25 mA was created. The source models the basic laws of beam formation in a unit cell of the future high-current injector of neutral atoms of high energy (~ 1 MeV) for fusion applications.

In the field of physics and technology of particle accelerators, SR sources, and FELs:

1) A conceptual design of accelerator complex with electron-positron colliding beams—"Super Charm/Tau Factory"—was developed. It is among the six projects recommended to the Government Commission on High Technologies and Innovations for consideration in regard to establishment of "MEGA-Science" facilities in Russia.

2) A record value of the "colliding beam parameter" was reached on the electron-positron collider VEPP-2000; an experiment with two detectors, SND and CMD-3, was conducted in the energy range of 1,000 to 2,000 MeV with a record integrated luminosity.

3) The installation for high-voltage electron cooling of proton beam for the COSY storage ring (Jülich, Germany) was designed, constructed, and tested successfully. It has a record rate of cooling.

4) For the first time in the world, a nanosecond-resolution method of controlling formation and growth of nanoparticles of the condensed phase of chemical reaction products of detonation at explosion was implemented with the use of synchrotron radiation of the VEPP-3 storage ring.

5) A unique 119-pole superconducting wiggler of record radiation brightness in the X-ray range, designed and built by BINP, was successfully tested on the synchrotron radiation source ALBA-CELLS (Spain).

6) A conceptual design was developed for the fourth-generation SR X-ray source based on energy recovery linac with radiation brightness several orders of magnitude larger than that of the European and U.S. X-ray sources under construction. The project is among the six projects recommended to the Government Commission on High Technologies and Innovations in regard to establishment of "MEGA-Science" facilities in Russia.

In December 2011, the General Assembly of the Russian Academy of Sciences elected Nikolay Sergeevich Dikansky a full member of the Russian Academy of Sciences and Nikolai Vinokurov and Pavel Logachev corresponding members of the Russian Academy of Sciences. Thus, 5 full Academy members

and 7 corresponding Academy members are currently working at the Institute.

Budker award of the Siberian Branch of Russian Academy of Sciences for the work "Optimization of the dynamic aperture of the electron-positron supercollider Charm-Tau Factory in Novosibirsk" was awarded to P.A. Piminov.

Personalized Premium of the Novosibirsk Region Government for young scientists in the nomination of "creation or development of instrumentation, techniques, technologies, and new scientific and technical products" for 2011 was awarded to A.L. Solomakhin for his work on "Multi-channel dispersion interferometer for measuring electron density on up-to-date installations with magnetic confinement of fusion plasma".

Young scientists A.L. Solomakhin (research topic: "Multi-channel dispersion interferometer for measuring electron density on up-to-date installations with magnetic confinement of fusion plasma") and D.E. Berkaev (research topic: "Modernization of the automation system of the accelerator complex VEPP-2000") became the winners of the competition for grants from the Novosibirsk Region Government on conduction of applied research and completion of development activities in 2012.

Government scholarships for graduate students of Novosibirsk region for 2012 were awarded to BINP graduate students V.I. Aleinik and A.Yu. Vlasov.

A.V. Sudnikov with the project "Study of the phenomena of reconnection of magnetic field lines in the multi-plug trap GOL-3" was awarded a grant by the results of Novosibirsk mayor contest among young scientists and engineers in 2011.

Four scientific collectives of the Institute, headed by RAS academy members Skrinisky, Kruglyakov, and Kulipanov and Professor Onuchin, have the status of leading scientific schools, which is awarded by the Council on Grants at the President of the Russian Federation. This Council awarded prizes to two teams of young scientists of the Institute as young candidates of science.

In 2011, three Dissertation Councils that are entitled to accept doctoral (candidate) thesis continued their work at the Institute. In total, 15 meetings were conducted, where 4 doctoral and 11 candidate theses were defended.

Over 50 excursions to the BINP facilities were organized for pupils, students, teachers, employees of other organizations, and guests of the Institute (about 1,500 visitors). Outreach lectures at Novosibirsk schools were given.

1

PARTICLE PHYSICS

1.1 CMD-3 DETECTOR

In 2011, several physics runs of experimental data taking were performed, in which parameters of the detector were optimized for work with the VEPP-2000 collider; systems of the detector were calibrated and recording of information as foreseen by the physical program was started.

From February to June 2011, data were collected in the energy range of 1.05 to 2.0 GeV in the center of mass system. In order to reduce systematic errors we performed the scanning twice, first increasing and then decreasing the beam energy. As a result, experimental data were collected at 40 energy points with step of 25 MeV in the center of mass system. The integrated luminosity was obtained to be 22 pb^{-1} .

Fig.1.1.1 shows a photograph of the CMD-3 detector in the experimental hall of VEPP-2000. One can see the plates of the scintillation counters for detection of muons, which were installed on the detector in 2011. Besides that, the detector was equipped with time-of-flight counters for separation of events of neutron-antineutron pair production near the threshold.

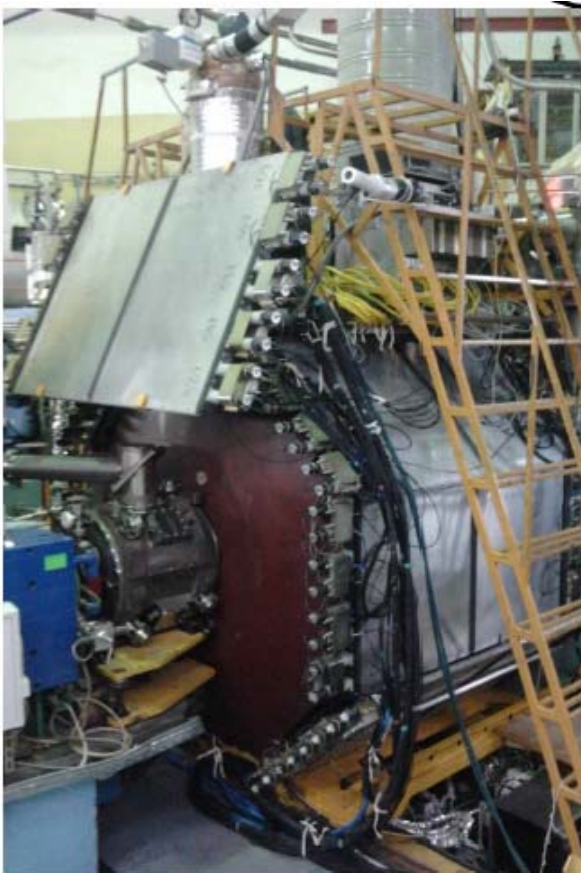


Fig. 1.1.1. CMD-3 detector in the experimental hall of the VEPP-2000 collider.

In 2011, the digitizing electronics plate AWF-32 has been developed. It will substitute the plates A32 of the KLYUKVA standard at data reading from the liquid-xenon calorimeter and Z-chamber of the CMD-3 detector. A few prototypes of AWF-32 were made and tested in the data acquisition system of CMD-3. The obtained results corresponded to the expected parameters. Full-scale production of the boards AWF-32 is to be completed in 2012.

The data collected allows a basis for the study of the processes of multihadron production. In particular, the production cross sections of four and six pions were measured in the energy range of 1.0 to 2.0 GeV in the center of mass system. Fig. 1.1.2 shows the preliminary results of the measurements of the cross section for the $e^+e^- \rightarrow 3(\pi^+\pi^-)$ process. The black circles show the CMD-3 results, and comparison the empty circles show the results of the BaBar detector. The vertical line indicates the threshold for proton-antiproton pair production.

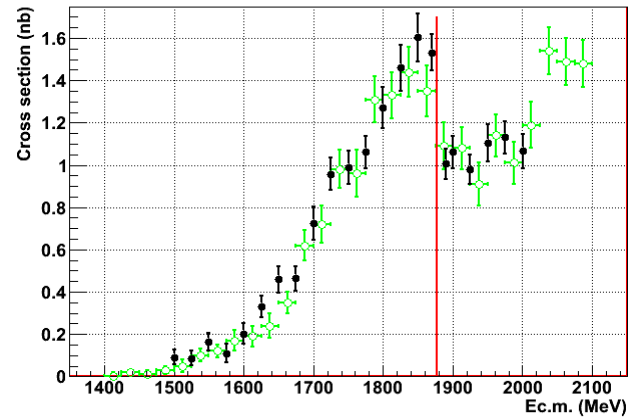


Fig. 1.1.2. Cross section for the $e^+e^- \rightarrow 3(\pi^+\pi^-)$ process vs. energy. Black circles: results of the experiment with CMD-3; empty circles: BaBar data. The vertical line indicates the threshold for the proton-antiproton pair production.

Another important physical result of the data analysis was the measurement cross sections for proton-antiproton pair production as shown in Fig.1.1.3. The analysis used a luminosity integral of just 3 pb^{-1} , the accuracy of measuring the cross section corresponded the BaBar results obtained after a eight years of work. There are already results of processing of information relating to energies in the beam of above 950 MeV, where nucleons have enough energy to fly through the vacuum tube that surrounds the collision place. At lower energies, they get stuck in the tube and the main criterion for selection of such events should be a peak in antiproton annihilation in the vacuum tube. Analysis of this energy region is in progress.

In addition, for calibration of VEPP-2000 beam energy, an energy region near the ϕ -meson resonance was scanned in June 2011.

The luminosity integral was 1.1 pb^{-1} . Experimental data collected at four energy points made a basis for determination of the ϕ -meson excitation curve and parameters of this resonance in the $\phi \rightarrow K_L K_S$ decay channel. Comparison of the values of these parameters with the world's averages made it possible to calibrate the energy scale of the VEPP-2000 collider.

To improve the momentum resolution of the tracking system, we studied the possibility of detector operation with a superconducting solenoid magnetic field of 13 kG instead of a previously used value of 10 kG. All systems of the detector demonstrated stable operation in this mode. Processing of the information collected showed that, the resolution improved by 15-20%, momentum according to our expectation .

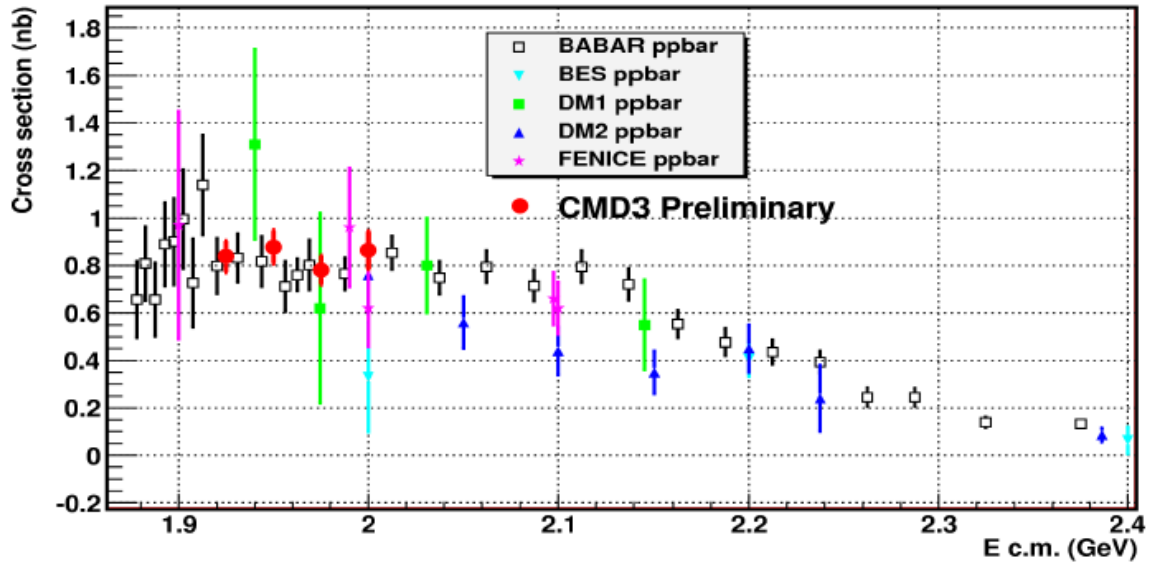


Fig.1.1.3. Cross section for proton-antiproton pair production vs. energy in the center of mass frame in comparison with other experiments.

1.2. THE SND DETECTOR

1.2.1. Detector performance and experiments at VEPP-2000

In December 2010 and in the first half of 2011, a successful experimental session of data taking was held with the SND detector at the VEPP-2000 collider. At the beginning of the session a collider tuning was performed at the beam energy of 750 MeV. The accumulated experimental data sample, collected during the tuning phase, corresponds to an integrated luminosity of 600 nb^{-1} . During the second half of December a detailed scan of the ϕ -meson resonance energy region was performed. Integrated luminosity of 650 nb^{-1} was accumulated at 10 energy points for beam energies from 505 to 514 MeV. These data was used for the collider energy scale calibration. After correcting for the revealed energy shift, experimental scan was repeated in the ϕ -meson region with an integrated luminosity of about 600 nb^{-1} .

In January 2011, a scan of the center of mass energy range from 1 to 2 GeV has began. The scanning step was chosen equal to 25 MeV. This energy interval was scanned twice: first upward in the increment steps of 50 MeV, and then from the top to downward with the same step but with the energy points shifted by 25 MeV. The scan was completed in June 2011. In Fig. 1.2.1 integrated luminosity versus time (days) is shown for this experiment, called MHAD2011. After the MHAD2011 experiment, a short session of the ϕ -meson scan was performed with integrated luminosity of about 0.8 pb^{-1} . The total integrated luminosity accumulated by SND detector in the 2010÷2011 season was about 25 pb^{-1} . About 1.7 million events were recorded. In the experiment, the average data recording speed was 435 Hz.

All subsystems of the detector have shown a stable and satisfactory performance during the data taking. Loss of statistics due to detector faults or due to the data acquisition system malfunctioning constituted not more than 5%.

During the data taking, new preamps of the calorimeter electronics were tested. These new preamps are expected to enhance the reliability of the calorimeter and significantly simplify the repair of faulty channels. The new electronics were installed in the 26 channels of the calorimeter first layer. During the seven months of operation under conditions of the real experiment, no single channel with the new preamps failed. In autumn 2011, new preamps were installed in the half of the calorimeter first layer channels (260 channels).

During 2011, a permanent improvement of the SND data acquisition system continued. It mainly affected the system of operational control of the detector state by using experimental events. To the existing performance control programs for the calorimeter, the tracking system and the scintillation counters, new ones were added to control the performance of the Cerenkov counters and muon tubes, to measure the energy thresholds in the calorimeter and its

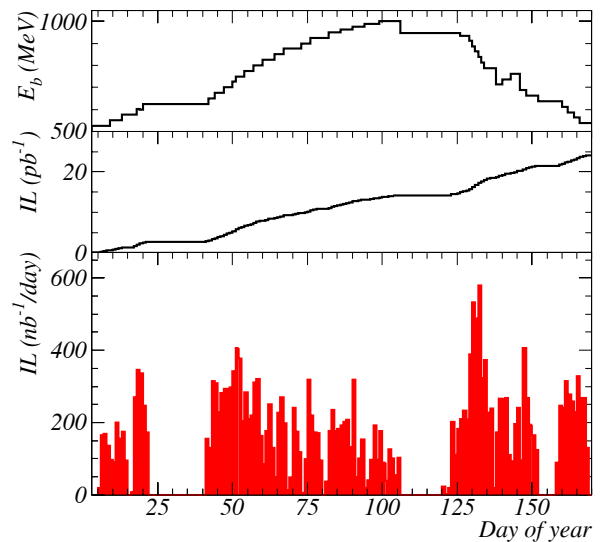


Figure 1.2.1: The integrated luminosity versus time for the MHAD2011 experiment. The upper graph shows the beam energy at which the data set was collected. The middle one shows the change in the accumulated integrated luminosity during the experiment. The bottom graph shows the distribution of integrated luminosities accumulated per day.

firing time. Gas mixture control system was assembled and put into operation. Significant improvements were also made in the operator interface. In April 2011, the first version of the preliminary event reconstruction procedure was ready and the data collected in 2010 were processed by using this procedure. The preliminary event reconstruction produces reconstructed events grouped by individual classes (flows): collinear, charged, neutral, etc. The use of preliminary reconstruction reduces the number of events about 20 times and allows to save the subsequent processing time. Preliminary reconstruction of the data recorded in 2011, was completed by December.

1.2.2. The first results of the experiments

To measure the cross section of the process $e^+e^- \rightarrow \omega\pi^0 \rightarrow \pi^0\pi^0\gamma$, data collected in the first half of 2010 in the energy interval $2E = 1.1\div 1.9 \text{ GeV}$ were used. The luminosity was measured by using events of the process $e^+e^- \rightarrow \gamma\gamma$ and the integrated luminosity used was about 4 pb^{-1} .

Events with no charged particles and 5 or more registered photons whose total energy deposition in the calorimeter was more than the energy of one beam were selected. Additional selection criteria included a few limitations on the values of the likelihood function aimed to select events in which five photons satisfy the energy-momentum conservation law and in which there is a candidate for the decay $\omega \rightarrow \pi^0\gamma$.

In Fig. 1.2.2. the cross section of the process under study, obtained in this work, is shown, as well as the results of previous measurements by the detectors SND, CMD-2, CLEO and DM2.

The figure also shows the result of the joint approximation of the SND results obtained in this experiment and in the experiment conducted in 2000. To approximate the cross section, the vector dominance model taking into account the $\rho(770)$, $\rho(1450)$ and $\rho(1700)$ intermediate states was used. The results of this work were published in the journal "JETP Letters".

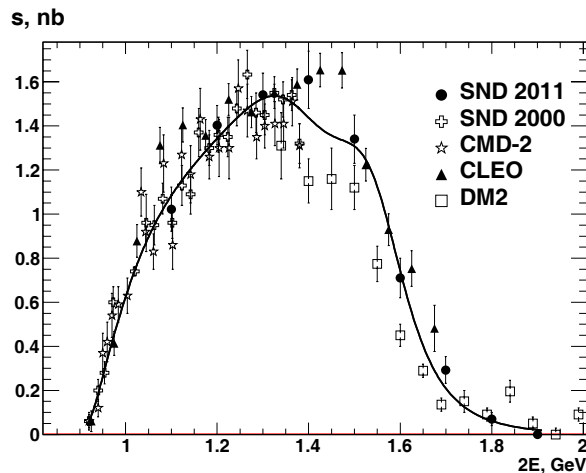


Figure 1.2.2: Cross section of the process $e^+e^- \rightarrow \omega\pi^0 \rightarrow \pi^0\pi^0\gamma$. The figure shows the experimental results of SND 2011, SND 2000, CMD-2, CLEO and DM2. The curve represents the result of the joint approximation of the SND 2011 and SND 2000.

Using the 2010 data with the integrated luminosity of about 4 pb^{-1} , the cross section of the process $e^+e^- \rightarrow \pi^+\pi^-\pi^0$ was measured. Events were selected according to the following criteria: 2 central tracks, two photons, the spatial angle between the charged particles is more than 40° , the total energy deposition in the calorimeter is in the range of $0.3 \div 0.8$ of the center-of-mass energy, χ^2 of the kinematic reconstruction is less than 30. The number of events of the process under study $e^+e^- \rightarrow \pi^+\pi^-\pi^0$ was determined by using the Gaussian fit to the $m_{\gamma\gamma}$ distribution of the selected events taking into account the remaining contribution from the background process $e^+e^- \rightarrow \pi^+\pi^-\pi^0\pi^0$. The resulting cross section is shown in Fig. 1.2.3.

Preliminary results of the $e^+e^- \rightarrow \pi^+\pi^-\pi^0\pi^0$ process cross section measurements has been obtained in the energy range from 1 to 2 GeV (see Fig. 1.2.4.). In this energy range the $\rho(1450)$ and $\rho(1700)$ intermediate states give the major contribution to the cross section. Our results are consistent with the previous measurements by SND in the energy range below 1.4 GeV, as well as with the results of BaBar detector obtained by the radiative return method.

The statistical uncertainty of our measurements is smaller than of the previous measurements and is $\simeq 2\%$.

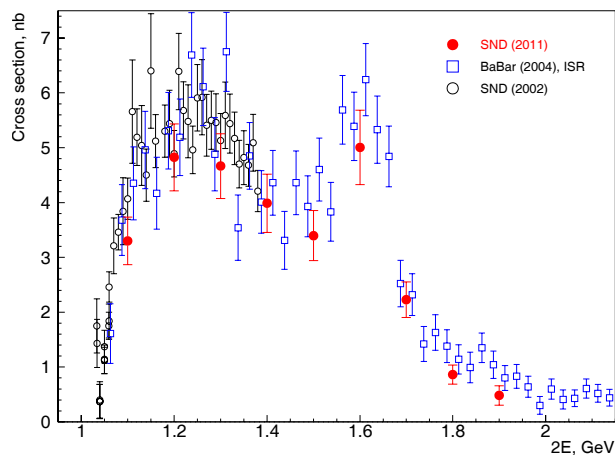


Figure 1.2.3: The cross section of the process $e^+e^- \rightarrow \pi^+\pi^-\pi^0$ in comparison with the results of previous experiments SND (VEPP-2M) and BaBar.

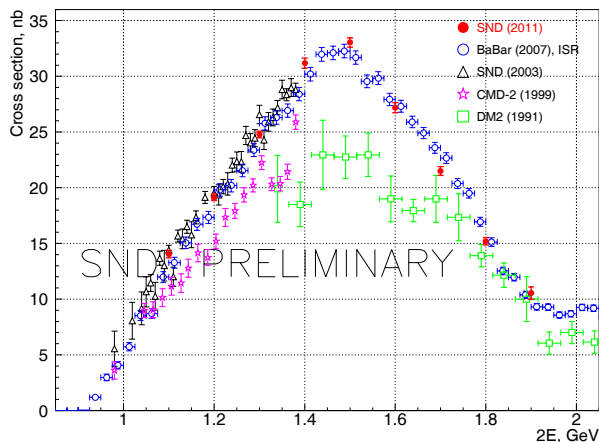


Fig 1.2.4: The $e^+e^- \rightarrow \pi^+\pi^-\pi^0\pi^0$ process cross section as measured by SND at VEPP-2000 and the results of previous experiments.

To measure the cross section of the process $e^+e^- \rightarrow p\bar{p}$, events with the antiproton annihilation in the wall of the vacuum chamber were used from the statistics recorded at an energy near the threshold. At energies above 1910 MeV, events with collinear tracks of the proton and antiproton having a high density of ionization in the drift chamber were selected. The detection efficiency was determined from the MCsimulation. To determine the background cross section, similar selection criteria were applied to events with energies below the $p\bar{p}$ threshold. The resulting cross section is shown in Fig. 1.2.5 in comparison with the currently most accurate results obtained by the BaBar detector.

To determine the $e^+e^- \rightarrow n\bar{n}$ process cross section,

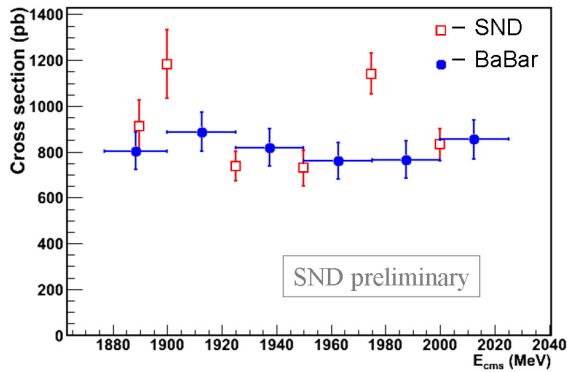


Fig 1.2.5: Preliminary SND results on the $e^+e^- \rightarrow p\bar{p}$ cross section measurement. Only statistical errors are shown for the SND results.

the background events containing tracks and photons emanating from the beam collision point were excluded. Remaining beam background events were suppressed by high threshold on the calorimeter energy deposition of about 1 GeV. The cosmic ray background was suppressed by using the muon system and the RF phase timing. The detection efficiency was determined from the MC simulation. The resulting cross section is shown in Fig. 1.2.6. in comparison with the only previous measurement by the FENICE detector.

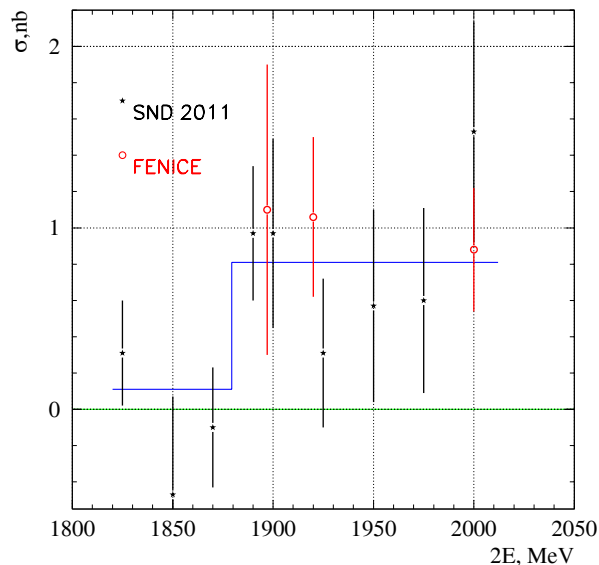


Fig 1.2.6: The measured $e^+e^- \rightarrow n\bar{n}$ cross section. Only statistical errors are shown. The results of the FENICE experiment are also indicated.

In 2011 work continued on the VEPP-2000 beam energy measurement system based on the Compton backscattering. In the experimental hall the following apparatuses were installed: CO laser as the primary photons source, an entrance vacuum chamber to guide the laser radiation into the collider vacuum chamber, high-purity germanium detector (HPGe) to register the backscattered Compton gamma quanta and measure their energy. The background conditions were studied when working in the VEPP-2000 hall. The counting rate in the absence of beams was 30 Hz. In the presence of the average total current of 80 mA, average load of the detector was about 1200 Hz. At that the live time was about 90%.

1.3. DETECTOR KEDR

The KEDR detector is an universal magnetic detector working on the e^+e^- collider VEPP-4M in the energy region from 2 to 11 GeV in the center of mass system.

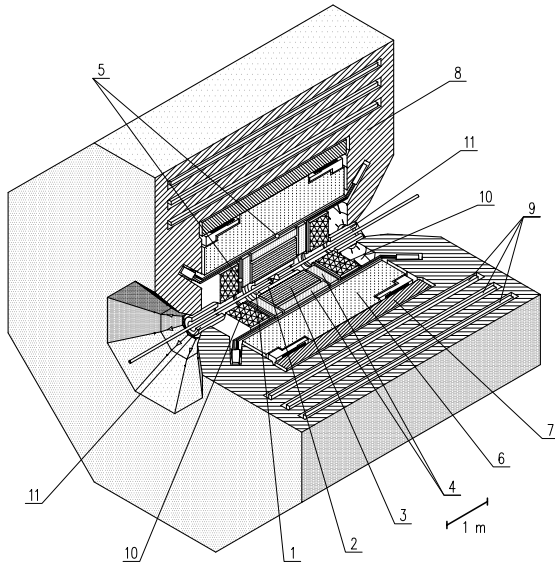


Figure 1.3.1: The KEDR detector. 1 – vacuum chamber of the collider, 2 – vertex detector, 3 – drift chamber, 4 – aerogel Cherenkov counters, 5 – time of flight counters, 6 – liquid krypton barrel electromagnetic calorimeter, 7 – superconducting solenoid, 8 – magnet yoke, 9 – muon chambers, 10 – end cap electromagnetic calorimeter based on CsI crystals, 11 – compensating solenoid.

The main systems of the KEDR detector are shown in Fig. 1.3.1. Besides this, the detector includes the system of detection of the scattered electrons for study of the $\gamma\gamma$ physics, and the luminosity monitor. Parameters of the detector are similar to those of the best detectors, operating in the world in this energy region.

1.3.1 Modernization of the KEDR detector for experiments in high energy region

It was decided to perform repair work and modernization KEDR detector systems in connection with moving to the energy region $W = 4 - 8$ GeV. Those works were initiated in May 2011. The most important results of works of 2011 on the modernization and improvement of the detector systems operation are described below:

- A disassembling of the KEDR detector was performed. All detector systems were pulled out, the vacuum chamber was dismantled.

- To increase the magnetic field from 6 kG to 10-12 kG a new source of power to feed the main superconducting solenoid and compensating coils is created on modern element base.

- At the cryogenic station of BINP in August-September 2011 new compressors were installed, which will extend the continuous operation between preventive stops.

- In connection with the increase of the field, in December 2011 work was completed to reinforce the detector elements, which provide fixing of the built-in ring, as well as supporting and defining the position of compensating coils, the central vacuum chamber, and the end-cap calorimeters with respect to the orbit of the VEPP-4M.

- New electronics of the muon chambers was developed and tested. Currently it is being produced and installed on the blocks of the system (88 blocks, 552 channels).

- For the end-cap calorimeter on base of CsI crystals a new construction to support crystals and combine their to units was built. The number of units was reduced from 8 to 4. This will reduce the systematic errors in calculations of luminosity in simulation settings and so on, associated with inaccurate knowledge of the position of crystals.

- New fixing of PMT of the aerogel Cherenkov counters was developed and tested, which prevents rotation of photodetectors in fields up to 20 kG. New fasteners were placed in second layer of the system.

- New modification of photomultipliers with three microchannel plates for aerogel Cherenkov counters system was performed for decrease degradation of photocathode.

1.3.2 Beam test of FARICH prototype

FARICH (Focusing Aerogel RICH) is a promising detector for charged particles identification in a wide momentum range. It is a detector of Cherenkov rings with a radiator of multilayer "focusing" aerogel. The works are carried out by the aerogel group of the KEDR detector with the extracted electron beam at the VEPP-4M.

1.3.3 Extracted electron beam

In 2009–2010 a new experimental facility, extracted electron beam of up to 3 GeV energy, was built at the VEPP-4M accelerator. (Fig. 1.3.2). To obtain the beam, one uses bremsstrahlung photons generated on a movable probe which is introduced into the halo of the beam of the accelerator. Conversion of gammas occurs before the dipole magnet in the experimental hall. The magnet is used to select electrons of certain momentum. Project momentum resolution reaches 0.5% at the highest energy of secondary electrons. For the measurement of electron trajectories 7 one-coordinate drift chambers with designed resolution of 0.3 mm are used. 2 scintillation counters are used to make a trigger signal and 4 veto counters are used to suppress side particles. Energy of electron is measured with the NaI-crystal calorimeter.

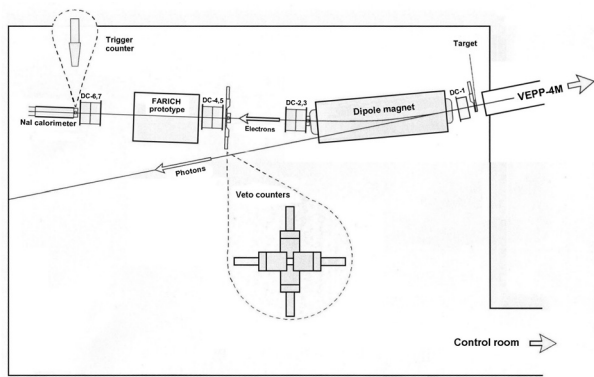


Figure 1.3.2: Test beam facility layout.

Fig. 1.3.3 shows a photo of the experimental hall with the test beam components and the FARICH prototype installed.

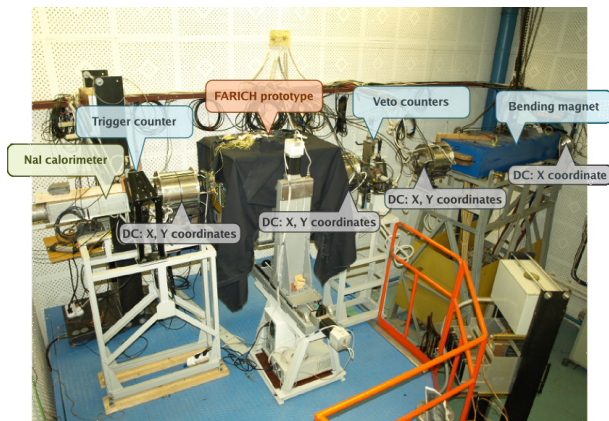


Figure 1.3.3: Experimental hall with the test beam components and the FARICH prototype.

During 2010–2011 experiments were carried out to tune the setup and to measure the beam parameters. The best results were obtained with the VEPP-4M beam energy of 3.5 GeV and beam current of 10 mA. Electron rates after the bending magnet in the experimental hall were measured to be 50–100 cps for the electron energy of 1.4 GeV and accelerator beam life time of 3000 s.

1.3.4 Works with FARICH

This technique is being developed in BINP SB RAS since 2004. A Monte Carlo simulation program was created that is able to deal with different configurations of aerogel layers and photon detectors. Boreskov Institute of Catalysis produced the world's first monolithic multilayer aerogel sample with the specific refractive indexes of layers. Projects of FARICH detectors were proposed for several HEP experiments: SuperB (Italy), PANDA (FAIR, Germany), ALICE (LHC, CERN), Super- c - τ -factory (BINP SB RAS). FARICH detectors for all

these projects have been simulated and their parameters have been calculated: particle velocity resolution, particle separation parameters, number of photoelectrons.

Conceptual design of the Super- c - τ -factory includes the FARICH system that covers 98% of full solid angle and comprises 17 m² area of radiator and 21 m² of photon detectors. The total number of channels of the detector is about 1 million. Silicon photomultipliers with 9 mm² active area are to be used. Cherenkov radiator is the 4-layer aerogel of 35 mm thickness with 200 mm focal distance, having refractive index of 1.07 in the most dense layer. Simulation has shown that the system will allow us to separate muons and pions from the Cherenkov threshold of pions in the aerogel (0.4 GeV/c) up to 1.7 GeV/c at the level higher than 3 standard deviations. This will allow to effectively use the system in a search for the $\tau \rightarrow \mu\gamma$ lepton-flavor-violating decay that if found can signalize about the new physics beyond the Standard Model. Such the μ/π -separation can not be possibly obtained using any other detector including DIRC, which worked at the BaBar experiment (SLAC), and DIRC analogues which are being developed for some future HEP experiments.

In 2010–2011 a prototype of the FARICH detector has been created at BINP SB RAS. MRS APD silicon photomultiplier produced by CPTA company (Moscow) with an active area size 2.1×2.1 mm² was chosen as a detector of photons. An array of 32 such photodetectors constitutes the detector for registration photons of Cherenkov radiation from aerogel. To read the signal two 16-channel discriminator-amplifier boards made in INR RAS (Moscow) are used. To digitize the signal one 64-channel TDC board in VME standard produced by firm CAEN (Italy) is used. The design of the prototype allows one to test the multi-layer aerogel radiators with a length of focus from 50 to 700 mm. Also a package of programs for the system of data collection from the FARICH prototype was written. Calibrations of the photon detectors with the help of picosecond laser were carried out. The time resolution of channels is 0.4–1 ns, dark counts rate is 2–8 Hz, channel dead time — 20 ns.

In April – May, 2011 the prototype was successfully tested with the extracted beam at an energy of electrons around 1 GeV. The resolution along the radius of Cherenkov ring for one photon for the 4-layer block of focusing aerogel with focusing length of 93 mm was measured. Resolution was 1.1 mm, in good agreement with the result, obtained from the simulation. Fig. 1.3.4 shows the distribution of hits in the plane of the photodetectors vs track's position (left picture: one can see three elements of ring) and the density of photoelectrons as a function of ring radius for one of the photomultipliers. The quality of aerogel is consistent with the calculations and does not introduce additional error.

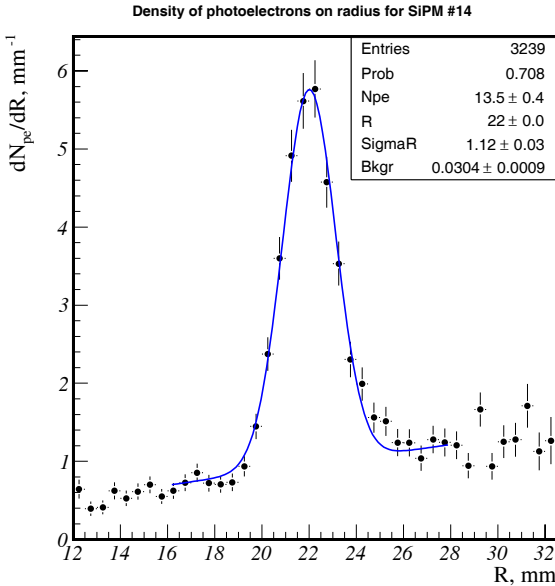
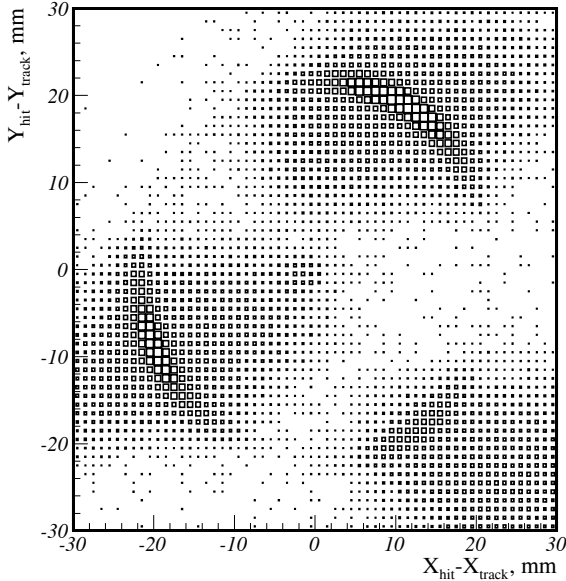


Figure 1.3.4: 2D distribution of hits wrt track's position (top) and photoelectron density as function of ring radius for the channel 14 (down). Line shows a fit with Gaussian and linear background.

1.4 RESULTS OF WORK OF THE KEDR DETECTOR AT THE VEPP-4M COLLIDER IN 2011

In the season 2011 the KEDR detector continued the experiment at the VEPP-4M collider, processing the statistics collected earlier and the new one. The most important results are the following.

— Collection of statistics: in 2011 the luminosity inte-

gral 2.1 pb^{-1} at the $\psi(2S)$ -meson, 1.4 pb^{-1} in the energy interval $2E=3.1 - 3.7 \text{ GeV}$ scanning, and 0.16 pb^{-1} at the energy $2E=7.0 \text{ GeV}$ was written.

— Analysis of experiment on search for narrow resonances in the energy region $2E=1.85 - 3.1 \text{ GeV}$ was completed.

— Analysis of experiment on measurement of parameters of the $\psi(3770)$ -meson was completed, the mass, the full and the electronic width were obtained.

— Measurement of parameters of the $\psi(2S)$ -meson: precision in the mass value was improved, the value $\Gamma_{ee} \times Br(\psi(2S) \rightarrow \text{hadrons})$, the full and the electronic widths were obtained.

— Measurement of the τ -lepton mass using full statistics was continued.

Description of these works in some detail follows below.

1.4.1 Search for narrow resonances

In 2011 analysis of the experiment on search for narrow resonances in the energy region $2E=1.85 - 3.1 \text{ GeV}$ was completed. Method of measurement and the data analysis were published elsewhere.

Fig. 1.4.1 shows the value of the upper limit on the product of the electron width and the probability of the narrow resonance decay to hadrons in the energy range 1.85 - 3.1 GeV.

The dependence of the detection efficiency on the type of final state and its cms energy has been obtained using the J/ψ -meson hadronic decays. Fig. 1.4.1 does not include the uncertainty, with which the beam energy spread in the storage ring is known. The final value of limit on the value of $\Gamma_{ee}^R \times Br(R \rightarrow \text{hadrons})$ in region $2E = 1.85 - 3.1 \text{ GeV}$ is equal to

$$\Gamma_{ee}^R \times Br(R \rightarrow \text{hadrons}) < 120 \text{ eV, 90\% CL.}$$

The value of this limit is four times lower than the previous one obtained at the collider ADONE.

1.4.2 Measurement of the $\psi(3770)$ -meson parameters

In 2010 final results of the experiment on measurement of the $\psi(3770)$ -meson parameters were obtained.

For processing we used statistics of 2.6 pb^{-1} , collected in three scans of the $\psi(2S)$ - $\psi(3770)$ region in 2004–2006. For the first time effect of interference of resonant and non-resonant $D\bar{D}$ -mesons pairs production (in latter case with different form-factor models) on $\psi(3770)$ parameters was studied in detail. Systematic uncertainties connected with choice of the form of non resonant cross section were studied.

Visible cross section of the process $e^+e^- \rightarrow \text{hadrons}$ is shown in Fig. 1.4.2.

The following values of the $\psi(3770)$ -meson mass and full width were obtained:

$$M = 3779.2_{-1.7}^{+1.8} {}_{-0.7}^{+0.5} {}_{-0.3}^{+0.3} \text{ MeV,}$$

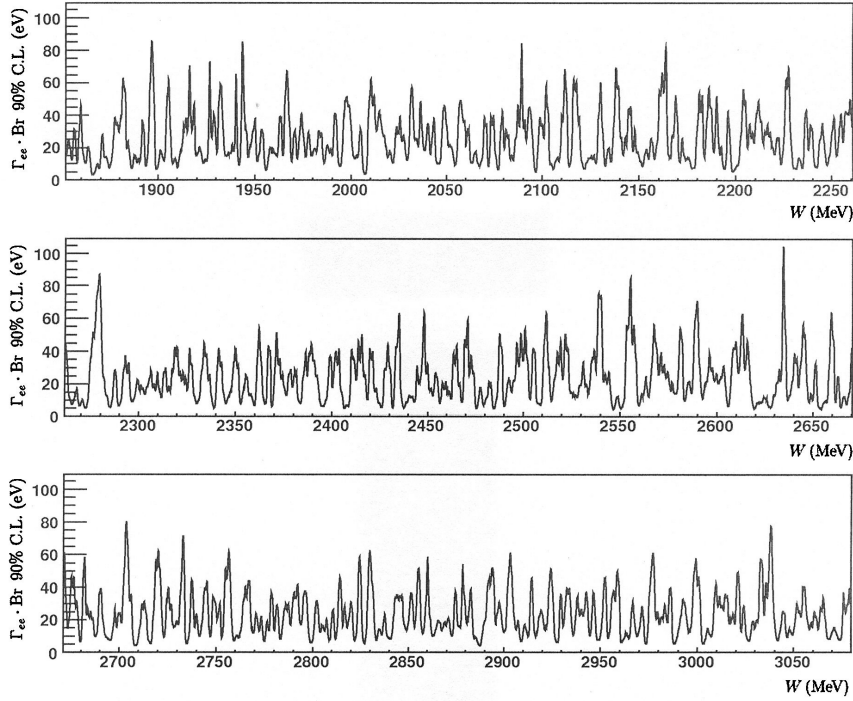


Figure 1.4.1: Upper limit on the product of the narrow resonance electron width and the probability of its decay to hadrons in the energy range $2E=1.85 - 3.1$ GeV.

$$\Gamma = 24.9^{+4.6}_{-4.0} {}^{+0.5}_{-0.6} {}^{+0.5}_{-0.2} \text{ MeV.}$$

Statistical, systematic and model uncertainty of results are presented consistently. Interference leads to two-valued result for the electronic width:

$$(1) \Gamma_{ee} = 154^{+79}_{-58} {}^{+17}_{-9} {}^{+13}_{-25} \text{ eV,}$$

$$(2) \Gamma_{ee} = 414^{+72}_{-80} {}^{+24}_{-26} {}^{+90}_{-10} \text{ eV,}$$

Article on the work submitted for publication.

1.4.3 Measurement of the $\psi(2S)$ -meson parameters

In 2011 processing of statistics, collected for the study of the properties of $\psi(2S)$ -meson, was continued. New results are presented in this section.

Measurement of the mass.

In 2011 an accuracy of the mass measurement of the $\psi(2S)$ -meson in comparison with the result, published in 2003 (for scanning 2002), was noticeably improved. The new value was obtained from the analysis of the data of 2004 and 2006, as well systematic errors were done more accurate.

$$M = 3686.114 \pm 0.007 \pm 0.011 {}^{+0.002}_{-0.012} \text{ MeV.}$$

This value is within one standard error consistent with the table value $M_{\psi(2S)} = 3686.093 \pm 0.034$ MeV and has two times better accuracy.

Data of different measurements are shown in Fig. 1.4.3. The results were accepted for publication.

Measurement of $\Gamma_{ee} \times Br(\psi(2S) \rightarrow \text{hadrons})$

In 2011, the analysis was performed with the purpose of measuring the value of $\Gamma_{ee} \times Br(\psi(2S) \rightarrow \text{hadrons})$. The following result was obtained:

$$\Gamma_{ee} \times Br(\psi(2S) \rightarrow \text{hadrons}) =$$

$$2.233 \pm 0.015 \pm 0.037 \pm 0.020 \text{ keV.}$$

Data of the KEDR detector allow us to calculate the value Γ_{ee} . Using the above result for

Using the above results for $\Gamma_{ee} \times Br(\psi(2S) \rightarrow \text{hadrons})$ independent averages (PDG2010) for the $Br(\psi(2S) \rightarrow \text{hadrons})$ and $Br(\psi(2S) \rightarrow e^+e^-)$ we obtain the following value of the full and electronic widths Γ_{ee} for the $\psi(2S)$ -meson:

$$\Gamma = 296 \pm 2 \pm 8 \pm 3 \text{ keV.}$$

$$\Gamma_{ee} = 2.282 \pm 0.015 \pm 0.038 \pm 0.021 \text{ keV.}$$

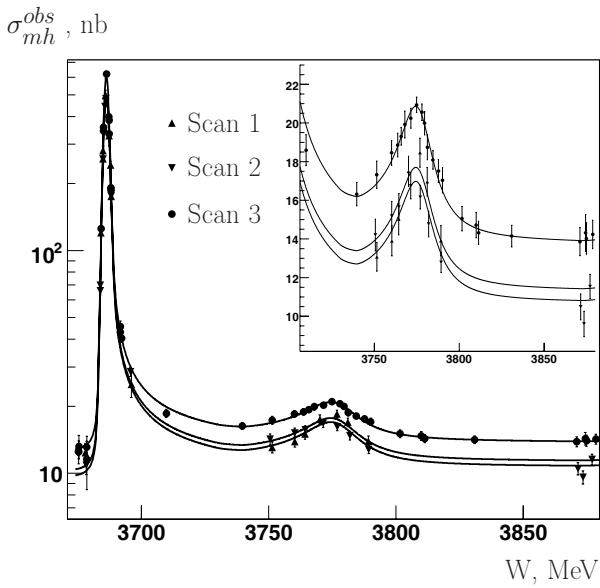


Figure 1.4.2: Visible cross section of the process $e^+e^- \rightarrow \text{hadrons}$ in three scans as a function of the center mass energy. The lines are the result of a common fit for three scans.

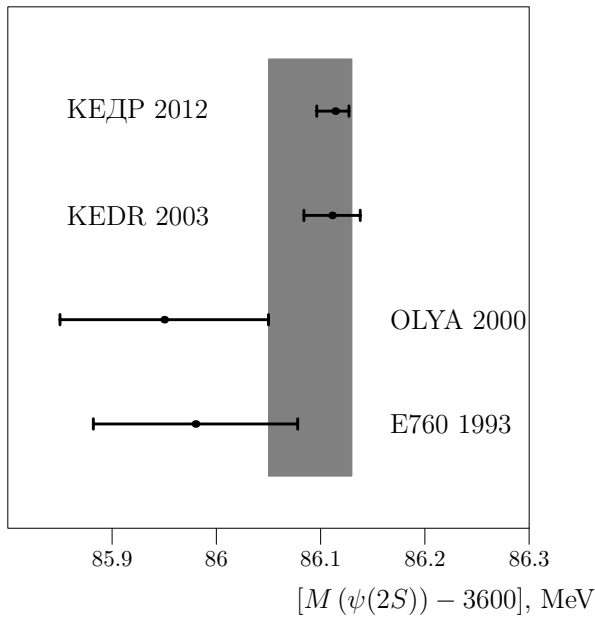


Figure 1.4.3: The mass of the $\psi(2S)$ according to the different experiments and the average value (shown as vertical band).

The achieved accuracy of determination of partial widths $\psi(2S)$ in two times exceeds the accuracy of similar measurements carried out in the previous experiments (see Fig. 1.4.4).

The results will be published in 2012.

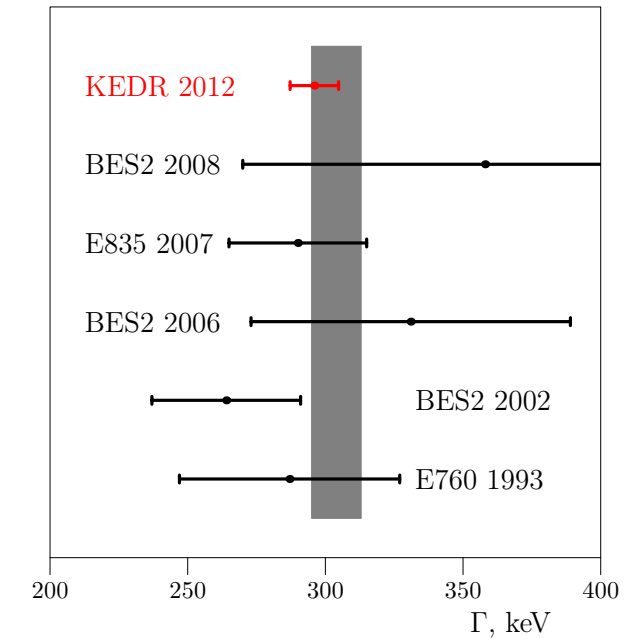
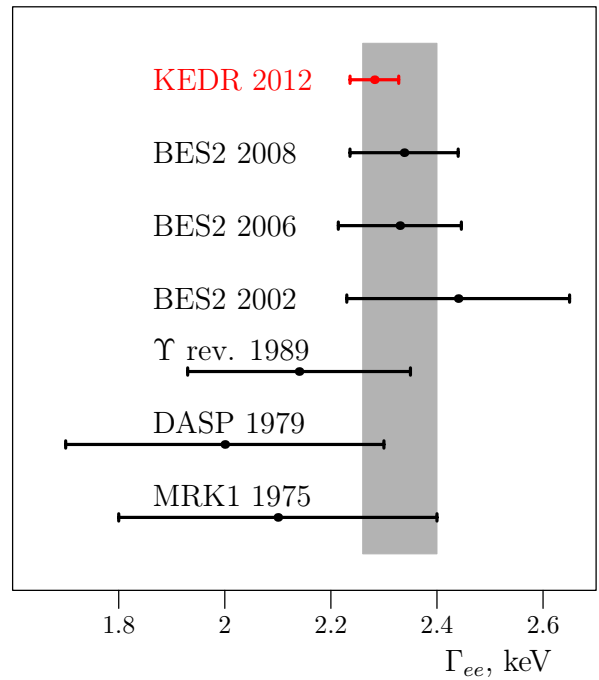


Figure 1.4.4: Electronic and full width $\psi(2S)$ according to data from different experiments. Vertical bands show the average values from the PDG-2010.

1.4.4 Measurement of the τ -lepton mass

The lepton universality principle is one of the fundamental principles of the Standard Model. It consists in requirement of equality of weak interaction constants for leptons e^\pm, μ^\pm, τ^\pm .

The $\mu - \tau$ universality requires that it should be satisfied the equality

$$\left(\frac{G_\tau}{G_\mu}\right)^2 = \left(\frac{m_\mu}{m_\tau}\right)^5 \left(\frac{t_\mu}{t_\tau}\right) Br(\tau \rightarrow e\nu_\tau\bar{\nu}_e) \cdot \frac{F_{cor}(m_\mu, m_e)}{F_{cor}(m_\tau, m_e)} \equiv 1$$

(Since $Br(\mu \rightarrow e\nu_\mu\bar{\nu}_e) = 1$). Using the PDG-2010 data, for the experimental value of this ratio one obtains a value 1.0029 ± 0.0045 , which is less than by one σ different from 1. The main contribution to the error give uncertainties with which the life time of the τ -lepton ($\pm 0.34\%$) and the value $Br(\tau \rightarrow e\nu_\tau\bar{\nu}_e)$ ($\pm 0.28\%$) are known. Error in the average value of the τ -lepton mass is $\pm 0.009\%$, its contribution to the presented above ratio is small now ($\pm 0.045\%$). The value of this error was diminished noticeably, after inclusion in the PDG tables our measurement of the m_τ with the best in the world precision (2007). Nevertheless, the measurement of the τ -lepton mass with the best possible accuracy remains an interesting task and can be claimed in the future. Such experiment with participation of physicists from the Budker INP has been started at the e^+e^- -collider in Beijing in 2011.

In 2011, we continued analysis of the full statistics, which was recorded (15.2 pb^{-1}), in order to improve the precision of the value of mass of the τ -lepton, to diminish the systematic errors of the measurement.

The following value of the mass was obtained:

$$m_\tau = 1776.69_{-0.19}^{+0.17} \pm 0.15 \text{ MeV} .$$

We are continuing analysis of the systematic errors, it is possible that this result will be improved.

1.4.5 Conclusion

In conclusion, it should be noted that work done with the KEDR detector under the title "In experiments with KEDR detector at VEPP-4M with the best in the world precision parameters of the $\psi(2S)$ and $\psi(3770)$ mesons have been measured and the most sensitive limit on narrow resonances cross section in the energy region $2E=3.1 - 3.7$ GeV has been achieved" was recognized the best work of the Budker INP in 2011 in the field of particle physics and fundamental interactions.

In 2011 results of experiments with the KEDR detector were published in 4 articles and 5 preprints, 3 reports were submitted at Scientific session-conference section of NF OFN RAS "Physics of fundamental interactions" (November, Moscow), 2 reports were submitted at conference "From ϕ to ψ " (September, Novosibirsk), one report was submitted at the 22nd International Conference on Magnet Technology (September, Marseille), one report was submitted at the XXIst Europhysics Conference on High Energy Physics (July, Grenoble), one report was submitted at the International conference on hadron spectroscopy HADRON 11 (June, Munich), one report was submitted at the 8th International Workshop of QWG (October, Darmstadt), and one doctoral dissertation was defended. 2 papers were published and 6 reports on international and Russian workshops as well as a talk on the experimental seminar at BINP SB RAS were presented regarding the experimental works with FARICH.

This work was done with partial support by grants RFBR 09-02-01143-a, 10-02-00871-a, 10-02-00904-a, 11-02-00558-a, 11-02-01064-a, 11-02-01422-a, 11-02-05024-b, the Russian President Grant for State support of leading scientific schools NSh-6943.2010.2, the Integration Project SB RAS 100 (2009 - 2011), as well as with financial support from the Ministry of Education and Science of Russia.

1.5 DETECTORS FOR HEP

In 2011, a lot was done within the upgrade of the detector electronics.

KEDR:

1. New discriminators for the muon system were fabricated (being installed at the moment).
2. The power backup unit for the valves of the cryogenic system was finished.
3. The second version of the control module for these valves was developed and built.
4. A prototype was made and a control unit of the forevacuum station is being adjusted.
5. The chamber electronics of the crypton calorimeter were repaired, and restoration of the CsI calorimeter with partial replacement of amplifiers is underway.

SND:

1. Spare modules for the trigger were made and tested: the logic of the tracks and that of the calorimeter (a stand was made for their inspection)
2. New front-end electronics were made for the first layer of the calorimeter and a half of it was mounted on the detector up and started operation.
3. Similar electronics for the second and third layers of the calorimeter were developed and are being fabricated now.
4. A prototype of the waveform registration module for the calorimeter was made and used for research on the possible time resolution of the calorimeter.
5. The time resolution of the calorimeter trigger was improved almost 3 times through correction of the modules of the primary trigger interface.

1.6 X-RAY DETECTORS

In 2011, development of registration equipment to study the dynamics of explosions was conceptualized. The existing detector DIMEX has a one-coordinate scale, which is a significant limitation in some experiments. There are plans to design a multi-coordinate detector, in which silicon microstrip structures will be used as recording elements. The work on drawing up technical specifications for the development and production of samples of such structures is underway.

In 2011, a contract on the supply of the X-ray detector OD-3M to the Institute of Crystallography, RAS (Moscow) was fulfilled. One more detector of this type was installed in beam line 5 of the VEPP-3 SR source instead of the detector OD-3, which had been in use there for several years.

In 2011, samples of information boards were made, as well as a stand to test them. The boards are intended for the detector OD-4, designed for experiments on wide-angle scattering on SR. Instead of a wire structure, such as in OD-3M, a multistage gas electron multiplier (GEM) is used in OD-4. This allows, together with a high gas gain (over 10,000), making a detector in the form of an arc with an arbitrary angular aperture. A lot was done on the

development of the topology of the motherboard and software of the detector.

1.7 OTHER WORKS

Active participation in the works associated with the development of the new data collection system for the detector BELLE-II (KEK, Japan) was continued. Twelve 16-channel shaper-amplifiers boards were made for the barrel part of the calorimeter on CsI(Tl) crystals.

The 2nd version of the collector module for reading data from the boards of the driver amplifiers was designed and passed to the production department.

1.8 MICROSTRUCTURE GASEOUS DETECTORS

Development of detectors based on gas electron multipliers (GEMs) was continued in 2011. The work went in several directions:

1) development of two-phase cryogenic avalanche detectors (CRADs) on the basis of thick GEMs (THGEMs) for low-background experiments on the search for dark matter and registration of coherent scattering of neutrinos on nuclei, as well as for medical imaging;

2) study of infrared (IR) scintillations in gaseous and liquid Ar at cryogenic temperatures;

3) modernization of the system for scattered electrons in the KEDR experiment; and

4) participation in collaborations RD51 at CERN on the development of micro-structure gas detectors and TPC for the International Linear Collider.

1.8.1 Two-phase cryogen avalanche detectors (CRADs) on the basis of thick gas electron multipliers (THGEMs)

The main objective of this project is development of methods for detecting neutrinos and dark matter and medical imaging via developing so-called cryogenic avalanche detectors (CRADs) based on liquid Ar and Xe, i.e. cryogenic detectors with electron avalanche amplification that is realized in the detection medium. The avalanche amplification is brought into effect by means of gas electron multipliers (GEMs), which work in dense noble gases at cryogenic temperatures. Such a wide range of application of CRADs is based on the GEM unique property, which had been revealed in our previous projects, of high gains in dense noble gases at cryogenic temperatures. GEM-based CRADs may be applied to registration of coherent scattering of neutrinos on nuclei and search for dark matter with the use of two-phase (liquid-gas) Ar and Xe, as well as in positron emission tomography (PET) with liquid or two-phase Xe. An important goal of the project is to increase the CRAD sensitivity in low-background experiments, to the single-electron counting mode. Besides other means, this will be achieved through the use of a combined multiplier that

consists of thin and thick GEMs, as well as by optical reading from the GEMs with the help of high-power Geiger avalanche photodiodes (G-APDs) in the near infrared (IR) range, see Fig. 1.8.1. Another aim of the project is to develop a real-life CRAD with a volume of 10 liters, applicable to operation in Ar and Xe. The response of the detector to recoils of nuclei will be studied; the recoils will be induced by neutron scattering and simulate a signal from coherent scattering of neutrinos and dark matter. Results of these studies will be used in the designing of a 100-liter detector of a volume, which will be sufficiently big for full-scale experiments on coherent scattering of neutrinos, search for dark matter, and PET. The application to medical imaging, PET, coherent scattering of neutrinos on nuclei, and remote monitoring of nuclear reactors via measuring the neutrino flux, may be of considerable commercial interest in the field of nuclear non-proliferation.

The intensive study of the CRADs on the new upgraded facility with a cryogenic chamber of a volume of 9 liters was continued in 2011.

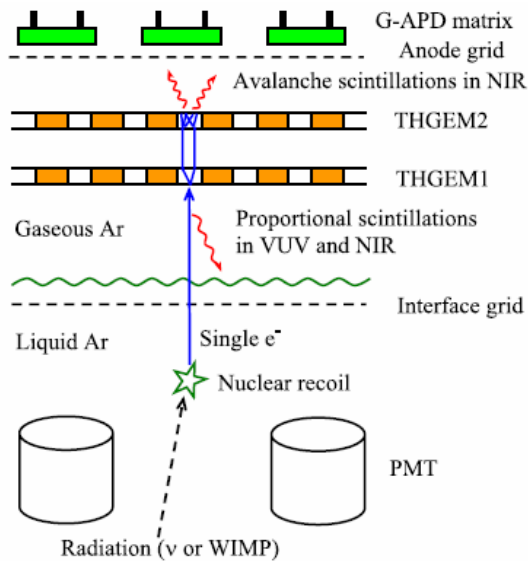


Fig. 1.8.1. Scheme and principles of operation of two-phase cryogenic avalanche detector (CRAD) in Ar. The detector is based on thick gas electron multipliers (THGEMs) with optical readout using Geiger avalanche photodiodes (G-APDs) and intended for low-background experiments on registration of coherent scattering of neutrinos on nuclei and search for dark matter.

A two-phase THGEM-based CRAD was studied for the first time in Xe, both with charge reading and with optical reading of signal with the use of Geiger avalanche photodiode (G-APD). The two-phase CRAD with an active area of $2.5 \times 2.5 \text{ cm}^2$ was shown to work stably in the two-phase CRAD in Xe: the charge gain was as high as 600 with a rather low noise level (a few Hz): see Fig. 1.8.2. On the other hand, the maximum gain achieved was 5 times lower than in two-phase Ar.

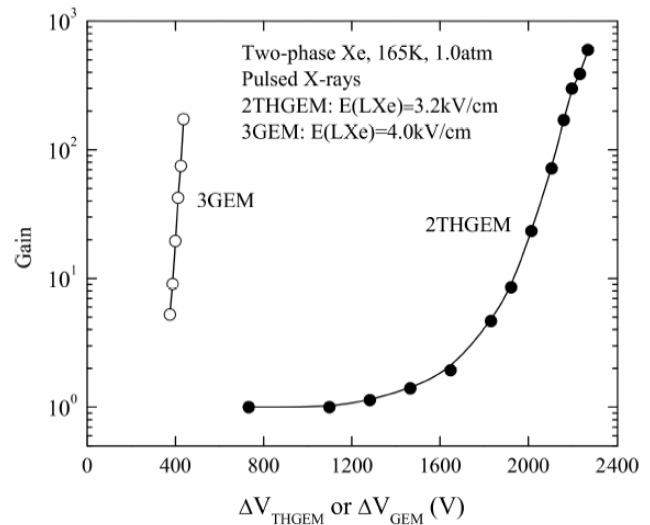


Fig. 1.8.2. Gain characteristics of the two-stage THGEM in the two-phase CRAD in Xe. The characteristic of a three-stage GEM is shown for comparison.

Further studies on optical reading were carried out with a combined THGEM/G-APD multiplier in gaseous Xe in the near-IR range (to 1,000 nm) at 200 K. Fig. 1.8.3 (above), in particular, shows the spectrum of infrared scintillations in Xe and Ar, as well as the efficiency of photon detection with G-APD. Fig. 1.8.3 (bottom) presents a typical optical and charge signals from the combined THGEM/G-APD multiplier at a charge gain of 350 and exposure to 60 keV X-rays. At a charge gain of 350, the optical signal amplitude was 0.07 photoelectrons per primary (before the amplification) electron at a G-APD angle of view of $\pm 70^\circ$. This is an order of magnitude lower than the amplitude attained in Ar in a two-phase mode with a similar charge gain. The weaker optical signal corresponds to smaller overlapping of the spectra of IR scintillations and G-APD sensitivity in Xe as compared with Ar.

Thus, it is concluded that the charge gain in the two-phase CRAD in Xe may be sufficient for PET applications. On the other hand, the gain is insufficient for the maximum-sensitivity detectors required for low-background experiments; two-phase CRADs in Ar are still more preferable.

The studies on cryogenic avalanche detectors will be continued in 2012 in the following directions:

- operation of THGEM and combined THGEM/GEM multipliers with an active area of $10 \times 10 \text{ cm}^2$ in the two-phase CRAD in Ar and Ar + N₂;
- operation of two-phase THGEM-based CRAD in Ar with a liquid layer thickness of 5 cm;
- study of a two-phase CRAD in Ar with optical readout from a THGEM with a G-APD matrix of 3×3 elements.

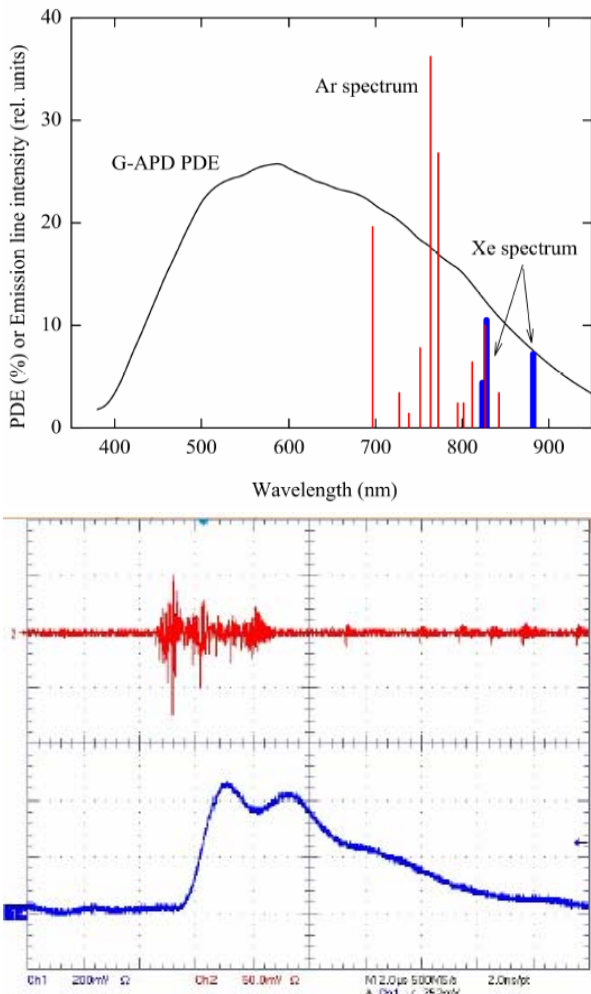


Fig. 1.8.3. Above: spectra of scintillations in gaseous Ar and Xe in the near-IR range and the spectrum of photon detection efficiency in the G-APD. Bottom: typical optical (upper scan) and charge (lower scan) signals from the combined THGEM/G-APD multiplier in gaseous Xe at 200 K at a charge gain of 350 and exposure to X-rays of an energy of 60 keV.

1.8. 2. Investigation into infrared (IR) scintillations in gaseous and liquid Ar at cryogenic temperatures

The successful results on optical reading of avalanche scintillations in Ar in the combined THEM/GAPD multiplier initiated studies on the primary and secondary IR scintillations in gaseous and liquid Ar at cryogenic temperatures. That resulted in 2011 in the first-time measurement of the yield of primary and secondary (proportional) scintillations in gaseous and liquid Ar in the range of 400 to 1000 nm. A new method for measuring the scintillation yield was developed for this purpose. This method involves G-APDs sensitive in the near infrared region of the spectrum and working in a

time-resolved photon counting mode. Below are presented the results of these studies.

For gaseous Ar, primary scintillations were proved to emit in the near IR range. Their yield (the fast component) amounted to $17,000 \pm 3,000$ photons/MeV in the range of 690 to 1,000 nm (Fig. 1.8. 4, above). This is comparable with the yield of scintillations in the VUV range for gaseous Ar and Xe.

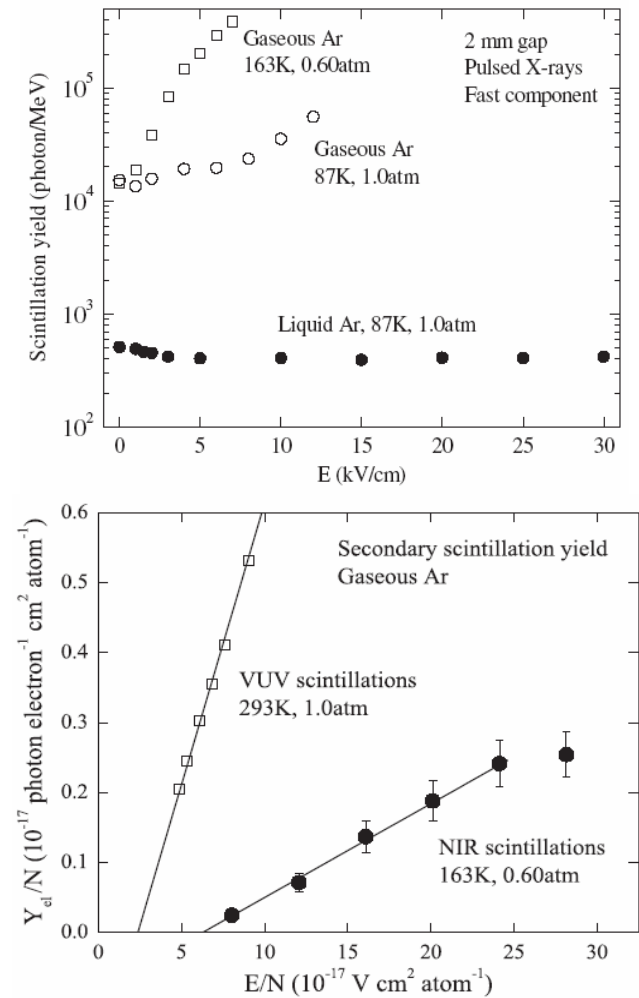


Fig. 1.8.4. Above: scintillation yield in gaseous and liquid Ar at cryogenic temperatures vs. electric field; the primary scintillation area corresponds to a field <1 kV/cm. Bottom: reduced yield of the secondary scintillations (electroluminescence) vs. reduced electric field in the near IR and VUV region.

The yield of primary scintillations (the fast component) in liquid Ar was significantly lower (Fig. 1.8.4, above): 510 ± 90 photons/MeV in the range of 400 to 1,000 nm. Nevertheless, it is comparable with the light yield of fast solid scintillators used in HEP calorimetry.

There were proportional scintillations (electroluminescence) found in the near IR field in gaseous Ar (Fig. 1.8.4, bottom). The parameter of electroluminescence proportionality (the slope in Fig. 1.8.4,bottom) at 163 K amounted to 13 photons per

electron per kV, which is slightly less than in the VUV region. However, proportional scintillations can significantly increase the light yield in the IR region as compared with primary scintillations, up to hundreds of thousands of photons per MeV.

Opposite to gaseous Ar, no proportional scintillations were observed in liquid Ar, up to an electric field of 30 kV/cm.

Research on infrared scintillations in noble gases will be continued in 2012.

1.8.3. Modernization of the system for scattered electrons in the KEDR experiment

The system for registration of scattered electrons is an essential part of the KEDR experiment and allows detecting electrons that are scattered through small angles from the collision place. These electrons are a characteristic feature of photon-photon interactions and their registration and accurate momentum measurement is an important physical task.

For the purpose of attaining ultimate electron-momentum resolution, which is determined by beam parameters in the accelerator, and improving the separation of signal from background, each of the eight stations of the system was equipped with a detector based on a triple GEM with two-coordinate readout. The detectors allow measuring the coordinate in the orbital plane with a resolution of ~ 0.1 mm. In the direction perpendicular to the orbital plane, the spatial resolution will be ~ 0.25 mm in the area of ± 1 cm from the orbit and ~ 1 mm in a larger distance. For the required parameters to be attained, a special design of the readout plane was developed, with a variable angle of the stereo strips. The detectors are 125*100 mm to 250*100 mm in size, depending on the type of the station.

During 2010, the system of GEM-based detectors (GEM-SRSE) was completely launched and began continuous operation in the data acquisition system of KEDR. During the season of 2010-2011 (November 2010 to March 2011), the system was involved in the collection of statistics in the energy range of 3.2 GeV to 8 GeV. Figs. 1.8.5 and 1.8.6 show the gas amplification factor and efficiency of all the 8 detectors of the system in dependence on the time since the beginning of the season.

It is evident that the detectors have operated stably for a long time at a high gain of 20,000 to 40,000 and efficiency of 95 to 97%, with no signs of breakdown and subsequent damage to the structure of the detectors and electronics.

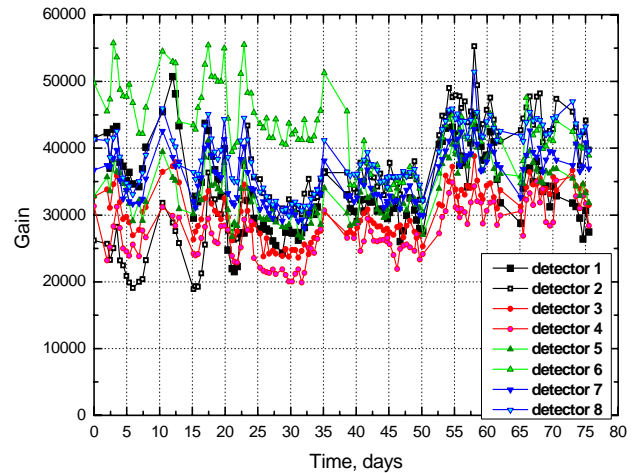


Fig. 1.8.5. Gas amplification coefficient of the GEM-SRSE detectors vs. time.

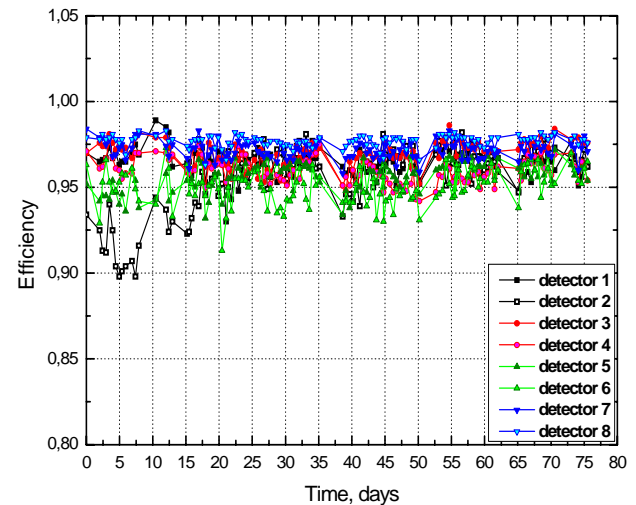


Fig. 1.8.6. Efficiency of the GEM-SRSE detectors vs. time.

1.8.4. Participation in collaborations

The BINP group of microstructure gas detectors participates in the international collaboration RD51 at CERN, which is aimed at the development of microstructure gas detectors and was formed in 2008. In 2011, the BINP group continued its participation in this collaboration.

Besides, the group continued its participation in the development of the TPC for the International Linear Collider (ILC). Currently, the cascaded GEM seems to be the most likely candidate for the end registering detector of the TPC.

The work on cryogenic avalanche detectors was supported by grants from the federal target program "Scientific and scientific-pedagogical staff of innovative Russia" (for 2009-2012), Ministry of Education and Science Contracts P682 and P980 (for 2009-2013), and RF Government grant 11.G34.31.0047 (for 2011-2013).

1.9 EXPERIMENT BELLE

1.9.1. Main results

- A method has been developed to take into account interference in the decays $B^\pm \rightarrow K^\pm \eta_c^{(0)}$, parameters of the η_c и η_c' charmonia as well as products of the branching fractions have been measured.

- A model-independent method of the measurement of the branching fraction for the decay $\Lambda_c^+ \rightarrow p K^- \pi^+$ was developed.

- Charged bottomonium-like states Z(10610) and Z(10650) were discovered. A model considering them as four-quark bound systems of BB^* and B^*B^* mesons, respectively.

- A search for lepton-flavor-violating decays $\tau \rightarrow l V^0$ was completed.

- A search for CP-violation was performed in the decay $\tau^\pm \rightarrow K_S^0 \pi^\pm \nu_\tau$.

- A search for lepton-flavor-violating decays $\tau \rightarrow l hh'$ was continued.

- A new shaper-digitizer in the VME standard was developed and constructed, its characteristics measured.

- Mechanical and electrical specifications for the new VME crate were developed.

- Measurements of the light output and non-uniformity were performed for pure CsI crystals produced in Kharkov.

1.9.2. Data analysis of the Belle experiment

The BINP group is actively participating in the Belle experiment at KEK, Tsukuba, Japan, both in its design

and construction and maintenance of the world largest calorimeter on CsI crystals. In 2010 the Belle detector was stopped for an upgrade, also upgraded is the KEKB collider. Analysis of the collected data is in progress.

Study of the η_c and $\eta_c(2S)$ charmonia in B decays

A group of BINP scientists has studied properties of the η_c and its excited state $\eta_c(2S)$. These particles are bound states of c and anti-c quarks (so called charmonia). Their source was considered to be a B meson decay into K meson and charmonium, followed by the charmonium decay into hadrons, $K_S K \pi$. B meson decays into the same final state ($KK_S K \pi$), but without the intermediate charmonium state, are referred to as the non-resonant contribution. interference with which amplitude leads to a considerable model error of the measurement of B meson and charmonium decays branching product. To decrease this model error, the estimation of the interference using the 2D fit of $\cos\theta$ (cosine of the angle between a K meson from the B decay and a K_S meson) and $K_S K \pi$ invariant mass distributions was performed. The fit results are shown in Fig. 1.9.1. The proposed procedure of taking the interference into account for the first time contains no assumptions about the interference phase or absolute value, i.e., is model independent. Results of this study are the B meson and charmonium decays branching product and the mass and width values of the η_c and $\eta_c(2S)$ mesons. Due to the large data sample size, the results have small statistical errors and allow the improvement of the corresponding world average values. The results were published in journal Physics Letters B.

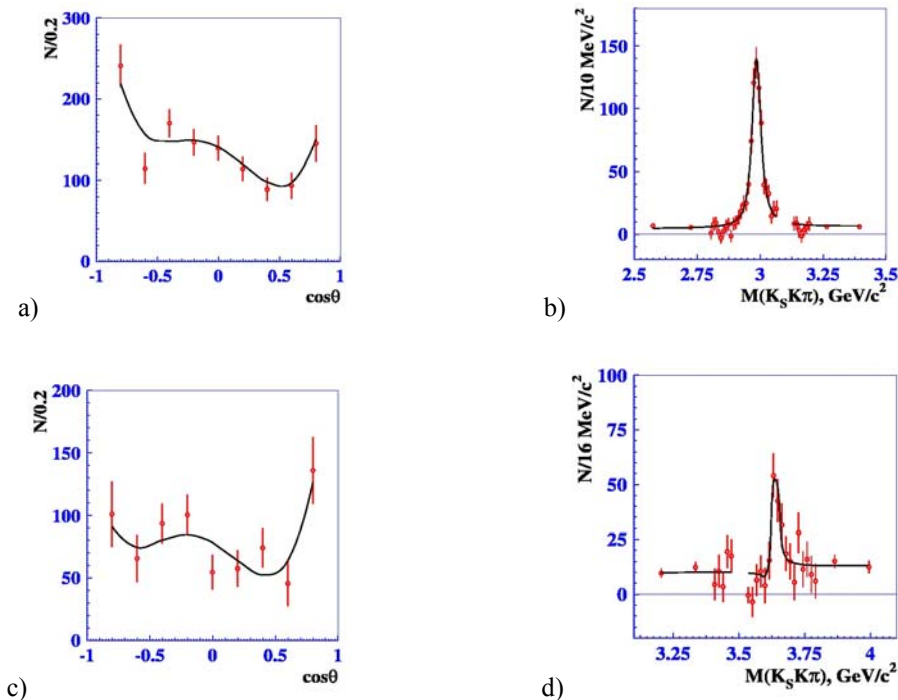


Fig. 1.9.1. Projections of the 2D fit of the $\cos\theta$ and $K_S K \pi$ distributions in case of η_c (a, b) и $\eta_c(2S)$ (c, d) meson decays.

Model-independent measurement of the branching fraction of $\Lambda_c^+ \rightarrow pK^-\pi^+$

The absolute value of the branching fraction of the decay $\Lambda_c^+ \rightarrow pK^-\pi^+$ is an important quantity for physics of heavy quarks since probabilities of the majority of other decays of the Λ_c^+ baryon have been measured relative to this mode. The absolute value of this branching fraction, $(5.0 \pm 1.3)\%$, has a large 26% uncertainty mainly due to the theoretical models. The BINP group has developed a model-independent method to determine this branching fraction based on the selection of the exclusive process $e^+e^- \rightarrow \Lambda_c^+ p^- D^0$ by two different ways: (1) reconstruction of Λ_c^+ in recoil mass (Fig.1.9.2(a)) and (2) search for this process with Λ_c^+ detection in the invariant mass of $pK^-\pi^+$, e.g., $D^{(*)0}$ reconstruction in recoil mass (Fig.1.9.2 (b)). The ratio of (2) to (1) gives a sought for result with an uncertainty of about 10% (taking into account systematic effects). This analysis is close to completion and will be published after its discussion by the collaboration.

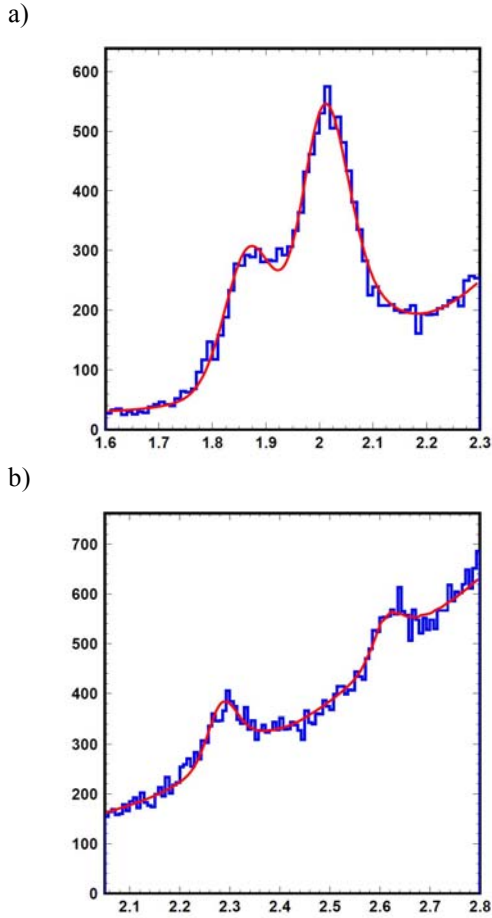


Fig. 1.9.2. (a) Recoil mass of $(D^0 p)$ in GeV/c^2 for the process $e^+e^- \rightarrow \Lambda_c^+ p^- D^0$, $D^0 \rightarrow K^-\pi^+$. A peak in the right part is $\Lambda_c(2625)^+$. (b) Recoil mass of $(\Lambda_c^+ p^-)$ in GeV/c^2 for the process $e^+e^- \rightarrow \Lambda_c^+ p^- D^{(*)0}$, $\Lambda_c^+ \rightarrow pK^-\pi^+$.

Discovery of exotic $Z(10610)$ and $Z(10650)$ states

In 2008 analysis of the data collected by Belle in the $Y(5S)$ region showed that the probabilities of the $Y(5S) \rightarrow Y(nS)\pi^+\pi^-$ transitions, where $n=1, 2, 3$, are almost two orders of magnitude larger than expected. By 2010 an integrated luminosity larger than 120 fb^{-1} was collected near $Y(5S)$ and allowed full amplitude analysis of the three-body decays $Y(5S) \rightarrow Y(nS)\pi^+\pi^-$, $n=1, 2, 3$, to be performed.

Analysis used completely reconstructed events of $Y(5S) \rightarrow Y(nS)\pi^+\pi^-$, where $Y(nS)$ was reconstructed by $Y(nS) \rightarrow \mu^+\mu^-$ decay. Reliable muon identification was possible due to the Belle KLM detector. To select a signal we plotted the dependence of the invariant mass of the muon pair on $MM(\pi^+\pi^-)$, where $MM(\pi^+\pi^-)$ is a missing mass for a pion pair calculated from energy-momentum conservation. The corresponding distribution is shown in Fig.1.9.3, where a signal of $Y(5S) \rightarrow Y(nS)\pi^+\pi^-$, $Y(nS) \rightarrow \mu^+\mu^-$ decays can be seen along the diagonal in the regions corresponding to $Y(nS)$ mass.

For further analysis we selected events satisfying a requirement common for all final states, $|MM(\pi^+\pi^-) - MM(\mu^+\mu^-)| < 150 \text{ MeV}/c^2$ and requirement $|MM(\pi^+\pi^-) - M_{Y(nS)}| < 50 \text{ MeV}/c^2$ to select a signal in the channel $Y(5S) \rightarrow Y(nS)\pi^+\pi^-$. For selected events the two-dimensional (Dalitz) distribution $M^2(Y(nS)\pi^+\pi^-)_{\text{max}}$ vs. $M^2(\pi^+\pi^-)$ was plotted. To determine the background distribution events in the sidebands $50 \text{ MeV}/c^2 < |MM(\pi^+\pi^-) - M_{Y(nS)}| < 150 \text{ MeV}/c^2$ have been used. Dalitz distributions for signal and background events of the decay $Y(5S) \rightarrow Y(2S)\pi^+\pi^-$ are shown in Fig.1.9.4.

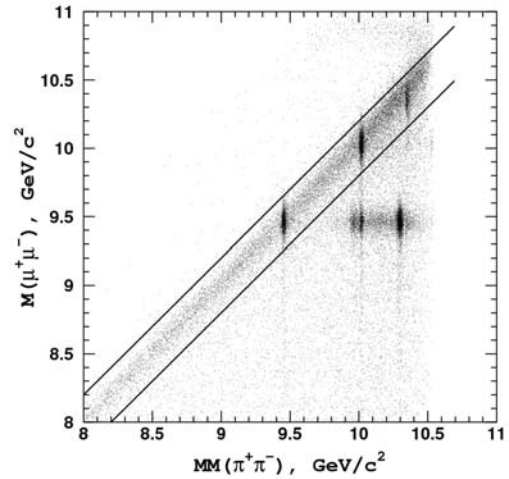


Fig. 1.9.3. Dependence $M(\mu^+\mu^-)$ vs. $MM(\pi^+\pi^-)$.

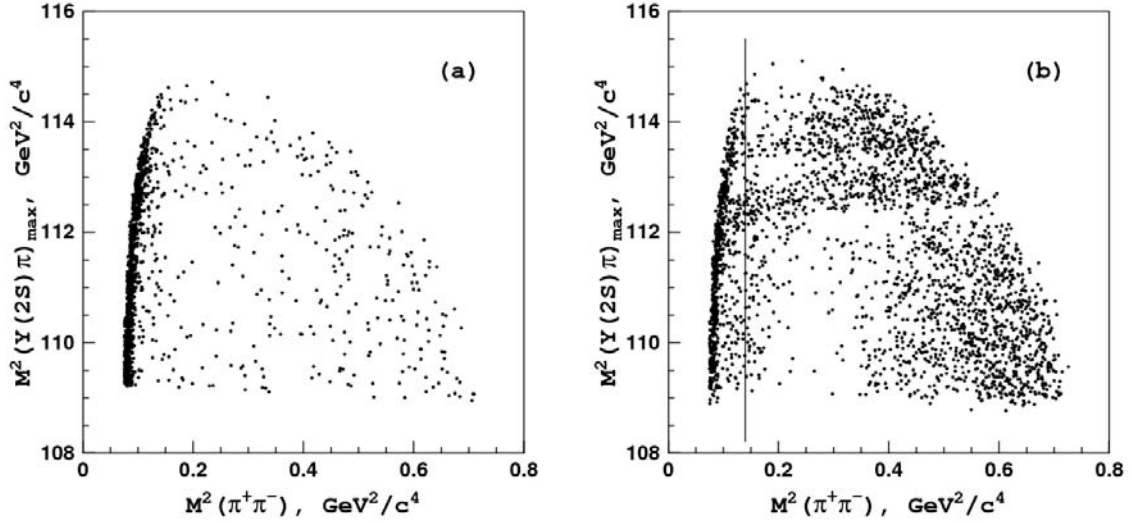


Fig. 1.9.4. Dalitz distributions for background (a) and signal (b) events in the decay $Y(5S) \rightarrow Y(2S)\pi^+\pi^-$.

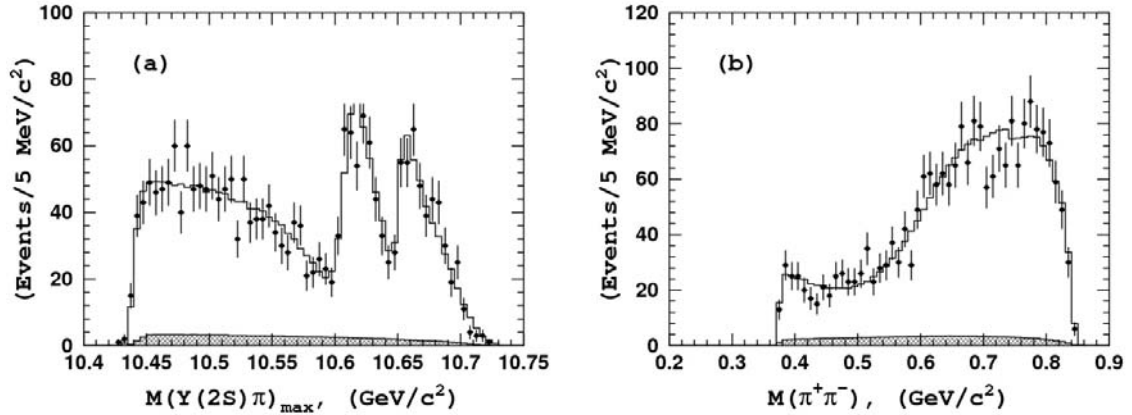


Fig. 1.9.5. Invariant mass distribution of the $Y(2S)\pi^\pm$ system (left) and $\pi^+\pi^-$ system (right) for signal events in the decay $Y(5S) \rightarrow Y(2S)\pi^+\pi^-$. Points – experimental data, the histogram – result of the fit, the shaded histogram shows the expected level of background events.

A significant background for the processes under study comes from decays $Y(5S) \rightarrow \mu^+\mu^-\gamma$, in which a photon further converts into a e^+e^- pair. Since tracks have small momentum, the Belle electron identification efficiency is small. However, such events can be rejected by the requirement $MM(\pi^+\pi^-) > 0.4 \text{ GeV}/c^2$. The background in the remaining part of the Dalitz plot agrees well with the uniform. One-dimensional distributions over the two-body invariant mass are shown in Fig. 1.9.5. The Dalitz distribution of signal events for all three final states was parameterized in the following common model:

$A_{Y\pi\pi} = A_{Z1} + A_{Z2} + A_{f_0} + A_{f_2} + A_{NR}$, where A_{Z1} and A_{Z2} – amplitudes of the $Y(5S)$ decay with formation of the intermediate Z states, A_{f_0} и A_{f_2} – amplitudes of $Y(5S) \rightarrow Y(nS)f_0(980)$ and $Y(5S) \rightarrow Y(nS)f_2(1270)$ decays, respectively, A_{NR} – the amplitude of the non-resonant decay. Experimental data were fit to the combination of the signal and background to determine the relative

phases and contributions of separate quasi-two-body amplitudes as well as mass and width of the Z states. In the subsequent analysis of the $h_b(1P)$ and $h_b(2P)$ production the ITEP group found that the main mechanism of the production of such states is a transition with intermediate production of one of these Z states $Y(5S) \rightarrow Z\pi^\pm \rightarrow h_b\pi^+\pi^-$. Results of the determination of the parameters of the Z states are listed in Table 1.9.1.

The most important result of this work is the first observation of charged bottomonium-like states. Moreover, the existence of decays $Z \rightarrow Y(nS)\pi^\pm$ makes classification of Z as two-quark systems impossible. A minimal quark content will be that of four quarks. The authors suggested to consider $Z(10610)$ as a system of bound B and B^* mesons and $Z(10650)$ as a system of bound B^*B^* mesons, respectively. Such a model is in good agreement with all observed properties of the Z states. This work was accepted for publication in journal Phys. Rev. Lett.

Table 1. Comparison of the parameters of the Z states measured in different final states.

Final state	$\Upsilon(1S)\pi^+\pi^-$	$\Upsilon(2S)\pi^+\pi^-$	$\Upsilon(3S)\pi^+\pi^-$	$h_b(1P)\pi^+\pi^-$	$h_b(2P)\pi^+\pi^-$
$M[Z_b(10610)], \text{ MeV}/c^2$	$10611 \pm 4 \pm 3$	$10609 \pm 2 \pm 3$	$10608 \pm 2 \pm 3$	$10605 \pm 2^{+3}_{-1}$	10599^{+6+5}_{-3-4}
$\Gamma[Z_b(10610)], \text{ MeV}$	$22.3 \pm 7.7^{+3.0}_{-4.0}$	$24.2 \pm 3.1^{+2.0}_{-3.0}$	$17.6 \pm 3.0 \pm 3.0$	$11.4^{+4.5+2.1}_{-3.9-1.2}$	13^{+10+9}_{-8-7}
$M[Z_b(10650)], \text{ MeV}/c^2$	$10657 \pm 6 \pm 3$	$10651 \pm 2 \pm 3$	$10652 \pm 1 \pm 2$	$10654 \pm 3^{+1}_{-2}$	10651^{+2+3}_{-3-2}
$\Gamma[Z_b(10650)], \text{ MeV}$	$16.3 \pm 9.8^{+6.0}_{-2.0}$	$13.3 \pm 3.3^{+4.0}_{-3.0}$	$8.4 \pm 2.0 \pm 2.0$	$20.9^{+5.4+2.1}_{-4.7-5.7}$	$19 \pm 7^{+11}_{-7}$
Rel. normalization	$0.57 \pm 0.21^{+0.19}_{-0.04}$	$0.86 \pm 0.11^{+0.04}_{-0.10}$	$0.96 \pm 0.14^{+0.08}_{-0.05}$	$1.39 \pm 0.37^{+0.05}_{-0.15}$	$1.6^{+0.6+0.4}_{-0.4-0.6}$
Rel. phase, degrees	$58 \pm 43^{+4}_{-9}$	$-13 \pm 13^{+17}_{-8}$	$-9 \pm 19^{+11}_{-26}$	187^{+44+3}_{-57-12}	$181^{+65+74}_{-105-109}$

Studies of τ -lepton decay

Analysis of a search for lepton-flavor-violating decays $\tau \rightarrow lV^0$, where $l = e, \mu$, and $V = \rho^0, \omega, \phi, K^{*0}$, anti- K^{*0} , 10 different decay modes in total, has been completed. A data sample for analysis was 854 fb^{-1} or 782×10^6 produced τ -lepton pairs. In all the modes a signal did not exceed an expected background, so that upper limits for the corresponding branching fractions can be set: $B(\tau \rightarrow eV^0) < (1.8 - 4.8) \times 10^{-8}$, $B(\tau \rightarrow \mu V^0) < (1.2 - 8.4) \times 10^{-8}$ at 95% confidence level. These limits are by a factor of 5.7 stricter than in previous Belle experiments and are also stricter than those at BaBar. The improvement is due to an increase of statistics as well as stronger suppression of the background processes. This work has been published in journal Physics Letters B.

Also completed is a search for CP-violation in $\tau^\pm \rightarrow K_S^0 \pi^\pm \nu_\tau$. Analysis used a data sample of 699 fb^{-1} . Using $(162.2 \pm 0.4) \times 10^3$ decays $\tau^+ \rightarrow K_S^0 \pi^+ \nu_\tau$ and $(162.0 \pm 0.4) \times 10^3$ decays $\tau^- \rightarrow K_S^0 \pi^- \nu_\tau$, CP-asymmetry has been measured in four bins of invariant mass of the $K_S^0 \pi^\pm$ -system (Fig.1.9.6). In all bins the asymmetry is compatible with zero with $O(10^{-3})$ accuracy allowing to set upper limits on the CP-violation parameter $|T(\eta_s)| < 0.026$ at 95% confidence level, an order of magnitude stronger than previously. This work has been published in Physical Review Letters. Analysis is in progress to search for lepton-flavor violating decays $\tau \rightarrow l'hh'$, where $l = e, \mu$, $h = \pi^\pm, K^\pm$.

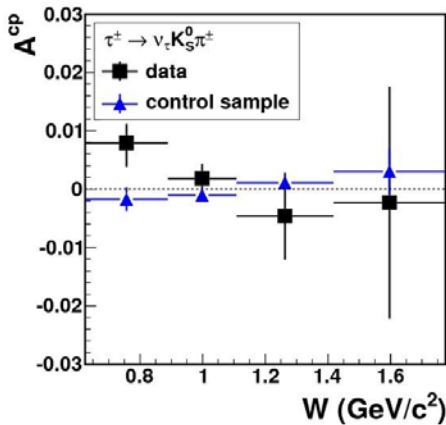


Fig. 1.9.6. Measured CP-asymmetry.

1.9.3. Detector upgrade

The upgrade of both the detector (Belle II) and the collider to increase the luminosity up to $8 \times 10^{35} \text{ cm}^{-2} \text{ s}^{-1}$ is in progress. The new experiment will allow a measurement of all angles of the unitarity triangle with a few percent precision and, perhaps, will give an opportunity to go beyond the Standard Model. Besides the study of the CP-violation mechanism, a large data sample accumulated in this experiment will allow new results on physics of B and D mesons, and τ -lepton decay to be obtained.

Increase of the luminosity and background rate imposes new requirements on the detector subsystems. To provide efficient calorimeter operation, it has to be upgraded. The BINP group participates in the upgrade of the calorimeter. It has developed and proposed the scheme of the calorimeter upgrade.

For the barrel part of the calorimeter, the counter electronics will be replaced by the scheme with pipeline readout followed by the data fit with a known response function. Such a procedure allows the determination of both the energy and signal arrival time. Time information allows the suppression of the rate of fake clusters to be realized.

For the end caps, where the background conditions are most severe, the first stage includes the electronics upgrade and then the replacement of the CsI(Tl) scintillation crystals by the crystals of non-activated CsI with a smaller decay time. This will allow a 30 times improvement of the counter time resolution, and taking into account a fit of the signal shape, will provide background suppression by a factor of more than 150.

In 2011 BINP completed development and constructed the first version of the shaper-digitizer module in VME standard (Fig.1.9.7). This module will be a main unit of the new electronic system. It forms signals from counters, performs digitization of the signal shape with a frequency of about 2 MHz followed by digital processing to reconstruct a pulse height and its arrival time. In addition, the module forms a fast analogous signal to be used for a neutral trigger. Compared to the previous version, the new module has significantly smaller duration of the trigger signal to decrease dead time of the neutral trigger during continuous injection. The module has an additional option of calibrating separately each of 16 channels, an important feature to tune and calibrate trigger.

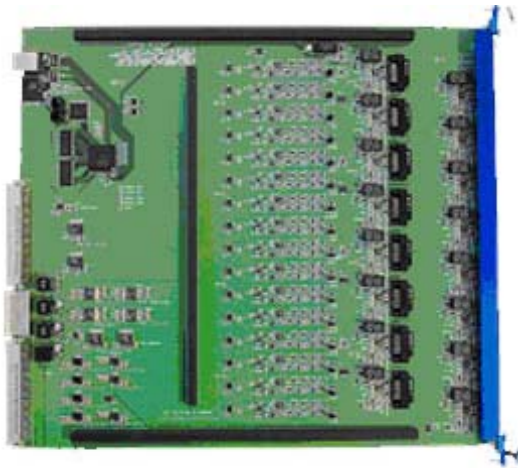


Fig. 1.9.7. Module of 16-channel shaper-digitizer in VME standard

Measurements of shaper-digitizer characteristics were performed. Using signals from cosmics a signal shape at the digitization input has been measured in detail. The shape shown in Fig. 1.9.8(a) corresponds to the expected one and a channel-to-channel deviation is less than 2%. A unit linearity was measured using a calibrating generator. The deviation from linearity does not exceed 0.3% (Fig. 1.9.9). The energy equivalent of incoherent noises was 300 keV, while for coherent noise it was 20 keV. A signal shape for a trigger channel (Fig. 1.9.8(b)) corresponds to the expected one, совпадающие с ожиданием, adjustment of the transformation coefficients was performed.

12 test modules will be constructed at the beginning of 2013. Preparation of stands for module measurement and passportization in mass production is in progress.

Mechanical and electrical specifications for a new VME crate were developed. They are chosen in such a way that a crate provides operation of 12 shaper-digitizer modules without noise increase. Production of such crates started.

At the next stage of upgrade crystals of pure в торцевой части калориметра планируется установить кристаллы чистого CsI will be installed at the endcap calorimeter. The Kharkov Institute of Scintillation Materials is considered as a possible supplier of crystals. Light output and non-uniformity were measured for a set of crystals produced in Kharkov. Their parameters are consistent with those of the previous set. 50 test crystals have been ordered. Tests of radiation hardness are planned.

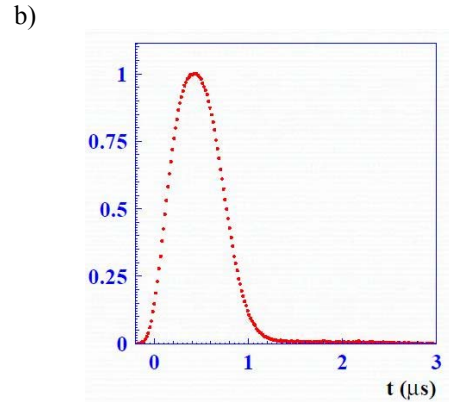
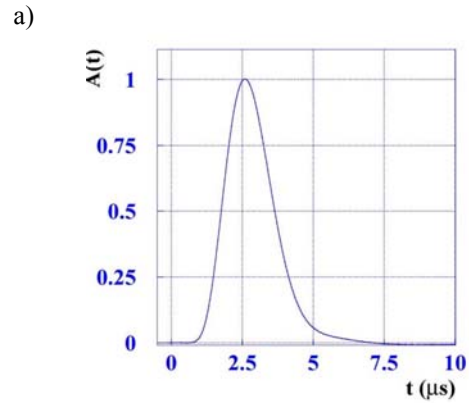


Fig. 1.9.8. (a) Shape of shaper-digitizer signal. (b) Shape of trigger signal.

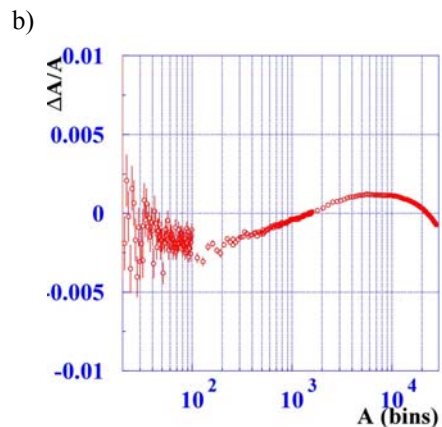
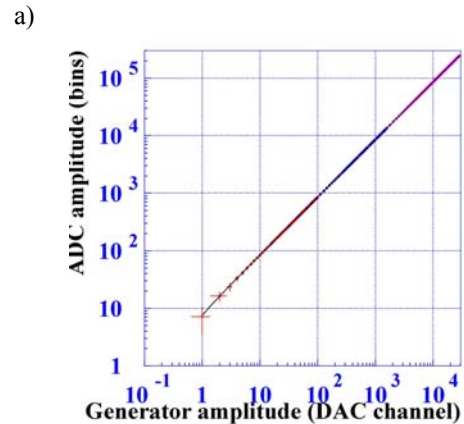


Fig. 1.9.9. (a) Shaper-digitizer response. (b) Module deviation from linearity.

1.10 BABAR EXPERIMENT

Experiments with the BABAR detector were carried out on the e^+e^- collider PEP-II at SLAC (USA) since 1999 to 2008. Processing of data accumulated in the experiment is going on. The BABAR collaboration includes about 600 physicists representing 72 institutes from 12 countries, with 11 BINP members among them. In 2011, the collaboration published 29 papers and about 100 analysis are currently in process.

The main objectives of the BABAR experiment is to study CP violation in decays of B mesons, precise measurement of the decays of B and D mesons and τ leptons, and search for their rare decays. Although the design of the detector and collider were optimized for the study of CP asymmetry, this practically did not reduce the potential of the experiment in relation to other processes.

BINP participants of the collaboration are engaged in the analysis of data on the measurement of the matrix element V_{ub} of the CKM matrix, measurement of cross sections for e^+e^- annihilation into hadrons using the radiative return, and study of two-photon processes with registration of scattered electrons.

The radiative return method was developed by BINP physicists and consists in study of processes with emission of hard photon by initial particles, so that the rest of energy goes into hadron production at much lower energies, down to the production threshold. This allows us to study the exclusive processes of e^+e^- annihilation into hadrons with hadron mass ranging from the threshold up to 5-6 GeV/ c^2 .

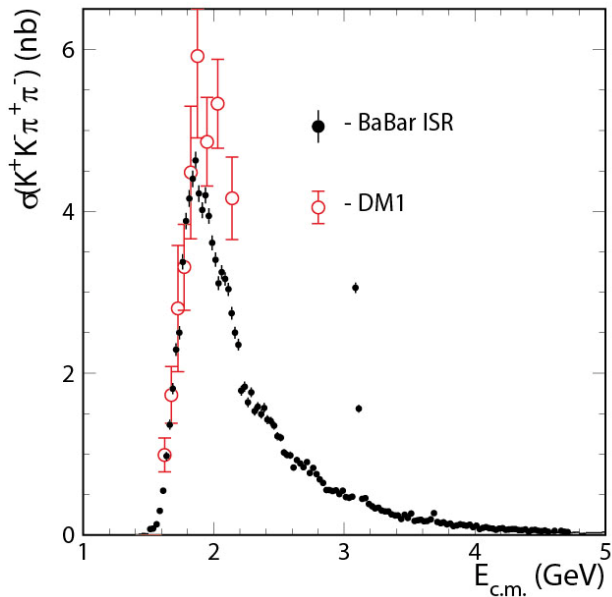


Fig.1.10.1 Cross section for $e^+e^- \rightarrow K^+K^-\pi^+\pi^-$ as a function of $E_{c.m.}$, as measured in the process of radiative return on the BABAR detector (shaded circles). Direct measurement with the DM1 detector is shown with unshaded circles. Only statistical errors are shown.

Analysis of the $e^+e^- \rightarrow K^+K^-\pi^+\pi^-$ and $K^+K^-\pi^0\pi^0$ processes using all data recorded in the BABAR experiment was completed and published in 2011. The resulting cross section (Fig. 1.10.1) in the region from the threshold to $E_{c.m.} = 5\text{GeV}$ is the most precise measurement so far. The $e^+e^- \rightarrow K^+K^-\pi^0\pi^0$ process (Fig.1.10.2) has not been studied before.

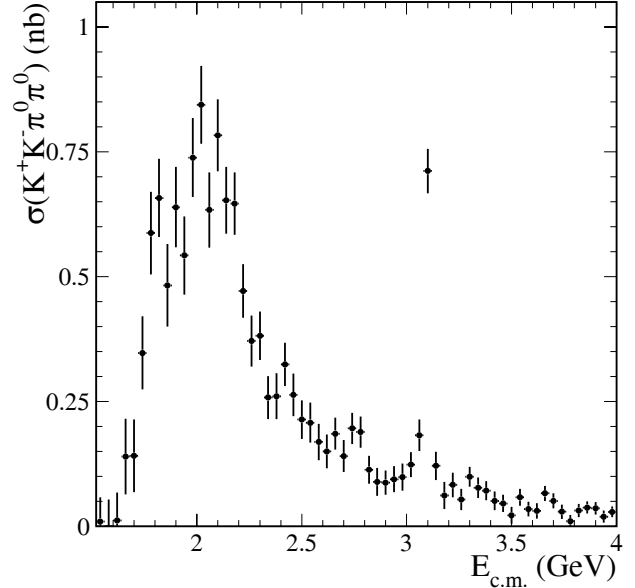


Fig.1.10.2 Cross section for the $e^+e^- \rightarrow K^+K^-\pi^0\pi^0$ process as a function of $E_{c.m.}$, as measured in the process of radiative return on the BABAR detector. Only statistical errors are shown.

Data sample allows to study in detail the intermediate states, such as $K^*(892)K\pi$, $KK\rho(770)$, $K_1(1420)K\pi$, and $\phi(1020)\pi\pi$, where the pion pair may be charged or neutral.

In the course of the study of the $e^+e^- \rightarrow K^+K^-\pi^+\pi^-$ reaction, a previously unknown resonance with a mass of 2175 MeV/ c^2 was discovered in events in which the K^+K^- pair forms the $\phi(1020)$ resonance and $\pi^+\pi^-$ or $\pi^0\pi^0$ are produced from the $f_0(980)$ decay. The cross section for the $e^+e^- \rightarrow \phi(1020)f_0(980)$ process is shown in Fig.1.10.3.

The small width of the resonance, around 80 MeV, indicates its exotic origin. With that, $Y(2175)$ is observed only when the $\pi\pi$ pair forms the $f_0(980)$ resonance, which itself is a candidate for an exotic four-quark state. The existence of the $Y(2175)$ resonance was confirmed in experiments with the Belle detector in Japan and on the BES in China. Currently, there is no generally accepted theoretical interpretation for this state.

At present, BINP physicists work on the measurement of the parameter V_{ub} with higher precision and measurement by the radiative return method of cross sections for the $e^+e^- \rightarrow p\bar{p}$, $e^+e^- \rightarrow K_S K_L$, and $e^+e^- \rightarrow K_S K^+\pi^0$ processes.

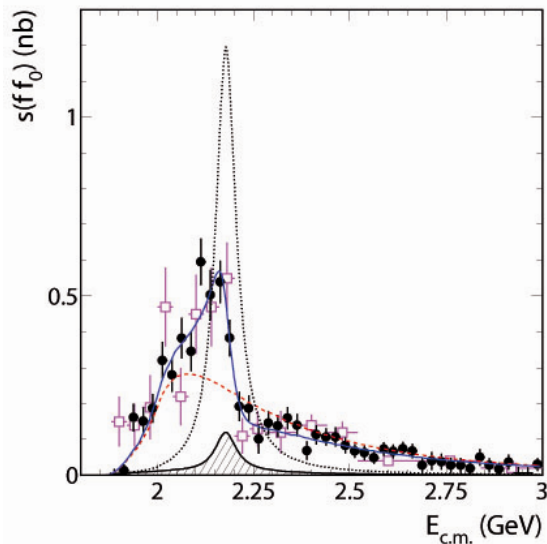


Fig. 1.10.3 Cross section for $e^+e^- \rightarrow \phi(1020)f_0(980)$, as measured in the decays to $K^+K^-\pi^+\pi^-$ final states (shaded circles) and $K^+K^-\pi^0\pi^0$ (unshaded circles). The solid and dashed lines represent the result of fitting with two resonances ($\phi(1680)+Y(2175)$) and one ($\phi(1680)$) resonance, respectively. The shaded region and the dashed curve show the contribution of $Y(2175)$ for the two phases of interference.

1. 11 PARTICIPATION IN THE ATLAS EXPERIMENT AT THE LARGE HADRON COLLIDER (LHC)

For the experiments at the Large Hadron Collider, the year 2011 became the most successful so far. The "Annual Plan" of luminosity integral acquisition (1 inverse femtobarn) was completed by 17 June. In total, 5 inverse femtobarn were acquired in 2011, which is 110 times as much as in 2010. The main physical challenge was a search for the Higgs boson. This is a particle, by interacting with the field of which other particles acquire the mass. Analysis of all collected statistics was prepared and reported on December 13 (in just a month after the end of data taking). The Standard Model Higgs boson was excluded at a confidence level of 95% in the mass ranges of 112.9÷115.5, 131÷238, and 251÷466 GeV (see Fig.1.11.1). An excess of the number of events over the expected background level was observed in the area of invariant masses of around 126 GeV. The local significance of this excess for the Higgs boson decay channels into two photons, four leptons, and two W-bosons is respectively 2.8, 2.1, and 1.4 σ (standard deviations); the significance of a combination of the channels is equal to 3.5 σ . However, the global significance, i.e. the probability of finding such (or larger) fluctuation of the number of background events in the

wide Higgs boson mass range of 110÷600 GeV is estimated as 1.4%, which corresponds to only 2.2 σ . Thus, the acquired statistics is not enough to make definite conclusion that significant excess of signal over the Standard Model background is observed. It is planned to collect about 10 inverse femtobarn in 2012.

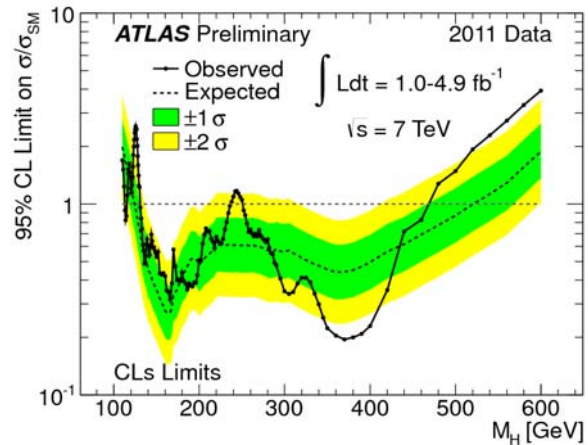


Fig. 1.11.1 Solid black line: ratio of the combined upper limit on the Standard Model Higgs boson production cross section to the cross-section expected in the Standard Model, as a function of the Higgs boson mass M_H . Dashed curve: the average expected (from the simulation) limit in the absence of signal. Green and yellow bands: the corresponding 68% and 95% areas for the expected limit.

About 50 papers based on data analysis from the ATLAS detector were published in 2011.

Physicists of the BINP group participated in the data collection in the experiment control room (ATLAS point 1) within the system of liquid-argon calorimeters. The work on the monitoring and analysis of data quality and calibration of the calorimeters was continued. Since spring 2009, in collaboration with the Universities of Pittsburgh and Irvine, BINP physicists are searching for heavy Majorana neutrinos in the channel with two leptons and two jets in the final state in the framework of the left-right symmetry model. This model can explain the nonzero mass of standard light neutrinos (which follows from the observation of their oscillations), as well as the emergence of asymmetry between matter and antimatter (the baryon number B and lepton number L may be violated separately provided that B-L remains constant).

All available statistics collected in 2010 (34.7 inverse picobarn) and 2.1 out of 5 inverse femtobarn acquired in 2011 were processed. The number of selected events in the data is consistent with the contribution of the Standard Model background processes, as expected from the simulation. This analysis allows one to exclude a wide range of masses of the right boson W_R (up to 2.2-2.5 TeV) and the Majorana neutrino N_1 (up to 1.5 TeV), see Fig. 1.11.2, which significantly improves the limit that was set at the Tevatron (the mass $W_R > 640$ GeV). Further

substantial progress requires increasing the energy of colliding protons in the LHC, from the current 3.5 TeV to the nominal 7 TeV (it is planned in 2014).

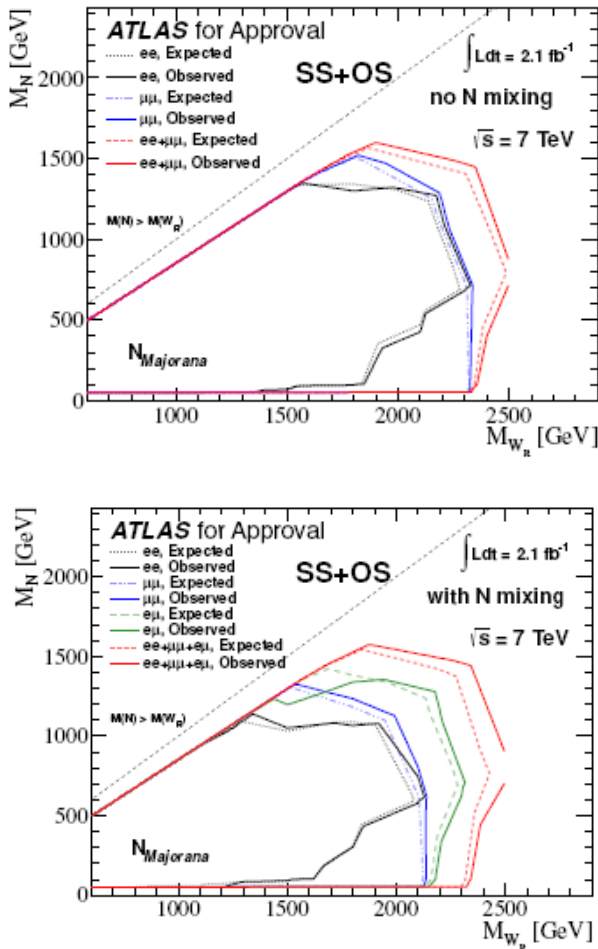


Fig. 1.11.2 Expected (from Monte-Carlo simulation) and observed 95% C.L. upper limits on the masses of the Majorana neutrino (M_N) and of the right intermediate boson (M_{WR}), for the no-mixing (top) and maximal-mixing between electron and muon Majorana neutrinos (bottom) scenarios. We combined results for leptons of the same sign (SS) and opposite sign (OS). 2.1 inverse femtobarn of 5 collected in 2011 were processed.

Much work is also done for development of the computer infrastructure and software. Data from the experiment of this scale (several petabytes of data input per year) can be stored and processed only with a well-

coordinated work of many powerful computing clusters around the world, using advanced technology of distributed computing GRID.

BINP programmers have made a substantial contribution to the creation and development of critical services and utilities to manage the distributed computing system (ATLAS GRID)–Monitoring of Data Replication and Information System.

The performance of the BINP GRID cluster is being improved; the network equipment is being upgraded. Cooperation with the NSU and SB RAS computer centers is developing. The access to external computing resources was implemented via the virtualization technology.

Since 2007, BINP experts take part in the activities of the administration system for experimental data collection, which deals with the exploitation and development of the computer software for the high-level trigger, a system responsible for building and filtering the events, and other subsystems of the data acquisition system. The equipment consists of about 2,300 servers with network support (in total, about 17,000 CPU cores), about 100 auxiliary control servers, 50 support servers for the control room of the detector ATLAS, as well as many other components of the IT infrastructure of the experiment.

Currently, a project of upgrade of the LHC for increasing the luminosity by an order of magnitude, up to $10^{35} \text{ cm}^{-2}\text{sec}^{-1}$, is being developed. In this regard, the activity on upgrade of the ATLAS detector for work at such luminosity is started. The BINP group takes part in an experiment to study the operation of ATLAS liquid-argon calorimeters at a luminosity of $10^{35} \text{ cm}^{-2}\text{sec}^{-1}$. To this end, mini-modules of the calorimeters (electromagnetic, hadronic, and forward) have been made and placed in a cryostat with liquid argon. The modules are irradiated with a 50 GeV extracted proton beam of U-70 accelerator in Protvino (the beam intensity can be varied in a wide range, $10^7 \div 10^{12}$ particles per second). The BINP group is fully responsible for the mini-module of the electromagnetic calorimeter and is involved in the data collection and analysis. As a result of these beam tests, the article was published in NIM.

2

ELECTRO – AND
PHOTONUCLEAR PHYSICS

2.1 EXPERIMENTS WITH INTERNAL TARGETS

I. In 2011, the first preparation was carried out and then an experiment was launched on the new measurement of the ratio of cross sections of elastic electron/positron scattering on proton: $R = \sigma_{e^+p} / \sigma_{e^-p}$.

It is known that measured R makes it possible to determine the contribution of two-photon exchange (TPE) to this process. Information on the TPE might explain the dramatic difference in the results of recent experiments on the measurements of proton form factors, which were performed at TJNAF, USA with the help of the polarization techniques, and previous (non-polarization) measurements, in which the proton form factors were determined via analysis of differential cross sections for the reaction on the assumption of validity of single-photon approximation.

TPE correction inclusion, however, runs into difficulties, both of theoretical (there are no correct calculations of TPE because excited states of proton in intermediate state are difficult to take into account) and experimental character. Attempts to determine the TPE contribution to the scattering cross-section were taken in the 70s. Unfortunately, they were associated with bad statistic accuracy of measurement, or angles of scattering of electrons/positrons were small (the TPE contribution is very small in this case).

In 2009, BINP carried out measurements of R at an energy of positron/electron beams of 1.6 GeV in two areas of the e^+/e^- scattering angle: 16 to 23 and 56 to 75 degrees. The measurements were performed on VEPP-3. A preliminary result was obtained, with accuracy much higher than that of the known data.

It is worth noting that they at TJNAF also conducted a similar experiment on the CLAS detector in February 2011; no details of the results have been reported yet. In 2012, an analogous experiment was started at the accelerator center DESY (Germany) on the storage ring DORIS. For this purpose, the newly-established collaboration OLYMPUS united the effort of researchers of 14 institutions.

It was scheduled for 2011 to carry out measurements on VEPP-3 in a new kinematic area – at a beam energy of 1 GeV and angles of positron/electron scattering of 67 to 105 degrees. The expected value of R in this area is approximately the same as in the experiment in 2009, in the second area of scattering angles (56 to 75 degrees). The expected accuracy of the new measurement, however, will be approximately twice as high. Fig. 2.1.1 shows the kinematic ranges of all the mentioned experiments in the plane of commonly used parameters: four-momentum transfer squared Q^2 and virtual photon polarization ϵ .

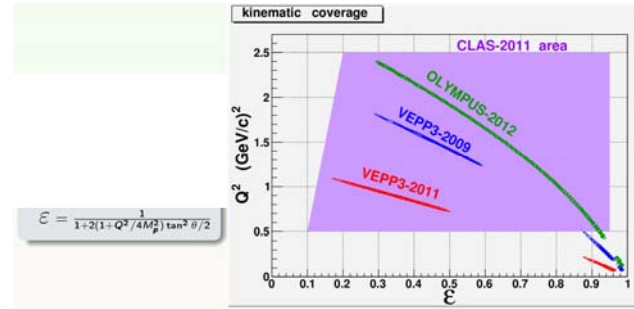


Fig. 2.1.1 Kinematic areas of 3 experiments on the measurement of cross sections for elastic scattering of electrons/positrons on proton $R = \sigma_{e^+p} / \sigma_{e^-p}$.

A series of works was done for preparation of the experiment. A code was created for simulation of elastic and inelastic (with emission of a photon) scattering of electrons and positrons of VEPP-3 beams on the protons of the target, which made it possible to accurately calculate the radiative corrections, which are required for analysis of experimental results at separation of the TPE contribution, with the use of ep -scattering cross sections calculated recently by the theorists of the Institute. MC simulation of the detector was conducted for elastic scattering and for emission of a photon. This simulation allowed us to select the optimal configuration of the detector (see Fig. 2.1.2). The MA1 and MA2 systems register electrons/positrons scattered at angles of about 20 degrees (recoil protons falling into the LA1 or LA2 detectors). Events of this sort are used for monitoring of luminosity. The MA2 system is also equipped with an electromagnetic calorimeter for measurement of the energy of scattered electrons/positrons. This will restore the full kinematics of the events in which elastic scattering is accompanied by emission of a photon and, if it falls into one of the calorimeters of the LA1 or LA2 systems, the recoil proton is registered by the detectors of the LA2 system. This class of events will verify the predictions from calculations with radiative corrections. Finally, electrons/positrons scattered through large angles and registered by the LA1 and LA2 systems (in this case, recoil protons fall into MA1 or MA2 detectors) give the class of events for determination of the TPE contribution.

In addition, the target was upgraded; its faulty elements were repaired; the operation stability was adjusted; the target was operated for a long period of time; additional cryopumps were installed into the pumping system of the experimental straight section; calorimeters and their support systems were mounted. During the summer shutdown of the complex, the target and detector were mounted on the VEPP-3 storage ring. Then the equipment was tested and adjusted. At the same time, the installation for the Compton back scattering was moved from VEPP-4 to VEPP-3 for measurement of the energy of electron/positron beams.

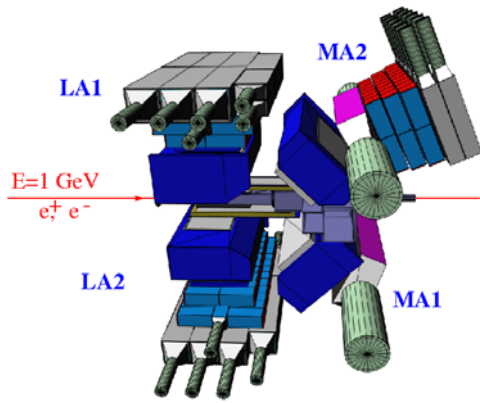


Fig. 2.1.2. Schematic representation of the particle detection systems.

Statistics collection began in late September, with breaks for planned outages and work of SR groups. The effectiveness of the collection, measured in the integral of the electron/positron beam current at a constant target thickness of about 10^{15} at/cm², gradually increased. The total integral of beam current as on January 21, 2012 was 61.2 kC or 367 pb⁻¹ (see Fig. 2.1.3).

Fig. 2.1.4 shows the preliminary results of the ongoing experiment on the specified integral luminosity (right panel) and previous measurements at an energy of 1.6 GeV (left panel). In both cases, the radiative corrections (taking into account the contribution to R from processes with emission of real photons) were made. The results of the known measurements of R close to our measurements in the kinematic parameters are also shown, as well as theoretical predictions by Blunden et al, Phys. Rev.C72(2005) 0364612. The integral of luminosity of the experiment is expected to reach 600 pb⁻¹.

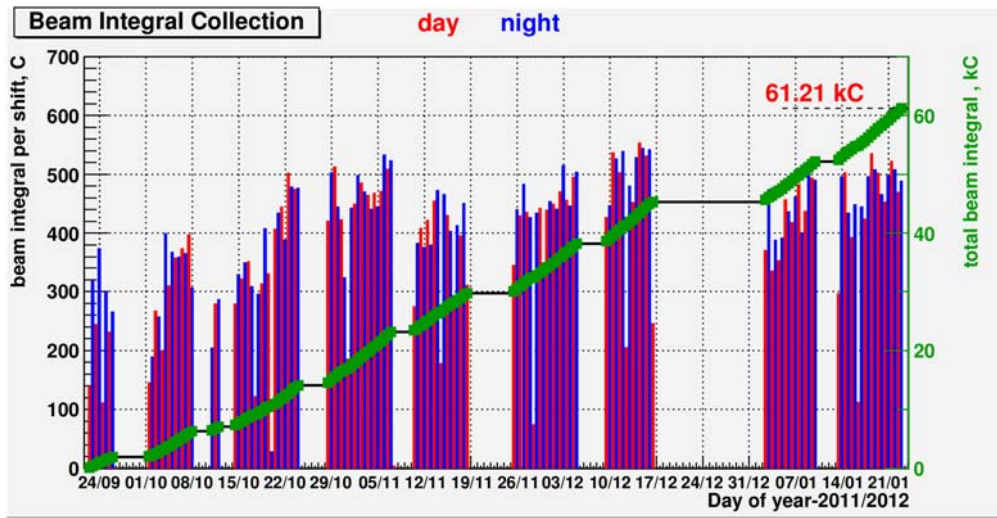


Fig. 2.1.3. Integrals of beam current per shift (histogram) and total integral of beam current vs. time (black solid line).

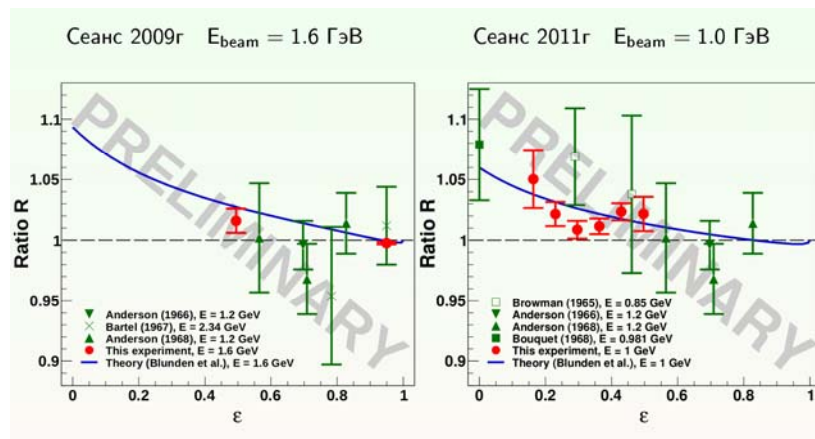


Fig. 2.1.4 Preliminary results on the measurement of R on VEPP-3 vs. ϵ for the ongoing experiment and the experiment in 2009. The known world data are also shown. Curves: theoretical predictions by Blunden et al.

3

THEORETICAL
PHYSICS

3.1. STRONG INTERACTION

Integration by parts: An introduction

A.G. Grozin

Int. J. Mod. Phys. A **26** (2011) 2807–2854

Integration by parts is used to reduce scalar Feynman integrals to master integrals.

HQET heavy-heavy vertex diagram with two velocities

A.G. Grozin, A.V. Kotikov.

arXiv:1106.3912 [hep-ph]

The one-loop HQET heavy-heavy vertex diagram with arbitrary powers of all three denominators and arbitrary residual energies is investigated. Various particular cases in which the result becomes simpler are considered.

Simultaneous decoupling of bottom and charm quarks

A.G. Grozin, M. Höschele, J. Hoff, M. Steinhauser

J. High Energy Phys. **09** (2011) 066

We compute the decoupling relations for the strong coupling, the light quark masses, the gauge-fixing parameter, and the light fields in QCD with heavy charm and bottom quarks to three-loop accuracy taking into account the exact dependence on m_c/m_b . The application of a low-energy theorem allows the extraction of the three-loop effective Higgs-gluon coupling valid for extensions of the Standard Model with additional heavy quarks from the decoupling constant of α_s .

DRA method: Powerful tool for the calculation of the loop integrals.

R. Lee

Proceedings of ACAT2011 conference.

We review the DRA method of the calculation of multiloop integrals.

Analytic Epsilon Expansions of Master Integrals Corresponding to Massless Three-Loop Form Factors and Three-Loop $g-2$ up to Four-Loop Transcendentality Weight

R. Lee and V. Smirnov

JHEP **1102** (2011) 102. arXiv: 1010.1334

We evaluate analytically higher terms of the epsilon-expansion of the three-loop master integrals corresponding to three-loop quark and gluon form factors and to the three-loop master integrals contributing to the electron $g-2$ in QED up to the transcendentality weight typical to four-loop calculations, i.e. eight and seven, respectively. The calculation is based on a combination of a method recently suggested by one of the authors (R.L.) with other techniques: sector decomposition implemented in FIESTA, the method of Mellin–Barnes representation, and the PSLQ algorithm.

Application of the DRA method to the calculation of the four-loop QED-type tadpoles

R. Lee and I. Terekhov

JHEP **1101** (2011) 068. arXiv: 1010.6117

We apply the DRA method to the calculation of the four-loop ‘QED-type’ tadpoles. For arbitrary space-time dimensionality D the results have the form of multiple convergent sums. We use these results to obtain the epsilon-expansion of the integrals around $D=3$ and $D=4$.

Master Integrals for Four-Loop Massless Propagators up to Transcendentality Weight Twelve

R. N. Lee, A. V. Smirnov and V. A. Smirnov

Nucl.Phys. **B856** (2012) 95-110. arXiv: 1108.0732

We evaluate a Laurent expansion in dimensional regularization parameter $\epsilon = (4 - d)/2$ of all the master integrals for four-loop massless propagators up to transcendentality weight twelve, using a recently developed method of one of the present coauthors (R.L.) and extending thereby results by Baikov and Chetyrkin obtained at transcendentality weight seven. We observe only multiple zeta values in our results. Therefore, we conclude that all the four-loop massless propagator integrals, with any integer powers of numerators and propagators, have only multiple zeta values in their epsilon expansions up to transcendentality weight twelve.

On Epsilon Expansions of Four-loop Non-planar Massless Propagator Diagrams

R. N. Lee, A. V. Smirnov and V. A. Smirnov

Eur.Phys.J. **C71** (2011) 1708. arXiv: 1103.3409

We evaluate three typical four-loop non-planar massless propagator diagrams in a Taylor expansion in dimensional regularization parameter $\epsilon = (4 - d)/2$ up to transcendentality weight twelve, using a recently developed method of one of the present coauthors (R.L.). We observe only multiple zeta values in our results.

BFKL equation for the adjoint representation of the gauge group in the next-to-leading approximation at $N=4$ SUSY

V.S. Fadin and L. N. Lipatov

Phys. Lett. B **706** (2012) 470-476. arXiv:1111.0782 [hep-th].

We calculate the eigenvalues of the next-to-leading kernel for the BFKL equation in the adjoint representation of the gauge group $SU(N_c)$ in the $N=4$ supersymmetric Yang-Mills model. These eigenvalues are used to obtain the high energy behavior of the remainder function for the 6-point scattering amplitude with the maximal helicity violation in the kinematical regions containing the Mandelstam cut contribution. The leading and next-to-leading singularities of the corresponding collinear anomalous dimension are calculated in all orders of perturbation theory. We compare our result with the known collinear limit and with the recently suggested ansatz for the remainder function in three loops and obtain the full agreement providing that the numerical parameters in this ansatz are chosen in an appropriate way.

Connection between complete and Möbius forms of gauge invariant operators

V.S. Fadin, R. Fiore, A.V. Grabovsky and A. Papa
Nucl. Phys. **B 856** (2012) 111-124. arXiv:1109.6634 [hep-th].

We study the connection between complete representations of gauge invariant operators and their Möbius representations acting in a limited space of functions. The possibility to restore the complete representations from Möbius forms in the coordinate space is proven and a method of restoration is worked out. The operators for transition from the standard BFKL kernel to the quasi-conformal one are found both in Möbius and total representations.

Quasi-conformal shape of the BFKL kernel and impact factors for scattering of colourless particles

V.S. Fadin, R. Fiore, A.V. Grabovsky and A. Papa
AIP Conf. Proc. **1350** (2011) 224-227.

The NLO BFKL kernel in the Möbius representation is transformed to the quasi-conformal shape in theories containing fermions and scalars in arbitrary representations of the colour group. Corresponding transformations of impact factors of colourless particles are discussed.

Check of the gluon reggeization condition in the next-to-leading order: Quark part

M. G. Kozlov, A. V. Reznichenko and V. S. Fadin
Phys. Atom. Nucl. **74** (2011) 758-770 [Yad. Fiz. **74** (2011) 784-796].

The bootstrap condition for gluon production in the multi-Regge kinematics in the next-to-leading order is considered. The bootstrap conditions result from the requirement of compatibility of the Regge form of QCD amplitudes with the s -channel unitarity and represent non-linear restraints on the reggeized gluon trajectory and vertices. Their fulfillment provides the gluon reggeization, i.e. the Regge form of elastic and inelastic amplitudes. The condition under consideration remained only one to be checked. The demonstration of its fulfillment is the last step in the proof of the gluon reggeization in the next-to-leading approximation. In this paper this demonstration is presented for the quark part of the bootstrap condition.

NLO impact-factor for one-gluon production in the multi-Regge kinematics

M. G. Kozlov, A. V. Reznichenko and V. S. Fadin
Preprint Budker INP 2011-23; accepted by Yad. Fiz.

The one-loop correction to the impact-factor for one-gluon production at one-reggeon state transition into two-reggeon t -channel state. This impact-factor is a part of multi-particle production amplitudes in the multi-Regge kinematics. The correction under consideration is required for development of the theory of Regge and multi-Regge processes. In particular, it is necessary for the proof of the

multi-Regge form of production amplitudes in the next-to-leading logarithmic approximation. It permits one to complete verification of the last unproved bootstrap condition for the gluon reggeization and to prove in this approximation validity of the multi-Regge form. All necessary calculations are described and explicit expressions for the impact-factors at all possible colour states in the t -channel are presented.

Check of the gluon reggeization condition in the next-to-leading order: Gluon part

M. G. Kozlov, A. V. Reznichenko and V. S. Fadin
Phys.Atom.Nucl. **75** (2012) 493-506 [Yad.Fiz. **75** (2012)]

The last bootstrap condition which fulfillment was not checked till now is considered. This condition is a necessary part of the proof of the multi-Regge form of the high energy QCD amplitudes with gluon exchanges in the next-to-leading logarithmic approximation. The proof is based on the s -channel unitarity and permits to reproduce sequentially the multi-Regge form of the amplitudes in all orders of perturbation theory provided that definite nonlinear relations between the reggeon vertices and the gluon Regge trajectory, which are called bootstrap conditions, are fulfilled. All these conditions were obtained and fulfillment of all but one of them was proved before. In this paper verification of the last unproved condition – bootstrap condition for one-gluon production in the multi-Regge kinematics – is performed in the next to leading order. In our previous paper this verification was done for the fermion contributions; here the gluon contributions are considered and the proof of validity of the last bootstrap condition is completed.

Heavy quark spin structure in Z_b resonances

A.E. Bondar, A. Garmash, A.I. Milstein, R. Mizuk, and M.B. Voloshin.
Phys. Rev. D **84**, 054010 (2011).

We discuss the heavy quark spin structure of the recently observed "twin" resonances $Z_b(10610)$ and $Z_b(10650)$, assuming that these are mostly of a "molecular" type, i.e. that their internal dynamics is dominated by the coupling to meson pairs $B^* \bar{B} - B \bar{B}^*$ and $B^* \bar{B}^*$. We find that the state of the $b\bar{b}$ pair within the $Z_b(10610)$ and $Z_b(10650)$ resonances is a mixture of a spin-triplet and a spin-singlet of equal amplitude and with the phase orthogonal between the two resonances. Such a structure gives rise to specific relations between observable amplitudes that are in agreement with the data obtained recently by Belle. We also briefly discuss possible properties of the isotopically singlet counterparts of the newly found resonances, and also of their C (G) parity opposites that likely exist in the same mass range near the open B flavor threshold.

Nucleon polarization in the process $e^+e^- \rightarrow N\bar{N}$ near threshold

A.E. Bondar, V.F.Dmitriev, A.I. Milstein, V.M. Strakhovenko.

Physics Letters B 697, 159 (2011).

The process $e^+e^- \rightarrow N\bar{N}$ is studied nearby a threshold with account for polarizations of all initial and final particles. The nucleon polarization ζ^N reveals a strong energy dependence due to that of the nucleon electromagnetic form factors $G_E(Q^2)$ and $G_M(Q^2)$ caused by the final-state interaction of nucleons. It is shown that the modulus of the ratio of these form factors and their relative phase can be determined by measuring ζ^N along with the differential cross section. The polarization degree is analyzed using Paris $N\bar{N}$ optical potential for calculation of the form factors. It turns out that $|\zeta^N|$ is high enough in a rather wide energy range above the threshold. Being especially high for longitudinally polarized beams, $|\zeta^N|$ is noticeable even if both e^+e^- beams are unpolarized.

3.2. CP NONCONSERVATION

Can CP-violation be observed in heavy-ion collisions?

I.B. Khriplovich, A.S. Rudenko
Can. J. Phys. 89, 63-64 (2011)

We demonstrate that, at least at present, there is no convincing way to detect CP -violation in heavy-ion collisions.

$K_{l3\gamma}^+$ decays revisited: branching ratios and T -odd momenta correlations

I.B. Khriplovich, A.S. Rudenko
Phys. Atom. Nucl. 74, 1214-1222 (2011)

We calculate the branching ratios of the $K^+ \rightarrow \pi^0 l^+ \nu_l \gamma$ ($l = e, \mu$) decays, and the T -odd triple momenta correlations $\xi = \vec{q} \cdot [\vec{p}_l \times \vec{p}_\pi] / M_K^3$, due to the electromagnetic final state interaction, in these processes. The contributions on the order of ω^{-1} and ω^0 to the corresponding amplitudes are treated exactly. For the branching ratios, the corrections on the order of ω are estimated and demonstrated to be small. We compare the results with those of other authors. In some cases our results differ considerably from the previous ones.

$K_{l3\gamma}^0$ decays: branching ratios and T -odd momenta correlations

A.S. Rudenko
Phys. Rev. D 84, 016001 (2011)

The branching ratios of the $K^0 \rightarrow \pi^- l^+ \nu_l \gamma$ ($l = e, \mu$) decays, and the T -odd triple momenta correlations $\xi = \vec{q} \cdot [\vec{p}_l \times \vec{p}_\pi] / M_K^3$, due to the electromagnetic final state interaction, in these processes are calculated. The contributions on the order of ω^{-1} and ω^0 to the corresponding amplitudes are treated exactly. For the branching ratios and T -odd correlation in $K^0 \rightarrow \pi^- e^+ \nu_e \gamma$ decay, the corrections on the order of ω are estimated and demonstrated to be small. The results for the branching ratios are in good agreement with the previous ones. The T -odd triple momenta correlations in $K_{l3\gamma}^0$ decays are calculated for the first time. The values of the ξ -odd asymmetry are on the order of 10^{-3} and 10^{-2}

in the $K^0 \rightarrow \pi^- \mu^+ \nu_\mu \gamma$ and $K^0 \rightarrow \pi^- e^+ \nu_e \gamma$ decays, respectively.

3.3. QUANTUM ELECTRODYNAMICS

Coulomb effects in the spin-dependent contribution to the intra-beam scattering rate

V. M. Strakhovenko
Phys.Rev. ST. Accel. Beams, 14(2011)012803

Coulomb effects in the intra-beam scattering are taken into account in a way providing correct description of the spin-dependent contribution to the beam loss rate. It allows one to calculate this rate for polarized e^\pm beams at arbitrarily small values of the ratio $\delta\varepsilon/\varepsilon$, characterizing relative change of the electron energy in the laboratory system during scattering event.

Polarized positron production in amorphous targets

V. Strakhovenko
<http://indico.ihep.ac.cn/event/2210>
Invited talk given at the workshop "Posipol 2011", IHEP, Beijing, China, August 28-30, 2011

Depolarization during polarized positron production in amorphous targets is considered for the case where the electromagnetic shower is initiated by circularly polarized photons. It turns out that depolarization occurs mainly in bremsstrahlung from created positrons, while their elastic scattering and Compton scattering of initial photons are not important.

Pair photoproduction in a constant and homogeneous electromagnetic field

V.M. Katkov
Nuovo Cimento C, 34, No. 4 (2011) 1-7.

The process of pair photoproduction in an electromagnetic field of arbitrary configuration is investigated. At high energy the correction to the standard quasiclassical approximation (SQA) of the process probability has been calculated. In the region of intermediate photon energies where SQA is inapplicable the new approximation is used. The influence of weak electric field on the process in a magnetic field is considered. In particular, in the presence of this field the root divergence in the probability of pair creation on the Landau energy levels is vanished. For smaller photon energies the low energy approximations have been derived. At low photon energy the electric field action dominates and the influence of the magnetic field on the process occurs because of its interaction with the the magnetic moment of creating particles.

Pair creation by polarized photons in constant and homogeneous electromagnetic fields

V.M. Katkov
Book of abstracts of IX International symposium "RREPS-11", p.14.
September 12-16, 2011, Egham, United Kingdom.

The probability of pair creation by a polarized photon in a constant and homogeneous electromagnetic field of an arbitrary configuration is calculated with using the imaginary part of the diagonalized polarization operator. Separating of the photon energy divisions and the main characteristics of the process is the same as for the unpolarized case. Connected with a polarization state of photon the special features are considered.

Induced current in the presence of a magnetic flux tube of small radius

A.I. Milstein and I.S. Terekhov.
Phys. Rev. B 83, 075420 (2011).

The induced current density, corresponding to the massless Dirac equation in (2+1) dimensions in a magnetic flux tube of small radius is considered. This problem is important for graphene. In the case, when an electron can not penetrate the region of nonzero magnetic field, this current is the odd periodical function of the magnetic flux. If the region inside the magnetic tube is not forbidden for penetration of electron, the induced current is not a periodical function of the magnetic flux. However in the limit $R \rightarrow 0$, where R is the radius of magnetic flux tube, this function has the universal form which is independent of the magnetic field distribution inside the magnetic tube at fixed value of the magnetic flux.

Relativistic Coulomb Green's function in d -dimensions

R.N. Lee, A.I. Milstein and I.S. Terekhov.
ZhETF 140, 236 (2011) [JETP 113, 202 (2011)].

Using the operator method, the Green's functions of the Dirac and Klein-Gordon equations in the Coulomb potential $-Z\alpha/r$ are derived for the arbitrary space dimensionality d . Nonrelativistic and quasiclassical asymptotics of these Green's functions are considered in detail.

Effective field theories and spin-wave excitations in helical magnets

A.I. Milstein and O.P. Sushkov.
Phys. Rev B 84, 195138 (2011).

We consider two classes of helical magnets. The first class has magnetic ordering close to that of an antiferromagnet and the second class has magnetic ordering close to that of a ferromagnet. The first case is relevant to cuprate superconductors and the second case is realized in FeSrO_3 and FeCaO_3 . We derive the effective field theories for these cases and calculate the corresponding excitation spectra. We demonstrate that the "hourglass" spin-wave dispersion observed experimentally in the cuprates is a fingerprint of the "antiferromagnetic spin spiral state". We also show that quantum fluctuations are important for the "ferromagnetic spin spiral", as they influence qualitative features of the spin-wave dispersion.

3.4. GRAVITY

Path integral on the extreme field configurations

V. M. Khatsymovsky.
Intl. J. Mod. Phys. A, Vol. 26, No. 1, pp. 135-148 (2011).

The canonical Hamiltonian path integral measure obeys certain rule which relates such measure on the paths defined on the whole time axis to the measures on the paths defined on the regions constituting the time axis. We show that this "gluing" rule can be reproduced without referring to Hamiltonian formalism, by substituting field configurations with arbitrarily fast change of the fields at the boundary points of these regions into action and viewing the path integral in the sense of generalized function. Now the coordinate along which gluing proceeds can be not only the time.

The piecewise-flat (simplicial) minisuperspace gravity system is considered. Arbitrarily fast change of the (tangential component of) metric between the two 4-simplices with common 3-face is studied. That is, we generalize piecewise-flat ansatz by allowing tangential metric be function of the distance from the 3-face in the neighborhood of this 3-face. The action is non-degenerate (nonsingular) w. r. t. these additional generalized coordinates. The rule for gluing the path integral measures on separate 4-simplices is found. The resulting general expression covers a large variety of the measures including those usually used in numerical calculations and allows to specify the measure in some applications.

Attributing sense to some integrals in Regge calculus

V. M. Khatsymovsky.
J. Math. Phys., Vol. 52, No. 022502, pp. 1-14 (2011).

Regge calculus minisuperspace action in the connection representation has the form in which each term is linear over some field variable (scale of area-type variable with sign). We are interested in the result of performing integration over connections in the path integral (now usual multiple integral) as function of area tensors even in larger region considered as independent variables. To find this function (or distribution), we compute its moments, i. e. integrals with monomials over area tensors. Calculation proceeds through intermediate appearance of δ -functions and integrating them out. Up to a singular part with support on some discrete set of physically unattainable points, the function of interest has finite moments. This function in physical region should therefore exponentially decay at large areas and it really does being restored from moments. This gives for gravity a way of defining such nonabsolutely convergent integral as path integral.

Gravity action on the rapidly varying metrics

V. M. Khatsymovsky.
Gen. Rel. Grav., Vol. 43, No. 11, pp. 3127-3138 (2011).

We consider a four-dimensional simplicial complex and the minisuperspace general relativity system on it. The

metric is flat in the most part of the interior of every 4-simplex with exception of a thin layer of thickness $\propto \varepsilon$ along each three-dimensional face. In this layer the metric undergoes jump between the two 4-simplices sharing this face. At $\varepsilon \rightarrow 0$ this jump would become discontinuity. However, discontinuity of the (induced on the face) metric is not allowed in general relativity. Namely, the terms in the Einstein action tending to infinity at $\varepsilon \rightarrow 0$ arise. In the path integral approach, these terms lead to the pre-exponent factor with δ -functions requiring vanishing the discontinuities of the induced on the faces metric. That is, the 4-simplices fit on their common faces. The other part of the path integral measure corresponds to the action which is the sum of independent terms over the 4-simplices. Therefore this part of the path integral measure is the product of independent measures over the 4-simplices. The result obtained is in accordance with our previous one obtained from the symmetry considerations.

3.5. ASTROPHYSICS

Quark-mass variation effect on big bang nucleosynthesis

V.F. Dmitriev, J. Berengut, V.V. Flambaum.

Conference: Nuclear Physics in Astrophysics V, 3-8 April 2011, Eilat, Israel.

We calculate the effect of variation in the light-current quark mass, m_q , on standard big bang nucleosynthesis. A change in m_q at during the era of nucleosynthesis affects nuclear reaction rates, and hence primordial abundances, via changes the binding energies of light nuclei. It is found that a relative variation of $\Delta m_q/m_q = 0.016 + 0.005$ provides better agreement between observed primordial abundances and those predicted by theory. This is largely due to resolution of the existing discrepancies for ${}^7\text{Li}$. However this method ignores possible changes in the position of resonances in nuclear reactions. The predicted ${}^7\text{Li}$ abundance has a strong dependence on the cross-section of the resonant reactions ${}^3\text{He} (d, p) {}^4\text{He}$ and $t (d, n) {}^4\text{He}$. We show that changes in m_q at the time of BBN could shift the position of these resonances away from the Gamow window and lead to an increased production of ${}^7\text{Li}$, exacerbating the lithium problem.

3.6. NONLINEAR DYNAMICS AND QUANTUM, CHAOS

Quantum vacuum of strongly nonlinear lattices

O.V.Zhirov, A.S.Pikovskiy and D.L.Shepelyansky.

Phys. Rev. E **83**, 016202 (2011).

We study the properties of classical and quantum strongly nonlinear chains by means of extensive numerical simulations. Due to strong nonlinearity, the classical dynamics of such chains remains chaotic at arbitrarily low energies. We show that the collective excitations of classical chains

are described by sound waves whose decay rate scales algebraically with the wave number with a generic exponent value. The properties of the quantum chains are studied by the quantum Monte Carlo method and it is found that the low-energy excitations are well described by effective phonon modes with the sound velocity dependent on an effective Planck constant. Our results show that at low energies the quantum effects lead to a suppression of chaos and drive the system to a quasi-integrable regime of effective phonon modes.

Wigner crystal in snaked nanochannels

O.V. Zhirov, D.L. Shepelyansky.

e-print: arXiv:1102.1277v1 [cond-mat.mes-hall]

(2011);Eur. Phys. J. B **82**, 63-67 (2011).

We study the properties of a Wigner crystal in snaked nanochannels and show that they are characterized by a conducting sliding phase at low charge densities and an insulating pinned phase above a critical charge density. The transition between these phases has a devils staircase structure typical for the Aubry transition in dynamical maps and the Frenkel-Kontorova model. We discuss the implications of this phenomenon for charge density waves in quasi-one-dimensional organic conductors and for supercapacitors in nanopore materials.

Conference ECRYS-2011:

Wigner crystal in snaked nanochannels: outlook

O.V. Zhirov, D.L. Shepelyansky.

e-print: arXiv:1110.1812v1 [cond-mat.str-el] (2011);

Proceedings of ECRYS-2011, August 15-27, Cargese, France.

We study properties of Wigner crystal in snaked nanochannels and show that they are characterized by a conducting sliding phase at low charge densities and an insulating pinned phase emerging above a certain critical charge density. We trace parallels between this model problem and the Little suggestion for electron transport in organic molecules. We also show that in presence of periodic potential inside the snaked channel the sliding phase exists only inside a certain window of electron densities that has similarities with a pressure dependence of conductivity in organic conductors. Our studies show emergence of dynamical glassy phase in a purely periodic potential in absence of any disorder that can explain enormously slow variations of resistivity in organic conductors. Finally we discuss the KAM concept of superfluidity induced by repulsive Coulomb interaction between electrons. We argue that the transition from the sliding KAM phase to the pinned Aubry phase corresponds to the superfluid-insulator transition.

Classical Versus Quantum Dynamical Chaos: Sensitivity to External Perturbations, Stability and Reversibility

Valentin V. Sokolov, Oleg V. Zhirov, Yaroslev A. Kharkov.

Chaos Theory, "Topics on Chaotic Systems; Selected Papers from CHAOS2010 International Conference", World Scientific, pp. 59-76, (2011).

The extraordinary complexity of classical trajectories of typical nonlinear systems that manifest stochastic behavior is intimately connected with exponential sensitivity to small variations of initial conditions and/or weak external perturbations. In rigorous terms, such classical systems are characterized by positive *algorithmic complexity* described by the Lyapunov exponent or, alternatively, by the Kolmogorov-Sinai entropy. The said implies that, in spite of the fact that, formally, any however complex trajectory of a perfectly isolated (closed) system is unique and differentiable for any certain initial conditions and the motion is perfectly reversible, it is impractical to treat that sort of classical systems as closed ones. Inevitably, arbitrary weak influence of an environment crucially impacts the dynamics. This influence, that can be considered as a noise, rapidly effaces the memory of initial conditions and turns the motion into an irreversible random process.

In striking contrast, quantum mechanics of classically chaotic systems exhibit much weaker sensitivity and strong memory of the initial state. Qualitatively, this crucial difference could be expected in view of a much simpler structure of quantum states as compared to the complexity of random and unpredictable classical trajectories. However the very notion of trajectories is absent in quantum mechanics so that the concept of exponential instability seems to be irrelevant in this case. The problem of a quantitative measure of complexity of a quantum state of motion, that is a very important and nontrivial issue of the theory of quantum dynamical chaos, is the one of our concern. With such a measure in hand, we would be able to quantitatively analyze the stability and reversibility of quantum dynamics in the presence of external noise.

To solve this problem we point out first that individual classical trajectories are of minor interest if the motion is chaotic. Properties of all of them are alike in this case and rather the behavior of their manifolds carries really valuable information. Therefore the phase-space methods and, correspondingly, the Liouville form of the classical mechanics become the most adequate. It is very important that, opposite to the classical trajectories, the classical phase space distribution and the Liouville equation have direct quantum analogs. Hence, the analogy and difference of classical and quantum dynamics can be traced by comparing the classical ($W^{(c)}(I, \theta; t)$) and quantum (Wigner function $W(I, \theta; t)$) phase space distributions both expressed in identical phase-space variables but ruled by different(!) linear equations.

The paramount property of the classical dynamical chaos is the exponentially fast structuring of the system's phase space on finer and finer scales. On the contrary, degree of structuring of the corresponding Wigner function is restricted by the quantization of the phase space. This makes Wigner function more coarse and relatively "simple" as

compared to its classical counterpart. Fourier analysis affords quite suitable ground for analyzing complexity of a phase space distribution, that is equally valid in classical and quantum cases.

We demonstrate that the typical number of Fourier harmonics is indeed a relevant measure of complexity of states of motion in both classical as well as quantum cases. This allowed us to investigate in detail and introduce a quantitative measure of sensitivity to an external noisy environment and formulate the conditions under which the quantum motion remains reversible. It turns out that while the mean number of harmonics of the classical phase-space distribution of a non-integrable system grows with time exponentially during the whole time of the motion, the time of exponential upgrowth of this number in the case of the corresponding quantum Wigner function is restricted only to the Ehrenfest interval $0 < t < t_E$ - just the interval within which the Wigner function still satisfies the classical Liouville equation. We showed that the number of harmonics increases beyond this interval *algebraically*. This fact gains a crucial importance when the Ehrenfest time is so short that the exponential regime *has no time to show up*. Under this condition the quantum motion turns out to be quite stable and reversible. Quantitatively, the degree of reversibility of a chaotic quantum system subject to a persistent noise is characterized by the Purity of the quantum state at the moment of the time reversion.

Dynamical Quantum Chaos and Suppression of Quantum Coherence

Valentin V. Sokolov.

Electronic ArXiv of the Third Workshop on Nuclei and Mesoscopic Physics WNMP11, pp. 1-35, East Lansing, 2011.

In the light of the general problem of the quantum-classical correspondence principle, mechanisms of decoherence are discussed with reference to the quantum systems whose dynamics is chaotic in the classical limit. Though rapid decay of phase correlations is an underlying feature of the classical dynamical chaos, the so called "quantum chaos" is not, by itself, capable of destroying the quantum phase coherence. Basically, formation of incoherent mixed states is necessary on some stage of the evolution for decoherence to appear. Therefore interaction with an environment plays primary role. We demonstrate and compare the ways the decoherence phenomenon shows up in the temporal behavior of the relevant quantities like Peres fidelity, Shannon (information) and von Neumann (correlational) entropies when the evolution starts from a pure or mixed state. The time of complete decoherence is estimated. Connection with the problems of stability and reversibility of quantum chaotic dynamics is analyzed as well. At last, effects of decoherence and energy dissipation induced by interaction with a complicated many-body environment with a weak disorder are investigated within the framework of a microscopic model based on the general theory of the resonance scattering.

4

PLASMA PHYSICS
AND
CONTROLLED THERMONUCLEAR
FUSION

4.1 EXPERIMENTS ON THE GAS-DYNAMIC TRAP (GDT) FACILITY

In 2011, two series of experimental studies were conducted on the GDT facility, which gave significant scientific results. The first series of experiments was aimed at improving the longitudinal plasma confinement in the gas-dynamic trap with two ambipolar cells on the edges. In the course of the second series, heating with electron beam was tried for the first time on the GDT facility. Besides that, preparatory works for commissioning of the system of microwave heating of plasma at electron cyclotron resonance frequencies were underway. These works are described below in the form of three relatively independent parts.

4.1.1 Effect of ambipolar electric fields on longitudinal plasma losses in the gas-dynamic trap

This section describes experiments on the development of effective ambipolar barriers for suppression of longitudinal loss from the gas-dynamic trap, namely investigation cells the effect of ambipolar electric fields generated in additional end magnetic bottles ("ambipolar plugs") on the longitudinal confinement of plasma in the GDT. This research is a continuation of the cycle of works in 2008-2009, when one ambipolar cell was used. At that time, with one such cell on one side of

the GDT, the longitudinal plasma flow from the central part of the trap was made about five times as small.

Additional cells—compact magnetic mirrors (CMs)—were integrated, one to each side of the GDT facility. Two of the CMs (east CM (E-CM) and west CM (W-CM)) with independent power supplies of magnetic coils were used in these experiments as "ambipolar cells" on both sides of the GDT. Fig. 4.1.1 shows the scheme of the experiment with the two ambipolar cells, while a photo of the GDT with two integrated CMs is presented in Fig. 4.1.2.

The power supply system of the GDT magnetic field was upgraded with a capacitor bank in a dedicated technology room. 1,000 IR-6-150 capacitors (6 kV, 150 μ F) in sections of 100 items were installed on shelves in the capacitor compartment, which gave an additional unit with 6 kV capacitor storages of total capacity of 150 mF. This unit consists of two independent modules of 500 capacitors (75 mF) with their own charging systems and allows independent creation of magnetic fields in the two compact magnetic mirrors (east and west). The charging system was able to charge the capacitor banks up to 6 kV, but for reasons of reliability and service life of the capacitors, the recommended voltage is 5.5 kV or less.

Thanks to the design of both CMs, two focused high-power beams of atomic hydrogen or deuterium could be injected normally to the axis of the system. In these experiments, each ambipolar cell comprised one injector of deuterium atoms (see Fig. 4.1.1).

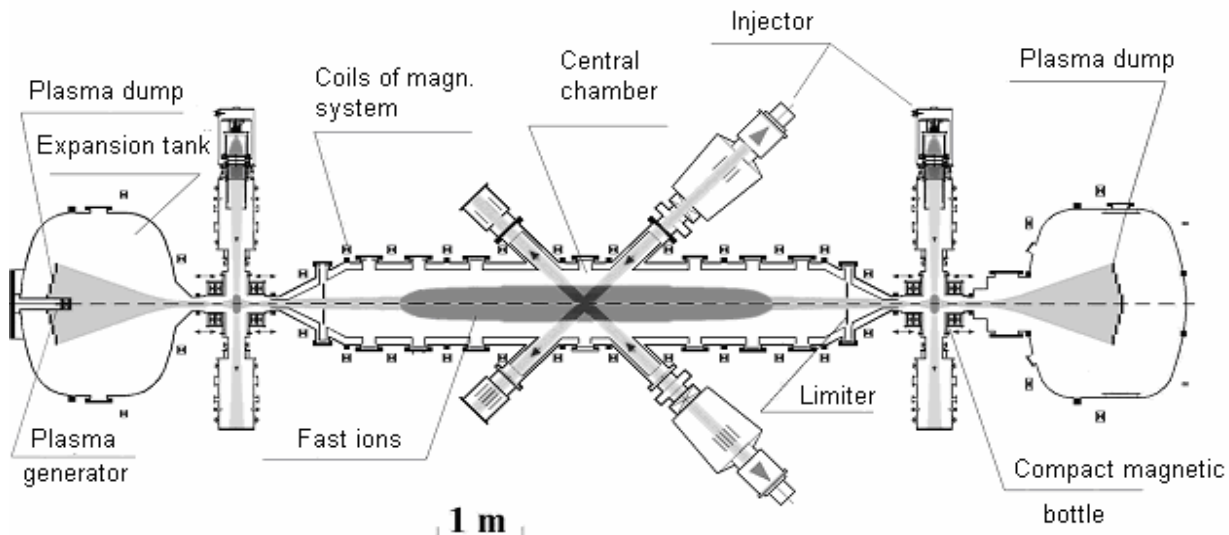


Fig. 4.1.1. Scheme of the experiment with two compact magnetic mirrors.



Fig. 4.1.2. View of the GDT facility with two compact magnetic mirrors.

For better working conditions of the first wall, a few monolayers of titanium are to be sprayed on a specially prepared rough inner surface of the chamber just before the beginning of the experiment, using a ring-shaped arc titanium evaporator inside the chamber.

The first step in the experiments on plasma confinement by means of ambipolar barriers was attaining steady accumulation of fast ions in the two compact magnetic mirrors, which were to serve as ambipolar cells.

At the initial stage of the experiment, both the compact magnetic mirrors were filled with the warm flowing "target" plasma from the central chamber of the GDT. Typically, the density of the flowing plasma was $n_0 \leq 10^{13} \text{ cm}^{-3}$, and its electron temperature was comparable with that in the central part of the GDT, about 100 eV. Then, with a delay of 200 μs from the beginning of injection of atoms in the central part of the GDT, focused beams of deuterium atoms with energy $E = 20 \div 25 \text{ keV}$, duration 4 ms, and a power of about 0.5 MW were injected into the CMs, one beam to a CM, normally to the axis of the system. Ionization of atoms in a CM led to formation of plasmoids, consisting of fast deuterium ions with strongly anisotropic distribution and density several times as large as the density of the background isotropic plasma.

The accumulation of fast ions in the CMs could be observed via the growth of electron density. Fig. 4.1.3 presents the linear density of electrons in modes with and without injection of focused atom beams into the CMs. These measurements were carried out in the west CM (W-CM) with the use of a dispersion interferometer. In the

first approximation, the linear density of hot ions corresponds to the linear density of electrons because the amount of warm target plasma in the plasmoid area is small. Accumulation of fast ions in the second CM (E-CM) run in a similar way, controlled through attenuation of the atom beam and with a diamagnetic probe.

Fig. 4.1.4 presents the density profile of hot ions in the equatorial plane of the west CM, obtained with an analyzer of charge-exchange atoms. The profiles were constructed for the time interval from 2 ms to 3 ms after the start of injection into the compact magnetic mirrors. The profiles were normalized to the linear density of fast ions, which was calculated from the linear density of electrons, which was derived from readings of the dispersion interferometer (see Fig. 4.1.3). So obtained maximum density of fast ions in the center of the CM was $1.1 \times 10^{13} \text{ cm}^{-3}$.

The increased density of fast anisotropic ions in the end CMs led to formation of an ambipolar potential "hump" in these plugs, which prevented loss of ions of the target plasma from the central part of the GDT.

The main purpose of the experiments was to investigate the CMs as ambipolar plugs for improvement of longitudinal confinement. Main attention was paid to the measurements of the radial profiles of electron temperature and density in the main magnetic bottle of the GDT, measurements of longitudinal plasma loss through the CMs, and the magnitude of the ambipolar potential drop in modes with and without injection of beams of atoms into the end compact magnetic mirrors. These studies demonstrated ambipolar plasma confinement in

the GDT with two ambipolar plugs in a regime of moderate plasma parameters, which was proved by a substantially smaller density of the warm ion flux from the GDT through the CM sections on the east and west ends in modes with injection of beams of atoms into the CMs than in modes without it.

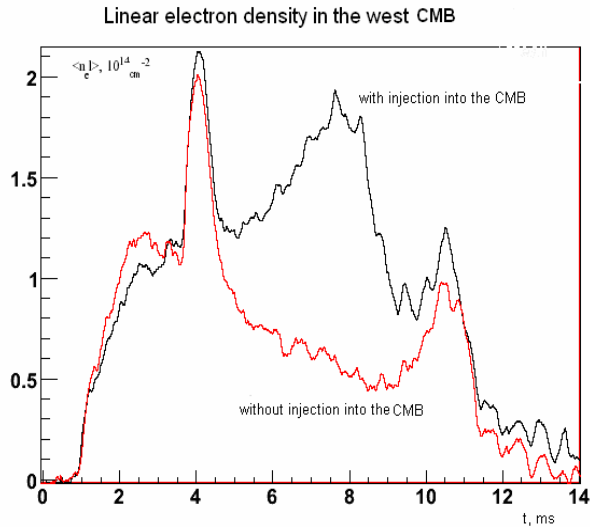


Fig. 4.1.3. Linear density of electrons in the west CMB.

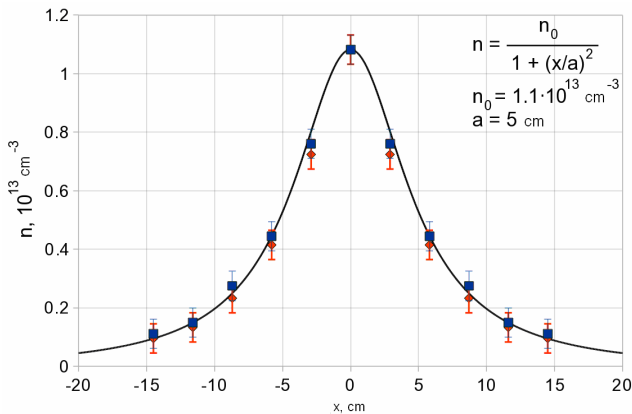


Fig. 4.1.4. Density profile of hot ions in the equatorial plane of the west CMB.

The main diagnostics means for the degree of suppression of the longitudinal loss were a pyroelectric bolometer and a grid probe, located next to each other on a movable rod. Two identical sets of a bolometer and a grid probe were placed in the east and west expanders at a point with the mirror ratio $R_d = 0.7$ (see Fig. 4.1.1). They were used in the measurement of the temporal and radial dependences of the absolute density of ion flux into the expanders. It is worth noting that the bolometer-and-probe system could not be installed on the east side on radii near the axis of the system since this area was projected on the cathode of the arc source of initial plasma.

Fig. 4.1.5 presents radial profiles of ion flux in the west expander in modes with injection of atom beams into both the CMs (triangles) and without it (diamonds), i.e.

with and without creation of a dense anisotropic plasmoid in the compact magnetic mirrors (in this case, the W-CM) and hence an ambipolar barrier on the way of warm ions from the center of the trap. For ease of comparison of the results, the radii in this and all subsequent figures are given in terms of magnetic flux on the central plane of the GDT. One can see from the figure that the ions flux through the W-CM got more than 2 times weaker with the ambipolar barrier was created in it.

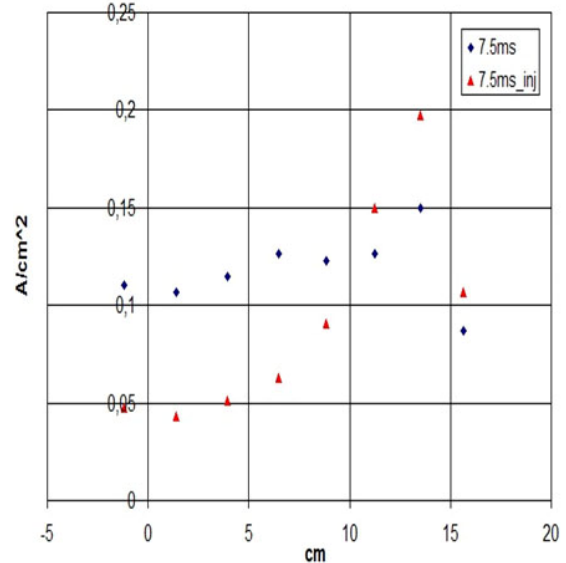


Fig. 4.1.5. Radial profiles of ion flux density measured with the grid probe in the expander near the west plasma absorber.

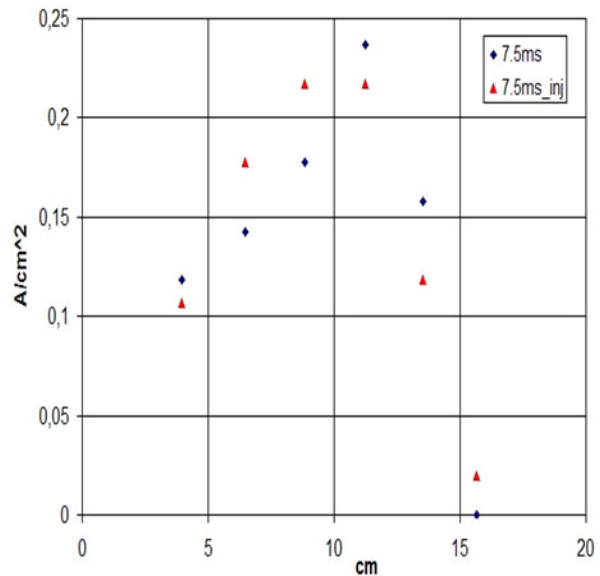


Fig. 4.1.6. Radial profiles of ion flux density measured with the grid probe in the expander near the east plasma absorber.

Fig. 4.1.6 shows the same profiles for the east expander. The weakening of the flux through the E-CM was less, perhaps, because of the gas conditions in the east expander, due to the arc plasma source in it.

Analyzing the spectrum of longitudinal energies of ions leaving the trap through an ambipolar plug, one can also measure the maximum value of the ambipolar potential in a given magnetic force line. In a natural way this value corresponds to the minimum energy of ions, i.e. the “shift” of the distribution function relative to the origin. The spectrum of longitudinal energies (or the longitudinal component of the velocity distribution function) of plasma ions leaving the trap through a plug was measured with a grid analyzer with scanning of the locking voltage. The analyzer was located in the area of the expander behind the W-CM. Fig. 4.1.7 shows the radial profiles of the plasma ambipolar potential measured by this method. Profile (a) corresponds to a mode with injection into the CMs; profile (b) is for a mode without injection, i.e. a free flux of plasma through the additional CMs; profile (c) illustrates the difference in the obtained profiles. According to the measurements, when dense bunches of hot ions were created in the end magnetic mirrors, the magnitude of the ambipolar potential jump in the CMs was ~ 100 V (see Fig. 4.1.7(c)), which is comparable with the electron temperature of the flowing-out target plasma in this mode.

The density and temperature of electrons in the central plane of the GDT were also measured in these experiments, by the method of Thomson laser scattering. The radial profile of the target plasma density changed with “switching on” the two ambipolar plugs, as shown in Fig. 4.1.8. As in the previous figure, profiles (a) and (b) correspond to modes with and without injection into the CMs, while profile (c) illustrates the difference.

The electron temperature of the plasma stayed virtually unchanged, which can be explained by the fact that the local energy balance of the system changed when the plasma density increased substantially. For example, the injection power remained unaffected during all the experiments and was determined by energy of the supply systems of the injectors. Therefore, with increasing plasma density the heating of the beams, as recalculated to ion-electron pair, reduced. On the other hand, an increase in the plasma density in a given force line led to a growth (up to 2 times on the axis!) of the flux incident on the plug, which, even with the ambipolar barriers, resulted in equalization of the fluxes, with and without ambipolar plugs. This effect was observed in the measurement of ion flux through the east CM (see Fig. 4.1.6). In this case, in some force lines, the flux on the probe through the ambipolar plug was even somewhat higher than that without the barrier potential.

However, we demonstrated experimentally that plasma density was increasing due to improved longitudinal confinement caused by formation of ambipolar barriers on the edges, which is a good stepping stone for further study of the ambipolar confinement in traps of the GDT type.

Let use these experimental data to estimate the time of longitudinal plasma confinement $\tau_{||}$ and the confinement parameter $n\tau_{||}$ for particles in the axial region

in modes with (denoted with * in the equations) and without injection of beams into both the CMs.

From the measurement data shown in Figs. 4.1.5 and 4.1.6, one can estimate the longitudinal plasma flow from the trap near the axis at the moment 7.5 ms in the mode without injection (without creating an ambipolar barrier) as

$$j_w(r=0, t=7.5 \text{ ms}) \approx j_E = j \approx 0.1 \text{ A/cm}^2$$

Here, j_w and j_E are the warm ion fluxes through the west and east CM, respectively. When the ambipolar barriers are created in the CMs, according to the measurement data, the flux of warm ions near the axis reduced about two times on the west side and remained at the same level on the east one:

$$j_w^* \approx j/2, \quad j_E^* \approx j.$$

Recall that * denotes parameters of the experiment with ambipolar locking.

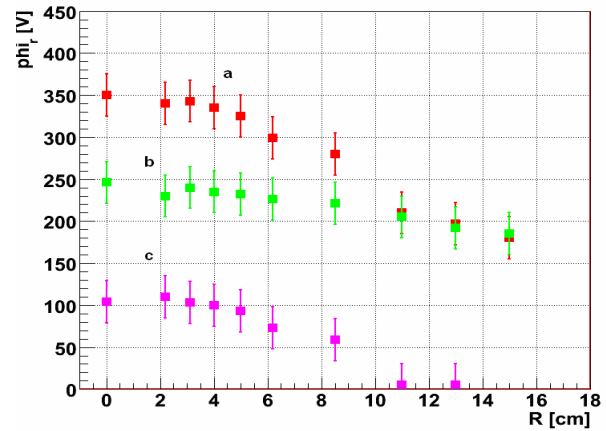


Fig. 4.1.7. Radial profile of ambipolar potential of plasma with (a) and without injection (b) into the CMs of the GDT; (c) illustrates the difference in the profiles.

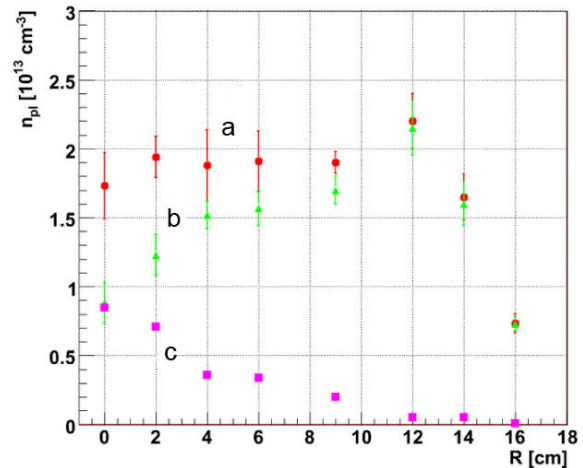


Fig. 4.1.8. Radial profile of plasma density in the central part of the GDT in modes without (triangles, a) and with injection (circles, b) of atom beams into the CMs. Squares (c) show the difference in the two profiles.

As one can see from Fig. 4.1.8, plasma density in the central part of the GDT near the axis increased 2 times with the ambipolar locking, i.e.

$$n^* = 2n.$$

The time of longitudinal confinement on the axial force tube can be estimated as the time of outlet of the plasma of the density n from a unit volume V of this tube in the flows j_W and j_E through the western and eastern plugs, respectively:

$$nV/\tau_{||} \propto j_W + j_E$$

Then, for the case without ambipolar blocking (only magnetic mirrors),

$$\tau_{||} \propto nV/2j,$$

whereas with ambipolar locking,

$$\tau_{||}^* \propto n^*V/(j+j/2) = 4nV/3j = (8/3) \cdot \tau_{||} \approx 2.7 \tau_{||}.$$

Thus, with the use of the ambipolar barriers, the time of longitudinal confinement of particles in the axial region of the GDT increased 2.7 times; $\tau_{||}^* \approx 2.7 \tau_{||}$. As for the parameter $n\tau_{||}$, which illustrates improvement in the longitudinal confinement,

$$n^*\tau_{||}^* \approx 5.4n\tau_{||}.$$

Similar calculations for other radii with subsequent averaging over the plasma filament cross section (<...>) give the following:

$$\langle \tau_{||}^* \rangle \approx 1.8 \langle \tau_{||} \rangle \quad \text{and} \quad \langle n^*\tau_{||}^* \rangle \approx 2.9 \cdot \langle n\tau_{||} \rangle,$$

respectively.

From these comparisons, one can conclude that in these experiments with ambipolar plugs of rather moderate parameters (the height of the potential hump was about the plasma temperature), the longitudinal confinement was improved more than 5 times on the axis of the facility and almost 3 times on the average over the plasma cross section.

The improved confinement of the target plasma in the GDT had a positive effect on the accumulation and containment of the population of fast ions in the central part of the GDT. From the results of measurements of local diamagnetism (MSE) one can get the maximum value of the relative plasma pressure $\beta_{\max} = 0.45$ and the maximum density of fast ions at the stop point $n_{f \max} \approx 4 \cdot 10^{14} \text{ cm}^{-3}$ (for the average ion energy $\langle E_f \rangle = 10 \text{ keV}$). These values are record ones for a GDT with an injection power of 4.5 MW (6 heating injectors in the central part).

To further investigate the influence of the effect of ambipolar locking on the parameters of plasma confined in the GDT, it was decided to increase the magnetic field in the central part of the GDT from 2.95 to 3.35 kG. The increase in magnetic field led to more pronounced results, demonstrating an augment in the plasma parameters due to the use of two ambipolar barriers. Fig. 4.1.9 shows the time dependence of the linear plasma density in the

central plane of the GDT according to the data of dispersion interferometer for a mode with high magnetic field. Upper curve (1): with injection of atom beams into both CMs; lower curve (2): without injection.

One can see from the figure that in this mode the injection of beams into the CMs, i.e. creation of ambipolar barriers, led to a significant increase in the density (the linear density increased almost 2 times!). The growth of the plasma density in this regime was limited by the developing MHD instability, as evidenced by plasma oscillations after 8 ms in the scale of Fig. 4.1.9.

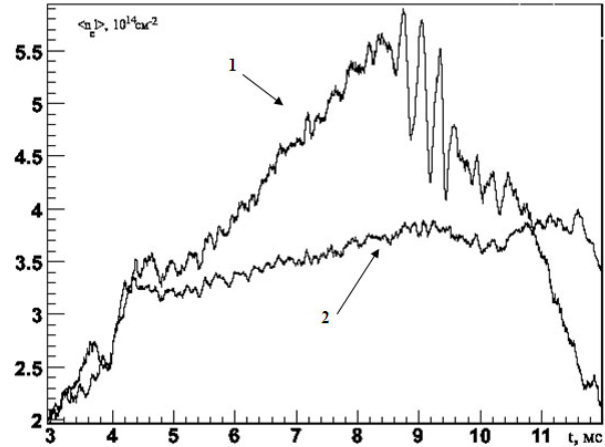


Fig. 4.1.9. Time dependence of the linear plasma density in the central plane of the GDT for a mode with high magnetic field. (1) with injection into both CMs and (2) without injection.

In modes with high magnetic field, the influence of the ambipolar potential on the maximum parameters of plasma density and temperature in the central part of the GDT demonstrated itself more clearly. According to Thomson scattering measurement, in a steady regime with high magnetic field and ambipolar plugs, the electron temperature on the axis at the time $t = 8 \text{ ms}$ was $T_e^* = 138 \pm 3.5 \text{ eV}$ at the density $n^* = (2.2 \pm 0.2) \cdot 10^{13} \text{ cm}^{-3}$. For comparison, at the same magnetic field value but without ambipolar locking (without injection of beams into the end CMs) the temperature was much lower: $T_e = 109 \pm 9 \text{ eV}$ and the density was more than 2 times lower: $n = (0.95 \pm 0.04) \cdot 10^{13} \text{ cm}^{-3}$.

Thus, in a mode with high magnetic field we managed to demonstrate a significant increase in the density and temperature due to the longitudinal confinement improvement with two ambipolar plugs in the form of end CMs and perpendicular injection of atomic beams into them.

To investigate the effectiveness of each of the ambipolar plugs we conducted special experiments with injection of beams, i.e. creation of an ambipolar barrier, into either the eastern or western CM. The results of these studies are presented in Fig. 4.1.10. As one can see, both the CMs had approximately the same efficiency and gave a half of the contribution to improvement of the confinement.

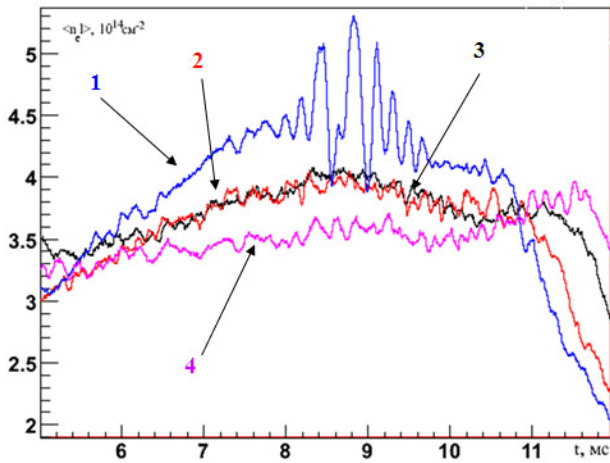


Fig. 4.1.10. Comparison of the effectiveness of the east and west CMs via the linear time dependence of plasma density $\langle n_e \rangle$ in the central plane of the GDT for modes with high magnetic field:

- 1 - injection of beams into both CMs (blue curve);
- 2 - injection of beam only into the east CM (red curve);
- 3 - injection of beam only into the west CM (black line);
- 4 - without injection of beams into the CMs (purple).

Examination of oscillations of the plasma potential and magnetic field in the region of ion cyclotron frequencies showed no Alfvén ion-cyclotron instability in these modes. This instability was observed earlier in experiments on the GDT with one compact magnetic bottle. This is due to the lower parameters of ion plasmoids in the CMs in these experiments and a threshold character of development of this microinstability.

In conclusion of the section, we present the main results obtained during the presented cycle of works:

- two end compact magnetic mirrors (CMs) were manufactured and installed on the GDT, with perpendicular injection of high-energy beams of hydrogen or deuterium atoms into them;
- accumulation and confinement of bunches of fast ions of a mean energy of 10-15 keV and a density several times as large as that of flowing target plasma were experimentally demonstrated;
- we demonstrated that two ambipolar barriers created in the compact magnetic mirrors on both sides of the GDT improve the longitudinal confinement. We observed a two-fold increase in the plasma density on the axis in the central part of the GDT, a decrease in the longitudinal loss, and a noticeable augment in the electron temperature. As a result, the parameter $n\tau_{||}$ increased more than 5 times relative to the mode with no ambipolar plugs.

4.1.2 Results of first experiments on plasma heating with electron beam on the GDT facility

High-power electron beams injected into the trap from behind-plug areas along the magnetic field play an important role in the experimental studies on the GDT and next-generation facilities on its basis. In this case, the electron beams have two functions:

- 1) additional heating of the electron component of plasma and
- 2) control of the radial profile of the electric potential of plasma, which is necessary to overcome the effect of MHD instabilities on the confinement of particles and energy.

Successful implementation of these functions requires determination of the following:

- 1) the possibility of injection of electron beam of a megawatt-range power through the plug unit, with a high degree of beam compression;
- 2) the range of densities of ion flux from the plasma, in which the electron beam generator can operate safely.

The solution to these problems was the main motive of the first series of experiments on electron beam injection into the GDT, which were held in late 2011.

An electron gun was developed for beam formation. The gun is schematically illustrated in Fig. 4.1.11. The LaB₆ cathode of 20 mm in diameter was heated by the electron beam from an additional "minor electron gun" with an electron energy of 1.5 keV. Such a two-stage scheme allowed us to minimize the power of heating of the main cathode unit and use air cooling. The anode was made as a molybdenum grid with a thickness of 0.5 mm and 37 hexagonally-ordered holes of 2.4 mm in diameter. The total area of the holes was 1.67 cm². The cathode was closed with a molybdenum mask of respective form. The electron gun is shown in Fig. 4.1.12.

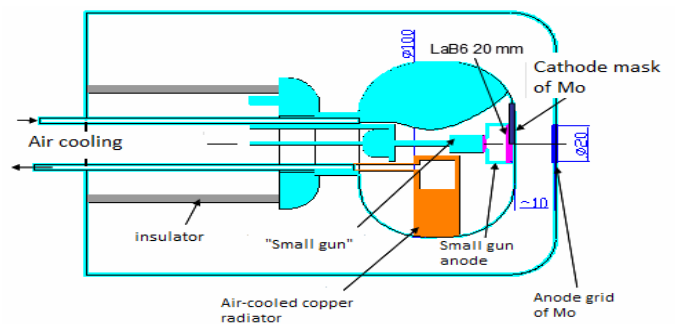


Fig. 4.1.11. Schematic representation of the electron gun developed for experiments on the GDT.



Fig. 4.1.12. Photo of the electron gun, prepared for installation on the GDT: view from the anode.

During the experiments on the GDT, parameters of the electron gun were as follows: the anode voltage was 40 kV; the beam current was 10 A; the duration of operation was 0.3 ms.

The electron gun was installed in one of the end expansion tanks of the GDT, as shown in Fig. 4.1.13.

At the initial stage of the experiment, the electron beam was injected in a mode without plasma generation, the residual gas pressure in the GDT not exceeding $3 \cdot 10^{-5}$ Pa. The beam current and energy were recorded with a movable collecting calorimeter installed

inside the trap near the opposite mirrors unit. The magnitude of magnetic field in the electron gun could be varied by means of a special coil mounted on the expansion tank. The measurements showed that for a beam compression degree in the range $K_{\text{egun}} = 60 \div 120$ (K_{egun} is the ratio of magnetic field in the plug to that in the anode gun area) the beam is transported into the trap without loss and detected by the collecting calorimeter.

To study the interaction of beam with plasma, we implemented a "decay" mode, in which the plasma generator filled the trap with warm plasma in 4 ms. The generator was located in the expansion tank opposite to the electron gun. Then the plasma flowed freely from the trap, its density decreasing exponentially with time. Switching the electron gun on at different moments of the outflow, one could inject electrons into the plasma of the density $n = 0 \div 3 \cdot 10^{13} \text{ cm}^{-3}$; the electron temperature of the plasma was several electron volts.

Fig. 4.1.14 shows a typical shape of signal pulse from the diamagnetic probe located in the central plane of the GDT facility. The amplitude of the signal pulse is proportional to the total energy of the plasma column. One can see from the measurements that the plasma energy increases linearly during all the time of electron beam injection and no steady state of plasma heating with the beam is achieved.

Fig. 4.1.15 shows the main result of this series of measurements, i.e. the dependence of the diamagnetic signal amplitude (energy transmitted by the beam to the plasma) on the degree of beam compression in the plug K_{egun} .

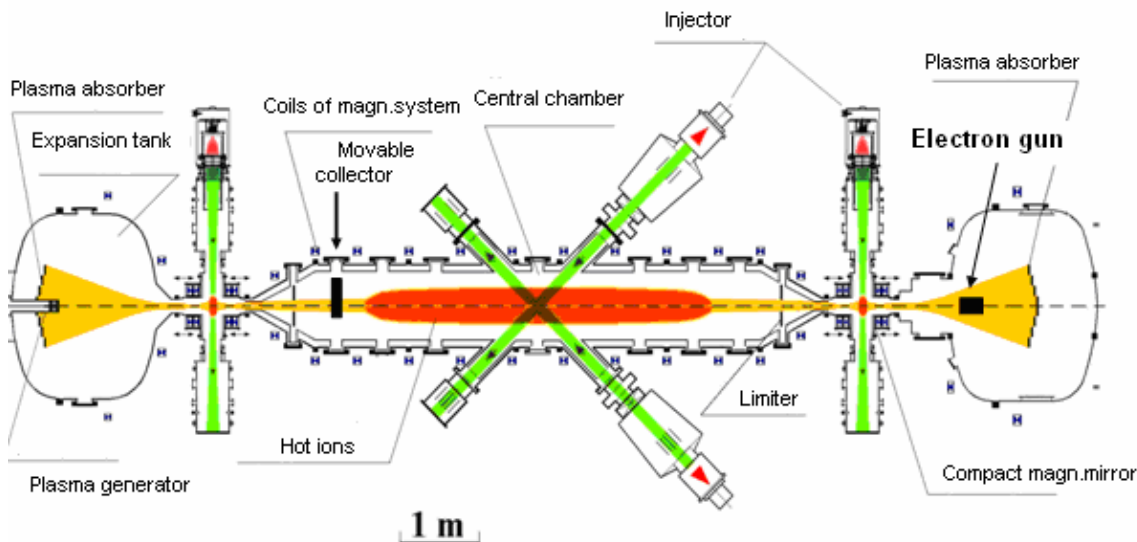


Fig. 4.1.13. Schematic representation of the GDT with the electron gun and a movable collect for with mounted calorimeter for measuring electron beam parameters.

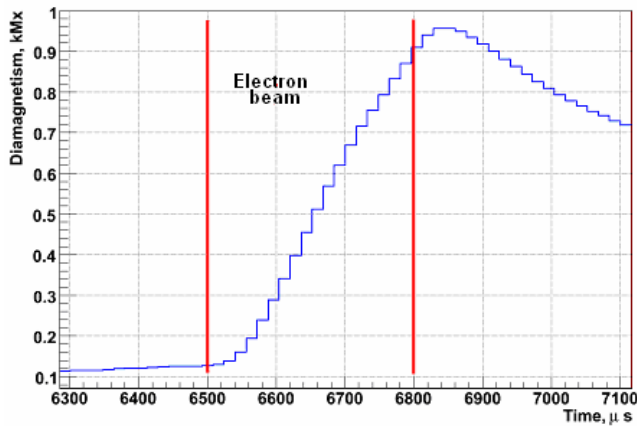


Fig. 4.1.14. Shape of signal pulse from the diamagnetic probe located in the central plane of the GDT. The pulse amplitude is proportional to the total energy content of the plasma.

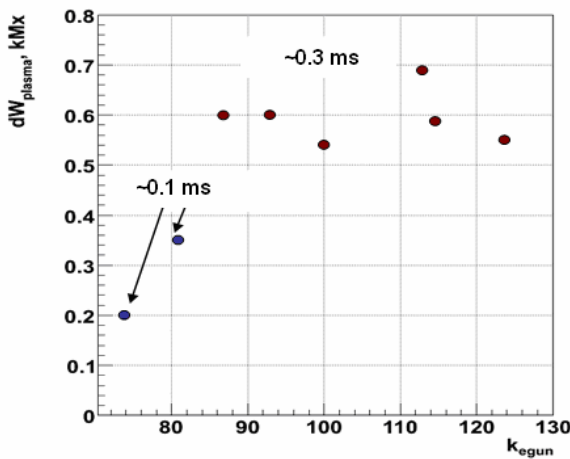


Fig. 4.1.15. Diamagnetic signal amplitude (energy transmitted by the beam to the plasma) vs. degree of beam compression in the plug K_{egun} .

One can see that at $K_{egun} = 85 \div 120$ the energy transferred by the beam to the plasma remains unchanged. Thus we conclude that in this range of compression degree, the beam is freely transported into the trap and interacts with the plasma. When $K_{egun} < 85$, the density of the ion flux on the anode exceeds 15 mA/cm^2 , which is the limit of reliable operation of the electron gun. The operation duration was reduced and restricted by breakdowns. Increase in the electron temperature was measured with a Langmuir probe and a laser-scattering system. The measurement results agree well with the scaling obtained in previous years on a number of pulse facilities with electron beam injection into plasma (Fig. 4.1.16). In a separate series of experiments with injection of atom beams it was shown that the electron beam does not affect confinement of hot ions.

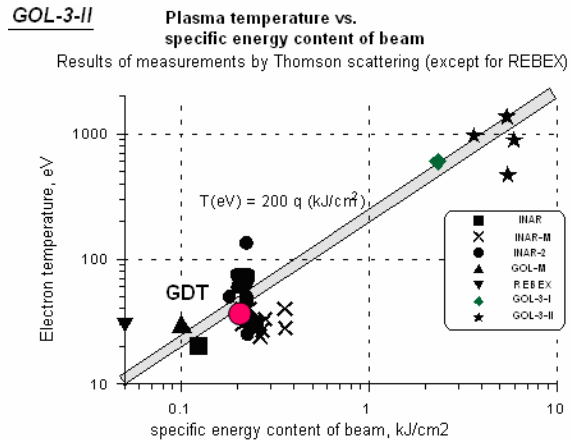


Fig. 4.1.16. Scaling of the dependence of electron temperature increase on specific energy content of the beam, obtained earlier on a number of pulsed facilities with electron beam injection into plasma. The round spot corresponds to the result of the experiment on the GDT facility.

Thus, the results of first experiments with electron beam injection on the GDT facility allow the following conclusions:

- the possibility of electron beam injection through a magnetic plug with a compression ratio of up to $K_{egun} = 120$ to the plasma of the GDT was demonstrated;
- the electron gun was shown to operate reliably at densities of plasma ion flux to the anode $0 < j_i < 15 \text{ mA/cm}^2$;
- the energy content of plasma is increasing linearly throughout the time of electron beam injection. In so doing, in the range $80 < K_{egun} < 120$, the energy transferred from the beam to the plasma does not depend on the degree of beam compression in the plug;
- the electron beam injection does not affect confinement of hot ions.

4.1.3 Development of the system for ECR heating of plasma in the gas-dynamic trap (GDT)

In 2011, BINP SB RAS together with Gycom Ltd. (Nizhny Novgorod) and the Institute of Applied Physics (IAP RAS) (Nizhny Novgorod) were actively working on the construction of the system for ECR heating of plasma on the GDT facility. Commissioning of the system and first experiments are planned for 2012. Below the results of the various stages of preparation and commissioning of the ECR heating system are presented.

During the initial phase of the project, two gyrotron modules were commissioned and tested and their performance was measured on the bench at Gycom Ltd. (Nizhny Novgorod). They were demonstrated to be able to reach the rated 450 kW at a radiation frequency of 54.4 GHz and a HVPS voltage of 70 kV. Precise measurements of individual phase characteristics of

microwave radiation on the output of the gyrotrons were performed. The measurement results were later on used in the design and manufacture of mirrors of quasioptical filters.

BINP together with the Institute of Applied Physics (Nizhny Novgorod) created a code for calculation of the propagation and absorption of electromagnetic radiation in an axially symmetric magnetic trap. Later on, this numerical code was used for numerical modeling of input of microwave radiation into plasma and its absorption in the area of plug units, where there are zones of electron cyclotron resonance.

The initial stage of the designing of elements for microwave plasma heating involved calculations to optimize the process of wave penetration into the plasma, wave propagation to the region of cyclotron resonance, and absorption of microwave power by the GDT plasma. A numerical modeling was performed for a wide range of plasma densities and microwave beam launching angles relative to the axis of symmetry of the plasma column. Fig. 4.1.17 shows an example of results of such calculations; above: separation of captured and uncaptured rays depending on the launching angle at a plasma density of $1.5 \cdot 10^{19} \text{ m}^{-3}$; bottom: rays launched at an angle of 55° for a set of plasma densities in the range $N_0 = 0.5 \div 2.5 \cdot 10^{19} \text{ m}^{-3}$.

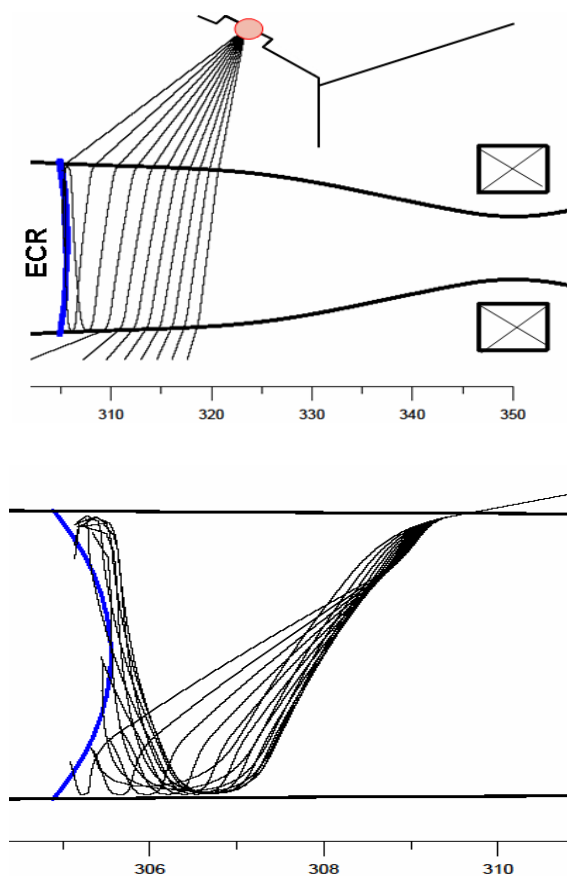


Fig. 4.1.17. Above: geometrical-optics rays for a set of launching angles of 15° to 70° at a plasma density of

$1.5 \cdot 10^{19} \text{ m}^{-3}$. Bottom: rays launched at an angle of 55° at plasma densities $N_0 = 0.5 \div 2.5 \cdot 10^{19} \text{ m}^{-3}$.

It is important to note that the power of microwave radiation introduced with the captured rays is absorbed with an efficiency of 100%. The simulation shows that the rays can be captured at a wide range of plasma densities for different radial density profiles corresponding to different experimental conditions. The most important results are summarized in Fig. 4.1.18, where the diagram "launching angle vs. plasma density" shows areas corresponding to captured beams. We examined three possible positions of the last mirror in the system for radiation injection into the plasma (see the inset in Fig. 4.1.18). In the course of optimization of the input device, we chose position 1 and a launching angle of 54° . These parameters allow efficient injection of radiation into a plasma of a density of $0.5 \div 2.5 \cdot 10^{19} \text{ m}^{-3}$ with launching angles of $50 \div 55^\circ$.

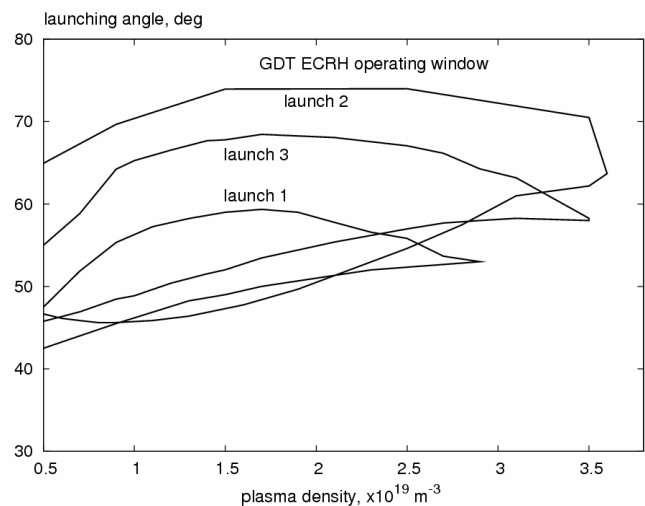


Fig. 4.1.18. Areas of efficient capture of beams in the diagram "launching angle vs. plasma density" for three positions of the last mirror of the system for radiation injection into the plasma. Position 1 was selected for the design.

Fig. 4.1.19 shows an example of the calculated spatial profiles that describe the density of absorbed power $Q(r)$ and $Q(z)$ in the (r, z) coordinates for parameters corresponding to Fig. 4.1.18. 10 geometrical-optics rays with launching angles of 50° to 55° were chosen for simulation of absorption of the quasi-optical beam being formed. The results of the calculations predict rather flat and broad radial density profiles of absorbed power with good localization ($\sim 4 \text{ cm}$) in the longitudinal direction. The lower graph in Fig.4.1.19 illustrates absorbed power vs. electron velocity $Q(v_{||})$. From this dependence it follows that in this scenario power is absorbed mainly by thermal electrons.

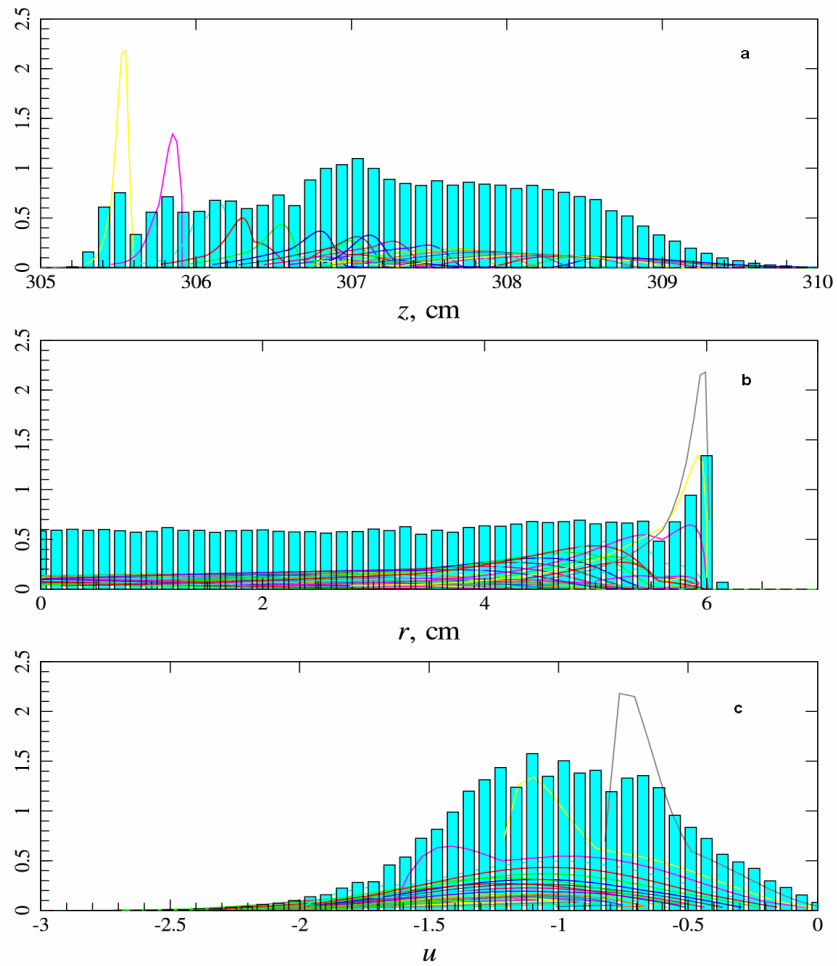


Fig. 4.1.19. Density profiles of absorbed power: (a) radial, (b) longitudinal, for a set of 10 rays with angles of 50° to 55° and the plasma density $N_0 = 1.5 \cdot 10^{19} \text{m}^{-3}$, (c) absorbed power density as a function of the electron velocity normalized to their thermal velocity $u = v_{\parallel} / v_{Te}$

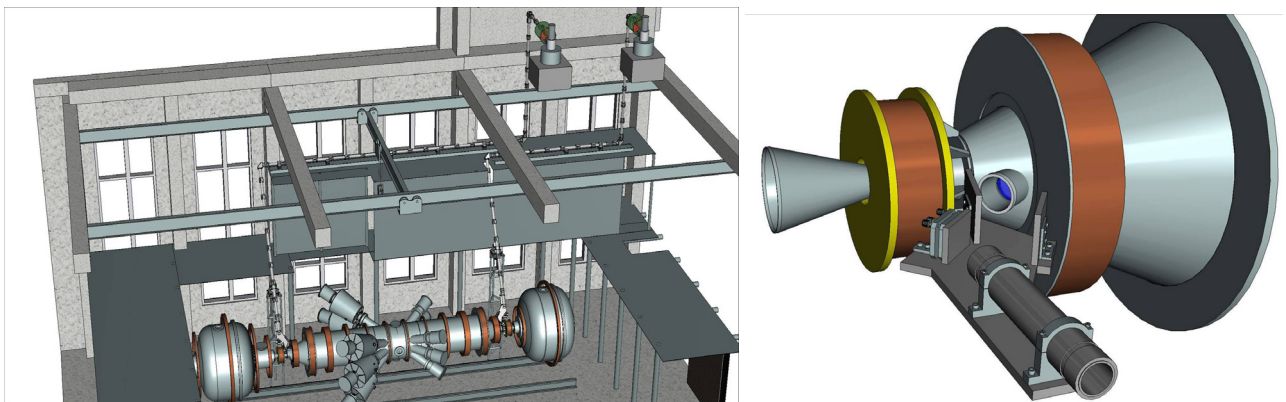


Fig. 4.1.20. 3D model of the GDT facility with the system of microwave heating (left). One of the units for microwave power input into the GDT facility (right).

The main conclusions from the numerical simulation can be summarized as follows:

1. It was shown that beams of microwave radiation with a frequency of 54.5 GHz injected at angles of 50° to 55° into the plasma near the plug units from the trap side can be efficiently captured and completely absorbed at the plasma density $N_0 = 0.5 \div 2.5 \cdot 10^{19} \text{ m}^{-3}$. These data form a basis for designing a system for ECR heating of plasma in the GDT.

2. The results of the calculations predict rather flat and broad radial density profiles of absorbed power with good localization ($\sim 4 \text{ cm}$) in the longitudinal direction

3. The chosen scenario of radiation injection into the plasma predicts radiation absorption mainly by thermal electrons.

The simulation and electrodynamic calculations performed in collaboration with the Institute of Applied Physics resulted in a statement of work for designing a system for microwave beam generation, transport, and injection into the plasma of the GDT facility.

The designing of all elements of the microwave heating system for the GDT facility were completed in July 2011. Holders and devices for adjustment of the waveguide lines were also designed, as well as the end elements of the GDT central vacuum chamber with windows for microwave radiation entry and movable valves with pneumatic actuators for protection of the windows during the application of titanium film preparing the first wall for the working pulse of the facility.

Fig. 4.1.20 shows a 3D model of the GDT facility with the system of microwave heating. The gyrotron modules with quasi-optical filters are arranged in a specialized room above the facility. Via the waveguides and waveguide corners, beams of microwave radiation are brought to the end parts of the magnetic trap, where the cyclotron resonance zones are located. Waveguide corners closest to the GDT facility contain a special system of mirrors, which allows microwave radiation polarization optimal for input into the plasma. Fig. 4.1.20 (right) shows the unit for input of microwave radiation beams into the plasma.

The preparation of the specialized room for the gyrotron modules and their mounting were completed by the end of 2011. The room was redecorated; the cryogenic magnets of the gyrotrons were installed and prepared for testing; all the electrical, vacuum, and gas connections were made; pipelines for process water and gaseous helium discharged from the cryogenic magnets were mounted; the mains were checked; the Ethernet line to the local network of the GDT system for control and data collection was mounted. The insulating vacuum volumes of the cryogenic magnets were pumped out.

Fig. 4.1.21 presents a photograph of the completely ready room at the stage of adjustment of the cryogenic magnets for gyrotron modules. Fig. 4.1.22 shows a photograph of one of the mounted cryogenic magnets, prepared for testing and installation of the gyrotrons.



Fig. 4.1.21. Adjustment of the cryogenic magnets for the gyrotron modules.

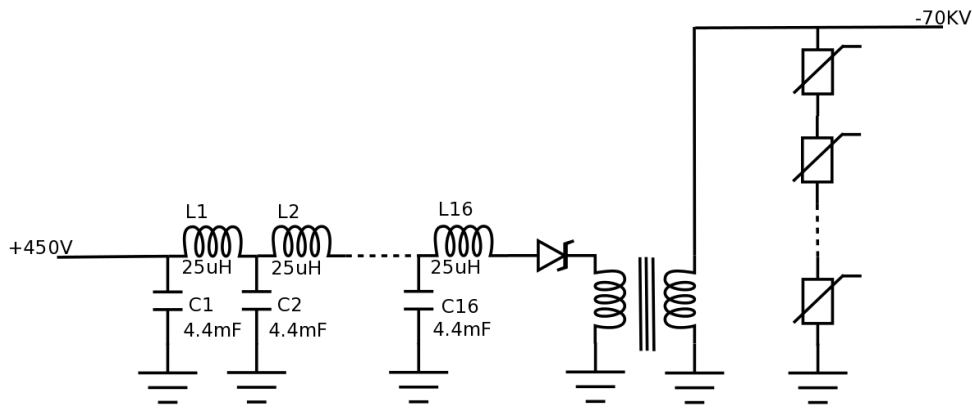


Fig. 4.1.22. Photo of one of the mounted cryogenic magnets, prepared for testing and installation of the gyrotrons.

For testing of the gyrotrons and conduction of the initial phase of experiments on the microwave heating of plasma, we fabricated a pilot version of the high-voltage power supply. Its schematic diagram is shown in Fig. 4.1.23.

The pilot version of high-voltage modulator has the following characteristics: output voltage of 70 kV, load current of up to 25 A, pulse duration of 300 μs , and repetition rate of 1/1 min.

The dimensions of the high-voltage modulator are 800*800*2000 mm. Its weight is about 200 kg. The modulator is set up as an LC line, which is connected to a step-up high-voltage transformer via a thyristor switch. Output voltage stabilization is performed by a set of zinc oxide varistors connected to the secondary winding of the transformer. The number of switched-on varistors is regulated by a scheme for step-wise stabilization of the output pulsed voltage with a step of 500 V. In case of breakdown of the load, the modulator is switched off till the end of the current pulse. The modulator was mounted and tested on a dummy load. Fig. 4.1.24 shows the pilot version of the high-voltage modulator in the course of testing.



HV modulator 300uS for Gyrotron

Fig. 4.1.23. Schematic diagram of the pilot version of the high-voltage modulator for powering the gyrotrons with operation duration of 300 microseconds.

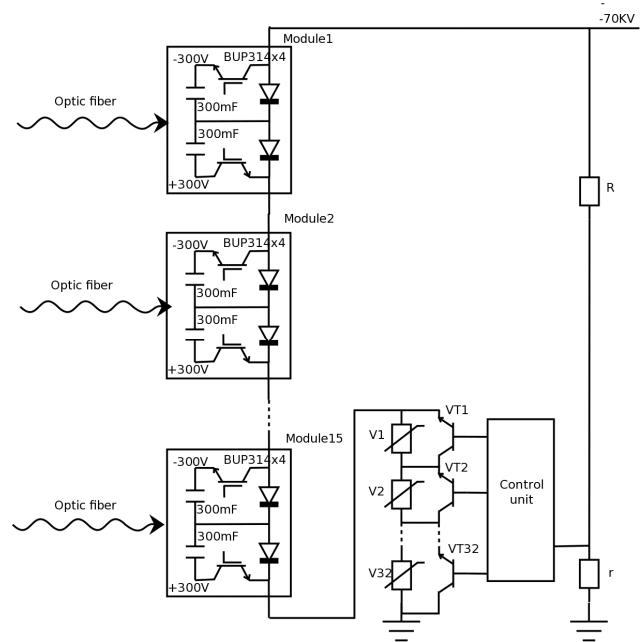


Fig.4.1.24. Testing of the pilot version of the high-voltage modulator.

With the pilot version of the high-voltage modulator we will be able to test the gyrotrons and start the first phase of experiments on ECR heating of plasma in the GDT. Then the pilot version will be replaced with a permanent modulator.

Fig. 4.1.25 presents a schematic diagram of a permanent high-voltage modulator with the following characteristics: output voltage of 70 kV, load current of up to 25 A at a pulse duration of up to 5 ms, and repetition rate of up to 1/1 min. Its dimensions are 600*1000* 000 mm and its weight is 800 kg. The modulator is set up as a capacitor energy storage circuit with IGBT transistor switch and output voltage stabilization via a set of series-connected varistors. The number of switched-on varistors is regulated by the circuit for step-wise stabilization of the output voltage in pulse

with a step of about 500 V. The modulator consists of 15 series-connected sections charged to a voltage of about 6 kV. Each section contains six series-parallel K75-28 capacitors (100 μ F/3000 V). Switching the capacitor voltage on the load is performed with BUP314D transistor switches connected in series. The capacitors are charged from two sealed lead accumulators (12 V/7 Ah) with energy sufficient for 200 to 300 pulses of the modulator. In case of breakdown in the load, the modulator is switched off till the end of the current pulse. Besides that, the modulator is turned off at a microwave breakdown in the output window of a gyrotron or in the waveguide tract.



HV modulator 5mS for Gyrotron

Fig. 4.1.25. Schematic diagram of the permanent high-voltage modulator with an operation duration of 5 ms for power supply to the gyrotrons.

All units of a separate section of the modulator were modeled and tested in an operation mode. The design documentation was drawn for the section and the modulator as a whole. The mounting, testing, and adjustment of the separate section version (see Fig. 4.1.26) are underway.

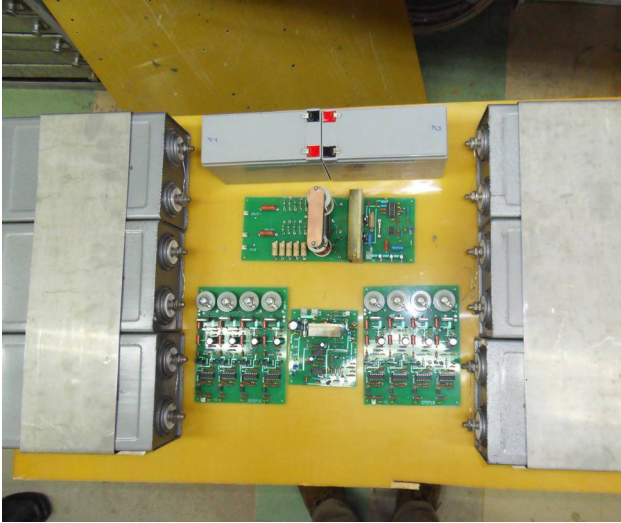


Fig. 4.1.26. Photo of a section of the permanent high-voltage modulator in the process of adjustment.

By the end of 2011, the functionality of separate components of the microwave heating of plasma was verified on the GDT facility. The cryogenic magnets were first to be tested. At a current of 60 A, we attained the magnetic induction value $B \approx 2.1$ T in the area of the gyrotron cavity, which agrees well with the rating values. It is worth noting that the cryogenic magnets were produced over 20 years ago and not exploited since the time of initial tests. Then the vacuum conditions inside the gyrotron were checked, as well as the operability of the ion pump, intended to maintain the working vacuum. The operating current of the ion pump was shown to be 100 microamperes or less, which indicates that vacuum conditions inside the gyrotron comply with the specification. At the present time, the switching-on of the gyrotrons and their testing with the pilot version of the high-voltage modulator are underway.

4.2 GOL-3 FACILITY

4.2.1 General description and operation regimes of GOL-3

GOL-3 is the unique electro-physical facility intended for studies of physics of fast collective plasma heating by a high-current relativistic electron beam of microsecond duration and for studies of physics of multiple-mirror confinement of high-temperature plasma in corrugated magnetic field. The main feature of plasma behavior in the facility is the key role of collective and non-linear processes. Scientific program of 2011 was targeted to several specific tasks of physics and technology of multiple-mirror confinement systems for a high-temperature plasma. Development of experimental base was continued in 2011 in parallel with experiments under scientific programs. New advances in a technology of generation of long-pulse electron beams with the plasma emitter were achieved. The diagnostic complex of GOL-3 was improved with several new diagnostics that will be described later in the text.

The 12-meter-long solenoid consists of 103 coils with an independent feed. In the regular multimirror configuration the magnetic field has 52 corrugation periods (cells of multimirror system) with 22 cm length, the field in maxima is 4.8 T, and in minima is 3.2 T. The mirror ratio of the corrugated field is 1.5. This means that the operating mode of GOL-3 corresponds to a "moderate corrugation regime". The solenoid terminates in single magnetic mirrors with the field of 8-9 T. The exit unit consists of the plasma creation system and exit expander tank with the end beam collector. Magnetic field strength decreases to 0.05 T at the collector surface reducing thereby specific heat flux at the surface. Metals therefore can be used as the material for the collector plate.

Typical experimental scenario is the following. Several gas-puff valves create required axial deuterium density distribution in a metal vacuum chamber $\varnothing 10$ cm, placed inside the solenoid. Then a special linear discharge creates a start plasma with length-averaged density of $(1\div 30) \cdot 10^{20} \text{ m}^{-3}$ and temperature ~ 2 eV. After that the relativistic electron beam is injected into this plasma with the following parameters in a standard regime: electron energy is ~ 0.8 MeV, current is ~ 25 kA, duration is ~ 12 μs , energy content is ~ 120 kJ, the beam diameter is ~ 4.1 cm (this value corresponds to 3.2 T magnetic field as in minima of corrugated magnetic field). Such a beam is formed in a slit relativistic diode of the beam generator U-2 and then it is transformed to a circular shape and compressed by a magnetic system of U-2. As a result of collective heating the plasma gets ion temperature $2\div 3$ keV (in the hottest part of the plasma column). Use of the multiple-mirror confinement scheme (the corrugated magnetic field) allows to confine the hot plasma much longer, than in a simple solenoidal trap.

4.2.2 Measurements of fast localized fluctuations in plasma density

Plasma fluctuations at scales much less than characteristic plasma size play a crucial role in anomalous losses of particle and energy of hot plasma across the confining magnetic field. Understanding of mechanisms of such anomalous transport is a key problem for a fusion reactor based on toroidal magnetic systems. On the contrary, in magnetic mirror confinement systems plasma fluctuations can play positive role both by reducing axial losses and by increasing plasma heating efficiency. Previous experiments on the GOL-3 device showed that plasma axial thermal conductivity decreases more than three orders of magnitude due to plasma turbulence driven during plasma heating process. Besides, it was stated that ion heating by hot plasma electrons occurred much faster than binary collision times. The likeliest mechanism of such fast ion heating involves plasma density fluctuations as a key element, as it follows from measurements. All this makes diagnostics of plasma density fluctuations in multiple-mirror trap GOL-3 extremely important.

Large scale plasma density fluctuations driven by relativistic electron beam during plasma heating were observed previously at GOL-3 with the use of multichannel Thomson scattering. These measurements were done on shot by-shot basis and required large number of plasma discharges. Upgrade of the Thomson scattering system in 2010 season made two measurements of plasma density and temperature during a single discharge possible. It was achieved with the use of two independent master oscillators that shared common path through the output gain sections of the laser system. As the result the laser system produces two output pulses with the following parameters: $\lambda = 1054$ nm, energy per pulse 10-20 J, pulse duration 20-40 ns, time delay between pulses 60-150 ns.

In the presented experiments Thomson scattering system has been modified for observation of plasma density profile. Measurements were performed at 8 spatial locations within 9 cm section across the plasma chamber and cover the entire plasma diameter. The measurements were aimed at observation of fast local dynamics of plasma density during injection of the electron beam into plasma. As the result fast (60-90 ns) plasma density fluctuations were detected. Typical plasma density profile with fast variation of density is shown in Fig. 4.2.1 (a) in contrast to a profile without such fast variations (b).

Analysis of obtained data shows with high confidence that random fast localized density fluctuations are observed. The future experiments will be aimed at specifying the mechanisms for observed localized density fluctuations. Such a dynamics of plasma density profiles might be associated with direct consequence of strong Langmuir turbulence as a wave collapse or can be produced by inhomogeneous plasma heating due to filamentation of the electron beam. The local dynamics of plasma density might also evidence of occurrence of the

above-mentioned fast ion heating mechanism driven by relaxation of flows of plasmas heated in local mirror traps of the multi mirror GOL-3 device.

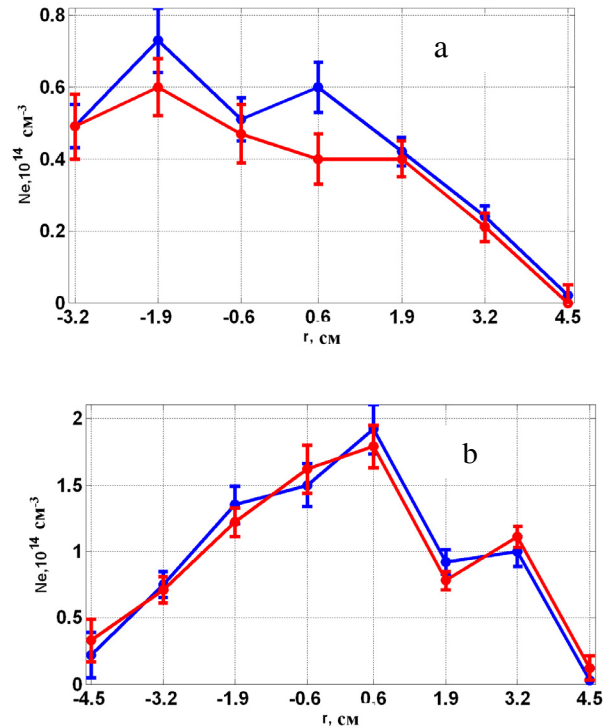


Fig. 4.2.1. Plasma density profiles for shots: a) with fast variations at -1.9 and 0.6 cm; b) without density variation recorded. The time interval between two profiles is less than 100 ns.

4.2.3 Studies of a sub-THz plasma radiation

The energy transfer from an electron beam to the plasma during its heating is based on the pumping of strong Langmuir turbulence by the beam that leads to the absorption of energy of plasma oscillations by electrons and to the suppression of electron heat transport along the magnetic field. At the same time high energy density of plasma oscillations also leads to generation of electromagnetic radiation from plasma in a wide frequency range, extending from the vicinity of the plasma frequency to twice this value. The possibility of such generation of radiation was predicted in the middle of last century by theory. It also was observed in astrophysics. Hence by studying a structure and dynamics of the emission spectrum of microwave radiation from the plasma, it is possible to obtain information about the beam-plasma interaction, as well as the processes that accompany the relaxation of the electron beam in plasma.

Radiometric diagnostics with the quasi-optical elements on the basis of the anisotropic selective surfaces were developed in 2009-2010 for registration of microwave radiation from the plasma in the vicinity of the

double plasma frequency. Using these diagnostics we found that the detectable electromagnetic radiation is present only at the stage of intense plasma heating which suggests that generation of the detected electromagnetic radiation is not directly caused by cyclotron motion of electrons, and being the plasma process.

Experiments were continued in 2011 to study emission of electromagnetic radiation from the plasma during injection of relativistic electron beam. The radiation was detected by using a spectrally-selective 4-channel quasioptical system, as well as broadband detectors and a calorimeter. The 4-channel spectroscopic system was equipped with new quasioptical elements that use isotropic selective surfaces. The filters had out-of-band transmission at -60 dB level. Spatial regularities of the radiation and the radiation spectrum were studied (see Fig. 4.2.2-4). In the experiments with the plasma density of $(1.5 \div 3) \cdot 10^{20} \text{ m}^{-3}$ the linear plasma frequency lies in the range of 120–170 GHz. Dependence on the longitudinal coordinate was measured with single-channel mobile broadband detectors tuned to the first and the second harmonic of the plasma frequency. As can be seen the axial distribution of the radiation near ω_p and $2\omega_p$ has a maximum near the point of beam injection into plasma. The maximum output power measured in the experiments at the plasma frequency reaches $\sim 5 \text{ kW/cm}^3$ and at double plasma frequency it is $\sim 1 \text{ kW/cm}^3$ (at coordinate $z = 83 \text{ cm}$). Assuming that generation of the radiation near double plasma frequency is due to the merge of two plasmons, such power may occur in plasma with electron temperature $\sim 1 \text{ keV}$ if energy density of plasma waves reaches $W/nT \sim 0.1$ that is consistent with previous studies of plasma heating with relativistic electron beams.

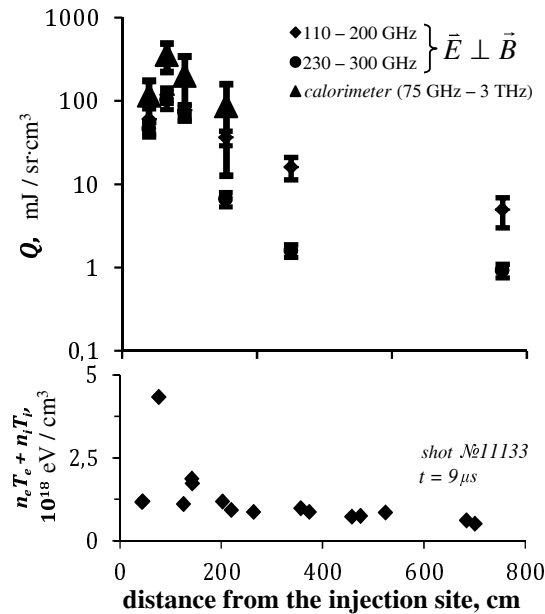


Fig. 4.2.2. Distribution of the radiated sub-THz energy per pulse (top) and the plasma pressure (bottom) along the device during the plasma heating phase at the

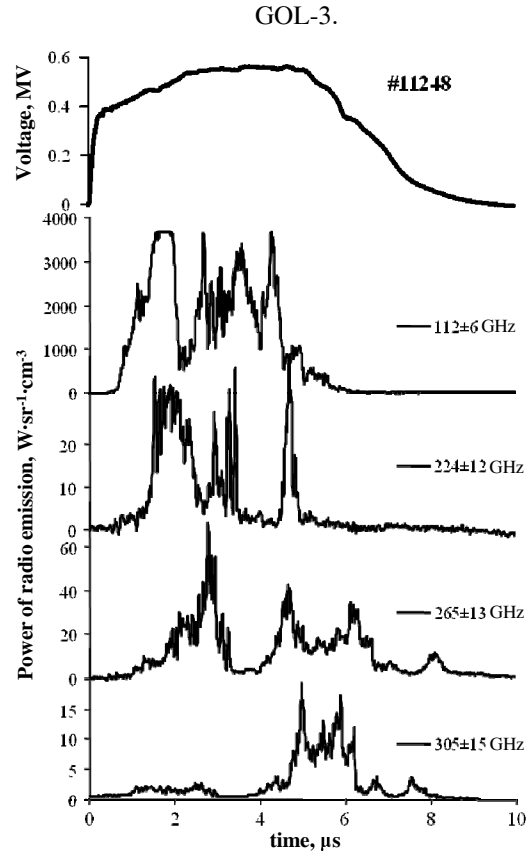


Fig. 4.2.3. Dynamics of the plasma radiation power in different spectral ranges.

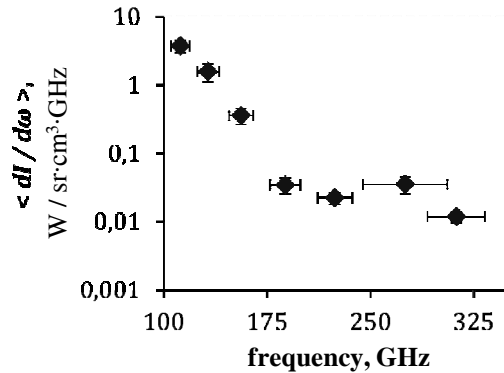


Fig. 4.2.4. Spectrum of sub-THz emission from GOL-3 at $n_e = (1.5 \div 3) \cdot 10^{20} \text{ m}^{-3}$ (averaged over the pulse duration).

4.2.4 Investigation of azimuthal rotation of plasma

Magnetic activity of the plasma was studied with the help of multichannel set of compact detectors measuring azimuthal component of magnetic field in the central part of vacuum chamber. Due to the freezing-in of the magnetic field into the plasma these results correspond to

oscillations of the effective magnetic boundary of the plasma.

Complex structure of the azimuthal distribution of the magnetic surface was observed. Modes with $m = 1, 2$ and 4 were found to be the most significant. Mode $m = 1$ has the largest amplitude of about 2 mm. This disturbance corresponds to the off-axis shift of the whole plasma column. Significant level of the first magnetic mode in common with the symmetric optical radiation of the plasma at the stage of its heating allows assuming the conversion of a co-axial current structure into a helical one. This process corresponds to the tearing instability predicted previously in numerical simulations. Evolution of spatial structure to the higher modes (i.e. current filamentation) with $3\div 4 \mu\text{s}$ timescale was also found (Fig. 4.2.5).

Plasma rotation with the angular velocity of up to $\omega \sim 10^6 \text{ s}^{-1}$ corresponding to the $E \times B$ drift in plasma with potential $\sim 1 \text{ kV}$ was observed (Fig. 4.2.6). At the stage of plasma cooling rotation decelerates to $\omega < 10^5 \div 10^4 \text{ s}^{-1}$. Periphery of the plasma rotates with constant velocity $\omega \sim 10^5 \text{ s}^{-1}$ in most experiments. Therefore during the injection of the relativistic electron beam and immediately after this stage the sheared rotation with the shift of nearby layers of up to $\varphi \sim 4\pi$ occurs.

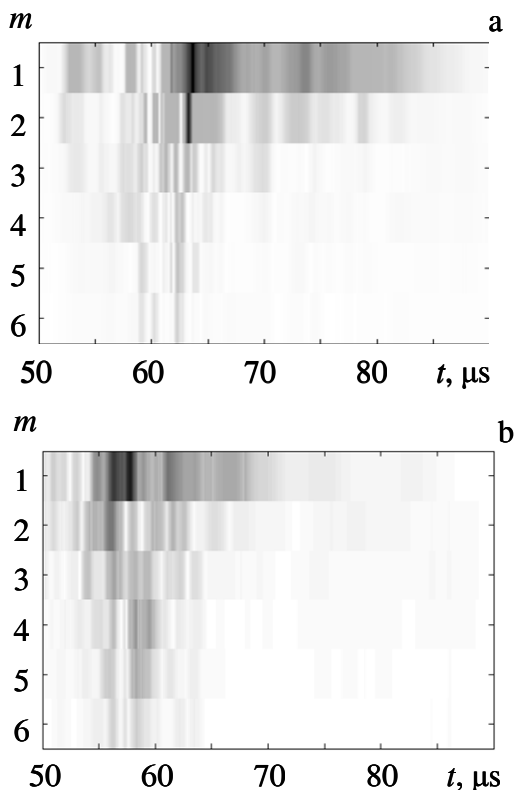


Fig. 4.2.5. Azimuthal modes in shots PL10630 (a) и PL10647 (b) with different plasma density. Black colour corresponds to the maximal amplitude of a selected mode. Injection of the relativistic electron beam begins in $t = 50 \mu\text{s}$. Shift to higher spatial modes during the injection ($50\text{--}60 \mu\text{s}$) is observed.

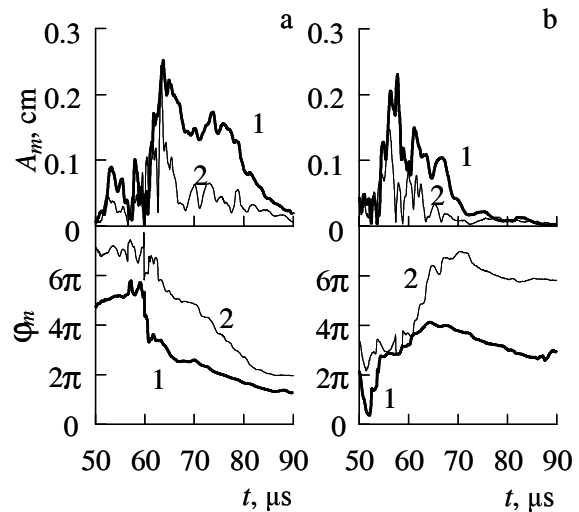


Fig. 4.2.6. Amplitude A_m and phase φ_m of azimuthal modes of effective current boundary. Shots PL10630 (a) and PL10647 (b). Labels (1) and (2) mark corresponding mode numbers. Phases of $m = 1$ и $m = 2$ modes are shifted by one turn (2π rad) for better plot perception.

The explanation of these events based on theory of the reconnection of magnetic field lines was supposed sposing analogy with the magnetic dynamo in astrophysics. Theoretical estimation shows that the filamentation of the current layers in GOL-3 for $\omega \sim 10^6 \text{ s}^{-1}$ occurs in $t \sim 3 \mu\text{s}$; agreeing well with experimental results. This effect agrees well with the magnetic events on the stage of plasma cooling observed previously.

4.2.5 The interferometer based on CO₂ laser

Interferometry is a traditional method of measuring the plasma density in plasma physics. Its methods are constantly being improved, taking into account parameters of the experiments conducted, determining of which are on the one hand, the density of the plasma, its dynamics and dimensions, and the other is a spectrum of vibrations of structural elements of a device. Since the inception of the GOL-3, and up to date on the device two-pass scheme of the Michelson interferometer is used.

In order to improve temporal resolution and increased sensitivity of the method existing two interferometers were substantially upgraded. CO₂ lasers ($\lambda = 10.6 \mu\text{m}$) as a radiation source and fast ($\sim 1 \text{ ns}$) HgCdTe detectors developed in ISP SB RAS were applied in them. The scheme of the interferometer is shown in Fig.4.2.7. The key elements of the CO₂ interferometer are calibration and remote control of the initial phase, which achieved by moving the mirror in the reference arm. As an example, Fig.4.2.8. shows raw interferograms obtained by these interferometers that were preset with different initial phases.

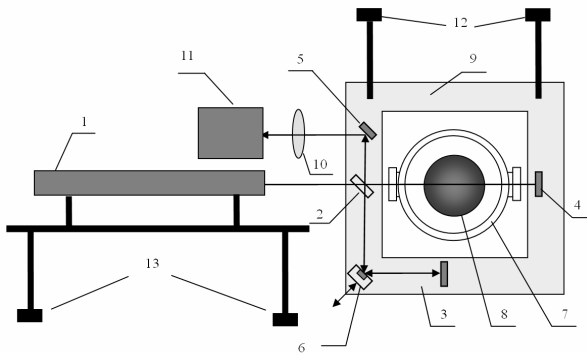


Fig. 4.2.7. Schematic diagram of the interferometer. Designations are the following, 1 is CO₂ laser, 2 is BaF₂ beam splitter, 3 ÷ 5 are mirrors, 6 is piezoelectric-positioned mirror, 7 is the plasma chamber with ZnSe windows, 8 is the plasma, 9 is the dielectric frame, 10 is BaF₂ lens, 11 is HgCdTe photodiode, 12 are base suspension rods, 13 are laser supports.

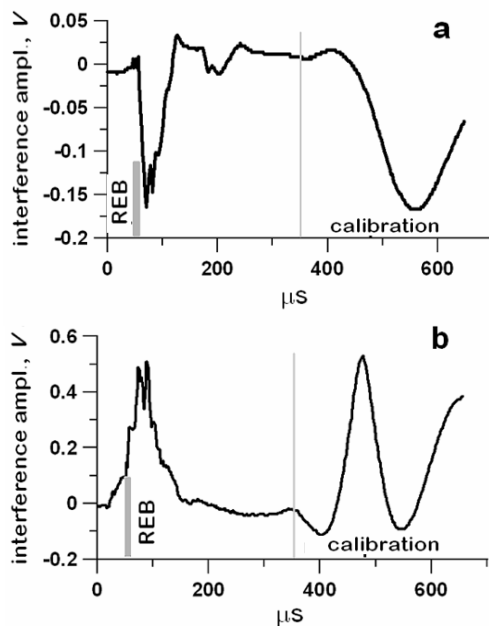


Fig. 4.2.8. Typical interferograms reflecting the dynamics of the plasma density in two cross-sections of GOL-3 corrugated trap: a) $z = 0.8$ m, b) $z = 9$ m.

4.2.6 Neutral Particle Analyzer

The Neutral Particle Analyzer with novel design was developed for investigations of fast ions population in GOL-3 facility (fig.4.2.9). The analyzer is capable to measure energy distribution of charge-exchange neutrals leaving plasma in a wide range of energies – from several hundreds of eV up to tens of keV, that allow to study both thermal component and population of fast ions in

plasma. The analyzer also separates and measures simultaneously atoms of hydrogen and deuterium that open possibilities for special experiments for study of fuel efficiency, longitudinal transport, mass dependence of ion confinement, etc.

Main parts of analyzer are a vacuum chassis, a stripping target with an electrostatic lens, a magnet-separator, a mass-separating capacitor, an ion detection unit, and a built-in calibration source. The magnet-separator represents C-shaped yoke with permanent NdFeB magnets. The magnet dimensions are 130×90×100 mm. Shape of magnet poles is optimized for focusing of the ions in two dimensions (horizontal and vertical) onto the detector array. After passing through the magnet ions travel in the transverse electric field of the capacitor that separates ions by masses. Distance between the capacitor plates is 15 mm, operation voltage is 8 kV. The shape of the plates is designed for constant deflection angle of ions with different energies in the capacitor. Analyzer is equipped by the built-in miniature ion source that allows performing in-situ calibration of sensitivity and instrumental functions of registration channels. Channeltrons with high dynamic range and output current are used for ion detection. The channeltrons may operate both in count and current mode and provide temporal resolution up to 10 μs.

Two analyzers were mounted on the plasma facilities MST (University of Wisconsin in Madison, USA) and C-2 (Tri Alpha Energy, USA). One example of the measurement of fast ions dynamics in the MST facility is shown in fig. 4.2.10. Neutral beam injection system operating at this facility creates population of fast ions with energies up to $E_{inj} = 23.4$ keV. After injection these fast ions are slowing down in the plasma and the high-energy cutoff of the ion distribution function shifts to lower energies. Fast ions with energy less than 10 keV are rapidly lost and don't confine in plasma. Magnetic reconnections that are shown by dashed lines in fig. 4.2.10 cause strong redistribution of plasma with partial or full loss of fast ions. Results of these measurements are in agreement with predictions of Monte-Carlo simulations of ion dynamics in the plasma.



Fig. 4.2.9. Neutral particle analyzer

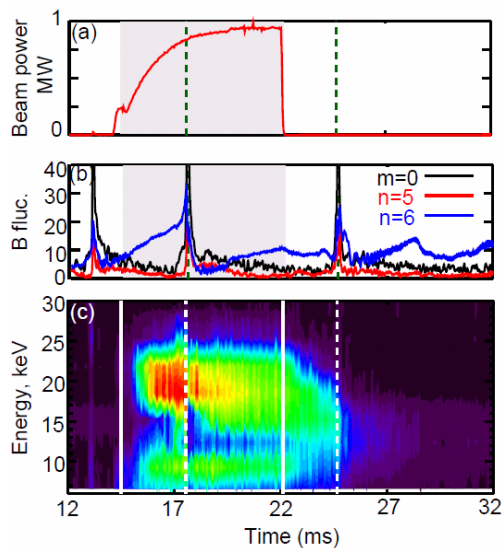


Fig. 4.2.10. Dynamics of fast ion population in the MST facility; (a) Neutral beam power density; (b) magnetic fluctuations with $m = 0$, $m = 1$, $n = 5,6$ tearing; (c) raw signals of 10 hydrogen channels of the analyzer. Dashed lines indicate two moments of strong magnetic reconnections.

4.2.7 Compact neutron detector with digital n - γ discrimination

In the experimental study of parameters of hot plasma ion component there is a need of efficient neutron detection with reliable discrimination of gamma radiation. Neutron detectors based on organic scintillators are usually used for this purpose. Shape of the scintillation pulse depends on type of incident fast particles. The fast neutron spectrometer based on single stilbene scintillator was developed for recording of long-pulse emission of neutrons from the plasma with sub-thermonuclear parameters using the data acquisition board ADC12500 with the sampling frequency of 500 MHz and the accuracy of 12 bits, with the ability to process scintillation pulse shapes in real time by a built-in high-speed digital processing unit.

The main task of the diagnostic is continuous recording of intense flux of fast (1-15 MeV) neutrons with the ability of gamma-ray discrimination by a pulse shape and correct processing of superimposed events. The difference of the developed method from traditional solutions with analog n - γ discrimination circuits and digital post-processing methods is the use of computing power of built-in real time FPGA-based streaming data processing unit. Analysis of shape of each scintillation pulse gives the value of its "fast" and "slow" components, as well as the arrival time. Stream processing of scintillation pulses increases by two orders the continuous recording time for a constant amount of on-board memory, and reduces the bandwidth requirements of communication with a control computer.

Due to the possibility to modify firmware of the processing unit, the detector can be flexibly and promptly adjusted for a wide range of tasks. In particular, similar detector was used to determine the shape of a neutron pulse of a borehole neutron generator in stroboscopic mode. Electronics for the detector is designed and manufactured in BINP.

Results of calibration of the neutron detector using radionuclide ^{252}Cf source, as well as the source of monoenergetic neutrons from deuterium accelerator tube shown that good discrimination of gamma-rays starting from neutron energy threshold of 0.3 MeV and the energy resolution of less than 10% for neutron energies 2.45 MeV are achieved – see Fig. 4.2.11.

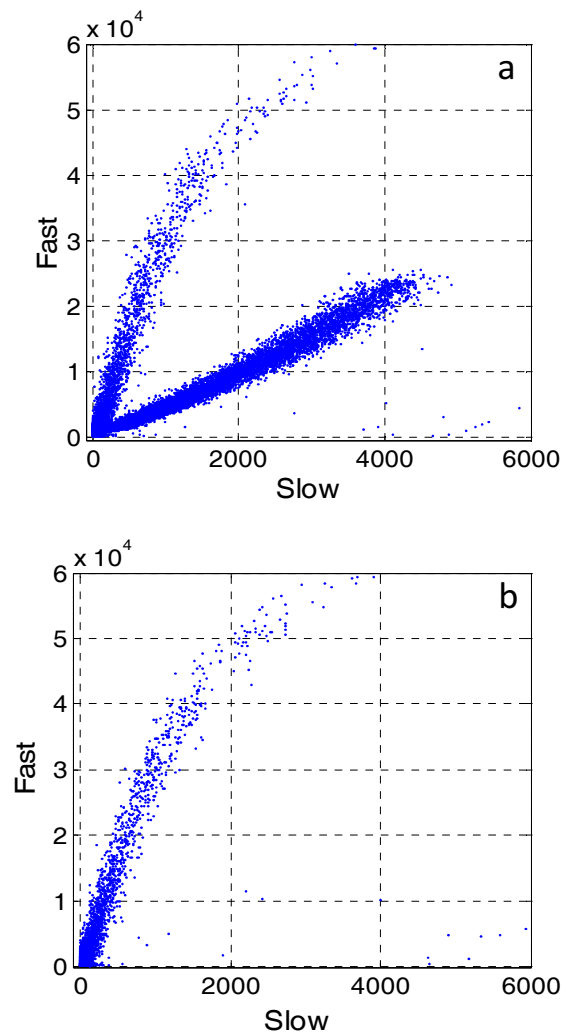


Fig. 4.2.11. Achieved degree of separation of neutrons and gammas for a pulsed generator of DD neutrons (2.45 MeV). Each dot with coordinates "fast" and "slow" corresponds to individual particle. (a) Data was measured during operation of the generator with two branches of which the lower corresponds to neutrons, and the upper corresponds to gamma rays. (b) Data was measured between pulses with only gamma-rays from the induced radioactivity left.

4.2.8 Development of methods for modeling diode systems with plasma electrodes

Development of methods for the numerical simulation of systems with open-emitting plasma boundaries was continued in 2011. Impact of a high-power plasma flow from the trap to the beam source and to its electron-optical characteristics should be considered in the design of sources of high-power electron beams intended for plasma heating in open magnetic traps. Algorithms for computation of shape of plasma boundaries in the low-temperature approximation of uniform emission from the surface were developed earlier for modeling of diodes with plasma electrodes. To account effects of thermal and directional movement of the plasma flow to characteristics of a diode, the problem of potential distribution in the gap between cathode and anode plasmas was solved and the results were applied in the computer code POISSON-2 for simulation of beam formation in systems with plasma emitters. The model also takes into account restriction of the emission fluxes orificing by the cathode and the anode apertures, leading to heterogeneity of emission of the plasma surface. Formation of an electron beamlet from a single cathode aperture of a plasma-cathode-based multiaperture source was simulated in the axisymmetric approximation. Conditions of the electron beam formation at the source with the design parameters (100 kV, 1 kA, 100 microseconds or more) were determined with features that allow 100-fold compression of the beam by guiding magnetic field, see Fig. 4.2.12. In the numerical simulation of the diode exposed by the incident plasma flow a lossless motion of particles accelerated in the diode gap through the cathode and anode apertures without leaking to metal electrodes of the diode was achieved. As was shown by earlier experiments, losses of current to diode surfaces are some of the reasons that limit duration of the beam.

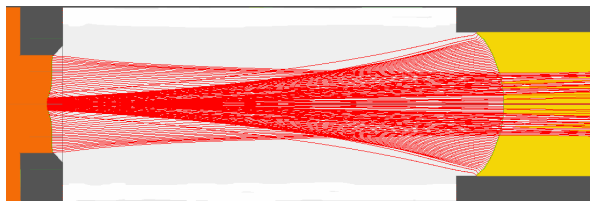


Fig. 4.2.12. Simulation of an electron beamlet in a single diode aperture. The left side is the cathode with a cathode plasma, the right one is the anode with a stream of plasma. Diameter of the cathode aperture is of 3 mm, anode one is 4.4 mm, the diode gap is 12 mm, the voltage is 100 kV, the electron current density averaged over the cathode aperture is 63 A/cm^2 , the ion current density at the anode is $\sim 1 \text{ A/cm}^2$, the diode current is 1.1 kA. The maximum pitch angle of electrons is $\sim 0.07 \text{ rad}$. The magnetic field is 0.05 T.

The next expected step is further development of the numerical model taking into account impact ionization processes in the working and residual gas in the diode gap. Influence of the distribution function of electrons and ions in the cathode and anode plasmas on the optics of the diode will be studied also.

4.2.9 Transportation of an intense submillisecond electron beam in a magnetic field of mirror configuration

The existing scheme of plasma heating in an open trap with a high-power long-pulse electron beam provides location of the beam injector in the output expander with a magnetic field $B_{\text{out}} \sim 0.1 \text{ T}$ or less. Formed in this field, the beam is transported further into a plasma chamber of the trap with the field $B_{\text{in}} \approx 5 \text{ T}$. Thus, when injected into the plasma, the beam must pass through a magnetic mirror with the mirror ratio $R = B_{\text{in}} / B_{\text{out}}$, which imposes corresponding restrictions on the starting pitch-angles of the beam. In 2011, as a part of the program on plasma heating with a submillisecond electron beam in GOL-3 a series of experiments was carried out to study the possibility of transportation of intense e-beam obtained in the source with a plasma emitter and multiple-aperture diode electron optical system (EOS) through the magnetic mirror with $R \approx 50$.

The work was done with a test bench beam source operated at accelerating voltage of 32 kV. The source was basically the same in design as the source installed in GOL-3. Beam pulse duration (limited by capabilities of high-voltage modulator) was about 0.25 ms. Layout of the bench experiments is shown in Fig.4.2.13.

According to the scenario of the experiment, quasi-uniform magnetic field of 0.02 - 0.04 T was formed at EOS place. At the same time the field of CSF was varied from shot to shot. Accordingly, the mirror ratio R was varied also from 5 to 70. The beam current passing through the magnetic mirror was registered with the Faraday cup. A fraction of the beam electrons with large pitch angles reflected back from the mirror was registered as an additional current deposition on the anode electrode. The sum of the current to Faraday cup and current deposition to the anode with a good accuracy corresponds to the beam emission current. With increasing mirror ratio a rapid growth of the current to the anode occurs. This gradually leads to a shortening of the beam pulse, and then to the diode shorting. A typical diagram of currents versus R with the magnetic field value at EOS of 0.025 T is shown in Fig. 4.2.15.

The experiments demonstrated that the electron beam, formed in the multiaperture diode with arc plasma cathode at accelerating voltage $U = 32 \text{ kV}$, with the emission current $I_e \approx 60 \text{ A}$ and pulse duration of 0.25 ms is transported with virtually no loss in the increasing magnetic field through the magnetic mirror with ratio $R > 50$.

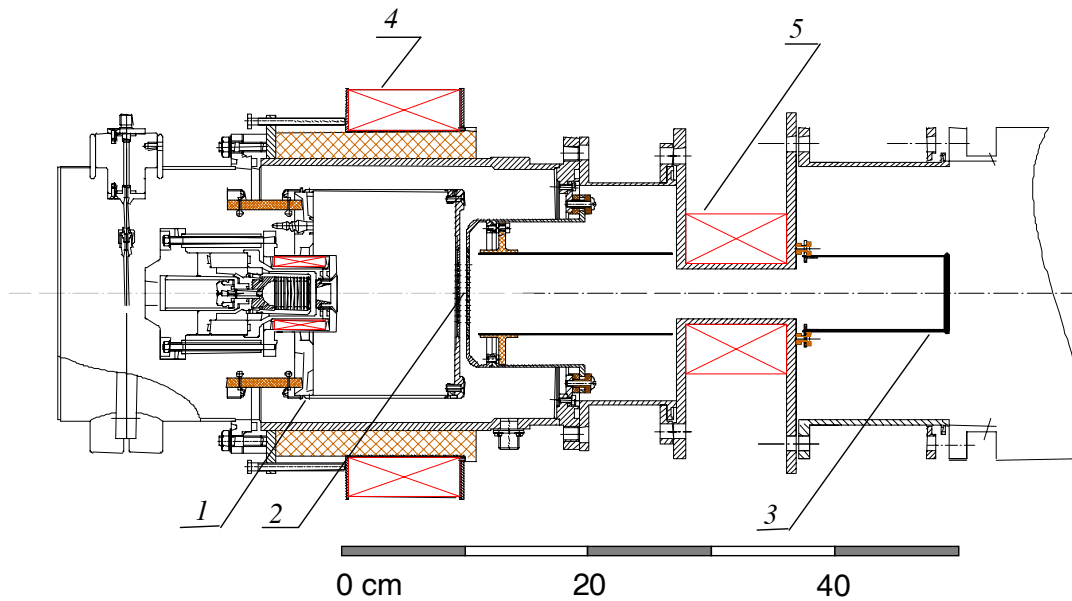


Fig. 4.2.13. Layout of the experiment: 1 – plasma emitter; 2 – multi-aperture EOS; 3 – Faraday cup; 4,5 – magnetic field coils.



Fig. 4.2.14. Multiaperture diode-type EOS, view from the anode side (beam transport tube is removed).

4.2.10 Summary

Experiments aimed at the development of a physical knowledge base for a mutimirror-trap-based fusion reactor are continued at the multimirror trap GOL-3. Physical data quality is improved both due to improvements of diagnostic equipment and due to dedicated experimental runs. New plasma heating technologies are developing in order to improve plasma parameters. Development of analytical and numerical models of plasma in GOL-3 is in progress. Applied research contracted by outer organizations was carried out.

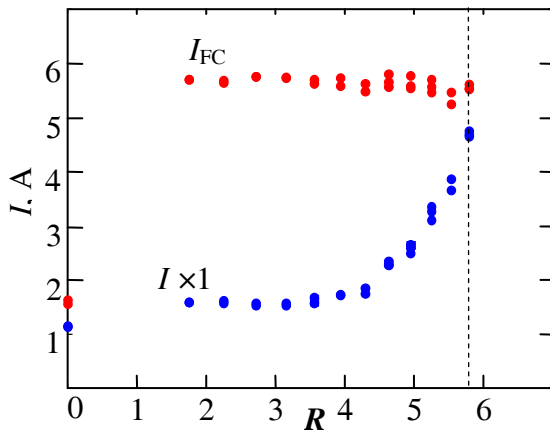


Fig. 4.2.15. Current to Faraday cup I_{FC} and current deposited on the anode I_a (multiplied by 10) versus mirror ratio R .

4.3 PLASMA THEORY

4.3.1 Nonneutral plasmas

The study of different transport regimes and descriptions of possible wave modes are important problems of the nonneutral plasma theory.

The trapped particle diocotron mode (TPDM) theory is presented in [Yu.A. Tsidulko, T.J. Hilsabeck, and T.M. O'Neil, *Physics of Plasmas*, 18, 084505 (2011)], where in contrast with the previous theory [T.J. Hilsabeck and T.M. O'Neil, *Phys. Plasmas*, 10, 3492 (2003)], the collisional and collisionless particle exchanges between trapped and passing particle populations are consistently taken into account. The corrected equation for TPDM perturbations is derived. In particular, it eliminates the "fast modes" predicted by the previous theory.

In some regimes of the neoclassic transport of nonneutral and quasineutral plasmas, the particles populating superbanana orbits yield the main contribution to the transport. The superbanana orbits contain parts where the particle dynamics is similar to the trapped particle dynamics and the parts where it is similar to the passing one. In the typical for nonneutral plasmas case, such orbits arise because of external field perturbations breaking the axial symmetry of the separatrix separating the passing and trapped particles. The theory describing the enhanced nonneutral plasma transport caused by the separatrix symmetry violation is presented in the papers [D.H.E. Dubin, C.F. Driscoll, and Yu.A. Tsidulko, *Phys.Rev.Lett.*, 105, 185003 (2010), D.H.E. Dubin, Yu.A. Tsidulko, *Physics of Plasmas*, 18, 062114 (2011)]. In particular, the plateau regime is studied where the diffusion and mobility do not depend on the collision rate. This regime takes place when the collisional energy change is negligible during the azimuthal drift time, while the collision rate is sufficient to distribution function relaxation in the parts of the orbits where the particle dynamics is close to the passing one. The effect of separatrix symmetry breaking on the damping rate of the trapped particle diocotron modes is also considered. The experimental verification of the theory is presented in [A.A. Kabantsev, D.H.E. Dubin, C.F. Driscoll, and Yu.A. Tsidulko, *Phys.Rev.Lett.*, 105, 205001 (2010)]. The results of the theory can be important for the problems of quasineutral plasma confinement, in particular, in stellarators.

4.3.2 Plasma surface interaction theory

A theoretical investigations of dust particles size distribution produced by brittle destruction under assumption of self-similarity are finished in 2011 year. It is shown that the value of distribution exponent points to type of destruction: surface or volumetric.

A theoretical investigations of elastic stress in non-uniformly heated solid. The elastic stress results in formation of large-scale cracks and production of dust particles.

4.3.3 Theory of plasma wakefield acceleration

Proton driven plasma wakefield acceleration has recently been proposed as a means of generating high energy electron beams.

In search of testing possibilities for this scheme, different options for a demonstration experiment with the CERN PS beam are considered. A possible magnetic compression of the PS bunches and resulting electric fields in the plasma are analyzed. Self-modulation of the proton bunch for different plasma densities and lengths is studied. It is found that the latter option offers interesting possibilities for a first experiment.

A high energy particle beam propagating in a uniform plasma is subject to the transverse two-stream instability that first transforms the beam into the train of microbunches and then quickly destroys that train by transverse wakefields. By the proper longitudinal inhomogeneity of the plasma density, it is possible to stop the instability action at the stage of microbunches and form the bunch train that can resonantly excite plasma wakefields over a long distance.

It is demonstrated that the performance of the self-modulated proton driver plasma wakefield accelerator is strongly affected by the reduced phase velocity of the plasma wave. Using analytical theory and particle-in-cell simulations, we show that the reduction is largest during the linear stage of self-modulation. As the instability nonlinearly saturates, the phase velocity approaches that of the driver. The deleterious effects of the wake's dynamics on the maximum energy gain of accelerated electrons can be avoided using side-injections of electrons, or by controlling the wake's phase velocity by smooth plasma density gradients.

The plasma wakefield amplitudes which could be achieved via the modulation of a long proton bunch are investigated. We find that in the limit of long bunches compared to the plasma wavelength, the strength of the accelerating fields is directly proportional to the number of particles in the drive bunch and inversely proportional to the square of the transverse bunch size. The scaling laws were tested and verified in detailed simulations using parameters of existing proton accelerators, and large electric fields were achieved, reaching 1 GV/m for LHC bunches. Energy gains for test electrons beyond 6 TeV were found in this case.

A unified model of electron penetration into linear plasma wakefields is formulated and studied. The optimum angle for side injection of electrons is found. At smaller angles, all electrons are reflected radially. At larger angles, electrons enter the wakefield with superfluous transverse momentum that is unfavorable for trapping. Separation of incident electrons into penetrated and reflected fractions occur in the outer region of the wakefield at some "reflection" radius that depends on the electron energy.

A new PWFA experiment, motivated by the very large energy carried by collider proton bunches, is planned at CERN. First experiments will use a long

(12cm) proton bunch from the SPS ring(450 GeV). The wakefields will result from the modulation of the proton bunch by a transverse twostream instability. Numerical simulations indicate that the peak accelerating gradient exceeds 100 MV/m. The wakefields will be sampled by a co-injected, low energy (~ 10 MeV) electron bunch. The plasma will be 5-10 meters long, with an electron density near 7×10^{14} particles per cubic centimeter. Various methods to seed the instability are investigated, among which: a cut bunch with a fast rising leading edge, a preceding short electron bunch, and a short laser pulse for fast ionization. Diagnostics are developed to measure the bunch current modulation, the electrons energy gain and the wakefields themselves. The long-term goal is to accelerate a trailing electron bunch from a few GeVs to more than 500 GeV in a single plasma cell.

4.4 BEAM INJECTORS OF HYDROGEN ATOMS AND IONS

4.4.1 Beam Injectors of Hydrogen Atoms

For plasma heating in tokamak COMPASS-D (Institute of plasma physics, Prague, Czech Rep.) two 300kW neutral beam injectors with 40keV hydrogen atoms energy and 300ms pulse duration were commissioned, the required parameters were achieved. Ion sources are based on RF discharge plasma emitters.

For accelerating facility RHIC (Brookhaven Nat. Lab., NY, USA) two atomic injectors with particle energy up to 10keV, beam current up to 4.5A, 0.5ms pulse duration and 1Hz operating frequency were launched. Because of the required high current density and small angle divergence, the formation system was assembled from 0.4mm thick molybdenum grids with high adjustment accuracy. Ion sources are based on arc-discharge plasma emitters.

4.4.2 Development of powerful continuous injector of beam of fast hydrogen atoms

Works under the project of powerful continuous injector of beam of fast hydrogen atoms with 500-1000 keV energy on the basis of negative ions are continued. Detailed designing of the basic elements of an injector comes to the end. Prototype of a source of negative ions of hydrogen is manufactured. Experimental test stand for acceleration of hydrogen negative ion beam with current ~5 A to energy 120 keV is prepared.

5

ELECTRON-POSITRON
COLLIDERS

5.1 WORK OF VEPP-2000 WITH ROUND BEAMS

Let us remind shortly the scheme and working principle of VEPP-2000 (Fig. 5.1). The complex consists of an injection part (ILU-B-3M), booster BEP (maximal energy of operation is 825 MeV now) and the VEPP-2000 ring (detectors SND and CMD-2 are installed in two interaction points, beams are focused with superconducting solenoids). The main ring works in round beam mode that supposes observance of the following conditions:

1. angular momentum $M_y = x'z - xz'$ conservation
2. small and equal β -functions at interaction point

$$\beta_x^* = \beta_z^*$$
3. equal emittances of two betatron modes $\varepsilon_x = \varepsilon_z$
4. equal betatron tunes $\nu_x = \nu_z$
5. small fractional parts of betatron tunes above an integer resonance $\{\nu\} = 0.1$

Because the VEPP-2000 energy changes in a wide range during long working time, the need of closed orbit correction as well as tuning optics of the storage ring arises inevitably. It is especially true for VEPP-2000 — the ring's magnets work at strong saturation. The main task for the VEPP-2000 closed orbit correction is its minimal deviation from magnetic axes of chosen elements. After correction of closed orbit one can

remember beam position in all BPM and use these data for further orbit revisions. We use 16 CCD cameras (they detect synchrotron radiation of electrons and positrons from dipole magnets) as BPM in VEPP-2000 ring, and also 4 pickups. CCD cameras are not fixed tightly, so their position is changed from time to time. Hence to correct the orbit by using data from CCD we need to make regular calibrations.

The procedure of tuning the ring consists of several stages. The first one is correcting the closed orbit (CO): we obtain CO response matrices in pickups to the variation of quads' gradients, by using SVD analysis we compute orbit deviation in lenses, then we know currents in correctors to adjust CO. This procedure requires 2–3 iterations, each takes about 10 minutes. Then we minimize currents in correctors. As a result it is possible to achieve the CO accuracy of about 0.5 mm.

The second stage of tuning is adjustment of optical functions. One of the main problems during commission and regular work of an accelerator is the detection and correction of errors in linear magnetic structure of a machine. The procedure begins from accumulation of response matrices in pickups and CCD cameras on the variation of dipole correctors. By help of SVD analysis we compute a working model, and then we correct currents in quads and solenoids. One iteration takes about 60 minutes, the whole procedure requires 3–4 iterations. As a result we get smooth beam sizes, projected β -function at IP, and zero dispersion function outside achromats (Fig. 5.1.2, Fig. 5.1.3).

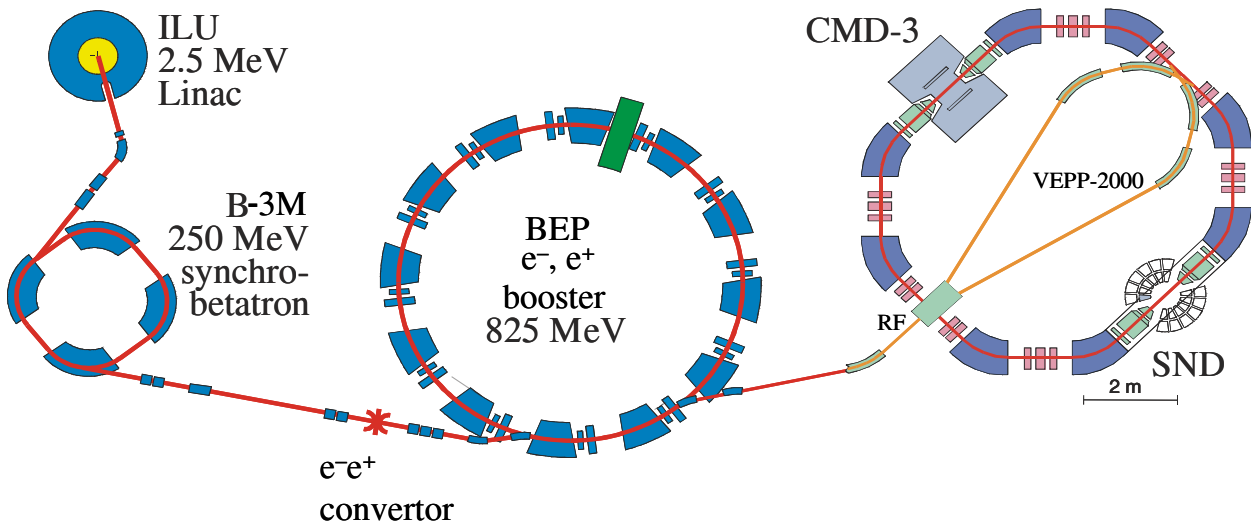


Fig. 5.1.1 Scheme of VEPP-2000 complex.

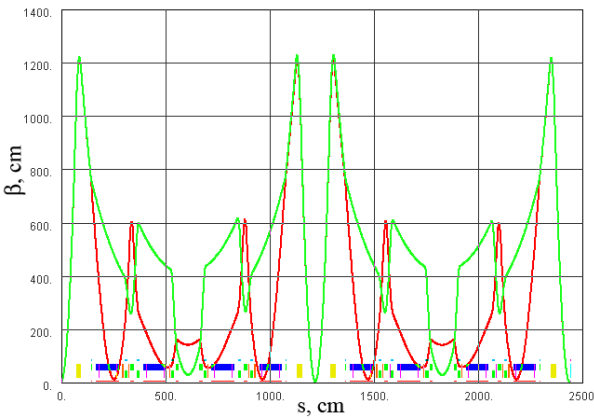
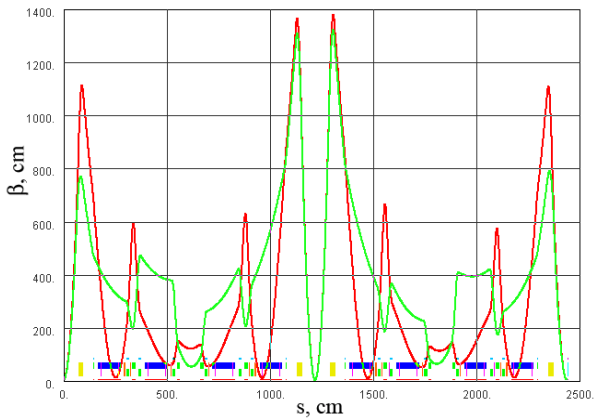


Fig. 5.1.2. The result of correcting optical functions.

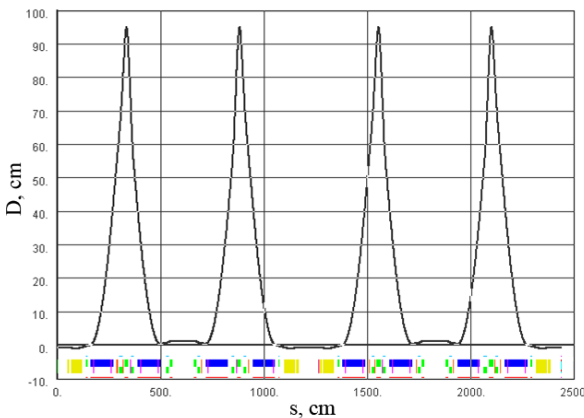


Fig. 5.1.3. Dispersion function is zero outside achromats.

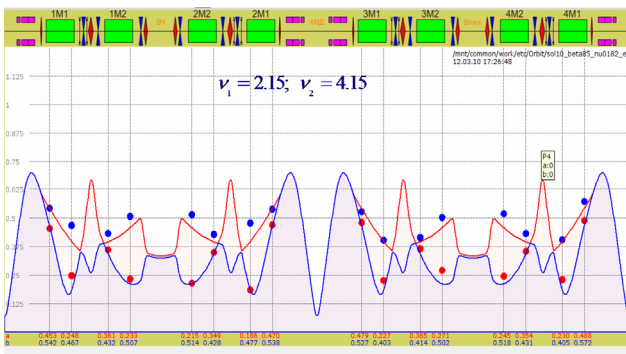


Fig. 5.1.4. Beam sizes in VEPP-2000 ring.

The last stage of the ring tuning is compensation of coupling by using families of skew quads to the level of < 0.003 . Independent control of working optics is made by measurements of beam sizes: at low currents without beam-beam effects the beam sizes should be equal to projected ones. In Fig. 5.1.4 the “natural” sizes at low beam currents (< 1 mA) are shown, one can see good agreement we get after optics correction.

The importance of adjusting the optical functions is demonstrated by the Fig. 5.1.5. As the correction procedure takes so long time we did it sometimes only. As a result optical functions and achromats were distorted, the luminosity was low. One can see essential increase in luminosity after all the corrections have been made.

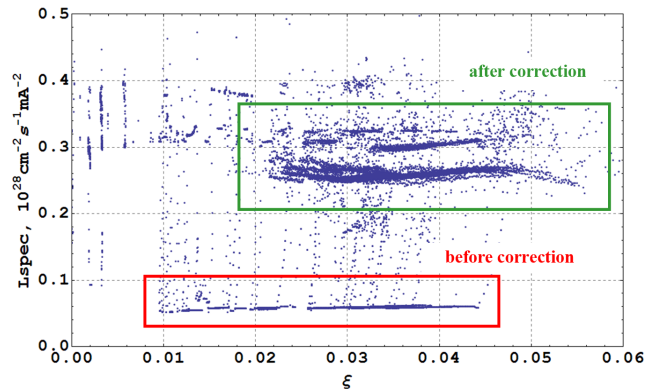


Fig. 5.1.5 Specific luminosity vs. ξ parameter at 900 MeV.

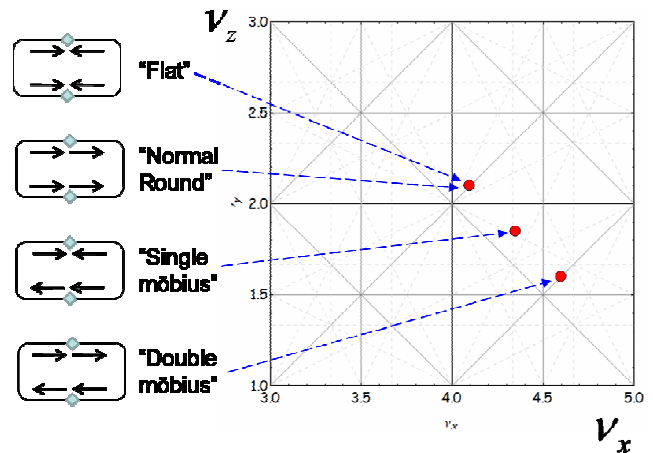


Fig. 5.1.6. Schemes of round beam.

There exists several variants of work with round beam (Fig. 5.1.6); they differ from each other by polarity of solenoids.

In “Möbius” scheme the working point is far from coupling resonance, this can be interesting from the non-linear dynamic point of view (tunes are near to other non-linear resonances). However, this scheme has much smaller dynamic aperture (Fig. 5.1.7, Fig. 5.1.8), therefore we abandoned its practical use, and the ring works near the coupling resonance.

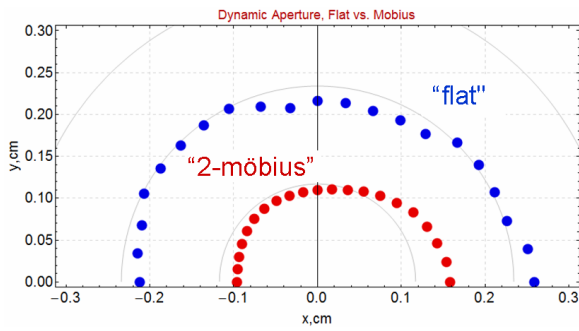


Fig. 5.1.7. Dynamic aperture simulation of flat and double möbius beams in SAD code.

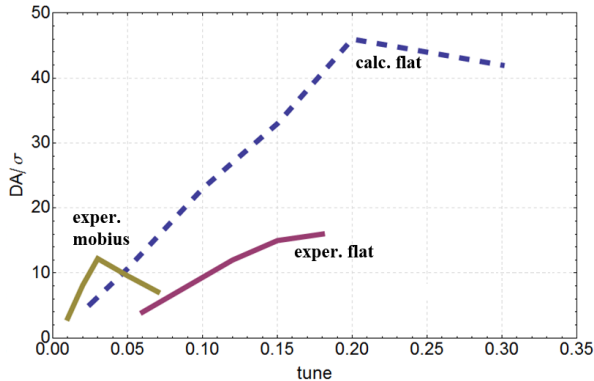


Fig. 5.1.8. Loss of kicked beam measured in pickups.

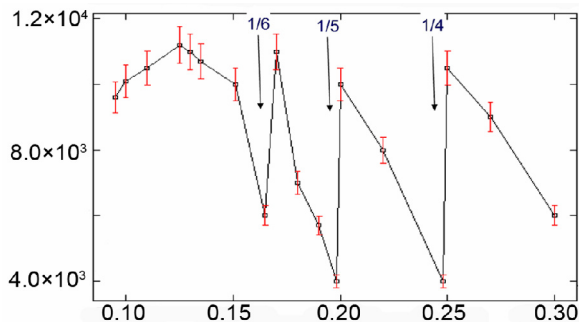


Fig. 5.1.9. Life time of 20 mA positron beam vs. working tune.

During practical work it is important to take into account the influence of high-order resonances on beam dynamics in ring.

Fig. 5.1.9 shows effect of high-order machine resonances, beam life time goes down considerably.

The situation is much more complicated with a presence of colliding beam (Fig. 5.1.10), the resonances of higher order appear.

This means the working point should be kept far from all these resonances with good accuracy.

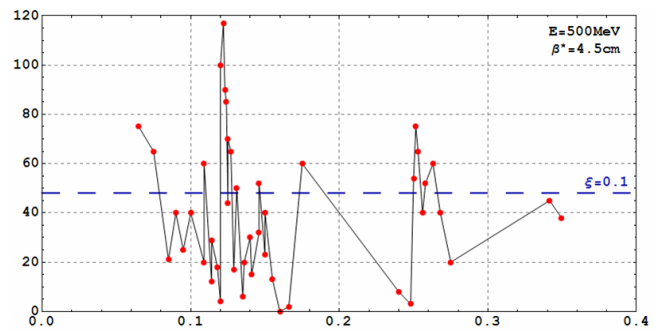


Fig. 5.1.10. Threshold current vs. working point.

Let us shortly describe the history of VEPP-2000 work in 2011. At the beginning of January we have tried “möbius” scheme of round beams. From January to mid-June there was luminosity accumulation in the energy range of 500–1000 MeV. The new season began with the replacement of inflector plates: old plates were made of stainless steel with μ slightly different from 1 that could adversely affect while working at low energy, the plates were replaced with copper ones. Then we carried out modification of vacuum chamber to input laser light from the system of energy calibration based on Compton backscattering. After all these activities with vacuum chamber it was needed to make degassing in so-called “warm” optics. In late November vacuum chamber damage occurred, after that we repaired bellows, and then got vacuum and degassing again. New Year began from input of CMD-3 field and calibrating energy on ϕ -meson with SND detector.

Fig. 5.1.11 shows the luminosity in various seasons, depending on beam energy. One can see, that in the 2009–2010 season the luminosity catastrophically went down. But in present season we solved some technical problems and achieved greater luminosity with the rise of energy. One of the possibilities to increase the luminosity at low energies is varying β -function at IP. We obtained projected energy of 1 GeV, and at 825 MeV there were best shifts with accumulation of 580 nb^{-1} in a day.

Progress at high energy was achieved due to several improvements in BEP and VEPP-2000. We modified sextupoles of BEP and increased BUMP power supply. This allowed us to raise practical energy of boosting the beam up to 825 MeV, but this seems to be a limit of BEP at its present state, hence we planned program of booster ring modernization to work with the beam at 1 GeV. The speedup of VEPP-2000 solenoids was made: there was a lag in solenoids' current during energy rise, therefore working point shifted to some resonances and we lost the beam. To fix this situation the program correction was made to the management of solenoids' currents. This allowed us to boost the beams to high energy.

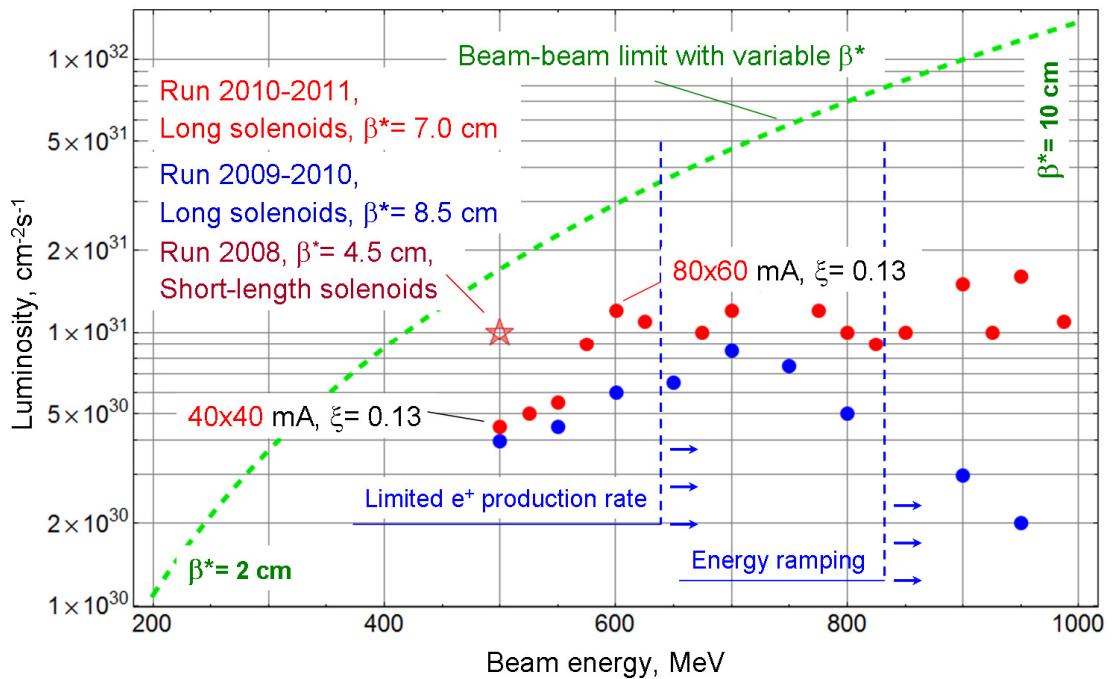
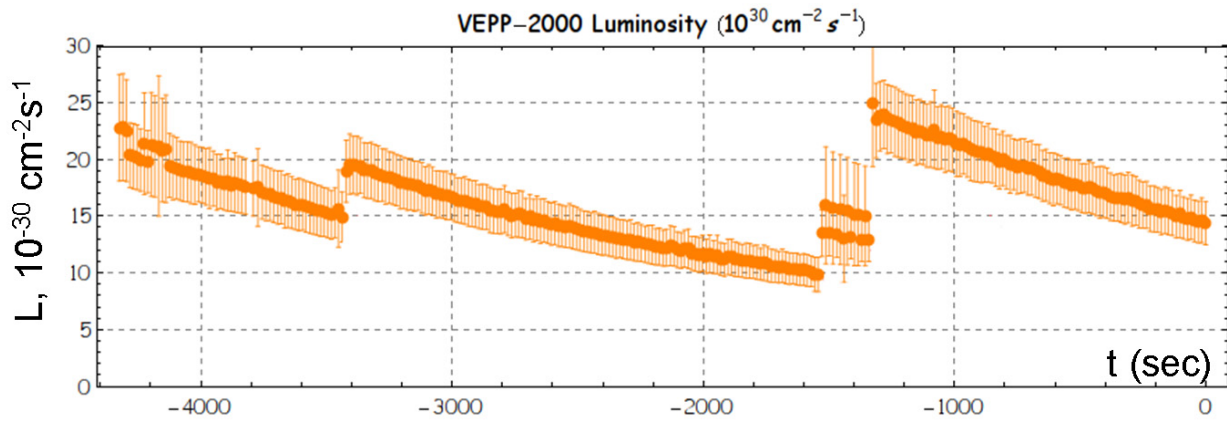


Fig. 5.1.11. Luminosity vs. energy.



E=	837.035	β^* =	8.50539	ν_0 =	0.181983	L_{nom} =	1.44769×10^{31}	ξ_{nom} =	0.0542719
I+=	62.45	I=-	79.3375	N+=	3.17547×10^{10}	N=-	4.03416×10^{10}		
β_{x^+} =	6.61923	β_{z^+} =	7.30896	β_{x^-} =	6.33846	β_{z^-} =	7.55464		
$\epsilon_{x^+}/\epsilon_0$ =	1.19075	$\epsilon_{z^+}/\epsilon_0$ =	1.28085	$\epsilon_{x^-}/\epsilon_0$ =	1.18568	$\epsilon_{z^-}/\epsilon_0$ =	1.29095		
σ_{x^+} =	0.0895587	σ_{z^+} =	0.0976045	σ_{x^-} =	0.0874519	σ_{z^-} =	0.0996221		
L_{spec} =	0.289726	L_{err} =	1.89×10^{30}	ξ =	0.0447				

Fig. 5.1.12. Luminosity measurement based on beam sizes.

Luminosity measurements on VEPP-2000 are carried out since 2007 using data from detectors. However, these measurements are slow enough and have big statistical error, fluctuate and are not always convenient for tuning the accelerator. As alternative method the independent measurement of luminosity based on beam sizes was implemented. To calculate the luminosity one should know sizes and intensities of colliding beams at IP. Even in a machine with one ring the sizes of electron and positron beams are different due to beam-beam effects:

dynamical emittance \mathcal{E} and β^* depend on current of counter beam. And besides linear effects there exists stochastic emittance growth by machine and nonlinear resonances, generated by beam-beam effects. This makes impossible to predict the dependence of luminosity on beam current in the case of strong colliding bunches.

The measurement of beam sizes directly at IP is technically impossible. However, the ring has 16 points to measure beam sizes with CCD cameras by synchrotron radiation from bending magnets: 8 points for each beam.

In the absence of counter beam the ring's optics is well known, transport matrixes between measuring points are known too, so all sizes can be reduced to one azimuth for comparison and analysis. Beam-beam effects change emittances of beams, as well as distort the focusing, but this perturbation is localized at IP, therefore all transport matrixes outside the IP remain the same.

Calculation of beam sizes and luminosity is made with such assumptions:

1. Optics of unperturbed ring is known including transport matrixes, dispersion function and momentum spread in the beam.
2. Two arcs between IPs remain identical each other, mirror symmetry is preserved.
3. Optics is uncoupled, so we can use independent 2x2 transport matrixes.

The described method of measuring the luminosity works fine in VEPP-2000 complex (Fig. 5.1.12). Besides the luminosity the code allows us to get some other beam parameters and track their change in time.

Data obtained with method are in good agreement with data from detectors (Fig. 5.1.13).

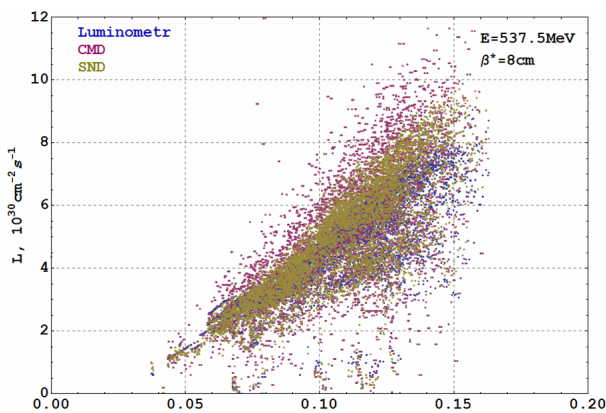


Fig. 5.1.13 Luminosity vs. ξ parameter

Fig. 5.1.14 and Fig. 5.1.15 show success in luminosity accumulation in 2010–2011 season.

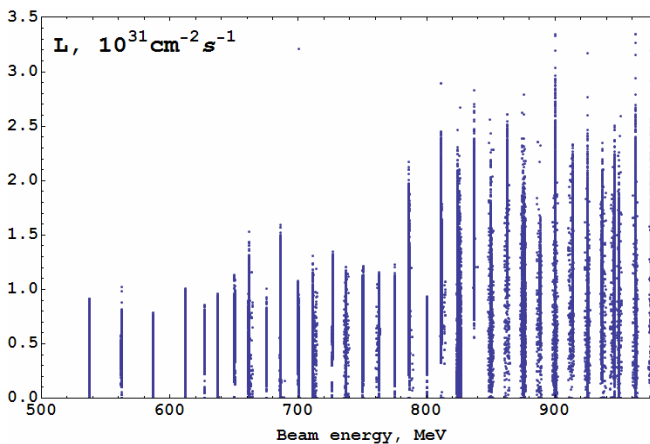


Fig. 5.1.14. Luminosity in 2010–2011.

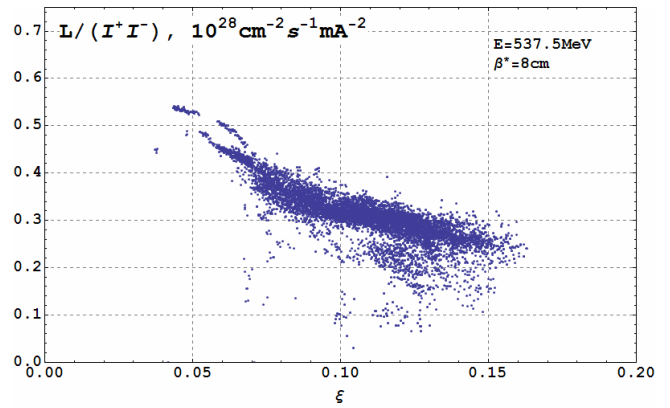


Fig. 5.1.15. Specific luminosity vs. ξ parameter.

Together with the team of SND detector there is a preparation to energy calibration based on Compton backscattering.



Fig. 5.1.16. Modification of vacuum chamber for Compton backscattering method.

5.2 VEPP-4 ACCELERATOR COMPLEX

The VEPP-4 acceleration complex is a unique facility for experiments with colliding electron-positron beams of high energy. The complex includes the "Positron" injector, multifunctional storage ring VEPP-3, and electron-positron collider VEPP-4M with the universal magnetic detector KEDR. The main purpose of VEPP-4M is the experimental study of the properties of elementary particles, resonance parameters, and cross sections for electron-positron annihilation.

5.2.1 Allocation of operation time

In 2011, HEP experiments with the KEDR detector were continued on the electron-positron collider VEPP-4M but with a smaller share of the operation time of the complex, due to the closedown of the detector for scheduled maintenance since March 23. The following experiments were prepared and conducted:

- two scans in the region of $2E = 3.1 \div 3.7$ GeV for the measurement of the parameter R, with the total integral $\int L dt \sim 1.4 \text{ pb}^{-1}$;
- acquisition of $\int L dt \sim 2.1 \text{ pb}^{-1}$ on the ψ (2s)-meson; and
- trial operation at the beam energy $E = 3.5$ GeV. The integral luminosity $\int L dt \sim 0.16 \text{ pb}^{-1}$ was acquired in two weeks.

There were also conducted experiments with SR beams extracted from the VEPP-3 and VEPP-4M storage rings. A series of experiments was carried out on VEPP-4M with a beam of high-energy γ quanta produced via conversion on the internal target ("extracted beam").

Besides that, some experimental time on VEPP-3 was allocated for the DEUTERON experiment with the internal target.

A number of experiments on the modernization of the VEPP-4M collider were performed:

- tuning of the RF system for operation at high energy (over 2 GeV);
- tests of the longitudinal feedback system at the beam energy $E = 3.5$ GeV;
- experiments with traversal feedback at the beam energy $E = 3.5$ GeV for generation of the maximum possible electron and positron currents.

The time of the complex was distributed mainly between the HEP experiments with the KEDR detector (14.8 %) and experiments using synchrotron radiation (20.7% on VEPP-3 + 2.8% on VEPP-4M), as well as the DEUTERON experiment on VEPP-3 (17.3%). Regular preventive maintenance (2.6%) was performed weekly. Time losses due to failures (6.2%) and repair were caused by the large amount, complexity, and wear and tear of the equipment, most of which has been operated for decades.

5.2.2 High-Energy Physics

In 2011, experiments on high energy physics with the KEDR detector were continued. Currently, the main experiment is the measurement of the cross section of e^+e^- annihilation into hadrons in a wide range of energy of 1.8 GeV to 8 GeV in the center-of-mass frame (the energy of particle beams is 0.9 GeV to 4 GeV). Besides that, a scanning of the ψ (2s)-meson was performed.

The cross section for e^+e^- annihilation into hadrons is usually characterized by the parameter R, the ratio of this cross section to the calculated cross section for annihilation into muons. The R value is one of the most important characteristics of the physics of quarks, which determines, among other things, the magnitude of the hadronic contribution to the muon anomalous magnetic moment and renormalization of the electromagnetic coupling constant. Measurement of R in the range of 5 to 7 GeV in the center-of-mass frame seems to be the most interesting. This interval had been studied previously only in experiments with the detectors MARK-I and Crystal Ball. However, the results of MARK-I are now considered erroneous, and the result of Crystal Ball has not been published in journals, so there are no reliable data included in the PDG.

In 2011, within the framework of measurement of R, collection of statistics was carried out in the beam energy range of 0.9 to 1.5 GeV. The monitoring of the beam parameters during the scanning was provided by the system for measuring beam energy and energy spread from the Compton back scattering (CBS) of laser photons. There were also conducted several high-precision measurements of beam energy by the resonance depolarization method, for calibration of the CBS system.

In this experiment, the main problem is the luminosity, which is significantly decreasing with reducing beam energy; theoretical calculations give $L \sim E^4$ dependence. In addition, since VEPP-4M was not planned to be used at such low energies, there arise problems contributing to the loss of luminosity. In particular, at low energy, the negative influence of the collective effects of beam dynamics and collision effects increases significantly, which reduces the ultimate beam currents.

Fig. 5.2.2 shows the luminosity measured during 2011 vs. beam energy in comparison with the theoretical curve $L_{\text{calc}} = L_{\text{max}} = 1.85 \text{ GeV} \cdot (E/1.85 \text{ GeV})^4$. As one can see in the figure, the maximum luminosity is mostly in good agreement with the theoretical curve.

The main results of the HEP experiments are the improved value of the ψ (2s)-meson mass, measured with the world's best precision, and the limit to the magnitude of narrow resonances in the region of $2E = 1.85 \div 3.1$ GeV.

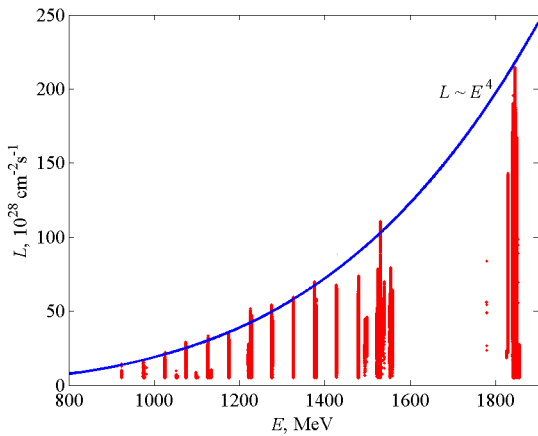


Fig. 5.2.2. Measured and calculated luminosity vs. beam energy.

5.2.3 Operation of VEPP-4 at energy $E = 3.5 \div 4 \text{ GeV}$

Fig. 5.2.3 presents VEPP-4M energy vs. time in one of the typical high-energy runs of the accelerator.

The maximum luminosity, reached at the energy $E = 3.5 \text{ GeV}$, amounted to $L_{\text{max}} = 3.7 \cdot 10^{30} \text{ cm}^{-2} \text{ sec}^{-1}$ with the average luminosity $L_{\text{av}} = 2.5 \cdot 10^{30} \text{ cm}^{-2} \text{ sec}^{-1}$. Both the values are limited by currents that can be stored in the VEPP-3 booster.

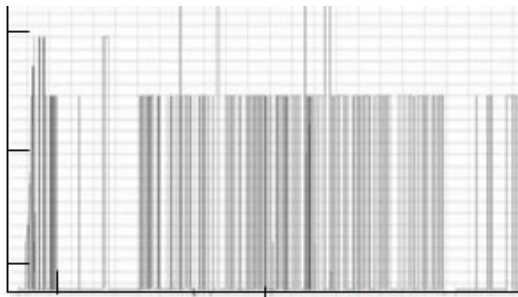


Fig. 5.2.3. Energy of the VEPP-4M collider vs. time during a month.

VEPP-4M will be used as an SR source at the energy $E = 3.5 \div 4 \text{ GeV}$; the maximum achievable beam current in the accelerator is therefore an important value, similarly to operation for luminosity. For the purpose of suppressing coherent instabilities, which hamper increase in beam current at high energy, the traverse feedback system (FB) was tested in the season of 2011. This technique had earlier proved to be effective at accelerator operation at energy injection from VEPP-3. The FB is the same efficient at beam acceleration in VEPP-4M and allows attaining a bunch current of up to 30 mA (Fig. 5.2.4). There is a reasonable hope of a total current of 50 to 60 mA in four bunches sequentially injected at operation for luminosity in the mode of "two e^- bunches per two e^+ bunches."

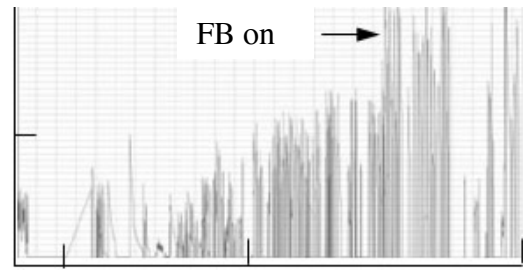


Fig. 5.2.4. Beam current per bunch on VEPP-4M vs. time during a month.

5.2.4 DEUTERON experiment on VEPP-3

Measuring the ratio of elastic scattering of electrons/positrons on a proton (R) allows one to determine the contribution of two-photon exchange (TPE) to the process. The necessity of taking the TPE into account was caused by a contradiction revealed in the measurements of the proton electromagnetic form factors. In 2009, R was measured on the VEPP-3 storage ring with a record precision. R measurements in another kinematic region (Fig. 5.2.5) started in 2011. This will make the precision two times better. The planned integral of luminosity, over 60 kilocoulombs, was acquired by the beginning of 2012 (Fig. 5.2.6).

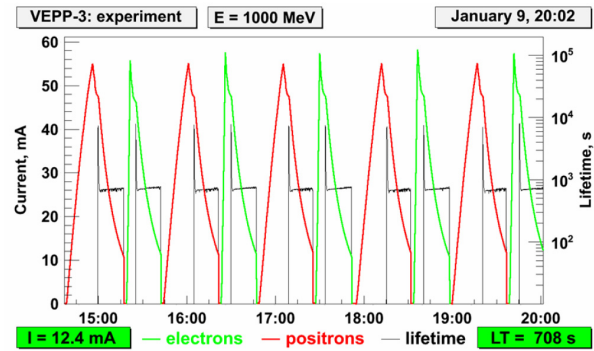


Fig. 5.2.5. Cycle of statistics collection in the DEUTERON experiment. The beam lifetime is determined by the interaction with the internal target (hydrogen jet).

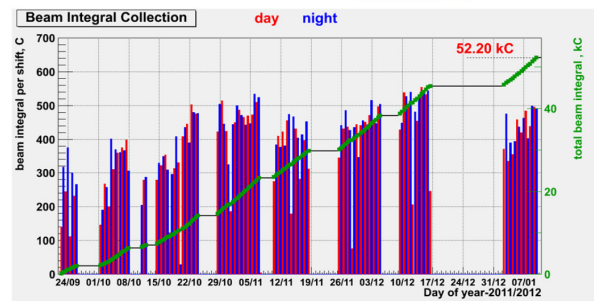


Fig. 5.2.6. Acquisition of luminosity on VEPP-3 in the DEUTERON experiment.

5.2.5 Extracted beam on VEPP-4M

Calibration of various systems of particle detectors for accelerators planned and under construction requires fluxes of γ quanta and electrons of known properties. Such beams are produced on VEPP-4M via scattering of electrons on either residual gas or a tungsten converter specially introduced into the vacuum chamber of the accelerator. The arising secondary particles come through a collimator into the equipped experimental hall (Fig. 5.2.7). The rated parameters of the beams of γ quanta and electrons are presented in Table. 5.2.1.

Table 5.2.1. Parameters of extracted beams of γ quanta and electrons

	electrons	γ quanta
Energy, GeV	0.1 ÷ 3.0	0.1 ÷ 3.0
$\frac{\sigma_E}{E}, \%$	0.5 ÷ 5.0	~ 1
Intensity, Hz	10 ÷ 1 000	1 000
Coordinate resolution, mm	0.5	-

In the spring of 2011, the FARICH prototype for the future Super-C τ factory and scintillation crystals for the COMET experiment (JPARC, Japan) were tested on the extracted beam. Both the experiments are to be continued in 2012.

5.2.6 Summer maintenance works on the VEPP-4 complex

The scheduled maintenance shutdown since the 1st of June was used for numerous works, including those requiring opening the vacuum chamber of VEPP-4M.

Below are listed fulfilled works on the upgrade of VEPP-4:

1. Hydraulic tests ("Positron").
2. Change of the windows and mirrors in the system for optical diagnostics of beam in the technical section of VEPP-4M.
3. Opening of the linear accelerator and repair of the tuning system.
4. Replacement of the SR absorber in insert "S" of VEPP-4M.
5. Installation of a mobile converter in the experimental section of VEPP-4M (for extracted beams).
6. Installation of a lens unit in the beam line from VEPP-3 to VEPP-4M.
7. Upgrade of the beam diagnostics system in the beam line from VEPP-3 to VEPP-4M.
8. Repair of the cavities of VEPP-4M.
9. Replacement of the thermal stabilization of the cavities of VEPP-4M.
10. Modernization of the adjustment units of the four magnets in semiring S.
11. Air conditioning of the room for surge generators.
12. Elimination of the VEPP-4M aperture limitation in pickup SRP4.

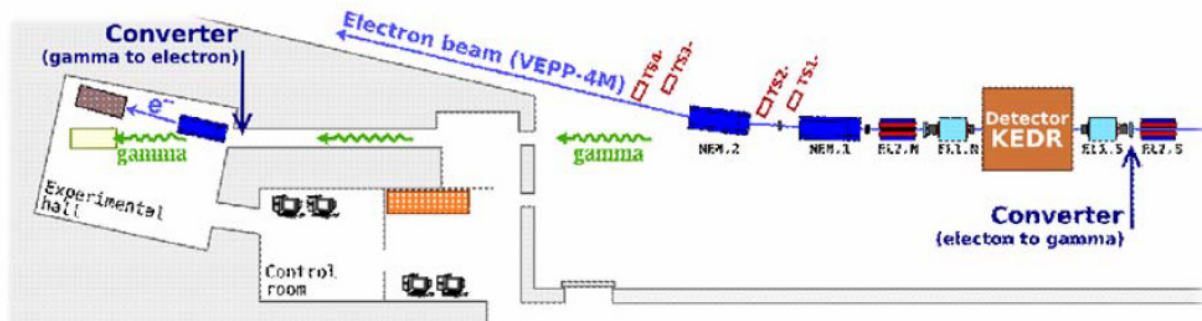


Fig.5.2.7. Extracted beam on VEPP-4M.

5.3 INJECTION COMPLEX

A lot was done in 2011 for the commissioning of the linear accelerator of positrons on the VEPP-5 injection complex. In particular, the accelerating structures of the positron linac were tested at high RF power (see Fig. 5.3.1), and the system for removal of electrons from the positron beam was fabricated and installed on the accelerator (see Fig. 5.3.2). The stored beam current sensor was mounted on the damping ring (see Fig. 5.3.3).



Fig. 5.3.1. Positron linac on the injection complex.

The positron linear accelerator was the last missing piece in the new injection complex. This complex is able to simultaneously provide a plenty of electrons and positrons for the BINP electron-positron colliders VEPP-2000 and VEPP-4M. Operation of these large facilities is required for the Institute basic research program on High Energy Physics. The injection complex of VEPP-5 has no analogues in Russia and is comparable with the world's best similar facilities. Moreover, its individual components and subsystems have record parameters, with no analogues in the world.

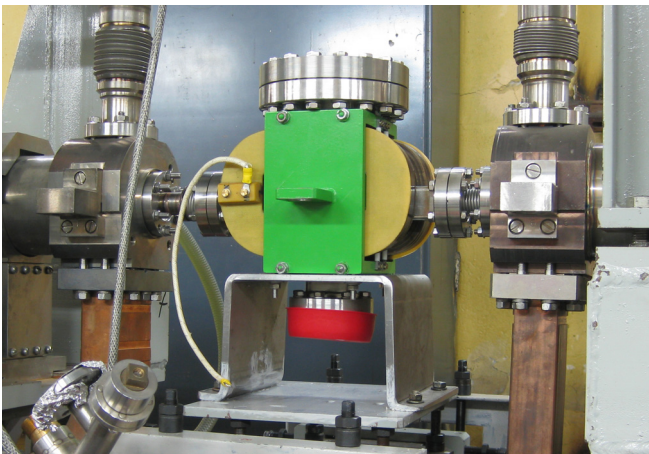


Fig. 5.3.2. Element of the system for removal of electrons from the positron beam.



Fig. 5.3.3. Stored beam current sensor of the damping ring before installation on the ring.

The installation of the equipment for the electron and positron beam transport lines (Fig. 5.3.4) on the VEPP-2000 (Fig. 5.3.6) and VEPP-4M (Fig. 5.3.5) colliders was continued in 2011. In particular, the main cable routes ensuring operation of the beam lines were laid and the main elements of these beam lines were mounted.



Fig. 5.3.4. Descent of beams in the tunnels for the beam transport lines of the injection complex.



Fig. 5.3.5. View of the beam transport line on VEPP-4M.



Fig. 5.3.6. View of the beam transport line on VEPP-2000.

5.4 LINEAR INDUCTION ACCELERATOR LIA-2

The linear induction accelerator LIA-2 was installed and commissioned on the internal prove ground of VNIITF (Snezhinsk) in 2011 (see Figs. 5.4.1 and 5.4. 2).

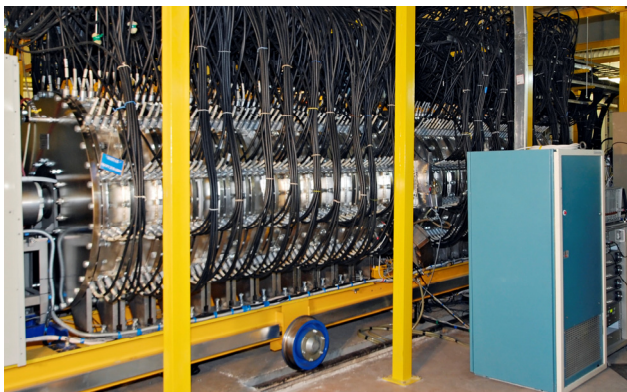


Fig. 5.4.1. View of the accelerator LIA-2 on the internal prove ground at VNIITF.



Fig. 5.4.2. View of the pulsed high-voltage power supply for LIA-2.

The linear induction accelerator LIA-2 was designed and manufactured by BINP in 2007-2010 as a prototype injector for a 20 MeV large induction accelerator intended for a promising new-generation radiographic complex.

The new machine is developed with the aim to achieve the highest possible beam quality, which will reduce the maximum transverse dimension of electron beam on the conversion target.

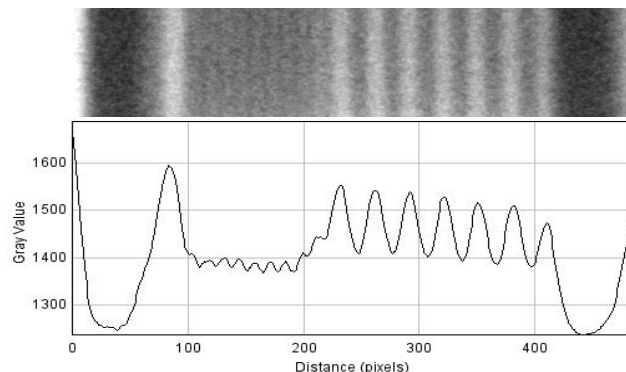


Fig. 5.4.3. Image and corresponding intensity profile of the tungsten target, recorded with LIA-2 in a standard setting of explosion experiment. The period of the target is 1 mm on the left and 3 mm on the right.

As a result, the beam size on the target was 1.5 mm at an energy of 2 MeV, current of 2 kA, and duration of 180 ns (full width at half maximum). The obtained parameters makes it possible to use LIA-2 as an independent radiographic facility with a transmission capability of up to 90 mm of lead equivalent and transverse diameter of X-ray source of 1.5 mm or less (full width at half maximum). Currently, LIA-2 operates as part of the radiographic complex in the main area of research at VNIITF. Fig. 5.4.3 shows the 0.5 mm maximum spatial resolution of the radiographic system based on the LIA-2.

5.5 ELECTRON BEAM WELDING

Works on the improvement of promising electron beam welding units developed and manufactured by BINP were continued in 2011. An experimental electron gun with indirectly-heated tungsten cathode was manufactured and successfully tested. Based on this experience, a prototype gun was created. An experimental bench for adjustment of subsystems of the electron-beam welder was created and put into operation. In fact, the bench is a universal electron beam welder with a vacuum volume of 0.3 m³ (see Figs. 5.5.1 and 5.5. 2).

We developed the scheme and fabricated the electronics of a unit for checking the weld seam for inhomogeneity of scattering and/or reflection of electrons and subsequent precise (from results of observation) aiming of electron beam at the seam during the welding

process. Fig. 5.5.3 shows the result of test welding of a stainless tube on the bench.

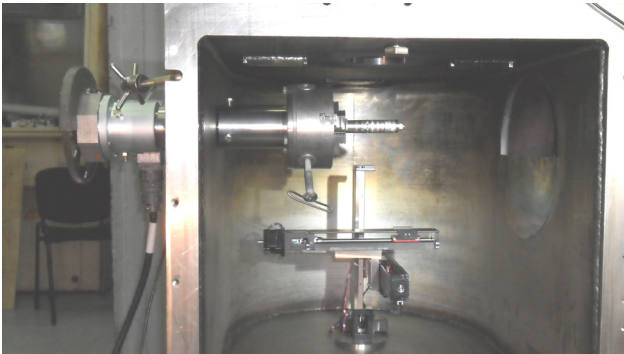


Fig. 5.5.1. Inside view of the experimental bench for adjustment of the electron-beam welder subsystems.



Fig. 5.5.2. Assembling the electron gun on the bench.



Fig. 5.5.3. Sample that was welded on the bench.

5.6 PRODUCTION OF QUADRUPOLE LENSES FOR NSLS-II

Brookhaven National Laboratory in the United States is currently constructing the NSLS-II source of synchrotron radiation. BINP had designed and manufactured quadrupole lenses of several types for the NSLS-II main ring. Lens parameters are presented in Table 5.6.1.

Table 5.6.1. Parameters of the NSLS-II quadrupole lenses.

Parameter	Unit	Types 9801 and 9802	Types 9804 and 9807
Amount		30/30	30/30
Aperture radius	mm	33	33
Yoke length	m	0.217	0.415
Magnetic field gradient	T/m	11	20.2
Magnetic field integral	T	2.8	8.8
Ampere-turns	kA	4.9	9.0

Below is given the quantity of lenses that were already produced.

Type 9801: 25 of 30; type 9802: 24 of 30; type 9804: 24 of 30; type 9807: 21 of 30. One can see the lenses in Fig. 5.6.1.

The measured harmonics of the fields of the completed NSLS-II quadrupoles in comparison with those of quadrupoles of a few SR sources are presented in Fig. 5.6.2. The vertical axis is the amplitude of harmonics relative to the fundamental one in the units of 10^{-4} , and abbreviated names of SR sources and the years of their commissioning are laid off in the horizontal axis. For all the quadrupoles, the measurement results were scaled to 75 % of the aperture and averaged over all the types of lenses. One standard deviation from the mean value is laid off as an error.

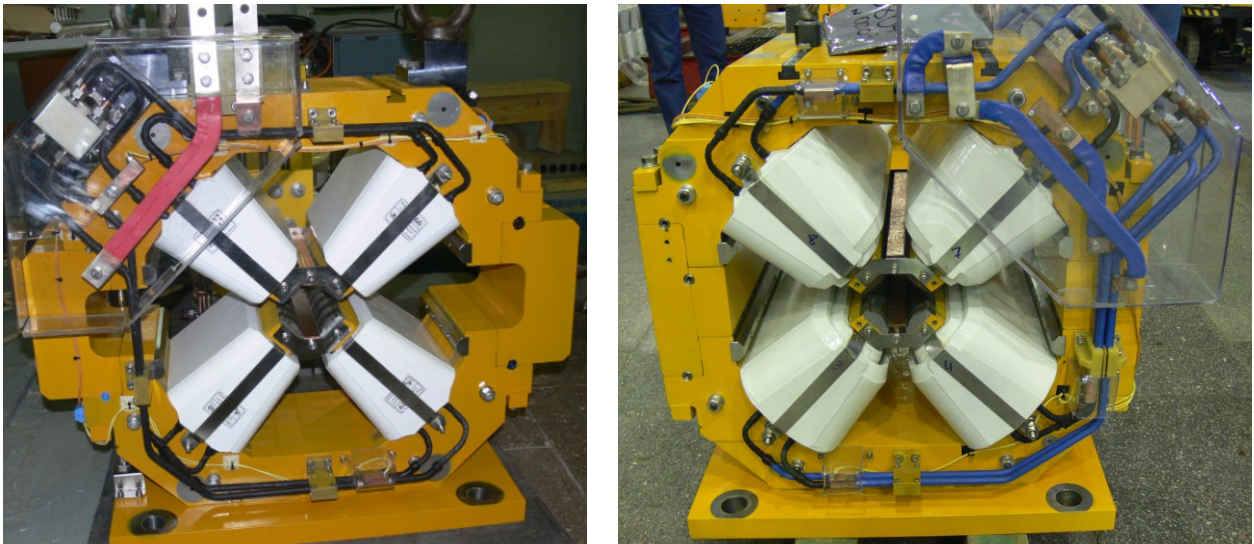


Fig. 5.6.1 NSLS-II quadrupole lenses.

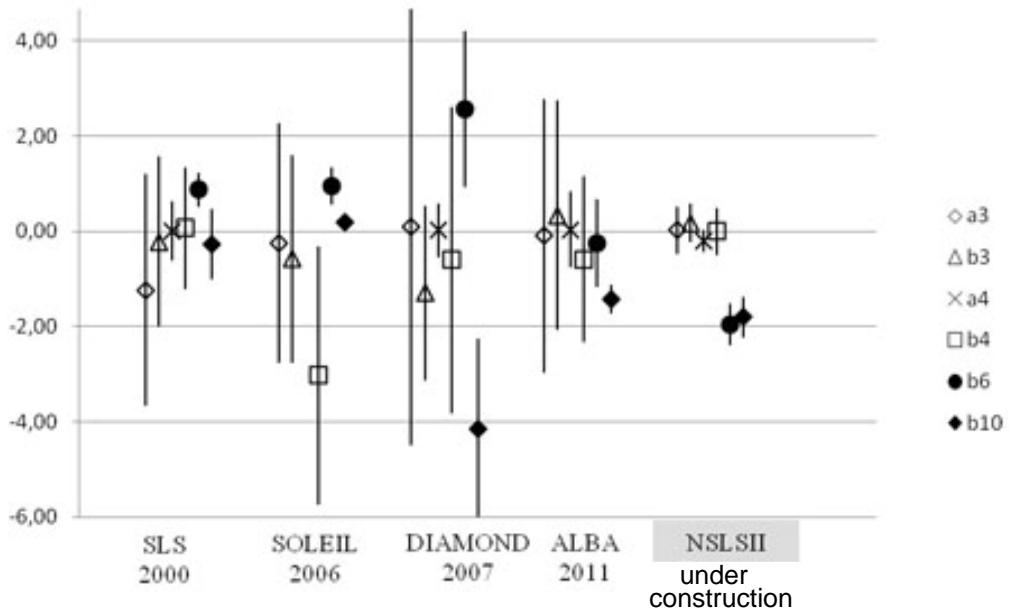


Fig. 5.6.2. Measured quality of the field of the NSLS-II quadrupoles as compared with other synchrotron radiation sources. The vertical axis is the amplitude of the harmonics relative to the main harmonic in the units of 10^{-4} .

5.7 ELECTRON COOLING SYSTEM

In 2011 the activities for the assembling of the electron cooler for the COSY synchrotron (Germany) have been continuous. An electrostatic accelerator of 34 high-voltage sections was assembled. Its testing resulted in a voltage of 1 MeV; joint operation of the electronic components of the sections was checked; Zig-Bee communication with the high-voltage sections was checked. Power transfer to the high-voltage sections was carried out using a cascade transformer. It was assembled, commissioned, and the power of about 10 kW was transferred in the electrostatic accelerator.

The new electron gun and collector with the Wien filter were tested on a purpose-designed "gun-collector" stand (see Fig. 5.7.1). The electron gun with four sectors is intended for experimental measurements of the transverse beam shape along the beam transport line and cooling section. A dedicated collector was designed and manufactured to be the electron beam

dump. Its parameters were investigated experimentally on the "gun-collector" stand. During the experiments, losses currents at the level of 10^{-5} and better, down to 10^{-6} , were attained. The HV terminal electronics, which were subsequently installed on the electrostatic accelerator, were adjusted on the stand.

During the commissioning, all the magnetic elements were assembled, installed, and powered. Magnetic field distributions were measured with a set of sensors along the trajectory of electrons. A beam with a current of 200 mA and energy of 60 kV was transmitted along the magnetic system.

The tests are to be completed at the beginning of 2012, and then the electronic cooling system will be delivered to Germany. The first tests demonstrated operation of the electron gun with creation of four spatially-separated electron beams. The beam size and shape changing along the magnetic system was measured using beam position monitors.

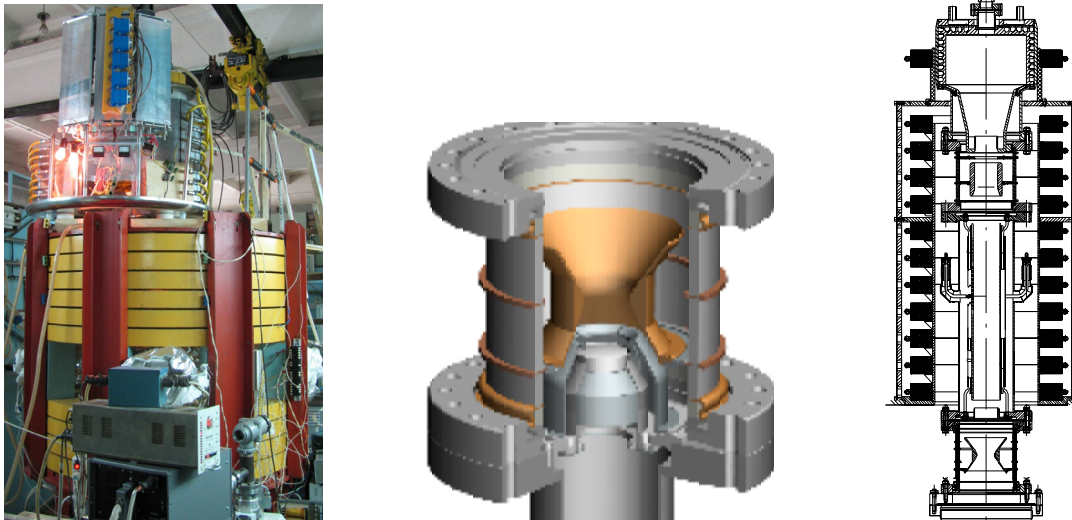


Fig. 5.7.1 "Gun-collector" stand, 4-electrode gun, and collector with the Wien filter (from left to right).



Fig. 5.7.2 Photos of the hall for testing the electron cooling system at 2 MW in early 2011 and November 2011.

5.8 ACCELERATOR MASS SPECTROMETER

Accelerator Mass Spectrometer (AMS) is intended for high-sensitivity analysis of isotopic composition of carbon. The content of radioactive carbon isotope of 14 amu in modern objects (plants and animals) is about 10^{-12} relative to the main isotope. When the object is dying out, the amount of radiocarbon is decreasing by half every 5730 years. The AMS sensitivity is restricted by the background of “foreign” ions that have passed through all the selection stages of the analyzer. Ions of close masses, ^{12}C , ^{13}C , ^{14}N , and ^{16}O , make the basis of the background flow. The processes of scattering, ionization, electron capture, and energy change, when ions exchange their charges in the electric field at interaction with the residual gas and walls of the vacuum equipment, reduce the selection capacity. The concept of the AMS, which was created by BINP, incorporates additional features for reducing the ion background. Tests conducted in 2011 showed the possibility of attaining a background of down to 10^{-15} , which corresponds to the age of more than 50 thousand years. First measurements of field samples were made: sediments of lakes Shira and Teletskoye, old trees dated by their annual rings, archaeological finds, and so on.

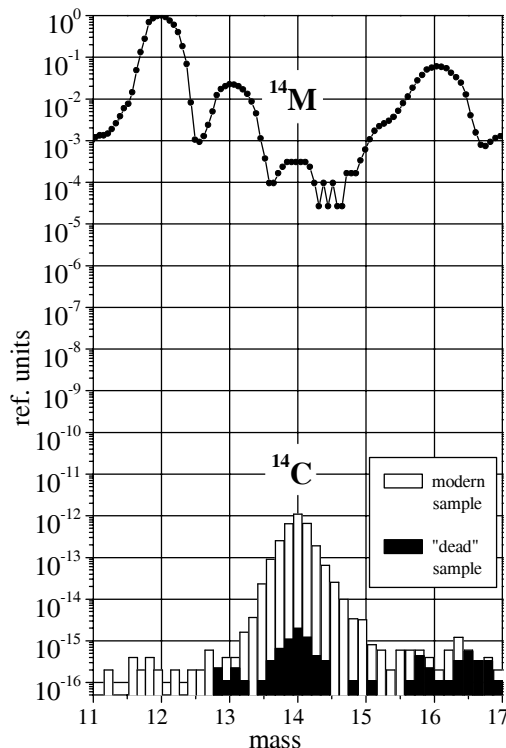


Fig. 5.8.1 Spectrum of present-day wood and pure graphite sample, in which C^{14} had already decayed and there was only low contamination background. The spectrum was normalized to the input current of C^{12} .

5.9 ION BEAM LIFETIME IN THE PRESENCE OF ELECTRONS IN ITS ORBIT

Experiments with strong modulation of electron energy were conducted on a facility of the Institute of Modern Physics, Lanzhou, China. To this end, BINP created a system for rapid modulation of electron beam energy. The system was installed on the electron cooling system at the Institute of Modern Physics (Lanzhou, China). An interesting phenomenon of abrupt shortening of ion beam lifetime at strong deviation of electron energy from the cooling optimum was revealed.

One can see from the figure that the ion beam lifetime exceeds 2000 seconds at small modulation, while at a 400 V modulation the lifetime decreases to 150 seconds! This phenomenon supports the view that this is development of coherent fluctuations in the ion beam. The first phenomena of this kind occurred on the CELSIUS facility and were called "electron heating". The phenomenon may significantly restrict ion beam parameters and its full understanding is important for the NICA project.

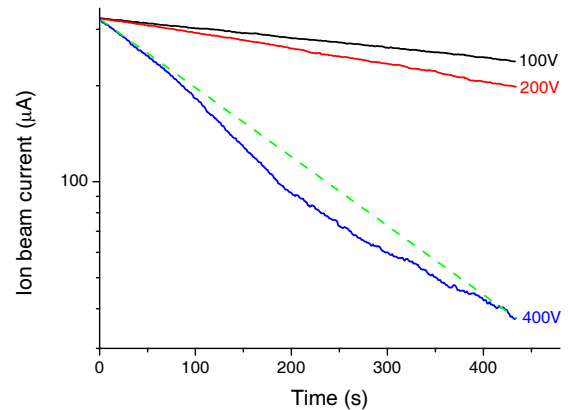


Fig. 5.9.1. Ion beam lifetime.

5.10 VACUUM SYSTEMS

5.10.1 Secondary emission and electron clouds

In 2011, BINP designed an experimental setup for laboratory creation and study of the behavior of electron clouds in the presence of magnetic field, for the following reasons:

- lack absence of experimental data on the interaction of low-energy electrons with a solid surface in the presence of strong magnetic fields.
- implementation of a relatively simple method of laboratory creation of electron clouds in laboratory conditions and study of their dynamics.
- investigation into the effect of charge exchange in a metal oxide layer on the yield of secondary electrons.

The experimental setup is shown in Fig. 5.10.1. All the main elements (C - thermo-cathode, M - modulator, D - diaphragm (grounded), BM1 - first beam monitor (a cylinder with adjustable potential capacity), Drift - drift cylinder with adjustable potential, BM2 - second beam monitor with adjustable potential, S - sample to study (grounded through a current meter)) are located in one line, along the lines of the magnetic field inside the superconducting solenoid. Table 5.10.1 shows sizes and relative arrangement of the elements.

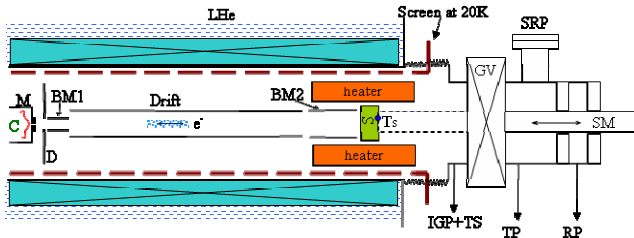


Fig. 5.10.1. Experimental setup.

A pulse measurement technique with a time resolution of about 3 ns was implemented on this facility. Matched coaxial lines were laid to the modulator, beam monitors, and sample. A beam of primary electrons $2 \div 100$ ns long was created via application of a voltage pulse to the modulator. The energy of primary electrons was determined by the potential of the cathode.

Table 5.10.1. Size of the components and their relative positions.

Component (from right to left)	Inner diameter [mm]	Length [mm]	Distance to the component on the right [mm]
C	-		0.25
M	0.5	2	3
D	4.5	1	1
BM1	4	10	0
Drift tube	7	325	1
BM2	7	59	$2 \div 3$ (to the sample)

After the interaction of the primary electrons with the sample, there arise secondary (mainly low-energy) electrons, the living space of which is limited by their movement only along the magnetic field lines, the negative potential of the cathode, and finally the sample surface. Thus, the electron cloud can dissipate only on the sample surface. How quickly this happens depends on the coefficient of effective reflection of secondary electrons from the sample surface. This parameter, which is important for predicting formation of electron cloud in accelerators, is extremely difficult to determine by direct measurements because of the complexities in managing electron flows of energy of 1 eV or less.

In 2011, a trial run of the setup was performed with the "warm" solenoid for a maximum field of 350 Gs. Fig. 5.10.2 shows typical time dependences of the currents of the monitors (Ibm1 and Ibm 2) and sample (Is).

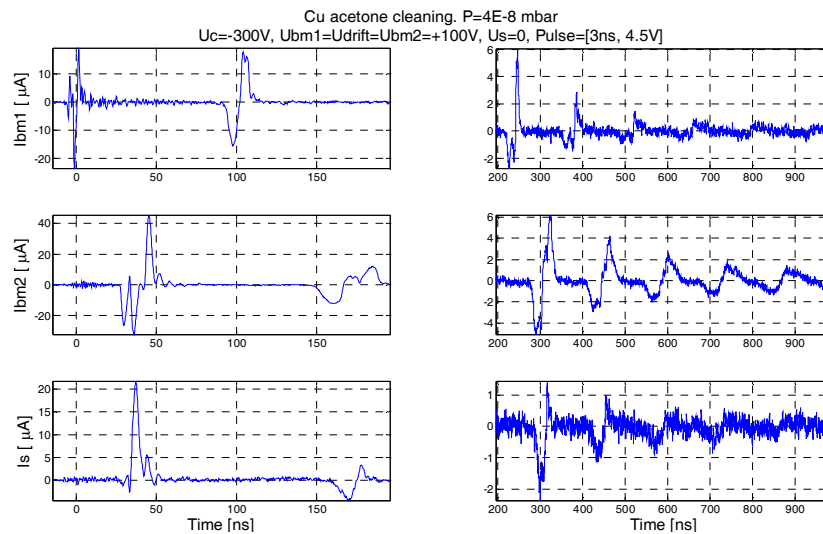


Fig.5.10.2. Currents of beam monitors Ibm1 & Ibm2 and the sample under study.

The coefficient of secondary electron emission can be defined for this method in two ways at least (see the left-hand graphs in Fig. 5.10. 2):

$$1. \quad SEY_{BM2 \text{ only}} = \frac{\int_{\text{over first positive pulse}} I_{BM2}(t) dt}{\int_{\text{over first negative pulse}} I_{BM2}(t) dt}$$

The integral in the denominator is equal to the charge of the primary electrons (the integral over the first pulse of the BM2 current, which corresponds to the entry of primary electrons into BM2). The integral in the numerator is equal to the charge of the cloud of secondary electrons (the current pulse at the time of departure of the secondary electrons from BM2).

2.

$$SEY_{BM2 + Is} = \frac{\int_{\text{over first positive pulse}} I_{BM2}(t) dt}{\int_{\text{over first positive pulse}} I_{BM2}(t) dt - \int_{\text{over first pulse}} I_s(t) dt}$$

Here, the charge in the pulse of primary electrons is determined via subtraction of the charge flowing through the sample during the interaction of the electrons with the surface from the charge of the secondary electron cloud. Fig. 5.10.3 shows the measured dependence of the secondary emission coefficient on the energy of primary electrons for a copper sample.

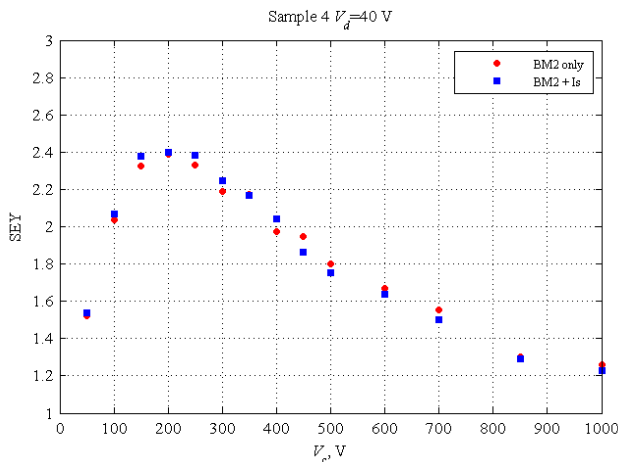


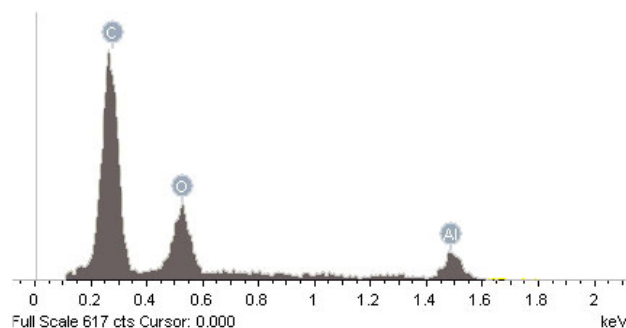
Fig. 5.10.3. Secondary emission coefficient of copper.

The right-hand graphs in Fig. 5.10.2 show a long-term dynamics of the electron cloud. One can see that the electrons "live" in a free state for a rather long time. This indicates high reflectivity of secondary electrons from the metal surface. To determine actual values of the reflection coefficient it is necessary to compare the experimental data with a computer simulation of the electron cloud dynamics in this configuration.

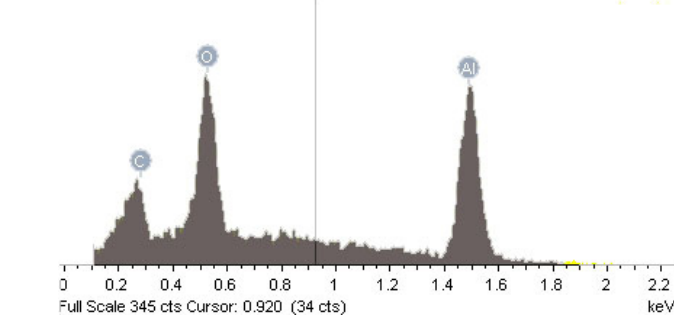
First experiments showed that the main obstacle to precise measurements is the fact that the control pulse of the modulator excites a high-frequency electromagnetic field. Next year, the thermo-cathode is planned to be replaced with a photocathode with a semiconductor RF laser. This will make the electromagnetic interference lower by order of magnitude and reduce the heat load. Besides, the measurement structure can be placed in a superconducting solenoid for experiments in a magnetic field of up to 13T.

5.10.2 Examination of the effectiveness of supersonic washing of aluminum chambers

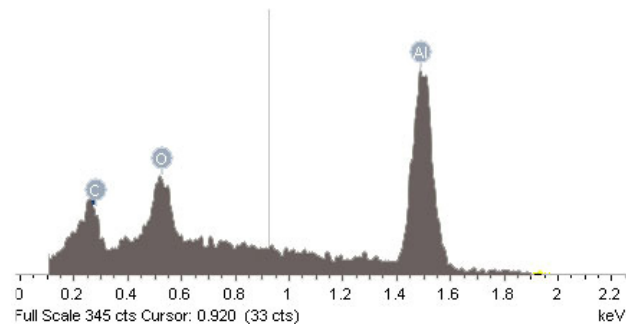
The degree of cleanness of the surface of parts before assembly significantly affects the ultimate pressure.



a) Hand cleaning with gasoline and alcohol.



b) Ultrasonic cleaning. Detergent NGL 17.40, T = 50 °C.



c) Oxide film was removed with a scraper immediately before the measurement of the spectrum.

Fig. 5.10.4. Fluorescence spectra at E_c=2kV.

In 2011, under a contract on the designing and manufacturing of vacuum chambers for the positron ring of the Super B Factory at KEK, the effectiveness of ultrasonic cleaning of articles of aluminum alloy 6063 in various solutions was examined by fluorescence spectra recorded with an electron microscope with the option of electron-probe X-ray fluorescence (EP-XRF) analysis (lab. 8-2). The electron energy was chosen somewhat higher than the excitation line of aluminum, i.e. its intensity was several times smaller than the intensity of the lines of the light elements in the superficial layers (mainly carbon and oxygen) for samples manually cleaned with alcohol. As expected, in this mode, the relative intensity of the carbon line proved to be very sensitive to the degree of surface cleaning.

Fig. 5.10.4 shows examples of the spectra. The sample which was manually washed with alcohol (Fig. 5.10.4a) demonstrates a pronounced dominance of the carbon peak. The best cleaning can be achieved via chemical etching or mechanical treatment of the surface with subsequent washing in the NGL 17.40 solution (Fig. 5.10.4b). The relative content of carbon after ultrasonic washing with the same detergent is almost the same as after the ideal method of cleaning: mechanical removal of the oxide with a scraper immediately right before placing the sample in the electron microscope chamber (Fig. 5.10.4c). In total, there were made more than 30 records of fluorescence spectra for samples with different histories of mechanical and chemical surface treatment. The main results are presented in Table 5.10.2.

N	Machining (dry milling)	Alcohol (slightly) by hand	Benzene + Alcohol by hand	Etching in NaOH, brightening in HNO ₃	Detergent NGL 17.40, 9.7 p.p.l, 20 min, 50°C in ultrasonic bath at workshop	Detergent NGL 17.40, 9.7 p.p.l, 20 min, 50°C in ultrasonic bath at laboratory right before* EP-XRF analyze.	Cl ₂ C-CHCl by hand	Cl ₂ C-CHCl in ultrasonic bath, 20 min	Scatched right before* EP-XRF analyze.	Atomic Composition %		
										Carbon	Oxygen	Aluminum
0										46	16	38
										36	13	51
1										5	12	83
										3,7	13,5	82,8
4										4,5	8,3	82,8
										4	8,3	87,7
5						3				3,2	11,8	85
						3				3,5	12,3	84
5 ¹								0.5		2,3	4,7	93
								0.5		2,7	5,3	92
6										14	14,5	71,5
										13,1	10,6	76,3
7										9,8	21,1	69,1
										Not measured		
8										7,5	11,8	80,7
										5,9	8,4	85,7
10						3				4	13,2	82,8
						3				3,4	13,8	82,8

Table 5.10.2. Main results of surface treatment of the samples of Al alloy 6063. Numbers in the green cells indicate the time in minutes before the sample was placed in the chamber of the electron microscope after the last treatment.

5.10.3 Vacuum system of the NSLS-II booster

During the designing of the vacuum system of the NSLS-II booster, the following tasks were accomplished:

- SR influence on the tolerance of the vacuum chambers.

The synchrotron radiation has a power of about 44 W/m (maximum in the defocusing magnets), which leads to uneven heating of the chamber in the place of incidence, by 60 degrees Celsius ($\Delta T = 62 \text{ }^\circ\text{C}$). With this non-uniform heating, the chamber undergoes mechanical stresses of about 114.5 MPa, while the acceptable limit is 150 MPa.

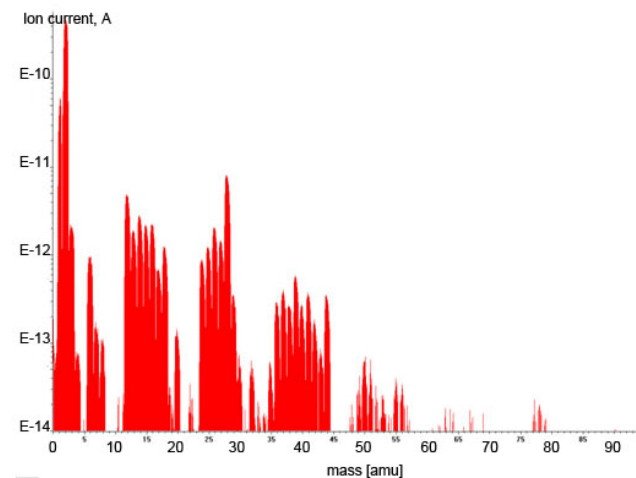
- Desorption under the SR exposure.

The calculations showed that, despite the pulsed mode of booster operation (the SR-intensity duty cycle is 1/7 with a repetition frequency of 2 Hz), desorption of gas under the SR influence will exceed the thermal desorption. The structure of the vacuum system was determined from the calculations of the dynamic pressure.

The residual gas pressure after accumulation of a current integral of about 1 A•h should be no worse than 10^{-7} Torr. The vacuum will be provided by ions pumps (72 pumps in total) from Gamma Vacuum with a pumping rate of 45 l/s, spaced by 2.3 meters on average.

The production of vacuum chambers for the bending sections, DC septum, and injection and extraction pulsed septa was completed. The technology for brazing of the BUMP chambers was developed.

All the vacuum elements were subjected to heating and vacuum tests: check for leaks (leakage below 10^{-10} l•Torr/sec); recording the spectra of residual gases; and determination of the coefficient of thermal gas liberation (below 10^{-12} l•Torr/sec/cm²). Fig. 10.1.5 shows a typical residual gas spectrum.



5.10.5. Spectrum of residual gases after heating.

5.10.4 Bellows units for the XFEL accelerator structure

In 2011, the designing and manufacturing of vacuum components for the XFEL continued. Over 3,000 elements of varying difficulty are to be fabricated and assembled. High requirements to the inner surface and geometry of the vacuum chambers made it necessary to develop new technologies. The most challenging process, in terms of technology, was the electrodeposition of uniform copper layer on the inner surface of the bellows units that are intended for operation in liquid helium for the XFEL linear accelerator. Joint work with EP2 and implementation of technological ideas of the electroplating department of EP2 resulted in a coating uniformity of 1.2 or better (ratio of thicknesses at the crest and inside of the bellows corrugation) with a high degree of coating quality reproducibility. Fig. 5.10.6 shows prototype expansion units. There are plans for year 2012 to launch small-scale production and manufacture 850 expansion units of this type.



Fig. 5.10.6. Bellows units for the XFEL accelerator structure.

5.11 WORKS ON THE ELECTRON-POSITRON FACTORIES AND BEAM PHYSICS

In 2011 two works were performing.

First, during approximately the last decade we begun to feel a kind of discomfort due to shortness in the description in the tutorial by D.V. Pestrikov “Lectures on coherent oscillations” (NSU, 1996) of the coherent beam-beam instabilities. These lacks have been removed in 2011 in the tutorial written by N.S. Dikansky, D.V. Pestrikov. Coherent oscillations of colliding bunches. Apart from careful and systematic descriptions of the coherent beam-beam instabilities in storage rings this tutorial helps students to improve their ability in solving such problems and to improve their knowledge in practical use of many standard as well as more peculiar techniques of the theory of the linear coherent oscillations. We carefully studied specific features of the Landau damping of the coherent oscillations of colliding bunches; using a rigid bunch model we described resonant cures of the coherent beam-beam oscillations; besides, we discussed specific features of the coherent oscillations of the colliding bunches with the compensation if their beam-beam kicks.

In the second publication we have studied a decrease in the strengths of the coherent beam-beam resonances with an increase in the lengths of the colliding bunches. Due to the phase averaging effect the increments of small coherent oscillations of the bunches of a finite length can be decreased up to 80% compared to their value, calculated for short bunches. The phase averaging reduction factor is larger the larger is the multipole number of the betatron coherent oscillations. For the bunches with flat cross section the waist in the vertical bunch envelope results in the hourglass amplifications of the increments of the coherent oscillations provided the lengths of colliding bunches are large. Since the collider luminosity decreases with an increase of the bunch length in the region, where the bunch length exceeds beta-function at the interaction point, the calculations for this parameter region may have only an academic worth.

In addition to the suppression of the oscillation increments in the phase-averaging region, the phase averaging effect for coherent oscillations is accompanied by excitations of the bunch synchro-betatron oscillation modes and by the coupling of the synchro-betatron modes. These two effects, generally, increase the widths of the stopbands of coherent beam-beam oscillations near the beam-beam resonances. Therefore, although the coherent beam-beam instability becomes weaker the net of the stopbands near the resonances becomes more densely compared to that, calculated for short bunches.

In general, the main features of the phase averaging effect for coherent beam-beam oscillations are found to be very similar to those, which were found for the incoherent ones.

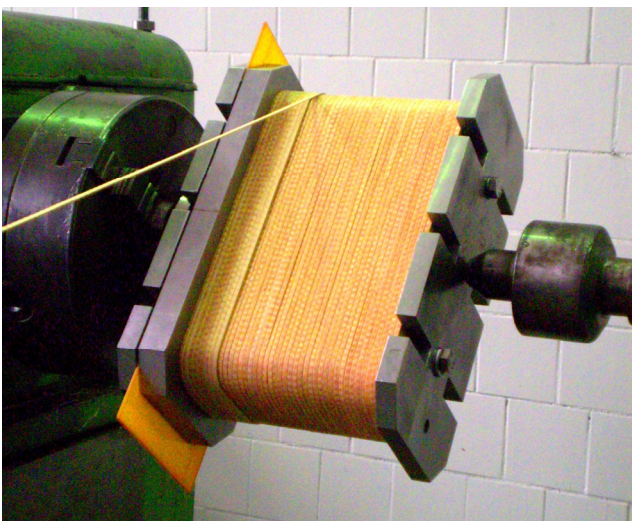
5.12 MAGNETS FOR THE KEK SUPER-B

In the frameworks of KEK and INP collaboration the testing and update of pulse magnet for KEK Super-B conversion system were performed. This work includes update of control and computing of magnet supply system. Also the control and monitoring system of vacuum in the magnet chamber was improved. Works aimed the resource test and update the operation of magnet jointly with near-placed electron-positron converter.

In the frameworks of contract between INP, KEK and Toyota Tshusho, production of magnets-correctors KEK Super-B was started. During 2011 were performed stages of design and magnets prototype production. Mass production of whole magnets number (290 units) is started. Magnets include two types correctors - vertical and horizontal with apertures 290 mm and 280 mm.



5.12.1. Conversion magnet of positron system.



5.12.2. Winding of magnet-corrector coil.

5.13 NSLS-II BOOSTER

Introduction

In May 2010, a contract was signed on the creation of the booster for the NSLS-II synchrotron, which is now constructed at Brookhaven National Laboratory (BNL), USA. The customer received the Preliminary Design in September 2010, and in January 2011 the customer was submitted the Final Design. In July 2011, the customer accepted the first serialized products. The booster should be assembled at the customer's site no later than July 2012. Acceptance of the booster operating with the required parameters is scheduled for February 2013.

BINP shall design and fabricate the magnetic, vacuum, extraction-injection, and diagnostics systems and power supplies and develop the control system. The RF system shall come from BNL. In addition, BINP shall participate in the assembly and testing of the booster at the BNL site. BINP shall also be responsible for commissioning of the booster and attainment of the required beam parameters.

Table 5.13.1. Rated parameters of the NSLS-II booster.

Perimeter	158.4 m
Injection energy, rated/minimum	200 MeV/170 MeV
Extraction energy, rated/maximum	3 GeV/3.15 GeV
Repetition rate	1 or 2 Hz
RF frequency	499.68 MHz \pm 10 kHz
Horizontal emittance at 3 GeV	<40 nm*rad
Pulse spread at extraction	<0.1%
Charge (long-pulse mode/single-pulse mode)	> 10 nC/0.5 nC
Efficiency of charge transfer from the linac to the main ring	> 75%
Operation hours per year	6, 000 hours
Unscheduled shutdown time	0.4% (24 hours per year)

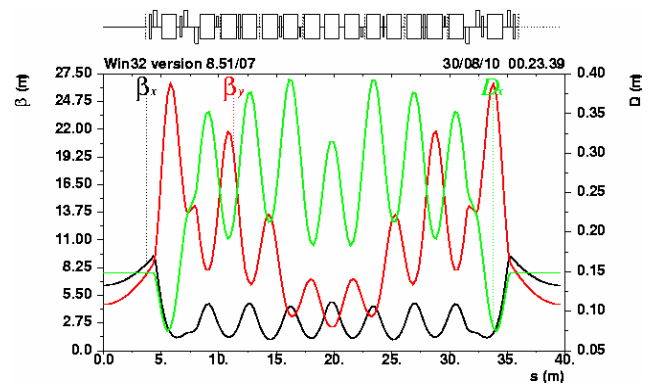


Fig. 5.13.1. Structural functions of one quarter of the booster.

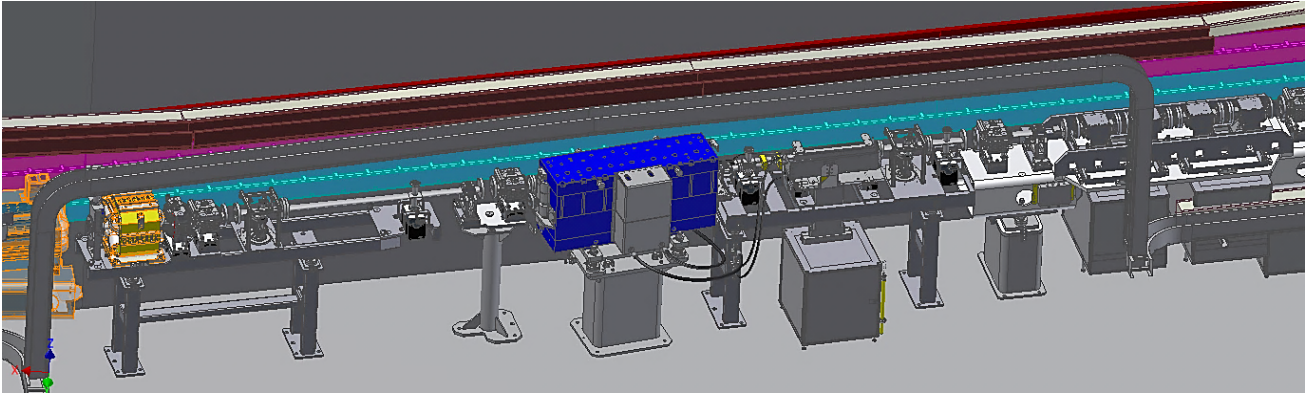


Fig.5.13.2. 3D integration of models from numerous designers. Extraction gap. 10 meters of the entire booster length (158 meters).

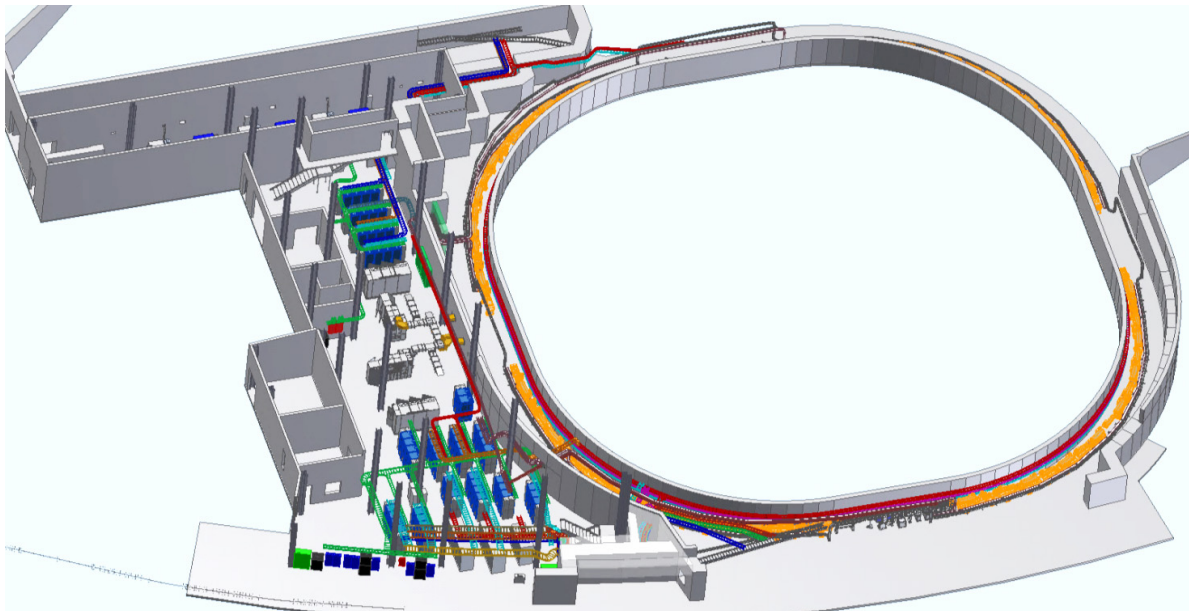


Fig.5.13.3 3D model of the entire NSLS-II booster.

5.13.1 Design

Designing of the entire booster and its components began in July 2010. Preliminary drawings were developed by September 2010 and presented to the customer at the PDR (Preliminary Design Review). The designing of the main elements of the booster was completed by the Final Design Review (FDR) in February 2011, and after approval by the customer the drawings were handed over to the production department. In spring 2011, the main effort was focused on the agreement of the injection and extraction gaps with the BNL representatives, which resulted in the creation of agreed 3D models, which were submitted to the customer in May 2011. Last booster units were designed and handed over to the production department in August, after which the activity was aimed

at completing the 3D model of the booster as a whole. The customer received the model in October 2011. Because of the large volume of work and tight deadlines, more than thirty members of the designing department were involved, which required integration of structures developed by different designers in one big project.

5.13.2 Magnetic system

The magnetic system includes 60 dipoles of two types, 24 quadrupoles, 16 sextupoles, and 39 bending magnets of three types. The dipole magnets have quadrupole and sextupole components. For the required field quality parameters to be attained, the dipole magnets were designed with special edge chamfers (Fig.5.13.4). All stamps were designed and manufactured by the BINP

production department. The accuracy of the plates made was 15 microns or better, and in some types of plates it was better than 5 microns. All the quadrupoles, sextupoles, and bending magnets and half of the dipoles were made in 2011.

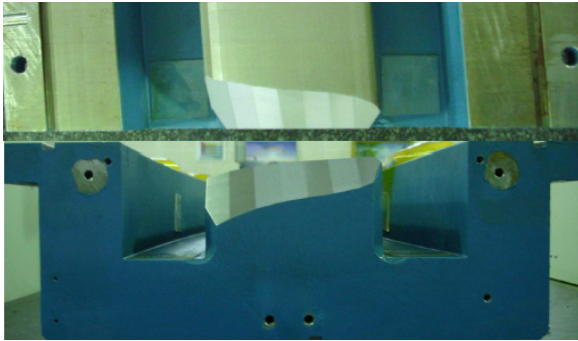


Fig.5.13.4. Final variant of the 3D chamfer on the BD dipole.

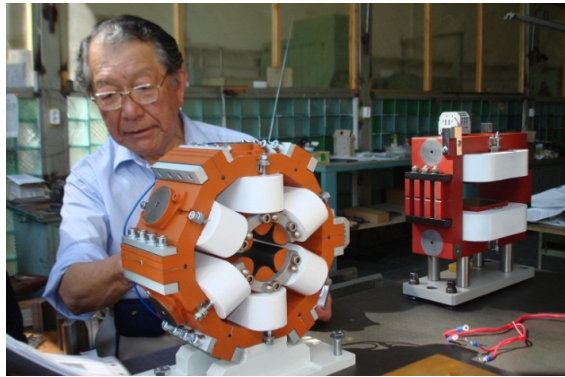


Fig.5.13.5. BNL Director Advisor on the project Satoshi Ozaki inspecting the first serialized magnets.



Fig.5.13.6. Two additional benches with rotating coils were constructed for the measurements of the quadrupoles and sextupoles.



Fig.5.13.7. For magnetic measurements of the dipoles (above), BNL provided a laser tracker and ¼" nonmagnetic corner reflectors, which were mounted on carriages with Hall sensors for the BD and BF dipoles (below). This allowed referring the magnetic measurement maps to the fiducials of the dipoles with accuracy better than 20 microns.

5.13.3 Vacuum system

The residual gas pressure after accumulation of a current integral of about 1 A*h should be 10^{-7} Torr or better. Ion pumps (72 pumps in total with an average spacing of 2.3 meters) create vacuum with a pump speed of 45 l/s.

A number of important tasks were accomplished:

a) the influence of eddy currents on the desorption of gases (the effect is insignificant since the eddy currents heat the chamber by 3 °C);

b) the effect of SR on the stability of the vacuum chambers. Synchrotron radiation has a power of about 44 W/m (maximum in the defocusing magnets), which leads to uneven heating of the chamber in the place of incidence (by 60 °C; $\Delta T = 62$ °C). As a result, the chamber undergoes mechanical stresses of about 114.5 MPa, while 150 MPa is maximally admissible;

c) the influence of SR on the desorption of gases. Calculations showed that, despite the pulsed mode of booster operation (duty cycle as to the SR intensity is 1/7 at a repetition frequency of 2 Hz), the SR-determined desorption of gas will exceed the thermal desorption. Fig.10.8. shows an example of calculation for one of the straight sections.

All vacuum elements were subjected to heating and vacuum tests (leakage test (leakage less than 10^{-10} l*Torr/sec), residual gas spectra measurement, and determination of the coefficient of thermal gas outgassing (10^{-12} l*Torr/sec/cm² or less)).

In 2011, about 100 of the 150 meters were completed (Fig.5.13.9). A brazing technology for chambers with webbings for the bump magnets was developed (Fig.5.13.10).

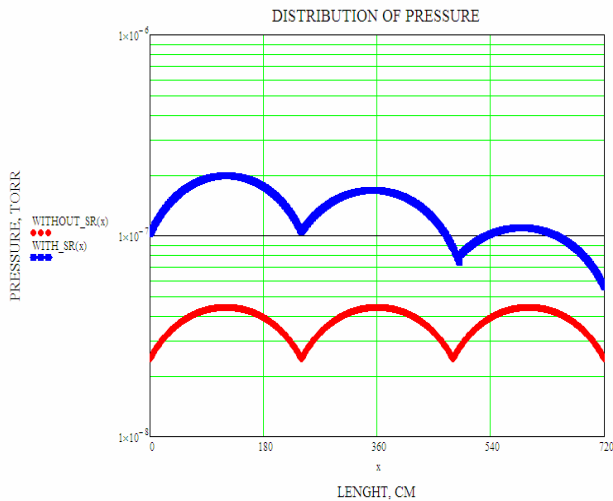


Fig.5.13.8. Pressure distribution as caused only by thermal desorption and in SR presence.



Fig.5.13.9. Completed vacuum chambers. Each is intended for two dipoles and has a pickup.

5.13.4 Diagnostics

In 2011, BINP staff fulfilled the main work on the development and manufacture of electrostatic pickups, betatron frequency measurement system, and means of optical diagnostics of beam (phosphor sensors and SR output ports).

Development of the electrostatic pickups was based on calculations involving both approximate analytical formulas and numerical simulation of electromagnetic fields. The pickup electrodes with vacuum inputs were taken from the MPF Products. In 2011, BINP produced the cases of the pickups and performed assembling and vacuum and electrical measurements.

Beam diagnostics in the NSLS-II booster will be performed with the following equipment:

Device	Beam parameters to measure	Quantity
Electrostatic pickups	Beam orbit and structure functions	37
DCCT	Average beam current and lifetime	1
FCT	Beam current distribution over bunches	1
Phosphor sensors	Single-flight beam image	6
SR output ports	Transverse dimensions of beam	2
Frequency measurement system	Betatron frequencies	1

The betatron frequency measurement system, which includes electronics for excitation of beam oscillations and processing of signals, a pickup and a kicker on strip lines, as well as software, was completely developed and manufactured by BINP. The system parameters allow one to measure beam betatron frequencies during beam acceleration in the booster; the measurement accuracy is 0.0005 or better; one measurement takes about 1 ms. The prototype of the system was tested with beam on VEPP-3.

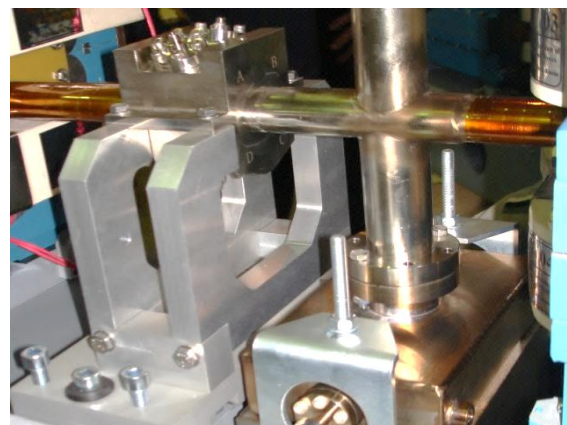


Fig.5.13.10. Cases of the pickups (above) and an assembled pickup on a girder (below).



Fig.5.13.11. Strip pickup (above) and electronics of the betatron frequency measurement system (below).

The phosphor sensors and SR output ports were designed by BINP. The phosphor screens are introduced into the vacuum chamber with a remotely controlled pneumatic actuator. High-accuracy adjustment of the mirrors that direct the output SR beam to the sensor is performed by electromechanical actuators. The light is registered with CCD cameras Prosilica GC1290. The units of mirrors for SR output were subjected to heating and vacuum tests. The phosphor sensors are around 70% ready now. The average beam current transducer Bergoz DCCT and fast beam current transducer Bergoz FCT were purchased for measuring the beam current intensity. BNL measured the characteristics of the beam current transducers.

5.13.5 Assembly of the modules of the booster ring at the BINP site

The regular part of the booster ring is supplied in the form of girder assemblies. A girder is a 500x300 mm rectangular steel profile with walls 16 mm thick and integrated components that provide the required rigidity, high-accuracy positioning, and fixation of the magnetic elements and girder assembly as a whole. The girders are produced based on BINP drawings at the pilot plant of the branch of ITAM SB RAS. A girder assembly consists of the magnetic elements set in the design position on the girder with the inserted vacuum chamber with pickups.

In December, pedestals for girder assemblies for all four arcs and five girder assemblies were dispatched to BNL.

5.13.6 Power Supplies

Power supplies for the dipole magnets (BF and BD) were made by Danfysik under BINP supervision. By the end of 2011, the production was completed and tests were started. BINP designed, fabricated, and tested a power supply providing the "1-cos" current shape at a frequency of 1 to 2 Hz and a maximum current of 750 A (Fig.5.13.12.). This power supply will be used for dynamical tests of the dipole magnets.

56 power supplies (6A/60V) for the steering and sextupole magnets in the format of 19" crates (8 power supply channels per crate) were designed and manufactured (see Fig.5.13.13).

3 power supplies (200A/200V) were designed and manufactured for the quadrupole magnets (Fig.5.13.14), as well as a source (500A/12V) for the DC "septum magnet" (Fig.5.13.13).

Generators for the pulsed "septum magnets" and "bump magnets" with pulse currents of up to 10 kA were designed and manufactured.

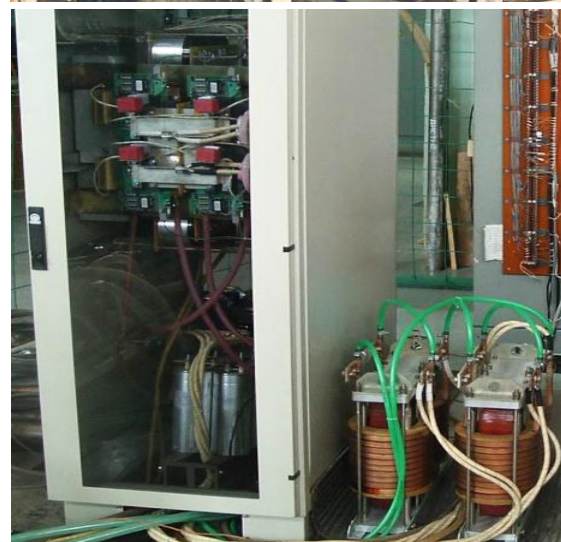


Fig.5.13.12. Power supplies for the BD dipole magnets (above). Power supply for dynamic tests at the BINP site (below).

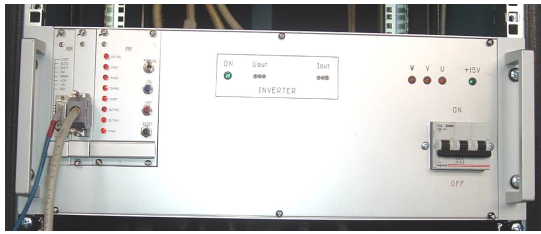


Fig.5.13.13. Power supply for the DC "septum magnet".



Fig.5.13.14. Power supplies for the quadrupole magnets (above). Power supplies for the corrector and sextupole magnets (below).

5.13.7 Injection-extraction system

Injection into the booster and extraction are performed in a single turn in the horizontal plane. A train, which is 300 nsec long and contains up to 150 bunches, is injected from the linac. Injection into the booster and extraction are realized with pulsed "septum magnets" and ferrite kickers, which are located outside the vacuum. The magnets have embedded thin-walled vacuum chambers of stainless steel, and the kickers contain ceramic vacuum chambers.

Single-shot injection into the booster is performed with a pulsed "septum magnet" and two ferrite kickers. The beam can be accumulated in the booster. To this end, there are two extra kickers installed in the injection section. The four kickers deflect the orbit of the circulating beam in such a way that the distance between the injected and circulating beams at the injection azimuth is minimal. The kickers are set up as modules. At the inlet, those are four freestanding modules with their own power supply. At the exit they are four successive modules powered from two sources.

Extraction from the booster involves the four "bump magnets", extraction ferrite kicker, pulsed septum, and C-shaped "septum magnet" with a constant field.

The "bump magnets" slowly, in 0.75 ms, bring the beam to the knife of the pulsed magnet, and the kicker kicks the beam into the aperture of the pulsed septum and further into the "DC septum."

All above elements were manufactured by BINP in 2011 and their testing was begun.

This system is characterized by quite stringent requirements to field stability in the magnets. For the extraction kicker, the amplitude instability and field inhomogeneity on a shelf 300 nsec long should not exceed $\pm 0.2\%$. For the pulsed and DC septums, the field stability should be no worse than $\pm 0.02\%$.

A dedicated stand was created for measurement of the pulsed elements—"bump magnets", "septum magnets", and kickers (Fig.5.13.15).

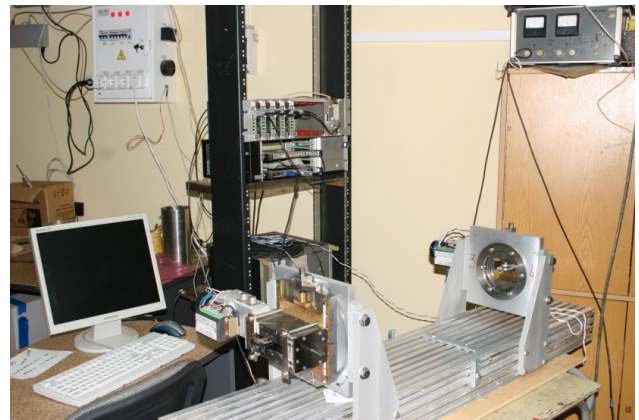


Fig.5.13.15. Stand for pulsed magnetic measurements.

The extraction "septum magnet" was measured (Fig.5.13.16.) and field stability was tested at operation from an actual 2 Hz generator, which showed that requirements to stability were met and magnetic field characteristics complied with the technical requirements. Magnetic measurements of the injection "septum magnet" are underway (Fig.5.13.17).



Fig.5.13.16. Extraction "septum magnet" with the vacuum chamber (top view).

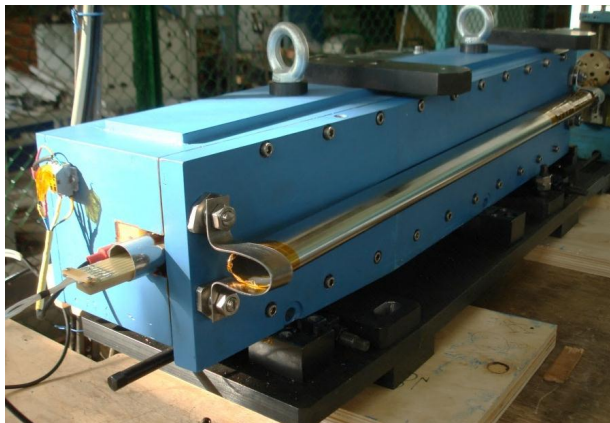


Fig.5.13.17. Injection "septum magnet" on the measurement stand.

Measurements of the "bump magnets" were performed using the vacuum chamber model. Measurements of the "bump magnets" with real vacuum chambers are coming. Two of the chambers are ready to date (Fig.5.13.18).

It was the first time when BINP manufactured ferrite kickers with built-in ceramic vacuum chambers. For the beam image currents to get closed, the inside of the chamber was coated with titanium nitride strips 4 μm thick and 3.5 mm wide (Fig.5.13.19).

Actually, there is no accelerator on which the extremely tough requirements to field stability in the kickers have been met. Typically, this is a level of about 1%. So, now they on the stand are intensely working on adjustment of the measurement systems and power supplies to achieve the required parameters (Fig.5.13.18).

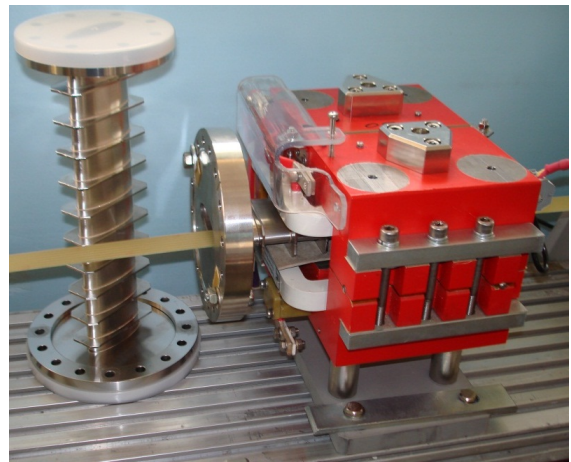


Fig.5.13.18. Thin-wall vacuum chamber with webbings for the "bump magnet" and the "bump magnet" on the measurement stand (above). Pulsed power generator for the "bump magnets" (below).



Fig.5.13.19. Ceramic vacuum chamber with the strip coating.

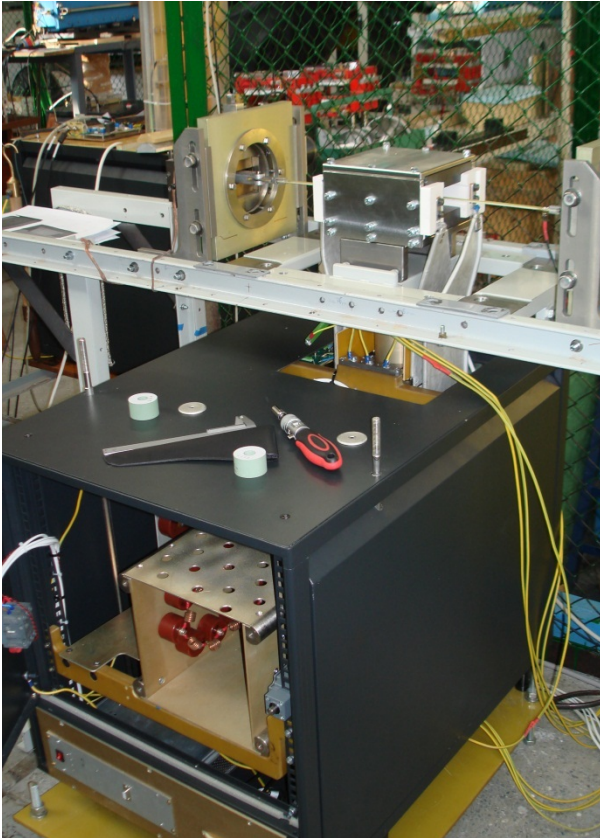


Fig.5.13.20. Ferrite kicker without the chamber and modulator on the measurement stand (below). Charger unit of the modulator kicker (above).

5.13.8 Control system

Functionally, the booster control system is divided into several parts:

- the booster magnetic system controls provide circulation of the injected and accelerated beams in the synchrotron ring;
- the pulsed magnets controls provide injection at the energy of 200 MeV and extraction of the accelerated beam at the energy of 3 GeV;
- the vacuum controls ensure maintenance of required vacuum in the booster ring;
- the beam diagnostics monitoring system allows the measurement of various parameters of the beam;

- the interlocks monitoring system supports safe and reliable operation of the power supplies, ramping and pulsed magnetic elements of the booster;

- the timing system provides mutual synchronization of all subsystems of the booster during the acceleration cycle, as well as lock the accelerated beam to the beam that circulates in the main ring of NSLS-II.

The booster control system is based on EPICS to be compatible with the NSLS-II main ring control system. In addition to the electronics of well-known suppliers (Agilent, ISC, GE, IBM, Emerson, and Allen Bradley), electronic modules designed by BNL is used: a PSC-PSI set for power supplies distributed control and a controller for processing signals from the pickup stations. The control system integrates various bus types: VME, cPCI, Euromechanics chassis, and PLC.

To provide the required stability of the injection/extraction pulsed systems, it is supposed to use BINP-designed ADCs: 200 MHz ADC200 and the signal integrator VsDC3.

Communication and synchronization of the processors, controllers, and various devices of the control system are carried out through 1Gb Ethernet, as well as through optical lines with a capacity of up to 125 MBytes/sec. A block diagram of the computers and electronics of the booster control system is shown in Fig.5.13.21.

The final design of the control system was completed in late 2010 – early 2011: the composition and quantity of computers and electronics modules were determined; then the hardware was purchased. Technical specifications for the power supply controllers (PSC-PSI) and all the details of the vacuum controls were determined.

During 2011, a stand for creation and testing of software was assembled at BINP. The stand comprises a full set of equipment included in the control system (Fig.5.13.22). The development of engineering screens for the power supplies testing is underway in parallel with the developing and testing of the firmware for the power supply controllers.

The first set of PLCs for control of the vacuum system of the beam transportation line from the linac to the booster (Fig.5.13.23) was assembled, tested, and shipped to BNL by the end of 2011.

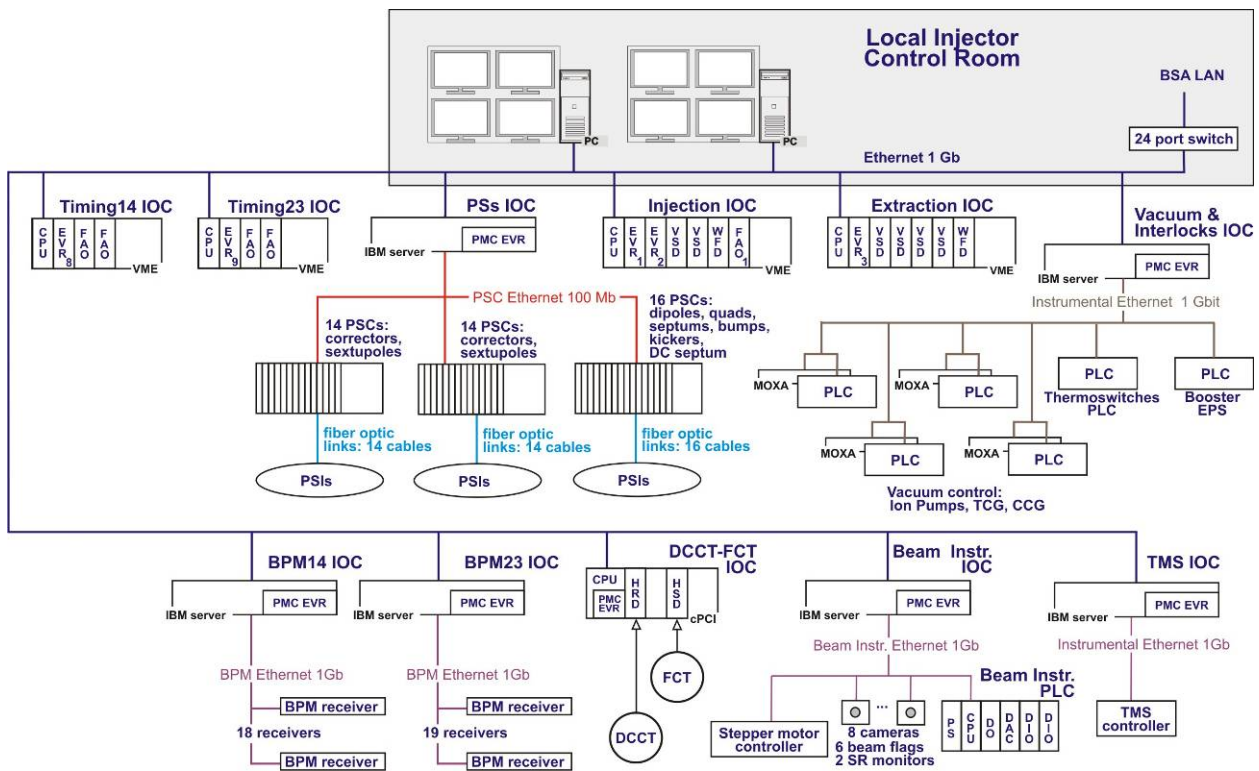


Fig.5.13.21. Block diagram of the control system of the NSLS-II booster.



Fig.5.13.22 Equipment for control of the power supplies.



Fig.5.13.23 Chassis with PLCs to control the vacuum of the beam transport line from the linac to the booster.

The following works on the software for the booster control were underway in 2011: development of EPICS databases for power supplies control and timing, development of engineering screens for the power supplies testing, creation of programs to work with the beam diagnostics electronics, development of the vacuum system control software.

6

SYNCHROTRON RADIATION AND
FREE ELECTRON LASER
RESEARCH

6.1. INTRODUCTION

The shared-use Siberian Synchrotron and Terahertz radiation Center (SSTRC) has been operating for more than thirty years on the basis of facilities and laboratories of the Institute of Nuclear Physics SB RAS.

The synchrotron radiation (SR) activity includes works on SR beams from the VEPP-3 and VEPP-4 storage rings, as well as the designing and development of systems for SR generation for Russian and foreign centers.

Another direction, associated with terahertz radiation, includes works with the use of radiation from Novosibirsk free electron laser (FEL) (in the range of 110-240 μm and 40-120 μm), as well as further development of Novosibirsk FEL and participation in international projects on this topic.

Besides that, undergraduate and graduate students are taught and trained at the center.

In 2011, 2028 hours were allocated for work on SR beams from VEPP-3 (1220 hours in 2010) and 180 hours for work on SR beams from VEPP-4 (294 hours in 2010). 10 stations on 7 SR extraction beam lines of the VEPP-3 storage ring and 2 SR stations on VEPP-4 were involved in experiments.

In 2011, Novosibirsk FEL worked for users for about 1000 hours. One of the two main tasks in 2011 was the organization of regular work at six user stations. The second task was the preparation for the commissioning of the third stage of Novosibirsk FEL.

Research groups from more than 50 institutes and other organizations carried out works at the stations.

6.2. WORK ON SR FROM VEPP-3

6.2.1. Station "Explosion (Extreme states of matter)"

The station "Explosion (Extreme states of matter)" is intended for registration of transmitted radiation and small-angle X-ray scattering (SAXS) for investigation into detonation and shock-wave processes.

Participating organizations:

Lavrentyev Institute of Hydrodynamics. SB RAS, Novosibirsk; Russian Federal Nuclear Center "All-Russian Research Institute of Technical Physics (VNIITF)", Snezhinsk; Institute of Solid State Chemistry and Mechanochemistry SB RAS, Novosibirsk; Budker Institute of Nuclear Physics SB RAS, Novosibirsk.

In 2011, the work was carried out with financial support under the following projects: SB RAS Integration project № 11; RAS Presidium comprehensive research program № 2-9 "Thermophysics and mechanics of extreme energy effects and the physics of strongly

compressed matter"; RFBR 08-03-00588-a; and RFBR 10-08-00859-a.

Examples of activity

Study of the dynamics of formation of condensed-phase nanoparticles during detonation of new TATB-based explosives at VEPP-3 SR station "Explosion" by the method of high-speed small-angle scattering

There were conducted experiments on SR-SAXS registration at detonation of high explosives (HE) on the basis of 1,3,5-triamino-2,4,6-trinitrobenzene (TATB) with additions of graphite and nanodiamonds.

Analysis of data on graphite-containing TATB indicates presence of nanoparticles, presumably of graphite, of $\sim 4\text{-}5$ nm in size, registered immediately behind the detonation front. Comparison of the SAXS signals from TATB and TATB/graphite mixtures shows that condensation of carbon in the TATB detonation products occurs into the graphite phase. The size of nanodiamonds registered is ~ 2 nm or less. One may assume that larger nanodiamonds fail (burn) in the explosion products. For mixtures of TATB with nanodiamonds, there is registered a SAXS signal from ultra-dispersed nanodiamonds (UDD) introduced into the charge. The signal from condensed nanoparticles at detonation of TATB is small as compared with the signal from the introduced UDD.

The size of scattering particles was derived from SAXS signals by an original technique using a special software package. The particles were assumed to be spherical and uniformly distributed in a homogeneous medium. The obtained and calibrated evolution of the particle size in experiments with samples of TATB/graphite and TATB/UDD is shown in Fig.6.2.1, where time $t=0$ corresponds to the passage of the detonation front. Fig.6.2.2 presents graphs of variation in the SAXS flow integrated over all angles for the same high explosives. One can see from the graphs that the introduction of nanodiamonds of ~ 5 nm in size (produced via explosion) does not lead to a marked increase in the size of the nanoparticles behind the detonation front. Parameters behind the detonation front in TATB do not contribute to increase in the size of particles already introduced.

Data on the dynamics of the integrated SAXS (Fig.6.2.2, below) also show that the integrated SAXS signal is proportional to the initial amount of introduced UDD, i.e. the amount of carbon nanoparticles condensed during the explosion (in the diamond form) is small as compared to that of the introduced particles.

There were also obtained the dynamics of the condensed-carbon particle size at detonation of BTF. The size of particles behind the detonation front is as large as 70 nm. The absence of hydrogen in BTF leads to a higher temperature in the detonation front.

Fig.6.2.3 presents data on the growth of the size of condensed nanoparticles at detonation of TATB,

TG50/50, and BTF. The particle size for BTF is an order of magnitude greater than that for TG50/50, which may be explained with the above-mentioned increase in the temperature in the detonation front. Other factors leading to such a significant increase in condensed nanoparticles require further study. It should be noted that a size of ~ 70 nm is the upper limit of our experimental setting, thus the final particle size may be larger. The presence of large particles in the products of BTF detonation has been noted earlier.

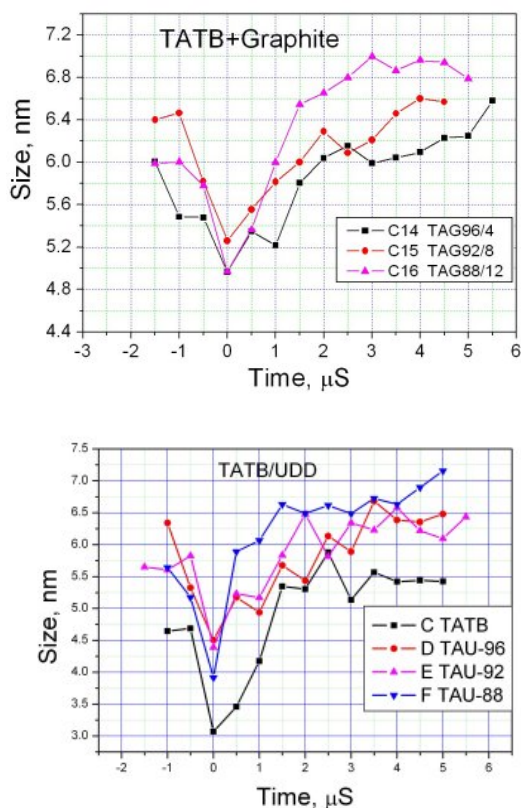


Fig. 6.2.1. Variation in the size of condensed-carbon nanoparticles at detonation of mixtures of TATB with additives of graphite (above) and UDD (below). TAG96/4 denotes a mixture of 96% of TATB and 4% of graphite by weight.

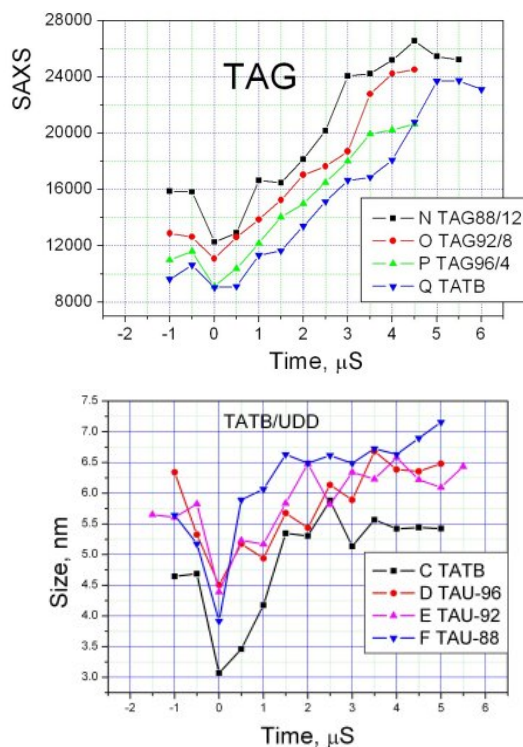


Fig. 6.2.2. Integrated SAXS vs. time for mixtures of TATB/graphite (above) and TATB/UDD (below). The zero time corresponds to the passage of the detonation front.

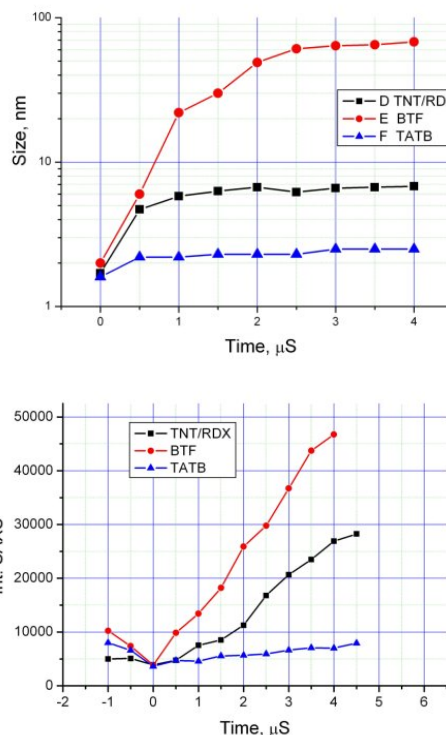


Fig. 6.2.3. Data on the growth of the size of condensed nanoparticles at detonation of TATB, TG50/50, and BTF.

6.2.2. Station "LIGA-technology and X-ray lithography"

The station is intended for experiments on X-ray lithography in thick resistive layers for production of microstructures, including X-ray masks.

Participating organizations:

Budker Institute of Nuclear Physics SB RAS, Novosibirsk; Institute of Cytology and Genetics SB RAS, Novosibirsk; Institute of Solid State Chemistry and Mechanochemistry SB RAS, Novosibirsk; Institute of Automation and Electrometry SB RAS, Novosibirsk; Vorozhtsov Institute of Organic Chemistry SB RAS, Novosibirsk.

In 2011, the work was carried out with the financial support under the following projects: SB RAS interdisciplinary integration project № 55 "X-ray LIGA technology for synthesis of 3D diffraction structures"; state contract № 16.513.11.3135 dated October 21, 2011 "Development of an experimental model of new-generation bioanalytical complex based on micro/nano fluid systems"; and State contact № OK-12-R-VK/2011 dated August 29, 2011 "X-ray microlithographer".

Within the framework of State contact OK-12-R-VK/2011 dated August 29, 2011, the equipment and software of the station "LIGA" was upgraded for the implementation of the X-ray microlithographer.

Examples of work

Development of technology for synthesis of 3D optical structures

A fundamentally new method of production of 3D microstructured structure-selective metal film grid elements for the IR and THz ranges was developed and implemented. It is based on a combination of formation of microstructures in thick polymer films (10-1000 μm) by means of X-ray lithography and chemical deposition of metallic silver on the entire surface of the polymer.

Deep X-ray lithography with sample scanning with a pattern in SR beam was used for creation of through microstructures in mylar films 10 microns thick and 40x40 mm PMMA sheets 1 mm thick. They at ISSCM SB RAS conducted chemical deposition of silver from a solution on a three-dimensional surface of a PMMA grid structure (Fig.6.2.4). So produced three-dimensional metallized films were tested as terahertz radiation filters. These three-dimensional films turned out to have properties close to those of thick metal grids and be an example of a new type of optical elements.

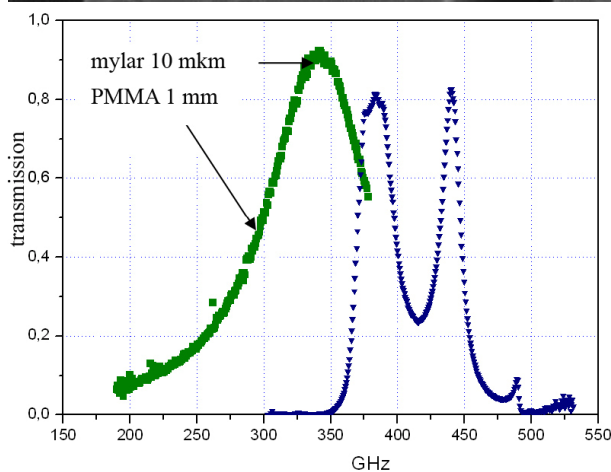
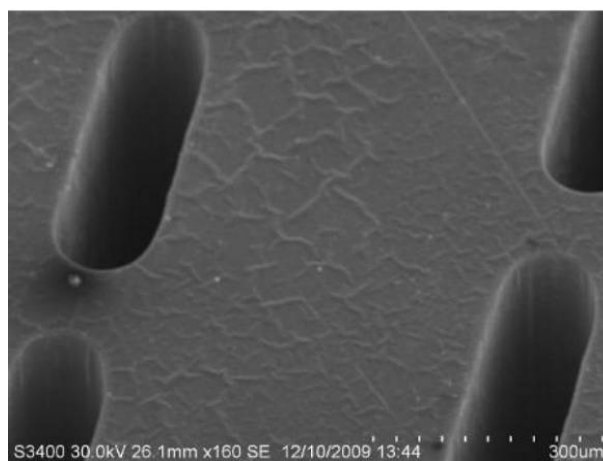


Fig. 6.2.4. Above: 3D silver film grid filters for terahertz radiation on a PMMA microstructured substrate 1 mm thick. Below: measured spectral dependence of the pass-band of these filters. LIGA master molds for replication of intraocular diffractive refractive lenses.

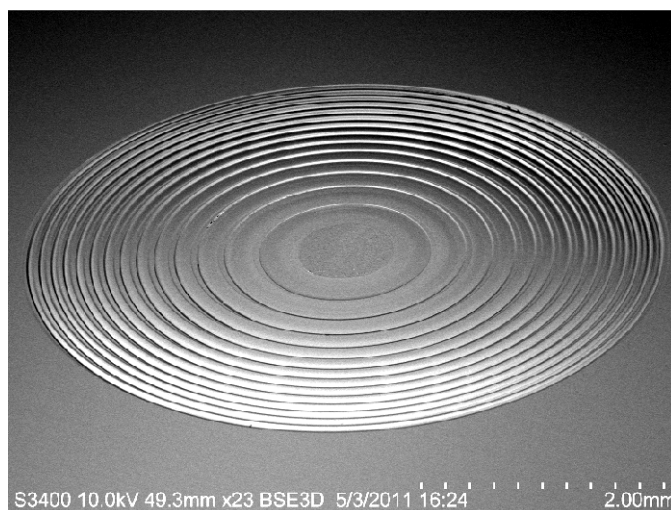


Fig. 6.2.5 SEM photo of an X-ray lithography replica in PMMA. The depth of the relief structures is 5 to 25 microns. The thickness of the solid resistive PMMA layer on a silicon substrate is 50 microns.

An important application area in diffractive optics is the formation of metal microstructure matrices for replication of polymer diffractive elements. Bifocal diffractive refracting intraocular lenses are an example of diffractive elements in demand. A joint project with the IAE SB RAS was aimed at the development of lithographic techniques of making microstructured relief surfaces of optical quality and the processes of formation of master molds for replication of lenses. In 2011, BINP was developing the following LIGA technologies: X-ray lithography and electro-nickel plating—for replication of relief microstructures of intraocular lenses.

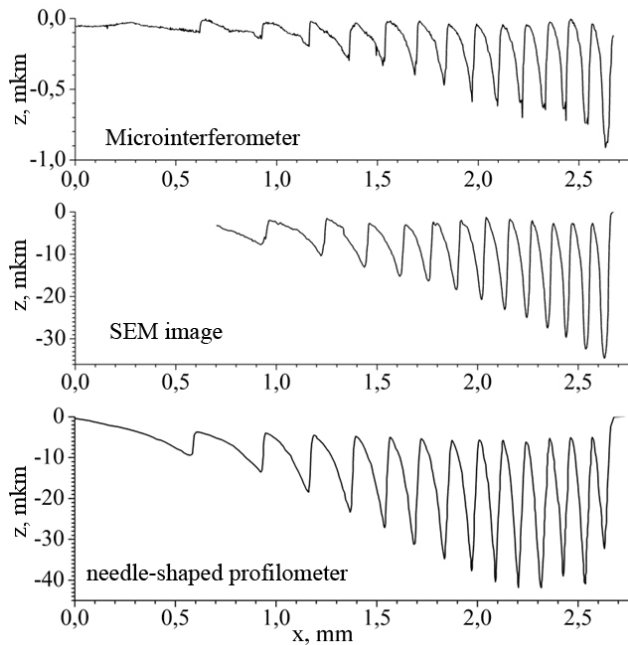


Fig. 6.2.6. Radial profiles of different replicas made using axisymmetric rotation under X-rays and measured by different methods.

3D continuous optical surfaces with smooth-wall microrelief were obtained for the first time by means of dynamic axisymmetric lithography in a quasi-solid PMMA layer formed of 950PMMA resist with a narrow distribution of molecular weights, in contrast to a sheet polymer. The X-ray lithography replicas presented in Fig.6.2.5 and Fig.6.2.6 were made via rotation of a substrate relative to a mask, the axis of rotation being adjusted. In so doing, in the radial coordinates the resist gets a dose D proportional to the angle φ of the arc in the transparent zone of the mask, with a coefficient determined by equation (6.2)1, and the profile depth z is determined by function (6.2)2 of the rate of development of the polymer layer ν , which is measured as a characteristic one for PMMA resist, in the form of equation (6.2)3, and the time of development τ .

$$D(r) = k\varphi(r)$$

$$k = It \cdot \iint \prod e^{-\mu_i(\lambda)d_i} \cdot \mu(\lambda)e^{-\mu(\lambda)z} d\lambda dz \quad (6.2)1$$

where It is the exposure dose, involving parameters of the synchrotron radiation source and exposure time; $\mu_i(\lambda)$ and $\mu(\lambda)$ are tabulated spectral linear absorption coefficients of the materials and media with a thickness d_i located in the SR beam before and after the resist layer, respectively; z is the coordinate directed into the resist.

$$z(r) = \nu\tau = \tau Ak\varphi^B \quad (6.2)2$$

where A and B are empirical constants,

$$\nu = AD^B \quad (6.2)3$$

Both the characteristic parameters of PMMA and profiles of the replicas made by the method of dynamic axially symmetric X-ray lithography were measured with varying doses and times of exposure. Thus, a basic function of process parameters was developed for simulation and design of any profile of relief lenses, including multifocal intraocular ones.

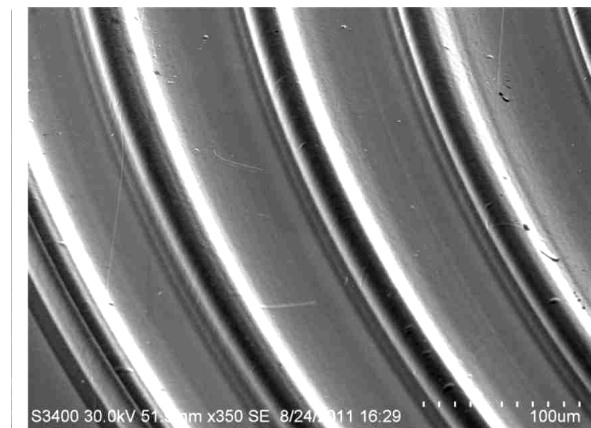
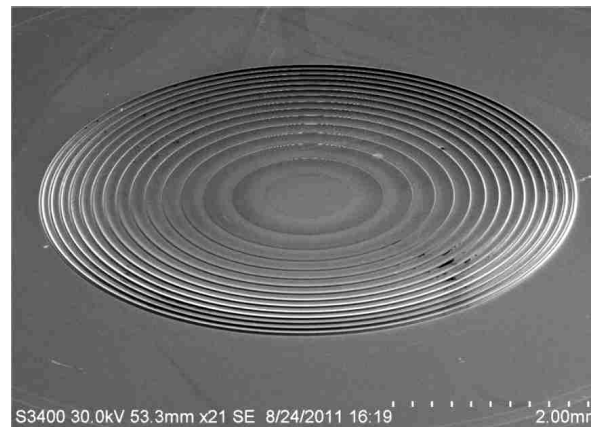


Fig. 6.2.7 Nickel galvanic master mold for replication of polymeric intraocular lenses (right: relief surface at high magnification of the scanning electron microscope).

Since forming is a mass-tech method of manufacture of polymer products, a galvanic bath for nickelizing of X-ray lithography replicas and production of nickel forms was designed and fabricated. The electroforming process was optimized as to the current density and design of the anode and cathode for manufacturing thick flat nickel forms with minimal internal stresses at an average nickel deposition rate of about 1 $\mu\text{m}/\text{min}$. Thanks to the weak adhesion of the gold electroplated substrate to polymers, a polymer replica can be easily separated from the nickel mold. The nickel mold surface, also of gold, simplifies the process of separation of polymer product (Fig.6.2.7).

The made replicas of PMMA and nickel relief lenses have the quality of optically clean surfaces with a roughness $R_a = 10 \div 30 \text{ nm}$ (Fig.6.2.8).

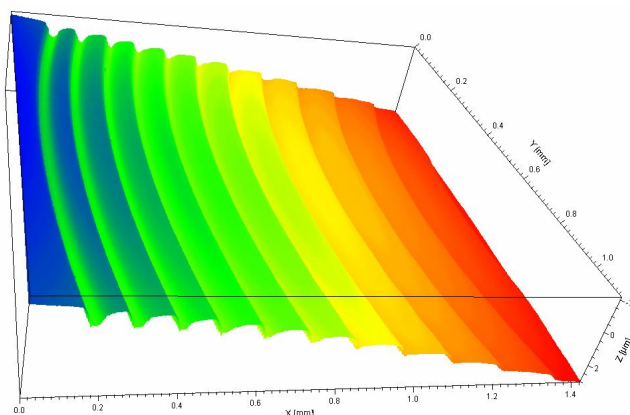


Fig. 6.2.8 Nickel mold surface for relief lens, scanned with the WLI microinterferometer. The surface roughness measured as the mean square deviation of the profile is about 10 nm.

6.2.3. Stations "Anomalous Scattering" and "Precision Diffraction"

The station "Anomalous scattering" is intended for precision studies of the structure of polycrystalline materials by the methods of X-ray diffractometry with high angular resolution.

Experiments performed:

Mesostructured materials;

Oxygen-conducting materials based on strontium cobaltites;

Oxygen-accumulating materials based on cobaltites of rare earth metals;

Catalysts for carbon-dioxide conversion of methane on the basis of Fe_3Al intermetallides;

Catalysts based on nanosized gold.

The station "Precision diffraction" is intended for studies of changes in the structure of polycrystalline materials under effect of high temperature and reacting media by the methods of time-resolved X-ray diffraction.

Materials studied:

Oxygen-conducting materials based on strontium cobaltites;

Oxygen-accumulating materials based on cobaltites of rare earth metals;

Catalysts for carbon-dioxide conversion of methane on the basis of Fe_3Al intermetallides;

Selective adsorbents of ammonia;

Cobalt-containing catalysts for the Fischer-Tropsch processes;

Iron-cobalt catalysts for synthesis of multiwalled carbon nanotubes;

Copper-nickel catalysts for synthesis of nitrogen-containing carbon nanofibers.

Participating organizations:

Boreskov Institute of Catalysis SB RAS; Nikolaev

Institute of Inorganic Chemistry SB RAS; Institute of

Solid State Chemistry and Mechanochemistry SB RAS;

Tomsk Polytechnic University.

Some studies were conducted with a complex of methods involving experiments at both stations. For example, catalysts for carbon-dioxide conversion of methane on the basis of intermetallides of nickel-aluminum and iron-aluminum were studied at the station "Anomalous Scattering" before and after the reactions, whereas *in situ* experiments on changes in the phase composition and structure of catalysts under reaction conditions were carried out at the station "Precision Diffraction". Iron-cobalt catalysts for synthesis of carbon nanotubes were subjected to a similar study.

Examples of works performed

Selective sorbents of ammonia

Development of absorption refrigeration machines with ammonia as the working fluid is a promising direction in energy-efficient technology. The operating temperature range, efficiency, and output of ammonia absorption refrigerating machines are directly dependent on the choice of sorbent. The perfect ammonia sorbent should have a low reactivation temperature, high dynamic capacity in a given range of temperatures and pressures, and thermal and mechanical stability. Traditional adsorbents (activated carbons and carbon fibers) and chemisorbents of ammonia (inorganic salts) do not meet both these requirements and therefore may not be the best option for any specific application of absorption refrigerating machines. In this connection synthesis of new sorption materials with properties that provide the most efficient operation of refrigeration units is a pressing task. "Salt in a porous matrix" composites (SPMC) are promising materials for use in absorption refrigerating machines since the use of inorganic salt gives the principal possibility of creating a material of high sorption capacity and low temperature of reactivation, whereas the porous matrix prevents aggregation of the salt in the process of ammonia absorption and helps to improve the sorption dynamics.

They at Boreskov Institute of Catalysis SB RAS have for a long time worked on the exploration of selective sorbents of water on the basis of alkaline-earth metal chlorides in a porous matrix. Since the physical characteristics of molecules of ammonia NH_3 and water H_2O are similar, it was suggested to use chlorides of calcium, strontium and barium to create SPMC for absorption of ammonia.

It is known from literature that chlorides of alkaline-earth metals absorb ammonia to form complexes of one, two, four and eight ammonias. As regards composite absorbers of water and methanol vapor, there is a known effect of changing sorption properties of the salt when it is placed into the pores of matrix. So, the influence of the carrier matrix on the sorption properties of the salt is likely to show in reactions with ammonia. Consequently, the sorption equilibrium of SPMC with ammonia requires a detailed study not only with absorption and thermodynamic methods but with structural ones too.

SPMC were studied by the X-ray diffraction methods on synchrotron radiation at the station "Precision diffractometry" with the use of the one-coordinate detector OD-3M-350 and X-ray reactor cell XRK-900 made by Anton Paar, Austria. The reactor cell allows X-ray measurements of sample in a reaction medium in the range from room temperature to 900°C and pressures from 10^{-2} mbar to 10 bar. Fig.6.2.9 presents the results of the experiment on changes in the phase composition of calcium chloride in a $\gamma\text{-Al}_2\text{O}_3$ porous matrix. The absorption was performed at a pressure of 1.6 bar and room temperature, and desorption at $T=100^\circ\text{C}$ and atmospheric pressure. It can be seen that in the course of absorption and desorption the system goes through a series of reversible reactions. During the reaction, there was registered a short-lived phase of a complex of four ammonias. This has not been registered earlier with X-rays.

The experiment was also carried out with barium chloride in various matrices. At a pressure of ammonia of ~ 5 bar, a $\text{BaCl}_2 \cdot 8\text{NH}_3$ phase of unknown structure was registered. Fig.6.2.10 presents X-ray photographs of barium chloride sample on vermiculite under normal conditions and in ammonia under pressure. The structure of the complex is being found out now.

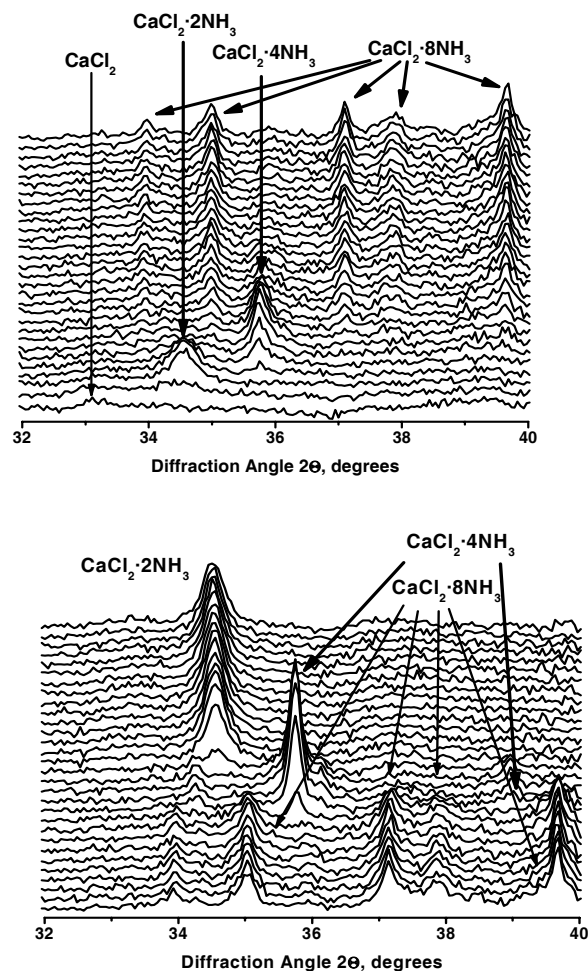


Fig. 6.2.9 Change in the phase composition of calcium chloride in the course of absorption (above) and desorption (below) of ammonia.

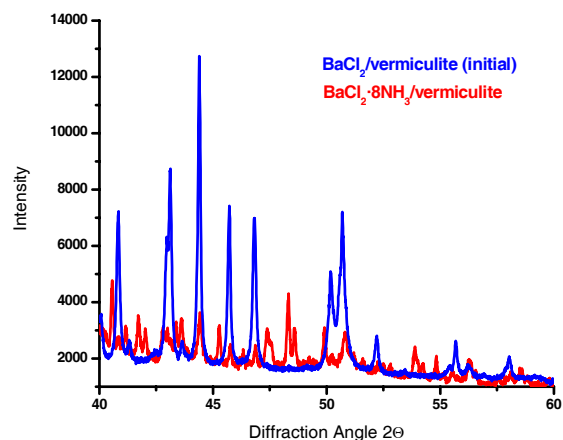


Fig. 6.2.10. X-ray photographs of barium chloride on vermiculite under normal conditions (blue) and at a pressure of ammonia of about 5 bar (red).

Cobalt-containing catalysts for the Fischer-Tropsch processes

Catalytic synthesis of olefins (double-bond hydrocarbons), liquid hydrocarbons, and ceresins (hydrocarbons with long branched chains) from hydrogen-enriched synthesis gas (a mixture of hydrogen and carbon monoxide in different proportions) produced from natural and associated gas is most effective with cobalt-containing catalysts. This work was aimed at the study of how the preparation method effects the anion composition and structure of hydroxide precursors of Co-Al catalysts and their catalytic properties in the Fischer-Tropsch synthesis reactions. The dynamics of changes in the composition and structure of hydroxide precursors of Co-Al catalysts in the processes of heat treatment and subsequent activation by various physicochemical methods, including X-ray diffraction *in situ* with the use of synchrotron radiation, were studied. Precursor compounds that were obtained by deposition of cobalt cations on γ - and δ -Al₂O₃ at conditions of hydrolysis of urea, have a structure of the hydroxalcite type and contain nitrate, carbonate and hydroxyl groups were shown to transform under heat treatment in an inert environment into oxide compounds of the spinel structure, Co_{3-x}Al_xO₄ (0 < x < 2). Hydrogen activation of oxide precursor leads to formation of particles of metallic cobalt through the intermediate formation of cobalt(II)-aluminum oxide phase. High activity and selectivity for C5+ hydrocarbons in the reactions of the Fischer-Tropsch synthesis is typical to this catalyst.

The X-ray diffraction study was carried out at the station "Precision Diffractometry". It reproduces all the main stages of preparation and activation of catalyst, except for the stage of deposition from solutions and the Fischer-Tropsch reaction itself. It was necessary to obtain particles of metallic cobalt or cobalt-aluminum alloy of 5 nm or less to provide large specific surface area of the active component of catalyst. The heating of the precursor in an inert atmosphere and the temperature increase during the reduction of cobalt from oxide were carried out slowly, at a rate of 2°C/min or less. In the course of the heating, there arose and disappeared an intermediate phase of unknown composition. In the resulting series of X-ray patterns one can see how the phase composition of the precursor changes during the heating to 250 °C in the inert atmosphere and with subsequent reduction in the atmosphere of pure hydrogen with temperature increasing from the room one to 650°C. There are observed intermediate phases of cobalt-aluminum oxides (Al)Co₃O₄ and CoO, as well as the final metal state of cobalt-aluminum nanoparticles.

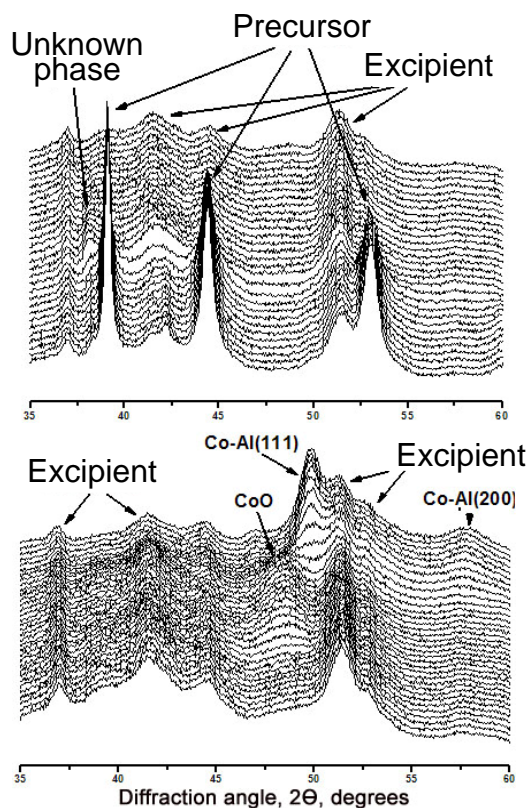


Fig. 6.2.11. X-ray patterns of the aluminum-cobalt catalyst during the activation process in the inert atmosphere (above) and reduction in hydrogen (below).

Ascertainment of the composition–structure–oxygen conductivity relationship in the class of cobaltites RBaCo₄O_{7+δ} (R=Y, Dy-Lu, δ=0, δ~1.5)

Compounds RBaCo₄O_{7+δ} (R=Y, Dy-Lu) have a unique ability to absorb and release oxygen. With their hexagonal close-packed structure, these oxides can absorb and release up to 1.5 formula units of oxygen at a relatively low temperature (300 to 400°C). Little is known on the structural changes occurring at their oxygen saturation. The only experimental determination of the structure was carried out by the results of exposure of YBaCo₄O_{8.1} to high-resolution neutron and synchrotron radiation. It was shown that, entering the structure, extra oxygen ions associate with cobalt ions. As a result, half of cobalt ions in triangular layers acquire octahedral coordination, and there arise zigzag chains of cobalt octahedra and tetrahedrons that remain from the previous structure. It is not known yet if the proposed structure model will fit cobaltites with rare-earth cations of other sizes Yb and Lu and fully oxygenated compounds.

They at the Institute of Inorganic Chemistry SB RAS have synthesized polycrystalline samples of RBaCo₄O_{7+δ} and maximumally saturated them with oxygen using a special technique and developed a technique of equilibrium saturation with oxygen. Judging by preliminary X-ray examinations, structural changes in rare earth elements of different sizes at sorption/desorption of oxygen may run in different ways.

To solve the task set it was necessary to study *ex situ* and *in situ* the structural transformation of oxygenated polycrystalline samples $\text{RBaCo}_4\text{O}_{7+\delta}$ (R=Y, Dy, Lu) with rare earth cations of different sizes at heating in air by the diffraction method with SR application.

It was found that the nature of structural changes at oxygen saturation is strongly dependent on the size of the rare-earth ion. In a compound with $\text{YBaCo}_4\text{O}_{7+\delta}$ the transition between the phases with $x=0$ and $x=1.4-1.5$ occurs abruptly, the structural symmetry changing from orthorhombic to hexagonal. Whereas in $\text{LuBaCo}_4\text{O}_{7+\delta}$ the transformation goes through an intermediate phase and does not lead to a change in the symmetry of the structure, and the unit cell parameters vary in directions that are opposite to those observed for the yttrium sample.

Fig.6.2.12 presents X-ray patterns of the $\text{YBaCo}_4\text{O}_{7+\delta}$ (a) and $\text{LuBaCo}_4\text{O}_{7+\delta}$ (b) samples under heating from room temperature to 500°C.

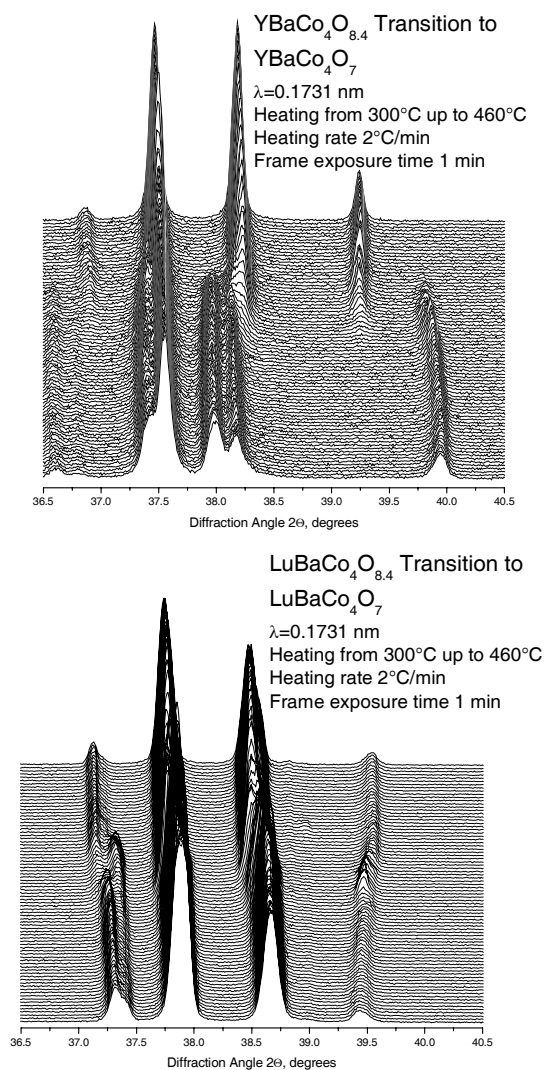


Fig. 6.2.12. Fragments of X-ray patterns of the $\text{YBaCo}_4\text{O}_{7+\delta}$ and $\text{LuBaCo}_4\text{O}_{7+\delta}$ samples during heating. Phase transition caused by the loss of oxygen.

Change in the phase composition of the Ni-Cu catalyst at growth of nitrogen-containing carbon nanofibers

Selective synthesis of carbon nanotubes (CNT) and nanofibers (CNF) of a given structure type and certain physical and chemical properties is an important area of nanotechnology in relation to a wide range of possible practical applications of such materials to chemistry, materials science, nanoelectronics, medicine, etc. Particular attention is paid to fine regulation of physical and chemical properties of carbon composites for purposeful synthesis of functional materials with desired characteristics. Modification of the carbon structure with heteroatoms (N, B, F, and Si) or decoration of carbon material with metals (Pt, Pd, Fe, Co, Ti, etc) is among the possible approaches.

Among the various methods of synthesis of nitrogen-containing carbon nanotubes (N-CNT) and nanofibers (N-CNF) (arc, laser ablation, and substitution of carbon atoms in the initial materials), the catalytic method is of a special interest, because of the relatively low temperature of the process and cost of the product, as well as its availability for large-scale production. Decomposition of carbon-containing compounds is performed with metals of the iron subgroup (Fe, Co, Ni) and their alloys as catalysts.

Now there is a conventional model of the formation of CNT and CNF on metal catalysts. It includes the following main steps: (1) decomposition of precursor molecules on the catalyst surface with formation of adsorbed carbon atoms, (2) diffusion of carbon atoms through a catalyst particle, and (3) formation of a nucleus and growth of a carbon tube or fiber.

There remains a rather ambiguous issue of the state of carbon on the surface of the catalyst particle and in the structure of the metal during the diffusion of carbon from the faces on which the decomposition of the precursor molecules occurs to the places of segregation of carbon atoms. It has been supposed that dissolution of carbon atoms in the volume of the catalyst particle is accompanied by formation of carbide. On the other hand, several studies have questioned the participation of carbides in the synthesis of CNF, assuming that the decomposition of carbon-containing precursors is accompanied by dissolution of carbon in the metal particle without formation of carbide.

Changes in the Ni-Cu catalyst in the course of decomposition of the $\text{C}_2\text{H}_4/\text{NH}_3$ mixture have been investigated *ex situ* earlier. It was shown that formation of N-CNF on the catalyst particle goes through the stage of formation of a supersaturated solid solution of carbon and nitrogen in a nickel-enriched alloy « $\text{NiCu}_x\text{C}_y\text{N}_z$ », which results in the lattice parameter of the alloy increasing to abnormally high values $a=0.3616 - 0.3706$ nm without destruction of its cubic structure. It is important that the formation of the « $\text{NiCu}_x\text{C}_y\text{N}_z$ » phase and its presence in

the system lasts for a period that is optimal for the synthesis for production of N-CNF with maximum nitrogen content in the material and maximum values of texture parameters.

This work was the first *in situ* study of the change in the state of Ni-Cu catalyst during the growth of N-CNF at decomposition of ethylene-ammonia mixture.

The phase composition of the initial Ni-Cu catalyst is represented by two metallic phases—a nickel-based alloy $\text{Ni}_{0.87}\text{Cu}_{0.13}$ ($a = 0.3536 \pm 0.0003$ nm) and copper-based alloy $\text{Cu}_{0.93}\text{Ni}_{0.07}$ ($a = 0.3609 \pm 0.0003$ nm). While the catalyst is being heated up to 550°C in the reactor cell in stream of hydrogen, the reflections shift towards smaller angles due to thermal expansion. No other changes in the state of the catalyst are observed at this stage of the experiment.

Significant changes in the structure of the Ni-Cu catalyst after decomposition of the $75\%\text{CH}_4/25\%\text{NH}_3$ mixture were observed earlier with the application of *ex situ* XFA. With the reaction going for 15 minutes, no maximums corresponding to the Ni-enriched alloy were detected. At the same time, in the X-ray patterns there was observed formation of a phase with an increased fcc lattice parameter $a = 0.3621 \div 0.3628$ nm, which exceeds the lattice parameter of pure copper ($a_{\text{Cu}} = 0.3615$ nm (ICDD PDF-2 #4-836) by an amount $\Delta a = 0.0006 \div 0.0013$ nm. The use of the anomalous scattering effect in addition to the usual method of X-ray diffractometry revealed that the phase with the increased fcc lattice parameter is nickel-based alloy « $\text{NiCu}_x\text{C}_y\text{N}_z$ », which forms at the initial stage of the reaction and exists for 15 minutes to 3 hours, depending on the temperature of the process. It was also noted that the Cu-enriched phase undergoes significant changes eventually.

Fig.6.2.13 (above) shows diffraction patterns of the Ni-Cu catalyst, which were produced *in situ* in the course of decomposition of the $75\%\text{C}_2\text{H}_4/25\%\text{NH}_3$ mixture at 550°C in the high-temperature X-ray reactor cell. From the first minutes of the reaction, there is observed a shift of the reflection relating to the Ni-enriched alloy towards smaller angles. The alloy lattice parameter increases, respectively. Over a period of 15 minutes of the reaction, the parameter raises from 0.3567 nm to 0.3585 nm. The position of the reflection related to the Cu-enriched alloy, in turn, does not change during the reaction. It is known that increase in the lattice parameter of a metal catalyst with growth of carbon materials is associated with the dissolution of carbon in the catalyst particle. In this case, on the basis of reference data, an increase in the lattice parameter by 0.0018 nm corresponds to a dissolution of ~ 2.5 at.% C.

With the cooling of the reactor cell in the stream of the reaction mixture, in the zone of 550 to 460°C the reflection of the Ni-enriched alloy continues shifting towards smaller angles, Fig.6.2.13 (below). This may be due to the ongoing saturation of the catalyst particles with

carbon and nitrogen. At a temperature of 460 to 440°C , there is a significant change in the diffraction pattern—one more reflection, with a parameter of ~ 0.3635 , nm can be seen in the X-ray pattern. With further cooling of the catalyst, its phase composition is no longer changing.

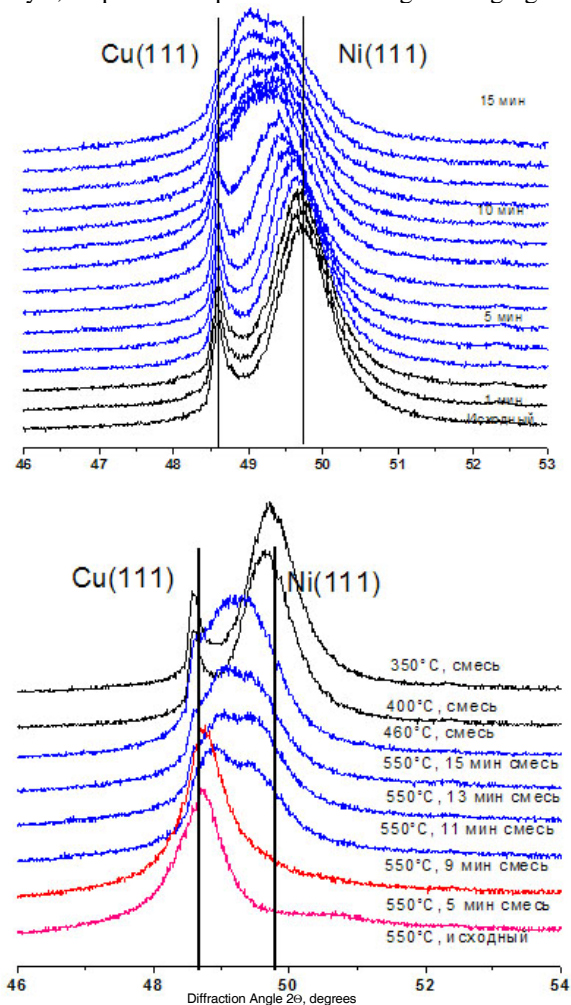


Fig. 6.2.13. Variation in the state of the Ni-Cu catalyst under the reaction conditions (above) and in the course of the cooling (below).

This experiment allows one to accurately determine the state of the Ni-Cu catalyst in the growth of N-CNF during the decomposition of the ethylene-ammonia mixture. When the reaction goes at 550°C , the catalyst is a two-phase system similar to the original state: Ni-enriched alloy and Cu-enriched alloy. In the course of reaction, carbon is being dissolved in the Ni-enriched alloy, the lattice parameter of the alloy simultaneously increasing by 0.018 Å. The Cu-enriched alloy seems to be not involved in the reaction since the reflections related to this phase remain unchanged during the process. This state of the catalyst remains at cooling in the stream of the reaction mixture to 440 – 460°C . There is an abrupt change in the state of the catalyst at a temperature of 440 – 460°C . It is still biphasic, but the Ni-enriched phase changes its

parameter a lot because of the anomalous absorption of carbon and nitrogen, and the reflections of this phase completely overlap the reflections present in the sample of the phase initially enriched with Cu. This new state of the catalyst, denoted as the «NiCu_xC_yN_z» phase, has a lattice parameter of 0.3635 nm, which is by 0.020 nm higher than the lattice parameter of pure Cu (0.3615 nm at this temperature). This significant increase in the parameter indicates that at this temperature, a large amount of carbon is being dissolved (> 15 at.%C). The data obtained allow one to conclude that the formation of carbon nanofibers during the decomposition of ethylene/ammonia mixture goes through the stage of carbon dissolution in the catalyst particle, but without formation of metal carbide.

Study of the active component of the Fe-Co catalysts for growth of multiwalled carbon nanotubes

In this case they used FeCo/CaCO₃ catalysts, with the active ingredient based on iron and/or cobalt and calcium carbonate as a carrier that were obtained by the Pechini method. The FeCo/CaCO₃ catalyst allows production of multiwall carbon nanotubes (MCNT) with an average diameter of 22 nm, a yield of more than 20 g/g of the catalyst in 30 minutes of synthesis at a temperature of 670 °C and a low content of impurities of amorphous carbon and metals.

Experimental data allow one to interpret the phase composition of the initial catalyst as a mixture of fine phases (8-10 nm from analysis of the coherent scattering area (CSA)) of calcium carbonate (in the lime form) and spinel-structure iron&calcium/cobalt oxides. When the catalyst is being heated (30 °C per minute) in a nitrogen stream (99% purity, 1.5 mL/sec), the interplanar distances are increasing due to the thermal expansion. At T~600 °C, calcium carbonate decomposes to calcium oxide. When the sample is hold at a temperature of 670 °C, there is observed a further change in the phase composition of the catalyst. With this method of catalyst preparation (polymerized complex precursors), there remains amorphous carbon in the volume of catalyst, and this amorphous carbon is able to reduce oxides of the metal. In addition, at this temperature, the system starts being agglomerated. Upon comparison of the experimental diffraction pattern of the catalyst heated up to 670 °C and kept at this temperature for 10 minutes with theoretical diffraction patterns at normal temperature, a conclusion was made that the system consists of a mixture of oxides of different types based on iron, calcium and cobalt of various composition. It should be noted that the agglomeration starts at temperatures below the temperature of the reaction (the oxide phase CSA size calculated from corresponding reflections is 25-30 nm, and that of the metal phase is about 50 nm).

Upon the hold-up of the catalyst, feeding of ethylene was started. The growth of carbon nanotubes leads to a

sharp increase in the volume of the system and displacement of the sample surface with respect to the X-ray beam, which results in a drastic distortion of the pattern and reduction in the intensity of the signals. Therefore diffraction patterns obtained before the sharp decrease in the background line were the most informative.

With the feeding of ethylene the researchers observed a further reduction of iron and cobalt oxides and formation of Fe-Co alloy. A detailed analysis of the peaks of the metal alloy, iron and cobalt oxide, and calcium oxide lets one to assert that there is no intermediate phases in the transition from the Co-Fe oxides to the metal alloy as the increase in the content of the reduced metals in the system stops almost simultaneously with the end of reduction of the metal oxides. The observed slight increase in the metal content may be due to the agglomeration of small metal particles unobservable because of instrumental limitations.

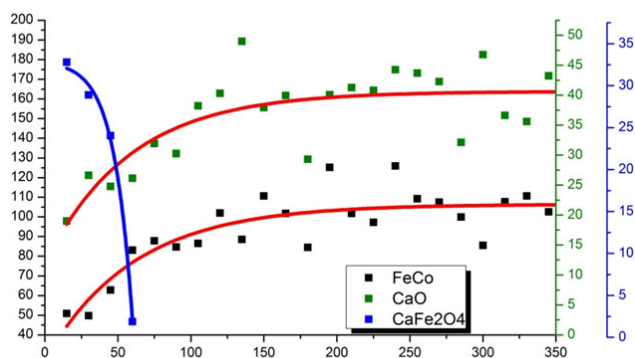


Fig. 6.2.14. Variation in the phase composition of the catalyst for synthesis of MCNT in the course of the reaction.

Complete reduction of the cobalt oxides is evidenced by the formation of alloy particles. Cobalt may be present either in a pure form (there are peaks typical to a face-centered lattice of cobalt) or in an alloyed form. Diffraction patterns of pure iron and an alloy particle can be distinguished only by the lattice parameter, which is distorted because of the high temperature, but the absence of cobalt reflections is sufficient for confirmation of the alloy particle existence. In addition, the alloy peaks gradually shift towards smaller angles (i.e. larger lattice parameters), which can be interpreted as saturation of the metal particle with carbon, in agreement with most today's theoretical mechanisms of growth of carbon nanotubes. The subsequent drop in the saturation of the metals (decrease in the lattice parameter of the alloy) may be interpreted as encapsulation of most metal particles because there are no changes in the average size and relative content of the particles.

To verify the idea of encapsulation of the metal, it was decided to raise the ethylene content in the reaction mixture up to 50% and hence increase the supersaturation of the metal particles and reduce the radius of the critical nucleus of carbon nanotube. No diminution in the alloy lattice parameter was observed, which may confirm the hypothesis formulated above.

Thus, we can assert that the reduction processes (and hence the subsequent agglomeration) of the alloy and its saturation (and supersaturation) with carbon go in parallel, and the ratio of their speeds can affect the final distribution of nanotubes by diameter. Moreover, the ratio of the specific quantities of carbon required for triggering a sharp increase in the volume corresponds approximately to the square root of the ethylene pressure ratio in these experiments. This fact suggests that the experiments are performed beyond the diffusion regions of reduction of the metal and decomposition of ethylene on its surface.

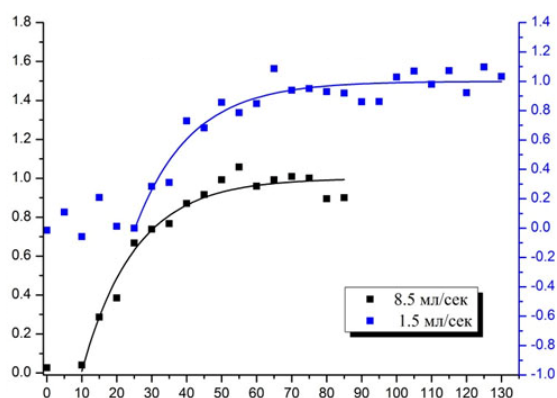


Fig. 6.2.15. Dynamics of reduction of the alloy at different flow rates of ethylene.

6.2.4 Station "X-ray fluorescence elemental analysis"

The station is intended for determination of the elemental composition of samples of various origin (geological rocks, biological tissues, aerosols, etc.) by the method of X-ray spectral fluorescence elemental analysis using synchrotron radiation (SR XFA). The elemental analysis can be performed both in a local mode and in a scanning one.

Participating organizations:

Nikolaev Institute of Inorganic Chemistry SB RAS, Novosibirsk; Sobolev Institute of Geology and Mineralogy SB RAS, Novosibirsk; Institute of Chemical Kinetics and Combustion SB RAS, Novosibirsk; Budker Institute of Nuclear Physics, Novosibirsk; Limnological Institute, Irkutsk.

Topics of work in 2011:

Application of synchrotron radiation X-ray fluorescence analysis to the study of bottom sediments of proglacial lake for reconstruction of the dynamics of the glacier of Chersky mountain (the Baikal Mountains, Eastern Siberia) over the past 160 years

The dynamics of the glacier of Chersky mountain in the Baikal Mountains were reconstructed from the elemental composition of bottom sediments of proglacial lake Gitara. The scheme of the study area is shown in Fig.6.2.16. The X-ray fluorescence analysis was performed via continuous scanning of an undeformed wet core. The work was done with the use of the equipment of the shared-use SCSTR under state contract 16.552.11.7044. The dynamics of the glacier were determined from the level of terrigenous elements supply with melt water ice to the proglacial lake. We separate five episodes (~ 1880, 1905, 1918, 1950, and since 1968 to present) of major advances in the glacier over the past 160 years.

The purpose of this work was to reconstruct the response of the glaciers of Baikal area (on the example of the glacier of Chersky mountain) to climate variations over last 160 years from a detailed study of the elemental composition of the bottom sediments of proglacial lake Gitara. The records of this period include important climatic alterations, such as the transition from the little ice age (LIA) to the present warming (PW) and the beginning of active human influence on the global climate.

The elemental composition of the core was studied at the Siberian center of SR, with the use of X-ray spectral fluorescence analysis via total scanning of an undeformed wet core in beams of synchrotron radiation ("SR XFA scan") with increments of 1 mm. The SR XFA station is equipped with a special scanning device. A sample can be moved by a distance of up to 400 mm, normally to the incident monochromatic radiation (and the direction of detection of characteristic fluorescence radiation). The minimum scanning step is 0.1 mm. In addition, the software applied allows one to check the presence of SR beam and recollect the spectrum in case of re-storage of the electron beam in the ring. The mechanical precision of the scanner was tested with a displacement gage (Burleigh Instruments, Inc.) with a resolution of 0.1 microns. The scanner deviates the position of the sample displacement from the actual position recorded by the gage. It is clear that the deviation does not exceed 100 μm throughout the 200 mm scan interval. This accuracy is quite acceptable for paleoclimatic studies. The spectra were processed with the program AXIL. Concentrations of the rock-forming elements K, Ca, Ti, Mn, and Fe and rare and scattered elements Ni, Cu, Zn, As, Br, Rb, Sr, Y, Zr, Nb, Mo, Ba, La, and Ce were found. The water content in the sediment was determined by drying at 60 °C. The data were processed by the statistical method of factor analysis.

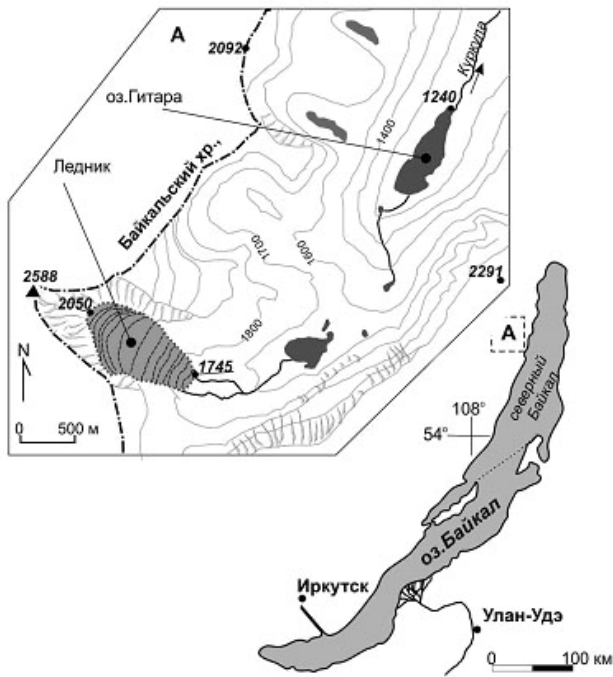


Fig. 6.2.16. Layout of the area of study.

The following main groups of elements that describe changes in the study area over the past 160 years can be marked out: the group reflecting the intensity of chemical weathering of the rocks and soils of the drainage basin of lake Gytara (Ca, Ti, V, Fe, Mn, Cu and Sr); the group associated with the organic autochthonous component of the lake (K, Br, and U); and the group marking the processes of physical weathering, in particular, surges of the glacier (Y, Th, Ga, Rb, Zr, Nb and the Rb/Sr ratio). The elemental composition variation along the core is shown in Fig.6.2.17.

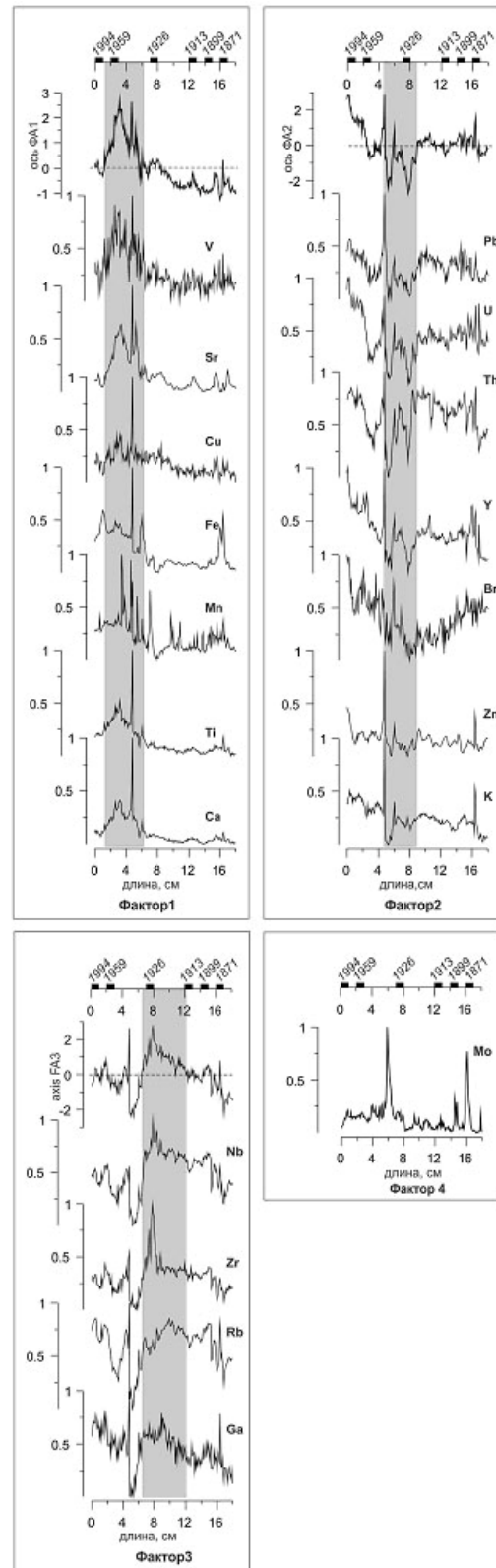


Fig. 6.2.17. Elemental composition variation along the core. The elements were grouped by the method of factor analysis (Factor 1-4). Gray rectangles: changes in the intensity of accumulation of the elements of each factor group. The element contents are given in normalized values between 0 and 1.

These data allow one to mark out five episodes when the glacier came into motion (~ 1880, 1905, 1918, 1950, and from 1968 to present) and the period of increasing intensity of chemical weathering of the drainage basin of the lake since 1930 to the present, with a peak around year 1960.

Distribution of chemical elements in the sediments of geothermal lakes in the caldera of volcano Uzon

In 2011, works were carried out under RFBR grant № 11-05-00655 and integration project №10.

A core of peat from Vydrinskoe bog was scanned for revealing horizons of abnormal concentrations of Zn and Cu for further study of the forms of compounds with S by means of electron microscope. These studies revealed clusters of micron-scale sulphides of Zn and Cu in peat horizons of 8000 to 11000 years (the early Holocene). Pelletes were subjected to SR XFA for interpretation of the absolute distribution of the elements of the K-Zr (Mo) group in the peat core and standard samples with the silicate and organic matrix (SBMP; SBMT).

Within the framework of integration project # 10, sediments of geothermal lakes of the caldera of volcano Uzon (Kamchatka) were sampled and scanned by the SR XFA method. The aim was to study the distribution of chemical elements by nuclear-geophysical methods, analyze the periodicities and reconstruct the paleoclimatic and physico-chemical conditions of formation.

The scanning was performed in 1 mm increments. The relative distribution of element concentrations in the sediment cores was determined. There are plans to analyze the samples by the method of atomic absorption in order to determine the absolute values of concentrations of the elements. The upper graph presents the distribution of the most pronounced chemical elements in the core of sediments of lake Vosmyoerka, obtained by SR XFA in 1 mm increments. The lower plot shows the distribution of As and Fe in a section of the sediment of the same interval, 1 mm increment, by SR XFA.

One can see that the relative concentration of the main elements (Sr, Y, Zr, and Mo) varies insignificantly throughout the study interval of the sediment core. Thus, one can hardly determine any changes in the physical and chemical conditions of formation of the sediment from the distribution of these elements in the sediment core, while the concentrations of As and Fe are continually changing, which can tell about variation in the physicochemical conditions of formation of the bottom sediments.

There are plans to perform statistical analysis of these data to identify patterns and periodicities, if any.

The works were carried out by members of the Institute of Geology and Mineralogy (IGM) SB RAS, Novosibirsk.

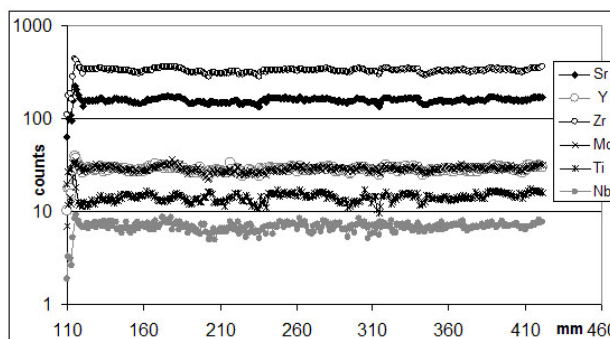


Fig.6.2.18

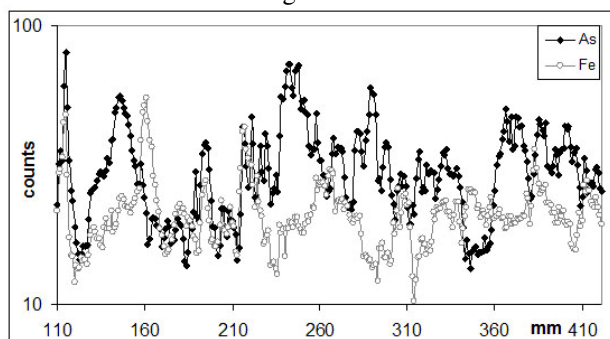


Fig. 6.2.19

6.2.5 Station "Diffractometry with hard X-rays"

Diffractometry in the hard X-rays. The station is intended for *in situ* diffraction studies at high pressures and high and low temperatures, as well as in the course of chemical reactions.

Participating organizations:

Institute of Solid State Chemistry and Mechanochemistry SB RAS, Institute of Geology and Mineralogy SB RAS, Institute of Inorganic Chemistry SB RAS, Institute of Catalysis SB RAS.

New equipment at the station:

A compact cell with a diaphragm actuator for pressurizing and resistive heating (DiaCell, England); the diameter of the working area of the anvils is 0.8 mm; the attainable parameters are 900 °C and 200 kbar. With the cell one can study minerals in conditions similar to those arising in the Earth's crust as deeply as 100 km.

The station was involved in the performance of the following integration and RFBR projects:

RFBR grant № 10-05-00483 "Structural evolution of Ca/Na zeolites and their microporous heterosilicate analogues at high pressure" (under the guidance of senior researcher of the Institute of Geology and Mineralogy SB RAS U.V. Seretkin);

RFBR grant № 11-05-01121 "Dynamics of lattice of microporous minerals at their interaction with aqueous medium at high pressure" (under the guidance of senior researcher of the Institute of Geology and Mineralogy SB RAS S.V. Goryainov)

SB RAS project on cooperation with outside organizations № 138 "Creating the fundamental principals of the effect of activation on the regulation of interaction of hard metals and their compounds with metal melts, aimed at creation of functional materials of a given structure and properties" (under the guidance of RAS member N.Z. Lyakhov).

Examples of the works:

1) *In situ* diffractometry (400°C, 20 kbar) of formation of a high-pressure water-containing phase (lawsonite) in the CaO-Al₂O₃-SiO₂-H₂O system

The method of diffraction survey was successfully tested in a high-pressure resistive-heating cell Helios DiaCell on the example of the study of the reaction "laumontite → lawsonite+quartz", which marks the transition from zeolite facies to the blue shale facies during metamorphism.

Lawsonite is one of few water silicates that are stable up to 1000 °C and 100 kbar and thus a probable carrier of water into the mantle. The reaction of its formation during decomposition of laumontite zeolite was first investigated *in situ* at 400 °C and 20 kbar, which corresponds to conditions of subduction wedge of the oceanic lithosphere. Powder diffraction measurements were carried out on the 4th SR beam line of VEPP-3 ($\lambda = 0.3685\text{\AA}$) with a detector image-plate MAR345. Fig.6.2.20. presents Debye patterns of the initial mineral laumontite (a) and products of its decomposition at 400°C and 20 kbar (b). The main phase here is lawsonite, and its texturing is clearly manifested in the lenticular shape of the Debye reflections.

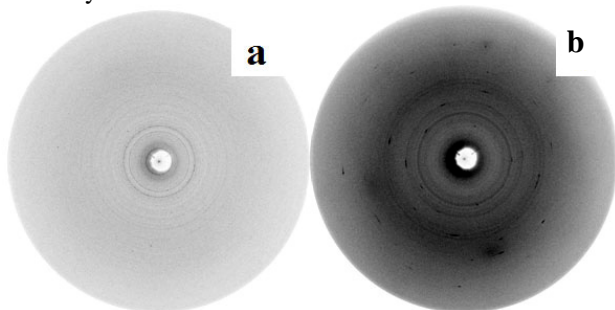


Fig. 2.6.20. Debye patterns of (a) laumontite at 0 kbar and (b) a mixture of phases resulting from its decomposition at 400°C and 20 kbar.

2) *Phase transition in natural (Mg, Fe)-cordierite at 45 kbar*

Powder diffraction measurements of natural cordierite compressed in an aqueous medium in a high-pressure chamber were performed with the aim of structural interpretation of the previously observed anomalous shifts in framework modes at a pressure of about 50 kbar. They found a twist at 44-50 kbar in the pressure dependence of the lattice parameters of cordierite (Fig.6.2.21), which confirms the presence of a phase transition. More precise determination of the

structure at 44 and 50 kbar indicates a redistribution of water molecules within the structural channels, apparently, due to the deformation of the channel-forming sixfold (Si,Al)O₄ tetrahedral rings. Since the total population of water positions is not increasing, the detected phase transition cannot be associated with hydration of the channels under the influence of the penetrating aquatic environment. The obtained structural data confirm the earlier findings of Raman spectroscopic studies that this transition marks a change in the compression mechanism from dominant shrinkage to deformation of framework structural units in ring silicates in the region of 50 kbar.

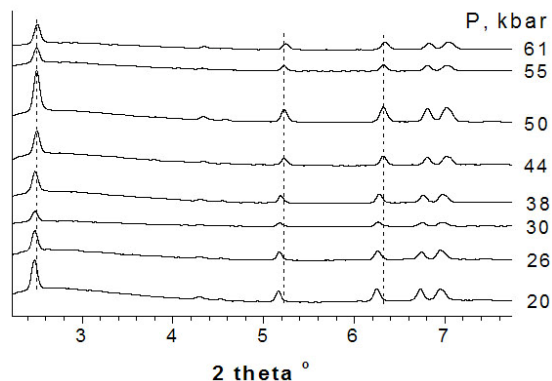


Fig. 6.2.21. Diffraction patterns of natural cordierite under compression in aquatic environment. The vertical dotted lines mark the position of the peaks at 44-50 kbar, where regular compression is violated due to the phase transition.

3) *Compressibility of natural stilbite and stellerite in aquatic environment*

The investigation of compressibility of natural zeolites stilbite and stellerite in water up to 60 kbar was aimed at the study of the effect of pressure-induced hydration on the elasticity of microporous aluminosilicates. The compression regularity violation associated with the hydration of the structure cavities is more clearly seen in stellerite, while not leading to phase transition. This distinguishes the behavior of these minerals from the previously studied group of fibrous zeolites, where superhydration results in significant structural deformation and volume surges.

In situ diffraction studies of interaction of copper with indium, tin and their eutectic alloy

The processes of interaction of solid and liquid metals are widely used in industry: soldering, welding, liquid-phase sintering, and mechanochemical alloying. Such interaction is often accompanied by formation of intermetallic compounds. There are two basic mechanisms of these processes. The first is diffusion, due to which atoms of one kind penetrate into a layer of another substance and chemical compounds arise in the boundary layer. The second mechanism is dissolution of the solid component or reaction product in the liquid

component and formation of crystallites either on the boundary between the solid and liquid phases or near the boundary of the liquid phase. Numerous researchers used different approaches to the study of the processes of chemical interaction of a massive solid metal with a metal melt. Most studies were conducted by microscopical methods on contact zone sections after cooling of sample. The aim of this study was to investigate the interaction on mechanocomposite powders. Mechanocomposites have large specific surface area, and their phase composition may be non-equilibrium.

At a temperature of 350 °C or less, the Cu-Sn system may contain four phases: solid copper-based solution; ϵ -phase, also denoted as the Cu_3Sn intermetallide; η -phase, also denoted as Cu_6Sn_5 intermetallide; and tin.

Mechanocomposites of copper with tin and copper with indium were prepared with different composition and time of mechanical activation. A preliminary analysis of diffraction patterns showed that mechanocomposites having 12 wt.% of tin and subjected to mechanical activation at 20g for 2 and 4 minutes consist of three phases: copper, tin, and η -bronze. One can assume that mechanocomposite particles are a copper nucleus covered with tin; η -phase formed at the interface between the copper and tin. Diffraction patterns from mechanocomposites of copper with tin and copper with indium subjected to mechanical activation at 60g for 20 minutes consisted of copper peaks, expanded and shifted towards small angles of diffraction. Thus, the sample was a metastable supersaturated solid solution of tin or indium in copper.

The test samples were prepared via co-rolling of mechanocomposite powder and tin foil. Tin is quite plastic and foil 50 microns thick can easily be rolled from it. A mechanocomposite powder portion of a weight resulting in a total composition corresponding to the ϵ -phase was evenly distributed inside a foil strip. After that, the foil was folded and spread flat between rollers to a thickness of 70-100 microns. Then, again, the foil was folded several times, and rolled to a thickness of 70-100 microns. The procedure was repeated 4-5 times. At the final stage, the resulting foil thickness was 50-70 microns. Samples to study were cut out of the foil. The samples were heated in two ways: (1) the temperature was raised to a temperature 5 °C below the melting temperature in the corresponding system and was maintained until the end of the interaction, (2) the temperature was raised rapidly to a temperature 5 °C above the melting temperature in the corresponding system and was maintained until the completion of the interaction.

At temperature below the temperature of liquid phase formation, the interaction in the copper-tin system can occur only via diffusion. Namely diffusion leads to the formation of the two phases (ϵ -phase and the η -phase) that can exist under these conditions. The diffusion mechanism is also corroborated by the form of the

diffraction patterns. Even rings and the absence of major reflections are also explained by diffusion processes during the formation of intermetallic compounds. One can see from the results of the diffraction studies that the formation of intermetallic compounds of copper and tin is much slower when a metastable solid solution of tin in copper is used. Tin atoms, replacing the copper atoms in the crystal lattice, distort it. This results in a slower movement of the vacancies and, hence, reduces the rate of diffusion.

The processes of interaction of the copper-based mechanocomposites with liquid tin are almost identical, which may be explained by the fact that the reaction product— η -phase—dissolves in the liquid tin and crystallizes in the boundary area.

The processes of interaction of copper-indium mechanocomposite and tin differ substantially. Heating up to 220 °C and subsequent exposure for 4 hours did not lead to a change in the phase composition—the solid solution of indium in copper and tin. With the temperature increasing up to 235 °C (the melting point of tin is 232 °C) and exposure for 0.5 hour there occurs a radical change in the diffraction pattern. Tin becomes liquid, there arises intermetallide of the η -phase type and diffraction peaks from the copper phase disappear.

These effects can be applied to the development of technology and solders for low-temperature and thermosetting soldering.

6.2.6 Station "X-ray microscopy and tomography"

The station "X-ray microscopy and tomography" is intended for the study of three-dimensional structure of samples with high spatial resolution.

Topics of works in 2011:

- Distribution of minerals in rocks obtained by the XCT method.
- Obtaining data on the microstructure of samples of high explosives and propellants by XCT with high spatial resolution.
- Control of the quality of X-ray masks for LIGA technology.
- Examination of archaeological finds by the non-destructive method of XCT.

Participating organizations:

Budker Institute of Nuclear Physics SB RAS, Novosibirsk; Sobolev Institute of Geology and Mineralogy SB RAS, Novosibirsk; Lavrentyev Institute of Hydrodynamics SB RAS, Novosibirsk; Institute of Chemical Kinetics and Combustion SB RAS, Novosibirsk; Institute of Archaeology and Ethnography SB RAS, Novosibirsk.

The works were carried out in the framework of:

1. RFBR grant № 09-05-00985-a "Zonal-sectorial structure of diamonds from kimberlite fields in Yakutia as reflection of the evolution of their formation";

2. SB RAS Interdisciplinary Integration Project № 51 "Environmental influence on the morphology, real structure and isotopic composition of carbon diamond";

3. SB RAS Project № 24 "Unknown pages in the history and culture of ancient civilizations in I century BC to 1 century AD (the Han Empire, Parthia, the Roman Empire, and the Hun Empire) by the results of interdisciplinary research of archaeological finds from the "Royal" tombs of Northern Mongolia".

Computerized X-ray tomography (CXT) makes it possible, in many cases, to optimize geological studies to determine the mineral (phase) composition and structural-textural features of rocks and industrial ores. The method is attractive with its non-destructiveness, simplicity of recording, and absence of the stage of preparation of objects (cutting, manufacturing of polished thin sections, spraying, etc.). That makes CXT a very popular instrument for the study of unique geological objects.

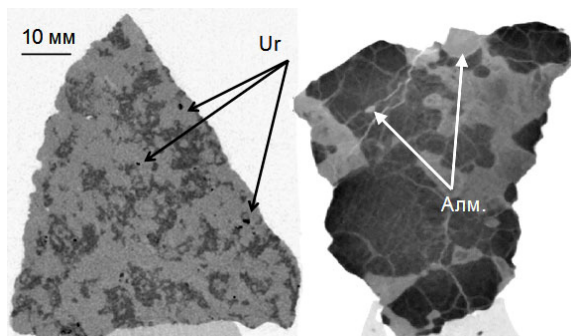


Fig. 6.2.22 (Left) distribution of minerals in uraniferous rock; (right) distribution of minerals in diamond-bearing rock.

Fig.6.2.22 presents virtual slices of rock samples obtained by CXT with a spatial resolution of 100 microns. It is clear that minerals with different X-ray absorption coefficients have contrasting borders, which gives clear distribution of minerals in the sample.

Our setup allows obtaining three-dimensional distribution of inhomogeneities in visibly-opaque high-energy materials (HEM) with a spatial resolution of 3-4 microns. The high sensitivity of our X-ray microscope to phase changes in radiation transmitted through object under study allows visualization of small density variations in an HEM volume. This feature is very important as HEMs are usually organic compounds, which are faint in X-rays.

A study of microinhomogeneities in a solid propellant under different conditions of crystallization is shown in Fig.6.2.23. The size and density of the inhomogeneities affect the resistance to detonation and combustion of the propellant.

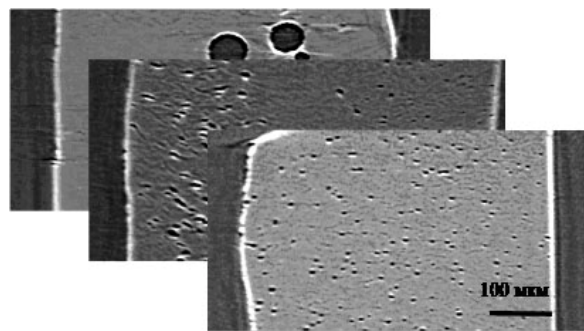


Fig. 6.2.23 Samples of HEMs based on FTDO/DNP mixture, obtained at different temperatures of crystallization.

Successful development of X-ray lithography methods of manufacturing of deep microstructures implies testing of the quality of manufactured X-ray masks. Traditional methods of visual inspection (optical and electron microscopy) can only control the topology of the picture and appearance of the X-ray masks but do not provide information on the thickness, density, porosity and defectiveness of the X-ray absorbing coating. That is why the method of micron-resolution X-ray microscopy became a popular technique of rapid quality control of masks produced at Budker Institute.

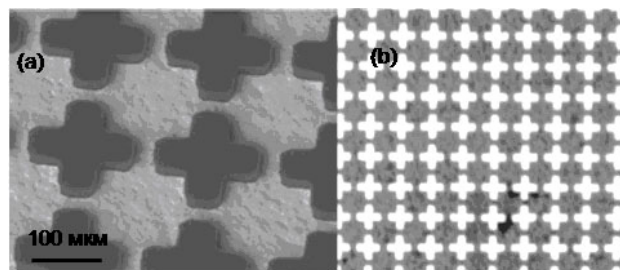


Fig. 6.2.24 Golden X-ray mask images obtained by scanning electron microscopy (a) and X-ray microscopy (b).

Fig.6.2.24 shows golden X-ray mask images obtained with a scanning electron microscope and a magnifier on asymmetrically cut crystals. One can see that though electron microscopy has a higher spatial resolution than that the X-ray images obtained, it gives information only on the surface of the objects. Images of defects hidden in the depths of the absorbing layer can be obtained only with analysis of micro-images in the X-ray range.

In some cases, when the investigated archaeological finds are too big for our installation (more than 45 mm), we make use of the tomograph on the basis of the low-dose digital X-ray machine "Siberia", designed and created at BINP.

An interesting example of such research is the study of an archaeological find – a clay sculpture of the head of an ancient man (Fig.6.2.25). A three-dimensional image with a spatial resolution of 1 mm was restored from 360

projections. One can see that the sculpture was based on a ram's skull, not a man's head as initially anticipated. Detailed study of the tomographic slices allows one to trace the sequence of modeling.

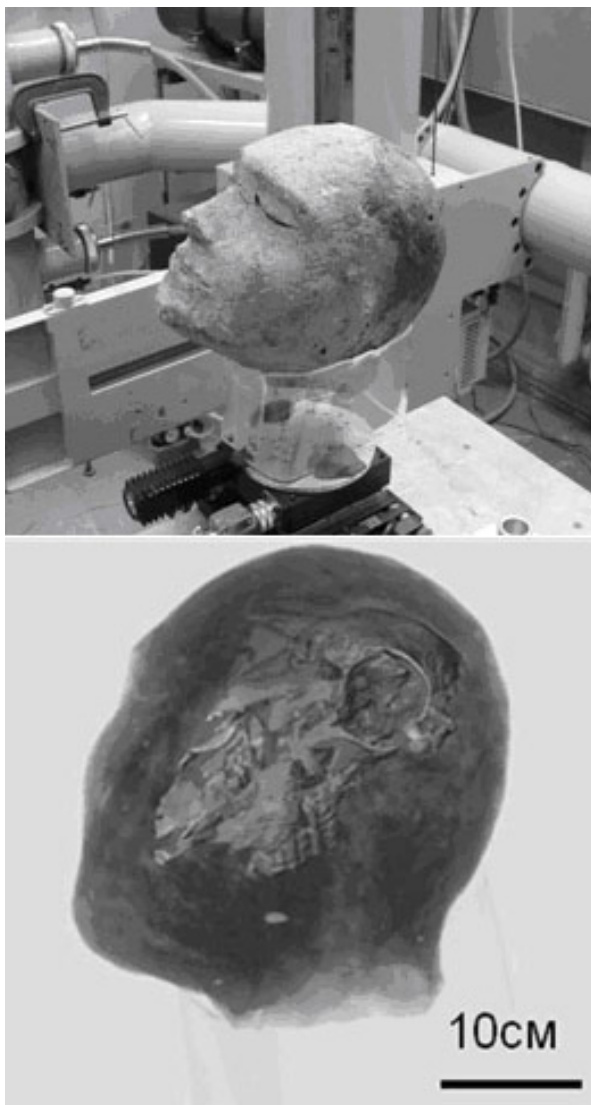


Fig. 6.2.25 Clay head photo (above) and a three-dimensional X-ray image of the head, obtained in the course of tomographic survey (below).

6.2.7. Station "Diffraction movie"

The station is intended for the X-ray diffraction study of the structural and phase transformations in solids in the course of chemical reactions by the methods of X-ray diffractometry. Upon the installation of the two-coordinate detector MarCCD the station is also used for research by the method of single-crystal diffraction and hence small amounts of substances can be investigated, as well as samples with a pronounced texture.

Participating organizations:

Boreskov Institute of Catalysis SB RAS, Novosibirsk; Nikolaev Institute of Inorganic Chemistry SB RAS, Novosibirsk; Institute of Hydrocarbons Processing SB RAS, Omsk; Institute of Solid State Chemistry and Mechanochemistry SB RAS, Novosibirsk.

Topics of works in 2011:

Investigation into decomposition of silver oxalate in a mesoporous matrix

Mesoporous structures of the SBA-15 or MCM-41 type are a hexagonal packing of long cylindrical cavities of up to tens of nanometers in diameter in a SiO_2 matrix. These cavities are of interest as carriers of catalysts resulting from decomposition of precursors. It is therefore important to establish how and where metal particles arise at this preparation method. Decomposition of silver oxalate was chosen to be a model system. This system is convenient because the decomposition process goes at relatively low temperatures and only silver is formed. Mesoporous structures yield a typical triplet in the small angle area, its position determined by such structural parameter as the distance between the centers of the pores.

Experiments were carried out at the station "Diffraction movie" on beam line 5 "b" in the small angle area and at the station on beam line 6 "b" in the large angle zone.

A change in the diffraction patterns in the small angle area is shown in Fig.6.2.26. Decomposition of silver oxalate is accompanied by decrease in the intensity of the first peak of the hexagonal structure and increase in the small-angle scattering. The first is presumably due to the diminution in the contrast because of the exit of silver heavy atoms from the pores, and the second is caused by formation of silver particles outside the channels.

The same process was investigated via diffraction in large angles. Dynamics of the diffraction patterns at growing temperature are shown in Fig.6.2.27a. It was found that the peak Ag (111) can be divided into two components—a broad peak and a narrow one (Fig.6.2.27b). This fact is interpreted as the existence of two classes of silver particles: with coherent scattering areas (CSAs) of ~ 270 Å and ~ 2500 Å. When the temperature reaches 280 °C, the CSA size increases to 550 Å and 10000 Å, respectively (Fig.6.2.28).

Based on these results an assumption was made that part of the silver forming in the course of decomposition of silver oxalate diffuses outside the channels of SBA-15 with formation of large metal particles, while some part remains in the channels, so the increase in the particle size is limited.

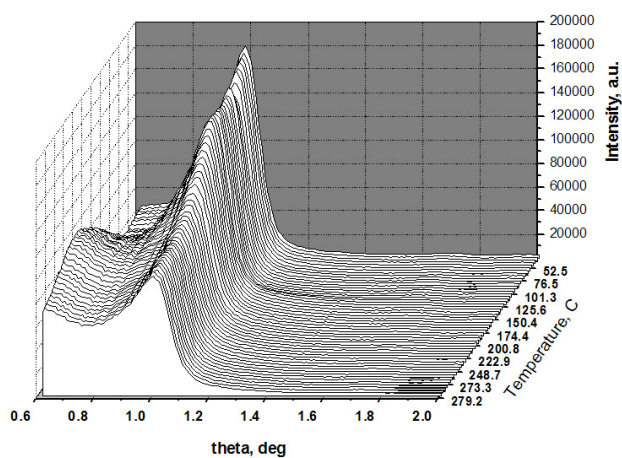


Fig. 6.2.26. Dynamics of the peaks in the small angle area at temperature growth.

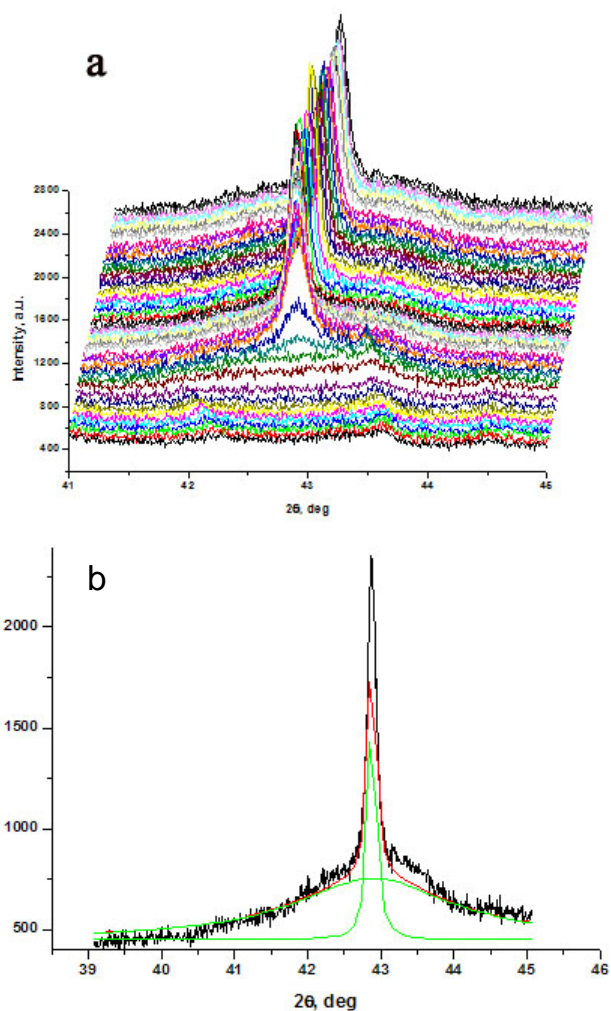


Fig. 6.2.27 (a) Dynamics of diffraction patterns in the large angle area, (b) the broad and narrow components of the peak Ag(111).

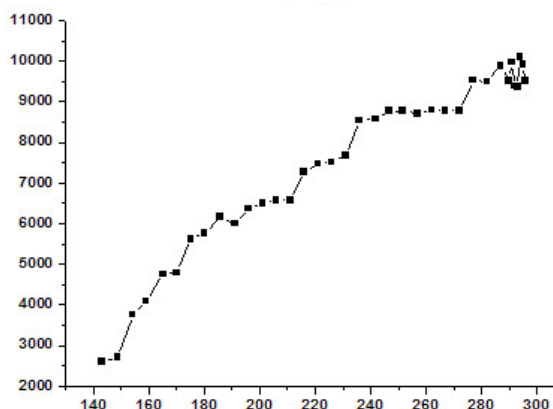
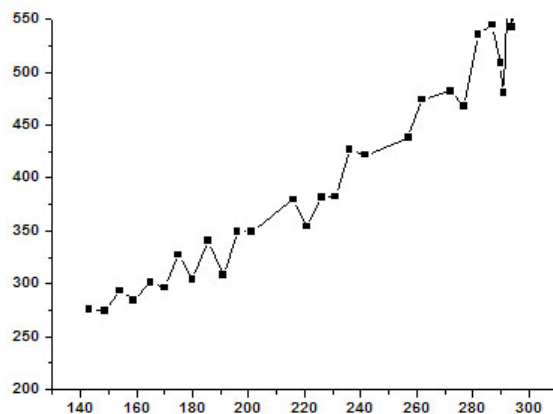


Fig. 6.2.28. Increase in the CSA size for the two types of Ag particles at temperature growth.

6.2.8. Station "EXAFS spectroscopy"

The station is intended for the study of the structure of local environment of atoms of a certain chemical element (the coordination number and interatomic distances). Depending on the applied methodology, the objects of analysis are the volume, surface, or surface layers.

Over 150 samples were investigated and more than 450 spectra were recorded at the EXAFS spectroscopy station in 2011. Over 40 publications were submitted and accepted for publication, including articles in peer-reviewed journals (over 10), articles in conference proceedings, and abstracts of conferences.

Participating organizations:

Institute of Catalysis SB RAS (Novosibirsk); Institute of Inorganic Chemistry SB RAS (Novosibirsk); Institute of Chemical Physics RAS (Moscow); Institute of General and Inorganic Chemistry RAS (Moscow); Rostov State University (Rostov); Institute of Organoelement Compounds RAS (Moscow); Institute of Petrochemical Synthesis RAS (Moscow); Institute of Hydrocarbons Processing SB RAS (Omsk); Saratov State University (Saratov); Institute of Chemical Kinetics and Combustion

SB RAS (Novosibirsk); Institute of Solid State Chemistry and Mechanochemistry SB RAS (Novosibirsk); Limnological Institute of SB RAS (Irkutsk); Hahn-Meitner-Institut (Berlin, Germany); Institute for Semiconductor Physics SB RAS (Novosibirsk); Institute of Coal Chemistry and Materials Science SB RAS (Kemerovo); Institute of Physical Chemistry and Electrochemistry RAS (Moscow); Institute of Geology and Mineralogy SB RAS (Novosibirsk); Institute of Metal Physics UB RAS (Ekaterinburg); Udmurt State University (Izhevsk); Physico-Technical Institute UB RAS (Izhevsk); Max-Planck-Institut für Kohlenforschung (Germany); Institute of High Temperature Processes & Chemical Engineering (Patras, Greece); Institute of Chemistry: Humboldt University (Berlin, Germany); Ohldeburg University (Ohldeburg, Germany); Åbo Akademi University (Turku, Finland); University of Oulu (Oulu, Finland); Centro de Nanociencias y Nanotecnología (UNAM, Ensenada, BC, Mexico); Instituto de Ciencia de Materiales de Sevilla (Spain); Centro Mixto CSIC-Universidad de Sevilla (Spain).

The works were carried out under RFBR projects 09-03-00369a, 09-03-00346a, 09-03-00780a, 08-03-00823a, 09-03-90424-Ukr_f_a, 09-03-00089a, 09-03-00133a, 09-03-00328a, AF-08 0391758a, 08-03-92502-NCNL, 09-03-00514a, 09-05-98019a, 08-02-00404a, 09-03-00780a, 09-03-00346a, 09-03-00540a, 09-03-01013a, DGAPA-PAPIIT - IN 1207063, FASI (contract 02.513.11.3203), RAS Presidium (contracts 20, 21, 24).

Main directions and summary of the works in 2011:

Development of techniques for the study of complex ultradiluted and multicomponent nanosystems

New capabilities of fluorescence XAFS spectroscopy with the use of multi-element detection system for the study of various nanoscale systems were shown. Energy-resolved registration of XAFS spectra by the fluorescence yield allows one to study samples with extremely low concentrations (less than 0.1%) and nanosystems of complex composition. The detector and the software were tried in the studies of the state of elements in "living" systems of microbial communities and nanostructured multicomponent Au-Pd catalysts.

The method of fluorescence XAFS spectroscopy and a 9-element communication processor were applied to the study of "living" systems of microbial communities from hydrothermal vents in the rift zone of Lake Baikal.

Researchers have recently got interested in unique microbial communities in the hydrothermal vents of Barguzin Depression (the rift zone of Lake Baykal). These communities, consisting of various types and classes of microorganisms, including cyanobacteria, form dense microbial mats 1 to 5 cm thick on the water surface. Microbial communities are a convenient model for investigation into the early ecosystem and processes of mineral formation. The XFA method had earlier showed

living microbial mats to accumulate several elements; in particular, content of germanium was found to be unusually high (~10-50 ppm). Because of methodological limitations, these objects are difficult to study by other SR methods. Of course, a direct structural study of the state and forms of stabilization of germanium would be very useful for understanding of the mechanisms of Ge accumulation. Such a study by XAFS, however, became possible only with the development of the unique 9-element communication processor with high-speed digital spectrometric channel and software.

The technique of fluorescence XAFS spectroscopy as applied to "living" systems was developed. A XAFS structural study of the status and characteristics of germanium stabilization in "living" microbial communities from hydrothermal sources of Barguzin depression was conducted. This approach was shown to be promising; it was found from analysis of the XANES and EXAFS data that germanium has a distorted oxygen environment. There may be various stabilized "living" forms of a complex structure differing crucially from inorganic oxide and carbonate forms.

Application of fluorescent XAFS Spectroscopy and 9-element communication processor to the investigation into low-percentage nanosized Au-Pd catalysts

New techniques for processing of natural raw materials from renewable resources are being actively developed today in the field of catalysis. Rational use of natural sugars and their selective heterogeneous oxidation into multifunctional organic acids is a topical task. These acids are in high demand in medicine and food industry and produced mainly via the expensive biotechnological method. Heterogeneous catalysts based on nanosized Au and Pd are expected to significantly improve the process efficiency and reduce the expenses. For example, a supported low-percentage catalytic nanosystem of Au-Pd/Al₂O₃-ZrO₂, (Au/Pd =5/1) has given a significant increase in the selectivity. Structural information obtained by the XAFS method is necessary for design of optimal catalysts with desired structural and functional properties. Such a study was impossible earlier because of the low concentration of supported Me and a significant background contribution from the "heavy" ZrO₂ matrix of the support. The use of the 9-element communication processor with high-speed digital spectrometric channel and software made it possible to obtain reliable information on bimetallic Au-Pd catalysts.

The technique of fluorescence XAFS spectroscopy as applied to low-percentage systems on "heavy" matrices was developed. A XAFS structural study of the state and characteristics of stabilization of Au and Pd in nanosized heterogeneous catalysts for oxidation of sugars was performed. This approach was shown to be promising. It was found that in the system there forms a Pd-Au nanosystem, which is responsible for the high selectivity of the catalyst. Variants of structural models were examined.

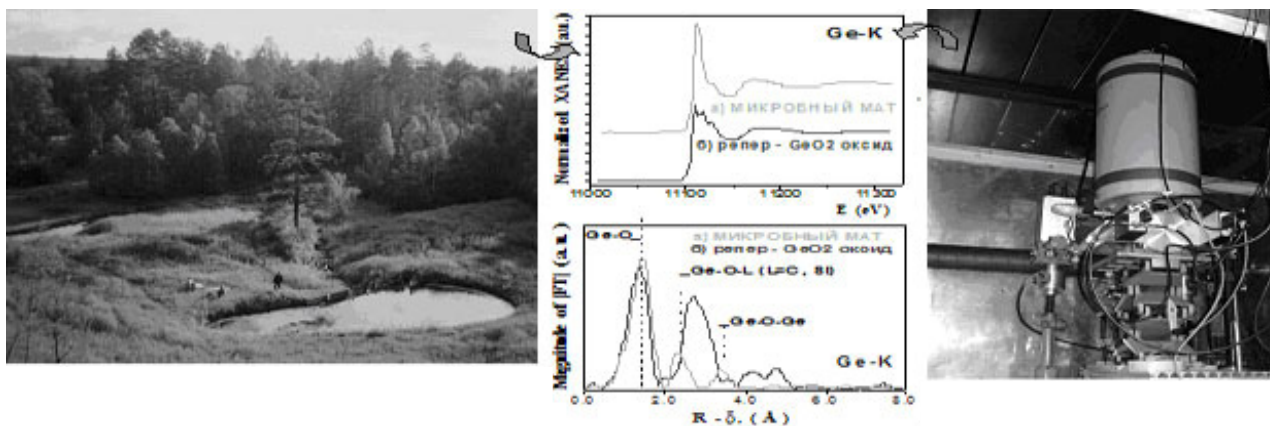


Fig. 6.2.29. Application of fluorescence XAFS spectroscopy and the 9-element communication processor to the study of "living" systems of microbial communities from hydrothermal vents in the rift zone of Lake Baikal.

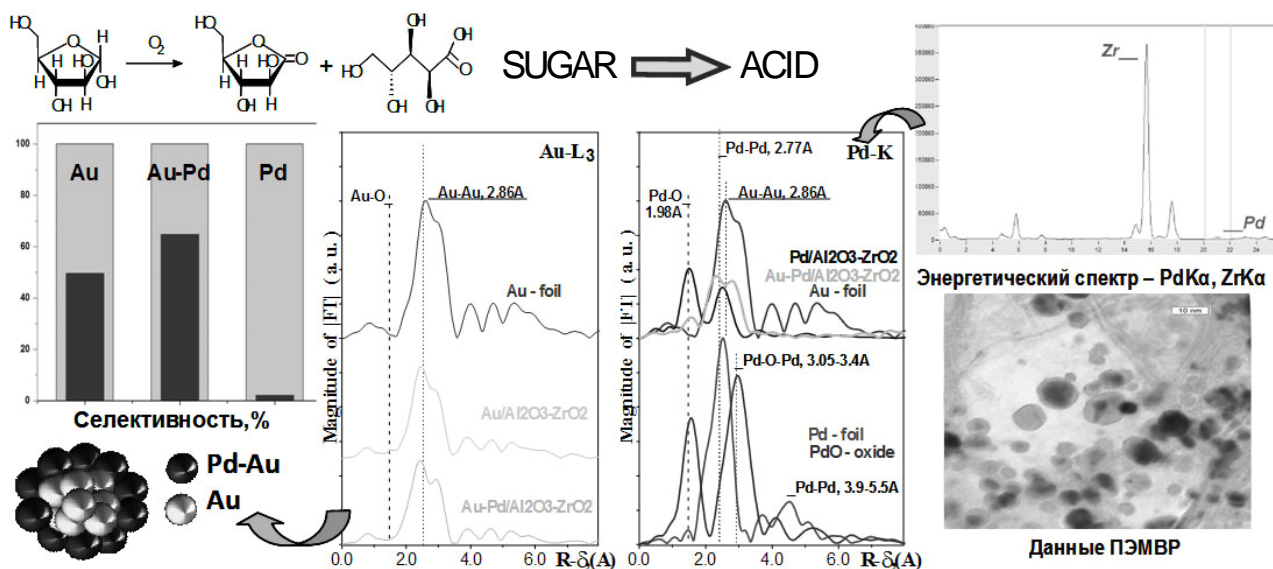


Fig. 6.2.30. Application of fluorescent XAFS spectroscopy and 9-element communication processor to the study of nanosized low-percentage Au-Pd catalysts.

Study of model multicomponent nanostructured catalysts for conversion of industrially important substrates

The methods of XAFS, XFA, and TEM were applied to the study of a model system of Cu-Cr-Fe, which is promising for the process of steam conversion of CO. This catalyst is a metastable disordered partially hydrated oxide Fe³⁺ promoted with ions of chromium (~ 9 at.%) and copper (4 to 7 at.%). The activity of the catalyst in the reaction of steam conversion of CO at low (less than 350°C) temperatures is much higher than the activity of the known Fe-containing catalysts. The results of the study suggest that copper cations in the initial samples are in the Cu²⁺ state in a tetragonally-distorted octahedral environment, while in a CO steam conversion reaction at

temperatures below 350 °C they are in the reduced state, in the form of ultrafine (less than 2 nm) particles of metallic Cu⁰. These particles define the high activity of the catalyst at temperatures below 350 °C.

The methods of XANES spectroscopy, EXAFS spectroscopy, electron microscopy, ICP elemental analysis, and X-ray diffraction were applied to a comprehensive study of bimetallic Pd-M (M = Co, Ni, Zn, Ag, Ce) palladium-containing nanoparticles produced from initial complexes of Pd(OOCMe)₂M(OH)₂ (M = Ni (II), Co (II), Zn (II)) and Pd(OOCMe)₄Ag₂(HOOCMe)₂. The structure and morphology of the bimetallic nanoparticles as well as the electronic state of the metal atoms have been studied. The catalytic properties of the bimetallic nanoparticles have been investigated in

comparison with the standard supported catalyst Pd/SiO₂ on the example of the reactions of catalytic decomposition of hydrazine and reduction of U(VI) to U(IV) with hydrazine and formic acid. The catalytic activity of Pd-Ni nanoparticles was found to exceed by far that of the standard supported catalyst Pd/SiO₂ with the same number of palladium atoms, while Pd-Co, Pd-Zn and Pd-Ag nanoparticles do not catalyze the reactions studied. Possible structural models were examined in detail.

Study of spatially correlated nanostructures and nanocomposite thin films on semiconductor compounds of the isoelectronic series of germanium

It is known that materials based on germanium and compounds of its isoelectronic series (Ge, GaAs, Zn (S) Se, etc.) are traditionally used in various fields of engineering and electronics. Nanoscale structures based on them have also recently come into wide use. This has led to the development of techniques (especially epitaxial) which allow production of orderly-arranged nanoobjects, e.g. quantum dots of Ge on the surface of single-crystal Si and GaAs and other semiconductor materials. The interest in nanocomposites based on dielectric matrices of semiconductors is also increasingly growing. Such structures can not only prevent charge transfer among individual quantum dots due to spatial separation of elements but also protect them from external influences. The use of matrix isolation makes it possible to significantly reduce the efficiency of recombination of excitons and electron-hole pairs on surface defects and defects of the semiconductor, thus enhancing the quantum yield of luminescence when nanocomposites are used in photovoltaic devices and opening up broad prospects for design of nanoelectronics elements (diodes and new-generation switches) based on such systems.

The methods of EXAFS, SEM, AFM, TEM, and XFA were applied to the studies of nanostructures based on Ge, ZnS, and ZnSe, produced by thermal evaporation of material in vacuum onto porous Al₂O₃ substrates. The synthesis was performed with varying modes of evaporation, condensation temperatures, and sizes of the pores of the substrate. General laws and mechanisms of the nanostructure formation were investigated, as well as their resistance to thermal treatment. It was shown that the geometrical arrangement and size of Ge nanofibers, consisting of small amorphous entities and nanostructures of ZnSe and ZnS, reproduces the porous structure of the template matrixes. It was revealed that smaller structures are highly reactive and annealing leads either to a change in the degree of crystallization or to phase transitions not typical to massive systems.

The methods of EXAFS, XPS, and XFA were applied to the study of promising semiconductor materials based on bulk compounds of Ga₂Se₃, GaAs and nanostructures of gallium arsenide. Powders of bulk Ga₂Se₃ and GaAs were prepared by grinding of

monocrystals; filamentary nanostructures of GaAs were obtained by thermal evaporation of the material on porous film of Al₂O₃. For bulk Ga₂Se₃ and GaAs it was shown that the structural data (interatomic distances and coordination numbers) agree well with the results of calculations of the structure from crystallographic parameters. The stoichiometry and atomic state of the samples were certified by XPS and XFA. It was found that filamentary nanostructures have a more disordered local structure as compared with bulk materials and are of nonstoichiometric composition.

Complex investigations into low-percentage (starting from ~ 1%) noble-metal nanostructured catalysts of new generation

The methods of XAFS (XANES/EXAFS) spectroscopy, XPS, and TEM were applied to the exploration of stabilization and state of Pd in low-percentage mono- and bimetallic palladium catalysts supported by oxide carriers. It was shown that the state of palladium oxide nanostructures formed on the surface of the support can be purposely varied from almost atomically dispersed to PdO nanoparticles. Possible variants of structural models were examined.

Currently, supported palladium catalyst nanosystems are widely used for processing of industrially important substances, e.g. for industrial carbon dioxide reforming of methane to synthesis gas by the membrane technology, as well as for neutralization of automotive emissions and industrial waste gases. The experiments were conducted with model low-percentage (~1%) catalysts Pd/Al₂O₃ and Pd-Mn/TiO₂, prepared by incipient wetting impregnation from aqueous solutions of palladium nitrate and palladium chloride and by the sol-gel method from bimetallic acetate precursor complexes. It was found that palladium in the samples was mostly in the form of ions Pd(2+) in immediate square-planar oxygen environment. No metallic phase of PdO was found within the precision of the method. The role of the second metal in the stabilization of the active ingredient was shown for the bimetallic catalysts. A detailed complex analysis of the structural data allows one to suggest formation of a defective nanophase of palladium oxide nucleation in the intermediates (at the stage of gel), this nanophase consisting both of residues (fragments) of the initial complexes of Pd-Mn, as well as PdO nanoparticles. Whereas in the resulting products (heterometallic nanocomposite catalysts) produced on the basis of heterobimetallic carboxylate complexes of palladium there goes formation of a highly dispersed palladium oxide nanophase stabilized on the oxide support TiO₂. It should be noted that possible distortions of the local structure (as compared with the reference massive PdO) of these nanoparticles are apparently associated with both the size effects and the influence of ions of the second metal, Mn. Defective surface nanophases MnO_x have been found, though apparently most manganese ions

penetrate into the subsurface structure of anatase. In so doing, isolated ions localized by their defects get stabilized and a complex interaction nanophase $\text{MnO}_x\text{-TiO}_y$ forms.

The methods of XAFS spectroscopy, electron microscopy, X-ray diffraction, X-ray photoelectron spectroscopy and elemental analysis were applied to the study of the characteristics of the state of the atoms of platinum and palladium in intermediate compounds and products (heterometallic nanoclusters and nanomaterials) resulting from thermal and redox transformations of initial complexes of palladium and platinum (promising precursors of catalytic systems). Platinum and palladium were found to exist in the initial complexes solely in the form of ions $\text{Pt}(2+)$ and $\text{Pd}(2+)$. Whereas after heat treatment in air, there forms a complex phase (metal + oxide) on the part of platinum and a highly dispersed oxide phase on the part of palladium. At soft reduction processing in hydrogen, there form mostly metallic platinum and palladium nanoparticles. It should be noted that no alloys seem to form (or the contribution of this phase is very small). Possible structural models were considered in detail.

Study of promising catalysts for processing of products of biomass fermentation into high-quality components of bio-diesel and bio-fuel

The methods of XAFS, XPS, XFA, HRTEM were applied to the study of the structural features of the active component of promising catalytic nanosystems $\text{Ta(W)-Re/Al}_2\text{O}_3$, which are used for the production of alkane and alkene fractions $\text{C}_4\text{-C}_{12+}$ —high-quality components of biofuels—from products of fermentation of renewable biomass. Even by most optimistic forecasts, organic fuel will be widely used for internal combustion engines until the beginning of the next century. That is why much attention is now paid to the search for alternative (non-related to oil sources) high-efficiency ways of development of the world energetics and petrochemicals on the basis of renewable resources. Conversion of renewable biomass into energy is one of the possible ways because fermentation products (ethanol, butanol, izopentanol, glycerine, etc.) can serve as fuel components, both in pure form and after catalytic processing, which provides more efficient and quality fuel components for bio-fuel.

Initial samples of catalysts were prepared by the sol-gel method from a variety of mono- and bimetallic complexes of precursors, via their deposition on the oxide carrier $\gamma\text{-Al}_2\text{O}_3$. No substantial signs of formation of mixed Ta(W)-O-Re oxide phases were detected. It was well established, however, that in these systems the active components strongly interact with the Al_2O_3 support, with formation of distorted oxide nanostructures: Ta(W)O_x , Ta(W)-O-Al , ReO_y , and $(\text{ReO}_3)_{\text{ads}}\text{-O-Al}$. It was found for the Ta(W)-Re systems that rhenium predominantly takes the form of $\text{Re}(7+)$, whereas tantalum and tungsten

mostly the form of $\text{Me}(5+)$. It was also found that the local environment of catalysts produced from bimetallic precursors has some differences from that of samples synthesized from mono-complexes. The genesis of the catalytic systems under study, the state of the metals (Ta, W, and Re) and the local environment were described in detail; the relationship between the structure and catalytic properties was shown. Possible variants of structural models were examined. The data of all the methods are in good agreement with each other.

They at IGIC RAS synthesized for the first time a series of new bimetallic PdM compounds ($m\text{-OOCMe}$) $_4\text{L}$ ($M = \text{Ni, Co, Zn, Mn}$; $\text{REE L} = \text{MeCN}$) with a structure of the type shown in Fig.6.2.31. Methods for selective synthesis of nanoparticles of any of the species below were perfected at EXAFS spectroscopy station.

A notable area of energy development is the creation of portable autonomous power supplies, including fuel cells and compact high-performance hydrogen generators on Rh/TiO_2 catalysts.

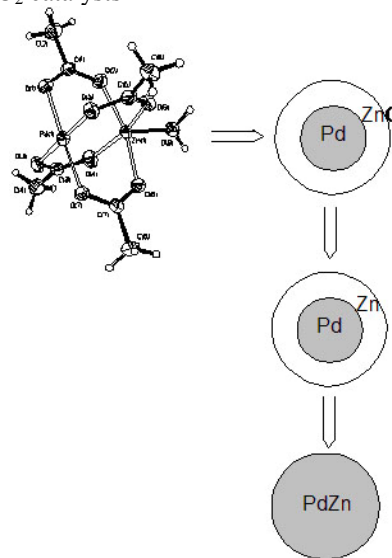


Fig. 6.2.31. Some of bimetallic PdZn nanoparticles are promising catalysts for processing of nuclear fuel and radioactive waste.

It was shown for the first time that the most effective catalysts comprise rhodium in the form of metal nanoparticles decorated with the carrier, as shown in Fig. 6.2.32. The activity of rhodium is caused by the appearance of a positive charge on the metal particles. With results obtained, the life of such sources can be extended.

Associated petroleum gases can be processed into more valuable products at the place of crude oil extraction, which makes the transportation of oil products more cost-effective. For instance, acetylene in associated petroleum gases can be hydrogenated to ethylene, which is a more valuable chemical raw material. Such solutions stimulate development of bimetallic $\text{Pd/Ga}_2\text{O}_3$ catalysts. It was shown for the first time that their activity is

determined by the formation of palladium-gallium alloy on the surface of palladium. The obtained results may be useful in development of catalysts of higher efficiency.

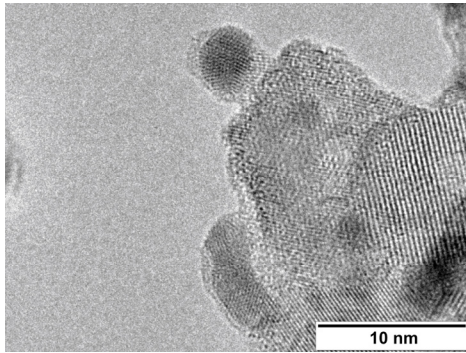


Fig. 6.2.32.

6.3 WORK ON SR BEAMS FROM VEPP-4M

6.3.1 Development of methodological support for the metrological station "Cosmos"

They at the station "Cosmos" were working on calibration of the spectral sensitivity of silicon photodiodes of the FDUK-100UV and AXUV-100A1 types. The calibration was carried out in the spectral range of 80-1200 eV with an accuracy of 2%. In addition, a study of the radiation resistance of the CCD matrix was done. These works resulted in the creation of methodological support to the station, which will be followed by certification of the methods developed. Furthermore, earlier designed technique for measuring the power of EUV radiation (80-120 eV) for the purposes of projection lithography was certified (certificate 113-01.00249-2011 dated October 20, 2011).

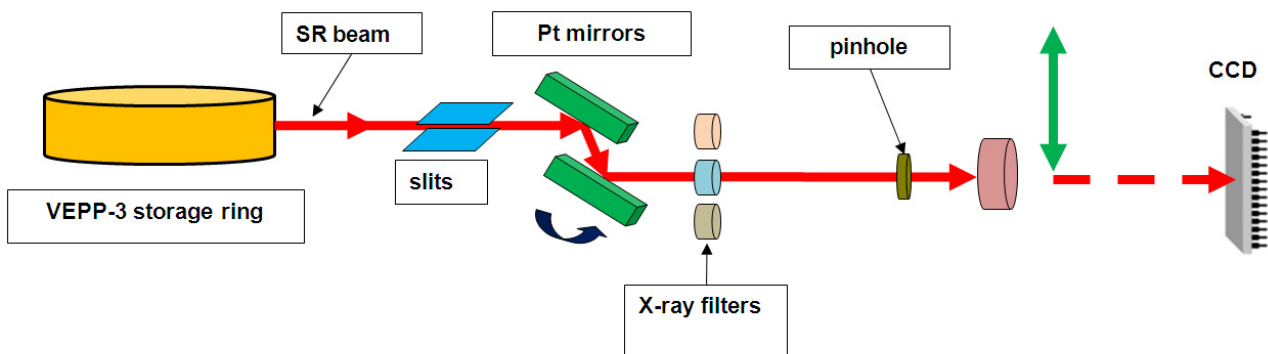


Fig. 6.3.1. White SR beam passes through a couple of mirrors and a filter and gets into the matrix. The calculations are verified via measurements of the power of quasi-monochromatic beam with a reference detector (these measurements are performed at a low current in the storage ring).

Examination of the radiation resistance of the CCD matrix

A 1x1 mm portion of the matrix was irradiated with the SR beam, which passed through the filter and mirrors of total external reflection (Fig.6.3.1). The SR spectral power coming on the matrix is shown in Fig.6.3.2.

The degradation results in the increasing dark current in the matrix area exposed to the radiation (Fig.6.3.3).

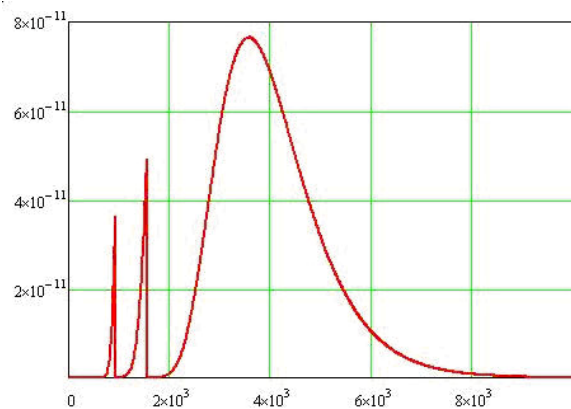


Fig. 6.3.2. Vertical: the spectral radiation power (W/eV) into an aperture of 1 mm² at the station "Cosmos" (30 meters to the point of emission; the storage ring current is 1 mA; the energy is 1800 eV). The filter: 1 micron of Cu + 10 microns of Al.

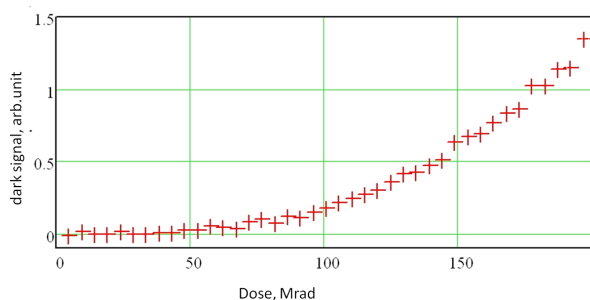


Fig. 6.3.3. Increase in the dark current in the matrix area as a function of the irradiation dose.

6.4 WORK WITH BEAMS OF TERAHERTZ RADIATION

6.4.1 Novosibirsk terahertz free electron laser

Novosibirsk free electron laser (FEL) is still a terahertz radiation source of world's highest power. The maximum average radiation power attained at a repetition rate frequency of 11.2 MHz is 500 Watts. In 2011, Novosibirsk FEL worked for users for about 1000 hours. In the standard mode of operation for users, at a repetition frequency of 5.6 MHz the average radiation power on the workstations depended on the wavelength and tuning of the accelerating system and was about 100 Watts. The FEL radiation is linearly polarized and fully spatially coherent; the wavelength is tunable in the range of 40 - 240 μm ; the relative spectral width is less than 1% (full width at half maximum); the pulse duration is less than 100 ps (full width at half maximum).

In 2011, works on the FEL were carried out by members of Budker Institute of Nuclear Physics SB RAS, Institute of Chemical Kinetics and Combustion SB RAS, Institute of Cytology and Genetics SB RAS, Institute of Inorganic Chemistry SB RAS, Rzhanov Institute of Semiconductor Physics SB RAS, Institute of Theoretical and Applied Mechanics, Design and Technological Institute of Scientific Instrument, and Scientific-Technological Center of Unique Instrumentation RAS (Moscow), as well as teachers, students and graduates of Novosibirsk State University and Novosibirsk State Technical University.

The main tasks in 2011 were the organization of regular work at the six user workstations and preparation to the commissioning of the third stage of Novosibirsk FEL.

6.4.2 Examples of experiments with THz radiation beams

Investigation into nonthermal effects of electromagnetic radiation on living systems of different levels of organization

Experiments on nonthermal effects of electromagnetic radiation on living systems of different levels of organization were continued. A special cuvet was made for exposure of biological samples to the radiation of the terahertz free electron laser (Fig.6.4.1).

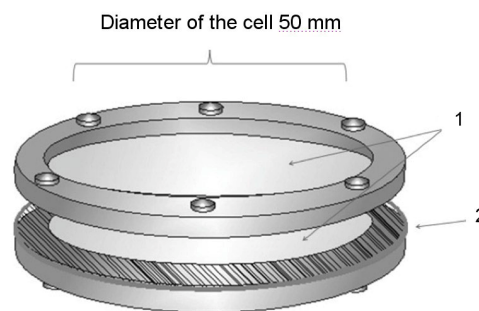


Fig. 6.4.1. Thz radiation transparent cuvet for exposure of objects. 1 - PP film 40 microns thick; 2 - Insert 40 microns thick.

The sample was placed between two stretched polypropylene films 40 microns thick. The cuvet volume was 50 ml with a distance between the films of 25 mm and a cuvet diameter of 50 mm. The beam cross section in the plane of the cuvet was an elongated ellipse. There was a special mechanism rotating the cuvet for the purpose of uniform exposure of sample. The axis of rotation passed through the edge of the ellipse.

Temperature of liquid samples at absorption of terahertz radiation was monitored with a highly sensitive imager TKVr SVIT101, produced by the Institute of Semiconductor Physics SB RAS, with a sensitivity of 0.027 $^{\circ}\text{C}$ or better. The imager allows dynamic registration of changes in temperature fields.

Determination of minimum reacting doses for different biosensors in dependence on time and power of irradiation

For correct interpretation of the effect of THz radiation on living objects is necessary to ensure uniform irradiation throughout the liquid sample volume with the sample temperature maintained within narrow limits. The characteristic length of absorption of terahertz radiation by water is about 50 microns. The cross section of the radiation beam in the plane of the sample is an elongated ellipse. That is why the above cuvet was used in the experiments. Since the volume of liquid sample in the cuvet remained unchanged and the temperature of the sample was to be maintained constant in all experiments, the average power density also remained unchanged. They varied the dose, changing the time of irradiation. The average power density

was 1.4 W/cm². The exposure time was 5, 10, and 15 minutes. The dose was 420 J/cm², 840 J/cm², and 1260 J/cm², respectively

At this stage of determination of terahertz radiation doses, the subjects of investigation were genosensor structures (*E.coli/pKatG-gfp*), which are sensitive to oxidative stress and were created on the basis of the catalase gene promoter. The theoretical possibility of involvement of a gene of response to oxidative stress caused by terahertz radiation has been shown earlier on the example of the *Dps* gene promoter (*E.coli/pDps-gfp* genosensor).

Involvement of genes maintaining homeostasis of transition metals associated with the control of redox reactions in *E.coli* cells in response to terahertz radiation was tested using the newly created genosensor structure based on the *copA* gene promoter.

Genosensor cells were irradiated as described above. The intensity of fluorescence of *Gfp* protein was determined with a flatbed fluorimeter. A series of experiments was carried out with exposure of cells of the *E.coli/pKatG-gfp* genosensor to terahertz radiation at wavelengths of 130 microns, 150 microns and 200 microns. Fig. 6.4.2 shows the level of fluorescence of the *Gfp* protein in the genosensor cells after a single exposure to terahertz radiation with a power density of 1.4 W/cm² and a wavelength of 130 microns during 15 minutes, as well as the level of fluorescence of the *Gfp* protein in the same cells induced by hydrogen peroxide of different concentrations (positive control). The values of fluorescence intensity in cells not exposed to any effects (negative control) were subtracted from the values of the experiment and positive control.

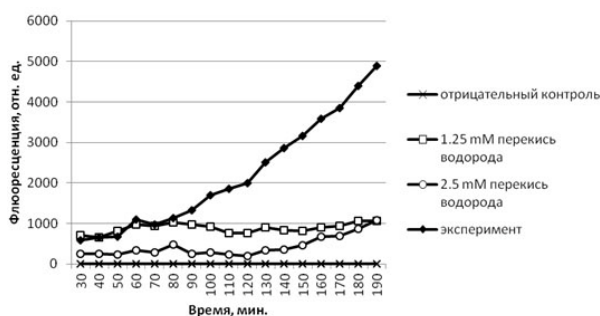


Fig. 6.4.2. Fluorescence of the *Gfp* protein in cells of the *E.coli/pKatG-gfp* genosensor as a result of exposure to terahertz radiation with a wavelength of 130 microns for 15 min. Negative control: non-irradiated cells. Positive control: induction with hydrogen peroxide H₂O₂.

Irradiation with terahertz radiation for 15 minutes at all above wavelengths results in induction of expression of the *Gfp* protein in cells of the *E.coli/pKatG-gfp* genosensor, whereas irradiation for 5 and 10 minutes gives no strongly pronounced response in the form of increased fluorescence intensity.

Cells of the *E.coli/pKatG-gfp* genosensor were shown to react similarly both to the presence of hydrogen peroxide in different concentrations and to terahertz radiation, the response of cells to terahertz radiation developing a little later though with significantly higher fluorescence intensity. It should be noted that different clones have different baseline fluorescence and different levels of response to the induction of *Gfp* synthesis with hydrogen peroxide. The number of cells in each image was approximately the same for each time slice, which indicates increase in the *Gfp* synthesis in cells of the *E.coli/pKatG-gfp* genosensor. Cells of the genosensor singly exposed to terahertz radiation keep producing *Gfp* for five hours, which corresponds to approximately eight life cycles.

Assessment of overall metabolic distress in organisms Escherichia coli, Chlorella vulgaris, and Daphnia magna under THz radiation

To estimate the total metabolic distress of organisms under the influence of THz radiation we selected a three-component test system consisting of organisms of different trophic levels. The test system consisted of prokaryotic and eukaryotic organisms that grow well in laboratory conditions and have high sensitivity to the most widespread environmental pollutants.

Composition of the test system

Escherichia coli belongs to the prokaryotes, heterotrophs. We used strain DH5 alpha, which is widely applied as a sanitary-indicative organism (Fig.6.4.3, A).

Chlorella vulgaris is referred to the lower plants, eukaryotes, autotrophs, producers (Fig.6.4.3, B). It is used at numerous laboratories around the world, hence there is an available global data bank on it.

Daphnia magna relates to the entomostracans, Cladocerae (Fig.6.4.3, C). This organism is frequently used for bioassays.

The test samples were exposed to radiation in the above mentioned cuvet with THz-transparent polypropylene windows (Fig.6.4.1). The thickness of the irradiated liquid layer was 40 microns for *Escherichia coli* and *Chlorella vulgaris*. For the case of *Daphnia magna* the inter-plate thickness was increased to 800 microns in accordance with the size of the object; 4 to 5 *Daphnia magna* individuals were placed in the cuvet at a time. The irradiation lasted for 1 hour. The temperature was maintained in accordance with Table 6.4.1 due to changes in the average radiation power.

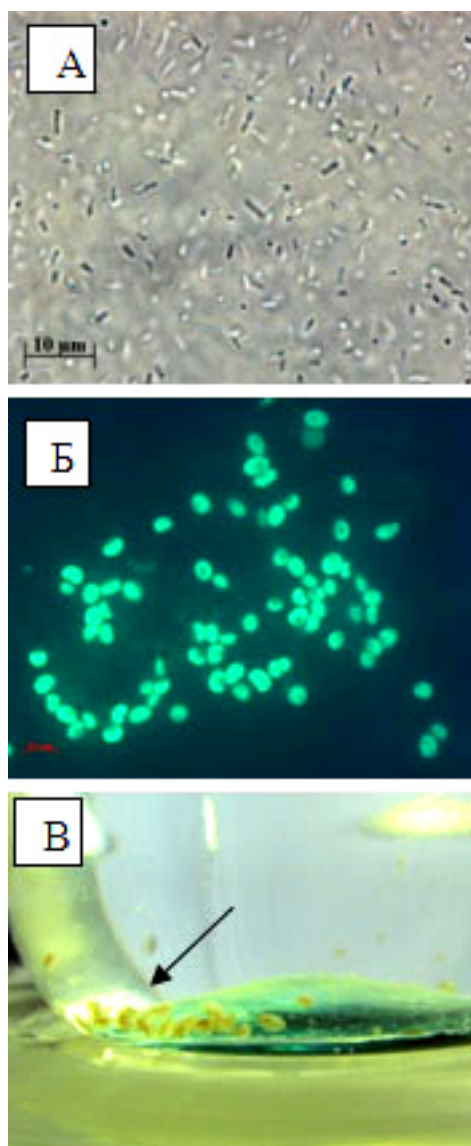


Fig. 6.4.3 Morphology of the test organisms used in the experiment: *Escherichia coli* (A), *Chlorella vulgaris* (B), and *Daphnia magna* (C); the arrow shows a concentration of *Daphnia magna* adults in the culture vessel.

Table 6.4.1. Temperature regimes in the experiment.

Object	Temperature, °C
<i>Escherichia coli</i>	36 ± 2 °C
<i>Chlorella vulgaris</i>	28 ± 2 °C
<i>Daphnia magna</i>	21 ± 2 °C

All the experiments were carried out in triple repetition and with observation of sterility rules.

The influence of THz radiation on *E.coli* was calculated from the variation in the number of colonies that grew on the Luria-Bertani agar in the control and

irradiated samples. In the experiments with *Chlorella vulgaris*, the optical density of the cell suspension before and after exposure to THz radiation was taken into account. In the experiments with *Daphnia magna*, the number of individuals that survived after being in the experimental cuvet was analyzed. Individuals that were not exposed to terahertz radiation were taken as control ones.

For comparability of the outcome, a toxicity index of the factor to estimate (TIF) was calculated from the test results:

$$TIF = TF_E/TF_C,$$

where TF_E is the value of the test function to register in the experiment and TF_C is that for the control samples. The TIF value varies from 0 to M, M being any positive quantity.

Formalization of the procedure for comparison of the results obtained was realized via the toxicity scale developed by R.R. Kabirov. The TIF mean value was used as a generalized criterion for TIF values obtained in different experiments. The index of toxicity for each solution to investigate and its toxicity class were determined from the resulting average value:

$$TIF_{av} = (TIF_1 + TIF_2 + TIF_3)/3$$

where TIF_{av} is the average value of the index of toxicity; TIF_1 , TIF_2 and TIF_3 are the toxicity indexes calculated for *Escherichia coli*, *Chlorella vulgaris*, and *Daphnia magna*, respectively.

Results of the experiments

Exposure of *Escherichia coli* cells to terahertz radiation resulted in stimulation of growth shown by the increase in the number of colonies (Table 6.4.2 and Fig. 6.4.4).

Experiments with *Chlorella vulgaris* demonstrated a significant increase in the optical density of cell suspension of the irradiated sample in comparison with the control ones (Table 6.4.3 and Fig. 6.4.5), which indicates a stimulating effect of THz radiation on the culture of *Chlorella vulgaris*.

In all experiments with *Daphnia magna* there was observed a partial loss of the individuals (Table 6.4.4 and Fig. 6.4.6).

Table 6.4.2. Quantity of *Escherichia coli* colonies.

	Quantity, CFU/ml
Control	9.5*10 ⁷ ±5%
Experiment	1.1*10 ⁸ ±5%

Table 6.4.3. Optical density of the *Chlorella vulgaris* culture before and after irradiation.

	Optical density, relative units.
Control	0.325 ± 15%
Experiment	0.715 ± 15%

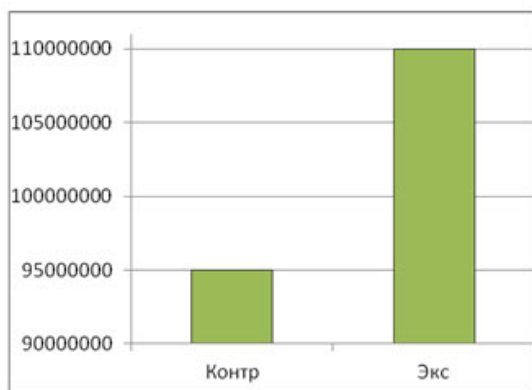


Fig. 6.4.4 Evolution of the *Escherichia coli* quantity caused by THz radiation. Left - control, right - exp.

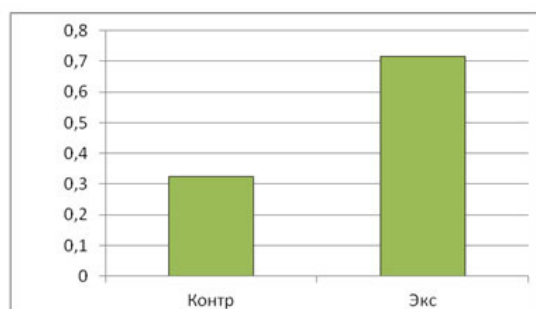


Fig. 6.4.5 Variation in the optical density of the *Chlorella vulgaris* culture in the control and experimental samples. Left - contr., right - exp.

Table 6.4.4. Number of *Daphnia magna* individuals before and after irradiation.

	Number of surviving individuals
Control	30 of 30
Experiment	24 of 30

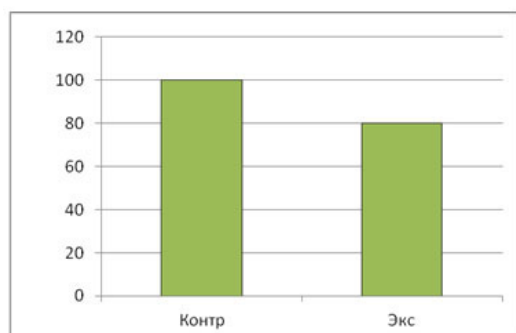


Fig. 6.4.6 Evolution of the *Daphnia magna* quantity (%) in the control and experimental samples.

Table 6.4.5 presents the values of the toxicity index of factor to estimate (TIF), calculated as

described above. One can see from Table 6.4.5 that the average value of TIF was 1.4.

Table 6.4.5. TIF values and the class of the toxicity of samples.

TIF for <i>E. Coli</i>	TIF for <i>C. vulgaris</i>	TIF for <i>D. Magna</i>	Total toxicity ABILITY (TIFav)	Class of toxicity
1.2	2.2	0.8	1.4	VI stimulation

Thus, the effect of THz radiation on metabolic stress in organisms of different trophic levels was tested on a standard test system. It was shown that radiation in this range does not inhibit the process of reproduction of test organisms. Moreover, in the case of *E. coli* and *C. Vulgaris* there was observed a stimulatory effect of the radiation on the organisms.

6.4.3 Third stage of Novosibirsk FEL

The second stage of the free electron laser (FEL) was constructed for moving towards higher frequencies in the terahertz frequency range. For creation of a free-electron laser operating in the frequency range of 3 - 8 THz, the world's first energy recovery linac (ERL) with two tracks was built and commissioned. The electron beam passes 4 times through the high-frequency resonators of the ERL. The build-up of the third stage of Novosibirsk FEL (10 - 50 THz) is underway.

The full-scale ERL uses the same RF accelerating structure as the first-stage ERL but is situated, in contrast to the latter, in a horizontal plane (see Fig.6.4.7). Thus, construction of one ERL does not require removal of the other one. The mode of operation is set via just a switching of the bending magnets.

The second-stage FEL is located on the second track of the ERL. The average power of its radiation is 0.5 kW, and the wavelength can be tuned from 40 to 80 microns. The average power of radiation of the first-stage and the second-stage FELs exceeds by far that of similar foreign installations. A high-power near-IR FEL for the wavelength range of 6 - 30 microns (the third-stage FEL) is to be mounted on the last track (40 MeV) of the ERL.

The magnet/vacuum system of the third stage of the FEL is located on the third and fourth tracks of the ERL. It consists of 10 bending magnets and 7 large and 26 small magnetic quadrupole lenses. Besides, it comprises vacuum chambers with ion pumps, electron beam position monitors, vacuum valves, and units for extraction of synchrotron radiation.

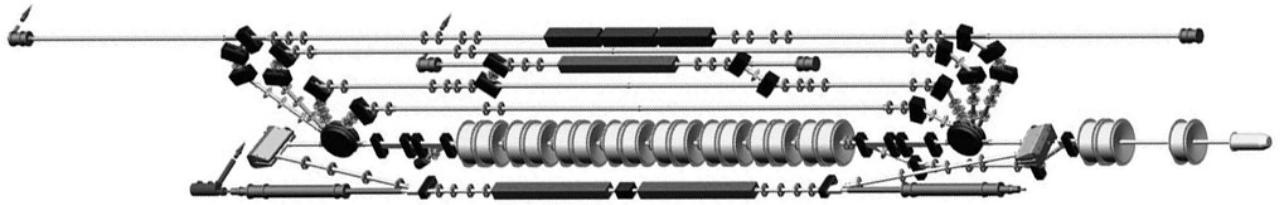


Fig. 6.4.7 General view of the magnetic system of the ERL.

Table 6.4.6 Main parameters of the undulators.

Material	Gap, cm	B, kG	Period d_w , cm	K	Number of periods	N, pcs
Neodymium-iron-boron	2.5-6.0	5.2-0.8	6	3.1-0.5	33	3

Along the ERL there should be placed focusing elements for transportation of electron beam, quadrupole lenses in this case. For an electron beam with a sufficiently large energy spread to arrive at the dump after passing through the system of undulators there should be a sizeable aperture at places with non-zero dispersion. In our system, we use two types of lenses, with apertures of 110 mm and 170 mm (the inscribed circle diameter).

For want of space in the accelerator room and need for access to all elements of the magnet-vacuum system, all elements of the latter are suspended from horizontal beams laid across the long hall of the accelerator.

Some elements are attached to the main beams through intermediate suspensions with devices for fine adjustment of their position.

The small bending magnets and the upper halves of the large quadrupole lenses were mounted the first. Then the small quadrupole lenses were placed on the aluminum supports as shown in Fig.6.4.9.



Fig. 6.4.9 Small quadrupole lenses (in the foreground, right) and the small bending magnets (in the background)

The vacuum system of the separate tracks of the ERL consists of the vacuum chambers of the bends, arranged symmetrically left and right; the vacuum chambers of the four straightforward sections; and the vacuum chamber of the bypass. Pumping is provided by eight ion pumps. Most of the vacuum chambers are made of aluminum, which has high thermal conductivity, is easy to process, and thus provides good cooling of the vacuum chambers. Besides, the atomic number of aluminum is relatively small, i.e. the average energy of the bremsstrahlung is reduced, and aluminum does not form radioactive substances under irradiation.

The apertures of the vacuum chambers were chosen with due account for the calculated envelope of electron beam and maximization of the energy acceptance of the ERL.

The vacuum chambers of the bends were made as boxes with water-cooled walls. Special tubes were designed, ordered and produced for the vacuum chambers of the straightforward sections. These tubes have a square outer cross-section, a central channel of 82 mm in diameter and water-cooling channels of 8 mm in diameter in the corners of the square. The tubes serve as distributed collimators for electron-beam. The undulators are installed in a box-like chamber. The vacuum system includes 25 capacitive sensors for determination of electron beam position and 10 units for observation of synchrotron radiation.

To improve the degree of electron bunching and reduce the power incident on the mirrors of the optical resonator of the third-stage FEL, it was proposed to modify the electron extraction by means of an optical klystron with a radiator placed in its buncher. Parameters of the undulators are presented in Table 6.4.6.

The magnetic units are mounted on the top and bottom supports of undulator. The supports, in turn, are fixed with driving screws attached to the frame. Rotating the screws, one can adjust the working gap of undulator and, hence, the amplitude of its field. All units of the undulators (except for purchased mechanical components) were made at the

experimental production of BINP. All the three undulators have been assembled by now (see Fig. 6.4.10).



Fig. 6.4.10 Assembling one of the three undulators of the third stage.

In addition, a station with a partially transparent mirror and a spectrometer was constructed for continuous measurement of the radiation spectrum.

6.4.4 Results of 2011 and plans for 2012

Main results of work in 2011:

Regular work was provided for the users of the first-stage FEL (wavelengths of 110-240 microns) and the second-stage FEL (wavelengths of 40-80 microns).

Construction of new stations was continued. A station was created for continuous measurement of radiation spectrum.

The assembly, commissioning and alignment of the elements of the four-track ERL for the third-stage FEL were completed.

Plans for 2012:

1. Commissioning of the four-track ERL.
2. Further work on the creation of the new stations.
3. Continuing designing and manufacture of components of the test stand of the RF injector.
4. Ongoing work of the user stations.
5. Magnetic measurements and correction of the magnetic field of the undulators of the third-stage FEL.

6.5 DESIGN AND DEVELOPMENT OF SPECIALIZED GENERATORS OF SR

In 2011, work continued on the development and production of various cryogenic superconducting

magnet systems for generation of synchrotron radiation.

A 7-pole prototype of the magnetic system of the 7.5 T multipole wiggler (Fig.6.5.1) with a magnetic gap of 26 mm and period of 200 mm for the CAMD-LSU storage ring (USA) was manufactured and successfully tested in February 2011. The fabrication of the full-size 15-pole magnetic system is underway. This wiggler has an extremely high stored energy of magnetic field: 800 kJ. This imposes specific requirements both on the system of coil protection at a quench and on the mechanical resistance of the copper liner to the influence of ponderomotive forces. The wiggler is planned to be mounted and commissioned directly on the CAMD-LSU storage ring in September 2012.

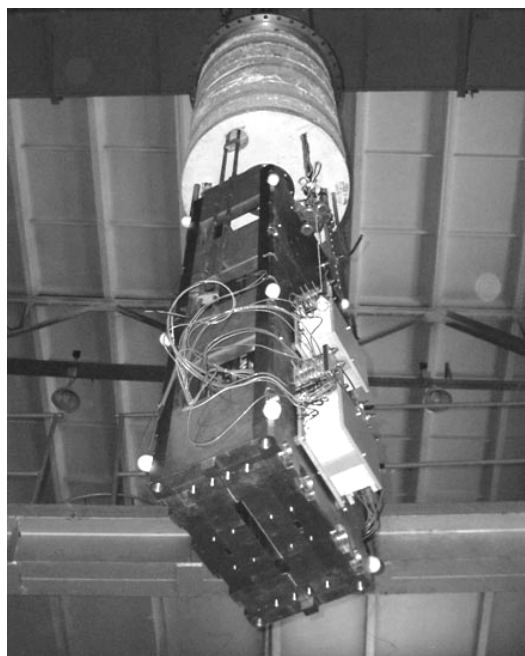


Fig. 6.5.1 Exterior view of the 7-pole prototype of the 7.5 T multipole superconducting wiggler for the LSU-CAMD storage ring (USA) before placement in the immersion cryostat.

In October 2011, a unique 119-pole superconducting wiggler with a working field of 2.1 T and a period length of 30 mm (Fig.6.5.2) was put into operation on the ALBA-CELLS SR source (Spain). The pole gap and the beam aperture are 12.6 mm and 8.5 mm, respectively. The total power of radiation in a horizontal angle of 2 mrad is about 16 kW at an electron beam current of 0.4 A and energy of 3 GeV. The wiggler was tested successfully with a 3 GeV electron beam. An X-ray beam of high brightness was extracted into the beamline to the experimental station "Powder diffraction". With an emittance of the ALBA-CELLS SR source of less than 5 nanometers and a maximum electron current of 0.4 A, the brightness of this beam will be among the highest in the world for 5-50 keV photons of continuous spectrum. For photon energies below 5 keV the radiation spectrum is of the undulator character.

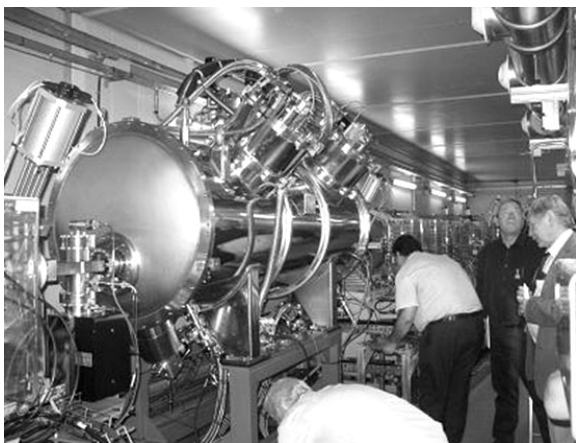


Fig. 6.5.2 T superconducting 119-pole wiggler on the ALBA-CELLS storage ring (Spain).

The full-size magnet system of the 63-pole wiggler (Fig.6.5.3) with a period of 51 mm, magnetic field of 4.0 T, and 15.2 mm pole gap for the Australian Synchrotron storage ring (Melbourne) was manufactured and successfully tested in an immersion cryostat in November 2011. An own cryostat for the wiggler is being fabricated now. The completed wiggler is to be tested in May 2012 and installed and commissioned directly on the Australian Synchrotron storage ring in July 2012.

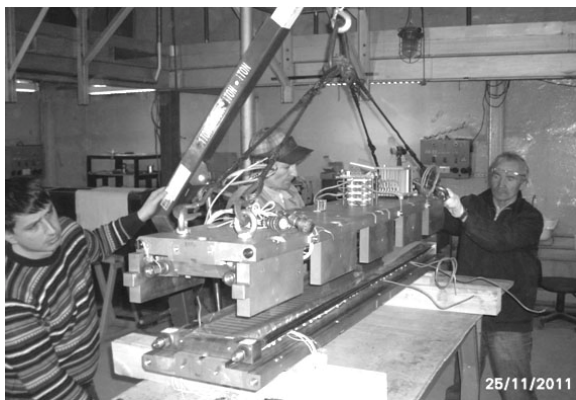


Fig. 6.5.3 Assembling the superconducting 63-pole magnet with a field of 4.0 T and a period of 51 mm for the Australian Synchrotron storage ring (Melbourne).

Along with new superconducting wigglers, insertion devices put into operation in recent years and working at various SR centers are becoming objects of increasing interest. For instance, the latest commissioned wiggler (ALBA-CELLS, Spain) allowed finding a few successful technical solutions, which led to a significant decrease in the liquid helium consumption and improved the general reliability of the cryostat. That is why, with the very first opportunity, they carried out a corresponding upgrade of some already existing wigglers. In particular, new-design

copper liners (Fig.6.5.4) were installed on two wigglers with fields of 3.5 T and 4.3 T, which have operated on the DLS storage ring (England) since 2006 and 2009, respectively. In addition, the scheme of cooling of special adapters on these two wigglers and a wiggler with a field of 3.6 T, operating since 2009 on the LNLS storage ring (Brazil), was upgraded. These adapters ensure smooth transition between the vacuum chamber and copper liners of the wigglers. These changes improved significantly the performance of the existing cryostats without substantial material expenses.

Another problem, associated the 7.5 T 21-pole wiggler operating since 2007 on the Siberia-2 storage ring at Kurchatov Institute in Moscow, was eliminated in November 2011. The problem was in mechanical instability of the copper liner in case of quench. This wiggler has a very high magnetic field (7.5 T) and large stored field energy (520 kJ), which, in case of quench, resulted in mechanical deformation of the copper liner due to the action of ponderomotive forces. The problem was solved via a significant optimization and modification of the design of the liner. The point is that the liner, which is a copper chamber of elliptic cross section, should meet rather contradictory requirements. On the one hand, the liner, which is actually designed to protect the vessel with liquid helium from heating because of the electron beam electromagnetic field, should have good electrical and thermal conductivity. On the other hand, the liner should have low electrical conductivity, since at a superconductivity quench there occurs an abrupt change in the magnetic field penetrating the walls of the liner, which induces currents and hence ponderomotive forces, which deform this liner. Additional calculations were performed and an optimal form of the liner cross section was found, corresponding to both requirements. Testing of the upgraded liner showed correctness of design selected.



Fig. 6.5.4 Installing the new liner on the 3.5 T multipole wiggler on the Diamond Light Source storage ring (England).

6.6 CONFERENCES, MEETINGS, AND SEMINARS

The fourth school of young specialists in synchrotron radiation was held at Budker Institute of Nuclear Physics SB RAS (BINP) on 10 to 13 October 2011. The School was

traditionally organized by BINP (Siberian Center for Synchrotron and Terahertz radiation).

The first such school was held at BINP in 1984, the second and third in 1985 and 1987. After a long break, this tradition was resumed in 2008.

School 2011 was attended by about sixty young scientists, including about fifteen people from various cities of Russia (mainly from Tomsk, as well as from Omsk, Yekaterinburg, and Irkutsk), the rest from Novosibirsk institutes, BINP among them. Unfortunately, a certain loss of interest in the SR School is observed – as few as 60 participants this year (100, 120, and 80 participants in 2008, 2009, and 2010, correspondingly), and even fewer people attended the lectures.

This school was combined with the third roving Russian-German seminar, which is held every year in different countries. In 2011 it was held in Russia, the cities of Moscow and Yekaterinburg preceding Novosibirsk. Ten young professionals from Germany and another ten from Russia participated in this seminar, which resulted in some amendments to the traditional program of the SR School. For example, all lectures of the first day were given by leading specialists in English.

As to the rest, the School traditionally covered the main areas of research on synchrotron radiation: small-angle diffraction, EXAFS, elemental analysis, LIGA technology, metrology, SR theory, and generation and application of terahertz radiation. As always, non-resident participants of the School were given an opportunity to get acquainted with the equipment of the Siberian SR center through introductory practice at its stations.

7

RADIOPHYSICS AND
ELECTRONICS

Introduction

BINP activity in the field of radio physics and electronics is concentrated mostly at the Radiophysics Laboratory. The main research area of the Laboratory is associated with the development and research of radiophysics systems for accelerators and charged particle storage rings, which in turn, are developed by the Institute in accordance with the government programs "Colliding beams", "High Energy Physics", "Synchrotron radiation", "Microwave Physics", and "Plasma Physics".

Under these programs, the Laboratory staff is engaged in the development of diverse electronic equipment: power, control, and diagnostics systems and computer control systems; RF accelerating systems and sources of RF and microwave energy. The Laboratory researches the behavior of charged particle beams in interaction with accelerating systems and other elements, and investigates components of accelerators and charged particle storage rings. It is obvious that the main results of the Laboratory activity are part of the common results of research and work carried out on the existing complexes: VEPP-4, VEPP-2000, FEL, and the Injection Complex, as well as the works on plasma physics.

Due their universality, some of the developments by the Laboratory became the basis for instruments and/or devices of an independent scientific or technological value. Some products are more or less used in works in other research areas of the Institute and performance of contracts with Russian and/or foreign research centers in the U.S., Germany, Switzerland, Japan, China, and South Korea.

It should be noted that year 2011 was particularly intense for the Laboratory 6 staff due to the huge amount of work on contracts with COSY (Germany), Brookhaven National Laboratory (USA), KAERI (Korea), TAE (USA), etc.

Below are some brief results of the works conducted by the Laboratory in 2011, as well as guidelines for works to be continued in the future.

7.1 POWER SUPPLIES FOR ELECTROPHYSICAL INSTALLATIONS

7.1.1. Stabilized current sources

Development of stabilized current sources for various electrophysical installations and their individual components is one of the main objectives of the Radio Physics Laboratory. Devices of this class include, first of all, DC sources for electromagnets of charged particle storage rings. The output current of such sources varies from a few amperes to tens of kiloamperes, which corresponds to an output power of tens of watts to hundreds of kilowatts and a few megawatts. Current sources, as a rule, are adjustable in a wide current range and have high accuracy of regulation and stabilization (error of 0.01% or less). Current sources are complex

electrophysical devices with computer control, monitoring, testing, and a complex system of interlocks and internal control devices. There are no analogues produced by the Russian industry.

Because of the long-term operation of power supplies and measuring equipment on physical facilities (accelerators and/or charged particle storage rings), the electronics becomes physically obsolete and loses its once best options. This inevitably leads to higher operating costs and forced stands of the complexes, which has to be taken into account at planning research works and finance.

- The long-term work on the upgrade of the electronics of the precise sources (the IST series) for feeding electromagnets was continued in 2011. Those are devices of a power of 50kW, 100kW, and 200kW, with thyristor control and a channel for ripple suppression. The sources are controlled by built-in single-channel 20-bit DACs (CEAC121). Current is measured with non-contact current transformers (DCCTs). Five stabilized current sources were upgraded in 2011. The upgrade included replacement of the electronics, intra-cabinet cabling, and capacitor banks. 18 sets of control electronics for the stabilized current sources were produced and adjusted, which provides modernization of a few sources of the IST series and 13 sources of the B-1000 type (1000 A, 20 V).

- A circuit for load current reverse was developed for IST current sources intended to power magnets of the K-500 beam line. Since the K-500 beam line is to transport both electrons and positrons from the injection complex to VEPP-2000 and VEPP-4, current polarity in the magnets is to be reversible. In 2011, the current reverse circuits were mounted in the power supplies of the K-500 beam line, as well as the power supply of the BEP magnetic system.

- Four modified power supplies of the IST series with an output current of up to 400 A and power of up to 200 kW were adjusted and put into operation in 2011. The thyristor rectifiers of these current sources are made by the Low-Voltage Equipment Plant (Rasskazovo, Tambov region) and contain control and current stabilization electronics designed and manufactured by BINP. The sources are used in the electron cooling installation developed by BINP for COSY. The modernization and operation of the main power supplies of BEP and VEPP-2000 was continued. Those are devices of the megawatt power range with current as high as 10 kA.

- The production of a number of original power supplies for electromagnets for the NSLS-II booster accelerator (BNL, USA) was completed in 2011. The booster can work at a repetition rate of up to 2 Hz, which imposes rather unique requirements on the power supplies. Along with high requirements to the current stabilization accuracy, the power supplies should have good dynamic characteristics. In particular, the time of current rise from the minimum to the nominal value should be 0.26 seconds or less for all the power supplies.

The total number of power supplies developed and manufactured for the booster magnets is over 50. Table 7.1 shows the basic parameters of the Lab 6 power supplies for NSLS-II.

- In 2011, the development and manufacture of precision current sources with an output of 10 kW, made with about 20 kHz power conversion, was continued. In particular, new high-precision four-quadrant power supplies of the HF-500 type (500A/12V) were developed and manufactured. The power supplies are to be delivered to BNL, USA (2 pcs.), and KAERI, Korea (4 pcs.).

- The development was completed and full-scale tests begun of a high-power (with an output current of 800 A and a maximum voltage of 400 V) precision arbitrary-shape current source. Such current sources are required for powering dipole magnets of synchrotrons and booster accelerators operated at a repetition frequency of 1-2 Hz.

- A significant amount of high-precision current sources for correctors was manufactured under a number of contracts. In particular, there were fabricated over 160 current sources of the MPS-6 type (output current of up to 6A), over 25 current sources of the MPS-20 type (output current of up to 20 A), and up to ten two-channel units of the SR-20-30 type (current stabilizers based on shunting of the coils of the magnets).

- Over 20 channels of precision current sources of the UM-1, UM-3, and UM-10 types with output currents of 1 A, 3 A, and 10 A, respectively, were made and put into operation. The sources are installed on the FEL, ELS, and LIA accelerator complexes.

Table 7.1.1

Power supply	Number	Max. current, A	Max voltage, V	Max power, W
BR-QF	1	157	207	32.496
BR-QD	1	85	49	4.200
BR-QG	1	126	73.2	9.22 9
BR-SXV	8	18	17.4	2.507
BR-SXH	8	18	17.4	2.507
BR-Corr	32	7	8.8	1.963
DC-septum	1	400	15	6.000

7.2. HV SOURCES OF STABILIZED DC VOLTAGE

The Laboratory has successfully developed HV sources of stabilized DC voltage for a wide range of power:

- tens of watts, for powering of electrostatic devices for deflection or focusing charged particle beams;
- hundreds of watts to tens of kilowatts, for powering of various high-voltage "direct action" accelerators;
- hundreds of kilowatts, for high-voltage powering of ion sources and atom injectors.

The high-voltage power supplies have high stability and accuracy of regulation; they are protected against short circuits and breakdowns.

7.2.1. High-voltage sources for atom injectors for diagnostics and heating of plasma in plasma installations

Designing and manufacture of powerful high-voltage sources for atom injectors for particle diagnostics and heating of plasma in experimental plasma installations

remains one of the important activities of the Laboratory. In particular, in 2011 the Laboratory:

- put into operation two high-voltage power supplies (40kV/15A/300ms) for the "heating" injectors for the Compass-D tokamak (Prague, Czech Republic), each consisting of 12 series-connected RF rectifiers fed from 12 controllable 10 kHz inverters.

- continued the development and manufacture of individual units of the high-voltage power supply for the high-power injector of negative ions, under a contract with TAE. The power supply has the following parameters: $U(\text{out}) = -660 \text{ kV}$, $I(\text{out}) = 10 \text{ A}$, $T(\text{pulse}) = 100 \text{ sec}$ and consists of six series-connected high-voltage rectifiers with an output voltage -110 kV, placed in one volume filled with insulating gas. Regulated AC voltage (2 kHz, 3 kW) is applied to these rectifiers from voltage inverters with a frequency of 2 kHz and output power of 500 kW each. The voltage inverters are now being developed by the Laboratory.

- The Laboratory is making a high-voltage source (-120 kV, 100 mA) for a stand of the source of negative ions at TAE, the U.S. The high-voltage source consists of a cascade generator and a regulable voltage inverter of high (20 kHz) frequency.

7.2.2. High-voltage power supplies for electron accelerating tubes

The development, improvement, and manufacture of components and assemblies of high-voltage power supplies for electron accelerating tubes were continued in 2011:

- elements of cascade generator (push-pull voltage multiplier) are used in the manufacture of high-voltage power supplies for the electron tube for a FEL and accelerating tube for a electron beam welder (EBW) for a beam current of up to 100 mA. The output voltage of the FEL high-voltage power supply is up to -300 kV and the EBW one is up to - 60 kV.

- a high-voltage rectifier with an output voltage of up to - 60 kV and a semiconductor high- frequency converter (20 kHz) were designed and manufactured for a high-power (up to 60 kW) EBW.

- a high-power (40 kW) resonance high-frequency converter (25 kHz) was developed for feeding an accelerating tube with a voltage of up to 2 MW for the electron cooling installation for the COSY accelerator, Germany.

- for recovery of the injector of electrons at KAERI (Korea), works were carried out on the reconstruction of the high-voltage power supply (-300 kV, 15 kW). A new adjustable low-frequency (500 Hz) resonance voltage inverter was made; preventive maintenance works were conducted for the -300 kV high-voltage rectifier.

One of the most complicated works in 2011 was the completion of the fabrication and the start of experiments on the electron cooling installation for COSY, Germany. A "high-voltage tower", creating an adjustable stabilized voltage of up to -2 MV, consists of cascade-connected high-voltage transformers. Auxiliary windings of the transformers are used for generation of variable current in solenoids, which are at corresponding high potentials. "The high-voltage tower" is a complex mix of power, control, and measurement electronics. A 15 kW collector is used as the electron beam dump of the electron cooling installation. An original voltage source of up to 15 kW at a high-voltage potential of -2 MV was designed and manufactured for generation of regulated voltage on the collector (1 - 5 kV).

7.2.3. Switch-mode power supplies for electromagnets of accelerator complexes

Production of a large number of pulse current generators was continued in 2011. In particular, 75 pulse-mode power supplies of the GID-25 type were made for the K-500 beam transport line. One radio rack comprises eight generators of the GID-25 type, automated control units, and two 4-channel units for rapid measurement of output current. All eight generators, placed in one rack, are powered from a common AC/DC 24V power supply.

Original pulse current generators MIG-100 were designed and manufactured for pulse-mode power supply of the focusing system of the linear pulse accelerator (LIA). Generators MIG-100 are capable of generating current pulses with an amplitude up to 800A. One radio rack comprises six generators. The system is equipped with computer control units and output pulse current meters.

7.3 DEVELOPMENT OF MEASUREMENT SYSTEMS AND AUTOMATION OF PHYSICAL EXPERIMENTS

The Laboratory participates in the following works on automation of facilities, stands, and large physics complexes:

- development and delivery of completed systems (control, monitoring, diagnostics, and computer systems) with subsequent participation in the adaptation of the systems to the physical facilities;

- development of elements of control, monitoring, and timing of power systems with subsequent complex delivery of these systems to accelerators and charged particle storage rings and study of their effect on the complex as a whole;

- delivery of individual standardized modules (CAMAC, VME, VISHNYA, Euromechanics) to existing or new installations and test facilities;

- development of new approaches, techniques, and, as a result, new devices that allow solving experimental tasks at a new level;

- upgrade of existing systems for automation, control, and diagnostics on existing physics facilities;

- repair and maintenance of several thousands of electronics units and entire systems developed by the Laboratory and being in use.

Equipment developed and manufactured by BINP is widely used not only at SB RAS, but also in many scientific organizations in Russia and abroad. Main results in 2011:

- commissioning at VNIITF (Snezhinsk) of the control system for the linear induction accelerator for pulsed radiography, which allowed conduction of first experiments with real objects;

- creation of the required hardware and software for a wide range of measurements of BINP-produced magnetic elements for the NSLS-II booster: dipole magnets, quadrupole and sextupole lenses, kickers, bumps, and septum magnets. To this end,

- one more Hall measurement system was manufactured and launched on the stand of EP-1;

- the second system for measurement of the multipole components of magnetic lenses was made; the system has very high accuracy parameters;

- electronics for measurement of pulsed magnets of the NSLS-II booster was designed, manufactured, and adapted;

- equipment for measurement of the kickers for injection/extraction on NSLS-II was constructed and put into operation;

- the system for measurement of pulse parameters of the dipole magnets of the NSLS-II booster was prepared for work;

- the stand for magnetic measurements for the COSY cooler was fabricated and put into operation.

- Fabrication, adjustment, and putting into operation of about 150 various units with the CAN-BUS interface for the systems for control and monitoring of electro physical installations. A detailed description of the modules is available on the site of the Laboratory. It should be noted that devices of this family are widely used in contract works. In recent years, more than half of the produced modules (a total of 1100 pieces) together with various power supplies and measurement and control systems were delivered under Russian and foreign contracts.

- Designing and manufacture of a required amount of high-precision digital integrators VSDC-3, intended to measure instantaneous values and shapes of pulsed magnetic fields.

- Modernization of waveform recorders ADC - 200ME. The new modules are intended for the monitoring and control systems of the NSLS-II booster.

- Adjustment and putting into operation of a set of electronics modules for powering and controlling the electron gun of the ion cooler (COSY).

- Designing and implementation of a wireless communication CAN channel for control of the electron gun of the ion cooler (COSY)

- Manufacture and commissioning of two versions (manually- and computer-controlled) electronics for the magnetic field adjustment system in the solenoid of the ion cooler (COSY)

- Participation in the development and implementation of the control system for the NSLS-II booster. The thermal switch inquiry system and cross-boxes for the vacuum control system and monitoring and security devices were designed and manufactured. Operation with the Allen-Bradley PLC was mastered; a set of software was written for testing of the components of the control system of the NSLS-II booster.

- Work on the creation of the control system for the four-track FEL was prolonged.

- Installation and commissioning of the new modulator of the electron gun of the FEL injector. The modulator has unique parameters: a pulse duration of 1 ns, an amplitude of 0 to 120V at a load of 25 Ohms, and a repetition rate of 0 to 90 MHz.

- Tests of the new timer (90 MHz) for the modulator of the injector gun.

- Continuation of the implementation of up-to-date intelligent controllers in control systems of physics facilities. One more batch of controllers and CAN-

Ethernet gateways for various installations of the Institute was fabricated.

- Completion of the replacement of obsolete equipment of the power control systems of the main magnetic elements of the VEPP-4 storage ring. For this purpose, a high-precision (0.002%) interpolating DAC with the MIL-STD-1553B interface was developed. The module software and hardware are compatible with the previous outdated design, which made it possible to keep the existing software of the control systems of the complex unchanged.

- Continuation of the development of a new power supply for electron beam welders with an option of indirect heating of cathode with electron beam. The aim is to create a cathode design with a significantly increased lifetime.

- System for joint search and electron beam aiming for the electron beam welder at EP-1. Modernization of the system to improve welding technology at the stand of laboratory 5-1 was continued.

- Conduction of real-condition tests of the two-channel precision current meter (a resolution of 2 to 3 fA) for ionization chambers. The meter is intended for experiments using synchrotron radiation. The results obtained allowed proceeding to the development of a production sample of the meter.

- Start of development of the time interval generator module for equipping numerous pulse systems of the K-500 beam line.

- Completion of the development of the system for monitoring of main parameters of the heat pump used in the cooling system of the accelerator complex.

- Fabrication and commissioning of the new electronics for the pickups of the VEPP-2000 complex.

- Development and fabrication of the new electronics for orbit measurement on the VEPP-3 complex.

- Fabrication and adjustment of electronics for the pickups of the electron cooling installation for the COSY accelerator.

- Development of the prototype unit for signal processing in the betatron frequency measurement system of the NSLS-II booster. Tests were performed on the VEPP-3 storage ring; relevant corrections were made and fabrication of a working system for NSLS-II started.

- Construction of a new automated high-precision stand for measurement of parameters of pickups. Parameters of the first batch of 7 pickups for the NSLS-II booster were measured. Parameters were also measured on a special stand for 3-strip sensors for the booster NSLS-II.

- New unit for matching and fast protection of the modulator of the klystron 5045 (the Injection Complex) for replacement of obsolete units, which were developed about 15 years ago.

- Development of a switch for powering of vacuum getter-ion. A prototype (50A/30V) was made.

- 12 capacitance and 12 upgraded ultrasonic hydrostatic sensors were developed and fabricated for the University of Montana (USA). 10 capacitance hydrostatic

sensors were made for KEK (Japan). Collaboration on the technical support to the hydrostatic system of monitoring of magnetic elements on the Tevatron accelerator (FNL, USA) was continued. The hydrostatic systems created by BINP Lab. 6-0 have operated at FNL for more than 10 years.

- Designing and manufacture of a prototype semiconductor RF generator with the option of amplitude modulation of an output 4 MHz voltage for powering the plasma emitter of the ion source of the diagnostic atom injector. The prototype, which provides an output power of 10 kW, was tested in operation in the atom injector. The development of a semiconductor RF generator with an output power of up to 20 kW was continued.

- A filament power supply with an emission pulse current of up to 2 kA. The power consumed from the current source is up to 2 kW in the continuous mode. A typical feature of the source is that the filament current rises within a few minutes (an adjustable parameter) with continuous monitoring of operation.

- Fabrication of 30 electrical drives of the ESHD-5 type for the stepper motors of VEPP-5.

- Automation of another two ovens for the gluing area of work EP-2.

The technical maintenance of earlier made electronic systems and their components in use at facilities at and beyond the Institute was continued.

Table 7.3.2 Family of devices with the CAN - BUS interface

Name	Brief description
CANDAC16	16-channel, 16-bit DAC; 8-bit input and output registers
CANADC40	40-channel, 24-bit ADC (class 0.03%); 8-bit input and output registers
CDAC20 CEDAC20	20-bit DAC; 5-channel, 24-bit ADC (class 0.003%); 8-bit input and output registers (VISHNYA and Euromechanics)
CEAC 51	20-bit DAC; 5-channel, 24-bit ADC (class 0.003%); 8-bit input and output registers (Euromechanics 3U)
CAC208 CEAC208	8-channel, 16-bit DAC; 20-channel, 24-bit ADC (class 0.003%); 8-bit input and output registers (VISHNYA and Euromechanics)
CEAC124	4-channel, 16-bit DAC; 12-channel, 24-bit ADC (class 0.003%); 4-bit input and output registers (Euromechanics 3U)
CEAC121	1-channel, 16-bit DAC; 12-channel, 24-bit ADC (class 0.003%); 4-bit input and output registers (Euromechanics 3U); for control of fast sources
CEAD20	20/40-channel, 24-bit ADC (class 0.003%); 4-bit input and output registers (Euromechanics 3U)
CGVI8	8-channel, 16-bit delayed pulse oscillator; 8-bit input and output registers
CPKS8	8-channel, 16-bit code-duty factor converter
SLIO24	CANbus interface: 24-bit bidirectional bus, built-in card
CKVCH	Commutator of RF signals 8-1, 2*(4-1) 4*(2-1)
CANIPP	CANbus interface: 2 branches of the BPM type
CANIVA	16-channel vacuum meter (current of ion pump)
CURVV	Universal input/output register (2 input and 4 output registers of 8 bits)
CIR8	Recorder of discrete signals (interrupt register, BSI, input/output registers)
CAC168	8-channel, 16-bit DAC; 16-channel, 24-bit ADC (class 0.03%); input and output registers; built-in card
CAN-DDS	CAN-DDS module: divider of input clock frequency with remotely tunable fractional coefficient
CAN- ADC3212	For closing the feedback loop in the thermal adjustment scheme of RF cavities.
CANGW	Ethernet-CAN/RS485 gateway
VME-CAN	VME-CAN interface
CEDIO_A	Multi-port input/output register
GZI-CAN	4-channel generator of delayed pulses, 80 ns - 10.28 μ s
VSDC2	Module for precision measurement of magnetic fields by the induction method, 2 channels
IVI1811	Time interval meter with a resolution of 0.5 ns

7.4 RESEARCH RELATED TO MODELING AND SOLUTION TO ELECTROSTATIC AND ELECTRODYNAMIC PROBLEMS OF ACCELERATOR PHYSICS

In 2011, the Laboratory continued calculating and designing elements of accelerators, both for the Institute and under international contracts. In so doing, the computational methods and software were developed and modernized for calculation, designing and computer modeling of the dynamics of charged particle beams, including the following:

- Under a contract on the creation of a powerful source of neutral particles, the final optimization of magnetic field in a plasma charge-exchange target was carried out; electron fluxes on the chamber walls were estimated; the final version of the magnetic system was passed to the designing department.

- Under the contract on the creation of a high-voltage installation for electron cooling (COSY), the Laboratory continued its work on the electron gun and collector. Stand measurements of the design were carried out; comparison of the data showed good agreement between the calculated and measured parameters.

- Works on the software for calculation of electrostatic and magnetostatic fields and electron and ion guns were continued. The pre- and post-processors in the software UltraSAM were significantly improved; errors revealed were eliminated.

Under the contract on the development of a prototype injector of high-energy atom beam based on a source of negative ions, the Laboratory carried out numerical simulation, including the following:

1. As part of the designing of a prototype atom injector with one "driver":

- calculation and optimization of the field of the plasma expander with peripheral permanent multipole magnets;

- calculation and optimization of the field of the magnetic filter of the plasma electrode;

- calculation and optimization of the deflecting magnet of the ion-optical system;

- calculation of electric fields in the ion-optical system of the prototype atom injector with one driver and "single-aperture extending";

- calculation of the trajectories of accelerated negative ions and co-accelerated electrons.

2. Similar calculations for the prototype high-voltage high-power atom injector with four drivers and a beam current of 1.5 A.

3. Calculations of beam passage from the ion source through the bending magnets and the accelerator for the prototype with four drivers and a 1.5A beam.

- Going on development of the Laboratory site <http://www.inp.nsk.su/activity/automation/index.ru.shtml>. This site should contribute to fuller and better use of developments by the Laboratory. For this purpose,

operation manuals (application notes) were added to descriptions of various modules. The site is updated regularly.

7.5 EQUIPMENT OF THE ACCELERATING STATIONS OF THE COLLIDER COMPLEX NICA

The collider is designed for experiments with gold nuclei at energy of 1 GeV/n to 4.5 GeV/n. The number of particles in each beam is $6.3 \cdot 10^9$ at an energy of 1 GeV/n and $5.5 \cdot 10^{10}$ at an energy of 4.5 GeV. The number of particles can be considered depending linearly on the energy. The beam current is 0.4 A at an energy of 4.5 GeV/n. The particle revolution frequency varies depending on the energy the experiment is conducted at, from 522 kHz to 587 kHz (12.45%). Each beam in the collider is moving in its own ring, which is a strong-focusing accelerator with a critical energy of 7.1 GeV/n. The distance between the axes of the vacuum chambers of each ring is 320 mm, and the diameter of their aperture is 100 mm in the places of location of the accelerating stations.

There should be four types of accelerating stations in each ring of the collider. The first type is a barrier station, which can be used for accumulation and acceleration of particles at energy of 600 MeV/n to 4.5 GeV/n. This station is to generate a sequence of accelerating and decelerating voltage pulses for ions. Depending on the particle energy, the pulse repetition frequency ranges from 473 kHz to 587 kHz. The pulse duration is 1/12 of the ion orbital period in the ring of the collider. The voltage of the pulses is 5 kV. The shift in time between the accelerating and decelerating pulses is 1/2 of the orbital period of particles in the ring. Ions are injected into the ring between accelerating and decelerating pulses, whereas particles are accumulated between decelerating and accelerating pulses. Accumulation is to be accompanied by electron or stochastic cooling.

The barrier station is a coaxial line filled with rings of amorphous iron type 5 TM. The line length is 0.9 m. Voltages from the sources are applied to the rings with the use of the switch transistors DRF1201. These voltages form a sequence of +5 kV, 0 V, -5 kV, 0V of a respective duration on the open part of the coaxial line. In the break of the vacuum chamber of each ring there is a cylindrical ceramic insulator. The open parts of the coaxial line are connected to the break.

For gold ions to be accelerated in the energy range of 600 MeV/n to 4.5 GeV/n, there has to be a pulsed accelerating station (zero-type accelerating station) operating together with the barrier system. This station is similar in design to the barrier system. The pulsed accelerating station should create "meander"-like voltage with a frequency of ion circulation in the accelerator and a voltage of ± 300 V. This ensures an ion acceleration rate of 120 eV/n per turn and ion acceleration of 4 GeV/n in about 70 seconds. The beginning of the accelerating

"meander" voltage pulse should be in the middle of the decelerating voltage pulse of the barrier station.

The barrier station and the pulsed accelerating station are located on the same base 2000 mm long (Fig.7.5.1). A heating cable is wound on the parts of the accelerator vacuum chamber that are located under the coaxial lines of the barrier and pulsed accelerating stations. There should be thermal insulation between the cable and the inner cylinders of the coaxial lines of stations. The heating cable is used for heating the vacuum chamber during the preparation of the required vacuum. The barrier and pulsed accelerating stations have a common vacuum pump MRN250.

At the ends of the vacuum chamber, which passes through the barrier station and pulsed accelerating station, there are two vacuum gates.

The second station creates a harmonic voltage at the 24th harmonic of the particle revolution frequency in the accelerator. The maximum accelerating voltage that can be created by one station is 25 kV. Each ring of the collider is to comprise four such stations, which can create an accelerating voltage of 100 kV.

The third stations operate at the 72nd harmonic of the ion revolution frequency. The maximum accelerating voltage of one of these stations is 125 kV. Each ring comprises eight stations. The accelerating voltage in each ring is up to 1 MV at this frequency.

All the stations are equipped with mechanical contactors of the accelerating gaps with a response time of $0.1 \div 0.2$ seconds.

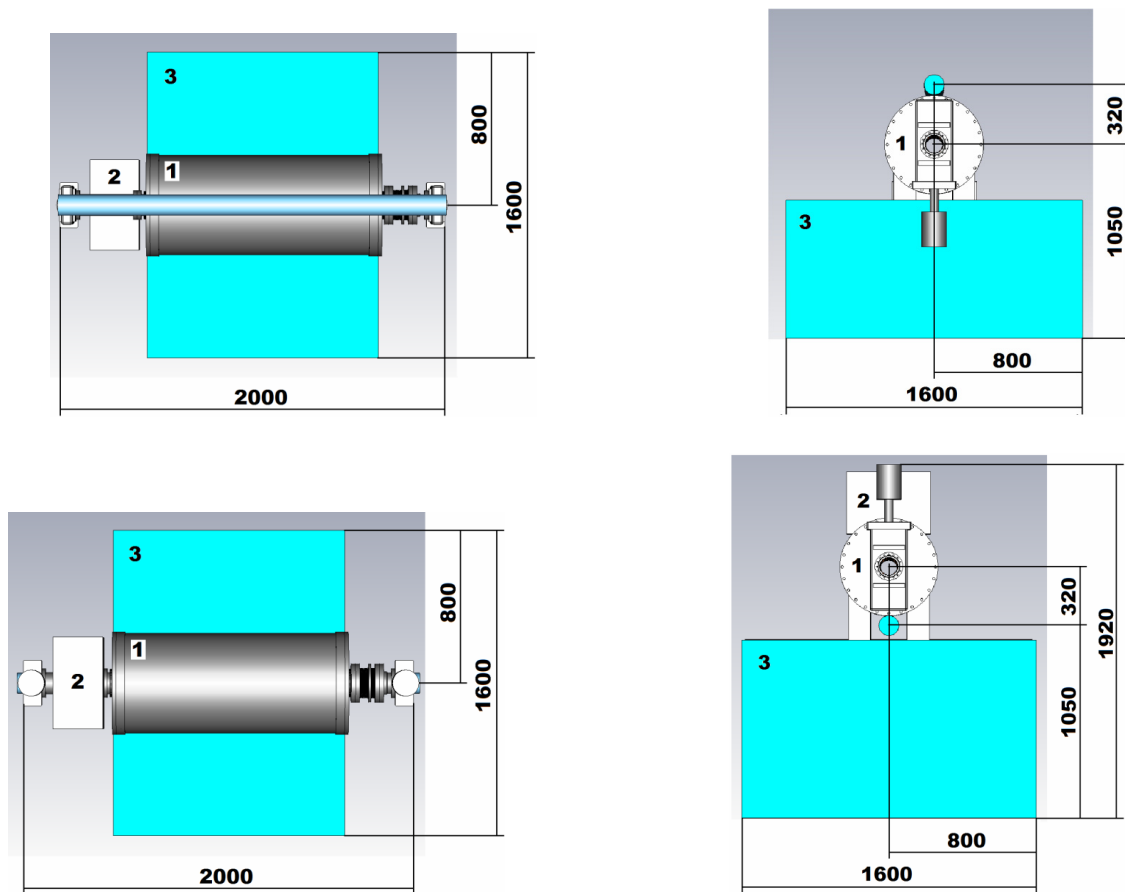


Fig. 7.5.1: Dimensions of the cavities of RF systems 1 and 0 for the lower and upper rings of the NICA collider: 1 – cavities, 2 – vacuum pumps, 3 – bases.

The acceleration systems work as follows. During injection of particles into the ring, the mechanical contactors of the accelerating gaps of the barrier and pulse stations are opened, and the gaps of the rest stations are closed with mechanical contactors. Voltage is applied only to the barrier station. Once the required ion current has been accumulated, the ions are accelerated up to the energy of the experiment. For this purpose, in accordance with the desired rate of acceleration, voltage on the pulsed

accelerating voltage station is switched on; the frequency of the pulse voltages of the barrier and pulsed accelerating voltage stations is increased; the fields in the magnetic systems of the accelerator ring are magnified. If the ion energy reaches the energy of the experiment, increase in the accelerating voltage frequency and magnetic fields is stopped; voltages on the barrier and pulsed accelerating voltage stations are switched off. Once the ion beam uniformly fills the entire accelerator, the mechanical

contactors short-circuit the accelerating gaps of the barrier station and pulse acceleration voltage station. After that, the electron or stochastic cooling is to reduce the energy spread of ions to such a value that the ions can be intercepted into twenty-four bunches. Then, the mechanical contactors of the accelerating stations of the 24th and 72nd harmonics are to open the accelerating gaps. Before that, the RF cavities of these stations should be tuned so that after opening the natural frequencies of the RF cavities of the second stations are tuned to a frequency located midway between the 24th and 25th harmonics of the revolution frequency of the ions, and the cavities of the third stations tuned to a frequency located midway between the 72nd and 73rd harmonics. In addition, the parasitic resonances of the accelerating cavities due to the connected tubes GU-92A should be pre-tuned so that their resonant frequencies are located in the middle of the harmonics of the revolution frequencies. Such tunings provide minimum increments for coherent synchrotron oscillations.

After that, voltage at the stations of the second type is slowly increased; the continuous beam is divided into 24 bunches; voltage at the stations of the 72nd harmonic is increased for reduction of the bunch length to the desired value ($\sigma = 0.6$ m). In this state, the RF systems of the collider are ready for experiments with colliding beams.

7.5.1 Cavities of RF system 2 (the 24th harmonic), NICA

High-frequency systems 2 are completely identical for the top and bottom rings of the NICA collider. The main parameters of one RF system are listed in Table 7.5.1.

Each RF system will consist of 4 cavities arranged in pairs. Each pair will be located on a common base. Dimensions of a two-cavity assembly for the upper and lower rings are shown in Figs. 7.5.2 and 7.5.3.

Calculation of the first higher monopole modes of cavity shows that the minimum width of the accelerating gap and its symmetrical arrangement can significantly reduce their influence on the beam.

A multipactor discharge in the RF cavity of system 2 was simulated with the code MPS, which determined the

areas in which a discharge may occur at voltages on the cavity of 2 to 4 kV and 5 to 8 kV. The central tubes of the coaxial electrodes will be coated with TiN, which will reduce the risk of a multipactor discharge.

Table 7.5.1 Parameters of RF system 2.

Parameter	Value
Revolution frequency	522 ÷ 587 kHz
Operation harmonic number	24
Operation frequency	12.528 ÷ 14.088 MHz
Full voltage	100 kV
Beam current	0.4 A
Number of cavities	4
Voltage on one cavity	25 kV

Parameters of the fundamental mode of cavity are presented in Table 7.5.2.

Table 7.5.2 Parameters of the cavity of RF system 2.

Parameter	Value
Operation frequency	12.528 ÷ 14.088 MHz
Operation frequency tuning range	~ 1.9 MHz
Characteristic impedance	15.4 ÷ 17.3 Ohm
Basic Q ($Q_{SLANS} \cdot 0.8$)	3, 570 ÷ 3, 750
Shunt resistance	54.8 ÷ 65.0 kOhm
Accelerating voltage	25 kV
Beam current	0.4 A
Power of RF losses in cavity	5.7 ÷ 4.8 kW

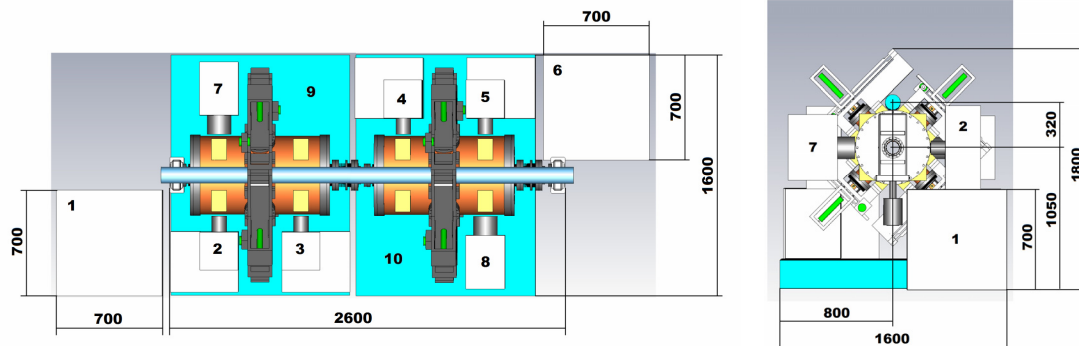


Fig.7.5.2. Overall dimensions of the RF cavities of system 2 for the bottom ring of the NICA collider: 1, 6 – racks of the air-cooling system of the generators; 2, 3, 4, 5 - RF generators, 7, 8 - vacuum pumps, 9, 10 - bases.

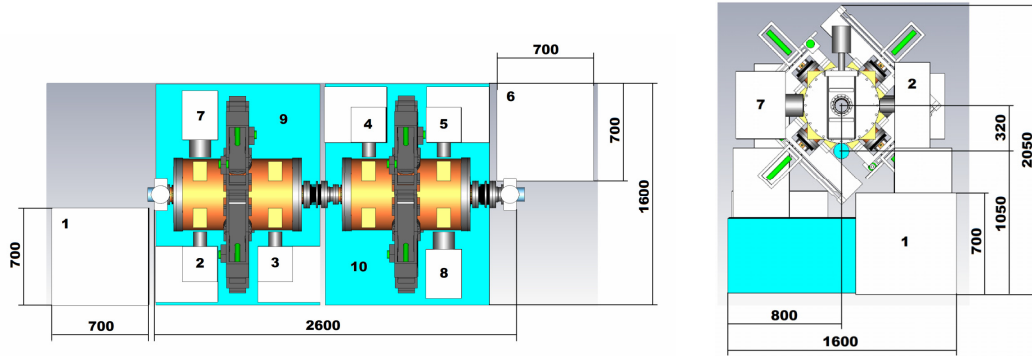


Fig.7.5.3. Overall dimensions of the RF cavities of system 2 for the upper ring of the NICA collider: 1, 6 – racks of the air-cooling system of the generators; 2, 3, 4, 5 - RF generators, 7, 8 - vacuum pumps, 9, 10 - bases.

7.5.2 Cavity of RF system 3 (the 72nd harmonic), NICA

characteristic impedances ($\rho_{\text{off-axis}}$) for a displacement of 1 mm are written in columns 4 and 8.

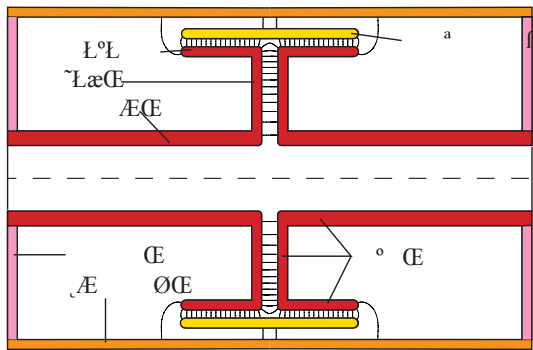


Fig.7.5.4 Schematic drawing of cavity of RF system 3

The revolution frequency range of 522÷587 kHz corresponds to ion energies of 600÷4500 MeV or velocities $\beta=0.877\div0.985$. The cavity is tuned to the 72nd harmonic of revolution frequency (37.584÷42.264 MHz) via variation of the capacitor of the accelerating gap. The four capacitor segments, placed symmetrically in azimuth around the capacitor of the accelerating gap, are synchronously moving in the radial direction. The mechanical adjustment displacement is 8.4 mm. Cavity characteristics in Table 3 are given for the two extreme values of β . The effective impedances are also presented (with due account of the transit factor).

Bunches in the collider are of the length $\sigma(\text{rms})=0.6\text{m}$. The envelope of the harmonic spectrum of the bunch current is shown in Fig. 7.5.5. The value of the envelope of the beam current harmonics at the higher-mode frequencies of the cavity in Table 7.5.4 is less than 10^{-7} A. Consequently, their influence on the excitation of coherent synchrotron oscillation modes can be neglected.

Table 7.5.5 presents characteristics of off-axis modes. Because of the mirror symmetry of the cavity, these modes have negligible impedances. The influence of symmetry violation was modeled via displacement of the capacitor segments in parallel to the axis. The effective

Table 7.5.3 Parameters of cavity of RF system 3.

Parameter	Value ($\beta = 0.877 \div 0.985$)
Operating frequency	37.584÷4.264 MHz
Operating frequency tuning range	~4.7 MHz (~12%)
Characteristic impedance	36.853÷42.51624 Ohm
Basic Q ($Q_{\text{SLANS}} \cdot 0.8$)	5, 494÷5, 816
Shunt resistance	252÷304 Ohms
Maximum accelerating voltage	125 kV
Maximum beam current	0.4 A
Maximum power of RF losses ($P_{\text{SLANS}}/0.8$)	38.6 ÷ 32.1 kW
Dimensions: diameter/length with a 15 mm wall thickness	520/750 mm

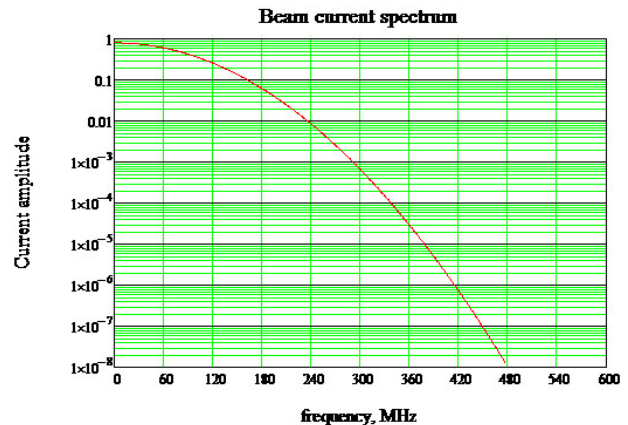


Fig. 7.5.5 Envelope of the harmonic spectrum of the beam current.

Table 7.5.4 Characteristics of monopole modes of cavity

Number	$\beta = 0.877$				$\beta = 0.985$			
	F, MHz	ρ , Ohm	R, kOhm	Q	F, MHz	ρ , Ohm	R, kOhm	Q
A	37.58339	36.853	252.1	6, 868	42.51624	41.86	304	7, 270
2	439.1537	0.239	1.5	6, 082	448.8326	0.157	2.0	12, 580
3	452.8919	0.077	1.1	13, 881	461.5183	1.419	5.4	3, 800
4	533.7109	10.112	60	5, 938	508.6281	6.31	36	5, 697
5	852.0069	2.369	39	16, 412	845.7928	3.98	65.6	16, 490

Table 7.5.5 Characteristics of monopole off-axis modes of cavity

Number	$\beta = 0.877$				$\beta = 0.985$			
	F, MHz	ρ , ohm	$P_{\text{off-axis.}}$, Ohm	Q	F, MHz	ρ , ohm	$P_{\text{off-axis.}}$, Ohm	Q
A	47.10234	$1.4 \cdot 10^{-16}$	$5.2 \cdot 10^{-4}$	7,876	59.0437	$7 \cdot 10^{-17}$	$1.2 \cdot 10^{-4}$	8,860
2	440.8700	$2.6 \cdot 10^{-19}$	0.066	6,402	449.4788	$1 \cdot 10^{-14}$	$7.5 \cdot 10^{-3}$	16,404
3	453.4763	$4 \cdot 10^{-20}$	0.021	12,344	469.7503	$2 \cdot 10^{-13}$	0.124	3,023
4	825.7762	$6 \cdot 10^{-16}$	$4 \cdot 10^{-7}$	11,441	790.6847	$7 \cdot 10^{-12}$	$8 \cdot 10^{-8}$	12,339
5	901.5797	$5 \cdot 10^{-19}$	$6 \cdot 10^{-4}$	26,879	900.2089	$3 \cdot 10^{-19}$	$5 \cdot 10^{-4}$	29,087

7.5.3 Water-cooling system

There are water-cooling channels laid in the walls of individual parts of the cavity. The maximum RF power losses on the surface of these parts (see Fig.7.5.5) are shown in Table 7.5.6.

Table 7.5.6. Maximum RF power losses ($P_{SLANS}/0.8$)

Name of cavity parts (see Fig.7.5.4)	Maximum RF power losses, kW
Shell	5.2
Wall	$2.3 \times 2 = 4.6$
Electrode =tube+disk+cylinder	$12.5 \times 2 = 25$
Segments of tuners	$0.91 \times 4 = 3.7$
Entire cavity	38.6

7.5.4 Multipactor discharge

Simulation with the code SLANS.

No multipactor discharge occurs in the accelerating gap.

A discharge arises in the volume of the cavity under the following conditions:

Table 7.5.7.

Accelerating voltage MV	Secondary emission coefficient
0.08	1.3
0.10	1.5
0.12	1.8
0.14	2.5
0.16	3.0
0.18	3.5

7.5.5 Suppression of multipactor discharge

Items 1, 2 and 3 below were modeled with the code ASRTRA; item 4 with the code SLANS; items 5 and 6 were not modeled. The effectiveness of multipactor discharge suppression by methods corresponding to items 5 and 6 was confirmed experimentally on the cavities of VEPP.

1. A TE mode at 1117 MHz suppresses the multipactor discharge, but this requires $4.2 \cdot 10^8$ W (mp2.1.in)

2. A symmetric mode at 47.2 MHz has almost no effect (mp2.2.in).

3. A symmetric higher mode at 453 MHz also has little effect on the multipactor (mp2.3.in).

4. Grooves on the central electrode slightly increase the secondary emission coefficient. Practically no suppression.

5. A ring at a high potential around the central core of 234 mm in diameter and a tube of 10 mm. The distance from the center of the axis is 177 mm. The power of RF losses is 400 Wt. Air- or water-cooling of the ring is required.

6. Coating of the inner surfaces of cavity (electrode and walls) with titanium nitride in a special chamber.

7.5.6 Cavity design

Fig. 7.5.7 shows the technical solutions in the design of individual units of the cavity.

7.6 RF INJECTOR OF THE MICROTRON-RECUPERATOR

The RF injector of the microtron-recuperator consists of an accelerating cavity for a frequency of 90 MHz with built-in controllable hot cathode. The RF injector is to replace the static injector installed on the microtron and allow attaining a record average beam current of 100 mA at injection into the microtron.

All the works associated with the manufacture of the RF injector by the experimental production department of BINP were completed in 2011. For the purpose of production of high vacuum, the cavity of the RF injector was baked out in a vacuum oven. Then the RF injector was mounted in the 11th building, where a test stand is now being created for it.

The tests include the training of the cavity at high RF power for attaining of high accelerating gradient. Then, once the hot cathode unit is installed in the cavity, tests with beam will be conducted.

At this point, the test stand is almost finished. The test stand includes, besides the cavity, a 100 kW RF generator on the tube GU-101A. The RF generator was assembled and tested at a dummy RF load. A 100-meter feeder connecting the generator with the cavity was made. The water-cooling system and the vacuum one were connected and tested. Control racks for the hot cathode were made and tested in various operation modes. The beam diagnostics system was created and installed on the stand. The connection and adjustment of the RF generator control rack are underway now.

Works on the stand are scheduled for 2012.

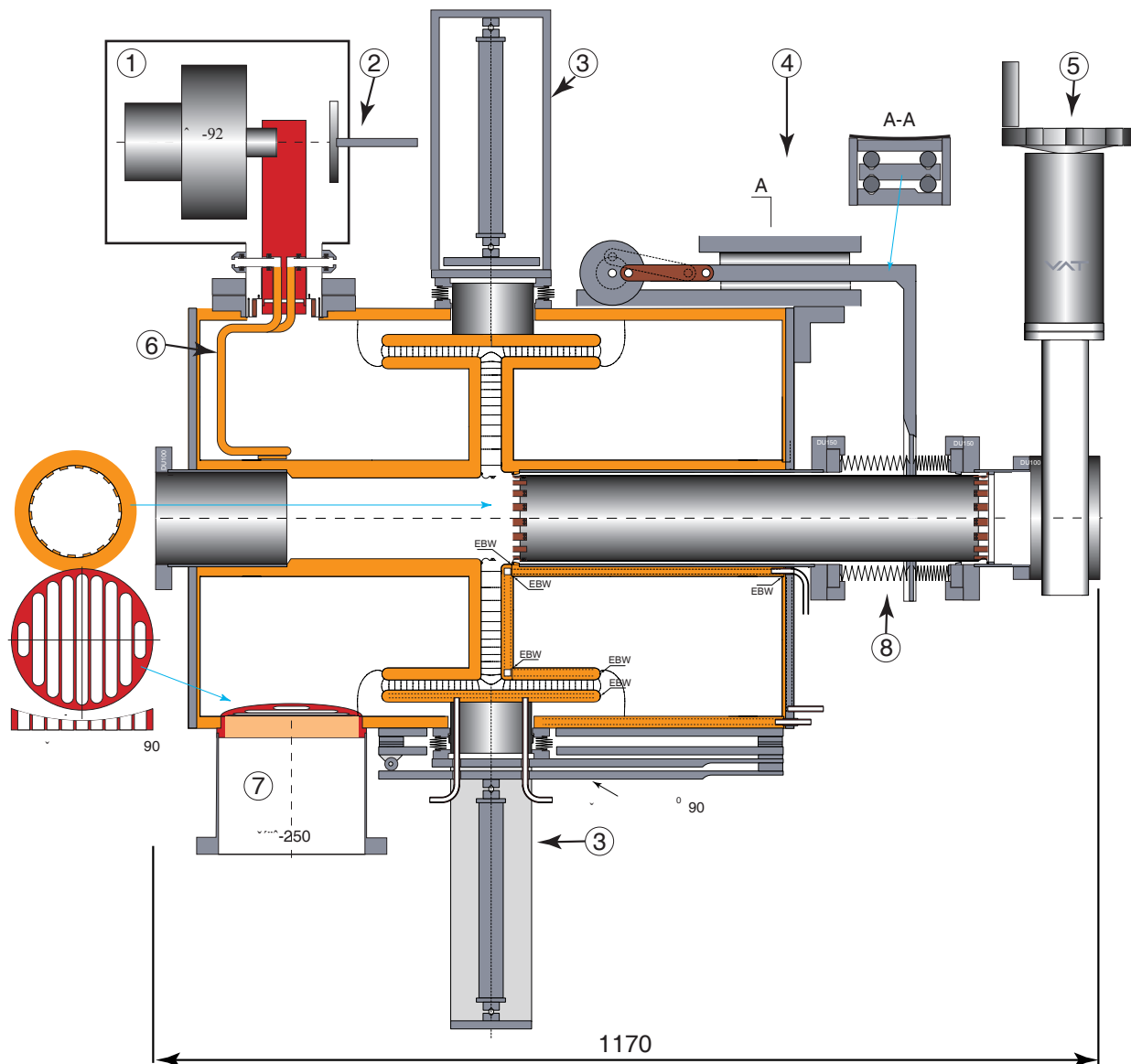


Fig.7.5.7. Arrangement of the cavity of station 3. 1 - RF generator on the tube GU-92A, 2 - tune-out of parasitic resonance frequency; 3 - play-free mechanism for retuning of the main operation frequency, 4 - mechanism for electric short-circuiting of the accelerating gap, 5 - vacuum gate valve, 6 - water-cooled loop for RF power input, 7 - branch pipe of ion pump, 8 - bellows assembly of the mechanism for short-circuiting of the accelerating gap.

7.7 DEVELOPMENT OF RF SYSTEM FOR HIGH-POWER CONTINUOUS INJECTOR OF BEAMS OF FAST HYDROGEN ATOMS

The Institute is working on the project of a high-power continuous injector of beams of fast hydrogen atoms with energies of 500÷1000 keV on the basis of negative ions. The project is based on separate formation and acceleration of beam of negative ions. Four RF-discharge emitters are used as a plasma source. An RF system was designed for supply of the emitters.

The system consists of four independent generators. The output stages of the generators are made on the tetrodes 4CW 50.000E (EIMAC USA); the pre-amplification stages are made on the transistors IXZ2210N50L. The output stage and the pre-stage are mounted in a 800x800x2100 mm cabinet of the "Euromechanics" standard.

The generators are controlled from one 600x800x2100 mm control rack of the "Euromechanics" standard. The rack comprises the control system for the generators, four modulators, power supply for the control grids of tetrodes, AC voltage distribution units, a cross-box, and an industrial computer.

The main parameters of the system are as follows:

Operation frequency	$4 \pm 3.5\%$ MHz
Power at load	$4 \times 40 = 160$ kW
Mode	Continuous
DC voltage across the "antenna" relative to the platform	120 kV
DC voltage across the platform relative to the "ground"	880 kV
Power consumed by the anode source from the 220/380 mains	400 kVA
Power consumed by the control rack from the 220/380 mains	15 kVA
Flow of deionized water cooling the tetrode 4CW50.000E	$4 \times 40 = 160$ l/min

The control system for the generators controls switching the generator on/off, protection of the tetrodes and power supplies at emergency operation, processing of analog signals, conversion of the analog signal levels to pass them to the ADC, and protection of personnel against electric shock.

The modulators ensure automatic tuning of the oscillator frequency and stabilization of the amplitude of RF voltage across the "antenna" of each channel. The oscillator frequency is retuned during an RF pulse so that the RF voltages on the control grid and anode of the tetrode are always opposite in phase. As a result, the resonance tuning of the anode circuit is maintained. The amplitude stabilization system also maintains a set RF pulse shape when the loss resistance in the plasma varies, as well as compensating for the influence of the power supply ripple.

The power supply of the control grids supplies bias voltage to the tetrodes.

By a command from the control unit, the AC voltage distribution unit provides 220/380 mains supply to the corresponding user.

The "cross box" and industrial computer perform timing and acquisition of data on the parameters of the system.

The anodes and screen grids of the generators are fed from a common source of high voltage power. The source is mounted in cabinets of the "Euromechanics" standard, connected in a line. The overall size of the source is 2700x800x2100 mm.

The output isolation transformer provides transfer of RF power to the antenna at a potential of 120 kV. The magnetic circuit of the transformer is composed of 56 ferrite (200 VNP) rings of 110x180x20 mm dimensions. The ferrites are produced by Neva-Ferrit (St. Petersburg). The transformer is placed in a tank of 700 mm in diameter and 870 mm in height, filled with SF₆ gas. The secondary

winding of the transformer has a center tap, which allows one to connect the antenna symmetrically and thus reduce parasitic radiation of RF power into the environment. The RF power from the transformer is transferred by a balanced shielded feeder.

The RF system of the experimental stand for acceleration of beam of negative hydrogen ions with a current of up to 1.5 A to an energy of 120 keV is a single channel of generator with a full-scale high-voltage power source. Elements of this system are now being fabricated by the pilot production department of BINP.

7.8 NEW 174 MHz RF SYSTEM FOR THE STORAGE RING OF THE ELECTRON-POSITRON BOOSTER (BEP)

The laboratory is working to create a new RF system for the storage ring of the electron-positron booster (BEP), which is the injector of the accelerator complex VEPP-2000. The new RF system will increase the energy of particles in the BEP from 0.9 to 1 GeV. The RF system operates at a frequency of 174 MHz (the 13th harmonic of the BEP revolution frequency) and consists of an accelerating cavity, RF power generator, and control system. The accelerating cavity of coaxial type for a maximum voltage of 120 kV has mechanisms for fine tuning of the fundamental and higher-order modes. The tetrode GU-92A is installed in the output stage of the RF generator with a maximum power of 20 kW. The pre-stages of the generator are made on transistors. The control system adjusts the amplitude and phase of the accelerating voltage and ensures synchronization at filling of the separatrices of the storage ring.

The design and technological study of the enclosure and central coaxial inserts of the cavity were finished in 2011. Preparation for their manufacture was begun. The power input for the cavity was made and its RF measurements were carried out. Designing of the feeder line connecting the generator with the cavity was begun. The output stage of the generator was fabricated and assembled; the systems for powering and cooling the stage are equipped with purchased products. New units of the control system are being fabricated and adjusted (part of electronics of the old RF system will be used in the control system).

7.9 PASSIVE SINGLE-MODE CAVITY FOR 816 MHz

In May 2011, BINP concluded a contract with the National Center for Synchrotron Radiation of China in Hefei (Hefei Light Source (HLS)) for the development and manufacture of a passive single-mode cavity for 816 MHz. This cavity will be used in the storage ring for increasing the bunch length. This will reduce the "Touschek effect" and increase the beam lifetime. The cavity operates at the fourth harmonic of the accelerating RF power. The cavity will be excited with the beam itself.

The required voltage level on the cavity is regulated via tuning the cavity out of the RF harmonic. A 3D modeling of the cavity was performed. An optimal form to meet the requirements to the fundamental and higher modes, as stated in the contract, was selected. The basic parameters of the operation mode and impedances of the high modes of the cavity to a frequency of 5 GHz were calculated. The cavity design was developed and optimal manufacturing techniques were chosen. The drawings were prepared for transfer to the production department.

7.10 ASSEMBLY AND TESTING OF THE RF GENERATOR FOR THE FEDERAL STATE UNITARY ENTERPRISE "RUSSIAN FEDERAL NUCLEAR CENTER-VNIIEF" (SAROV)

In accordance with the contract with the Federal State Unitary Enterprise "Russian Federal Nuclear Center-VNIIEF" (Sarov), BINP produced an RF generator of a continuous power of 180 kW at 100 MHz and sent it to the customer in July 2011. The equipment set includes an RF power amplifier, 100 kW dummy load, amplifier power supplies, and control system. Before shipment, the RF generator was tested at a rated power of 180 kW on a BINP stand.

In December 2011, a laboratory 6.2 team of 6 specialists traveled to Sarov to complete the work under the contract. Within 3 weeks, the BINP specialists unpacked, assembled, and tested the equipment at a maximum dummy load power of 100 kW. The tests were performed successfully; there was no criticism from the customer.

7.11 FURTHER DEVELOPMENT OF RF SYSTEM OF THE VEPP-4 STORAGE RING

For the purpose of raising the VEPP-4 energy to 4.2 GeV and above, works were carried out on the improvement of the reliability of the RF system of the storage ring. In 2011, the production department EP-1 finalized revision of the 181.8 MHz accelerating cavity, which was not installed in the storage ring earlier. All the units of the cavity were tuned, and its basic parameters were measured. One of the cavities, which was in an emergency state, was withdrawn from the technological gap of the VEPP-4 storage ring and replaced with the new cavity (Fig.7.11.1).

The cavity has vacuum gates on both sides. The cavity was warmed up with the gates closed, and a $2 \cdot 10^{-8}$ Torr vacuum was attained. Then the cavity was connected through a coaxial feeder to the distribution waveguide. Simultaneously, the RF generator and cabinets for bias rectifiers for 5 kV and 50 kV were inspected and tuned.

The RF generator was switched on for all five cavities installed in the technical gap. The total voltage was raised to 2.5 MW. The power of the generator was 65 kW. Currently, the RF training of the new cavity for multipactor suppression is underway. The removed cavity was passed to EP-1 for improvement.

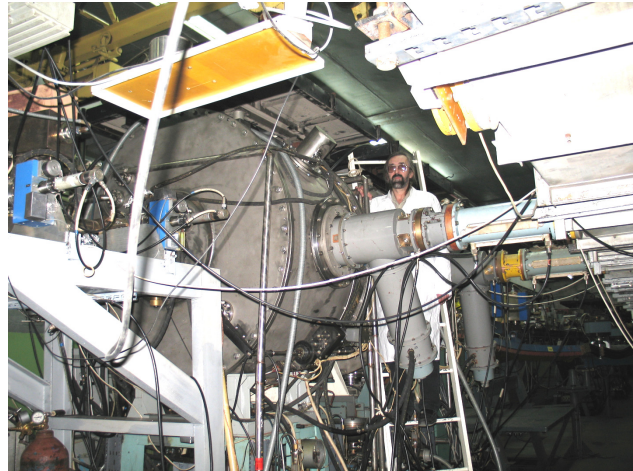


Fig.7.11.1 New 181.8 MHz cavity in the gap of the VEPP-4 storage ring.

7.12 UPGRADING THE RF SYSTEM OF THE MICROTRON FOR THE FEL

Works on the upgrade of the RF generator for the microtron for the FEL were continued. The tubes GU101A were gradually replaced with the tubes TN781 made by TALES. It was found that at operation of the output stage, consisting of two tubes GU101A and two tubes TN781, the cascade gets self-excited at a frequency of 800 MHz, which leads to destruction of the tubes TN781. According to the results of tests, a number of changes in the design of the stage were made for prevention of both self-excitation and destruction of tubes. The work will be continued as soon as new tubes TN781 arrive.

8

POWERFUL ELECTRON
ACCELERATORS AND
BEAM TECHNOLOGIES

8.1 DEVELOPMENT OF THE MODEL RANGE AND IMPROVE OF OPERATING CHARACTERISTIC OF ELV ACCELERATORS

In 2011, the Institute delivered ELV accelerators to the customers and carried out the contracts supervisions of accelerators being delivered earlier. In 2011 the greatest quantity of accelerators were supplied to the customers: there are 17. In present report new ELV accelerators of up to 100 kW power and of 0.8 to 1.5 MeV range energy are presented. The principle tendency of development of modern industrial accelerators as well as growth of the efficiency at the expense of adaptation to existing technological processes and more close integration with living auxiliary equipment are described. The experiments with extraction of electron beam into air at the laboratory stand equipped by ELV-6 accelerator were continued. The main part of the experiments was devoted to nanopowder production.

Radiochemical technologies with the use of electron accelerators as ionizing radiation sources were generally developed in the early sixties. By recent, they had strongly consolidated in world industrial production and, thereby, confirmed their efficiency as well as their uniqueness. The technological processes with the use of electron beams for polymer radiation modification, stimulation or initiation of chemical reactions, smoke purification, waste waters treatment, grain disinfection,

etc., are widely used in modern industry. A lot of accelerators are installed and operated in different science and research centers and applied-research laboratories. That leads to growth of radiation-modified goods production and development of new matters and technologies, where electron beams are used to obtain new and, sometimes, unique properties.

Budker Institute of Nuclear Physics (BINP) of Siberian Branch of Russian Academy of Sciences is one of the world leaders in the development, design, manufacture and application of electron accelerators of different series (such as DC accelerators of continuous action based on high-voltage rectifier, high-frequency accelerators, pulsed accelerators), the accelerated electron energy and power of which are much more. ELV-series accelerators are some of them. Their compact size and high functional quality allowed BINP to stand as a leading institution at industrial accelerators market as in Russia and abroad.

ELV-series DC accelerators of continuous action based upon high-voltage rectifier, which are recently produced by BINP, exceed maximum power range of separate accelerator from 20 to 100 kW and accelerated electron energy from 0.3 to 2.5 MeV (see Table 8.1.1 and Fig. 8.1.1). The accelerators meant for environmental purposes have a power up to 400 kW at maximum beam current up to 0.5 A.

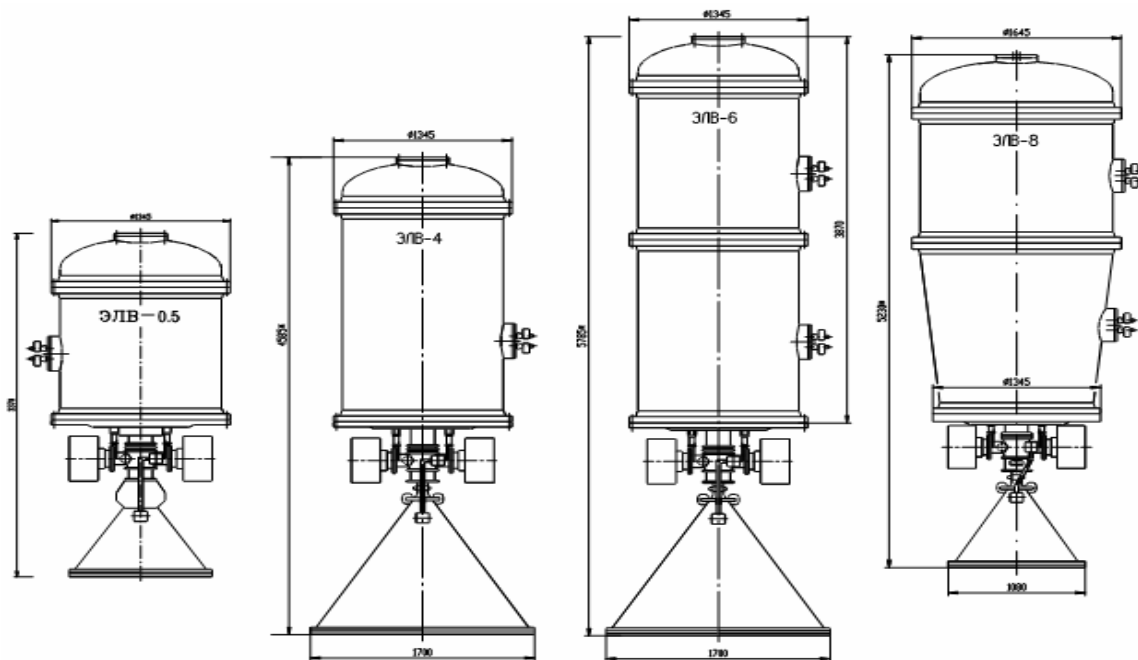


Fig.8.1.1. Character dimension of ELV-series accelerators ELV-0.5, ELV-4, ELV-6 and ELV-8 accelerators.

ELV-series DC accelerators of continuous action based upon high-voltage rectifier, which are recently produced by BINP, exceed maximum power range of separate accelerator from 20 to 100 kW and accelerated electron energy from 0.3 to 2.5 MeV (see Table 8.1.1 and Fig. 8.1.1). The accelerators meant for environmental purposes have a power up to 400 kW at maximum beam current up to 0.5 A.

Table 8.1.1

	Energy range MeV	Beam power kW	Max. beam current, mA
ELV mini	0.2...0.4	20	50
ELV-0,5	0.4...0.7	25	40
ELV-1	0.4...0.8	25	40
ELV-2	0.8...1.5	20	25
ELV-3	0.5...0.7	50	100
ELV-4	1.0...1.5	50	40
ELV-6	0.8...1.2	100	100
ELV-6M	0.75...1.0	160	200
ELV-8	1.0...2.5	100	50
PHAKEL (Flame)	0.5...0.8	500	800
ELV-12	0.8...1.0	400	400

Hard market conditions and growing demands for modified materials forms the industrial manufacturers needs in more powerful and effective electron accelerators enabling to increase the volume of production without compound and expensive inputs for change all equipment. Table 8.1.2 shows accelerator parameters of last 38 contracts. The part of these accelerators were already delivered, the rest are prepared to be supplied.

Table 8.1.2

Max. Electron energy, MeV	Max. Beam power, kW	Accelerator qty
1	100	11
1	70	1
1.5	100	14
2.5	100	10
2.5	50	1
0.7	20	1 (mobile)

As it is shown in Table 8.1.2 the needed accelerators are distributed enough evenly starting from 1 MeV energy in accordance with maximum energy. Most of them are of 100 kW power. That is why, at present, the development of ELV model range goes towards increase of accelerators power within the range of 1.0 to 1.5 MeV. Earlier, only ELV-6 accelerator had maximum required power of 1.2 MeV.

At the same time weigh and overall dimensions had been also changed. Those accelerators designed in new

dimension type extend power and energy range of more structure ELV-6 models enabling the following:

- production of more powerful electron beams, which accurately satisfy existing production needs, taking into account present and new industrial technologies;
- modification and/or replacement of accelerator equipment without changing the existing technological auxiliaries such as rewinding lines, takeup & payoff units, etc.

To solve those problems the design of cascade generator has been changed. The changes were made in primary winding with parallel inductive coupling to enhance heat sink as well as in connection circuit inside high-voltage rectifying section column. In previous models sequential connection circuit (Fig. 8.1.2a) was used and rectifying sections had been assembled in accordance with voltage doubling scheme.

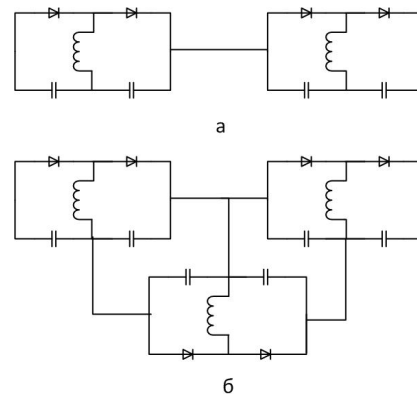


Fig. 8.1.2. Rectifying section schemes. The use of series-parallel switching (Fig. 8.1.2b) when each capacitor in a section is charged through correspondent diode of its own or neighbouring section enables to get more high-current column.

At series connection the voltage pulse form at capacitors corresponds to half wave rectification mode. At series-parallel connection it corresponds to full-wave rectification mode. Series-parallel diagram is similar to Gratz connection, but it provides the same protection of high-voltage rectifier elements (coils, diodes and capacitors) from overvoltage at gas or vacuum insulation breakdowns as doubler one. The parameters of new accelerators are (Fig. 8.1.3) are shown in Table 8.1.3.

Table 8.1.3

Accelerator	ELV 4-1	ELV 4-1.2	ELV 4-1.5
Maximum energy, MeV	1	1,2	1,5
Maximum beam current, mA	100	83	70
Beam power, kW	100	100	100

Together with manufacture of the accelerators mentioned above the mobile accelerators were developed. Fig. 4 shows the accelerator of 20 kW power and with up to 30 mA maximum beam current which was produced in cooperation with “EbTech” company (Republic of Korea). This accelerator is placed inside the trailer together with radiation protection. The main purpose of these accelerators is treatment of local pollutions.

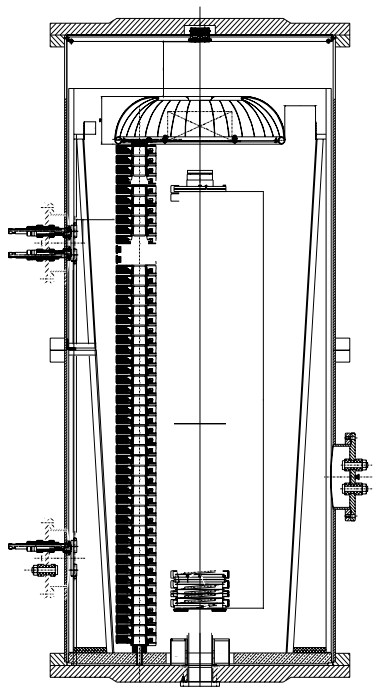


Fig. 8.1.3. Structure and dimensions of ELV4-1.2 accelerators.



Fig. 8.1.4. Mobile accelerator ELV.

Another important direction in development of accelerators is adaptation of accelerator complexes to present technological equipment and their integration with industrial technologies. So, to increase production efficiency in accordance with the customers needs, the scanning and beam extraction systems were modified. The length of extraction window was increased from 1600 mm up to 2000 mm (See. Fig. 8.1.5). This enabled to irradiate two and more types of products.



Fig.8.1.5. Modification of extraction window.

Other examples of integration allowing improvements in productive efficiency are information-measuring complex on visualization of accelerator current parameters and technological irradiation process (Fig.8.1.6) and under-beam transportation system developed in BINP.

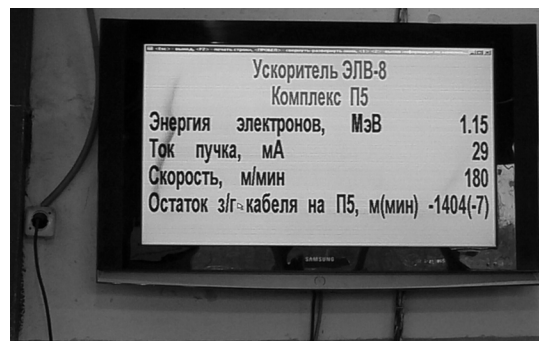


Fig.8.1.6. Parameters of accelerator ELV operation:

ELV-8 accelerator
Complex P5
Electron energy, MeV -> 1.15
Beam current, mA -> 29
Speed, m/min -> 180
Residue of loaded cable at P5 -> -1404(-7)

The construction of under-beam transportation system is shown in Fig. 8.1.7. It consists of 2 drums, one of which is driven and second one is driving and it is controlled by accelerator control system. This reduces the risk of stretching of irradiated products and prevents reduction of cable insulation diameter.

Recently, BINP holds leading positions among companies manufacturing irradiation equipment for industrial purposes. Considerable quantity of accelerators are installed and operated in different scientific centers, industry laboratories and production areas. Many companies using the accelerators of other manufacturers are purchasing ELV series accelerators. Gained experience of development and operation of ELV series accelerators enables to propose the customers the accelerators with parameters, which are no worse and in many respects exceed than the best world samples.



Fig.8.1.7. Under-beam transportation system.

8.1.1 Stand based on industrial ELV-6 accelerator with extraction of focused electron beam into air

ELV-6 accelerator with extraction of focused electron beam into air (electron energy 1,4 MeV) was used for testing of electron beam technologies in gaseous medium at air pressure. One of the directions of this testing was production of nanopowders by means of starting material evaporation method with the use of electron beam as an energy source. Over the evaporating material the flow of transporting gas arises. Depending on nanopowder composition being obtained, an air or inert gas are used as a transporting gas. The aerosol flow with nanoparticles, which is formed like this, is transported to nanoparticles collector at the filter. By means of similar method, not only compact and homogeneous nanoparticles had been obtained, but also there was got more complex formations, in particular, carbon nanotubes and nanohorns. Nanohorns achieved record big sizes up to 300 nm. Also, metal nanoparticles in silicon and silicon oxide coatings were obtained.

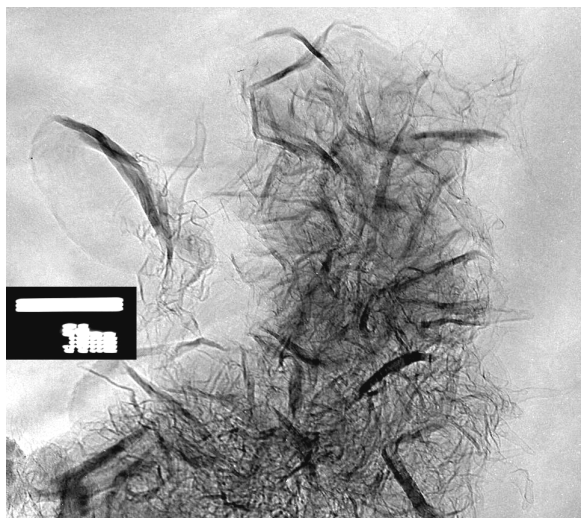


Fig. 8.1.8. Nanohorns produced by means of electron beam evaporation in inert gas medium at air pressure.

Other direction of our investigations was forming of coating on metallic substrate for different purposes. Beginning from 2009, the corrosion-resistant thick coatings were obtained by means of facing of tantalum and niobium powders onto titanic substrate. In that case, an advantage of the use of electron beam with electron energy within MeV range is in its high capacity to penetrate into powder materials and in capability to form homogeneous layers of alloys with fusion temperature up to 3000°C.

8.1.2 Nanoconstructions for medicine

In the beginning of 2006, the efforts to find medical application of superdispersed powders obtained by means of evaporation at ELV-accelerator had been taken. As soon as nanodimensional constructions enabling to visualize, *in-vivo*, the distribution of a temperature, oxygen, ferment and inflammatory processes activity the kinetically stable complexes of paramagnetic rare-earth ions and gel latex containing superdispersed ferromagnetics were proposed and investigated together with Nikolaev Institute of Inorganic Chemistry (NIIC) and Institute of Experimental Veterinary Science of Russian Academy Agricultural Sciences (IEVSRAAS). The highly sensitive NMR-thermoprobes were fluorine and lanthanide phosphoprous-containing complexes, the sensitivity of which was specified by the presence of lower lanthanide excited state partially settled at a room temperature and causing the thermosensitive paramagnetic shift of frequencies of NMR fluorine, hydrogen and phosphorus atoms belonging to a molecule of complex former. By means of combined analysis of lanthanide-induced paramagnetic increases of speeds of spin-lattice relaxation and lanthanide-induced shifts (LIS) in NMR spectra of the ligand nucleus the formation and the structure in a solution of a number of kinetically stable complexes of lanthanides (Ln) was studied. *In-vitro*, NMR investigation of thermodynamic of complex formation, stoichiometry and molecular structure of paramagnetic multiligand Ln complexes with porphyrins anions (Fig. 8.1.9), β -diketones (L), nitrate groups and ditiofosfina-mi (i - DBDTF) ftorhinolinom, as well as electroneutral phenanthroline, 2,2-bipiridil (2,2-bipy) and crown ethers in solution was carried out.

By example of LIS temperature dependence study (Fig.8.1.9) of Ln double-deck complexes with porphyrins, taking into account rotation of phenylic fragments of tetra-phenylic porphyrin anions, it was shown their use as nanodimensional thermal sensor NMR in solutions (minimum size being perpendicular to porphyrin anion plate is ~ 1.1 nm). The correlation between the growth of atomic number of cation Ln and increase of energy barrier of phenylic fragments rotation ($\Delta H_+ = 48$ (5) and 66 (7) kJ/mole correspondingly for Dy and Lu) was found. It is one of demonstrations of lantide compression leading to decrease of interplanar spacing between porphyrin anions

and growth of steric barrier at increase on Ln atomic number.

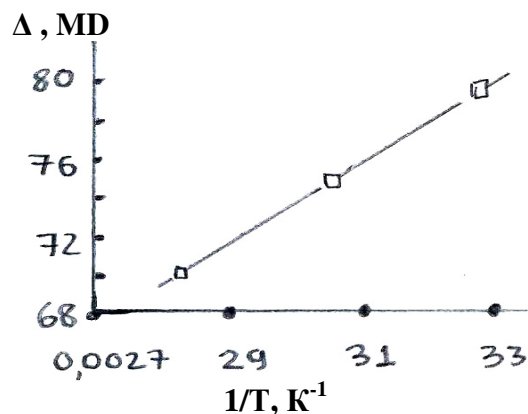


Fig. 8.1.9. Dependence of chemical shifts difference in 500 MHz¹ H NMR spectra between orthos-exo and orthos-endo atoms of anion porphyrin phenyl ring in the complexes [DyH(oep)(tpp)] from backward temperature.

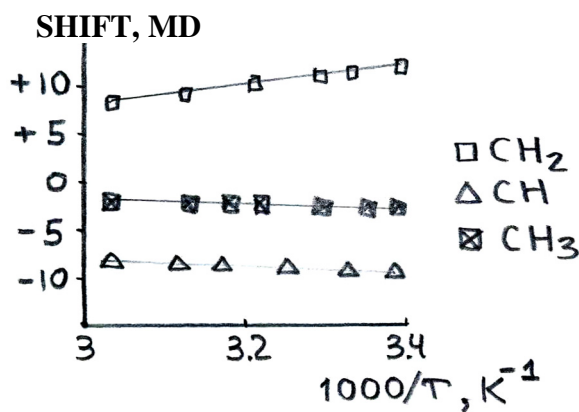


Fig. 8.1.10. Temperature dependence of paramagnetic lanthanide-induced shifts in 200 MHz ¹H NMR spectra of complex cations [Eu(ΠTA)₂(18-crown-6)]⁺ relative to corresponding protons of diamagnetic cation [La(ΠTA)₂(18-crown-6)]⁺; solution CDCl₃

The temperature dependences of LIS for CH₂ molecules of macro-cycle 18-crown-6 complexes indicating about possibility of their use as NMP-TSR (Fig.8.1.10) were also obtained. By means of NMR method the forming of kinetically stable Ln complexes with ethylenediaminetetraacetic acid (EDTA) in water solutions within pD range from 1.6 up to 8 was found out. During the study of temperature dependence of paramagnetic chemical shifts and possibility, *in vitro*, to use the complexes as NMR thermal sensors in water solutions the linear dependence of paramagnetic chemical shifts at ligand nuclei of Ln complexes on backward temperature was found out (Fig.8.1.10).

It is shown that in spite of complications conditioned by intra- and intermolecular dynamics, related problems of the study of stability, molecular structure, dynamics

and magnetochemistry features of complex compounds 4f-elements may be successfully solved by means of NMR methods. For complexes of Pr, Ho and Dy there were found the conditions enabled to show *in vitro* the possibility to use thermal sensors as subnanodimensional NMR in water solutions (Fig.8.1.11).

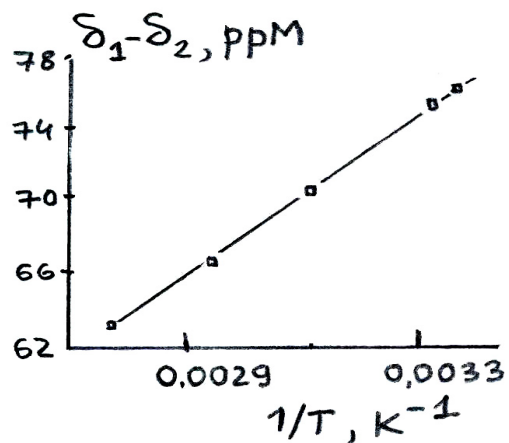


Fig. 8.1.11. Dependence of difference of ¹H NMR spectra for different groups CH₂ of complexes [HoEDTA] on $1/T$; solution – H₂O, pH=1.6

As a result of investigations it was shown that complexes Ln with EDTA may be used as NMR thermal sensors to solve thermometric problems in liquid, polymer and gel mediums as with the help of series NMR spectrometers and by means of magnetic-resonance micro-tomographs.

In cooperation with Nikolaev Institute of Inorganic Chemistry (NIIC) and Institute of Experimental Veterinary Science of Russian Academy of Agricultural Sciences (IEVSRAAS) the possibility to visualize boron distribution in animal organisms by means of NMR tomography was studied. *In vivo*, the sensitivity of NMR boron detection of about 300 mkg/g (in case of injection of microlatex boron preparation “magnicon”) was achieved.

Preparation “magnicon” developed in BINP SIB RAS contains, also, ferromagnetic powder. Its particles create magnetic field gradient observed in NMR upon the changes of speeds of proton relaxation.

To determine concentration of ferromagnetic particles *in vivo* in BINP the quantum magnetometer with laser pumping of paramagnetic rubidium-87 vapors was designed. The methodology of gastric diseases diagnostics with the use of magnetic particles suspension was proposed.

The method of obtaining the insoluble colloid basic bismuth sulfanilic salicylate, the perspective gastric radiopaque substance was developed.

As the perspective carcinotropic contrasting matters for PET cancer diagnostics the radioactive halogenated pyrimidines synthesized by the laboratory of radiation chemistry in the Institute of Chemical Biology and Fundamental Medicine of SB RAS had been investigated.

Accumulation of Br-77 and tritium-containing pyrimidine in mammary cellula of a mouse after its onetime injection into organism (in case of presence or absence of steroid hormones stimulation) was studied. After one-time nucleotide injection the activity accumulations continue during 45 minutes. Also, the bromodeoxyuridine accumulation rates (Fig. 8.1.12) were found.

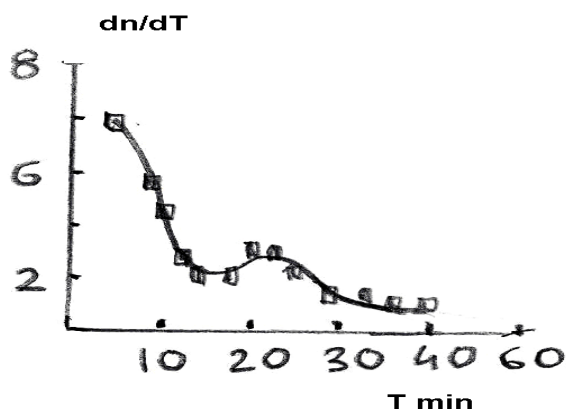


Fig. 8.1.12. Deoxyuridine accumulation rates relative unit: derivative of function.

In cooperation with the Institute of Experimental Veterinary Science the factors having an influence upon radioimmunity of collection salmonellae strain were studied. Antiradiation activity of chlortetracyclinum antibiotic was found out. By means of magnetic powders treated by bacterial DNA fragments, we succeeded in transforming of kalanchoe cells and achieving the agribacterial octopine secretion. To inject genetic make-up into the cell by means of magnetic powders the special permanent magnet with 3.5 Tesla/cm field gradient had been designed.

8.2 ILU ACCELERATORS AND THEIR APPLICATIONS

8.2.1 Accelerator supplies

Since 1983 the ILU accelerators are supplied for the industrial facilities and for the research establishments. The reliability and technical level of these machines is confirmed by the new supplies.

During the year of 2001 the accelerator ILU-10 with energy up to 5 MeV and power up to 50 kW was manufactured, mounted and tested in the BINP and then was disassembled, shipped and again assembled in Kazakhstan. This machine will work in the industrial line for sterilization of medical goods in the Park for Nuclear Technologies, city of Kurchatov, Kazakhstan.

The testing of the new 10 MeV 100 kW ILU-14 machine was continued during this year. The parameters achieved in BINP are as following:

Energy 7.5 MeV, pulse beam current of 560 mA, pulse repetition frequency 10 Hz, average beam current of 2.7 mA, beam power 20 kW

Energy 10 MeV, pulse beam current of 320 mA, pulse repetition frequency 25 Hz, average beam current of 3.8 mA, beam power 38 kW

The maximum beam power was restricted by the existing radiation shielding of the facility in BINP. By the end of 2012 the ILU-14 machine was shipped and mounted in the specially build bunker with the adequate radiation shield in the Federal Medical Biophysical Center named by A.I. Burnazyan, Moscow. The testing will be continued.

The new convertor for X-rays generation was specially designed for use with the ILU-14 machine. It was manufactured in 2011, its working energy is 7.5 MeV and working beam power up to 100 kW.

8.2.2 Modernization of the ILU machines

The new beam scanning and control system was developed in 2011. This system has the independent control and power supply. It permitted to improve the stability of beam scanning and decrease the dose variation in the irradiation zone.

The new modulators' synchronization system was developed especially for ILU-14 machine to decrease the load inequality between the 3 phases of the feeding net.

8.2.3 New technologies development

The research works were performed to develop the radiation-thermal synthesis of complex oxide compounds. The perovskite-like compounds for membrans were sintered under the Interdisciplinary Project of Siberian Branch №82 "Oxide permeability of the massive and deposited membranes based on perovskites with mixed conductivity".

The pilot works on radiation-thermal sintering of the fuel elements cells were carried out in collaboration with Borekov Institute of Catalysis, Novosibirsk.

The research activities in radiation treatment of the oil products were carried out under the Integration Project №5 of the Siberian Branch Presidium. The work was carried out in collaboration with Institute of Solid State Chemistry and Mechanochemistry, Novosibirsk, and Institute of Oil Chemistry, Tomsk.

The goudron irradiation was carried out to investigate the possibilities of its processing into more useful products. The modeling of this processes was performed using the various modeling materials(paraffin, other hydrocarbons, unsaturated hydrocarbons).

The test irradiations to study the radioresistivity of the microbes were carried out.

Various medical goods were subjected to electron beam treatment on the contract basis. The works were carried out on the ILU-6 and ILU-10 accelerators.

9

PHYSICS FOR MEDICINE

9.1 STATUS OF BNCT PROJECT

A promising approach in the treatment of several malignancies, primarily intractable brain tumors and melanomas, is the boron neutron capture therapy (BNCT). The method is based on the selective accumulation of non-toxic non-radioactive ^{10}B isotope in tumor and subsequent irradiation with epithermal neutrons. As a result of neutron absorption by boron a nuclear reaction $^{10}\text{B}(n,\alpha)^7\text{Li}$ occurs with a large release of energy. The release of energy leads to the death of the exact tumor cell, which contained the nucleus of boron. Clinical trials of the method on nuclear reactors have demonstrated its effectiveness in treating a variety of tumors, but the widespread adoption of BNCT in clinical practice requires a compact, safe and relatively inexpensive source of epithermal neutrons. The Institute of Nuclear Physics SB RAS has proposed and built, a prototype of epithermal neutron source based on the tandem accelerator with vacuum insulation, which provides the generation of neutrons in the reaction $^7\text{Li}(p,n)^7\text{Be}$. General view of the facility is shown in Figure 9.1.1.



Fig. 9.1.1 Tandem accelerator with vacuum insulation.

During 2011 the upgrade of the tandem accelerator was performed. The upgrade aimed at significant improvement of operating parameters: proton beam current, long-term stability of the proton beam energy, the overall stability of the facility. In the course of this work it was performed: increase of the diameters of diaphragms in accelerator electrodes, installation of a new charge-exchange target with a diameter increased to 16 mm, preparation of the technical elements correcting the voltage of the first accelerating electrode. For the measurement of high-power stationary proton beam it was produced a secondary-emission diagnostics with pick-up moving. The use of new diagnostics allows monitoring the beam profile and position in different parts of the high-energy path without destroying the beam at a proton current of 1.5 mA.

When training the accelerator after the increase of the diaphragms a dark current with high intensity was registered that caused partial melting of high-voltage electrode diaphragm. The analysis of the registered current and voltage of the accelerator, vacuum, power of gamma radiation, and also a numerical calculation of electrostatic fields and the trajectories of emitted electrons, allowed identifying the reasons for this undesirable phenomenon and making changes to prevent it.

A method of determining the linear thickness of the gas stripping target was proposed. The method is based on fixing the moment when the output current changes from negative into positive. The method enabled to set up a correspondence between the linear density of the target, gas flow and the residual gas pressure. It was demonstrated a good agreement between the experimentally measured output current and the calculated one. The pressure in the accelerating channel was estimated. It was formulated a procedure of setting gas flow system parameters to provide the required charge exchange of the beam.

At the entrance of the first electrode it was installed a beam detector having the possibility of measuring the radial distribution of current density. It was studied a focusing of the negative hydrogen ion beam in the accelerator, which allowed us to make a correction in the calculation to obtain agreement with experiment and optimize the acceleration of the beam.

The above-described work and modifications made it possible to provide a stable long-term generation of a proton beam with a current of 1.5 mA, which is more than 2 times higher than the previous values. Some ways are planned to obtain stable generation mode with a current of up to 3 mA.

To ensure long-term stabilization of the proton beam energy the special algorithm was proposed, the equipment was chosen and the experimental device was constructed. It allows us to stabilize the energy of the accelerated beam, using the feedback flux of gamma rays with energy 9.17 MeV from the threshold of the reaction $^{13}\text{C}(p,\gamma)^{14}\text{N}$. In a series of experiments verifying the functionality of the method we obtained a stable intensity of the 9.17 MeV line for about 2.5 hours and provided a long-term stability of the proton energy at the level of $\pm 0.1\%$.

This work is supported by the Ministry of Education and Science of Russian Federation.

9.2 X-RAY DETECTORS FOR MEDICINE AND SECURITY

9.2.1 Medical Radiography

BINP produced for JSC "Nauchpribor" (the city of Orel) eight 1536-channel detectors, which were supplied to medical institutions of Russia as part of digital scanning fluorographs FMTS-TM-O.

9.2.2 X-ray inspection system (XIS) "Sibscan" for screening of people

A new variant of the X-ray inspection system (XIS) of smaller dimensions (9.5 m³ instead of 15 m³) was manufactured and tested at airport.

Three detectors were fabricated for the XIS facilities produced by JSC "Nauchpribor."

A new design of the detector for the XIS facilities was developed with a spatial resolution of 1.6 mm and a smaller dose of radiation during inspection. The new detector uses only packaged chips and simpler printed circuit boards, which made it possible to do without complex and time-consuming ultrasonic welding and thus simplified the manufacturing technology and enhanced reliability of the detector. A pilot sample of such a detector was fabricated.

BIBLIOGRAPHY

List of publications

- [1] Silagadze Z.K. On the finslerian extension of the Schwarzschild metric. // Acta Phys. Pol. B, 2011. - Vol.42, N6. - P.1199-1206.
- [2] Gerasimov V.V., Knyazev B.A., Nikitin A.K., Zhizhin G.N. A way to determine the permittivity of metallized surfaces at terahertz frequencies. // Appl. Phys. Lett., 2011. - V.98, N17. - P.171912 -1-3.
- [3] Gerasimov V.V., Knyazev B.A., Nikitin A.K., Zhizhin G.N. A way to determine the permittivity of metallized surfaces at terahertz frequencies. // Appl. Phys. Lett. - 2011. - Vol.98, N17. - P.171912-1-3.
- [4] Kuznetsov S.A., Paulish A.G., Gelfand V., Lazorskiy P.A., Fedorinin V.N. Bolometric THz-to-IR converter for terahertz imaging. // Appl. Phys. Lett., 2011. - Vol.99, N2. - P.023501-1-3.
- [5] Beruete M., Navarro-Cia M., Kuznetsov S.A., Sorolla M. Circuit approach to the minimal configuration of terahertz anomalous extraordinary transmission. // Appl. Phys. Lett., 2011. - V.98, N1. - P.014106-1-3.
- [6] Mo X.-H., Zhang J.-Y., Zhang Q.-J., Achasov M., Cai X., Fu Ch.-D., Harris F., Liu Q., Muchnoi N., QIN Q., Qu H.-M., Wang Y.-F., Xu J.-Q., Zhang T.-B. Study of radiation background at the north crossing point of the BEPC II in collision mode. // Chinese Physics C, 2011. - V.35, N7. - P.642-655.
- [7] Kozyulin M.V., Silagadze Z.K. Light bending by a Coulomb field and the Aichelburg-Sexl ultraboost. // Eur. J. Phys., 2011. - V.32, N11. - P.1357-1365.
- [8] Aad G., Kazanin V.A., Kolachev G.M., Kotov K.Y., Malyshev V., Maslennikov A.L., Orlov I., Panin V.N., Peleganchuk S.V., Shamov A.G., Skovpen K., Soukharev A., Talyshev A., Tikhonov Y.A., Zaytsev A., et al. (ATLAS Collab.). Measurement of inclusive jet and dijet cross sections in proton-proton collisions at 7TeV centre-of-mass energy with the ATLAS detector. // Eur. Phys. J. C, 2011. - V.71, N2. - P.1512 (59 p.).
- [9] Aad G., ATLAS Collab., Bobrovnikov V.S., Bogdanchikov A., Kazanin V.A., Kolachev G.M., Korol A., Malyshev V., Maslennikov A.L., Orlov I., Peleganchuk S.V., Shamov A.G., Skovpen K., Soukharev A., Talyshev A., Tikhonov Y.A., Zaytsev A., et al. Measurement of the top quark-pair production cross section with ATLAS in pp collisions at radical $s=7$ TeV. // Eur. Phys. J. C, 2011. - V.71, N6. - P.1577 (36 p.).
- [10] Eidelman S.I., Fedotov G.V., Kuraev E.A., Sibidanov A.L. Monte-Carlo generator photon jets for the process $e+e- \rightarrow \gamma\gamma$. // Eur. Phys. J. C, 2011. - Vol.71, N6. - P.1597.
- [11] Aamodt K., ALICE Collab., Frolov A., Pestov Y. Production of pions, kaons and protons in pp collisions at radical $s=900$ GeV with ALICE at the LHC. // Eur. Phys. J. C, 2011. - V.71, N6. - P.1655-1678.
- [12] Aamodt K., ALICE Collab., Pestov Y. Strange particle production in proton-proton collisions at radical $s=0.9$ TeV with ALICE at the LHC. // Eur. Phys. J. C. 2011. - V.71, N5. - P.1594-1618.
- [13] Aad G., ATLAS Collab., Kazanin V.A., Malyshev V., Maslennikov A.L., Orlov I., Peleganchuk S.V., Tikhonov Yu.A., Zaytsev A. Studies of the performance of the ATLAS detector using cosmic-ray muons. // Eur. Phys. J. C, 2011. - V.71. - P.1-36.
- [14] Dimov G.I. Feasible scenario of startup and burnup of plasma in ambipolar D-T reactor. // Fusion Sci. Technol., 2011. - V.59, N1T. - P.208-210.
- [15] Ivanov A.A. Perspectives of development of magnetic mirror traps in Novosibirsk. // Fusion Sci. Technol., 2011. - V.59, N1T. - P.17-22.
- [16] Beklemishev A.D. Tail-waving system for active feedback stabilization of modes in open traps. // Fusion Sci. Technol., 2011. - V.59, N1T. - P.90-93.
- [17] Beklemishev A.D. Three-dimensional force-free equilibria in open traps driven electron beams. // Fusion Sci. Technol., 2011. - V.59, N1T. - P.184-186.
- [18] Miginsky S. Compact submillimeter FEL project [Electronic resource]. // Journal Korean Phys. Soc., 2011. - V.59, N5. - P.3246-3250.
- [19] Fatyanov A.G., Terekhov A.V. High-performance modeling acoustic and elastic waves using the parallel Dichotomy Algorithm. // Journal of Computational Physics, 2011. - V.230, N5. - P.1992-2003.

List of publications

- [20] Epifanov D. Electromagnetic calorimeters of the CMD-3 detector. // Journal of Physics: Conference Series, 2011. - V.293. - P.012009 (6p.).
- [21] Koop I.A., Bogomyagkov A.V., Otboev A.V. Longitudinally polarized electrons in Novosibirsk c-tau factory. // Journal of Physics: Conference Series, 2011. - V.295. - P.012160 (6p.).
- [22] Shatunov Yu.M. Polarized beam studies at Budker Institute. // Journal of Physics: Conference Series, 2011. - V.295. - P.012016 (9 p.).
- [23] Dmitriev V.F., Milstein A.I., Salnikov S.G. Spin-dependent part of p anti p interaction cross section and Nijmegen potential. // Journal of Physics: Conference Series, 2011. - V.295. - P.012088 (5p.).
- [24] Sadykov V.S., Mezentsseva N., Usoltsev V., Sadovskaya E., Ishchenko A., Pavlova S., Bepalko Yu., Kharlamova T., Zevak E., Salanov A., Krieger T., Belyaev V., Bobrenok O., Uvarov N., Okhlupin Yu., Smorygo O., Smirnova A., Singh P., Vlasov A., Korobeynikov M., Bryazgin A., Kalinin P., Arzhannikov A. Solid oxide fuel cell composite cathodes based on perovskite and fluorite structures. // Journal of Power Sources, 2011. - V.196, N17. - P.7104-7109.
- [25] Aad G., ATLAS Collab., Bobrovnikov V.S., Bogdanchikov A., Kazanin V.A., Kolachev G.M., Korol A., Malyshev V., Maslennikov A.L., Orlov I., Peleganchuk S.V., Shamov A.G., Skovpen K., Soukharev A., Talyshev A., Tikhonov Y.A., Zaytsev A., et al. Charged-particle multiplicities in pp interactions measured with the ATLAS detector at the LHC [Electronic resource]. // New Journal of Physics, 2011. - V.13, N5. - P.053033 (68p.).
- [26] Petrenko A.V. Calibrating the electron-optical model of the VEPP-5 damping ring. // Nuclear Experimental Technique, 2011. - V.54, N1. - P.8-15.
- [27] Bondar A., Buzulutskov A., Grebenuk A., Sokolov A., Akimov D., Alexandrov I., Breskin A. Geiger mode APD performance in a cryogenic two-phase Ar avalanche detector based on THGEMs. // NIM A, 2011. - V.628, N1. - P.364-368.
- [28] Ablikim M., BESIII Collab., Achasov M.N., Michnoi N.Yu., et al. Observation of χ_{c1} decaying into the p anti p K+K- final state. // Phys., 2011. - V.83, N11. - P.112009-1-9.
- [29] Khriplovich I.B., Rudenko A.S. Can CP-violation be observed in heavy-ion collisions? // Physics Procedia, 2011. - V.17. - P.123-125.
- [30] Skorodko T., Shwartz B., Zlomanczuk J., et al. Delta Delta excitation in proton-proton induced $\pi^0 \pi^0$ production. // Phys. Lett. B, 2011. - V.695, N1/4. - P.115-123.
- [31] Akhmetshin R.R., Aulchenko V.M., Banzarov V.Sh., Barkov L.M., Baru S.E., Bashtovoy N.S., Bondar A.E., Bragin A.V., Eidelman S.I., Epifanov D.A., Fedotov G.V., Gabyshev N.I., Grebenuk A.A., Grigoriev D.N., Ignatov F.V., Karpov S.V., Kazanin V.F., Khazin B.I., Koop I.A., Krokovny P.P., Kuzmin A.S., Logashenko I.B., Lukin P.A., Lysenko A.P., Mikhailov K.Yu., Okhapkin V.S., Perevedentsev E.A., Popov A.S., Redin S.I., Ruban A.A., Ryskulov N.M., Shatunov Yu.M., Shwartz B.A., Sibidanov A.L., Snopkov I.G., Solodov E.P., Yudin Yu.V., Zaitsev A.S., et al. Measurement of $\phi(1020)$ meson leptonic width with CMD-2 detector at VEPP-2M collider. // Phys. Lett. B, 2011. - Vol.695, N5. - P.412-418.
- [32] Aad G., ATLAS Collab., Bobrovnikov V.S., Bogdanchikov A., Kazanin V.A., Kolachev G.M., Korol A., Malyshev V., Maslennikov A.L., Maximov D.A., Orlov I., Peleganchuk S.V., Shamov A.G., Skovpen K., Soukharev A., Talyshev A., Tikhonov Y.A., Zaytsev A., et al. Measurement of the centrality dependence of J/psi yields and observation of Z production in lead-lead collisions with the ATLAS detector at the LHC. // Phys. Lett. B, 2011. - V.697, N4. - P.294-312.
- [33] Aad G., ATLAS Collab., Beloborodova O., Bobrovnikov V.S., Bogdanchikov A., Kazanin V.A., Kolachev G.M., Korol A., Malyshev V., Maslennikov A.L., Maximov D.A., Orlov I., Peleganchuk S.V., Shamov A.G., Skovpen K., Soukharev A., Talyshev A., Tikhonov Y.A., Zaytsev A., et al. Measurement of the Gamma(1S) production cross-section in pp collisions at radical s = 7 TeV in ATLAS. // Phys. Lett. B, 2011. - V.705, N1/2. - P.9-27.
- [34] Aamondt K., ALICE Collab., Pestov Y., et al. Rapidity and transverse momentum dependence of inclusive J/psi production in pp collisions at radical s = 7 TeV. // Phys. Lett. B, 2011. - V.704, N5. - P.442-455.
- [35] Aad G., ATLAS Collab., Beloborodova O., Bobrovnikov V.S., Bogdanchikov A., Kazanin V.A., Kolachev G.M., Korol A., Malyshev V., Maslennikov A.L., Maximov D.A., Orlov I., Peleganchuk S.V., Shamov A.G., Skovpen K., Soukharev A., Talyshev A., Tikhonov Y.A., Zaytsev A., et al. Search for quark contact interactions in dijet angular distributions in pp collisions at radical s = 7 TeV measured with the ATLAS detector. // Phys. Lett. B, 2011. - V.694, N4/5. - P.327-345.
- [36] Aamondt K., ALICE Collab., Pestov Y., et al. Suppression of charged particle production at large transverse

- momentum in central Pb-Pb collisions at $\sqrt{s} \text{NN} = 2.76 \text{ TeV}$. // *Phys. Lett. B*, 2011. - V.696, N1/2. - P.30-39.
- [37] Aamodt K., ALICE Collab., Pestov Y., et al. Two-pion Bose-Einstein correlations in central Pb-Pb collisions at $\sqrt{s} \text{NN} = 2.76 \text{ TeV}$. // *Phys. Lett. B*, 2011. - V.696, N4. - P.328-337.
- [38] Blinov A.E., Rudenko A.S. Upper limits on electric and weak dipole moments of W-boson. // *Phys. Lett. B*, 2011. - V.699, N4. - P.287-290.
- [39] Miyazaki Y., Arinstein K., Aulchenko V., Bondar A., Eidelman S., Epifanov D., Gabyshev N., Garmash A., Kuzmin A., Poluektov A., Shebalin V., Shwartz B., Usov Y., Vinokurova A., Zhilich V., Zhulanov V., Zyukova O., et. al. (Belle Collab.). Search for lepton-flavor-violating tau decays into a lepton and a vector meson. // *Phys. Rev. B*, 2011. - Vol.699, N4. - P.251-257.
- [40] Lees J.P., BABAR Collab., Blinov V.E., Buzykaev A.R., Buzykaev A.R., Druzhinin V.P., Golubev V.B., Kravchenko E.A., Onuchin A.P., Serednyakov S.I., Skovpen Yu.I., Solodov E.P., Todyshev K.Yu., Yushkov A.N., et al. Amplitude analysis of $B^0 \rightarrow K^+ \pi^- \pi^0$ and evidence of direct CP violation in $B \rightarrow K^* \pi$ decays. // *Phys. Rev. D*, 2011. - V.83, N11. - P.112010-1-21.
- [41] Lees J.P., BABAR Collab., Blinov V.E., Buzykaev A.R., Druzhinin V.P., Golubev V.B., Kravchenko E.A., Onuchin A.P., Serednyakov S.I., Skovpen Yu.I., Solodov E.P., Todyshev K.Yu., Yushkov A.N., et al. Analysis of the $D^+ \rightarrow K^- \pi^+ e^+ \nu_e$ decay channel. // *Phys. Rev. D*, 2011. - V.83, N7. - P.072001-1-35.
- [42] Choi S.-K., Arinstein K., Bondar A., Eidelman S., Epifanov D., Gabyshev N., Garmash A., Kuzmin A., Matvienko D., Poluektov A., Shebalin V., Vinokurova A., Zhilich V., Zhulanov V., Zyukova O., et. al. (Belle Collab.). Bounds of the width, mass difference and other properties of $X(3872) \rightarrow \pi^+ \pi^- J/\psi$ decays. // *Phys. Rev. D*, 2011. - Vol.84, N5. - P.052004-1- 16.
- [43] Lees J.P., BABAR Collab., Blinov V.E., Buzykaev A.R., Druzhinin V.P., Golubev V.B., Kravchenko E.A., Onuchin A.P., Serednyakov S.I., Skovpen Yu.I., Solodov E.P., Todyshev K.Yu., Yushkov A.N., et al. Branching fraction measurements of the color-suppressed decays anti B^0 to $D/\text{sab} (*)^0 \pi^0$, $D/\text{sab} (*)^0 \eta$, $D/\text{sab} (*)^0 \omega$, and $D/\text{sab} (*)^0 \eta'$ and measurement of the polarization in the decay anti $B^0 \rightarrow D/\text{sab} (*)^0 \omega$. // *Phys. Rev. D*, 2011. - V.84, N11. - P.112007-1-25.
- [44] Del Amo Sanchez P., BABAR Collab., Blinov V.E., Buzykaev A.R., Druzhinin V.P., Golubev V.B., Kravchenko E.A., Onuchin A.P., Serednyakov S.I., Skovpen Yu.I., Solodov E.P., Todyshev K.Yu., Yushkov A.N., et al. Dalitz plot analysis of $D^+ \rightarrow K^+ K^- \pi^+$. // *Phys. Rev. D*, 2011. - V.83, N5. - P.052001-1 - 20.
- [45] Lees J.P., BABAR Collab., Blinov V.E., Buzykaev A.R., Druzhinin V.P., Golubev V.B., Kravchenko E.A., Onuchin A.P., Serednyakov S.I., Skovpen Yu.I., Solodov E.P., Todyshev K.Yu., Yushkov A.N., et al. Evidence for the $h_b(1P)$ meson in the decay $\Gamma(3S) \rightarrow \pi^0 h_b(1P)$. // *Phys. Rev. D*, 2011. - V.84, N9. - P.091101-1-8.
- [46] Aamodt K., ALICE Collab., Pestov Y., et al. Femtoscopy of pp collisions at radical $s = 0.9$ and 7 TeV at the LHC with two-pion Bose-Einstein correlations. // *Phys. Rev. D*, 2011. - V.84, N11. - P.112004-1-22.
- [47] Sahoo H., Aulchenko V., Bondar A., Eidelman S., Epifanov D., Gabyshev N., Kuzmin A., Matvienko D., Shebalin V., Shwartz B., Vinokurova A., Zhilich V., Zhulanov V., et al. (Belle Collab.). First observation of radiative $B^0 \rightarrow \phi K^0 \gamma$ decays and measurements of their time-dependent CP violation. // *Phys. Rev. D*, 2011. - Vol.84, N7. - P.071101-1-6.
- [48] Ablikim M., BESIII Collab., Achasov M.N., Muchnoi N.Yu. First observation of the decays $X_{s1} \rightarrow \pi^0 \pi^0 \pi^0 \pi^0$. // *Phys. Rev. D*, 2011. - V.83, N1. - P.012006-1-7.
- [49] Ablikim M., BESIII Collab., Achasov M.N., Muchnoi N.Yu., Nikolaev I.B., et al. Higher-order multipole amplitude measurement in $\phi' \rightarrow \gamma X_{c2}$. // *Phys. Rev. D*, 2011. - V.84. - P.092006-1-9.
- [50] Pakhlova G., Arinstein K., Bondar A., Eidelman S., Epifanov D., Gabyshev N., Garmash A., Kuzmin A., Poluektov A., Shebalin V., Shwartz B., Vinokurova A., Zhilich V., Zhulanov V., Zyukova O., et al. (Belle Collab.). Measurement of $e^+e^- \rightarrow D_s^{(*)} + D_s^{(*)}$ cross sections near threshold using initial-state radiation. // *Phys. Rev. D*, 2011. - Vol.83, N1. - P.011101-1-7.
- [51] Del Amo Sanchez P., BABAR Collab., Blinov V.E., Buzykaev A.R., Druzhinin V.P., Golubev V.B., Onuchin A.P., Serednyakov S.I., Skovpen Yu.I., Solodov E.P., Todyshev K.Yu., Yushkov A.N. Measurement of the $B \rightarrow \text{anti } D/\text{sab} (*)^0 / D/\text{sab} (*)^0 / K$ branching fractions. // *Phys. Rev. D*, 2011. - V.83, N3. - P.032004-1-16.
- [52] Del Amo Sanchez P., BABAR Collab., Blinov V.E., Buzykaev A.R., Druzhinin V.P., Golubev V.B., Kravchenko E.A., Onuchin A.P., Serednyakov S.I., Skovpen Yu.I., Solodov E.P., Todyshev K.Yu., Yushkov A.N., et al. Measurement of the $B^0 \rightarrow \pi^- l^+ \nu$ and $B^+ \rightarrow \eta/\text{sab} (*)^0 / l^+ \nu$ branching fractions, the $B^0 \rightarrow \pi^- l^+ \nu$ and $B^+ \rightarrow \eta l^+ \nu$ form-factor shapes, and determination of $[V_{ub}]$. // *Phys. Rev. D*, 2011. - V.83, N5. - P.052011-1-16.

List of publications

- [53] Ha H., Bondar A., Eidelman S., Gabyshev N., Kuzmin A., Zhulanov V., et al. Measurement of the decay $B^0 \rightarrow \pi^+ l^- \nu$ and determination of $|V_{ub}|$. // Phys. Rev. D, 2011. - Vol.83, N7. - P.071101-1-6.
- [54] Del Amo Sanchez P., BABAR Collab., Blinov V.E., Buzykaev A.R., Druzhinin V.P., Golubev V.B., Kravchenko E.A., Onuchin A.P., Serednyakov S.I., Skovpen Yu.I., Solodov E.P., Todyshev K.Yu., Yushkov A.N., et al. Measurement of the $\gamma \gamma^* \rightarrow \eta$ and $\gamma \gamma^* \gamma \eta'$ transition form factors. // Phys. Rev. D, 2011. - V.84, N5. - P.052001-1-19.
- [55] Aad G., ATLAS Collab., Bobrovnikov V.S., Bogdanchikov A., Kazanin V.A., Kolachev G.M., Korol A., Malyshev V., Maslennikov A.L., Peleganchuk S.V., Skovpen K., Soukharev A., Talyshev A., Tikhonov Y.A., Zaytsev A., et al. Measurement of the inclusive isolated prompt photon cross section in pp collisions at radical $s=7$ TeV with the ATLAS detector. // Phys. Rev. D, 2011. - V.83, N5. - P.052005-1-31.
- [56] Lees J.P., BABAR Collab., Blinov V.E., Buzykaev A.R., Druzhinin V.P., Golubev V.B., Kravchenko E.A., Onuchin A.P., Serednyakov S.I., Skovpen Yu.I., Solodov E.P., Todyshev K.Yu., Yushkov A.N., et al. Measurement of the mass and width of the $D_{s1}(2536)^+$ meson. // Phys. Rev. D, 2011. - V.83, N7. - P.072003-1-14.
- [57] Ablikim M., BESIII Collab., Achasov M.N., Muchnoi N.Yu. Measurement of the matrix element for the decay $\eta' \rightarrow \eta \pi^+ \pi^-$. // Phys. Rev. D, 2011. - V.83, N1. - P.012003-1-10.
- [58] Aad G., ATLAS Collab., Bobrovnikov V.S., Bogdanchikov A., Kazanin V.A., Kolachev G.M., Korol A., Malyshev V., Maslennikov A.L., Orlov I., Peleganchuk S.V., Shamov A.G., Skovpen K., Soukharev A., Talyshev A., Tikhonov Y.A., Zaytsev A., et al. Measurement of underlying event characteristics using charged particles in pp collisions at radical $s = 900$ GeV and 7 TeV with the ATLAS detector. // Phys. Rev. D, 2011. - V.83, N11. - P.112001-1-34.
- [59] Lees J.P., BABAR Collab., Blinov V.E., Buzykaev A.R., Druzhinin V.P., Golubev V.B., Kravchenko E.A., Onuchin A.P., Serednyakov S.I., Skovpen Yu.I., Solodov E.P., Todyshev K.Yu., Yushkov A.N. et al. Measurements of branching fractions and CP asymmetries and studies of angular distributions for $B \rightarrow \phi \phi K$ decays. // Phys. Rev. D, 2011. - V.84, N1. - P.012001-1-13.
- [60] Bahinipati S., Arinstein K., Aulchenko V., Bondar A., Eidelman S., Gabyshev N., Poluektov A., Vinokurova A., et al. (Belle Collab.). Measurements of time-dependent CP asymmetries in $B \rightarrow D^{*\pm} \pi^\pm$ decays using a partial reconstruction technique. // Phys. Rev. D, 2011. - Vol.84, N2. - P.021101-1-7.
- [61] Chen P., Aulchenko V., Eidelman S., Kuzmin A., Matvienko D., Shwartz B., et al. (Belle Collab.). Observation of $B^- \rightarrow \text{anti } p \Lambda D^0$ at Belle. // Phys. Rev. D, 2011. - Vol.84, N7. - P.071501-1-7.
- [62] Del Amo Sanchez P., BABAR Collab., Blinov V.E., Buzykaev A.R., Druzhinin V.P., Golubev V.B., Kravchenko E.A., Onuchin A.P., Serednyakov S.I., Skovpen Yu.I., Solodov E.P., Todyshev K.Yu., Yushkov A.N., et al. Observation of $\eta'/\text{sub } c(1S)$ and $\eta'/\text{sub } c(2S)$ decays to $K^+K^- \pi^+\pi^-\pi^0$ in two-photon interactions. // Phys. Rev. D, 2011. - V.84, N1. - P.012004-1-9.
- [63] Lees J.P., BABAR Collab., Blinov V.E., Buzykaev A.R., Druzhinin V.P., Golubev V.B., Kravchenko E.A., Onuchin A.P., Serednyakov S.I., Skovpen Yu.I., Solodov E.P., Todyshev K.Yu., Yushkov A.N., et al. Observation of the baryonic B decay $\text{anti } B^0 \rightarrow \Lambda_{cb}^+/\text{sub } c/\text{ anti } \Lambda_{cb}^-$. // Phys. Rev. D, 2011. - V.84, N7. - P.071102-1-7.
- [64] Lees J.P., BABAR Collab., Blinov V.E., Buzykaev A.R., Druzhinin V.P., Golubev V.B., Kravchenko E.A., Onuchin A.P., Serednyakov S.I., Skovpen Yu.I., Solodov E.P., Todyshev K.Yu., Yushkov A.N., et al. Observation of the rare decay $B^+ \rightarrow K^+ \pi^0 \pi^0$ and measurement of the quasi-two-body contributions $B^+ \rightarrow K^*(892) \pi^0$, $B^+ \rightarrow f_0(980) K^+$, and $B^+ \rightarrow \chi_{c0}/K^+$. // Phys. Rev. D, 2011. - V.84, N9. - P.092007-1-11.
- [65] Lees J.P., BABAR Collab., Blinov V.E., Buzykaev A.R., Druzhinin V.P., Golubev V.B., Kravchenko E.A., Onuchin A.P., Serednyakov S.I., Skovpen Yu.I., Solodov E.P., Todyshev K.Yu., Yushkov A.N., et al. Searches for rare or forbidden semileptonic charm decays. // Phys. Rev. D, 2011. - V.84, N7. - P.072006-1-13.
- [66] Del Amo Sanchez P., BABAR Collab., Blinov V.E., Buzykaev A.R., Druzhinin V.P., Golubev V.B., Kravchenko E.A., Onuchin A.P., Serednyakov S.I., Skovpen Yu.I., Solodov E.P., Todyshev K.Yu., Yushkov A.N., et al. Searches for the baryon- and lepton-number violating decays $B^0 \rightarrow \Lambda_{cb}^+/\text{sub } c/l^-$, $B^- \rightarrow \Lambda_{cb}^-$, and $B^- \rightarrow \text{anti } \Lambda_{cb}^-$. // Phys. Rev. D, 2011. - V.83, N9. - P.091101-1-8.
- [67] Lees J.P., BABAR Collab., Blinov V.E., Buzykaev A.R., Druzhinin V.P., Golubev V.B., Kravchenko E.A., Onuchin A.P., Serednyakov S.I., Skovpen Yu.I., Solodov E.P., Todyshev K.Yu., Yushkov A.N., et al. Search for b \rightarrow u transitions in $B^+ \rightarrow [K^+ \pi^+ \pi^0]/\text{sub } D/K^+$ decays. // Phys. Rev. D, 2011. - V.84, N1. - P.012002-1-10.
- [68] Wang X.L., Eidelman S., Kuzmin A., Matvienko D., Shwartz B., Usov Y., Zhilich V., et al. (Belle Collab.). Search for charmonium and charmoniumlike states in $Y(2S)$ radiative decays. // Phys. Rev. D, 2011. - Vol.84, N7. - P.071107-1-7.

- [69] Aad G., ATLAS Collab., Beloborodova O., Bobrovnikov V.S., Bogdanchikov A., Kazanin V.A., Kolachev G.M., Korol A., Malyshev V., Maslennikov A.L., Maximov D.A., Orlov I., Peleganchuk S.V., Shamov A.G., Skovpen K., Soukharev A., Talyshev A., Tikhonov Y.A., Zaytsev A., et al. Search for contact interactions in dimuon events from pp collisions at radical $s = 7$ TeV with the ATLAS detector. // Phys. Rev. D, 2011. - V.84, N1. - P.0111101-1-18.
- [70] Ablikim M., BESSIII Collab., Achasov M.N., Muchnoi N.Yu., Nikolaev I.B., et al. Search for CP and P violating pseudoscalar decays into $\pi\pi$. // Phys. Rev. D, 2011. - V.84, N3. - P.032006-1-7.
- [71] Del Amo Sanchez P., BABAR Collab., Blinov V.E., Buzykaev A.R., Druzhinin V.P., Golubev V.B., Kravchenko E.A., Onuchin A.P., Serednyakov S.I., Skovpen Yu.I., Solodov E.P., Todyshev K.Yu., Yushkov A.N., et al. Search for CP violation in the decay $D^{+} \rightarrow K^{\circ}/\text{sub } s/ \pi^{+}$. // Phys. Rev. D, 2011. - V.83, N7. - P.071103-1-8.
- [72] Lees J.P., BABAR Collab., Blinov V.E., Buzykaev A.R., Druzhinin V.P., Golubev V.B., Kravchenko E.A., Onuchin A.P., Serednyakov S.I., Skovpen Yu.I., Solodov E.P., Todyshev K.Yu., Yushkov A.N., et al. Search for CP violation using T-odd correlations in $D^{+} \rightarrow K^{+} K^{\circ}/\text{sub } s/ \pi^{+}\pi^{-}$ and $D^{+}/\text{sub } s/ \rightarrow K^{+} K^{\circ}/\text{sub } s/ \pi^{+}\pi^{-}$ decays. // Phys. Rev. D, 2011. - V.84, N3. - P.031103-1-9.
- [73] Ablikim M., BESSIII Collab., Achasov M.N., Muchnoi N.Yu., Nikolaev I.B., et al. Search for η'_{c} decays into vector meson pairs. // Phys. Rev. D, 2011. - V.84, N9. - P.091102-1-7.
- [74] Seon O., Bondar A., Eidelman S., Gabyshev N., Kuzmin A., Usov Y., Vinokurova A., Zhilich V., Zhulanov V., Zykova O., et al. (Belle Collab.). Search for lepton-violating $B^{+} \rightarrow D^{-} l^{+} l^{+}$ decays. // Phys. Rev. D, 2011. - Vol.84, N7. - P.071106-1-7.
- [75] Del Amo Sanchez P., BABAR Collab., Blinov V.E., Buzykaev A.R., Druzhinin V.P., Golubev V.B., Onuchin A.P., Serednyakov S.I., Skovpen Yu.I., Solodov E.P., Todyshev K.Yu., Yushkov A.N. Search for the decay $B^{\circ} \rightarrow \gamma \gamma$. // Phys. Rev. D, 2011. - V.83, N3. - P.032006-1-11.
- [76] Del Amo Sanchez P., BABAR Collab., Blinov V.E., Buzykaev A.R., Druzhinin V.P., Golubev V.B., Onuchin A.P., Serednyakov S.I., Skovpen Yu.I., Solodov E.P., Todyshev K.Yu., Yushkov A.N. Studies of $\tau^{-} \rightarrow \eta K^{-} \nu_{\tau}$ and $\tau^{-} \rightarrow \eta \pi^{-} \nu_{\tau}$ at BABAR and a search for a second-class current. // Phys. Rev. D, 2011. - V.83, N3. - P.032001-1-10.
- [77] Ablikim M., BES III Co, Achasov M.N. Study of $a_0(980) - f_0(980)$ mixing. // Phys. Rev. D, 2011. - V.83, N3. - P.032003-1-11.
- [78] Del Amo Sanchez P., BABAR Collab., Blinov V.E., Buzykaev A.R., Druzhinin V.P., Golubev V.B., Onuchin A.P., Serednyakov S.I., Skovpen Yu.I., Solodov E.P., Todyshev K.Yu., Yushkov A.N. Study of $B \rightarrow \pi \ell \nu$ and $B \rightarrow \rho \ell \nu$ decays and determination of $|V_{ub}|$. // Phys. Rev. D, 2011. - V.83, N3. - P.P. 032007-1-45.
- [79] Ablikim M., BESIII Collab., Achasov M.N., Muchnoi N.Yu., Nikolaev I.B., et al. Study of $\chi/\text{sub } cJ/$ radiative decays into a vector meson. // Phys. Rev. D, 2011. - V.83, N11. - P.112005-1-9.
- [80] Lees J.P., BABAR Collab., Blinov V.E., Buzykaev A.R., Druzhinin V.P., Golubev V.B., Kravchenko E.A., Onuchin A.P., Serednyakov S.I., Skovpen Yu.I., Solodov E.P., Todyshev K.Yu., Yushkov A.N., et al. Study of dipion bottomonium transitions and search for the $h_b(1P)$ state. // Phys. Rev. D, 2011. - V.84, N1. - P.011104-1-9.
- [81] Lees J.P., BABAR Collab., Blinov V.E., Buzykaev A.R., Druzhinin V.P., Golubev V.B., Kravchenko E.A., Onuchin A.P., Serednyakov S.I., Skovpen Yu.I., Solodov E.P., Todyshev K.Yu., Yushkov A.N., et al. Study of $\Gamma(3S,2S) \rightarrow \eta$ $\Gamma(1S)$ and $\Gamma(3S,2S) \rightarrow \pi^{+}\pi^{-} \Gamma(1S)$ hadronic transitions. // Phys. Rev. D, 2011. - V.84, N9. - P.092003-1-8.
- [82] Aad G., ATLAS Collab., Bobrovnikov V.S., Bogdanchikov A., Kazanin V.A., Kolachev G.M., Korol A., Malyshev V., Maslennikov A.L., Orlov I., Peleganchuk S.V., Shamov A.G., Skovpen K., Soukharev A., Talyshev A., Tikhonov Y.A., Zaytsev A., et al. Study of jet shapes in inclusive jet production in pp collisions at radical $s=7$ TeV using the ATLAS detector. // Phys. Rev. D, 2011. - V.83. - P.052003-1-29.
- [83] Lees J.P., BABAR Collab., Blinov V.E., Buzykaev A.R., Druzhinin V.P., Golubev V.B., Kravchenko E.A., Onuchin A.P., Serednyakov S.I., Skovpen Yu.I., Solodov E.P., Todyshev K.Yu., Yushkov A.N., et al. Study of radiative bottomonium transitions using converted photons. // Phys. Rev. D, 2011. - V.84, N7. - P.072002-1-17.
- [84] Guler H., Arinstein K., Aulchenko V., Eidelman S., Kuzmin A., Poluektov A., Zhilich V., Zhulanov V. (Belle Collab.). Study of the $K^{+} \pi^{+} \pi^{-}$ final state in $B^{+} \rightarrow J/\psi K^{+} \pi^{+} \pi^{-}$ and $B^{+} \rightarrow \psi' K^{+} \pi^{+} \pi^{-}$. // Phys. Rev. D, 2011. - Vol.83, N3. - P.032005-1-29.
- [85] Ablikim M., BESSIII Collab., Achasov M.N., Muchnoi N.Yu., et al. Confirmation of the X(1835) and observation of the resonances X(2120) and X(2370) in $J/\psi \rightarrow \gamma \pi^{+} \pi^{-} \eta'$. // Phys. Rev. Lett., 2011. - V.106, N7. - P.072002-1-5.
- [86] Ablikim M., BESIII Collab., Achasov M.N., Mikolaev I.B., et al. $\eta \pi^{+}\pi^{-}$ resonant structure around 1.8 GeV/s/sab 2/ and $\eta(1405)$ in $J/\psi \rightarrow \omega \eta \pi^{+}\pi^{-}$. // Phys. Rev. Lett., 2011. - V.107, N18. - P.182001-1-6.

List of publications

- [87] Horii Y., Arinstein K., Aulchenko V., Eidelman S., Gabyshev N., Garmash A., Poluektov A., Shebalin V., Usov Y., Vinokurova A., Zhulanov V., et. al. (Belle Collab.). Evidence for the suppressed decay $B^- \rightarrow DK^-$, $D \rightarrow K^+ \pi^-$. // Phys. Rev. Lett., 2011. - Vol.106, N23. - P.231803-1-6.
- [88] Aad G., ATLAS Collab., Pestov Y., et al. Higher harmonic anisotropic flow measurements of charged particles in Pb-Pb collisions at $\sqrt{s} NN=2.76$ TeV. // Phys. Rev. Lett., 2011. - V.107, N3. - P.032301-1-10.
- [89] Li J., Arinstein K., Aulchenko V., Eidelman S., Gabyshev N., Garmash A., Kuzmin A., Poluektov A., Shebalin V., Shwartz B., Usov Yu., Vinokurova A., Zhilich V., Zhulanov V., et. al. (Belle Collab.). Observation of $B_s^0 \rightarrow J/\psi f_0(980)$ and evidence for $J/\psi f_0(1370)$. // Phys. Rev. Lett., 2011. - Vol.106, N12. - P.121802-1-5.
- [90] Ablikim M., BESIII Collab., Achasov M.N., Muchnoi N.Yu., et al. Observation of χ_{c1} decays into vector meson pairs $\phi\phi$, $\omega\omega$, and $\omega\phi$. // Phys. Rev. Lett., 2011. - V.107, N9. - P.092001-1-6.
- [91] Won E., Arinstein K., Bondar A., Eidelman S., Gabyshev N., Garmash A., Usov Y., Vinokurova A., Zhilich V., Zhulanov V., Zykova O., et. al. (Belle Collab.). Observation of $D^+ \rightarrow K^+ \eta^{(\prime)}$ and search for CP violation in $D^+ \rightarrow \pi^+ \eta^{(\prime)}$ decays. // Phys. Rev. Lett., 2011. - Vol.107, N22. - P.221801-1-6.
- [92] Del Amo Sanchez P., BABAR Collab., Blinov V.E., Buzykaev A.R., Druzhinin V.P., Golubev V., Onuchin A.P., Serednyakov S.I., Skovpen Yu.I., Solodov E.P., Todyshev K.Yu., Yushkov A.N., et al. Observation of the decay $B^- \rightarrow D/sab (*)+ /sub s/ K^- l^- \text{ anti } \nu_l$. // Phys. Rev. Lett., 2011. - V.107, N4. - P.041804-1-8.
- [93] Vossen A., Bondar A., Eidelman S., Gabyshev N., Garmash A., Shebalin V., Vinokurova A., Zhilich V., Zhulanov V., et. al. (Belle Collab.). Observation of transverse polarization asymmetries of charged pion pairs in $e^+ e^-$ annihilation near radical $\sqrt{s}=10.58$ GeV. // Phys. Rev. Lett., 2011. - Vol.107, N7. - P.072004-1-7.
- [94] Aad G., ATLAS Collab., Beloborodova O., Bobrovnikov V.S., Bogdanchikov A., Kazanin V.A., Kolachev G.M., Korol A., Malyshev V., Maslennikov A.L., Maximov D.A., Orlov I., Peleganchuk S.V., Schamov A.G., Skovpen K., Soukharev A., Talyshv A., Tikhonov Yu.A., Zaytsev A. Search for a standart model Higgs boson in the $H \rightarrow ZZ \rightarrow l+l^- \text{ nu anti nu}$ decay channel with the ATLAS detector. // Phys. Rev. Lett., 2011. - V.107, N22. - P.221801-16.
- [95] Ko B.R., Arinstein K., Bondar A., Eidelman S., Gabyshev N., Garmash A., Kuzmin A., Poluektov A., Shebalin V., Shwartz B., Vinokurova A., Zhilich V., Zhulanov V., Zykova O., et. al. (Belle Collab.). Search for CP violation in the decays $D^0 \rightarrow K_s^0 P^0$. // Phys. Rev. Lett., 2011. - Vol.106, N21. - P.211801-1-6.
- [96] Del Amo Sanchez P., BABAR Collab., Blinov V.E., Buzykaev A.R., Druzhinin V.P., Golubev V.B., Kravchenko E.A., Onuchin A.P., Serednyakov S.I., Skovpen Yu.I., Solodov E.P., Todyshev K.Yu., Yushkov A.N., et al. Search for production of invisible final states in single-photon decays of Gamma (1S). // Phys. Rev. Lett., 2011. - V.107, N2. - P.021804-1-7.
- [97] Socol Y., Kulipanov G.N., Matveenkov A.N., Shevchenko O.A., Vinokurov N.A. Compact 13.5-nm free-electron laser for extreme ultraviolet lithography [Electronic resource]. // Phys. Rev. Spec. Top. - Ac., 2011. - V.4, N14. - P.040702-1 - 040702-7.
- [98] Vinokurov N.A., Shevchenko O.A., Tcheskidov V.G. Variable-period permanent magnet undulators [Electronic resource]. // Phys. Rev. Spec. Top. - Ac., 2011. - V.4, N14. - P.040701-1 - 040701-7.
- [99] Smirnov A., Krivenko A.S., Murakhtin S.V., Savkin V.Ya., Korepanov S.A., Putvinski S. Neutral beam dump with cathodic arc titanium gettering. // Rev. Sci. Instrum., 2011. - V.82, N3. - P.033509-1-6.
- [100] Skuzovatov S.Yu., Zedgenizov D.A., Shatsky V.S., Ragozin A.L., Kuper K.E. Composition of cloudy microinclusions in octahedral diamonds from the Internatsional'naya kimberlite pipe (Yakutia). // Russian Geology and Geophysics, 2011. - V.52, N1. - P.85 - 96.
- [101] Kozlov A.S., Petrov A.K., Vinokurov N.A. Study of nano-objects of different nature by submillimeter laser ablation. // Avtometriy(Optoelectronics), 2011. - Vol.47, N4. - P.3-15.
- [102] Demyanenko M.A., Esaev D.G., Marchishin I.V., Ovsyuk V.N., Fomin B.I., Knyazev B.A., Gerasimov V.V. The use of uncooled microbolometer arrays for detection of radiation in terahertz spectral range (in Russian). // Avtometriya(Optoelectronics), 2011. - V.47, N5. - P.109-113.
- [103] Lotov K.V., Maslov V.I., Onishchenko I.N., Vesnovskaya M.S. To the mechanism of instability of cylindrical relativistic electron beam in plasma. // VANT. Ser. Physics of Plasma, 2011. - N1(71). - P.83-85.
- [104] Lotov K., Maslov V.I., Onishchenko I.N., Yarovaya I.P. Transformation ratio at interaction of long sequence of electron bunches with plasma. // VANT. Ser. Problems of Atomic Science and Technology, 2011. - V.73, N3. - P.87-91.

- [105] Zhmurikov E.I., Savchenko I.V., Stankus S.V., Tecchio L. Thermophysical properties easurements of graphite composites for the neutron target convertor (in Russian). // Vestnik NSU. Ser.: Physics, 2011. - Vol.6, N2. - P.77-84 .
- [106] Arbuzov V.S., Gorniker E.I., Kozyrev E.V., Kondakov E.V., Petrov V.M., Pilan A.M., Cheskidov V.G. Modernization of high power modular unit continuous-wave RF generators for electron accelerators. // Vestnik NSU. Ser.: Physics, 2011. - Vol.6, N3. - P.11-20.
- [107] Miginsky S. Project of a compact terahertz free electron laser (in Russian). // Vestnik NSU. Ser. Physics, 2011. - V.6, N1. - P.95-103.
- [108] Ivanov A.V. Calculation of the limiting perveance of a round beam partially filling a cylindrical vacuum chamber (in Russian). // Vestnik NSU. Ser.: Physics, 2011. - Vol.6, N2. - P.43-49.
- [109] Chernousov Yu.D., Levichev A.E., Pavlov V.M., Shamuilov G.K. Thin diaphragm in the rectangular waveguide. // Vestnik NSU. Ser. Physics, 2011. - Vol.6, N1. - P.44-49.
- [110] Vinokurov N.A., Kulipanov G.N., Skrinisky N.A. Free Electron Lasers, achievements and prospects (in Russian). // Vesti. Journal of Academy of Sciences, 2011. - V.81, N6. - P.520-524.
- [111] Mityanina N.V., Petrov V.M. Influence of feedback circuits in RF accelerating system and feeders between RF power generators and accelerating cavities on dipole synphase oscillations of bunches in circular accelerators. // JETP, 2011. - Vol.81, N10. - P.91-94.
- [112] Berkaev D.E., Shwartz D.B., Shatunov P.Yu., Rogovsky Yu.A., Romanov A.L., Koop I.A., Shatunov Yu.M., Zemlyansky I.M., Lysenko A.P., Perevedentsev E.A., Stankevich A.S., Senchenko A.I., Khazin B.I., Anisenkov A.V., gayazov S.E., Kozyrev A.N., Ryzhenenkov A.E., Shemyakin D.N., Epstein L.B., Serednyakov S.I., Astigeevich P.M., Kovrizhin D.P., Martin K.A., Obrazovsky A.E., Surin I.K., Kardopoltsev L.V., Belikov O.V., Gorchakov K.M., Kirpotin A.N., Skrinisky A.N. VEPP_2000 electron-positron collider at BINP. The first experiments (in Russian). // JETP, 2011. - Vol.140, N2(8). - P.247-255.
- [113] Choporova Yu.Yu., Vlasenko M.G., Gerasimov V.V., Irgalin T.N., Knyazev B.A., Cherkassky V.S. Recording and reconstruction of axial holograms of amplitude objects in the terahertz frequency band using a free electron laser (in Russian). // Izvestiya VUZov. Radiophysics, 2011. - T.LIV, N8/9. - P.649-655.
- [114] Poletica I.M., Ivanov Yu.F., Golkovsky M.G., Krylova T.A., Neresov A.D., Makarov S.A. Creating a new class of coatings by double electron-beam processing. // Advanced Materials, 2011. - N1. - P.71-81 (in Russian).
- [115] Shklyayev A.A., Romanyuk K.N., Latyshev A.V., Arzhannikov A.V. Effect of dislocations on the shape of islands during silicon growth on the oxidized Si(111) surface. // JETP Letters, 2011.- Vol.94 (6), P.442-445.
- [116] Batrakov A.M., Vagin P.V., Vobly P.D., Gurov D.S., Zubkov N.I., Ilyin I.V., Ogurtsov A.B., Tisher M., Utkin A.V., Havin N.G., Kholopov M.A., Shichkov D.S. Wigglers on permanent magnets intended to reduce the emittance of the synchrotron radiation source PETRA III (in Russian). // Surface. X-ray, Synchrotron and Neutron Techniques, 2011. - N11. - P.18-25.
- [117] Kosov A.V., Cooper E.A., Sheromov M.A. High vacuum ionization chamber with high spatial resolution for monitoring of SR beam. // Surface. X-ray, Synchrotron and Neutron Techniques, 2011. - N11. - P.44-48.
- [118] Gentshev A.N., Golubtsov S.K., Goldenberg B.G., Kondratiev V.I., Pindyurin V.F., Zelinsky A.G. Using graphite foil as a carrier membrane of LIGA templates. // Surface. X-ray, Synchrotron and Neutron Techniques, 2011. - N8. - P.19-24.
- [119] A.M. Batrakov, P.D. Voblyi, I.V. Ilyin, A.B. Ogurtsov, A.V. Utkin, D.S. Shichkov, M. Tisher, P.V. Vagin Complex of hardware and software tools for fine-tuning of damping wigglers of the PETRA III storager ring. // Surface. X-ray, Synchrotron and Neutron Techniques, 2011. - N11. - P.26-35.
- [120] B.G. Goldenberg, A. Yu. Abramsky, A. G. Zelinsky, A.I. Masliy, E.A. Maksimovskiy, V.I. Kondratiev, V.P. Korolkov, K.E. Cooper, E.V. Petrova, V.F. Pindyurin. Peculiarities in the manufacture of templates for deep X-ray technology at the Siberian Center for Synchrotron and Terahertz radiation. // Surface. X-ray, Synchrotron and Neutron Techniques, 2011. - N2. - P.61-68.
- [121] A.M. Semenov, V.V. Anashin, N.F. Goncharova, V.A. Ushakov, A.V. Filipchenko, L.M. Shchegolev. Status and description of the TNK vacuum system. // Surface. X-ray, Synchrotron and Neutron Techniques, 2011. - N11. - P.39-43.
- [122] V.A. Bezhanov, E.I. Zinin, D.N. Karimov, V.V. Mikhailin, S.P. Chernov Spectroscopic studies of wide-gap fluoride crystals doped with ions of rare-earth elements under X-ray excitation. // Surface. Physics. Chemistry. Mechanics,

List of publications

2011. - N1. - P.48-52.
- [123] A.V. Petrenko Calibration of the electron-optical model of the cooling storage ring of the VEPP-5 injection complex. // Instruments and Experimental Techniques, 2011. - N1. - P.12-19.
- [124] Bryazgin A.A., Bezuglov V.V., Chernov, Cheskidov V.G., Faktorovitch B.L., Kokin E.N., Korobeynikov M.V., Makarov I.G., Ostreiko G.N., Panfilov A.D., Radchenko V.M., Serdobintsev G.V., Sidorov A.V., Tarnetsky V.V., Tiunov M.A. ILU-14 industrial electron linear accelerator with a modular structure. // Instruments and Experimental Techniques (Online). A, 2011. - Vol.54, N3. - P.295-311. [PTE, 2011. - N3. - C.5-21].
- [125] Kabantsev A.A., Dubin D.H.E., Tsidulko Y.A., Driscoll C.F. Chaotic neoclassical transport at azimuthally perturbed or wave-mingled separatrix. // Fusion Sci. Technol., 2011. - V.59, NIT. - P.150-153.
- [126] Listopad A., Davydenko V., Freutel S., Ivanov A., Schweer B., Zlobinski M. Characterization of RUDI neutral beam parameters by optical diagnostics. // Fusion Sci. Technol., 2011. - V.59, NIT. - P.274-276.
- [127] Dimov G.I., Emelev I.S., Vobly P.D., Kobets V.V., Tiunov M.A. Multicusp trap with circular geometry for confinement of low-temperature plasma. // Fusion Sci. Technol., 2011. - V.59, NIT. - P.211-213.
- [128] Skovorodin D.I., Beklemishev A.D. Numerical kinetic model of axial confinement in a mirror trap. // Fusion Sci. Technol., 2011. - V.59, NIT. - P.199-201.
- [129] Astrelin V., Burfakov A., Vshivkov V., Vshivkov K., Medvedev S., Shvab I., Yakunkin N. Numerical modeling of plasma dynamics in non-uniform magnetic field. // Fusion Sci. Technol., 2011. - V.59, NIT. - P.313-315.
- [130] Driscoll C.F., Kabantsev A.A., Dubin D.H.E., Tsidulko Y.A. Overview of transport, damping, and wave couplings from separatrix dissipation in an axisymmetric plasma. // Fusion Sci. Technol., 2011. - NIT. - P.170-175.
- [131] Timofeev I.V., Terekhov A.V. Simulations of turbulent plasma heating by powerful electron beams. // Fusion Sci. Technol., 2011. - V.59, NIT. - P.70-73.
- [132] Shikhovtsev I.V., Averbukh I.I., Belov V.P., Davydenko V.I., Deichuli P.P., Ivanov A.A., Kapitonov V.A., Podyminogin A.A., Sorokon A.V. A continuously operated 70 mA, 50 keV proton source plasma diagnostic and other applications. // Fusion Sci. Technol., 2011. - V.59, NIT. - P.283-285.
- [133] Bagryansky P.A., Anikeev A.V., Beklemishev A.D., Donin A.S., Ivanov A.A., Korzhavina M.S., Kovalenko Y.V., Kruglyakov E.P., Lizunov A.A., Maximov V.V., Murakhtin S.V., Prikhodko V.V., Pinzhenin E.I., Pushkareva A.N., Savkin V.Y., Zaytsev K.V. Confinement of hot ion plasma with $\beta=0.6$ in the gas dynamic trap. // Fusion Sci. Technol., 2011. - V.59, NIT. - P.31-35.
- [134] Batkin V.I., Bobylev V.B., Burdakov A.V., Davydenko V.I., Ivanov A.A., Kapitonov V.A., Mekler K.I., Polosatkin S.V., Postupaev V.V., Rovenskikh A.F., Sorokina N.V., Sulyaev Yu.S., Trunev Yu.A. Development of new neutral beam injection system on GOL-3 Facility. // Fusion Sci. Technol., 2011. - V.59, NIT. - P.262-264.
- [135] Prikhodko V.V., Bagryansky P.A., Beklemishev A.D., Kolesnikov E.Y., Kotelnikov I.A., Maximov V.V., Pushkareva A.N., Soldatkina E.I., Tsidulko Y.A., Zaytsev K.V. Low-frequency oscillations of plasma in the Gas Dynamic Trap. // Fusion Sci. Technol., 2011. - V.59, NIT. - P.94-97.
- [136] Anderson J.K., Almagri A.F., Chapm B.E., Davydenko V.I., Deichuli P., Hartog D.J., Forest C.B., Fiksel G., Ivanov A.A., Liu D., Nornberg M.D., Sarff J.S., Stupishin N., Waksman J. Majority ion heating neutral beam injection and confinement of fast ions in the madison symmetric torus reversed field pinch. // Fusion Sci. Technol., 2011. - V.59, NIT. - P.27-30.
- [137] Shatilov D., Levichev E., Simonov E., and Zobov M. Application of frequency map analysis to beam-beam effects study in crab waist collision scheme. // APS Journals, Phys. Rev. ST, Accel. Beams, 21 January 2011. - Vol.14, Issue 1. - (13 pages).
- [138] E.V. Abakumova, M.N. Achasov, V.E. Blinov, X. Cai, H.Y. Dong, C.D. Fu, F.A. Harris, V.V. Kaminsky, A.A. Krasnov, Q. Liu, X.H. Mo, N.Yu. Muchnoi, I.B. Nikolaev, Q. Qin, H.M. Qu, S.L. Olsen, E.E. Pyata, A.G. Shamov, C.P. Shen, K.Yu.T. odyshev, G.S. Varner, Y.F. Wang, Q. Xiao, J.Q. Xu, J.Y. Zhang, T.B. Zhang, Y.H. Zhang, A.A. Zhukov. The beam energy measurement system for the Beijing electron-positron collider. // NIM A, 2011. - V.659. - P.21-29.
- [139] Abakumova E.V., Zhukov A.A., Krasnov A.A. Flat flange connection based on copper sealing plate with step form of cross-section. // Vacuum Technique and Technology, 2011. - V.21, N1. - P.41-44 (in Russian).
- [140] Abakumova E.V., Anashin V.V., Balewski K., Boespflug R., Gusev G.A., Levichev E.B., Krasnov A.A., Kuzminykh V.S., Nagorny B., Pupkov Yu.A., Semenov A.M., Smaluk V.V., Tischer M., Wedekind H-P., Zapfe K.,

- Zhukov A.A., Zolotarev K.V. Vacuum system of PETRA III damping wiggler section. // *Vacuum Technique and Technology*, 2011. - V.21, N2. - P.85-89 (in Russian).
- [141] Bondar A.E., Dmitriev V.F., Milstein A.I., Strakhovenko V.M. Nucleon polarization in the process $e+e- \rightarrow N$ anti N near threshold. // *Phys. Lett. B*, 2011. - V.697, N2. - P.159-163.
- [142] Milstein A.I., Terekhov I.S. Induced current in the presence of a magnetic flux tube of small radius. // *Phys. Rev. B*, 2011. - V.83, N7. - P.075420-1-5.
- [143] Lee R.N., Milstein A.I., Terekhov I.S. Relativistic Coulomb Green's function in d dimensions. // *JETP*, 2011. - Vol.113. - P. 202. [*ZhETF*, 2011. Vol.140, N2(8). - P.236-240].
- [144] A.E. Bondar, A. Garmash, A.I. Milstein, R. Mizuk, and M.B. Voloshin. Heavy quark spin structure in Z_b resonances. // *Phys. Rev. D*, 2011. - Vol.84. - P.054010.
- [145] Milstein A.I., Sushkov O.P. Effective field theories and spin-wave excitations in helical magnets. // *Phys. Rev. B*, 2011. - Vol.84, N19. - P.195138-1-13.
- [146] A.S. Rudenko. $K_{13\gamma}^0$ decays: branching ratios and T-odd momenta correlations. // *Phys. Rev. D*. - Vol.84. - P.016001.
- [147] Khriplovich I.B., Rudenko A.S. Can CP-violation be observed in heavy-ion collisions? // *Can. J. Phys.*, 2011. - Vol.89. - P.63-64.
- [148] Khriplovich I.B., Rudenko A.S. $K_{13\gamma}^+$: decays revisited: branching ratios and T-odd momenta correlations. // *Phys. Atom. Nucl.*, 2011. - Vol.74, N8. - P.1214-1222; [*Yadernaya Fizika*, 2011, - V.74, N8. - P.1243-1251].
- [149] Khatsymovsky V. M. Path integral on the extreme field configurations. // *Int. J. Mod. Phys. A*, 2011. - Vol.26, N1. - P.135-148.
- [150] Khatsymovsky V.M. Attributing sense to some integrals in Regge calculus. // *J. Math. Phys.*, 2011. - Vol.52, N2. - P.022502-1-14.
- [151] Khatsymovsky V.M. Gravity action on the rapidly varying metrics. // *Gen. Rel. Grav.*, 2011. - V.43, N11. - P.3127-3138.
- [152] Valentin V. Sokolov, Oleg V. Zhirov, Yaroslev A. Kharkov. Classical versus quantum dynamical chaos: sensitivity to external perturbations, stability and reversibility. // *World Scientific*, 2011. - P.59-76.
- [153] Grozin A.G. Integration by parts: An introduction. // *Int. J. Mod. Phys. A*, 2011. - Vol.26. - P.2807-2854.
- [154] Grozin A.G., Hörschele M., Hoff J., Steinhauser M. Simultaneous decoupling of bottom and charm quarks. // *J. High Energy Phys.*, 2011. - Vol.09. - P.066.
- [155] Strakhovenko V.M. Coulomb effects in the spin-dependent contribution to the intra-beam scattering rate. // *Phys. Rev. ST. Accel. Beams*, 2011, Vol.14. - P.012803.
- [156] Katkov V.M. Pair photoproduction in a constant and homogeneous electromagnetic field. // *Nuovo Cimento C*, 2011. - Vol.34, N4. - P.1-7.
- [157] Fadin V.S. and Lipatov L.N. BFKL equation for the adjoint representation of the gauge group in the next-to-leading approximation at $N=4$ SUSY. // *Phys. Lett. B*, 2012. - Vol.706. - P.470-476. [arXiv:1111.0782 [hep-th]].
- [158] Fadin V.S., Fiore R., Grabovsky A.V. and Papa A. Connection between complete and forms of gauge invariant operators. // *Nucl. Phys. B*, 2012. - Vol.856. - P.111-124. [arXiv:1109.6634 [hep-th]].
- [159] Fadin V.S., Fiore R., Grabovsky A.V. and Papa A. Quasi-conformal shape of the BFKL kernel and impact factors for scattering of colourless particles. // *AIP Conf. Proc.*, 2011. - Vol.1350. - P.224-227.
- [160] Kozlov M.G., Reznichenko A.V. and Fadin V.S. Check of the gluon reggeization condition in the next-to-leading order: Quark part. // *Phys. Atom. Nucl.*, 2011. - Vol.74. - P.758-770. [*Yad. Fiz.*, 2011. - T.74, N5. - P.784-796].
- [161] Lee R. and Smirnov V. Analytic epsilon expansions of master integrals corresponding to massless three-loop form factors and three-loop $g-2$ up to four-loop transcendentality weight. // *JHEP*, 2011. - Vol.1102. - P.102. [arXiv: 1010.1334].
- [162] Lee R. and Terekhov I. Application of the {DRA} method to the calculation of the four-loop {QED}-type tadpoles. // *JHEP*, 2011. - Vol.1101. - P.068. [arXiv: 1010.6117].
- [163] Lee R.N., Smirnov A.V. and Smirnov V.A. Master integrals for four-loop massless propagators up to transcendentality weight twelve. // *Nucl. Phys. B*, 2011. - Vol.856. - P.95-110. [arXiv: 1108.0732].
- [164] Lee R.N., Smirnov A.V., Smirnov V.A. On epsilon expansions of four-loop non-planar massless propagator

- diagrams. // Eur. Phys. J. C, 2011. - Vol.71, N8. - P.1707. [arXiv: 1103.3409].
- [165] Zhiron O.V., Pikovsky A.S., Shepelyansky D.L. Quantum vacuum of strongly nonlinear lattices. // Phys. Rev. E, 2011. - Vol.83, N1. - P.016202-1-7.
- [166] Zhiron O.V., Shepelyansky D.L. Wigner crystal in snaked nanochannels. // Eur Phys.J. B, 2011. - Vol.82, P.63-67.
- [167] Stibunov V.N., Barkov L.M., Dmitriev V.F., Fix A.I., Gauzshtein V.V., Loginov A.Yu., Levchuk M.I., Mishnev S.I., Nikolenko D.M., Osipov A.V., Rachek I.A., Sadykov R.S., Shestakov Yu.V., Sidorov A.A., Toporkov D.K., Zevakov S.A. Tensor analyzing power component T21 of a π^- -meson photoproduction on a deuteron. // Journal of Physics: Conference Series. 2011. - N.295. - P.012115.
- [168] Barkov L.M., Gauzshtein V.V., Dmitriev V.F., Dusaev R.R., Zevakov S.A., Loginov A.Yu., Mishnev S.I., Nikolenko D.M., Osipov A.V., Rachek I.A., Sadykov R.Sh., Sidorov A.A., Stibunov V.N., Toporkov D.K., Shestakov Yu.V. Investigation of the reaction $\gamma d \rightarrow pp\pi^-$ with high-momentum of protons. // Izvestiya Vuzov. Physics, 2011. - Vol.54. - N11/2. - P.4-6 (in Russian).
- [169] Gauzshtein V.V., Zevakov S.A., Loginov A.Yu., Nikolenko D.M., Rachek I.A., Sadykov R.Sh., Sidorov A.A., Stibunov V.N., Toporkov D.K., Shestakov Yu.V. Measurement of the tensor analyzing power components in the photoproduction reaction of π^- -mesons on the deuterons. // Izvestiya Vuzov. Physics, 2011. - Vol.54. - N11/2. - P.7-13 (in Russian).
- [170] Aad G., ..., Anisenkov A., Beloborodova O., Bobrovnikov V.S., Bogdanchikov A., Kazanin V.A., Kolachev G.M., Korol A., Malyshev V., Maslennikov A.L., Maximov D.A., Orlov I., Peleganchuk S.V., Skovpen K., Schamov A.G., Soukharev A., Talyshv A., Tikhonov Yu.A., Zaytsev A., et al. (ATLAS Collab.). Search for new phenomena in final states with large jet multiplicities and missing transverse momentum using $\sqrt{s} = 7$ TeV pp collisions with the ATLAS detector. // IHEP, 2011. - Vol.1111. - P.099.
- [171] Aad G., ..., Anisenkov A., Beloborodova O., Bobrovnikov V.S., Bogdanchikov A., Kazanin V.A., Kolachev G.M., Korol A., Malyshev V., Maslennikov A.L., Maximov D.A., Orlov I., Peleganchuk S.V., Skovpen K., Schamov A.G., Soukharev A., Talyshv A., Tikhonov Yu.A., Zaytsev A., et al. (ATLAS Collab.). Search for massive colored scalars in four-jet final states in $\sqrt{s} = 7$ TeV proton-proton collisions with the ATLAS detector. // Eur. Phys. J. C, 2011. - Vol.71. - P.1846. [arxiv.org 1109.6833].
- [172] Aad G., ..., Anisenkov A., Beloborodova O., Bobrovnikov V.S., Bogdanchikov A., Kazanin V.A., Kolachev G.M., Korol A., Malyshev V., Maslennikov A.L., Maximov D.A., Orlov I., Peleganchuk S.V., Skovpen K., Schamov A.G., Soukharev A., Talyshv A., Tikhonov Yu.A., Zaytsev A., et al. (ATLAS Collab.). Measurement of the inclusive and dijet cross sections of b-jets in pp collisions at $\sqrt{s} = 7$ TeV with the ATLAS detector. // Eur. Phys. J. C, 2011. - Vol.71. - P.1846. [arxiv.org 1109.6833].
- [173] Aad G., ATLAS Collab., Beloborodova O., Bobrovnikov V.S., Bogdanchikov A., Kazanin V.A., Kolachev G.M., Korol A., Malyshev V., Maslennikov A.L., Maximov D.A., Orlov I., Peleganchuk S.V., Shamov A.G., Skovpen K., Soukharev A., Talyshv A., Tikhonov Y.A., Zaytsev A., et al. Search for the Standard Model Higgs boson in the decay channel $H \rightarrow ZZ/\text{sub} (*) \rightarrow 4 l$ with the ATLAS detector. // Phys. Lett. B, 2011. - V.705, N5. - P.435-451. [arxiv.org 1109.5945].
- [174] Aad G., ATLAS Collab., Beloborodova O., Bobrovnikov V.S., Bogdanchikov A., Kazanin V.A., Kolachev G.M., Korol A., Malyshev V., Maslennikov A.L., Maximov D.A., Orlov I., Peleganchuk S.V., Shamov A.G., Skovpen K., Soukharev A., Talyshv A., Tikhonov Y.A., Zaytsev A., et al. Measurement of the fragmentation function and transverse profile in proton-proton collisions at a center-of-mass energy of 7 TeV with the ATLAS detector. // Eur. Phys. J. C, 2011. - Vol.71, N11. - P.1795. [arxiv.org 1109.5816].
- [175] Aad G., ATLAS Collab., Beloborodova O., Bobrovnikov V.S., Bogdanchikov A., Kazanin V.A., Kolachev G.M., Korol A., Malyshev V., Maslennikov A.L., Maximov D.A., Orlov I., Peleganchuk S.V., Shamov A.G., Skovpen K., Soukharev A., Talyshv A., Tikhonov Y.A., Zaytsev A., et al. Search for the higgs boson in the $H \rightarrow WW \rightarrow l \nu jj$ decay channel in pp collisions at radical $s = 7$ TeV with the ATLAS detector. // Phys. Rev. Lett., 2011. - Vol.107, N23. - P.231801-1-18.
- [176] Aad G., ATLAS Collab., Beloborodova O., Bobrovnikov V.S., Bogdanchikov A., Kazanin V.A., Kolachev G.M., Korol A., Malyshev V., Maslennikov A.L., Maximov D.A., Orlov I., Peleganchuk S.V., Shamov A.G., Skovpen K., Soukharev A., Talyshv A., Tikhonov Y.A., Zaytsev A., et al. Search for a Standard Model Higgs boson in the $H \rightarrow ZZ \rightarrow l+l-\nu^-$ decay channel with the ATLAS detector. // Phys. Rev. Lett., 2011. - Vol.107. - P.221802. [arxiv.org 1109.3357].
- [177] Aad G., ATLAS Collab., Beloborodova O., Bobrovnikov V.S., Bogdanchikov A., Kazanin V.A., Kolachev G.M.,

- Korol A., Malyshev V., Maslennikov A.L., Maximov D.A., Orlov I., Peleganchuk S.V., Shamov A.G., Skovpen K., Soukharev A., Talyshev A., Tikhonov Y.A., Zaytsev A., et al. Search for a heavy neutral particle decaying into an electron and a muon using 1 fb⁻¹ of ATLAS data. // *Eur. Phys. J. C*, 2011. - Vol.71. - P.1809. [arxiv.org 1109.3089].
- [178] Aad G., ATLAS Collab., Beloborodova O., Bobrovnikov V.S., Bogdanchikov A., Kazanin V.A., Kolachev G.M., Korol A., Malyshev V., Maslennikov A.L., Maximov D.A., Orlov I., Peleganchuk S.V., Shamov A.G., Skovpen K., Soukharev A., Talyshev A., Tikhonov Y.A., Zaytsev A., et al. Search for the Standard Model Higgs boson in the two photon decay channel with the ATLAS detector at the LHC. // *Phys. Lett. B*, 2011. - V.705, N5. - P.452-470. [arxiv.org 1108.5895].
- [179] Aad G., ATLAS Collab., Beloborodova O., Bobrovnikov V.S., Bogdanchikov A., Kazanin V.A., Kolachev G.M., Korol A., Malyshev V., Maslennikov A.L., Maximov D.A., Orlov I., Peleganchuk S.V., Shamov A.G., Skovpen K., Soukharev A., Talyshev A., Tikhonov Y.A., Zaytsev A., et al. Measurement of the Z to tau tau cross section with the ATLAS detector. // *Phys. Rev. D*, 2011. - Vol.84, P.112006, 16p.
- [180] Aad G., ATLAS Collab., Beloborodova O., Bobrovnikov V.S., Bogdanchikov A., Kazanin V.A., Kolachev G.M., Korol A., Malyshev V., Maslennikov A.L., Maximov D.A., Orlov I., Peleganchuk S.V., Shamov A.G., Skovpen K., Soukharev A., Talyshev A., Tikhonov Y.A., Zaytsev A., et al. Search for dilepton resonances in pp collisions at $\sqrt{s} = 7$ TeV with the ATLAS detector. // *Phys. Rev. Lett.*, 2011. - Vol.107. -P272002, 5p. [arxiv.org 1108.1582].
- [181] Aad G., ATLAS Collab., Beloborodova O., Bobrovnikov V.S., Bogdanchikov A., Kazanin V.A., Kolachev G.M., Korol A., Malyshev V., Maslennikov A.L., Maximov D.A., Orlov I., Peleganchuk S.V., Shamov A.G., Skovpen K., Soukharev A., Talyshev A., Tikhonov Y.A., Zaytsev A., et al. Search for a heavy gauge boson decaying to a charged lepton and a neutrino in 1 fb⁻¹ of pp collisions radical $s = 7$ Tev using the ATLAS detector. // *Phys. Lett. B*, 2011. - V.705, N1/2. - P.28-46. [arxiv.org 1108.1316].
- [182] Aad G., ATLAS Collab., Beloborodova O., Bobrovnikov V.S., Bogdanchikov A., Kazanin V.A., Kolachev G.M., Korol A., Malyshev V., Maslennikov A.L., Maximov D.A., Orlov I., Peleganchuk S.V., Shamov A.G., Skovpen K., Soukharev A., Talyshev A., Tikhonov Y.A., Zaytsev A., et al. Inclusive search for same-sign dilepton signatures in pp collisions at $\sqrt{s} = 7$ TeV with the ATLAS detector. // *JHEP*, 2011. - Vol.1110. - P.107, 21p. [arxiv.org 1108.0366].
- [183] Aad G., ATLAS Collab., Beloborodova O., Bobrovnikov V.S., Bogdanchikov A., Kazanin V.A., Kolachev G.M., Korol A., Malyshev V., Maslennikov A.L., Maximov D.A., Orlov I., Peleganchuk S.V., Shamov A.G., Skovpen K., Soukharev A., Talyshev A., Tikhonov Y.A., Zaytsev A., et al. Measurement of the inclusive isolated prompt photon cross section in collisions at $\sqrt{s} = 7$ TeV with the ATLAS detector using 35 pb⁻¹. // *Phys. Lett. B*, 2011. - Vol.706. - P.150-167. [arxiv.org 1108.0253].
- [184] Aad G., ATLAS Collab., Beloborodova O., Bobrovnikov V.S., Bogdanchikov A., Kazanin V.A., Kolachev G.M., Korol A., Malyshev V., Maslennikov A.L., Maximov D.A., Orlov I., Peleganchuk S.V., Shamov A.G., Skovpen K., Soukharev A., Talyshev A., Tikhonov Y.A., Zaytsev A., et al. Search for neutral MSSM Higgs boson decaying to $\tau^+\tau^-$ pairs in proton-proton collisions at $\sqrt{s} = 7$ TeV with the ATLAS experiment. // *Phys. Lett. B*. 2011. - Vol.705. - P.174-192, 8p. [arxiv.org 1107.5003].
- [185] Aad G., ATLAS Collab., Beloborodova O., Bobrovnikov V.S., Bogdanchikov A., Kazanin V.A., Kolachev G.M., Korol A., Malyshev V., Maslennikov A.L., Maximov D.A., Orlov I., Peleganchuk S.V., Shamov A.G., Skovpen K., Soukharev A., Talyshev A., Tikhonov Y.A., Zaytsev A., et al. Properties of jets measured from tracks in proton-proton collisions at center-of-mass energy radical $s = 7$ TeV with the ATLAS detector. // *Phys. Rev. D*, 2011. - Vol.84. - P.054001-1- 27. [arxiv.org 1107.3311].
- [186] Aad G., ATLAS Collab., Beloborodova O., Bobrovnikov V.S., Bogdanchikov A., Kazanin V.A., Kolachev G.M., Korol A., Malyshev V., Maslennikov A.L., Maximov D.A., Orlov I., Peleganchuk S.V., Shamov A.G., Skovpen K., Soukharev A., Talyshev A., Tikhonov Y.A., Zaytsev A., et al. Measurement of the transverse momentum distribution of Z/gamma* bosons in proton-proton collisions at radical $s = 7$ TeV with the ATLAS detector. // *Phys. Lett. B*, 2011. - V.705, N5. - P.415-434. [arxiv.org 1107.2381].
- [187] Aad G., ATLAS Collab., Beloborodova O., Bobrovnikov V.S., Bogdanchikov A., Kazanin V.A., Kolachev G.M., Korol A., Malyshev V., Maslennikov A.L., Maximov D.A., Orlov I., Peleganchuk S.V., Shamov A.G., Skovpen K., Soukharev A., Talyshev A., Tikhonov Y.A., Zaytsev A., et al. Measurement of multi-jet cross sections in proton-proton collisions at a 7 TeV center-of-mass energy. // *Eur. Phys. J. C*, 2011. - V.71, N11. - P.1763 (27p). [arxiv.org 1107.2092].
- [188] Aad G., ATLAS Collab., Beloborodova O., Bobrovnikov V.S., Bogdanchikov A., Kazanin V.A., Kolachev G.M., Korol A., Malyshev V., Maslennikov A.L., Maximov D.A., Orlov I., Peleganchuk S.V., Shamov A.G., Skovpen K., Soukharev A., Talyshev A., Tikhonov Y.A., Zaytsev A., et al. Measurement of dijet production with a veto on

- additional central jet activity in pp collisions at $\sqrt{s} = 7$ TeV using the ATLAS detector. // JHEP, 2011. - Vol.1109. - P. 053, 17p. [arxiv.org 1107.1641].
- [189] Aad G., ATLAS Collab., Beloborodova O., Bobrovnikov V.S., Bogdanchikov A., Kazanin V.A., Kolachev G.M., Korol A., Malyshev V., Maslennikov A.L., Maximov D.A., Orlov I., Peleganchuk S.V., Shamov A.G., Skovpen K., Soukharev A., Talyshev A., Tikhonov Y.A., Zaytsev A., et al. Search for diphoton events with large missing transverse energy with 36 pb⁻¹ of 7 TeV proton-proton collision data. // Eur. Phys. J. C, 2011. - Vol.71, N10. - P.1744 (21p.).
- [190] Aad G., ATLAS Collab., Beloborodova O., Bobrovnikov V.S., Bogdanchikov A., Kazanin V.A., Kolachev G.M., Korol A., Malyshev V., Maslennikov A.L., Maximov D.A., Orlov I., Peleganchuk S.V., Shamov A.G., Skovpen K., Soukharev A., Talyshev A., Tikhonov Y.A., Zaytsev A., et al. Search for new phenomena with the monojet and missing transverse momentum signature using the ATLAS detector in $\sqrt{s} = 7$ TeV proton-proton collisions. // Phys. Lett. B, 2011. - Vol.705. - P.294-312, 7p. [arxiv.org 1106.5327].
- [191] Aad G., ATLAS Collab., Beloborodova O., Bobrovnikov V.S., Bogdanchikov A., Kazanin V.A., Kolachev G.M., Korol A., Malyshev V., Maslennikov A.L., Maximov D.A., Orlov I., Peleganchuk S.V., Shamov A.G., Skovpen K., Soukharev A., Talyshev A., Tikhonov Y.A., Zaytsev A., et al. Measurement of the Upsilon(1S) production cross-section in pp collisions at $\sqrt{s} = 7$ TeV in ATLAS. // Phys. Lett. B, 2011. - Vol.705. - P.9-27, 24p. [arxiv.org 1106.5325].
- [192] Aad G., ATLAS Collab., Beloborodova O., Bobrovnikov V.S., Bogdanchikov A., Kazanin V.A., Kolachev G.M., Korol A., Malyshev V., Maslennikov A.L., Maximov D.A., Orlov I., Peleganchuk S.V., Shamov A.G., Skovpen K., Soukharev A., Talyshev A., Tikhonov Y.A., Zaytsev A., et al. Search for heavy long-lived charged particles with the ATLAS detector in pp collisions at radical $s = \sqrt{s}$ TeV. // Phys. Lett. B, 2011. - Vol.703, N4. - P.428-446. [arxiv.org 1106.4495].
- [193] Aad G., ATLAS Collab., Beloborodova O., Bobrovnikov V.S., Bogdanchikov A., Malyshev V., Maslennikov A.L., Maximov D.A., Orlov I., Kazanin V.A., Korol A., Peleganchuk S.V., Schamov A.G., Skovpen K., Soukharev A., Talyshev A., Tikhonov Y.A., Zaytsev A., et al. Limits on the production of the standart model Higgs boson in pp collisions at radical $s = 7$ TeV with the ATLAS detector. // Eur. Phys. J. C, 2011. - Vol.71, N9. - P.1728 (30 p.). [arxiv.org 1106.2748].
- [194] Aad G., ATLAS Collab., Beloborodova O., Bobrovnikov V.S., Bogdanchikov A., Malyshev V., Maslennikov A.L., Maximov D.A., Orlov I., Kazanin V.A., Korol A., Peleganchuk S.V., Schamov A.G., Skovpen K., Soukharev A., Talyshev A., Tikhonov Y.A., Zaytsev A., et al. Measurement of $W\gamma$ and $Z\gamma$ production in proton-proton collisions at $\sqrt{s} = 7$ TeV with the ATLAS Detector. // JHEP, 2011. - Vol.1109. - P.072, 25p. [arxiv.org 1106.1592].
- [195] Aad G., ATLAS Collab., Beloborodova O., Bobrovnikov V.S., Bogdanchikov A., Kazanin V.A., Kolachev G.M., Korol A., Malyshev V., Maslennikov A.L., Maximov D.A., Orlov I., Peleganchuk S.V., Skovpen K., Soukharev A., Talyshev A., Tikhonov Y.A., Zaytsev A., et al. Measurement of the $W^+ W^-$ cross section in radical $s = 7$ TeV pp collisions with ATLAS. // Phys. Rev. Lett., 2011. - Vol.107, N4. - P.041802-1-18. [arxiv.org 1104.5225].
- [196] Aad G., ATLAS Collab., Beloborodova O., Bobrovnikov V.S., Bogdanchikov A., Kazanin V.A., Kolachev G.M., Korol A., Malyshev V., Maslennikov A.L., Maximov D.A., Orlov I., Peleganchuk S.V., Shamov A.G., Skovpen K., Soukharev A., Talyshev A., Tikhonov Y.A., Zaytsev A., et al. Search for pair production of first or second generation leptiquarks in proton-proton collisions at radical $s = 7$ TeV using the ATLAS detector at the LHC. // Phys. Rev. D, 2011. - Vol.83, N11. - P.112006-1-24. [arxiv.org 1104.4481].
- [197] Aad G., ATLAS Collab., Beloborodova O., Bobrovnikov V.S., Bogdanchikov A., Kazanin V.A., Kolachev G.M., Korol A., Malyshev V., Maslennikov A.L., Maximov D.A., Orlov I., Peleganchuk S.V., Shamov A.G., Skovpen K., Soukharev A., Talyshev A., Tikhonov Y.A., Zaytsev A., et al. Search for contact interactions in dimuon events from pp collisions at $\sqrt{s} = 7$ TeV with the ATLAS detector. // Phys. Rev. D, 2011. - Vol.84. - P.011101, 18p. [arxiv.org 1104.4398].
- [198] Aad G., ATLAS Collab., Beloborodova O., Bobrovnikov V.S., Bogdanchikov A., Kazanin V.A., Kolachev G.M., Korol A., Malyshev V., Maslennikov A.L., Maximov D.A., Orlov I., Peleganchuk S.V., Shamov A.G., Skovpen K., Soukharev A., Talyshev A., Tikhonov Y.A., Zaytsev A., et al. Measurement of the differential cross-sections of inclusive, prompt and non-prompt J/ψ production in proton-proton collisions at radical $s = 7$ TeV. // Nucl. Phys. B, 2011. - V.850, N1/3. - P.387-444. [arxiv.org 1104.3038].
- [199] Aad G., ATLAS Collab., Beloborodova O., Bobrovnikov V.S., Bogdanchikov A., Kazanin V.A., Kolachev G.M., Korol A., Malyshev V., Maslennikov A.L., Maximov D.A., Orlov I., Peleganchuk S.V., Shamov A.G., Skovpen K., Soukharev A., Talyshev A., Tikhonov Y.A., Zaytsev A., et al. Measurement of the inelastic proton-proton

- cross-section at $\sqrt{s} = 7$ TeV with the ATLAS detector. // *Nature Commun.*, 2011. - Vol.2. - P.463, 6p. [arxiv.org 1104.0326].
- [200] Aad G., ATLAS Collab., Beloborodova O., Bobrovnikov V.S., Bogdanchikov A., Kazanin V.A., Kolachev G.M., Korol A., Malyshev V., Maslennikov A.L., Maximov D.A., Peleganchuk S.V., Schamov A.G., Skovpen K., Soukharev A., Talyshev A., Tikhonov Y.A., Zaytsev A., et al. Search for supersymmetric particles in events with lepton pairs and large missing transverse momentum in radical $s=7$ TeV proton-proton collisions with the ATLAS experiment. // *Eur. Phys. J. C*, 2011. - V.71, N7. - P.1682 (19p). [arxiv.org 1103.6214].
- [201] Aad G., ATLAS Collab., Beloborodova O., Bobrovnikov V.S., Bogdanchikov A., Kazanin V.A., Kolachev G.M., Korol A., Malyshev V., Maslennikov A.L., Maximov D.A., Orlov I., Peleganchuk S.V., Schamov A.G., Skovpen K., Soukharev A., Talyshev A., Tikhonov Y.A., Zaitsev A., et al. Search for an excess of events with an identical flavour lepton pair and significant missing transverse momentum in radical $s=7$ TeV proton-proton collisions with the ATLAS detector. // *Eur. Phys. J. C*, 2011. - V.71, N7. - P.1647 (17p). [arxiv.org 1103.6208].
- [202] Aad G., ATLAS Collab., Beloborodova O., Bobrovnikov V.S., Bogdanchikov A., Kazanin V.A., Kolachev G.M., Korol A., Malyshev V., Maslennikov A.L., Maximov D.A., Orlov I., Peleganchuk S.V., Shamov A.G., Skovpen K., Soukharev A., Talyshev A., Tikhonov Y.A., Zaytsev A., et al. Search for high mass dilepton resonances in pp collisions at radical $s = 7$ TeV with the ATLAS experiment. // *Phys. Lett. B*, 2011. - V.700, N3/4. - P.163-180. [arxiv.org 1103.6218].
- [203] Aad G., ATLAS Collab., Beloborodova O., Bobrovnikov V., Bogdanchikov A., Kazanin V.A., Kolachev G.M., Korol A., Malyshev V., Maslennikov A.L., Maximov D.A., Orlov I., Peleganchuk S.V., Schamov A.G., Skovpen K., Soukharev A., Talyshev A., Tikhonov Y.A., Zaytsev A., et al. Search for a heavy particle decaying into an electron and a muon with the ATLAS detector in radical $s=7$ TeV pp collisions at the LHC. // *Phys. Rev. Lett.*, 2011. - V.106, N25. - P.251801-1-18. [arxiv.org 1103.5559].
- [204] Aad G., ATLAS Collab., Beloborodova O., Bobrovnikov V., Bogdanchikov A., Kazanin V.A., Kolachev G.M., Korol A., Malyshev V., Maslennikov A.L., Maximov D.A., Orlov I., Peleganchuk S.V., Schamov A.G., Skovpen K., Soukharev A., Talyshev A., Tikhonov Y.A., Zaytsev A., et al. Search for supersymmetry in pp collisions at $\sqrt{s} = 7$ TeV in final states with missing transverse momentum and b-jets. // *Phys. Lett. B*, 2011. - Vol.701. - P.398-416, (9p). [arxiv.org 1103.4344].
- [205] Aad G., ATLAS Collab., Beloborodova O., Bobrovnikov V.S., Bogdanchikov A., Kazanin V.A., Kolachev G.M., Korol A., Malyshev V., Maslennikov A.L., Maximov D.A., Orlov I., Peleganchuk S.V., Shamov A.G., Skovpen K., Soukharev A., Talyshev A., Tikhonov Y.A., Zaytsev A., et al. A search for new physics in dijet mass and angular distributions in pp collisions at radical $s = 7$ TeV measured with the ATLAS detector. // *New Journal of Physics*, 2011. - V.13. - P.053044 (44p). [arxiv.org 1103.3864].
- [206] Aad G., ATLAS Collab., Beloborodova O., Bobrovnikov V.S., Bogdanchikov A., Kazanin V.A., Kolachev G.M., Korol A., Malyshev V., Maslennikov A.L., Maximov D.A., Orlov I., Peleganchuk S.V., Shamov A.G., Skovpen K., Soukharev A., Talyshev A., Tikhonov Y.A., Zaytsev A., et al. Measurement of the W charge asymmetry in the $W \rightarrow \mu \nu$ decay mode in pp collisions at radical $s = 7$ TeV with the ATLAS detector. // *Phys. Lett. B*, 2011. - V.701, N1. - P.31-49. [arxiv.org 1103.2929].
- [207] Aad G., ATLAS Collab., Beloborodova O., Bobrovnikov V.S., Bogdanchikov A., Kazanin V.A., Kolachev G.M., Korol A., Malyshev V., Maslennikov A.L., Maximov D.A., Orlov I., Peleganchuk S.V., Shamov A.G., Skovpen K., Soukharev A., Talyshev A., Tikhonov Y.A., Zaytsev A., et al. Search for stable hadronising squarks and gluinos with the ATLAS experiment at the LHC. // *Phys. Lett. B*, 2011. - V.701, N1. - P.1-19. [arxiv.org 1103.1984].
- [208] Aad G., ATLAS Collab., Beloborodova O., Bobrovnikov V.S., Bogdanchikov A., Kazanin V.A., Kolachev G.M., Malyshev V., Maslennikov A.L., Orlov I., Peleganchuk S.V., Shamov A.G., Skovpen K., Soukharev A., Talyshev A., Tikhonov Y.A., Zaytsev A. e.a. Measurements of underlying-event properties using neutral and charged particles in pp collisions at radical $s = 900$ GeV and radical $s = 7$ TeV the ATLAS detector at the LHC. // *Eur. Phys. J. C*, 2011. - V.71, N5. - P.1636 (24p). [arxiv.org 1103.1816].
- [209] Aad G., ATLAS Collab., Beloborodova O., Bobrovnikov V.S., Bogdanchikov A., Kazanin V.A., Kolachev G.M., Korol A., Malyshev V., Maslennikov A.L., Maximov D.A., Orlov I., Peleganchuk S.V., Shamov A.G., Skovpen K., Soukharev A., Talyshev A., Tikhonov Y.A., Zaytsev A., et al. Search for high-mass states with one lepton plus missing transverse momentum in proton-proton collisions at radical $s = 7$ TeV with the ATLAS detector. // *Phys. Lett. B*, 2011. - Vol.701, N1. - P.50-69. [arxiv.org 1103.1391].
- [210] Aad G., ATLAS Collab., Beloborodova O., Bobrovnikov V.S., Bogdanchikov A., Kazanin V.A., Kolachev G.M.,

- Korol A., Malyshev V., Maslennikov A.L., Maximov D.A., Orlov I., Peleganchuk S.V., Shamov A.G., Skovpen K., Soukharev A., Talyshev A., Tikhonov Y.A., Zaytsev A., et al. Search for squarks and gluinos using final with jets and missing transverse momentum with the ATLAS detector radical $s = 7$ TeV proton-proton collisions. // Phys. Lett. B, 2011. - V.701, N2. - P.186-203. [arxiv.org 1102.5290].
- [211] Aad G., ATLAS Collab., Beloborodova O., Bobrovnikov V.S., Bogdanchikov A., Kazanin V.A., Kolachev G.M., Korol A.A., Malyshev V., Maslennikov A.L., Maximov D.A., Orlov I., Peleganchuk S.V., Shamov A.G., Skovpen K., Soukharev A., Talyshev A., Tikhonov Y.A., Zaytsev A., et al. Measurement of dijet azimuthal decorrelations in pp collisions at radical $s=7$ TeV. // Phys. Rev. Lett., 2011. - V.106, N17. - P.172002-1-17. [arxiv.org 1102.2696].
- [212] Aad G., ATLAS Collab., Beloborodova O., Bobrovnikov V.S., Bogdanchikov A., Kazanin V.A., Kolachev G.M., Korol A.A., Malyshev V., Maslennikov A.L., Maximov D.A., Orlov I., Peleganchuk S.V., Shamov A.G., Skovpen K., Soukharev A., Talyshev A., Tikhonov Y.A., Zaytsev A., et al. Search for supersymmetry using final states with one lepton, jets, and missing transverse momentum with the ATLAS detector in radical $s=7$ TeV pp collisions. // Phys. Rev. Lett., 2011. - V.106, N13. - P.131802-1-19. [arxiv.org 1102.2357].
- [213] Aad G., ATLAS Collab., Bobrovnikov V.S., Bogdanchikov A., Kazanin V.A., Kolachev G.M., Korol A., Malyshev V., Maslennikov A.L., Orlov I., Peleganchuk S.V., Shamov A.G., Skovpen K., Soukharev A., Talyshev A., Tikhonov Y.A., Zaytsev A., et al. Search for massive long-lived highly ionising particles with the ATLAS detector at the LHC. // Phys. Lett. B, 2011. - V.698, N5. - P.353-370. [arxiv.org 1102.0459].
- [214] Aad G., ATLAS Collab., Bobrovnikov V.S., Bogdanchikov A., Kazanin V.A., Kolachev G.M., Korol A., Malyshev V., Maslennikov A.L., Orlov I., Peleganchuk S.V., Shamov A.G., Skovpen K., Soukharev A., Talyshev A., Tikhonov Y.A., Zaytsev A., et al. Luminosity determination in pp collisions at radical $s=7$ TeV using the ATLAS detector at the LHC. // Eur. Phys. J. C, 2011. - V.71, N4. - P.1630 (37 p.); [arxiv.org 1101.2185].
- [215] Aad G., ATLAS Collab., Bobrovnikov V.S., Bogdanchikov A., Kazanin V.A., Kolachev G.M., Korol A., Malyshev V., Maslennikov A.L., Orlov I., Peleganchuk S.V., Shamov A.G., Skovpen K., Soukharev A., Talyshev A., Tikhonov Y.A., Zaytsev A., et al. Measurement of the production cross section for W-bosons in association with jets in pp collisions at radical $s = 7$ TeV with the ATLAS detector. // Phys. Lett. B, 2011. - V.698, N5. - P.325-345. [arxiv.org 1012.5382].
- [216] Aad G., ATLAS Collab., Bobrovnikov V.S., Bogdanchikov A., Kazanin V.A., Kolachev G.M., Korol A.A., Malyshev V., Maslennikov A.L., Orlov I., Peleganchuk S.V., Shamov A.G., Skovpen K., Soukharev A., Talyshev A., Tikhonov Y.A., Zaytsev A., et al. Search for diphoton events with large missing transverse energy in 7 TeV proton-proton collisions with the ATLAS detector. // Phys. Rev. Lett., 2011. - V.106, N12. - P.121803--19. [arxiv.org 1012.4272].
- [217] Maslennikov A.L., Skovpen K., Tikhonov Yu., et al. Search for heavy Majorana neutrino and WR in dilepton plus jets events with the ATLAS detector in pp collisions at $\sqrt{s} = 7$ TeV. // ATLAS Conference Note ATLAS-CONF-2011-064. [http://cdsweb.cern.ch/record/1337072].
- [218] Achasov M.N., Beloborodov K.I., Berdyugin A.V., Bogdanchikov A.G., Bukin D.A., Vasiljev A.V., Golubev V.B., Dimova T.V., Druzhinin V.P., Kardapoltsev, L.V. Koop I.A., Korol A.A., Koshuba S.V., Pakhtusova E.V., Serednyakov S.I., Silagadze Z.K., Skrinsky A.N., Kharlamov A.G., Shatunov Yu.M. Search for $e^+ e^- \rightarrow f^0(600) \gamma$, $f_0(980)\gamma$, $f_0(1350) \gamma$, and $f_2(1270) \gamma$ processes in the energy range from 1.05 GeV to 1.38 GeV. // J. Exp. Theor. Phys., 2011. - Vol.113. - P.75-79. [ZhETF, 2011. - Vol.140. - N7. - P.87-91].
- [219] Achasov M.N., Beloborodov K.I., Berdyugin A.V., Bogdanchikov A.G., Bukin D.A., Vasilev A.V., Golubev V.B., Dimova T.V., Druzhinin V.P., Koop I.A., Korol A.A., Koshuba S.V., Pakhtusova E.V., Serednyakov S.I., Silagadze Z.K., Skrinsky A.N., Shatunov Yu.M. Search for the $e^+e^- \rightarrow K^{\pm} K_S^0 \pi^{\pm}$ process on the VEPP-2M $e^+ e^-$ collider. // J. Exp. Theor. Phys., 2011. - Vol.113. - P.433-434. [ZhETF, 2011. - T.140, N3(9). - C.497-498].
- [220] Achasov M.N., Barnyakov A.Yu., Beloborodov K.I., Berdyugin A.V., Berkaev D.E., Bogdanchikov A.G., Botov A.A., Bukin D.A., Vasiljev A.V., Golubev V.B., Dimova T.V., Druzhinin V.P., Zemlyansky I.M., Kardapoltsev L.V., Kovrizhin D.P., Koop I.A., Korol A.A., Koshuba S.V., Martin K.A., Obrazovsky A.E., Pakhtusova E.V., Rogovsky Yu.A., Romanov A.L., Serednyakov S.I., Silagadze Z.K., Skovpen K.Yu., Skrinsky A.N., Surin I.K., Tikhonov Yu.A., Usov Yu.V., Kharlamov A.G., Shatunov P.Yu., Shatunov Yu.M., Shwarts D.B., Shtol D.A. Measurement of the cross section for the $e^+e^- \rightarrow \omega\pi^0 \rightarrow \pi^0\pi^0\gamma$ process in the energy range of 1.1 - 1.9 GeV. // JETP Lett., 2011. - Vol.94, N10. - P.734-737. [ZhETF, 2011. - N10. - C.796-799].
- [221] Kharlamov A.G. Study of the process $e^+e^- \rightarrow \pi^+ \pi^- \pi^0 \pi^0$. // LAP LAMBERT Academic Publishing (2011-09-19) (2011) ISBN: 978-3-8443-5574-1. 116 p.

- [222] V.V. Anashin, V.M. Aulchenko, E.M. Baldin, A.K. Barladyan, A.Yu. Barnyakov, M.Yu. Barnyakov, S.E. Baru, I.Yu. Basok, I.V. Bedny, O.L. Beloborodova, A.E. Blinov, V.E. Blinov, A.V. Bobrov, V.S. Bobrovnikov, A.V. Bogomyagkov, A.E. Bondar, A.R. Buzykaev, S.I. Eidelman, Yu.M. Glukhovchenko, V.V. Gulevich, D.V. Gusev, S.E. Karnaev, G.V. Karpov, S.V. Karpov, T.A. Kharlamova, V.A. Kiselev, S.A. Kononov, K.Yu. Kotov, E.A. Kravchenko, V.F. Kulikov, G.Ya. Kurkin, E.A. Kuper, E.B. Levichev, D.A. Maksimov, V.M. Malyshev, A.L. Maslennikov, A.S. Medvedko, O.I. Meshkov, A.I. Milstein, S.I. Mishnev, I.I. Morozov, N.Yu. Muchnoi, V.V. Neufeld, S.A. Nikitin, I.B. Nikolaev, I.N. Okunev, A.P. Onuchin, S.B. Oreshkin, I.O. Orlov, A.A. Osipov, S.V. Peleganchuk, S.G. Pivovarov, P.A. Piminov, V.V. Petrov, A.O. Poluektov, D.N. Shatilov, G.E. Pospelov, V.G. Prisekin, A.A. Ruban, V.K. Sandyrev, G.A. Savinov, A.G. Shamov, B.A. Schwartz, E.A. Simonov, S.V. Sinyatkin, Yu.I. Skovpen, A.N. Skrinsky, V.V. Smaluk, A.V. Sokolov, A.M. Sukharev, E.V. Starostina, A.A. Talyshev, V.A. Tayursky, V.I. Telnov, Yu.A. Tikhonov, K.Yu. Todyshev, G.M. Tumaikin, Yu.V. Usov, A.I. Vorobiov, A.N. Yushkov, V.N. Zhilich, V.V. Zhulanov, A.N. Zhuravlev. Measurement of $B(J/\psi \rightarrow \eta_c \gamma)$. // Intern. Journal of Modern Physics: Conference Series, 2011, Vol.2. - P.188-192.
- [223] Barnyakov A.Yu., Barnyakov M.Yu., Basok I.Yu., Blinov V.E., Bobrovnikov V.S., Borodenko A.A., Buzykaev A.R., Gulevich V.V., Danilyuk A.F., Kononov S.A., Kravchenko E.A., Kuyanov I.A., Onuchin A.P., Ovtin I.V. Focusing Aerogel RICH for particle identification and momentum measurement. // NIM A, 2011. - Vol.639. - P.290-293.
- [224] Barnyakov A.Yu., Barnyakov M.Yu., Beloborodov K.I., Bobrovnikov V.S., Buzykaev A.R., Golubev V.B., Gulevich B.V., Danilyuk A.F., Kononov S.A., Kravchenko E.A., Martin K.A., Onuchin A.P., Porosev V.V., Serebnyakov S.I. Status of aerogel production in Novosibirsk. // NIM A, 2011. - Vol.639. - P.225-226.
- [225] Adam J., Grigoriev D.N., Ignatov E.V., Popov A.S., Khazin B.I., Yudin Yu.V., et al. (MEG Collab.). Calibration and monitoring of the MEG experiment by a proton beam from a Cockcroft-Walton accelerator. // NIM, 2011.- Vol. A641. - P.19-32.
- [226] Adam J., Grigoriev D.N., Ignatov F., Khazin B.I., Popov A., Yudin Yu.V., et al. (MEG Collab.). New limit on the lepton-flavor-violating decay $\mu^+ \rightarrow e^+ \gamma$. // Phys. Rev. Lett., 2011. - Vol.107, N17. - P.171801-1-5.
- [227] Voronin K.A., Grigoriev D.N., Ukraintsev Yu.G. Effective examination of the passenger on transport. // Airports International, 2011. - release N7 (36). - P.37-39.
- [228] Voronin K.A., Grigoriev D.N., Ukraintsev Yu.G. Contactless examination of the passenger on transport. // Airports. Progressive Technologies, 2011. - N3 (52). - P.12-15.
- [229] Neustroyev V.A., Ukraintsev Yu.G. Modern approaches and diagnostics technique anatomically contracted pelvis. Programs of modeling of bears. // Medical Business, 2011. - release №5 (205). - P.44-45.
- [230] Baru S.E., Talyshev A.A., Telnov V.I., Ukraintsev Yu.G., Usov Yu.V., Shamanaeva L.I., and Shamov A.G. Trigger of the KEDR detector. // Instruments and Experimental Techniques, 2011. - Vol.54, N3. - P.335-349 .
- [231] Babichev E.A., Baru S.E., Grigoriev D.N., Groshev V.R., Leonov V.V., Papishev P.A., Porosev V.V., Savinov G.A., Shayakhmetov V.R., Shekhtman L.I., Tikhonov Yu.A., Ukraintsev Yu.G., Yurchenko Yu.B. High-resolution detectors for medical applications synchrotron radiation research. // NIM A, 2011. - Vol.628, N1. - P.440-443.
- [232] Rachek I.A., Arenhovel H., Barkov L.M., Belostotsky S.L., Dmitriev V.F., Gauzshteyn V.V., Gilman R., Gramolin A.V., Holt R.J., Lazarenko B.A., Loginov A.Yu., Mishnev S.I., Nelyubin V.V., Nikolenko D.M., Osipov A.V., Potterveld D.H., Sadykov R.Sh., Shekhtman L.I., Shestakov Yu.V., Sidorov A.A., Stibunov V.N., Toporkov D.K., De Vries H., Zevakov S.A. Photoreactions with tensor-polarized deuterium target at VEPP-3. // Journal of Physics: Conference Series, 2011. - Vol.295. - P.012106.
- [233] Aulchenko V.M., Beloborodova O.L., Bobrov A.V., Bondar A.E., Kudryavtsev V.N., Shamov A.G., Shekhtman L.I., Zhilich V.N., Zhulanov V.V. Operation of the triple-GEM detectors in the tagging system of the KEDR experiment on the VEPP-4M collider [Electronic resource]. // Journal of Instrumentation, 2011. - Vol.6. - P.07001.
- [234] Titov V.M., Prueel E.R., Ten K.A., Lukjanchikov L.A., Merzhievsky L.A., Tolochko B.P., Zhulanov V.V., Shehtman L.I. Application experience of synchrotron radiations for research of detonation processes. // Physics of Burning and Explosion, 2011, N6. - P.3-16 (in Russian).
- [235] Baru S.E. Modern approach to safety precautions for transport and their conformity to new calls of terrorism. // Airports International, 2011, N2. - P.86-87 (in Russian).
- [236] Baru S.E. Safety on an air transport – new calls and new approaches. // Airports International, 2011, N2. - P.22-25.
- [237] Aaij R., Bobrov A., Bondar A., Eidelman S., Krokovny, Poluektov A., Shekhtman L., et al. (LHCb Collab.). First observation of $B_s \rightarrow D_s^{*+} X_{\mu\nu}$ decays. // Phys. Lett. B, 2001. - Vol.698. - P.14.

List of publications

- [238] R. Aaij, A. Bobrov, A. Bondar, S. Eidelman, P. Krokovny, A. Poluektov, L. Shekhtman, et al. (By LHCb Collab.). First observation of $B_s \rightarrow J/\psi f_0(980)$ decays. // *Phys. Lett. B*, 2011. - Vol.698. - P.115.
- [239] Aaij R., Bobrov A., Bondar A., Eidelman S., Krokovny, Poluektov A., Shekhtman L., et al. (LHCb Collab.). Measurement of J/ψ production in pp collisions at $\sqrt{s}=7$ TeV. // *Eur. Phys. J. C*, 2011. -Vol.71. - P.1645.
- [240] Aaij R., Bobrov A., Bondar A., Eidelman S., Krokovny, Poluektov A., Shekhtman L., et al. (LHCb Collab.). Determination of f_s/f_d for 7 TeV pp collisions and measurement of the $B^0 \rightarrow D^- K^+$ branching fraction. // *Phys. Rev. Lett.*, 2011. - V.107, N21. - P.211801-1-7.
- [241] Aaij R., Bobrov A., Bondar A., Eidelman S., Krokovny, Poluektov A., Shekhtman L., et al. (LHCb Collab.). Measurement of V^0 production ratios in pp collisions at $\sqrt{s} = 0.9$ and 7 TeV. B. // *JHEP*, 2011. - Vol.1108. - P.034.
- [242] Aaij R., Bobrov A., Bondar A., Eidelman S., Krokovny, Poluektov A., Shekhtman L., et al. (LHCb Collab.). Measurement of the inclusive ϕ cross-section in pp collisions at radical $\sqrt{s} = 7$ TeV. // *Phys. Lett. B*, 2011. - V.701, N3. - P.267-273.
- [243] Aaij R., Bondar A., Bobrov A., Eidelman S., et al. (By LHCb Collab.). Measurements of the branching fractions for $B_s \rightarrow D_s^- \pi\pi\pi$ and $\Lambda_b^0 \rightarrow \Lambda_c^+ \pi\pi\pi$. // *Phys. Rev. D*, 2011. - V.84, N9. - P.092001-1-19.
- [244] Aaij R., Bobrov A., Bondar A., Eidelman S., Krokovny, Poluektov A., Shekhtman L., et al. (LHCb Collab.). First observation of the decay $B_s^0 \rightarrow D^0 K^{*0}$ and a measurement of the ratio of branching fractions $\mathcal{B}(B_s^0 \rightarrow D^0 K^{*0})/\mathcal{B}(B^0 \rightarrow D^0 \rho^0)$. // *Phys. Lett. B*, 2011. - Vol.706. - P.32.
- [245] Aaij R., Bobrov A., Bondar A., Eidelman S., Krokovny, Poluektov A., Shekhtman L., et al. (LHCb Collab.). Search for CP violation in $D \rightarrow K^- K^+ \pi^+$ decays. // *Phys. Rev. D*, 2011. - Vol.84, N11. - P.112008-1-13. [arXiv:1110.3970].
- [246] Aaij R., Bobrov A., Bondar A., Eidelman S., Krokovny, Poluektov A., Shekhtman L., et al. (LHCb Collab.). Search for the rare decays $B_s^0 \rightarrow \mu^+ \mu^-$ and $B^0 \rightarrow \mu^+ \mu^-$. // *Phys. Lett. B*, 2011. - Vol.699, N5. - P.330-340. - [arXiv:1112.1600].
- [247] Skorodko T., Shwartz B., et al. (CELSIUS-WASA Collab.). The $pp \rightarrow pp\pi^0\pi^0$ reaction and its limiting case, fusion to quasi-bound He-2, in search of the ABC effect. // *Int. J. Mod. Phys. A*, 2011. - Vol.26, 702 (2011).
- [248] Skorodko T., Shwartz B., et al. (CELSIUS-WASA Collab.). Exclusive measurement of the $pp \rightarrow nn\pi^+\pi^-$ reaction at 1.1 GeV. // *Eur. Phys. J. A*, 2011. - Vol.47. - P.108.
- [249] Shwartz B.A. Measurement of hadronic cross sections at VEPP-2M and VEPP-2000. // *Nucl. Phys. B. Proc. Suppl.*, 2011. - Vol.218. - P.219-224.
- [250] Banerjee S., Shwartz B., et al. Status report from Tau subgroup of the HFAG. // *Nucl. Phys. Proc. Suppl.*, 2011. - Vol.218. - P.329.
- [251] Bondar A., Buzulutskov A., Grebenuk A., Shemyakina E., Sokolov A., Akimov D., Alexandrov I., Breskin A. // On the low-temperature performances of THGEM and THGEM/G-APD multipliers in gaseous and two-phase Xe. [Electronic resource]. // *Journal of Instrumentation*, 2011. - Vol.6. - P.07008.
- [252] Buzulutskov A., Bondar A., Grebenuk A. Infrared scintillation yield in gaseous and liquid argon. // *EPL*. - 2011. - Vol.94. - P.52001.
- [253] Anashin V.V., Aulchenko V.M., Baldin E.M., Barladyan A.K., Barnyakov A.Yu., Barnyakov M.Yu., Baru S.E., Basok I.Yu., Bedny I.B., Beloborodova O.L., Blinov A.E., Blinov V.E., Bobrov A.V., Bobrovnikov V.S., Bogomyagkov A.V., Bondar A.E., Buzykaev A.R., Eidelman S.I., Glukhovchenko Yu.M., Gulevich V.V., Gusev D.V., Karnaev S.E., Karpov G.V., Karpov S.V., Kharlamova T.A., Kiselev V.A., Kononov S.A., Kotov K.Yu., Kravchenko E.A., Kulikov V.F., Kuper E.A., Kurkin G.Ya., Levichev E.B., Maksimov D.A., Malyshev V.M., Maslennikov A.L., Medvedko A.S., Meshkov O.I., Mishnev S.I., Morozov I.I., Muchnoi N.Yu., Neufeld V.V., Nikitin S.A., Nikolaev I.B., Okunev I.N., Onuchin A.P., Oreshkin S.B., Orlov I.O., Osipov A.A., Peleganchuk S.V., Petrov V.V., Piminov P.A., Pivovarov S.G., Poluektov A.O., Pospelov G.E., Prisekin V.G., Ruban A.A., Sandyrev V.K., Savinov G.A., Shamov A.G., Shatilov D.N., Shwartz B.A., Simonov E.A., Sinyatkin S.V., Skovpen Yu.I., Skrinsky A.N., Smaluk V.V., Sokolov A.V., Sukharev A.M., Starostina E.V., Talyshev A.A., Tayursky V.A., Telnov V.I., Tikhonov Yu.A., Todyshev K.Yu., Tumaikin G.M., Usov Yu.V., Vorobiov A.I., Yushkov A.N., Zhilich V.N., Zhulanov V., Zhuravlev A.N. Tau lepton mass determination at KEDR. // *Nucl. Phys. B. Proc. Suppl.*, 2011. - Vol. 218. - P.155-159.
- [254] Todyshev K.Yu., Anashin V.V., Aulchenko V.M., Baldin E.M., Barladyan A.K., Barnyakov A.Yu., Barnyakov M.Yu., Baru S.E., Basok I.Yu., Beloborodova O.L., Blinov A.E., Blinov V.E., Bobrov A.V., Bobrovnikov V.S., Bogomyagkov A.V., Bondar A.E., Buzykaev A.R., Eidelman S.I., Grigoriev D.N., Glukhovchenko Yu.M., Gulevich V.V., Gusev D.V., Karnaev S.E., Karpov G.V., Karpov S.V., Kharlamova T.A., Kiselev V.A., Kolmogorov

- V.V., Kononov S.A., Kotov K.Yu., Kravchenko E.A., Kudryavtsev V.N., Kulikov V.F., Kurkin G.Ya., Kuper E.A., Levichev E.B., Maksimov D.A., Malyshev V.M., Maslennikov A.L., Medvedko A.S., Meshkov O.I., Mishnev S.I., Morozov I.I., Muchnoi N.Yu., Neufeld V.V., Nikitin S.A., Nikolaev I.B., Okunev I.N., Onuchin A.P., Oreshkin S.B., Orlov I.O., Osipov A.A., Peleganchuk S.V., Pivovarov S.G., Piminov P.A., Petrov V.V., Poluektov A.O., Prisekin V.G., Ruban A.A., Sandryev V.K., Savinov G.A., Shamov A.G., Shatilov D.N., Shwartz B.A., Simonov E.A., Sinyatkin S.V., Skrinsky A.N., Smalyuk V.V., Sokolov A.V., Sukharev A.M., Starostina E.V., Talyshev A.A., Tayursky V.A., Telnov V.I., Tikhonov Yu.A., Tumaikin G.M., Usov Yu.V., Vorobiov A.I., Yushkov A.N., Zhilich V.N., Zhulanov V.V., Zhuravlev A.N. Search for narrow resonances in e^+e^- annihilation between 1.85 and 3.1 GeV with the KEDR detector. // *Phys. Lett. B*, 2011. - Vol.703, N5. - P.543-546.
- [255] Eidelman S.I. Tau lepton lifetime determination at Belle. // *Nucl. Phys. B. Proc. Suppl.*, 2011. - Vol.218. - P.172-177.
- [256] Cherepanov V., Eidelman S. Decays $\tau \rightarrow \eta(\eta') \pi \pi^0 \nu_\tau$ and CVC. // *Nucl. Phys. B. Proc. Suppl.*, 2011. - Vol.218. - P.231-236.
- [257] Matvienko D.V., Kuzmin A.S., Eidelman S.I. A model of $B \rightarrow D^+ \omega \pi$ decay. // *JHEP*, 2011. - 1109. - P.129.
- [258] Druzhinin V.P., Eidelman S.I., Serednyakov S.I., Solodov E.P. Hadron production via e^+e^- collisions with initial state radiation. // *Rev. Mod. Phys.*, 2011. - Vol.83. - P.1545.
- [259] Brambilla N., Eidelman S., Levichev E., et al. Heavy quarkonium: progress, puzzles, and opportunities. // *Eur. Phys. J. C*, 2011. - Vol.71, N2. - P.1534 (178p.).
- [260] Aushev T., Aulchenko V., Arinstein K., Bondar A., Eidelman S., Epifanov D., Gabyshev N., Garmash A., Krokovny P., Kuzmin A., Matvienko D., Poluektov A., Shebalin V., Shwartz B., Usov Yu., Vinokurova A., Zhilich V., Zhulanov V., Zyukova O., et al. (Belle Collab.). Study of the decays $B \rightarrow D_{s1}(2536) + D^{(*)}$. // *Phys. Rev. D*, 2011. - Vol.83. - P.051102, Erratum - *Phys. Rev. D*, 2011. - Vol.83. - P.059902.
- [261] Bhardwaj V., Aulchenko V., Arinstein K., Bondar A., Eidelman S., Epifanov D., Gabyshev N., Garmash A., Krokovny P., Kuzmin A., Matvienko D., Poluektov A., Shebalin V., Shwartz B., Usov Yu., Vinokurova A., Zhilich V., Zhulanov V., Zyukova O., et al. (Belle Collab.). Observation of $X(3872) \rightarrow J/\psi \gamma$ and search for $X(3872) \rightarrow \psi' \gamma$ in B decays. // *Phys. Rev. Lett.*, 2011. - Vol.107. - P.091803.
- [262] M. Bischofberger., Aulchenko V., Arinstein K., Bondar A., Eidelman S., Epifanov D., Gabyshev N., Garmash A., Krokovny P., Kuzmin A., Matvienko D., Poluektov A., Shebalin V., Shwartz B., Usov Yu., Vinokurova A., Zhilich V., Zhulanov V., Zyukova O., et al. ((Belle Collab.)). Search for CP violation in $\tau \rightarrow K_S^0 \pi \nu_\tau$ decays at Belle. // *Phys. Rev. Lett.*, 2011. - Vol.107. - P.131801.
- [263] Vinokurova A., Aulchenko V., Arinstein K., Bondar A., Eidelman S., Epifanov D., Gabyshev N., Garmash A., Krokovny P., Kuzmin A., Matvienko D., Poluektov A., Shebalin V., Shwartz B., Usov Yu., Vinokurova A., Zhilich V., Zhulanov V., Zyukova O., et al. (Belle Collab.). Study of $B^\pm \rightarrow K^\pm (K_S^0 K \pi)^0$ decay and determination of η_c and $\eta_c(2S)$ parameters. // *Phys. Lett. B*, 2011. - Vol.706. - P.139.
- [264] Dikansky N.S., Pestrikov D.V. Coherent oscillations of colliding bunches. // A tutorial: RIC NGU, 2011, 9 quires, Novosibirsk (in Russian).
- [265] Pestrikov D.V. Phase averaging of the coherent head-on beam-beam instability. // *NIM in Phys. Res., A*, 2011. - Vol.640. - P.19-28.
- [266] Barzakh A. E., Lhersonneau G., Batist L. Kh., Alyakrinskiy O., et al. Secondary neutrons as the main source of neutron-rich fission products in the bombardment of a thick U target by 1 GeV protons. // *European Physical Journal A*, May 2011. - Vol.47, Issue 5, N70. DOI: 10.1140/epja/i2011-11070-y.
- [267] Bak P.A., Batrakov A.M., Kadyrov R.A., Logachev P.V., Pavlenko A.V., Panov A.N., Sazansky V.Ya., Fatkin G.A. Control system of linear induction accelerator for X-ray system: structure, hardware, the results of the pilot operation. // *Avtometriy(Optoelectronics)*. - 2011. - Vol.47, N3. - P.120-131 (in Russian).
- [268] Parkhomchuk, V.V., Rastigeev S.A. Accelerator mass spectrometer of the center for collective use of the Siberian Branch of the Russian Academy of Sciences, Novosibirsk. // *Surface: Investigation X-Ray, Synchrotron and Neutron Techniques*, Dec. 2011, Vol.5, Issue 6. - P.1068-1072.
- [269] Parkhomchuk, V.V., Rastigeev S.A. Accelerator mass spectrometer of the center for collective use of the Siberian Branch of the Russian Academy of Sciences, Novosibirsk. // [<http://www.springerlink.com/content/g171063r56ql7p11/>].
- [270] Meng Lingjie, Ma Xinwen, Vasily Parkhomchuk, Yang Xiaodong, Mao Lijun, Li Jie, Ma Xiaoming, Yan Tailai, Vladimir Reva, Xia Jiawen, Yuan Youjin, Xu Hushan, Yang Jiancheng Test of detuning system for dielectronic recombination experiment at the CSRm. // 2011 (sended at NIM).

List of publications

- [271] Volkov V. (BINP, Novosibirsk, Russia), Knobloch J. and Matveenko A. (Helmholtz-Zentrum, Berlin, Germany). Beam breakup instability suppression in multicell superconducting RF guns. // *Physical Review. Special Topics: Accelerators and Beams*, 2011. - Vol.14. - P.054202.
- [272] Caldwell A, Lotov K, Pukhov A. and Xia G. Plasma wakefield excitation with a 24 GeV proton beam. // *Plasma Phys. Control. Fusion*, 2011. - Vol.53, N1. - P.014003.
- [273] Lotov K.V. Controlled self-modulation of high energy beams in a plasma. // *Phys. Plasmas*, 2011. - Vol.18, N2. - P.024501-1-4.
- [274] Arakcheev A.S., Lotov K.V. Formation of Small Dust Particles by Brittle Destruction. // *Fusion Science & Technology*, 2011. - Vol.59, N1T. - P.265-267.
- [275] Pukhov A., Kumar N., Tuckmantel T., Upadhyay A., Lotov K., Muggli P., Khudik V., Siemon C., Shvets G. Phase velocity and particle injection in a self-modulated proton-driven plasma wakefield accelerator. // *Phys. Rev. Lett.*, 2011. - Vol.107, N14. - P.145003-1-5.
- [276] Caldwell A., Lotov K.V. Plasma wakefield acceleration with a modulated proton bunch. // *Phys. Plasmas*, 2011. - Vol.18, N10. - P.103101-1-9.
- [277] I.A. Kotelnikov, A.V. Borodin, A.P. Shkurinov. Multiphoton ionization of atoms by a two-color laser pulse. // *JETP*, 2011. - Vol.112. - N6. - P.946-951. [*ZhETF*, 2011. - Vol.139, N6, P.1081-1087].
- [278] Kotelnikov I.A., Equilibrium of high- β plasma with sloshing ions above the mirror instability threshold. // *Fusion Science and Technology*, January 2011. - Vol.59, N1T. - P.47-50.
- [279] Prikhodko V.V., Bagryansky P.A., Beklemishev A.D., Kolesnikov E.Yu., Kotelnikov I.A., Maximov V.V., Pushkareva A.H., Soldatkina E.I., Tsidulko Yu.A., Zaytsev K.V. Low-Frequency oscillations of plasma in the gas dynamic trap. // *Fusion Science and Technology*, 2011. - Vol.59, N1T. - P.9-16,
- [280] Dubin D.H.E., Tsidulko Yu.A. Neoclassical transport and plasma mode damping caused by collisionless scattering across an asymmetric separatrix. // *Physics of Plasmas*, 2011. - V.18, N6. - P.062114-1-17.
- [281] Tsidulko Yu.A., Hilsabeck T.J., O'Neil T.M. Particle fluxes through the separatrix in the trapped particle diocotron mode. // *Physics of Plasmas*, 2011. - V.18, N8. - P.084505-1-4.
- [282] Aleynic V., Burdakov A., Davydenko V., Ivanov A., Kanygin V., Kuznetsov A., Makarov A., Sorokin I., Taskaev S. BINP accelerator based epithermal neutron source. // *Applied Radiation and Isotopes*, 2011. - V.69, N12. - P.1635-1638.
- [283] Aleynic V., Bayanov B., Burdakov A., Makarov A., Sinitsky S., Taskaev S. New technical solution for using the time-of-flight technique to measure neutron spectra. // *Applied Radiation and Isotopes*, 2011. - V.69, N12. - P.1639-1641.
- [284] Kandiev Ya., Kashaeva E., Malyshkin G., Bayanov B., Taskaev S. Optimization of the target of an accelerator-driven neutron source through Monte Carlo numerical simulation of neutron and gamma transport by the PRIZMA code. // *Applied Radiation and Isotopes*, 2011. - N12. - P.1632-1634.
- [285] Taskaev S.Yu. VITA means life. // *Science from first hand*, 2011. - N4(40). - P.88-95 (in Russian).
- [286] Davydenko V., Ivanov A., Kolmogorov A., Zelenski A. Production of high brightness H- beam by charge exchange of hydrogen atom beam in sodium jet. // *AIP Conf. Proc.*, 2011. - Vol.1390. - P.393-400.
- [287] Zelenski A., Atoian G., Davydenko V., Ivanov A., Kolmogorov A., Ritter J., Steski D., Zubets V. The RHIC polarized source upgrade. // *Journal of Physics: Conference Series*, 2011. - Vol.295. - P.012147.
- [288] Chirkov A.Y., Ryzhkov S.V., Bagryansky P.A., Anikeev A.V. Plasma kinetics models for fusion systems based on the axially-symmetric mirror devices. // *Fusion Sci. Technol.*, 2011. - V.59, N1T. - P.39-42.
- [289] Akhmetov T.D., Ivanov A.A., Prikhodko V.V. Possible further steps for upgrading the GDT device. // *Fusion Sci. Technol.*, 2011. - V.59, N1T. - P.43-46.
- [290] Anikeev A.V., Bagryansky P.A., Chernoshtanov I.S., Korzhavina M.S., Prikhodko V.V., Tsidulko Y.A. Study of microinstabilities in anisotropic plasmoid of thermonuclear ions. // *Fusion Sci. Technol.*, 2011. - V.59, N1T. - P.104-107.
- [291] Solomakhin A.L., Bagryansky P.A., Beil W., Dreier H., Ivanenko S.V., Khilchenko A.D., Kovalenko Yu.V., Kvashnin A.N., Lambert H.T., Lizunov A.A., Lvovskiy A.V., Savkin V.Ya. Measurement of plasma density in modern devices by dispersion interferometer. // *Fusion Sci. Technol.*, 2011. - V.59, N1T. - P.120-123.

- [292] Sidorov A.V., Bagryansky P.A., Beklemishev A.D., Izotov I.V., Prikhodko V.V., Razin S.V., Skalyga V.A., Zorin V.G. Non-equilibrium heavy gases plasma MHD-stabilization in axisymmetric mirror magnetic trap. // *Fusion Sci. Technol.*, 2011. - V.59, N1T. - P.112-115.
- [293] Anikeev A.V., Dagan R., Fischer U. Numerical of the fusion-fission hybrid system based on Gas Dynamic Trap for transmutation of radioactive wastes. // *Fusion Sci. Technol.*, 2011. - V.59, N1T. - P.162-165.
- [294] Anikeev A.V., Bagryansky P.A., Fischer U., Noack K., Tsidulko Y.A. The GDT based neutron source as a driven in a sub-critical burner of radioactive wastes. // *Fusion Sci. Technol.*, 2011. - V.59, N1T. - P.220-222.
- [295] Bagryansky P.A., Maximov V.V., Pinzhenin E.I., Prikhodko V.V. DD product yield in the GDT central cell. // *Fusion Sci. Technol.*, 2011. - V.59, N1T. - P.256-258.
- [296] Abdrashitov G.F., Abdrashitov A.G., Deichuli P.P., Donin A.S., Khilchenko A.D., Lizunov A.A., Moiseev D.V., Murakhtin S.V., Sorokin A.V., Zubarev P.V. Neutral beam system of the Gas Dynamic Trap. // *Fusion Sci. Technol.*, 2011. - V.59, N1T. - P.280-282.
- [297] Lvovskiy A.V., Solomakhin A.L. Line plasma density measurement in the Gas Dynamic Trap with dispersion interferometer. // *Fusion Sci. Technol.*, 2011. - V.59, N1T. - P.298-300.
- [298] Smirnov A., Krivenko A.S., Murakhtin S.V., Savkin V.Y., Korepanov S.A., Putvinski S. Neutral beam dump utilizing cathodic arc titanium evaporation. // *Fusion Sci. Technol.*, 2011. - V.59, N1T. - P.271-273.
- [299] Dreiser H., Bagryansky P., Baumgarten N., Biel W., Lambertz H.T., Lehnen M., Lizunov A., Solomakhin A. First results from the modular multi-channel dispersion interferometer at the TEXTOR tokamak. // *Rev. Sci. Instrum.*, 2011. - V.82, N6. - P.063509-1-4.
- [300] Chirkov A.Yu., Ryzhkov S.V., Bagryansky P.A., Anikeev A.V. Thermonuclear regimes of axial symmetric open system with power neutral beams injection. // *Applied Physics*, 2011, N5. - P.57-63.
- [301] Lizunov A.A., Den Hartog D.J., Donin A.S., Ivanov A.A., Prikhodko V.V. Note: multi-point measurement of [B] in the gas-dynamic trap with a spectral motional Stark effect diagnostic. // *Rev. Sci. Instrum.*, 2011. - V.82, N8. - P.086105-1-3.
- [302] Burdakov A.V., Arzhannikov A.V., Astrelin V.T., Beklemishev A.D., Ivanov A.A., Kotelnikov I.A., Kruglyakov E.P., Polosatkin S.V., Postupaev V.V., Sinitsky S.L., Timofeev I.V., Zhukov V.P. Concept of fusion reactor based on multiple-mirror trap. // *Fusion Sci. Technol.*, 2011. - V.59, N1T. - P.9-16.
- [303] Shoshin A.A., Arzhannikov A.V., Burdakov A.V., Chebotarev V.V., Garkusha I.E., Ivanov I.A., Kuklin K.N., Makarov M.A., Makhlai V.A., Marchenko A.K., Mekler K.I., Rovenskikh A.F., Polosatkin S.V., Postupaev V.V., Sinitsky S.L., Tereshin V.I. Plasma-surface interaction during iter type I ELMS: comparison of simulation with QSPA KH-50 and the GOL-3 facilities. // *Fusion Sci. Technol.*, 2011. - V.59, N1T. - P.57-60.
- [304] Kandaurov I., Astrelin V., Avrorov A., Burdakov A., Bykov P., Derevyankin G., Kapitonov V., Kurkuchekov V., Rovenskikh A., Sinitsky S., Truneev Yu., Yarovoy V. Submillisecond electron beam for plasma heating in multi-mirror trap GOL-3. // *Fusion Sci. Technol.*, 2011. - V.59, N1T. - P.67-69.
- [305] Arzhannikov A.V., Burdakov A.V., Kuznetsov S.A., Makarov M.A., Mekler K.I., Postupaev V.V., Rovenskikh A.F., Sinitsky S.L., Sklyarov V.F. Subterahertz emission at strong REB-plasma interaction in multimirror trap GOL-3. // *Fusion Sci. Technol.*, 2011. - V.59, N1T. - P.74-77.
- [306] Postupaev V.V., Arzhannikov A.V., Astrelin V.T., Batkin V.I., Burdakov A.V., Burmasov V.S., Ivanov I.A., Ivantsivsky M.V., Kuklin K.N., Kuznetsov S.A., Makarov M.A., Mekler K.I., Polosatkin S.V., Popov S.S., Rovenskikh A.F., Shoshin A.A., Sinitsky S.L., Sklyarov V.F., Sorokina N.V., Sudnikov A.V., Sulyaev Yu.S., Vyacheslavov L.N. Experiments with «THIN» electron beam at GOL-3. // *Fusion Sci. Technol.*, 2011. - V.59, N1T. - P.144-149.
- [307] Sudnikov A.V., Burdakov A.V., Ivanov I.A., Makarov M.A., Mekler K.I., Polosatkin S.V., Postupaev V.V., Rovenskikh A.F., Sinitsky S.L., Sulyaev Y.S. MHD activity in GOL-3 at the stage of plasma cooling. // *Fusion Sci. Technol.*, 2011. - V.59, N1T. - P.187-189.
- [308] Ivanov I.A., Burdakov A.V., Ivanenko V.G., Makarov M.A., Mekler K.I., Polosatkin S.V., Postupaev V.V., Rovenskikh A.F., Sinitsky S.L., Sudnikov A.V., Shoshin A.A., Shchudlo I.M. Stabilization of relativistic electron beam by dense plasma cloud in GOL-3 expander. // *Fusion Sci. Technol.*, 2011. - V.59, N1T. - P.196-198.
- [309] Polosatkin S., Belykh V., Davydenko V., Fiksel G., Ivanov A., Kapitonov V., Khilchenko A., Khilchenko V.,

List of publications

- Mishagin V., Tiunov M. Advanced neutral particle analyzer for fusion plasma diagnostics. // *Fusion Sci. Technol.*, 2011. - V.59, N1T. - P.259-261.
- [310] Davydenko V.I., Ivaniv A.A., Deichuli P.P., Belov V.P., Gorbovsky A.I., Mishagin V.V., Shikhovtsev I.V., Sorokin A.V., Stupishin A.V., Shulzhenko G.I., Fiksel G., Schweer B. Development of focused neutral beams with small angular divergence for plasma heating and diagnostics. // *Fusion Sci. Technol.*, 2011. - V.59, N1T. - P.128-131.
- [311] Shoshin A.A., Arzhannikov A.V., Burdakov A.V., Kuklin K.N., Ivanov I.A., Mekler K.I., Polosatkin S.V., Postupaev V.V. Structure modification of different graphite and glassy carbon surfaces under high power action by hydrogen plasma. // *Fusion Sci. Technol.*, 2011. - V.59, N1T. - P.268-270.
- [312] Sorokina N., Burdakov A., Makarov M., Mekler K., Polosatkin S., Postupaev V., Rovenskikh A., Sinitsky S., Stepanov V. Study of plasma on the GOL-3 facility by imaging VUV spectroscopy. // *Fusion Sci. Technol.*, 2011. - V.59, N1T. - P.286-288.
- [313] Popov S.S., Vyacheslavov L.N., Ivantsivskiy M., Burdakov A.V., Kasatov A.A., Polosatkin S.V., Postupaev V.V. Upgrading of Thomson scattering system for measurements of spatial dynamics of plasma heating in GOL-3. // *Fusion Sci. Technol.*, 2011. - V.59, N1T. - P.292-294.
- [314] Burmasov V.S., Boblylev V.B., Ivanov A.A., Ivanenko S.V., Kasatov A.A., Kasatov D.A., Kuklin K.N., Popov S.S., Puryga E.A., Rovenskikh A.F., Sklyarov V.F. CO₂ interferometer for GOL-3 multimirror trap. // *Fusion Sci. Technol.*, 2011. - V.59, N1T. - P.301-303.
- [315] Arzhannikov A.V., Makarov M.A., Sinitsky S.L., Stepanov V.D. Energy spectrum of electrons in flow from plasma column heated by REB at GOL-3 facility. // *Fusion Sci. Technol.*, 2011. - V.59, N1T. - P.304-306.
- [316] Postupaev V.V., Arzhannikov A.V., Burdakov A.V., Ivanov I.A., Ivantsivsky M.V., Kuklin K.N., Makarov M.A., Mekler K.I., Polosatkin S.V., Popov S.S., Rovenskikh A.F., Sinitsky S.L., Sudnikov A.V., Sulyaev Yu.S., Vyacheslavov L.N. Experiments with gradual-energy-growth electron beam at GOL-3. // *Fusion Sci. Technol.*, 2011. - V.59, N1T. - P.307-309.
- [317] Astrelin V., Burdakov A., Kandaurov I., Postupaev V., Sinitsky S., Timofeev I. Physical basis for the use of long pulse electron beam in multi-mirror trap. // *Fusion Sci. Technol.*, 2011. - V.59, N1T. - P.310 - 312.
- [318] Astrelin V.T., Burdakov A.V., Vshivkov V.A., Vshivkov K.V., Medvedev S.V., Shvab I.V., Yakunkin N.A. Numerical modeling of plasma dynamics in non-uniform magnetic field. // *Fusion Sci. Technol.*, 2011. - V.59, N1T. - P.313-315.
- [319] Koop I.A., Logatchev P.V., Otboev A.V., Parkhomchuk V.V., Shatilov D.N., Shatunov P.Y., Shatunov Y.M., Shiyankov S.V., Shwartz D.B., Skrinsky A.N., et al. The electron-ion scattering experiment ELISE at the International Facility for Antiproton and Ion Research (FAIR): A conceptual design study. // *NIM A*, 2011. - Vol.637. - P.60-76.
- [320] Golkovsky M.G., Prozorenko P.S., Chakin I.K., Eliseev V.S., Bardakhanov S.P. Production of nanopowders of various materials by evaporation of starting material using a focused electron beam released into environment with atmospheric pressure (in Russian). // *Izvestia VUZov. Physics*, 2011. - Vol 54, N1/2. - P.171-177.
- [321] Tolochko B.P., Antokhin E.I., Yukhin Yu.M., Eliseev V.S., Golkovsky M.G., Lyakhov N.Z. Method for production of ultrafine powder of bismuth. // Patent RU 2426625 C1, Application: 2010117096/02 dated 29.04.2010.
- [322] Golkovsky M.G., Chakin I.K., Prozorenko P.S., Batayev A.A., Batayev V.A., Zhuravina T.V. Method of formation of anticorrosive coating on titanium products. // Positive conclusion given on application № 2010128692/02 (040721), the filing date 09.07.2010.
- [323] Golkovsky M.G., Zhuravina T.V., Bataev I.A., Bataev A.A., Veselov S.V., Bataev V.A., Prikhodko E.A. Cladding of tantalum and niobium on titanium by electron beam injected in atmosphere. // *Advanced Materials Research*, 2011. - Vol.314-316. - P.23-27. [doi:10.4028/www.scientific.net/AMR.314-316.23].
- [324] Babailov S.P., Goryunova A.V., Dudnikov A.V. Magnitoresonansnye termosensornye reagenty na osnove paramagnitnyh tris-diizobutilditiofosfatnyh kompleksov evropiya (iii) s 2,2 - bipiridilom dlya kontrolya temperatury v rastvorah. // *J. Structural Chemistry*. - in press.
- [325] Kalashnikov V.V., Bryazgin A.A., Sidorov A.V. Hardware disinfection development for medical goods. // *Medical Business, Moscow*, 2011. - N5(205). - P.70-71 (in Russian).
- [326] Bezuglov V.V., Bryazgin A.A., Voronin L.A., Gorbunov V.A., Kokin E.N., Korobeynikov M.V., Lukin A.N., Makarov I.G., Maximov S.A., Panfilov A.D., Podobaev V.S., Radchenko V.M., Sidorov A.V., Tarnetskiy, V.V., Tiunov M.A., Tkachenko V.O., Faktorovich B.L., Shtarklev E.A., Chernov K.N. Sterilization complexes based on ILU-type electron accelerators. // *Nuclear Science and Techniques*, Feb. 2011. - Vol.22, N1. - Shanghai, China. ISSN 1001-8042. CN 31 – 1559 / TL.

REPORTS ON THE CONFERENCES

- [327] Knyazev B.A. Advances in real-time terahertz imaging using the Novosibirsk free electron laser: imaging devices and applications. // 19th Intern. Conf. on Advanced Laser Technologies (ALT'11), 3-8 Sept. 2011, Golden Sands, Bulgaria: Book of Abstr., Inst. of Electronics of the Bulg. AS, 2011. - P.101.
- [328] Makarov S.V., Golosov E.V., Golosova O.A., Ionin A.A., Kolobov Yu.R., Kudryashov S.I., Ligachev A.E., Seleznev L.V., Sinitsyn D.V., Korolkov V.P., Samsonov R.V., Masliy A.I., Medvedev A.Zh., Goldenberg B.G. Modification of surface optical properties of solids by femtosecond laser pulses. // 19th Intern. Conf. on Advanced Laser Technologies (ALT'11), Golden Sands, Bulgaria, 3 - 8 Sept. 2011: Book of Abstr.: Inst. of Electronics of the Bulg. AS, 2011.- P.76.
- [329] Popik V.M., Gerlinskaya L.A., Goryachkovskaya T.N., Kolchanov N.A., Moshkin M.P., Peltek S.E. Complex estimates of nanoparticles with living objects by the example of the domestic mice. // 2nd Intern. School "Nanomaterials and Nanotechnology in Living Systems. Safety and nanomedicine," Sept. 19-24. 2011, Moscow Region. - Proc. Reports. Moscow: Moscow State University. 2011. - P.134.
- [330] V.M. Popik, L.A. Gerlinskaya, T.N. Goryachkovskaya, N.A. Kolchanov, M.P. Moshkin, S.E. Peltek. Comprehensive assessment of the contact of nanoparticles and living objects on the example of house mice (in Russian). // 2nd Intern. School "Nanomaterials and Nanotechnology in Living Systems. Safety and nanomedicine," Sept. 19-24. 2011, Moscow Region. - Proc. Reports. Moscow: Moscow State University, 2011. - P. 32.
- [331] Choporova Y.Yu., Cherkassky V.S., Knyazev B.A. In-line and reference-beam holography experiments on Novosibirsk free electron [Electronic resource]. // 36th Intern. Conf. on Infrared Millimeter, and Terahertz Waves (IRMMW-THz 2011), Houston, Texas, USA, Oct. 2 - 7, 2011. - S.1, 2011.
- [332] Knyazev B.A., Cherkassky V.S., Chesnokov E.N., Choporova Y.Yu., Dem'yanenko M.A., Esaev D.G., Gerasimov V.V., Getmanov Ya.V., Goryachkovskaya T.N., Kolobanov E.I., Kubarev V.V., Kulipanov G.N., Medvedev L.E., Naumova E.V., Nikitin A.A., Nikitin A.K., Miginsky S.V., Peltek S.E., Persov B.Z., Pickalov V.V., Popik V.M., Prinz V.Ya., Salikova T.V., Scheglov M.A., Serednyakov S.S., Shevchenko O.A., Skrinisky A.N., Vinokurov N.A., Vlasenko M.G., Zaigraeva N.S. Novosibirsk terahertz free electron laser: facility development and new experimental results at the user stations [Electronic resource]. // 36th Intern. Conf. on Infrared Millimeter, and Terahertz Waves (IRMMW - THz 2011), Houston, Texas, USA, Oct. 2 - 7, 2011. - S.1, 2011.
- [333] Gerasimov V.V., Knyazev B.A., Nikitin A.K., Zhizhin G.N. Terahertz surface plasmon generation and study using a free-electron laser and uncooled detectors [Electronic resource]. // 36th Intern. Conf. on Infrared Millimeter, and Terahertz Waves (IRMMW - THz 2011), Houston, Texas, USA, Oct. 2 - 7, 2011.- S.1, 2011.
- [334] Vlasenko M.G., Pickalov V.V., Rodionov D.G., Knyazev B.A. Tomography using a high-power terahertz free electron laser [Electronic resource]. // 36th Intern. Conf. on Infrared Millimeter, and Terahertz Waves (IRMMW - THz 2011), Houston, Texas, USA, Oct. 2 - 7, 2011. - S.1, 2011.
- [335] Knyazev B.A., Cherkassky V.S., Choporova Y.Yu., Gerasimov V.V., Vlasenko M.G., Dem'yanenko M.A., Esaev D.G., Nikitin A.K., Kulipanov G.N., Vinokurov N.A. High-power monochromatic terahertz radiation: metrological aspects. // Proc. of the 20th IMEKO TS2 Sympos. on Photonics in Measurement (20th ISPM), May 16 - 18, 2011, Linz, Austria. - Aachen: Shaker, 2011.- P.141-145.
- [336] Kuznetsov S.A., Paulish A.G., Gelfand A.V., Lazorskiy P.A., Fedorinin V.N., Arzhannikov A.V. THz imaging system based on THz-to-IR converter. // Proc. of the 20th IMEKO TS2 Sympos. on Photonics in Measurement (20th ISPM), May 16 - 18, 2011, Linz, Austria. - Aachen: Shaker, 2011. - P.135-140.
- [337] Gerasimov V.V., Knyazev B.A., Nikitin A.K., Zhizhin G.N. Experiments on generation of surface plasmons using terahertz radiation of a free-electron laser. // Strong microwaves and terahertz waves: sources and applications: 8th Intern. Workshop, Nizhny Novgorod - St.-Peterburg, Russia, July 9 - 16, 2011: Proc. - Nizhny Novgorod: Inst. of Appl. Physics RAS, 2011.- P.247-248.
- [338] Kulipanov G.N. High power NovoFEL: developments and new results. // Strong microwaves and terahertz waves: sources and applications: 8th Intern. Workshop, Nizhny Novgorod - St.-Peterburg, Russia, July 9 - 16, 2011: Proc. - Nizhny Novgorod: Inst. of Appl. Physics RAS, 2011.- P.26-27.
- [339] Knyazev B.A. Imaging with a high-power monochromatic terahertz source: techniques and applications. // Strong microwaves and terahertz waves: sources and applications: 8th Intern. Workshop, Nizhny Novgorod - St.-Peterburg, Russia, July 9 - 16, 2011: Proc. - Nizhny Novgorod: Inst. of Appl. Physics RAS, 2011.- P.219 -220.
- [340] Choporova Yu.Yu., Cherkassky V.S., Knyazev B.A. In-line and reference-beam holography experiments at Novosibirsk free electron laser. // Strong microwaves and terahertz waves: sources and applications: 8th Intern.

List of publications

- Workshop, Nizhny Novgorod - St.-Peterburg, Russia, July 9 - 16, 2011: Proc. - Nizhny Novgorod: Inst. of Appl. Physics RAS, 2011.- P.240-241.
- [341] Esaulkov M.N., Borodin A.V., Kuricyn I.I., Kotelnikov I.A., Shkurinov A.P. Role of the multiphoton ionization in generation of broadband terahertz radiation from optical breakdown plasma. // Strong microwaves and terahertz waves: sources and applications: 8th Intern. Workshop, Nizhny Novgorod - St.-Peterburg, Russia, July 9 - 16, 2011: Proc. - Nizhny Novgorod: Inst. of Appl. Physics RAS, 2011.- P.242-243.
- [342] Kubarev V.V., Kulipanov G.N., Chesnokov E.N., Shevchenko O.A. Ultra-fast phenomena on powerful terahertz NovoFEL. // Strong microwaves and terahertz waves: sources and applications: 8th Intern. Workshop, Nizhny Novgorod - St.-Peterburg, Russia, July 9 - 16, 2011: Proc. - Nizhny Novgorod: Inst. of Appl. Physics RAS, 2011.- p.258-259.
- [343] Bondar A., Buzulutskov A., Grebenuk A., Sokolov A., Akimov D., Alexandrov I., Breskin A. Geiger mode APD performance in a cryogenic two-phase Ar avalanche detector based on THGEMs. // Proc. of the 12th Intern. Vienna Conf. on Instrumentation (VCI 2010), Vienna, Austria, Febr. 15 - 20, 2010. - Amsterdam: Elsevier, 2011.- P.364-368.
- [344] Babichev E.A., Baru S.E., Grigoriev D.N., Groshev V.R., Leonov V.V., Papishev P.A., Porosev V.V., Savinov G.A., Shayakhmetov V.R., Shekhtman L.I., Tikhonov Yu.A., Ukraintsev Yu.G., Yurchenko Yu.B. High-resolution detectors for medical applications and synchrotron radiation research. // Proc. of the 12th Intern. Vienna Conf. on Instrumentation, Vienna, Austria, Febr. 15 - 20, 2010. - Amsterdam: Elsevier, 2011.- P.440-443.
- [345] Gerasimov V.V., Knyazev B.A., Nikitin A.K. Visualization of the field of surface plasmons generated by terahertz radiation from Novosibirsk free electron laser. // VIII All-Russia Workshop on Radiophysics of Millimeter and Submillimeter Wavelengths, March 1-4, 2011, Nizhny Novgorod: Theses. - Nizhny Novgorod: Alekseev NSTU 2011. - P.28-29.
- [346] Arzhannikov A.V., Burdakov A.V., Kalinin P.V., Kuznetsov S.A., Makarov M.A., Mekler K.I., Polosatkin S.V., Postupaev V.V., Rovenskikh A.F., Sinitsky S.L., Sklyarov V.F., Stepanov V.D., Sulyaev Yu.S., Tumm M.K.A., Vyacheslavov L.N. Generation by Strongly Turbulent Plasma with High Current REB. // VIII All-Russia Workshop on Radiophysics of Millimeter and Submillimeter Wavelengths, March 1-4, 2011, Nizhny Novgorod: Theses. - Nizhny Novgorod: Alekseev NSTU 2011. - P.17-18.
- [347] Kuznetsov S.A., Arzhannikov A.V., Paulish A.G., Gelfand A.V., Kubarev V.V., Sorolla M. Microstructural quasi-optical selective elements for the submillimeter range. // VIII All-Russia Workshop on Radiophysics of Millimeter and Submillimeter Wavelengths, March 1-4, 2011, Nizhny Novgorod: Theses. - Nizhny Novgorod: Alekseev NSTU 2011. - P.16-17.
- [348] Kubarev V.V., Klimov A.E., Paschin V.S., Chaplik A.V., Prints V.Ya., Naumova A.V., Okotrub A.V., Chesnokov E.N. Terahertz radiation in the studies of solids, semiconductors, metamaterials, and ultrafast spectroscopy of gases. // VIII All-Russia Workshop on Radiophysics of Millimeter and Submillimeter Wavelengths, March 1-4, 2011, Nizhny Novgorod: Theses. - Nizhny Novgorod: Alekseev NSTU 2011. - P.15.
- [349] B.A. Knyazev, N.A. Vinokurov, V.M. Vedernikov, M.G. Vlasenko, P.D. Voblyi, A.A. Galt, V.V. Gerasimov, Ya.V. Getmanov, E.N. Dementyev, I.A. Dovzhenko, M.A. Demyanenko, D.G. Esaev, N.S. Zaigraeva, E.I. Kolobanov, V.V. Kubarev, G.N. Kulipanov, L.E. Medvedev, S.V. Miginsky, L.A. Mironenko, A.K. Nikitin, V.K. Ovchar, I.G. Palchikova, B.Z. Persov, V.V. Pickalov, V. M. Popik, T.V. Salikova, S.S. Serednyakov, A.N. Skrinsky, M.F. Stupak, V.G. Cheskidov, V.S. Cherkassky, Yu.Yu. Choporova, O.A. Shevchenko, M.A. Shcheglov. Novosibirsk free electron laser: commissioning of the secondstage and experiments in quasioptics // VIII All-Russia Workshop on Radiophysics of Millimeter and Submillimeter Wavelengths, March 1-4, 2011, Nizhny Novgorod: Theses. - Nizhny Novgorod: Alekseev NSTU 2011. - P.11-12.
- [350] K.V. Zolotarev, G.N. Kulipanov, N.A. Mezentsev, S.V. Sinyatkin, A.V. Filipchenko. Analysis of the possibilities of generation of undulator radiation for EUV lithography on Zelenograd SR source [Electronic resource]. // VIII National Conference «X-ray, Synchrotron Radiation, Neutrons and Electrons for the Study of Nanosystems and Materials. Nano-Bio-Info-Cognitive Technology»: RSNE - NBIC 2011: cont. All-Russia Workshop on the Application of X-rays for Materials Research, Moscow, November 14-18, 2011: Proc. Reports. - Moscow: IC RAS - SIC KI, 2011. - P.499.
- [351] A.V. Daryin, I.A. Kalugin, Ya.V. Rakshun. Analytical microstratigraphy using synchrotron radiation [Electronic resource] // VIII National Conference «X-ray, Synchrotron Radiation, Neutrons and Electrons for the Study of Nanosystems and Materials. Nano-Bio-Info-Cognitive Technology»: RSNE - NBIC 2011: cont. All-Russia Workshop on the Application of X-rays for Materials Research, Moscow, November 14-18, 2011: Proc. Reports.

- Moscow: IC RAS - SIC KI, 2011. - P.536.
- [352] Ya.V. Rakshun, V.A. Chernov, N.A. Mezentsev, G.N. Kulipanov, M.A. Kholopov, D.S. Sorokoletov. Hardware-methodical complex for studies by the method of X-ray absorption spectroscopy in the soft X-rays [Electronic resource]. // VIII National Conference «X-ray, Synchrotron Radiation, Neutrons and Electrons for the Study of Nanosystems and Materials. Nano-Bio-Info-Cognitive Technology»: RSNE - NBIC 2011: cont. All-Russia Workshop on the Application of X-rays for materials research, Moscow, November 14-18, 2011: Proc. Reports. - Moscow: IC RAS - SIC KI, 2011. - P.551.
- [353] V.A. Chernov, A.V. Kosov, Ya.V. Rakshun, N.A. Mezentsev. X-ray beam position sensor on the basis of grazing incidence mirrors [Electronic resource]. // VIII National Conference «X-ray, Synchrotron Radiation, Neutrons and Electrons for the Study of Nanosystems and Materials. Nano-Bio-Info-Cognitive Technology»: RSNE - NBIC 2011: cont. All-Russia Workshop on the Application of X-rays for Materials Research, Moscow, November 14-18, 2011: Proc. Reports. - Moscow: IC RAS - SIC KI, 2011. - P.558.
- [354] V.I. Kondratiev, B.P. Tolochko, I.L. Zhogin, A.V. Kosov, B.Ya. Pirogov. Soft X-ray introscope on matrix-readout storage screens with [Electronic resource]. // VIII National Conference «X-ray, Synchrotron Radiation, Neutrons and Electrons for the Study of Nanosystems and Materials. Nano-Bio-Info-Cognitive Technology»: RSNE - NBIC 2011: cont. All-Russia Workshop on the Application of X-rays for Materials Research, Moscow, November 14-18, 2011: Proc. Reports. - Moscow: IC RAS - SIC KI, 2011. - P.501.
- [355] L.I. Shekhtman, V.M. Aulchenko, V.V. Zhulanov, P.A. Papishev, V.M. Titov, B.P. Tolochko, M.R. Sharafutdinov. Coordinate detector OD-4 with large angular aperture for high-resolution diffraction studies [Electronic resource]. // VIII National Conference «X-ray, Synchrotron Radiation, Neutrons and Electrons for the Study of Nanosystems and Materials. Nano-Bio-Info-Cognitive Technology»: RSNE - NBIC 2011: cont. All-Russia Workshop on the Application of X-rays for Materials Research, Moscow, November 14-18, 2011: Proc. Reports. - Moscow: IC RAS - SIC KI, 2011. - P.520.
- [356] V.N. Korneev, V.A. Shlektarev, A.V. Zabelin, V.M. Aulchenko, B.P. Tolochko, N.I. Ariskin, N.F. Lanina, A.A. Vasina. Small-angle X-ray stations on the basis of cylindrical zoomers for nanostructure studies using synchrotron radiation [Electronic resource]. // VIII National Conference «X-ray, Synchrotron Radiation, Neutrons and Electrons for the Study of Nanosystems and Materials. Nano-Bio-Info-Cognitive Technology»: RSNE - NBIC 2011: cont. All-Russia Workshop on the Application of X-rays for Materials Research, Moscow, November 14-18, 2011: Proc. Reports. - Moscow: IC RAS - SIC KI, 2011. - P.502.
- [357] D.S. Sorokoletov, Ya.V. Rakshun, A.V. Daryin, V.V. Maximovovskaya, M.A. Kholopov. Upgrade of the SR-XRF station for development of the method of scanning microanalysis [Electronic resource]. // VIII National Conference «X-ray, Synchrotron Radiation, Neutrons and Electrons for the Study of Nanosystems and Materials. Nano-Bio-Info-Cognitive Technology»: RSNE - NBIC 2011: cont. All-Russia Workshop on the Application of X-rays for Materials Research, Moscow, November 14-18, 2011: Proc. Reports. - Moscow: IC RAS - SIC KI, 2011. - P.556.
- [358] N.F. Lanina, A.A. Vasina, A.A. Vasilieva, V.N. Korneev, A.V. Zabelin, V.V. Stepanova, T.A. Kupriyanova, A.A. Legkodymov, S.Ch. Kundu. Molecular and nanostructural studies of various natural and biotechnological silk structures [Electronic resource]. // VIII National Conference «X-ray, Synchrotron Radiation, Neutrons and Electrons for the Study of Nanosystems and Materials. Nano-Bio-Info-Cognitive Technology»: RSNE - NBIC 2011: cont. All-Russia Workshop on the Application of X-rays for Materials Research, Moscow, November 14-18, 2011: Proc. Reports. - Moscow: IC RAS - SIC KI, 2011. - P.64.
- [359] E.I. Majewski, V.M. Aulchenko, A.A. Vasina, A.V. Zabelin, V.N. Korneev, G.N. Kulipanov, T.A. Kupriyanova, N.F. Lanina, V.P. Letyagin, V.V. Stepanova, V.G. Stankevich, B.P. Tolochko, M.R. Sharafutdinov. Nanostructural measurements of epithelial tissue in cancer pathology [Electronic resource]. // VIII National Conference «X-ray, Synchrotron Radiation, Neutrons and Electrons for the Study of Nanosystems and Materials. Nano-Bio-Info-Cognitive Technology»: RSNE - NBIC 2011: cont. All-Russia Workshop on the Application of X-rays for Materials Research, Moscow, November 14-18, 2011: Proc. Reports. - Moscow: IC RAS - SIC KI, 2011. - P.65.
- [360] A.A. Vasina, N.F. Lanina, M.A. Sheromov, V.D. Vasiliev, M.I. Samoilovich. The role of the external field of forces in the structural dynamics of multidomain proteins of the immunoglobulin superfamily on the example of fibrillar muscle protein titin [Electronic resource]. // VIII National Conference «X-ray, Synchrotron Radiation, Neutrons and Electrons for the Study of Nanosystems and Materials. Nano-Bio-Info-Cognitive Technology»: RSNE - NBIC 2011: cont. All-Russia Workshop on the Application of X-rays for Materials Research, Moscow, November 14-18, 2011: Proc. Reports. - Moscow: IC RAS - SIC KI, 2011. - P.10.

List of publications

- [361] A.N. Nikolenko, A.V. Gorlovoi, D.V. Ivlyushkin, A.A. Legkodymov, V.V. Lyakh, M.R. Mashkovtsev, V.F. Pindyurin, N.S. Shadrin. Synchrotron radiation station “Cosmos”: hardware - methodical complex for metrology works in the soft X-ray and VUV ranges [Electronic resource]. // VIII National Conference «X-ray, Synchrotron Radiation, Neutrons and Electrons for the Study of Nanosystems and Materials. Nano-Bio-Info-Cognitive Technology»: RSNE - NBIC 2011: cont. All-Russia Workshop on the Application of X-rays for Materials Research, Moscow, November 14-18, 2011: Proc. Reports. - Moscow: IC RAS - SIC KI, 2011. - P.507.
- [362] E.I. Zhmurikov, I.V. Savchenko, S.V. Stankus, L. Teccio. Thermalphysic properties of graphite composites for nuclear engineering [Electronic resource]. // VIII National Conference «X-ray, Synchrotron Radiation, Neutrons and Electrons for the Study of Nanosystems and Materials. Nano-Bio-Info-Cognitive Technology»: RSNE - NBIC 2011: cont. All-Russia Workshop on the Application of X-rays for Materials Research, Moscow, November 14-18, 2011: Proc. Reports. - Moscow: IC RAS - SIC KI, 2011. - P.245.
- [363] A.N. Gentshev, B.G. Goldenberg, A.D. Nikolenko, V.F. Pindyurin, I.V. Poletaev. Instalaltion for soft X-ray lithography on VEPP-4 [Electronic resource]. // VIII National Conference «X-ray, Synchrotron Radiation, Neutrons and Electrons for the Study of Nanosystems and Materials. Nano-Bio-Info-Cognitive Technology»: RSNE - NBIC 2011: cont. All-Russia Workshop on the Application of X-rays for Materials Research, Moscow, November 14-18, 2011: Proc. Reports. - Moscow: IC RAS - SIC KI, 2011. - P.532.
- [364] V.V. Maximovskaya, K.V. Zolotarev, V.A. Chernov, N.A. Mezentsev, Ya.V. Rakshun. Instalaltion for X-ray fluorescence analysis at total external reflection at the XRF-SR station on VEPP-3 [Electronic resource]. // VIII National Conference «X-ray, Synchrotron Radiation, Neutrons and Electrons for the Study of Nanosystems and Materials. Nano-Bio-Info-Cognitive Technology»: RSNE - NBIC 2011: cont. All-Russia Workshop on the Application of X-rays for Materials Research, Moscow, November 14-18, 2011: Proc. Reports. - Moscow: IC RAS - SIC KI, 2011. - P.547.
- [365] B.P. Tolochko, I.L. Zhogin, N.A. Mezentsev, E.B. Levichev, G.N. Kulipanov, V.M. Aulchenko, K.A. Ten. “Detonation” experimental Station on synchrotron radiation of a 100-pole superconducting wiggler of VEPP-4. // VIII National Conference «X-ray, Synchrotron Radiation, Neutrons and Electrons for the Study of Nanosystems and Materials. Nano-Bio-Info-Cognitive Technology»: RSNE - NBIC 2011: cont. All-Russia Workshop on the Application of X-rays for Materials Research, Moscow, November 14-18, 2011: Proc. Reports. - Moscow: IC RAS - SIC KI, 2011. - P.532
- [366] A.V. Daryin, I.A. Kalugin, K.V. Zolotarev, Ya.V. Rakshun. Analytical microstratigraphy using scanning microanalysis on synchrotron radiation beams. // VII All-Russia. Conference on X-Ray Analysis, 19-23 September, 2011, Novosibirsk. - Abstracts, Novosibirsk: Publishing House of SB RAS, 2011. - P.165.165.
- [367] T.A. Kupriyanova, M.N. Filippov, A.A. Vasina, A.A. Vasilieva, N.F. Lanina, A.A. Viryus, A.A. Legkodymov, S.Ch. Kundu. X-ray analysis of silk with the use of synchrotron radiation. // VII All-Russia. Conference on X-Ray Analysis, 19-23 September, 2011, Novosibirsk. - Abstracts, Novosibirsk: Publishing House of SB RAS, 2011. - P.168.
- [368] A.V. Daryin, I.A. Kalugin, K.V. Zolotarev, Ya.V. Rakshun. Analytical microstratigraphy using scanning microanalysis on synchrotron radiation beams [Electronic resource]. // VII All-Russia. Conference on X-Ray Analysis, 19-23 September, 2011, Novosibirsk. - Abstracts, Novosibirsk: Publishing House of SB RAS, 2011. - P.165.
- [369] Chernoshtanov I.S., Tsidulko Yu.A. Alfvén ion-cyclotron instability in a mirror trap with highly anisotropic hot ion component [Electronic resource]. // XXXVIII Intern. (Zvenigorod) Conference on Plasma Physics and Controlled Fusion, Zvenigorod (Moscow reg.), February 14-18, 2011. - . - M.: PLASMAIOFAN, 2011. - C.MC 2 - 03.
- [370] Lotov K.V., Maslov V.I., Onischenko I.N. Long train of relativistic electron bunches as a driver in plasma wakefield accelerator. [Electronic resource]. // XXXVIII Intern. (Zvenigorod) Conference on Plasma Physics and Controlled Fusion, Zvenigorod, 2011, 14-18 Febr. 2011. - M.: PLASMAIOFAN, 2011. - C.MC 2 - 05.
- [371] Ivantsivsky M.V., Burdakov A.V., Vyacheslavov L.N., Ivanov I.A., Kasatov A.A., Makarov M.A., Mekler K.I., Polosatkin S.V., Popov S.S., Postupaev V.V., Rovenskikh A.F., Sinitsky S.L. Measurement of non-Maxwellian electron distribution function dynamics in different space points on GOL-3 facility [Electronic resource]. // XXXVIII Intern. (Zvenigorod) Conference on Plasma Physics and Controlled Fusion, 14-18 Febr., 2011, Zvenigorod. - M.: PLASMAIOFAN, 2011.-C.MC 1 - 07.

- [372] Kasatov A.A., Popov S.S. Pulsed light source with a smooth spectrum from a xenon lamp for the calibration of Thomson scattering system [Electronic resource]. // XXXVIII Intern. (Zvenigorod) Conference on Plasma Physics and Controlled Fusion, Zvenigorod (Moscow reg.), February 14-18, 2011. - M.: PLASMAIOFAN, 2011.- C.PC 1 - 16.
- [373] Skovorodin D.I., Beklemishev A.D. Ambipolar potential influence on longitudinal losses from mirror trap in semicollision mode research [Electronic resource]. // XXXVIII Intern. (Zvenigorod) Conference on Plasma Physics and Controlled Fusion, Zvenigorod (Moscow reg.), February 14-18, 2011. - M.: PLASMAIOFAN, 2011.- C.MC 1 - 06.
- [374] Skovorodin D.I., Beklemishev A.D. Ambipolar potential influence on longitudinal losses from mirror trap in semicollision mode research. // Theses of XXXVIII Intern. (Zvenigorod) Conference On Plasma Physics And Controlled Fusion, Zvenigorod (Moscow reg.), February 14-18, 2011. - M.: PLASMAIOFAN, 2011.- P.52.
- [375] Sklyarov V.F., Burdakov A.V., Kuznetsov S.A., Mekler K.I., Polosatkin S.V., Postupaev V.V., Rovenskikh A.F. Sinitsky S.L. Investigation of emission of submillimeter electromagnetic radiation at turbulent plasma heating on the GOL-3 device. [Electronic resource]. // XXXVIII Intern. (Zvenigorod) Conference on Plasma Physics and Controlled Fusion, 14-18 February, 2011, Zvenigorod. - M.: PLASMAIOFAN, 2011. - C.MC 1 - 03.
- [376] Kurkuchekov V.V., Kandaurov I.V., Trunev Yu.A., Multi-aperture electron beam source with arc plasma emitter in external magnetic field [Electronic resource]. // XXXVIII Intern. (Zvenigorod) Conference on Plasma Physics and Controlled Fusion, Zvenigorod, 14-18 Febr., 2011. - M.: PLASMAIOFAN, 2011. - C.TC 1 - 05.
- [377] Dimov G.I., Emelev I.S., Vobly P.D., Kobets V.V., Tiunov M.A. Multipole trap of ring geometry for low temperature plasma confinement [Electron resource]. // XXXVIII Intern. (Zvenigorod) Conference on Plasma Physics and Controlled Fusion, Zvenigorod, 14-18 Febr., 2011. - M.: PLASMAIOFAN, 2011.- S.Pb. 1 - 06.
- [378] Avrorov A.P., Astrelin V.T., Burdakov A.V., Bykov P.V., Derevyankin G.E., Kandaurov I.V., Kapitonov V.A., Kurkuchekov V.V., Rovenskikh A.F., Sinitsky S.L., Trunev Yu.A., Yarovoi V.A. Prototype of the source of submillisecond electron beam for the GOL-3 facility [Electronic resource]. // XXXVIII Intern. (Zvenigorod) Conference on Plasma Physics and Controlled Fusion, Zvenigorod, 14-18 Febr., 2011. - M.: PLASMAIOFAN, 2011. - S.Pb. 1 - 09.
- [379] Chernoshtanov I.S., Tsidulko Yu.A. Spirally symmetric solutions of Vlasov-Maxwell equations [Electronic resource]. // XXXVIII Intern. (Zvenigorod) Conference on Plasma Physics and Controlled Fusion, Zvenigorod (Moscow reg.), February 14-18, 2011. M.: PLASMAIOFAN, 2011.- C.MC 2 - 04.
- [380] Chernoshtanov I.S., Tsidulko Yu.A. Alfvén ion-cyclotron instability in a mirror trap with highly anisotropic hot ion component. // Theses of XXXVIII Intern. (Zvenigorod) Conference on Plasma Physics and Controlled Fusion, Zvenigorod, 14-18 Febr., 2011. - M.: PLASMAIOFAN, 2011. - P.84.
- [381] Lotov K.V., Maslov V.I., Onischenko I.N. Long train of relativistic electron bunches as a driver in plasma wakefield accelerator. // Theses of XXXVIII Intern. (Zvenigorod) Conference on Plasma Physics and Controlled Fusion, Zvenigorod, 2011, 14-18 Febr., 2011. - M.: PLASMAIOFAN, 2011. - P.315.
- [382] Dimov G.I., Emelev I.S., Vobly P.D., Kobets V.V., Tiunov M.A. Multipole trap with ring geometry for low-temperature plasma confinement. // Theses of XXXVIII Intern. (Zvenigorod) Conference on Plasma Physics and Controlled Fusion, Zvenigorod, 2011, 14-18 Febr., 2011. - M.: PLASMAIOFAN, 2011. - P.204.
- [383] Beklemishev A.D. Project of new-generation open trap in INP: "Trap with turbulent plugs". // Theses of XXXVIII Intern. (Zvenigorod) Conference on Plasma Physics and Controlled Fusion, Zvenigorod, 2011, 14-18 Febr., 2011. - M.: PLASMAIOFAN, 2011. - P.19.
- [384] Chernoshtanov I.S., Tsidulko Yu.A. Spirally symmetric solutions of Vlasov-Maxwell equations. // Theses of XXXVIII Intern. (Zvenigorod) Conference on Plasma Physics and Controlled Fusion, Zvenigorod, 2011, 14-18 Febr., 2011. - M.: PLASMAIOFAN, 2011. - P.85.
- [385] Klimov A.E., Kubarev V.V., Paschin N.S., Shumsky V.N. Injection current in PbSnTe:In under ThZ radiation. // X Russian Conference on Semiconductor Physics, 19-23 September, 2011, Nizhny Novgorod. - Proceedings: Nizhny Novgorod: Lobachevsky NSU, 2011. - P.169.
- [386] Chistokhin I.B., Pchelyakov O.P., Tishkovsky E.G., Maksimov V.V., Ivanov A.A., Pinzhenin E.I. Silicon avalanche diodes for direct detection of nuclear particles. // X Russian Conference on Semiconductor Physics "Semiconductors-2011", 19-23 Sept., 2011, Nizhny Novgorod. - Theses: Nizhny Novgorod, Lobachevsky NSU, 2011. - P.242.

List of publications

- [387] Gauzshteyn V.V., Dusaev R.R., Zevakov S.A., Loginov A.Yu., Nikolenko D.M., Rachek I.A., Sidorov A.A., Stibunov V.N., Toporkov D.K., Shestakov Yu.V. Measurement of the differential cross section of the reaction $\gamma d \rightarrow pp\pi^-$ with high-momentum of protons. // 8th Intern. Conference “Nuclear and Radiation Physics”, 20-23 September, 2011, Almaty, Kazakhstan: Theses. - Almaty, 2011. - P.142.
- [388] Gauzshtein V.V., Gramolin A.V., Zevakov S.A., Loginov A.Yu., Nikolenko D.M., Rachek I.A., Sidorov A.A., Stibunov V.N., Toporkov D.K., Shestakov Yu.V. Measurement of the tensor analyzing power components in the photoproduction reaction of negative pi-mesons on the polarized deuterons. // 8th Intern. Conference “Nuclear and Radiation Physics”, 20-23 September, 2011, Almaty, Kazakhstan: Theses. - Almaty, 2011. - P.143.
- [389] Gauzshtein V.V., Gramolin A.V., Zevakov S.A., Loginov A.Yu., Nikolenko D.M., Rachek I.A., Sidorov A.A., Stibunov V.N., Toporkov D.K., Shestakov Yu.V. Incoherent photoproduction of neutral pi-mesons from tensor polarized deuterons. // 8th Intern. Conference “Nuclear and Radiation Physics”, 20-23 September, 2011, Almaty, Kazakhstan: Theses. - Almaty, 2011. - P.74.
- [390] Antokhin E.I., Eliseev V.S., Klimenko A.S., Tolochko B.P., Okotrub A.V. Synthesis of nanocarbon structures on an industrial electron accelerator and their application. // 8th Intern. Conference “Nuclear and Radiation Physics”, 20-23 September, 2011, Almaty, Kazakhstan: Theses. - Almaty, 2011. - P.340.
- [391] Smaluk V., Bekhtenev E., Cherepanov V., Karpov G., Kuzminykh V., Meshkov O., Singh O., Pinayev I., Vetter K. Beam diagnostics for the NSLS-II booster [Electronic resource]. // 10th European Workshop on Beam Diagnostics and Instrumentation for Particle Accelerators (DIPAC 2011), Hamburg, Germany, May 16 - 18, 2011: Proc. - S.I, 2011. - P.29-31. MOPD01.
- [392] Oreshonok V.V., Cherepanov V.P., Smaluk V.V., Sukhanov D.P. Broadband digital feedback system for the VEPP-4M electron-positron collider [Electronic resource]. // 10th European Workshop on Beam Diagnostics and Instrumentation for Particle Accelerators (DIPAC 2011), Hamburg, Germany, May 16 - 18, 2011: Proc. - S.I, 2011. - P.224-226. [JACoW, MOPD82].
- [393] Meshkov O.I., Smaluk V.V., Sukhanov D.P., Galashov E.N., Dorokhov V., Zhuravlev A.N., Kiselev V.A. Experimental comparison of performance of various fluorescent screens applied for relativistic electron/positron beam imaging [Electronic resource]. // 10th European Workshop on Beam Diagnostics and Instrumentation for Particle Accelerators (DIPAC 2011), Hamburg, Germany, May 16 - 18, 2011: Proc. - S.I, 2011.- P.558-560.
- [394] Anashin V.V., Krasnov A.A., Ovchar V.K., Smaluk V.V., Sukhanov D.P. Installation for measurements of secondary emission yield and electron cloud lifetime in magnetic field [Electronic resource]. // 10th European Workshop on Beam Diagnostics and Instrumentation for Particle Accelerators (DIPAC 2011), Hamburg, Germany, May 16 - 18, 2011: Proc. - S.I, 2011. - P.236-238.
- [395] Velikanov Yu.M., Veremeenko V.F., Vinokurov N.A., Galt A.A., Dovzhenko B.A., Kozak V.R., Kuper E.A., Medvedev L.E., Medvedko A.S., Serednyakov S.S. Control system for magnet power supplies for Novosibirsk free electron laser [Electronic resource]. // 13th Intern. Conf. on Accelerator and Large Experimental Physics Control Systems 10 - 14 Oct. 2011, WTC Grenoble, France: Contributions to the Proc. - S.I, 2011.- P.480-482.
- [396] Panov A., Bak P., Bolkhovityanov D. LIA-2 power supply control system [Electronic resource]. // 13th Intern. Conf. on Accelerator and Large Experimental Physics Control Systems (ICALEPCS 2011), 10-14 Oct. 2011, WTC Grenoble, France: Contributions to the Proc. - S.I, 2011. - P.926-928.
- [397] Cheblakov P., Karnaev S., Serednyakov S., Louie W., Tian Y. NSLS-II booster power supplies control [Electronic resource]. // 13th Intern. Conf. on Accelerator and Large Experimental Physics Control Systems (ICALEPCS 2011), 10-14 Oct. 2011, WTC Grenoble, France: Contributions to the Proc. - S.I, S.a. - P.1018- 1020.
- [398] Cheblakov P., Karnaev S., Long J.D. NSLS-II booster timing system [Electronic resource] // 13th Intern. Conf. on Accelerator and Large Experimental Physics Control Systems (ICALEPCS 2011), 10-14 Oct. 2011, WTC Grenoble, France: Contributions to the Proc. - S.I, 2011. - P.1003-1005.
- [399] Bolkhovityanov D., Cheblakov P. PCI hardware support in LIA-2 control system [Electronic resource]. // 13th Intern. Conf. on Accelerator and Large Experimental Physics Control Systems (ICALEPCS 2011), 10-14 Oct. 2011, WTC Grenoble, France: Contributions to the Proc. - S.I, 2011. - P.916-918.
- [400] Ivanyushenkov Y., Abliz M., Doose C., Kasa M., Trakhtenberg E.M., Vasserman I.B., Mezentssev N.A., Tsukanov V.M., Lev V.H. Development status of a magnetic measurement system for the APS superconducting undulator [Electronic resource]. // 2011 Particle Accelerator Conf., March 28 - April 1, 2011, New York, USA. - S.I, 2011. -

P.1286-1288.

- [401] Zelenski A., Ritter J., Zubets V., Steski D., Atoian G., Davydenko V., Ivanov A., Kolmogorov A. High-intensity, high-brightness polarized and unpolarized beam production incharge-exchange [Electronic resource]. // 2011 Particle Accelerator Conf., March 28 - April 1, 2011, New York, USA. - S.I, 2011. - P.2555-2557.
- [402] Bogomyagkov A.V., Levichev E.B., Piminov P.A. Interaction region design of Super-ct-factory in Novosibirsk [Electronic resource]. // 2011 Particle Accelerator Conf., March 28 - April 1, 2011, New York, USA.- S.I, 2011. - P.2264-2266.
- [403] Gurov S., Batrakov A., Emanov F., Kobets V., Polukhin V., Tsyganov A., Vobly P., Yaskina T., Jago S., Shih J., Tomlinson S. Large aperture quadrupole magnets for ISIS TS-1 and TS-2 [Electronic resource]. // 2011 Particle Accelerator Conf., March 28 - April 1, 2011, New York, USA. - S.I, 2011. - P.1103-1105.
- [404] Blinov V., Kiselev V., Nikitin S., Nikolaev I., Smaluk V. Measurement of the energy dependence of Touschek electron counting rate [Electronic resource]. // 2011 Particle Accelerator Conf., March 28 - April 1, 2011, New York, USA. - S.I, 2011. - P.426-428.
- [405] Gurov S., Akimov A., Anchugov O., Batrakov A., Belikov O., Bekhtenev E., Cheblakov P., Cherepanov V., Chernyakin A., Cheskidov V., Churkin I., Dubrovin A., Erokhin A., Gorchakov K., KarnaeV S., Karpov G., Kiselev V., Kobets V., Konstantinov V., Kolmogorov V., Korepanov A., Kuper E., Kuzminykh V., Levichev E., Mamkin V., Medvedko A., Meshkov O., Nefedov N., Neyfeld V., Okunev I., Petrov V., Petrichenkov M., Polyansky A., Pureskin D., Rakhimov A., Ruvinskiy S., Rybitskaya T., Schegolev L., Semenov A., Senkov D., Serednyakov S., Shiyankov S., Shvedov D., Sinyatkin S., Smaluk V., Sukhanov A., Tsukanova L., Utkin A., Yaminov K., Zhirkova A., Elkaer A., Shaftan T., Ganetis G., Willeke F., Sharma S., Flliller R., Singh O., Pinaev I., Hseuh H., De Long J., Tian Y., Yong H. Status of NSLS-II booster [Electronic resource]. // 2011 Particle Accelerator Conf., March 28 - April 1, 2011, New York, USA. - S.I, 2011. - P.1864-1866. [JACoW, WEP201].
- [406] Wittmer W., Bertsche K., Chao A., Novokhatski A., Nosochkov Y., Seeman J., Sullivan M.K., Wienands U., Bogomyagkov A.V., Levichev E., Nikitin S., Piminov P., Shatilov D., Sinyatkin S., Vobly P., Okunev I.N., et al. SuperB: next-generation e+e- B-factory collider [Electronic resource]. // 2011 Particle Accelerator Conf., March 28 - April 1, 2011, New York, USA. - S.I, 2011. - P.690-692. [SLAC-PUB-14286].
- [407] Petrichenkov M.V., Chudaev V.Ya. The new approximation of dose attenuation curve in concrete [Electronic resource]. // 2011 Particle Accelerator Conf., March 28 - April 1, 2011, New York, USA. - S.I, 2011. - P.2217-2219.
- [408] Zolkin T., Skrynsky A. Usage of Li-rods for ionization cooling of muons [Electronic resource]. // 2011 Particle Accelerator Conf., March 28 - April 1, 2011, New York, USA. - S.I, 2011. - P.226-228.
- [409] Dementyev E.N., Medvedko A.S., Serednyakov S.S., Shubin E.N., Tcheskidov V.G., Vinokurov N.A. Software and capabilities of the beam position measurement system for Novosibirsk free electron laser [Electronic resource]. // 13th Intern. Conf. on Accelerator and Large Experimental Physics Control Systems (ICALEPCS 2011), 10 - 14 Oct. 2011, WTC Grenoble, France: Contributions to the Proc. - S.I, 2011. - P.422-424.
- [410] Gudkov B.A., Selivanov P.A., Kozak E.A., Kuper E.A., Serednyakov S.S., Tararyshkin S.V. Temperature measurement system of Novosibirsk free electron laser [Electronic resource] // 13th Intern. Conf. on Accelerator and Large Experimental Physics Control Systems (ICALEPCS 2011), 10-14 Oct. 2011, WTC Grenoble, France: Contributions to the Proc. - S.I, 2011. - P.1044-1046.
- [411] Schlenker S., Arfaoui S., Franz S., Gutzwiller O., Tsaroichas C.A., Mindur B., Hartert J., Zimmermann S., Talyshev A., et al. The ATLAS detector control system. // 13th Intern. Conf. on Accelerator and Large Experimental Physics Control Systems (ICALEPCS 2011), 10-14 Oct. 2011, WTC Grenoble, France: Contributions to the Proc. - S.I, 2011. - P.5-8.
- [412] Adakin A., Chubarov D., Nikultsev V., Belov S., Kaplin V., Sukharev A., Zaytsev A., Kuchin N., Lomakin S., Kalyuzhny V. Virtualized high performance computing infrastructure of Novosibirsk scientific center [Electronic resource]. // 13th Intern. Conf. on Accelerator and Large Experimental Physics Control Systems (ICALEPCS 2011), 10-14 Oct. 2011, WTC Grenoble, France: Contributions to the Proc. - S.I, 2011. - P.630-633.
- [413] Jago S.J.S., Shih J., Tomlinson S.F.S., Gurov S. Quadrupole magnet with an integrated dipole steering element for the ISIS beam transport line [Electronic resource]. // 2nd Intern. Particle Accelerators Conf. (IPAC 2011), 4-9 Sept. 2011, Kursaal, San Sebastian, Spain. - S.I, 2011. - P.2445-2447.
- [414] Krushchev S.V., Lev V.K., Mezentsev N.A., Miginsky E.G., Shkaruba V.A., Syrovatin V.M., Tsukanov V.M.,

List of publications

- Volkov A.A., Campmany J., Einfeld D. Superconducting 119-pole wiggler for ALBA light source [Electronic resource] // 2nd Intern. Particle Accelerators Conf. (IPAC 2011), 4-9 Sept. 2011, Kursaal, San Sebastian, Spain. - S.I, 2011. - P.3302-3304.
- [415] Dietrich J., Kamerdzhiev V., Bryzgunov M.I., Goncharov A.D., Panasyuk V.M., Parkhomchuk V.V., Reva V.B., Skorobogatov D.N. Status of the 2 MeV electron cooler for COSY/HESR [Electronic resource]. // Workshop on Beam Cooling and Related Topics (COOL 11), Sept. 12 - 16, 2011, Pansionat «Dubna», Alushta, Ukraine. - S.I, 2011. - P.15-18.
- [416] Gabard A., George D., Negrazus M., Rivkin L., Vrankovic V., Kolokolnikov Yu., Vobly P. A 2.9 tesla room temperature superbend magnet for the swiss light source at PSI [Electronic resource]. // 2nd Intern. Particle Accelerators Conf. (IPAC 2011), 4-9 Sept. 2011, Kursaal, San Sebastian, Spain. - S.I, 2011. - P.3038-3040.
- [417] Getmanov Ya.V., Shevchenko O.A., Vinokurov N.A. Longitudinal stability of ERL with two accelerating RF structures [Electronic resource]. // 2nd Intern. Particle Accelerators Conf. (IPAC 2011), 4-9 Sept. 2011, Kursaal, San Sebastian, Spain. - S.I, 2011. - P.1509-1511.
- [418] Eliseev A.V., Brovko O.I., Meshkov I.N., Sidorin A.O., Trubnikov V., Kurkin G.Y., Petrov V.M. RF systems and bunch formation at NICA [Electronic resource]. // 2nd Intern. Particle Accelerators Conf. (IPAC 2011), 4-9 Sept. 2011, Kursaal, San Sebastian, Spain. - S.I, 2011. - P.2511-2513.
- [419] Litvinenko V.N., Vobly P., Kholopov M., Shevchenko O., et al. Coherent electron cooling demonstration experiment [Electronic resource]. // 2nd Intern. Particle Accelerators Conf. (IPAC 2011), 4-9 Sept. 2011, Kursaal, San Sebastian, Spain. - S.I, 2011. - P.3442-3444.
- [420] Neumann A., Volkov V., et al. First characterization of a fully superconducting RF photoinjector cavity [Electronic resource]. // 2nd Intern. Particle Accelerators Conf. (IPAC 2011), 4-9 Sept. 2011, Kursaal, San Sebastian, Spain. - S.I, 2011. - P.41-43.
- [421] Kamps T., Anders W., Barday R., Jankowiak A., Knobloch J., Kugeler O., Matveenko A., Neumann A., Quast T., Rudolph J., Schubert S., Volker J., Kneisel P., Nietubyc R., Sekutowicz J., Smedley J., Volkov V., Weinberg G., Will I. First demonstration of electron beam generation and characterization with an all superconducting radiofrequency (SRF) photoinjector [Electronic resource]. // 2nd Intern. Particle Accelerators Conf. (IPAC 2011), 4-9 Sept. 2011, Kursaal, San Sebastian, Spain. - S.I, 2011. - P.3143-3145.
- [422] W. Wittmer (FRIB, Michigan State University, East Lansing, Mi, USA), K. Bertsche, A. Chao, A. Novokhatski, Y. Nosochkov, J. Seeman, M. K. Sullivan, U. Wienands, S. Weathersby (SLAC, Menlo Park, Ca, USA), A.V. Bogomyagkov, E. Levichev, S. Nikitin, P. Piminov, D. Shatilov, S. Sinyatkin, P. Vobly, I.N. Okunev (BINP, Novosibirsk, RU), B. Bolzon, L. Brunetti, A. Jeremie (IN2P3-LAPP), Annecy-le-Vieux, F.M.E. Biagini, R. Boni, M. Boscolo, T. Demma, A. Drago, M. Esposito, S. Guiducci, S. Liuzzo, M. Preger, P. Raimondi, S. Tomassini, M. Zobov (INFN/LNF, Frascati, Roma, IT), E. Paoloni (INFN & Universit`a di Pisa, IT), P. Fabricatore, R. Musenich, S. Farinon (INFN & Universit`a di Genova, IT), S. Bettoni (CERN, Geneva, CH), F. Poirier, C. Rimbault, A. Variola (LAL, Orsay), F.M. Baylac, O. Bourrion, N. Monseu, C. Vescovi (LPSC, Grenoble), F.A. Chanc'e, CEA, Saclay, F). Status of the Super-B factory design. // Proc. of the Meeting of the Division of Particles and Fields of the American Physical Society (DPF-2011), August 8-13, 2011, Providence, Rhode Island, USA.
- [423] Wittmer W., Bogomyagkov A., Koop I., Levichev E., Nikitin S., Okunev I., Piminov P., Sinyatkin S., Shatilov D., Vobly P., et al. Status of the Super-B factory design. // Proc. of the Meeting of the Division of Particles and Fields of the American Physical Society (DPF-2011), August 8-13, 2011, Providence, Rhode Island, USA. [E-print: arXiv:1110.2167, 2011].
- [424] Bogomyagkov A.V. Super-c-tau in Novosibirsk. // Intern. Workshop on e+e- collisions from Phi to Psi (PHIPSI11), September 19 - 22, 2011, BINP, Novosibirsk.
- [425] Semenov A.M., Anashin V.V., Krasnov A.A., Hseuh H.-C., Shaftan T. NSLS-II booster vacuum system. // Proc. of XVIII Science-Technical Conference «Vacuum Technique and Technology», 2011, Sudak. - P.331-334.
- [426] Gurov S.M., Akimov A.V., Anchugov O.V., Batrakov A.M., Belikov O.V., Bekhtenev E.A., Burenkov D.B., Cheblakov P.B., Cherepanov V.P., Chernyakin A.D., Cheskidov V.G., Churkin I.N., Elkaer A., Erokhin A.I., Fliller R., Gorchakov K.M., Gurov D.S., Ganetis G., Hseuh H., Karnaev S.E., Karpov G.V., Kiselev V.A., Kobets V.V., Konstantinov V.M., Kolmogorov V.V., Korepanov A.A., Kuper E.A., Kuzminykh V.S., Levichev E.B., J. De Long, V.R. Mamkin, A.S. Medvedko, O.I. Meshkov, N.B. Nefedov, V.V. Neyfeld, I.N. Okunev, Petrov V.V., Petrichenkov M.V., Philipchenko A.V., Polyansky A.V., Pureskin D.N., Rakhimov A.R., Ruvinskiy S.I., Schegolev L.M., Semenov A.M., Senkov D.V., Serednyakov S.S., Shaftan T.V., Sharma S., Shichkov D.S., Singh O., Shiyankov S.V., Shvedov D.A., Sinyatkin S.V., Smaluk V.V., Sukhanov A.V., Tian Y., Utkin A.V., Willeke F.,

- Yaminov K.R., Yong H. Status of NSLS-II Booster. // XXII Intern. Workshop on Charged Particle Accelerators (IWCPA2011), September 22 - 28, 2011, Alushta, Ukraine.
- [427] Nikolenko D.M., Rachek I.A., Shestakov Yu.V., Toporkov D.K. Possibility to obtain a polarized hydrogen molecular target. // XIV Intern. Workshop on Polarized Sources, Targets and Polarimetry, 12-16 September, 2011, St. Petersburg, Russia. - Conference Proc., p.73-75.
- [428] Obrazovsky A.E. Preliminary results on e^+e^- to hadrons from SND detector at VEPP-2000 collider. // XIV International Conference on Hadron Spectroscopy (Hadron 2011), 13 - 17 June, 2011, Muenchen. [<http://www.slac.stanford.edu/econf/C110613>].
- [429] Achasov M.N., Aulchenko V.M., Barnyakov, A.Yu. Beloborodov K.I., Berdugin A.V., Bogdanchikov A.G., Botov A.A., Bukin D.A., Golubev V.B., Grevtsov K.A., Dimova T.V., Druzhinin V.P., Kardapoltsev, L.V. Kharlamov A.G., Kovrizhin D.P., Korol A.A., Koshuba S.V., Kravchenko E.A., Martin K.A., Obrazovsky A.E., Onuchin A.P., Pakhtusova E.V., Serednyakov S.I., Shatunov Yu.M., Shtol D.A., Shukaev A.N., Silagadze Z.K., Skovpen K.Yu., Skrinsky A.N., Surin I.K., Tikhonov Yu.A., Usov Yu.V., Vasiljev A.V., Vesenev V.M. Spherical Neutral Detector for experiments at VEPP-2000 e^+e^- collider. // Intern. Workshop on e^+e^- Collisions from ϕ to Ψ , 19 - 24 September, 2011, BINP, Novosibirsk. - To be publ. Nuclear Physics B (Proc. Supplements).
- [430] Achasov M.N., Barnyakov A.Yu., Beloborodov K.I., Berdyugin A.V., Bogdanchikov A.G., Botov A.A., Bukin D.A., Golubev V.B., Grevtsov K.A., Druzhinin V.P., Kasaev A.S., Kardapoltsev L.V., Kharlamov A.G., Koop I.A., Kovrizhin D.P., Korol A.A., Koshuba S.V., Lysenko A.P., Martin K.A., Obrazovsky A.E., Pakhtusova E.V., Rogovsky Yu.A., Romanov A.L., Serednyakov S.I., Shatunov P.Yu., Shatunov Yu.M., Shtol D.A., Shwartz D.B., Silagadze Z.K., Skovpen K.Yu., Skrinsky A.N., Surin I.K., Tikhonov Yu.A. Vasiljev A.V. First SND detector results on hadron cross sections at VEPP-2000 e^+e^- collider. // XXI Europhysics Conference on High Energy Physics (EPS-HEP2011), 21 - 27 July, 2011, Grenoble, Rhones Alpes, France. - Electronic resource: [Proc. of Science (EPS-HEP2011) 174].
- [431] Serednyakov S.I. First results of SND experiments at VEPP-2000. // Intern. Workshop on e^+e^- collisions «From ϕ to Ψ », 19 - 24 September, 2011, BINP, Novosibirsk.
- [432] Golubev V.B. First results on the nucleon form factors from SND. // Intern. Workshop on e^+e^- collisions «From ϕ to Ψ », 19 - 24 September, 2011, BINP, Novosibirsk.
- [433] Achasov M.N. Search for LFV in e^+e^- interactions. // Intern. Workshop on e^+e^- collisions «From ϕ to Ψ , 19 - 24 September, 2011, BINP, Novosibirsk.
- [434] Kardapoltsev L.V. Preliminary results from SND experiment at VEPP-2000 e^+e^- collider. // PANIC 11, 24-29 July, 2011, USA, Cambridge, Massachusetts at the Massachusetts Institute of Technology (MIT).
- [435] Telnov V.I., Photon collider project. // Talk at Intern. Conference on the Structure and the Interactions of the Photon including the 19th International Workshop on Photon-Photon Collisions (PHOTON2011), SPA, Belgium, May 22 - 27, 2011. - [<http://www.photon11.be/>], [<http://agenda.irmp.ucl.ac.be/getFile.py/access?contribId=8&sessionId=6&resId=0&materialId=slides&confId=924>].
- [436] Telnov V.I., Photon collider at CLIC. Talk at Intern. Workshop on Future Linear Colliders (LCWS2011), Granada, Spain, 26 - 30 September, 2011. - [<http://www.ugr.es/~lcws11/>], [<http://ilcagenda.linearcollider.org/getFile.py/access?contribId=247&sessionId=58&resId=1&materialId=slides&confId=5134>].
- [437] E.M. Baldin, V.V. Anashin, V.M. Aulchenko, A.K. Barladyan, A.Yu. Barnyakov, M.Yu. Barnyakov, S.E. Baru, I.V. Bedny, O.L. Beloborodova, A.E. Blinov, V.E. Blinov, A.V. Bobrov, V.S. Bobrovnikov, A.V. Bogomyagkov, A.E. Bondar, D.V. Bondarev, A.R. Buzykaev, S.I. Eidelman, Yu.M. Glukhovchenko, V.V. Gulevich, D.V. Gusev, S.E. KarnaeV, G.V. Karpov, S.V. Karpov, T.A. Kharlamova, V.A. Kiselev, S.A. Kononov, K.Yu. Kotov, E.A. Kravchenko, V.F. Kulikov, G.Ya. Kurkin, E.A. Kuper, E.B. Levichev, D.A. Maksimov, V.M. Malyshev, A.L. Maslennikov, A.S. Medvedko, O.I. Meshkov, S.I. Mishnev, I.I. Morozov, N.Yu. Muchnoi, V.V. Neufeld, S.A. Nikitin, I.B. Nikolaev, I.N. Okunev, A.P. Onuchin, S.B. Oreshkin, I.O. Orlov, A.A. Osipov, S.V. Peleganchuk, S.G. Pivovarov, P.A. Piminov, V.V. Petrov, A.O. Poluektov, I.N. Popkov, V.G. Prisekin, A.A. Ruban, V.K. Sandyrev, G.A. Savinov, A.G. Shamov, D.N. Shatilov, B.A. Shwartz, E.A. Simonov, S.V. Sinyatkin, Yu.I. Skovpen, A.N. Skrinsky, V.V. Smaluk, A.V. Sokolov, A.M. Sukharev, E.V. Starostina, A.A. Talyshev, V.A. Tayursky, V.I. Telnov, Yu.A. Tikhonov, K.Yu. Todyshev, G.M. Tumaikin, Yu.V. Usov, A.I. Vorobiov, A.N. Yushkov, V.N. Zhilich, V.V. Zhulanov, A.N. Zhuravlev. (KEDR Collab.). Recent results from the KEDR detector at the VEPP-4M e^+e^- collider. // XXI Europhysics Conference on High Energy Physics, 21-27 July 2011, Grenoble, Rhones Alpes, France. - Electronic resource: [Proc. of Science (EPS-HEP2011) 174].
- [438] A.K. Barladyan, V.V. Anashin, V.M. Aulchenko, E.M. Baldin, A.Yu. Barnyakov, M.Yu. Barnyakov, S.E. Baru,

- I.V. Bedny, O.L. Beloborodova, A.E. Blinov, V.E. Blinov, A.V. Bobrov, V.S. Bobrovnikov, A.V. Bogomyagkov, A.E. Bondar, D.V. Bondarev, A.R. Buzykaev, S.I. Eidelman, Yu.M. Glukhovchenko, V.V. Gulevich, D.V. Gusev, S.E. Karnaev, G.V. Karpov, S.V. Karpov, T.A. Kharlamova, V.A. Kiselev, S.A. Kononov, K.Yu. Kotov, E.A. Kravchenko, V.F. Kulikov, G.Ya. Kurkin, E.A. Kuper, E.B. Levichev, D.A. Maksimov, V.M. Malyshev, A.L. Maslennikov, A.S. Medvedko, O.I. Meshkov, S.I. Mishnev, I.I. Morozov, N.Yu. Muchnoi, V.V. Neufeld, S.A. Nikitin, I.B. Nikolaev, I.N. Okunev, A.P. Onuchin, S.B. Oreshkin, I.O. Orlov, A.A. Osipov, S.V. Peleganchuk, S.G. Pivovarov, P.A. Piminov, V.V. Petrov, A.O. Poluektov, I.N. Popkov, V.G. Prisekin, A.A. Ruban, V.K. Sandryev, G.A. Savinov, A.G. Shamov, D.N. Shatilov, B.A. Shwartz, E.A. Simonov, S.V. Sinyatkin, Yu.I. Skovpen, A.N. Skrinsky, V.V. Smaluk, A.V. Sokolov, A.M. Sukharev, E.V. Starostina, A.A. Talyshev, V.A. Tayursky, V.I. Telnov, Yu.A. Tikhonov, K.Yu. Todyshev, G.M. Tumaikin, Yu.V. Usov, A.I. Vorobiov, A.N. Yushkov, V.N. Zhilich, V.V. Zhulanov, A.N. Zhuravlev (KEDR Collab.). Superconducting magnet system for the KEDR detector. // 22nd Intern. Conference on Magnet Technology, 12 - 16 September, 2011, Marseille, France.
- [439] K.Yu. Todyshev, V.V. Anashin, V.M. Aulchenko, E.M. Baldin, A.K. Barladyan, A.Yu. Barnyakov, M.Yu. Barnyakov, S.E. Baru, I.V. Bedny, O.L. Beloborodova, A.E. Blinov, V.E. Blinov, A.V. Bobrov, V.S. Bobrovnikov, A.V. Bogomyagkov, A.E. Bondar, D.V. Bondarev, A.R. Buzykaev, S.I. Eidelman, Yu.M. Glukhovchenko, V.V. Gulevich, D.V. Gusev, S.E. Karnaev, G.V. Karpov, S.V. Karpov, T.A. Kharlamova, V.A. Kiselev, S.A. Kononov, K.Yu. Kotov, E.A. Kravchenko, V.F. Kulikov, G.Ya. Kurkin, E.A. Kuper, E.B. Levichev, D.A. Maksimov, V.M. Malyshev, A.L. Maslennikov, A.S. Medvedko, O.I. Meshkov, S.I. Mishnev, I.I. Morozov, N.Yu. Muchnoi, V.V. Neufeld, S.A. Nikitin, I.B. Nikolaev, I.N. Okunev, A.P. Onuchin, S.B. Oreshkin, I.O. Orlov, A.A. Osipov, S.V. Peleganchuk, S.G. Pivovarov, P.A. Piminov, V.V. Petrov, A.O. Poluektov, I.N. Popkov, V.G. Prisekin, A.A. Ruban, V.K. Sandryev, G.A. Savinov, A.G. Shamov, D.N. Shatilov, B.A. Shwartz, E.A. Simonov, S.V. Sinyatkin, Yu.I. Skovpen, A.N. Skrinsky, V.V. Smaluk, A.V. Sokolov, A.M. Sukharev, E.V. Starostina, A.A. Talyshev, V.A. Tayursky, V.I. Telnov, Yu.A. Tikhonov, G.M. Tumaikin, Yu.V. Usov, A.I. Vorobiov, A.N. Yushkov, V.N. Zhilich, V.V. Zhulanov, A.N. Zhuravlev (KEDR Collab.). Recent results from KEDR. // Intern. Conference «From Phi to Psi», 19-24 September 2011, BINP SB RAS, Novosibirsk.
- [440] V.N. Zhilich, V.V. Anashin, V.M. Aulchenko, E.M. Baldin, A.K. Barladyan, A.Yu. Barnyakov, M.Yu. Barnyakov, S.E. Baru, I.V. Bedny, O.L. Beloborodova, A.E. Blinov, V.E. Blinov, A.V. Bobrov, V.S. Bobrovnikov, A.V. Bogomyagkov, A.E. Bondar, D.V. Bondarev, A.R. Buzykaev, S.I. Eidelman, Yu.M. Glukhovchenko, V.V. Gulevich, D.V. Gusev, S.E. Karnaev, G.V. Karpov, S.V. Karpov, T.A. Kharlamova, V.A. Kiselev, S.A. Kononov, K.Yu. Kotov, E.A. Kravchenko, V.F. Kulikov, G.Ya. Kurkin, E.A. Kuper, E.B. Levichev, D.A. Maksimov, V.M. Malyshev, A.L. Maslennikov, A.S. Medvedko, O.I. Meshkov, S.I. Mishnev, I.I. Morozov, N.Yu. Muchnoi, V.V. Neufeld, S.A. Nikitin, I.B. Nikolaev, I.N. Okunev, A.P. Onuchin, S.B. Oreshkin, I.O. Orlov, A.A. Osipov, S.V. Peleganchuk, S.G. Pivovarov, P.A. Piminov, V.V. Petrov, A.O. Poluektov, I.N. Popkov, V.G. Prisekin, A.A. Ruban, V.K. Sandryev, G.A. Savinov, A.G. Shamov, D.N. Shatilov, B.A. Shwartz, E.A. Simonov, S.V. Sinyatkin, Yu.I. Skovpen, A.N. Skrinsky, V.V. Smaluk, A.V. Sokolov, A.M. Sukharev, E.V. Starostina, A.A. Talyshev, V.A. Tayursky, V.I. Telnov, Yu.A. Tikhonov, K.Yu. Todyshev, G.M. Tumaikin, Yu.V. Usov, A.I. Vorobiov, A.N. Yushkov, V.V. Zhulanov, A.N. Zhuravlev (KEDR Collab.). KEDR tagger. // Intern. Conference «From Phi to Psi», 19-24 September 2011, BINP SB RAS, Novosibirsk.
- [441] S.I. Eidelman, V.V. Anashin, V.M. Aulchenko, E.M. Baldin, A.K. Barladyan, A.Yu. Barnyakov, M.Yu. Barnyakov, S.E. Baru, I.V. Bedny, O.L. Beloborodova, A.E. Blinov, V.E. Blinov, A.V. Bobrov, V.S. Bobrovnikov, A.V. Bogomyagkov, A.E. Bondar, D.V. Bondarev, A.R. Buzykaev, Yu.M. Glukhovchenko, V.V. Gulevich, D.V. Gusev, S.E. Karnaev, G.V. Karpov, S.V. Karpov, T.A. Kharlamova, V.A. Kiselev, S.A. Kononov, K.Yu. Kotov, E.A. Kravchenko, V.F. Kulikov, G.Ya. Kurkin, E.A. Kuper, E.B. Levichev, D.A. Maksimov, V.M. Malyshev, A.L. Maslennikov, A.S. Medvedko, O.I. Meshkov, S.I. Mishnev, I.I. Morozov, N.Yu. Muchnoi, V.V. Neufeld, S.A. Nikitin, I.B. Nikolaev, I.N. Okunev, A.P. Onuchin, S.B. Oreshkin, I.O. Orlov, A.A. Osipov, S.V. Peleganchuk, S.G. Pivovarov, P.A. Piminov, V.V. Petrov, A.O. Poluektov, I.N. Popkov, V.G. Prisekin, A.A. Ruban, V.K. Sandryev, G.A. Savinov, A.G. Shamov, D.N. Shatilov, B.A. Shwartz, E.A. Simonov, S.V. Sinyatkin, Yu.I. Skovpen, A.N. Skrinsky, V.V. Smaluk, A.V. Sokolov, A.M. Sukharev, E.V. Starostina, A.A. Talyshev, V.A. Tayursky, V.I. Telnov, Yu.A. Tikhonov, K.Yu. Todyshev, G.M. Tumaikin, Yu.V. Usov, A.I. Vorobiov, A.N. Yushkov, V.N. Zhilich, V.V. Zhulanov, A.N. Zhuravlev. (KEDR Collab.). Recent results from the KEDR detector. // XIV Intern. Conference on Hadron Spectroscopy (HADRON 11), June 13-17, 2011, Munich, Germany.
- [442] S.I. Eidelman, V.V. Anashin, V.M. Aulchenko, E.M. Baldin, A.K. Barladyan, A.Yu. Barnyakov, M.Yu. Barnyakov, S.E. Baru, I.V. Bedny, O.L. Beloborodova, A.E. Blinov, V.E. Blinov, A.V. Bobrov, V.S. Bobrovnikov, A.V. Bogomyagkov, A.E. Bondar, D.V. Bondarev, A.R. Buzykaev, Yu.M. Glukhovchenko, V.V. Gulevich, D.V. Gusev, S.E. Karnaev, G.V. Karpov, S.V. Karpov, T.A. Kharlamova, V.A. Kiselev, S.A. Kononov, K.Yu. Kotov, E.A.

- Kravchenko, V.F. Kulikov, G.Ya. Kurkin, E.A. Kuper, E.B. Levichev, D.A. Maksimov, V.M. Malyshev, A.L. Maslennikov, A.S. Medvedko, O.I. Meshkov, S.I. Mishnev, I.I. Morozov, N.Yu. Muchnoi, V.V. Neufeld, S.A. Nikitin, I.B. Nikolaev, I.N. Okunev, A.P. Onuchin, S.B. Oreshkin, I.O. Orlov, A.A. Osipov, S.V. Peleganchuk, S.G. Pivovarov, P.A. Piminov, V.V. Petrov, A.O. Poluektov, I.N. Popkov, V.G. Prisekin, A.A. Ruban, V.K. Sandryev, G.A. Savinov, A.G. Shamov, D.N. Shatilov, B.A. Shwartz, E.A. Simonov, S.V. Sinyatkin, Yu.I. Skovpen, A.N. Skrinsky, V.V. Smaluk, A.V. Sokolov, A.M. Sukharev, E.V. Starostina, A.A. Talyshev, V.A. Tayursky, V.I. Telnov, Yu.A. Tikhonov, K.Yu. Todyshev, G.M. Tumaikin, Yu.V. Usov, A.I. Vorobiov, A.N. Yushkov, V.N. Zhilich, V.V. Zhulanov, A.N. Zhuravlev (KEDR Collab.). Properties of the J/ψ , $\psi(2S)$ and $\psi(3770)$ at KEDR. // 8 Intern. Workshop of QWG, October 4-7, 2011, Darmstadt, Germany.
- [443] V.E. Blinov, V.V. Anashin, V.M. Aulchenko, E.M. Baldin, A.K. Barladyan, A.Yu. Barnyakov, M.Yu. Barnyakov, S.E. Baru, I.Yu. Basok, S.E. Bedny, O.L. Beloborodova, A.E. Blinov, A.V. Bobrov, V.S. Bobrovnikov, A.E. Bondar, A.R. Buzykaev, A.I. Vorobiov, V.V. Gulevich, L.V. Dneprovsky, V.N. Zhilich, V.V. Zhulanov, G.V. Karpov, S.V. Karpov, S.A. Kononov, K.Yu. Kotov, E.A. Kravchenko, V.N. Kudryavtsev, A.S. Kuzmin, V.F. Kulikov, E.A. Kuper, E.B. Levichev, D.A. Maksimov, V.M. Malyshev, A.L. Maslennikov, A.S. Medvedko, N.Yu. Muchnoi, S.A. Nikitin, I.B. Nikolaev, A.P. Onuchin, S.B. Oreshkin, I.O. Orlov, A.A. Osipov, S.V. Peleganchuk, S.G. Pivovarov, A.O. Poluektov, G.E. Pospelov, V.G. Prisekin, A.A. Ruban, V.A. Rodyakov, G.A. Savinov, Yu.A. Skovpen, A.N. Skrinsky, V.V. Smaluk, R.G. Snopkov, A.V. Sokolov, A.M. Sukharev, A.A. Talyshev, V.A. Tayursky, V.I. Telnov, Yu.A. Tikhonov, K.Yu. Totyshev, Yu.V. Usov, T.A. Kharlamova, A.G. Shamov, B.A. Shwartz, L.I. Shekhtman, A.I. Shusharo, A.N. Yushkov. The review of results from the KEDR detector. // Scientific Session-Conference of NP Section of DPN of RAS "Physics of Fundamental Interactions", 21 - 25 November, 2011, ITEP, Moscow.
- [444] A.M. Sukharev, V.V. Anashin, V.M. Aulchenko, E.M. Baldin, A.K. Barladyan, A.Yu. Barnyakov, M.Yu. Barnyakov, S.E. Baru, I.Yu. Basok, S.E. Bedny, O.L. Beloborodova, A.E. Blinov, V.E. Blinov, A.V. Bobrov, V.S. Bobrovnikov, A.E. Bondar, A.R. Buzykaev, A.I. Vorobiov, V.V. Gulevich, L.V. Dneprovsky, V.N. Zhilich, V.V. Zhulanov, G.V. Karpov, S.V. Karpov, S.A. Kononov, K.Yu. Kotov, E.A. Kravchenko, V.N. Kudryavtsev, A.S. Kuzmin, V.F. Kulikov, E.A. Kuper, E.B. Levichev, D.A. Maksimov, V.M. Malyshev, A.L. Maslennikov, A.S. Medvedko, N.Yu. Muchnoi, S.A. Nikitin, I.B. Nikolaev, A.P. Onuchin, S.B. Oreshkin, I.O. Orlov, A.A. Osipov, S.V. Peleganchuk, S.G. Pivovarov, A.O. Poluektov, G.E. Pospelov, V.G. Prisekin, A.A. Ruban, V.A. Rodyakov, G.A. Savinov, Yu.A. Skovpen, A.N. Skrinsky, V.V. Smaluk, R.G. Snopkov, A.V. Sokolov, A.A. Talyshev, V.A. Tayursky, V.I. Telnov, Yu.A. Tikhonov, K.Yu. Totyshev, Yu.V. Usov, T.A. Kharlamova, A.G. Shamov, B.A. Shwartz, L.I. Shekhtman, A.I. Shusharo, A.N. Yushkov. Measurement of ψ -mesons parameters. // Scientific Session-Conference of NP Section of DPN of RAS "Physics of Fundamental Interactions", 21 - 25 November, 2011, ITEP, Moscow.
- [445] K.Yu. Totyshev, V.V. Anashin, V.M. Aulchenko, E.M. Baldin, A.K. Barladyan, A.Yu. Barnyakov, M.Yu. Barnyakov, S.E. Baru, I.Yu. Basok, S.E. Bedny, O.L. Beloborodova, A.E. Blinov, V.E. Blinov, A.V. Bobrov, V.S. Bobrovnikov, A.E. Bondar, A.R. Buzykaev, A.I. Vorobiov, V.V. Gulevich, L.V. Dneprovsky, V.N. Zhilich, V.V. Zhulanov, G.V. Karpov, S.V. Karpov, S.A. Kononov, K.Yu. Kotov, E.A. Kravchenko, V.N. Kudryavtsev, A.S. Kuzmin, V.F. Kulikov, E.A. Kuper, E.B. Levichev, D.A. Maksimov, V.M. Malyshev, A.L. Maslennikov, A.S. Medvedko, N.Yu. Muchnoi, S.A. Nikitin, I.B. Nikolaev, A.P. Onuchin, S.B. Oreshkin, I.O. Orlov, A.A. Osipov, S.V. Peleganchuk, S.G. Pivovarov, A.O. Poluektov, G.E. Pospelov, V.G. Prisekin, A.A. Ruban, V.A. Rodyakov, G.A. Savinov, Yu.A. Skovpen, A.N. Skrinsky, V.V. Smaluk, R.G. Snopkov, A.V. Sokolov, A.A. Talyshev, V.A. Tayursky, V.I. Telnov, Yu.A. Tikhonov, Yu.V. Usov, T.A. Kharlamova, A.G. Shamov, B.A. Shwartz, L.I. Shekhtman, A.I. Shusharo, A.N. Yushkov. Measurement of $\psi(3770)$ parameters. // Scientific Session-Conference of NP Section of DPN of RAS "Physics of Fundamental Interactions", 21 - 25 November, 2011, ITEP, Moscow.
- [446] Kravchenko E.A., Barnyakov A.Yu., Barnyakov M.Yu., Basok I.Yu., Blinov V.E., Bobrovnikov V.S., Borodenco A.A., Buzykaev A.R., Danilyuk A.F., Gulevich V.V., Kononov S.A., Kuyanov I.A., Onuchin A.P., Ovtin I.V., Talyshev A.A. Status of FARICH. // Intern. Workshop: XVI SuperB General Meeting, April, 2011, Frascati, Italy.
- [447] Kravchenko E.A., Barnyakov A.Yu., Barnyakov M.Yu., Basok I.Yu., Blinov V.E., Bobrovnikov V.S., Borodenco A.A., Buzykaev A.R., Danilyuk A.F., Gulevich V.V., Kononov S.A., Kuyanov I.A., Onuchin A.P., Ovtin I.V., Talyshev A.A. Test beam results on focusing aerogel. // Intern. Workshop: XVII SuperB Workshop and Kick off Meeting, May - June, 2011, Elba, Italy.
- [448] Kononov S.A., Barnyakov A.Yu., Barnyakov M.Yu., Basok I.Yu., Blinov V.E., Bobrovnikov V.S., Borodenco A.A., Buzykaev A.R., Danilyuk A.F., Gulevich V.V., Kravchenko E.A., Kuyanov I.A., Onuchin A.P., Ovtin I.V., Talyshev A.A. Development of the FARICH detector for the upgrade of the ALICE HMPID system. // Workshop "ALICE Upgrade Forum", June, 2011, CERN, Switzerland.
- [449] Danilyuk A.F., Barnyakov A.Yu., Barnyakov M.Yu., Bobrovnikov V.S., Buzykaev A.R., Kononov S.A.,

- Kravchenko E.A., Onuchin A.P. Synthesis of silica aerogels. // VI Scientific Conference "Supercritical Fluids: Fundamentals, Technology and Innovation", July 2011, Listvyanka, Russia.
- [450] Kravchenko E.A., Barnyakov A.Yu., Barnyakov M.Yu., Bobrovnikov V.S., Buzykaev A.R., Kononov S.A., Onuchin A.P. Investigation of PMT ageing in Novosibirsk. // Intern. Conference "1st SuperB Collaboration Meeting", September, 2011, London, Great Britain.
- [451] Kravchenko E.A., Barnyakov A.Yu., Barnyakov M.Yu., Basok I.Yu., Blinov V.E., Bobrovnikov V.S., Borodenco A.A., Buzykaev A.R., Danilyuk A.F., Gulevich V.V., Kononov S.A., Kuyanov I.A., Onuchin A.P., Ovtin I.V., Talyshev A.A. The experiment with the FARICH prototype at the extracted beam of the VEPP-4M. // Experimental Seminar of BINP, October 2011, Novosibirsk, Russia.
- [452] Kravchenko E.A., Barnyakov A.Yu., Barnyakov M.Yu., Basok I.Yu., Blinov V.E., Bobrovnikov V.S., Borodenco A.A., Buzykaev A.R., Danilyuk A.F., Gulevich V.V., Kononov S.A., Kuyanov I.A., Onuchin A.P., Ovtin I.V., Talyshev A.A. Development of a detector of Cherenkov rings on the basis of the focusing aerogel. // Scientific Session-Conference of NP Section of DPN of RAS "Physics of Fundamental Interactions", 21 - 25 November, 2011, ITEP, Moscow.
- [453] Buzulutskov A. Presentation of BINP activity. // Participation in 8th RD51 Collaboration Meeting, 2-3 September 2011, Kobe, Japan.
- [454] Buzulutskov A., Advances in Cryogenic Avalanche Detectors (review). // 2nd Intern. Conference on Micro-Pattern Gaseous Detectors, 29 August - 1 September 2011, Kobe, Japan (to be publ. in JINST).
- [455] Biberdorf E.A., Popova N.I. New possibilities of extended package GALA-4.0. // Ershov's Computer Science Conference «Science Intensive Applied Software», 27 June - 1 July, 2011, Academgorodok, Novosibirsk. - Theses of reports: A.P. Ershov Institute of Informatics Systems SB RAS, 2011.
- [456] Sokolov Valentin V. Dynamical quantum chaos and suppression of quantum coherence. // Third Workshop on Nuclei and Mesoscopic Physics (WNMP11), East Lansing, March 5 - 9, USA. - P.1-35. - [Electronic ArXiv].
- [457] Katkov V.M. Pair creation by polarized photons in constant and homogeneous electromagnetic fields. // IX Intern. Symposium (RREPS-11), September 12-16, 2011, Egham, United Kingdom. - Book of abstracts, P.14.
- [458] Strakhovenko V. Polarized positron production in amorphous targets. // Invited Talk Given at the Workshop «Posipol 2011», August 28-30, 2011, IHEP, Beijing, China. - [<http://indico.ihep.ac.cn/event/2210>].
- [459] Fadin V.S. Connection between "standard" and "quasi-conformal" BFKL kernels and impact factors for colourless particles. // Presented talk: International Workshop "Low x Meeting", June 3-7, 2011, Santiago de Compostela, Spain.
- [460] Fadin V.S. Möbius representation of BFKL equation. // Presented talk: GGI Workshop "High-Energy QCD after the Start of the LHC", September 11 - 30, 2011, Florence, Italy.
- [461] Fadin V.S. Möbius representation of BFKL equation. // Scientific Session-Conference of NP Section of DPN of RAS "Physics of Fundamental Interactions", 21 - 25 November, 2011, ITEP, Moscow.
- [462] Lee R. DRA method: Powerful tool for the calculation of the loop integrals. // Proc. of Conference on 14th Intern. Workshop on Advanced Computing and Analysis Techniques in Physics Research (ACAT2011), September 5 - 9, 2011, Uxbridge, London, UK.
- [463] Dmitriev V.F., Berengut J., Flambaum V.V. Quark-mass variation effect on big bang nucleosynthesis. // Conference: Nuclear Physics in Astrophysics V, 3-8 April, 2011, Eilat, Israel.
- [464] Logachev P., Akimov A., Bak P., Batazova M., Batrakov A., Boimelshtein Yu., Bolkhovityanov D., Eliseev A., Emanov F., Fatkin G., Korepanov A., Kulenko Ya., Kuznetsov G., Nikolaev I., Ottmar A., Pachkov A., Panov A., Pavlov O., Starostenko D. Performance of 2 MeV, 2 kA, 200 ns linear induction accelerator with ultra low beam emittance for X-ray flash radiography [Electronic resource]. // 2nd Intern. Particle Accelerators Conf. (IPAC 2011), 4-9 Sept. 2011, Kursaal, San Sebastian, Spain. - S.I, 2011. - P.1906-1908.
- [465] Fatkin G., Bak P.A., Batrakov A.M., Logachev P.V., Panov A., Pavlenko A.V., Sazansky V.Ya. Control system for linear induction accelerator LIA-2: the structure and hardware [Electronic resource]. // 13th Intern. Conf. on Accelerator and Large Experimental Physics Control Systems (ICALEPCS 2011), 10-14 Oct. 2011, WTC Grenoble, France: Contributions to the Proc. - S.I, 2011. - P.502-505.
- [466] Bryzgunov M., Buble A., Gosteev V., Panasyuk V., Parkhomchuk V., Reva V. Magnetic system of electron cooler for COSY [Electronic resource]. // Workshop on Beam Cooling and Related Topics (COOL 11), Sept. 12 - 16, 2011, Pansionat «Dubna», Alushta, Ukraine. - S.I, 2011. - P.114-117. [<http://www.JACoW.org>].

- [467] Bryzgunov M.I., Bubley A.V., Chekavinskiy V.A., Gusev I.A., Ivanov A.V., Kondauron M.N., Panasyuk V.M., Parkhomchuk V.V., Pureskin D.N., Putmakov A.A., Reva V.B., Senkov D.V., Skorobogatov D.N. Electron collector for 2 MeV electron cooler for COSY [Electronic resource]. // Workshop on Beam Cooling and Related Topics, Sept. 12 - 16, 2011, Pansionat «Dubna», Alushta, Ukraine. - S.I, S.a. - P.103-106.
- [468] Bryzgunov M., Bubley A., Ivanov A., Parkhomchuk V., Reva V., Kruchkov A. Electron GUN with variable beam profile for COSY cooler [Electronic resource] // Workshop on Beam Cooling and Related Topics (COOL 11), September 12 - 16, 2011, Pansionat «Dubna», Alushta, Ukraine. - S.I, 2011. - P.99-102.
- [469] Bocharov V.N., Bryzgunov M.I., Bubley A.V., Cheskidov V.G., Fedotov M.G., Parkhomchuk V.V., Reva V.B. System for measurement of magnetic field line straightness in solenoid of electron cooler for COSY [Electronic resource]. // Workshop on Beam Cooling and Related Topics (COOL 11), Sept. 12 - 16, 2011, Pansionat «Dubna», Alushta, Ukraine. - S.I, 2011. - P.107-110.
- [470] Reva V.B., Alinovsky N., Batrakov A.M., Bedareva T.V., Bekhtenev E.A., Belikov O.V., Bocharov V.N., Borodich V.V., Bryzgunov M.I., Bubley A.V., Chekavinskiy V.A., Cheskidov V.G., Dovzhenko B.A., Erokhin A.I., Fatkin G.A., Fedotov M.G., Goncharov A.D., Gorchakov K.M., Gosteev V.K., Gusev I.A., Ivanov A.V., Karpov G.V., Koisin Yu.I., Kondauron M.N., Kryuchkov A.M., Lisitsyn A.D., Lopatkin I.A., Mamkin V.R., Medvedko A.S., Panasyuk V.M., Parkhomchuk V.V., Poletaev I.V., Polukhin V.A., Protopopov A.Yu., Pureskin D.N., Putmakov A.A., Semenov E.P., Senkov D.V., Skorobogatov D.N., Zapiatkin N.P. The first commission results of the high voltage magnetized cooler for COSY [Electronic resource]. // Workshop on Beam Cooling and Related Topics (COOL 11), Sept. 12 - 16, 2011, Pansionat «Dubna», Alushta, Ukraine. - S.I, 2011. - P.37-42.
- [471] Dietrich J., Kamerzhiev V., Bryzgunov M.I., Goncharov A.D., Panasyuk V.M., Parkhomchuk V.V., Reva V.B., Skorobogatov D.N. Progress of the 2 MeV electron cooler development for COSY-Julich/HESR [Electronic resource]. // 2nd Intern. Particle Accelerators Conf., (IPAC 2011), 4-9 September, 2011, Kursaal, San Sebastian, Spain. - S.I, 2011. - P.3427-3429. [<http://accelconf.web.cern.ch/AccelConf/IPAC2011/papers/thps002.pdf>].
- [472] Dietrich J., Kamerzhiev V., Bryzgunov M.I., Goncharov A.D., Panasyuk V.M., Parkhomchuk V.V., Reva V.B., Skorobogatov D.N. Status of 2 MeV electron cooler for COSY - Julich/HESR [Electronic resource]. // 2011 Particle Accelerator Conf., March 28 - April 1, 2011, New York, USA. - S.I, 2011. - P.1918-1920.
- [473] Parkhomchuk V.V., Reva V.B. The advance technology extraction for therapy ions beam from carbon storage ring with electron cooling [Electronic resource]. // Workshop on Beam Cooling and Related Topics (COOL 11), Sept. 12 - 16, 2011, Pansionat «Dubna», Alushta, Ukraine. - S.I, 2011. - P.43-47.
- [474] Parkhomchuk V.V. The incomprehensible problems in dynamic of the beams BINP SD RAS (Novosibirsk). // IX Intern. Workshop to the Memory Prof. V.P. Sarantsev, 17-21 September, 2011, Alushta, Ukraina.
- [475] Parkhomchuk V.V., Rastigeev S.A. Ion selection in the BINP accelerator mass-spectrometer. // IX Intern. Workshop to the Memory Prof. V.P. Sarantsev 17-21 September, 2011, Alushta, Ukraina.
- [476] Rastigeev S.A., Frolov A.R. Goncharov A.D., Klyuev V. F., Konstantinov E.S., Kutnykova L.A., Parkhomchuk V.V., Petrozhitskii A.V. Development of the BINP AMS complex at CCU SB RAS. // XXII Intern. Particle Accelerator Seminar. 27-28 October, 2011, BINP, Novosibirsk (will be published "Problems of Atomic Science and Technology" (VANT)). [<http://www.kipt.kharkov.ua/conferences/ihepnp/2011/iwcpa/index.html>].
- [477] Biryuchevsky Yu.A., Gorniker E.I., Kendjebulatov E.K., Krutikhin S.A., Kurkin G.Ya., Petrov V.M., Pilan A.M. Status of 174 MHz RF system for BEP. // XXII Intern. Workshop on Charged Particle Accelerators, September 22 - 28, 2011, Alushta, Ukraine.
- [478] Aleshaev A., Belov S., Kozak V., Piskunov G., Tararyshkin S. The Problems of control of large electro-physical installations as the pre-requisite for developing original CPU architectures. // Proc. of the 2nd Intern. Conference on the History of Computers and Informatics in the Soviet Union and Russian Federation (SORUCOM-2011), 12-16 September, Veliky Novgorod, Russia.
- [479] Lotov K.V., Maslov V.I., Onischenko I.N. Long train of relativistic electron bunches as a driver in plasma wakefield accelerator. // XXXVIII Intern. Zvenigorod Conference on Plasma Physics and Controlled Fusion, Zvenigorod, 2011. - Abstracts. - M: «PLAZMAIOFAN». - P.315. - Electronic resource: [C.Ty 2-05] (in Russian).
- [480] Xia G., Caldwell A., Lotov K., Pukhov A., Assmann R., Zimmermann F., Huang C., Vieira J., Lopes N., Fonseca R.A., Silva L.O., An W., Joshi C., Mori W., Lu W., Muggli P. A proposed experimental test of proton-driven plasma wakefield acceleration based on CERN SPS [Electronic resource]. // 2011 Particle Accelerator Conference, March 28 - April 1, 2011, New York, USA. - S.I, 2011. - P.718-720.

List of publications

- [481] Lotov K.V. Self-organization of long proton beams in plasma wakefield accelerator. // Laser and Plasma Accelerator Workshop 2011, Shanghai & Wuzhen, China, 2011. - Abstracts.
- [482] Muggli P., Lotov K., Yakimenko V., Assmann R., Zimmermann F., Pukhov A., Silva L.O., Fonseca R.A., Lopes N.C., Russo C., Vieira J.M., Huang C., Caldwell A., Xia G., An W., Joshi C., Lu W., Mori W. Proton-driven plasma wakefield acceleration experiments at CERN. // Intern. Particle Accelerator Conference 2011 (IPAC-2011), September 4-9, 2011, San Sebastian, Spain. - Abstracts, p.WEPZ037.
- [483] Borodin A.V., Esaulkov M.N., Frolov A.A., Kotelnikov I.A., Kuritsin I.I., Shkurinov A.P. Generation and detection of broadband THz radiation from the optical breakdown plasma: from basic mechanisms to applications. // 19th Intern. Conf. on Advanced Laser Technologies (ALT'11), Golden Sands, Bulgaria, 3 - 8 Sept. 2011: Book of Abstr. - Sofia: Inst. of Electronics Bulg. Acad. of Sciences, 2011. - P.100.
- [484] Borodin A.V., Esaulkov M.N., Kuricyn I.I., Kotelnikov I.A., Shkurinov A.P. Role of the field ionization in generation and polarization of broadband terahertz radiation from optical breakdown plasma. // 19th Intern. Conference on Advanced Laser Technologies (ALT'11), Golden Sands, Bulgaria, 3 - 8 Sept. 2011. - Book of Abstracts. - Sofia: Inst. of Electronics Bulg. Acad. of Sciences, 2011.- P.145-146.
- [485] Taskaev S., Aleynik V., Burdakov A., Ivanov A., Kuznetsov A., Makarov A., Sorokin I. Vacuum-insulation tandem accelerator for boron neutron capture therapy [Electronic resource]. // 2nd Intern. Particle Accelerators Conference (IPAC 2011), 4-9 September, 2011, Kursaal, San Sebastian, Spain. - S.1, 2011. - P.3615-3617.
- [486] Aleynik V., Bayanov B., Burdakov A., Kasatov D., Makarov A., Sinitskiy S., Schudlo I. and Taskaev S. New technical solution for using the time-of-flight technique to measure neutron spectra. The front edge of BNCT development. // Proc. of 6th Young Researchers Boron Neutron Capture Therapy Meeting, December 4-8, 2011, Hsinchu, Taiwan (R.O.C). - P.152-157.
- [487] Listopad A., Davydenko V., Ivanov A., Mishagin V., Coenen J., Savkin V., Shulzhenko G. and Uhlemann R. Use of focusing multi-slit ion optical system at the diagnostic neutral beam injector RUDI. // 14th Intern. Conference on Ion Sources, 12-16 September, 2011, Giardini Naxos, Italy. - Book of Abstracts, p.96.
- [488] Deichuli P.P., Davydenko V.I., Belov V.P., Gorbovsky A.I., Dranichnikov A.N., Ivanov A.A., Sorokin A.V., Mishagin V.V., Abdrashitov A.G., Kolmogorov V.V., Kondakov A.A. Commissioning of heating neutral beams for COMPASS-D tokamak. // 14th Intern. Conference on Ion Sources, 12-16 September, 2011, Giardini Naxos, Italy. - Book of Abstracts, p.183.
- [489] Davydenko V.I., Ivanov A.A. Thermal regime of LaB6 of plasma linear device. // 2nd Intern. Workshop on Plasma Material Interaction Facilities for Fusion Research, 19-21 September 2011, Jülich, Germany. [http://www2.fz-juelich.de/ief/ief-4/_pmif/abstracts/pdf/Abstracts_PMIF_2011.pdf].
- [490] Bagryansky P.A., Beklemishev A.D., Korzhavina M.S., Lizunov A.A., Maximov V.V., Murakhtin S.V., Pinzhenin E.I., Prikhodko V.V., Pushkareva A.N., Savkin V.Ya., Soldatkina E.I., Solomakhin A.L., Zaytsev K.V. Review of plasma confinement research recent results in gas dynamic trap. // Proc. of XXXVIII Intern. Conference on Plasma Physics and Controlled Fusion, 14-18 February, 2011, Zvenigorod, 2011. - M.: PLASMAIOFAN, 2011. P.35.
- [491] Solomakhin A.L., Bagryansky P.A., Ivanenko S.V., Kvashnin A.N., Kovalenko Yu.V., Lizunov A.A., Savkin V.Ya., Khilchenko A.D. Multichannel dispersion interferometer for plasma density and position control. // Proc. of XXXVIII Intern. Conference on Plasma Physics and Controlled Fusion, 14-18 February, 2011, Zvenigorod, 2011. - M.: PLASMAIOFAN, 2011. P.40.
- [492] Lvovsky A.V., Bagryansky P.A., Kvashnin A.N., Prikhodko V.V., Solomakhin A.L., Khilchenko A.D. Investigations of plasma confinement in gas dynamic trap in experiments with compact mirror by dispersion interferometer. // Proc. of XXXVIII Intern. Conference on Plasma Physics and Controlled Fusion, 14-18 February, 2011, Zvenigorod, 2011. - M.: PLASMAIOFAN, 2011. P.51.
- [493] M.: PLASMAIOFAN, 2011. - P.51. [Electronic resource. - M.: PLASMAIOFAN, 2011.- C.MC 1 - 02]. Pinzhenin E.I., Ivanov A.A., Maksimov V.V., Pchelyakov O.P. Direct registration of low energy particles by array of avalanche diodes for GDT device. // Proc. of XXXVIII Intern. Conference on Plasma Physics and Controlled Fusion, 14-18 February, 2011, Zvenigorod, 2011. - M.: PLASMAIOFAN, 2011. P.48.
- [494] Brednikhin S.A., Kardapoltsev L.V., Ivanov A.A., Prikhodko V.V., Frolov S.A., Yurov D.V. Plasma and neutron processes simulation in a fission-fusion system based on the gas dynamic trap. Proc. of XXXVIII Intern. Conference on Plasma Physics and Controlled Fusion, 14-18 February, 2011, Zvenigorod, 2011. - M.: PLASMAIOFAN, 2011. P.36.

- [495] Brednikhin S.A., Frolov S.A., Lezhnin S.I., Anikeev A.V., Bagryansky P.A., Prikhodko V.V., Yurov D.V. Simulations of fusion-fission system with neutron source based on gas dynamic trap. // Proc. of 7th Intern. Scientific and Technical Conference «Ensuring the Safety of Nuclear Power Plants with WWR», 17-20 May, 2011, Podolsk. - P.31.
- [496] Yurov D.V., Ivanov A.A., Prikhodko V.V. Zero-dimensional model of GDT plasma evolution. // Proc. of XI National School-Conference of Young Scientists “Actual Problems of Thermophysics and Physical Hydrodynamics”, 17-19 October, 2010, Novosibirsk. - P.108.
- [497] Anikeev A.V. Optimization of the neutron source based on gas dynamic trap for transmutation of radioactive wastes. // Proc. of XXXVIII Intern. Conference on Plasma Physics and Controlled Fusion, 14-18 February, 2011, Zvenigorod, 2011. - M.: PLASMAIOFAN, 2011. P.99.
- [498] 228. Gaspodchikov E.D., Shalashov A.G., Smolyakova O.B., Bagryansky P.A., Malygin V.I., Gorbatushkov V.N., Amirov V.Kh., Thumm M. Design of auxiliary ECR heating system for the Gas Dynamic Trap. // Strong microwaves and terahertz waves: sources and applications. // 8th Intern. Workshop, July 9-16, 2011, Nizhny Novgorod - St.-Peterburg, Russia.- Nizhny Novgorod: Inst. of Appl. Physics RAS, 2011. - P.175-176.
- [499] Bagryansky P.A., Gaspodchikov E.D., Shalashov A.G., Smolyakova O.B., Malygin V.I., Gorbatushkov V, Amirov V.Kh., Thumm M. Design of auxiliary ECR heating system for the Gas Dynamic Trap. // 38th EPS Conference on Plasma Physics, June 27 - July 1, 2011, Strasbourg, France. - Report PD2.04.
- [500] Anikeev A.V. Optimisation of the neutron source based on Gas Dynamic Trap for transmutation of radioactive wastes. // Workshop on Fusion for Neutrons and Sub-Critical Nuclear Fission (FUNFI), September 12-15, 2011, Villa Monastero Varenna (Lecco), Italy,1 (to be publ.: Proc. of the Am. Inst. of Physics).
- [501] Anikeev A.V. The Plasma neutron source as a driver in a sub-critical reactor. // Abstracts of Humboldt-Kolleg “Cooperation and Networking of Universities and Research Institutes - study by doing research”, 6-10 October 2011, Chieinru, Moldova.
- [502] Sklyarov V.F., Burdakov A.V., Kuznetsov S.A., Mekler K.I., Polosatkin S.V., Postupaev V.V., Rovenskikh A.F., Sinitsky S.L. Investigation of emission of submillimeter electromagnetic radiation at turbulent plasma heating on the GOL-3 device. // Abstracts of XXXVIII Intern. (Zvenigorod) Conference on Plasma Physics and Controlled Fusion, 14-18 February, 2011, Zvenigorod. - M.: PLASMAIOFAN, 2011. - P.49.
- [503] Ivantsivsky M.V., Burdakov A.V., Vyacheslavov L.N., Ivanov I.A., Kasatov A.A., Makarov M.A., Mekler K.I., Polosatkin S.V., Popov S.S., Postupaev V.V., Rovenskikh A.F., Sinitsky S.L. Measuring of dynamics of non Maxwellian electron distribution function in different space points on the GOL-3 device. // Abstracts of XXXVIII International (Zvenigorod) Conference on Plasma Physics and Controlled Fusion, 14-18 February, 2011, Zvenigorod. - M.: PLASMAIOFAN, 2011. - P.53. [Electronic resource. M.: PLASMAIOFAN, 2011. - C.MC 1 - 07].
- [504] Sorokina N.V., Burdakov A.V., Makarov M.A., Mekler K.I., Polosatkin S.V., Postupaev V.V., Rovenskikh A.F., Sinitsky S.L. Investigation of space structure of plasma with image-VUV-spectrometer on the GOL-3 device. // Abstracts of XXXVIII International (Zvenigorod) Conference on Plasma Physics and Controlled Fusion, 14-18 February, 2011, Zvenigorod. - M.: PLASMAIOFAN, 2011. - P.67.
- [505] Kasatov A.A., Popov S.S. A pulse light source with smooth spectrum on the base of Xe-lamp for calibrating of Thomson scattering system. // Abstracts of XXXVIII International (Zvenigorod) Conference on Plasma Physics and Controlled Fusion, February, 14-18 February, 2011, Zvenigorod. - P.214. [Electronic resource. M.: PLASMAIOFAN, 2011. - C.MC 1 - 16].
- [506] Kurkuchekov V.V., Kandaurov I.V., Trunev Yu.A. The multi-aperture source of the electron beam with arc plasma emitter in external magnetic field. // Abstracts of XXXVIII International (Zvenigorod) Conference on Plasma Physics and Controlled Fusion, 14-18 February, 2011, Zvenigorod. - P.321. [Electronic resource. M.: PLASMAIOFAN, 2011. - C.TC 1 - 05].
- [507] Astrelin V.T., Bagryansky P.A., Karpov I.E., Trunev Yu.A. Characteristics of electron beam generated in the diode with flow of anode plasma incidences onto thermo emission cathode. // Abstracts of XXXVIII International (Zvenigorod) Conference on Plasma Physics and Controlled Fusion, 14-18 February, 2011, Zvenigorod. - P.324. - [Electronic resource: M.: PLASMAIOFAN, 2011.- C.TC 1 - 08].
- [508] Avrorov A.P., Astrelin V.T., Burdakov A.V., Bykov P.V., Derevyankin G.E., Kandaurov I.V., Kapitonov V.A., Kurkuchekov V.V., Rovenskikh A.F., Sinitsky S.L., Trunev Yu.A., Yarovoi V.A. Prototype of the source of

List of publications

- submillisecond electron beam for the GOL-3 facility. // Abstracts of XXXVIII International (Zvenigorod) Conference on Plasma Physics and Controlled Fusion, 4-18 February, Zvenigorod. - P.325. [Electronic resource: M.: PLASMAIOFAN, 2011. - C.TC 1 - 09].
- [509] Puryga E.A., Ivanova A.A., Ivanenko S.B., Kvashnin A.N., Khilchenko A.D., Vyacheslavov L.N. System of data registration for laser scattering diagnostics. // Abstracts of XIV All-Russia Conference "High Temperature Plasma Diagnostics", Zvenigorod. - P.54-56.
- [510] Sulyaev Yu.S., Puryga E.A., Khilchenko A.D., Kvashnin A.N., Polosatkin S.V., Rovenskikh A.F., Burdakov A.V. Universal spectrometer of thermonuclear neutrons based on registrator ADC 12500. // Abstracts of XIV All-Russia Conference «High Temperature Plasma Diagnostics», Zvenigorod. - P.69-70.
- [511] Sudnikov A.V., Burdakov A.V., Ivanov I.A., Makarov M.A., Mekler K.I., Rovenskikh A.F., Polosatkin S.V., Postupaev V.V., Sinitsky S.L., Sorokina N.V., Sulyaev Yu.S. Investigation of MHD plasma activity in the GOL-3 device. // Abstracts of XIV All-Russia Conference «High Temperature Plasma Diagnostics», Zvenigorod. - P.115-116.
- [512] Burmasov V.S., Bobylev V.B., Ivanova A.A., Ivanenko S.V., Kasatov A.A., Kasatov L.A., Kruglyakov E.P., Kuklin K.N., Popov S.S., Postupaev V.V., Puryga E.A., Rovenskikh A.F., Sklyarov V.F. IR- interferometer for investigation of sub thermonuclear plasma in multimirror trap GOL-3. // Abstracts of XIV All-Russia Conference "High Temperature Plasma Diagnostics", Zvenigorod. - P.115-116.
- [513] Zubarev D.V., Kvashnin A.N., Moiseev D.V., Postupaev V.V., Rovenskikh A.F., Khilchenko A.D., Khilchenko V.A.. System of synchronization of GOL-3 device. // Abstracts of XIV All-Russia Conference «High Temperature Plasma Diagnostics», Zvenigorod. - P.121-122.
- [514] Arzhannikov A.V., Burdakov A.V., Vyacheslavov L.N., Ivantsivsky M.V., Kasatov A.A., Kuznetsov S.A., Makarov M.A., Mekler K.I., Postupaev V.V., Popov S.S., Sinitsky S.L., Sklyarov V.F. Diagnostic complex for investigation of subTHz-emission generation at beam-plasma interactions on the GOL-3 device. // Abstracts of XIV All-Russia Conference "High Temperature Plasma Diagnostics", Zvenigorod. - P.125-126.
- [515] Beklemishev A., Astrelin V., Burdakov A., Ivanov A., Ivanov I., Postupaev V., Sinitsky S. Fusion prospects of axisymmetric traps with multi-mirror end plugs. // 38th EPS Conference on Plasma Physics, June 27 - July 1, 2011, Strasbourg, France. - [<http://ocs.ciemat.es/EPS2011PAP/pdf/P1.045.pdf>].
- [516] Arzhannikov A.V., Burdakov A.V., Burmasov V.S., Kalinin P.V., Ivanov I.A., Kuznetsov S.A., Makarov M.A., Mekler K.I., Polosatkin S.V., Postupaev V.V., Popov S.S., Rovenskikh A.F., Sinitsky S.L., Sklyarov V.F., Stepanov V.D., Sulyaev Yu.S., Thumm M.K.A., Vyacheslavov L.N.. Subterahertz electromagnetic emission of strong turbulent plasma driven by high current REB. // 38th EPS Conference on Plasma Physics, June 27 - July 1, 2011, Strasbourg, France. - [<http://ocs.ciemat.es/EPS2011PAP/pdf/P2.006.pdf>].
- [517] A.V. Burdakov, A.A. Ivanov, E.P. Kruglyakov. Study of high-b plasma stability and transverse losses in the experiments on modern magnetic mirrors. // 38th EPS Conference on Plasma Physics, Strasbourg, June 27 - July 1, 2011, France. - [<http://ocs.ciemat.es/EPS2011PAP/pdf/P2.011.pdf>].
- [518] Liu D., Almagri A.F., Anderson J.K., Belykh V.V., Chapman B.E., Davydenko V.I., Deichuli P., Hartog D.J., Den, Eilerman S., Fiksel G., Forest C.B., Ivanov A.A., Nornberg M.D., Polosatkin S.V., Sarff J.S., Stupishin N. and Waksman J. Fast ion confinement studies in the MST reversed field pinch. // 38th EPS Conference on Plasma Physics, June 27 - July 1, 2011, Strasbourg, France. - P.2.101. [<http://ocs.ciemat.es/EPS2011PAP/pdf/P2.101.pdf>].
- [519] Postupaev V.V., Arzhannikov A.V., Burdakov A.V., Ivanov I.A., Ivantsivsky M.V., Kuklin K.N., Kuznetsov S.A., Makarov M.A., Mekler K.I., Polosatkin S.V., Popov S.S., Rovenskikh A.F., Sinitsky S.L., Sklyarov V.F., Sorokina N.V., Sudnikov A.V., and Vyacheslavov L.N. Advances in plasma heating and confinement in multiple-mirror trap GOL-3. // 38th EPS Conference on Plasma Physics, June 27 - July 1, 2011, Strasbourg, France. - [<http://ocs.ciemat.es/EPS2011PAP/pdf/P5.044.pdf>].
- [520] Ginzburg N.S., Peskov N.Yu., Sergeev A.S., Arzhannikov A.V., Kalinin P.V., Sinitsky S.L., Thumm M. Powerful masers and lasers with two-dimensional distributed feedback. // Strong microwaves and terahertz waves: sources and applications: 8th Intern. Workshop, Nizhny Novgorod - St.-Peterburg, Russia, July 9 - 16, 2011: Proc. - Nizhny Novgorod: Inst. of Appl. Physics RAS, 2011. - P.57-58.
- [521] Kalinin P.V., Arzhannikov A.V., Kuznetsov S.A., Sinitsky S.L., Ginzburg N.S., Malkin A.M., Peskov N.Yu., Sergeev A.S., Zaslavsky V.Yu. Short-wavelength tunable Bragg reflectors based on coupling of propagating and

- cutoff waves: modeling and «cold» tests. // Strong microwaves and terahertz waves: sources and applications: 8th Intern. Workshop, Nizhny Novgorod - St.-Peterburg, Russia, July 9 - 16, 2011: Proc. - Nizhny Novgorod: Inst. of Appl. Physics RAS, 2011. - P.86-87.
- [522] Sinitsky S.L., Arzhannikov A.V., Astrelin V.T., Ginzburg N.S., Kalinin P.V., Kuznetsov S.A., Peskov N.Yu., Sergeev A.S., Stepanov V.D., Thumm M., Zaslavsky V.Yu. Planar FEM driven by two microsecond sheet E-beams. // Strong microwaves and terahertz waves: sources and applications: 8th Intern. Workshop, Nizhny Novgorod - St.-Peterburg, Russia, July 9 - 16, 2011: Proc. - Nizhny Novgorod: Inst. of Appl. Physics RAS, 2011.- P.131-132.
- [523] Arzhannikov A.V., Burdakov A.V., Kalinin P.V., Kuznetsov S.A., Makarov M.A., Mekler K.I., Polosatkin S.V., Postupaev V.V., Rovenskikh A.F., Sinitsky S.L., Sklyarov V.F., Stepanov V.D., Sulyaev Yu.S., Thumm M.K.A., Vyacheslavov L.N. Subterahertz generation by magnetized plasma at two-stream instability of high current 1-MeV REB. // Strong microwaves and terahertz waves: sources and applications: 8th Intern. Workshop, Nizhny Novgorod - St.-Peterburg, Russia, July 9 - 16, 2011: Proc. - Nizhny Novgorod: Inst. of Appl. Physics RAS, 2011.- P.209-210.
- [524] Kuznetsov S.A., Arzhannikov A.V., Paulish A.G., Gelfand A.V., Lazorskiy P.A. Ultra-thin submillimeter wave absorbers for bolometric applications. // Strong microwaves and terahertz waves: sources and applications: 8th Intern. Workshop, Nizhny Novgorod - St.-Peterburg, Russia, July 9 - 16, 2011: Proc. - Nizhny Novgorod: Inst. of Appl. Physics RAS, 2011.- P.237-238.
- [525] Sadykov V.A., Usoltsev V.V., Eremeev N.F., Salanov A.N., Mezentseva N.V., Kharlamova T.S., Pavlova S.N., Bobrenok O.F., Ulihin A.S., Uvarov N.F., Smorygo O.L., Arzhannikov A.V., Kalinin P.V., Thumm M.K.A. Microwave sintering of functional layers in design of planar solid oxide fuel cells. // Strong microwaves and terahertz waves: sources and applications: 8th Intern. Workshop, Nizhny Novgorod - St.-Peterburg, Russia, July 9 - 16, 2011: Proc. - Nizhny Novgorod: Inst. of Appl. Physics RAS, 2011. - P.295-296.
- [526] Beklemishev A., Anikeev A., Burdakov A., Ivanov A., I. Ivanov, Postupaev V and Sinitsky S. GDT-based Neutron Source with Multiple-mirror End Plugs. // Workshop on Fusion for Neutrons and Sub-Critical Nuclear Fission, Villa Monastero Varenna (Lecco), Italy, September 12-15, 2011 (to be published in Proc. of the Am. Inst. of Physics).
- [527] Liu D., Almagri A.F., Anderson J.K., Den Hartog D.J., Eilerman S., Nornberg M.D., Sarff J.S., Waksman J., Belykh V.V., Deichuli P., Davydenko V.I., Ivanov A.A., Polosatkin S., Stupishin N. Studies of fast ion confinement in the MST Reversed Field Pinch. // Bulletin of the American Physical Society. - DPP11 Meeting of the American Physical Society, BAPS.2011.DPP.PO4.3, 2011.
- [528] S. Eilerman, A.F. Almagri, J.K. Anderson, D.J. Den Hartog, S.T.A. Kumar, D. Liu, R.M. Magee, M.D. Nornberg, J. Waksman, V.V. Belykh, S. Polosatkin, J. Titus, G. Fiksel. Time-resolved measurements of the energetic ion distribution in MST. // Bulletin of the American Physical Society. - DPP11 Meeting of the American Physical Society, BAPS.2011.DPP.BP9.80, 2011.
- [529] S. Korepanov, R. Klary, A. Smirnov, S. Dettrick, S. Murakhtin, S. Polotkin. Fast ion diagnostics for the C-2 experiment. // Bulletin of the American Physical Society. - DPP11 Meeting of the American Physical Society, BAPS.2011.DPP.CP9.99, 2011.
- [530] Liu D., Almagri A.F., Anderson J.K., Chapman B.E., Davydenko V.I., Deichuli P., Hartog D.J. Den, Eilerman S., Fiksel G., Forest C.B., Ivanov A.A., Koliner J., Nornberg M.D., Polosatkin S.V., Sarff J.S., Stupishin N. and Waksman J. Neutral beam injection experiments in the MST reversed field pinch. // 12th IAEA Technical Meeting on Energetic Particles and Instabilities. - P.123.
- [531] Shoshin A.A., Burdakov A.V., Ivanov I.A., Kuklin K.N., Polosatkin S.V., Postupaev V.V. Spectroscopic study of interaction of high power plasma stream with lithium-carbon composites at multimirror trap GOL-3. // 2nd International Workshop on Plasma Material Interaction Facilities for Fusion Research (PMIF 2011), 19-21 September 2011, Jülich, Germany. - Abstracts, P.20.
- [532] Sudnikov A.V., Burdakov A.V., Ivanov I.A., Makarov M.A., Mekler K.I., Rovenskikh A.F., Polosatkin S.V., Postupaev V.V., Sinitsky S.L. Investigation of MHD dynamics of plasma under heating with relativistic electron beam. // Abstracts of V All-Russian Young Conference «Innovative Aspects of Fundamental Investigations on Actual Problems of Physics», Moscow. - P.103.
- [533] Bryazgin A.A. Industrial HF electron accelerators (ILU). // Report on 8th International Conference “Nuclear and Radiation Physics”, 20-23 September, 2011, Almaty, Kazakhstan.

List of publications

- [534] Burdakov A.V., Kalinin P.V., Kuznetsov S.A., Makarov M.A., Mekler K.I., Popov A.A., Postupaev V.V., Rovenskikh A.F., Sinitsky S.L., Sklyarov V.F., Stepanov V.D., Sulyaev Yu.S., Thumm M.K.A., Vyacheslavov L.N. Emission of submm-radiation by strong turbulent plasma at two-stream instability of high current REB. // 36th Intern. Conf. on Infrared, Millimeter, and Terahertz Waves (IRMMW - THz 2011), Houston, Texas, USA, Oct. 2 - 7, 2011. - Electronic resource S.I, 2011: [www.irmmw-thz2011.org, W5.45].
- [535] Arzhannikov A.V., Kalinin P.V., Sinitsky S.L., Kuznetsov S.A., Ginzburg N.S., Malkin A.M., Peskov N.Yu., Sergeev A.S., Zaslavsky V.Yu., Thumm M. Advanced Bragg structures based on coupling of propagating and cutoff waves: modeling and «cold» tests. // 36th Intern. Conf. on Infrared, Millimeter, and Terahertz Waves, Houston, Texas, USA, Oct. 2-7, 2011. - [www.irmmw-thz2011.org, Tu5.24].
- [536] Arzhannikov A.V., Astrelin V.T., Ginzburg N.S., Kalinin P.V., Kuznetsov S.A., Peskov N.Yu., Sergeev A.S., Sinitsky S.L., Stepanov V.D., Thumm M., Zaslavsky V.Yu. Generation of MW radiation in a two-channel planar FEM with combined electrodynamic system. // 36th International Conference on Infrared, Millimeter, and Terahertz Waves (IRMMW-THz 2011), Houston, Texas, Oct. 2-7, 2011. - [www.irmmw-thz2011.org, Tu5.25].
- [537] Ginzburg N.S., Peskov N.Yu., Sergeev A.S., Arzhannikov A.V., Kalinin P.V., Sinitsky S.L., Thumm M. Powerful masers and lasers with two-dimensional distributed feedback. // 36th Intern. Conf. on Infrared, Millimeter, and Terahertz Waves (IRMMW - THz 2011), Houston, Texas, USA, Oct. 2 - 7, 2011. - USA, 2011. - [www.irmmw-thz2011.org, Tu5.25].
- [538] Polosatkin S., Belykh V., Clary R., Davydenko V., Fiksel G., Ivanov A., Kapitonov V., Liu D., Mishagin V., and Tiunov M. Neutral particle analyzer for studies of fast ion population in plasma. // 2nd Intern. Conference: Frontiers in Diagnostic Technologies, 28-30 November 2011, Frascati, Italy. - N65, 2011.
- [539] Sulyaev Yu.S., Puryga E.A., Khilchenko A.D., Kvashnin A.N., Polosatkin S.V., Rovenskikh A.F., Burdakov A.V., Grishnyaev E.S. Multi-purpose fast neutron spectrum analyzer with real-time signal processing. // 2nd Intern. Conference: Frontiers in Diagnostic Technologies, 28 - 30 November 2011, Frascati, Italy. - N74, 2011.
- [540] Popov S.S., Burdakov A.V., Ivantsivsky M.V., Kasatov A.A., Polosatkin S.V., Postupaev V.V., Vyacheslavov L.N. 68-Two-pulse Thomson Scattering System for measurements of fast fluctuation of electron density profile in multi-mirror trap GOL-3. // 2nd Intern. Conference: in Diagnostic Technologies, 28 - 30 November 2011, Frascati, Italy. - N68, 2011.
- [541] Biagini M.E., SuperB Accelerators Team, Bogomiagkov A., Koop I., Levichev E., Nikitin S., Okunev I., Piminov P., Sinyatkin S., Shatilov D., Vobly P., et al. The SuperB project: accelerator status and R&D [Electronic resource]. // 2nd Intern. Particle Accelerators Conf., (IPAC 2011), 4 - 9 Sept. 2011, Kursaal, San Sebastian, Spain. - Proc. S.I, 2011. - P.3684-3686. [THPZ003].
- [542] Rogovsky Yu.A., Berkaev D.E., Koop I., Kyrpotin A.N., Nesterenko I., Romanov A.L., Shatunov Y.M., Shwartz D.B. Beam measurements with visible synchrotron light at VEPP-2000 collider. // [Electronic resource] 10th European Workshop on Beam Diagnostics and Instrumentation for Particle Accelerators (DIPAC 2011), Hamburg, Germany, May 16 - 18, 2011. - Proc.- S.I, 2011.- P.140-142.
- [543] Rogovsky Yu.A., Nesterenko I. Calibration of the electrostatic beam position monitors for VEPP-2000. // [Electronic resource] DIPAC 2011: 10th European Workshop on Beam Diagnostics and Instrumentation for Particle Accelerators (DIPAC 2011), Hamburg, Germany, May 16 - 18, 2011. - Proc.- S.I, S.a. 2011.- P.68-70.
- [544] Rogovsky Yu.A., Bekhtenev E.A. Pickup beam measurement system at the VEPP-2000 collider. E.A. // [Electronic resource] 10th European Workshop on Beam Diagnostics and Instrumentation for Particle Accelerators (DIPAC 2011), Hamburg, Germany, May 16 - 18, 2011. - Proc.- S.I, 2011.- P.203-205.
- [545] Zolkin T., Koop I., Perevedentsev E. Numerical studies of non-linear dynamics in BEP [Electronic resource]. // 2011 Particle Accelerator Conference, March 28 - April 1, 2011, New York, USA. - S.I, 2011. - P.1636-1638.
- [546] Berkaev D., Kirpotin A., Koop I., Lysenko A., Nesterenko I., Otboev A., Perevedentsev E., Rogovsky Y., Romanov A., Shatunov P., Shatunov Yu., Shwartz D., Skrinisky A., Zemlyansky I. Round beam collisions at VEPP-2000 [Electronic resource]. // 2nd Intern. Particle Accelerators Conf., (IPAC 2011), 4-9 September, 2011, Kursaal, San Sebastian, Spain. - S.I, 2011. - P.1926-1930.
- [547] Shatunov Yu.M. Round beam collisions at VEPP-2000. Proc. of Intern. Workshop on e+e- collisions from Phi to Psi (PHIPSI11), September 19 - 24, 2011, BINP, Novosibirsk.
- [548] Koop I.A. Experimental and theoretical research of beam-beam effects of round beams. // IV Cherenkov Readings, Moscow, 12 April, 2011.

- [549] Koop I.A. Experimental research of beam-beam effects of round beams. // IX Intern. Seminar on the Problems of Charged Particles Accelerators in Memory of Prof. V.P. Sarantsev, 17-21 September, 2011, Alushta, Ukraine.
- [550] Kuksanov N.K., Fadeev S.N., Golubenko Yu.I., Kogut D.A., Korchagin A.I., Lavruhin A.V., Nemytov P.I., Salimov R.A., Domarov E.V. Development of ELV-type accelerators and increasing of its exploitation parameters. // XXII Intern. Seminar for Charged Particle Accelerator, 22-28 September, 2011, Alushta, Ukraine.
- [551] Golubenko Yu.I., Kogut D.A., Kuksanov N.K., Nemytov P.I., Chakin I.V. Support for measurement of parameters of ELV-type accelerators and technological equipment. // XXII Intern. Seminar for Charged Particle Accelerator, 22-28 September, 2011, Alushta, Ukraine.
- [552] L.A. Merzhievsky, E.V. Karpov, E.O. Avseyko, M.V. Korobeinikov, E.A. Shtarklev. Effect of ionizing radiation on the mechanical properties of polymers (Electronic resource) // Proc. of V Russian Scientific-Technical Conference "Resource and Diagnostics of Materials and Structures" April 25-29, 2011, Yekaterinburg. - IES UB RAS, 2011. [CD ROM, gate-fold "Publications"].
- [553] L.A. Merzhievsky, E.V. Karpov, E.O. Avseyko, M.V. Korobeinikov, E.A. Shtarklev. Effect of ionizing radiation on the mechanical properties of polymers. // Proc. of V Russian Scientific-Technical Conference «Resource and Diagnostics of Materials and Structures» April 25-29, 2011, Yekaterinburg. - P.99.
- [554] L.A. Merzhievsky, E.V. Karpov, E.O. Avseyko, M.V. Korobeinikov, E.A. Shtarklev. Effect of ionizing radiation on the mechanical properties of polymers. // Proc. of II All-Russian Conference "Deformation and fracture of heterogeneous media and structures", October 10-14, 2011, Novosibirsk.
- [555] Auslender V.L., Bryazgin A.A., Bezuglov V.V., Chernov K.N., Cheskidov V.G., Faktorovich B.L., Kuznetsov G.I., Korobeynikov M.V., Lukin A.N., Makarov I.G., Ostreiko G.N., Panfilov A.D., Podobaev V.S., Serdobintsev G.V., Shtarklev E.N., Sidorov A.V., Tarnetsky V.V., Tiunov M.A., Tkachenko V.O. Last results on 7.5-10 MeV High-Power accelerator ILU-14 for E-beam and X-ray processing. Poster paper. // Intern. Meeting on Radiation Processing (IMRP 2011), 13-16 June, 2011, Montreal, Canada.

Preprints 2011

- 1 V.E. Blinov, V.G. Prisekin. Investigation of cathode aging and cathode wires autoemission in drift chambers. // Novosibirsk. - 24p, Preprint: INP 2011-2 (in Russian).
- 2 G.S. Villevald, T.A. Vsevolozhskaya V.N. Karasyuk, G.I. Silvestrov. The measurements results in the proton synchrotron elements. // Novosibirsk. - 20p, Preprint: INP 2011-5 (in Russian).
- 3 D.E. Berkaev, E.V. Bykov, V.P. Kozak, S.V. Tararyshkin. Time to Digital Converter. // Novosibirsk. - 16p, Preprint: INP 2011-6 (in Russian).
- 4 Averbukh, Yu.M. Glukhovchenko, V.V. Petrov, V.G. Cheskidov. Synchrotron B-4 accelerating system. // Novosibirsk. - 23p, Preprint: INP 2011-7 (in Russian).
- 5 V.V. Petrov, Yu.A. Pupkov. BINP testing of radiation resistance of the materials used for production of accelerator magnetic systems. Novosibirsk. - 28p, Preprint: Budker INP 2011-13.
- 6 I.I. Pupkov, Max Klein, Davide Tommasini. Models of dipole magnets for LHeC, CERN, made of grain-oriented electric steel. // Novosibirsk. - 26p, Preprint: INP 2011-14 (in Russian).
- 7 S.Yu. Taskaev. Neutron Capture Therapy: Accelerator Concept. I. Accelerators (review). // Novosibirsk. - 21p, Preprint: INP 2011-15 (in Russian).
- 8 O.I. Lavric, N.A. Moor, B.P.Tolochko, G.N. Kulipanov. Proteins involved in DNA repair as the most essential subjects of X-ray studies. // Novosibirsk. - 15p, Preprint: INP 2011-17 (in Russian).
- 9 V.I. Aleinik, A.A. Ivanov, A.S. Kuznetsov, I.N. Sorokin. Static high-voltage processes at the work of ccelerator-tandem with vacuum insulation. // Novosibirsk. - 14p, Preprint: INP 2011-19 (in Russian).
- 10 A.N. Aleshaev, V.V. Anashin, O.V. Anchugov, A.M. Batrakov, E.A. Bekhtenev, V.E. Blinov, A.V. Bogomyagkov, A.E. Bondar, D.B. Burenkov, S.P. Vasichev, V.F. Veremeenko, S.A. Glukhov, Yu.M. Glukhovchenko, O.P. Gordeev,

- V.N. Erokhov, V.N. Zhilich, A.I. Zhmaka, A.N. Zhuravlev, E.I. Zinin, V.V. Kaminsky, V.I. Kaplin, S.E. Karnev, G.V. Karpov, V.A. Kiselev, V.R. Kozak, G.I. Kuznetsov, G.N. Kulipanov, E.A. Kuper, G.Ya. Kurkin, E.B. Levichev, V.R. Mamkin, A.S. Medvedko, O.I. Meshkov, A.I. Mikaiylov, L.A. Mironenko, S.I. Mishnev, I.I. Morozov, N.Yu. Muchnoi, V.V. Neifeld, S.A. Nikitin, I.B. Nikolaev, D.M. Nikolenko, V.K. Ovchar, I.N. Okunev, A.P. Onuchin, V.V. Oreshonok, V.N. Osipov, V.V. Petrov, V.M. Petrov, P.A. Piminov, O.A. Plotnikova, A.V. Polyansky, Yu.A. Pupkov, V.V. Repkov, E.A. Rotov, V.K. Sandyrev, V.V. Svischev, I.K. Sedlyarov, A.N. Selivanov, E.A. Simonov, S.V. Sinyatkin, A.N. Skrinsky, V.V. Smalyuk, E. Starostina, D.P. Sukhanov, S.V. Tararyshkin, Yu.A. Tikhonov, D.K. Toporkov, G.M. Tumaikin, I.F. Utyupin, M.G. Fedotov, A.D. Khilchenko, V.M. Tsukanov, V.P. Cherepanov, I.N. Churkin, A.G. Shamov, D.N. Shatilov, D.A. Shvedov, S.V. Shiyankov, E.I. Shubin. VEPP-4 Accelerator Facilities. // Novosibirsk. - Preprint: INP 2011-20 (in Russian).
- 11 P.M. Astigeevich, M.N. Achasov, V.M. Aulchenko, A.Yu. Barnyakov, K.I. Beloborodov, A.V. Berdyugin, D.E. Berkaev, V.E. Blinov, A.G. Bogdanchikov, A.A. Botov, D.A. Bukin, A.V. Vasiljev, V.M. Vesenev, E.A. Vlasenko, V.B. Golubev, K.A. Grevtsov, T.V. Dimova, V.P. Druzhinin, I.M. Zemliansky, L.V. Kardapoltsev, A.N. Kirpotin, I.A. Koop, D.P. Kovrizhin, A.A. Korol, S.V. Koshuba, E.A. Kravchenko, A.Yu. Kulpin, A.P. Lysenko, K.A. Martin, I.N. Nesterenko, A.E. Obrazovsky, A.P. Onuchin, E.V. Pakhtusova, E.A. Perevedentsev, Yu.A. Rogovsky, A.L. Romanov, S.I. Serednyakov, Z.K. Silagadze, A.A. Sirotkin, K.Yu. Skovpen, A.N. Skrinsky, I.K. Surin, A.I. Tekutiev, Yu.A. Tikhonov, Yu.V. Usov, A.G. Kharlamov, P.Yu. Shatunov, Yu.M. Shatunov, D.A. Shtol, A.N. Shukaev, D.B. Shwartz. Beginning of the experiments with SND detector. at the collider VEPP-2000. // Novosibirsk. - Preprint: INP 2011-21 (40p) (in Russian).
- 12 M.G. Kozlov, A.V. Reznichenko, V.S. Fadin. NLO Impact-factor for one gluon production in the multi-Regge kinematics. // Novosibirsk. - 35p, Preprint: INP 2011-23 (in Russian).
- 13 M.G. Kozlov, A.V. Reznichenko, V.S. Fadin. Check of the gluon reggeization condition in the next-to-leading order. Gluon part. // Novosibirsk. - 31p, Preprint: INP 2011-24 (in Russian).
- 14 S.V. Miginsky. An Effective Numerical Scheme for Parabolic Partial Differential Equations. // Novosibirsk. - 14p, Preprint: Budker INP 2011-25.
- 15 V.S. Fadin, R. Fiore, A.V. Grabovsky, A. Papa. Transfer of gauge invariant operators from complete to Möbius representation and vice versa. // Novosibirsk. - 20p, Preprint: Budker INP 2011-27.
- 16 V.V. Anashin, S.V. Khrushchev, V.E. Panchenko, K.V. Zolotarev. Beryllium absorber of SR from 8.5 T superconducting bending magnet of 2.2 GeV / 1 A storage ring. // Novosibirsk. - 15p, Preprint: INP 2011-29 (in Russian).
- 17 A.E. Bondar, A.O. Poluektov, V.S. Vorobyev. Quantum correlations of $D^0\bar{D}^0$ studies of CP-violation of B- and D-mesons. Novosibirsk. - 38p, Preprint: INP 2011-30 (in Russian).
- * * *
- 18 A.G. Grozin, A.V. Kotikov. HQET heavy-heavy vertex diagram with two velocities. // arXiv:1106.3912 [hep-ph].
- 19 Zhiron O.V., Shepelyansky D.L. Wigner crystal in snaked nanochannels: outlook. // Proc. of ECRYS-2011, August 15-27, Cargese, France. E-print: arXiv:1110.1812v1 [cond-mat.str-el] (2011);
- 20 Zhiron O.V., Shepelyansky D.L. Wigner crystal in snaked nanochannels. // E-print: arXiv:1102.1277v1 [cond-mat.mes-hall] (2011).
- 21 V. Lotov. Optimum angle for side injection of electrons into linear plasma wakefields. // E-print: arXiv:1109.6081 [physics.acc-ph].
- 22 A. Caldwell, K.V. Lotov. Plasma Wakefield Acceleration with a Modulated Proton Bunch. // E-print: arXiv:1105.1292 [physics.acc-ph].
- 23 A.S. Arakcheev, K.V. Lotov. Analytical model of brittle destruction based on hypothesis of scale similarity. // E-print: arXiv:1105.1928 [physics.plasm-ph].
- 24 A. Pukhov, N. Kumar, T. Tuckmantel, A. Upadhyay, K. Lotov, P. Muggli, V. Khudik, C. Siemon, and G. Shvets. Phase velocity and particle injection in a self-modulated proton-driven plasma wakefield accelerator. // E-print: arXiv:1108.0071 [physics.plasm-ph].
- 25 K.Yu. Todyshev, V.V. Anashin, V.M. Aulchenko, E.M. Baldin, A.K. Barladyan, A.Yu. Barnyakov, M.Yu. Barnyakov, S.E. Baru, I.Yu. Basok, O.L. Beloborodova, A.E. Blinov, V.E. Blinov, A.V. Bobrov, V.S. Bobrovnikov, A.V.

- Bogomyagkov, A.E. Bondar, A.R. Buzykaev, S.I. Eidelman, D.N. Grigoriev, Yu.M. Glukhovchenko, V.V. Gulevich, D.V. Gusev, S.E. Karnaev, G.V. Karpov, S.V. Karpov, T.A. Kharlamova, V.A. Kiselev, V.V. Kolmogorov, S.A. Kononov, K.Yu. Kotov, E.A. Kravchenko, V.N. Kudryavtsev, V.F. Kulikov, G.Ya. Kurkin, E.A. Kuper, E.B. Levichev, D.A. Maksimov, V.M. Malyshev, A.L. Maslennikov, A.S. Medvedko, O.I. Meshkov, S.I. Mishnev, I.I. Morozov, N.Yu. Muchnoi, V.V. Neufeld, S.A. Nikitin, I.B. Nikolaev, I.N. Okunev, A.P. Onuchin, S.B. Oreshkin, I.O. Orlov, A.A. Osipov, S.V. Peleganchuk, S.G. Pivovarov, P.A. Piminov, V.V. Petrov, A.O. Poluektov, V.G. Prisekin, A.A. Ruban, V.K. Sandyrev, G.A. Savinov, A.G. Shamov, D.N. Shatilov, B.A. Shwartz, E.A. Simonov, S.V. Sinyatkin, A.N. Skrinsky, V.V. Smaluk, A.V. Sokolov, A.M. Sukharev, E.V. Starostina, A.A. Talyshev, V.A. Tayursky, V.I. Telnov, Yu.A. Tikhonov, G.M. Tumaikin, Yu.V. Usov, A.I. Vorobiov, A.N. Yushkov, V.N. Zhilich, V.V. Zhulanov, A.N. Zhuravlev. Search for narrow resonances in e^+e^- annihilation between 1.85 and 3.1 GeV with the KEDR Detector. // E-Print: arXiv:1107.2824 [hep-ex].
- 26 V.V. Anashin, V.M. Aulchenko, E.M. Baldin, A.K. Barladyan, A.Yu. Barnyakov, M.Yu. Barnyakov, S.E. Baru, I.Yu. Basok, I.V. Bedny, O.L. Beloborodova, A.E. Blinov, V.E. Blinov, A.V. Bobrov, V.S. Bobrovnikov, A.V. Bogomyagkov, A.E. Bondar, A.R. Buzykaev, S.I. Eidelman, Yu.M. Glukhovchenko, V.V. Gulevich, D.V. Gusev, S.E. Karnaev, G.V. Karpov, S.V. Karpov, T.A. Kharlamova, V.A. Kiselev, S.A. Kononov, K.Yu. Kotov, E.A. Kravchenko, V.F. Kulikov, G.Ya. Kurkin, E.A. Kuper, E.B. Levichev, D.A. Maksimov, V.M. Malyshev, A.L. Maslennikov, A.S. Medvedko, O.I. Meshkov, A.I. Milstein, S.I. Mishnev, I.I. Morozov, N.Yu. Muchnoi, V.V. Neufeld, S.A. Nikitin, I.B. Nikolaev, I.N. Okunev, A.P. Onuchin, S.B. Oreshkin, I.O. Orlov, A.A. Osipov, S.V. Peleganchuk, S. G. Pivovarov, P.A. Piminov, V.V. Petrov, A.O. Poluektov, D.N. Shatilov, G.E. Pospelov, V.G. Prisekin, A.A. Ruban, V.K. Sandyrev, G.A. Savinov, A.G. Shamov, B.A. Shwartz, E.A. Simonov, S.V. Sinyatkin, Yu.I. Skovpen, A.N. Skrinsky, V.V. Smaluk, A.V. Sokolov, A.M. Sukharev, E.V. Starostina, A.A. Talyshev, V.A. Tayursky, V.I. Telnov, Yu.A. Tikhonov, K.Yu. Todyshev, G.M. Tumaikin, Yu.V. Usov, A.I. Vorobiov, A.N. Yushkov, V.N. Zhilich, V.V. Zhulanov, A.N. Zhuravlev. Measurement of J/ψ leptonic width with the KEDR detector. // E-print: arXiv:1110.0328 [hep-ex], 2011.
- 27 K.Yu. Todyshev, V.V. Anashin, V.M. Aulchenko, E.M. Baldin, A.K. Barladyan, A.Yu. Barnyakov, M.Yu. Barnyakov, S.E. Baru, I.Yu. Basok, O.L. Beloborodova, A.E. Blinov, V.E. Blinov, A.V. Bobrov, V.S. Bobrovnikov, A.V. Bogomyagkov, A.E. Bondar, A.R. Buzykaev, S.I. Eidelman, D.N. Grigoriev, Yu.M. Glukhovchenko, V.V. Gulevich, D.V. Gusev, S.E. Karnaev, G.V. Karpov, S.V. Karpov, T.A. Kharlamova, V.A. Kiselev, V.V. Kolmogorov, S.A. Kononov, K.Yu. Kotov, E.A. Kravchenko, V.N. Kudryavtsev, V.F. Kulikov, G.Ya. Kurkin, E.A. Kuper, E.B. Levichev, D.A. Maksimov, V.M. Malyshev, A.L. Maslennikov, A.S. Medvedko, O.I. Meshkov, S.I. Mishnev, I.I. Morozov, N.Yu. Muchnoi, V.V. Neufeld, S.A. Nikitin, I.B. Nikolaev, I.N. Okunev, A.P. Onuchin, S.B. Oreshkin, I.O. Orlov, A.A. Osipov, S.V. Peleganchuk, S.G. Pivovarov, P.A. Piminov, V.V. Petrov, A.O. Poluektov, V.G. Prisekin, A.A. Ruban, V.K. Sandyrev, G.A. Savinov, A.G. Shamov, D.N. Shatilov, B.A. Shwartz, E.A. Simonov, S.V. Sinyatkin, A.N. Skrinsky, V.V. Smaluk, A.V. Sokolov, A.M. Sukharev, E.V. Starostina, A.A. Talyshev, V.A. Tayursky, V.I. Telnov, Yu.A. Tikhonov, G.M. Tumaikin, Yu.V. Usov, A.I. Vorobiov, A.N. Yushkov, V.N. Zhilich, V.V. Zhulanov, A.N. Zhuravlev. Measurement of $\psi(3770)$ parameters. // E-print: arXiv:1109.4205 [hep-ex]. 2011.
- 28 K.Yu. Todyshev, V.V. Anashin, V.M. Aulchenko, E.M. Baldin, A.K. Barladyan, A.Yu. Barnyakov, M.Yu. Barnyakov, S.E. Baru, I.Yu. Basok, O.L. Beloborodova, A.E. Blinov, V.E. Blinov, A.V. Bobrov, V.S. Bobrovnikov, A.V. Bogomyagkov, A.E. Bondar, A.R. Buzykaev, S.I. Eidelman, D.N. Grigoriev, Yu.M. Glukhovchenko, V.V. Gulevich, D.V. Gusev, S.E. Karnaev, G.V. Karpov, S.V. Karpov, T.A. Kharlamova, V.A. Kiselev, V.V. Kolmogorov, S.A. Kononov, K.Yu. Kotov, E.A. Kravchenko, V.N. Kudryavtsev, V.F. Kulikov, G.Ya. Kurkin, E.A. Kuper, E.B. Levichev, D.A. Maksimov, V.M. Malyshev, A.L. Maslennikov, A.S. Medvedko, O.I. Meshkov, S.I. Mishnev, I.I. Morozov, N.Yu. Muchnoi, V.V. Neufeld, S.A. Nikitin, I.B. Nikolaev, I.N. Okunev, A.P. Onuchin, S.B. Oreshkin, I.O. Orlov, A.A. Osipov, S.V. Peleganchuk, S.G. Pivovarov, P.A. Piminov, V.V. Petrov, A.O. Poluektov, V.G. Prisekin, A.A. Ruban, V.K. Sandyrev, G.A. Savinov, A.G. Shamov, D.N. Shatilov, B.A. Shwartz, E.A. Simonov, S.V. Sinyatkin, A.N. Skrinsky, V.V. Smaluk, A.V. Sokolov, A.M. Sukharev, E.V. Starostina, A.A. Talyshev, V.A. Tayursky, V.I. Telnov, Yu.A. Tikhonov, G.M. Tumaikin, Yu.V. Usov, A.I. Vorobiov, A.N. Yushkov, V.N. Zhilich, V.V. Zhulanov, A.N. Zhuravlev. Measurement of main parameters of the $\psi(2S)$ resonance. // E-print: arXiv:1109.4215 [hep-ex]. Sep. 2011.
- 29 Bondar A., Buzulutskov A., Grebenuk A. **Infrared scintillation yield in gaseous and liquid argon.** // E-print: arXiv:1102.1825, 2011.
- 30 Bondar A., Buzulutskov A., Grebenuk A., Shemyakina E., Sokolov A., Akimov D., Alexandrov I., Breskin A. On the low-temperature performances of THGEM and THGEM/G-APD multipliers in gaseous and two-phase Xe. // E-print: arXiv:1103.6126, 2011.

- 31 Buzulutskov A., Advances in Cryogenic Avalanche Detectors (review). // [E-print: arXiv:1112.6153, 2011].
- 32 Aaij R., Bobrov A., Bondar A., Eidelman S., Krokovny, Poluektov A., Shekhtman L., et al. (LHCb Collab.). Observation of J/ψ pair production in pp collisions at $\sqrt{s}=7$ TeV. // [arXiv:1109.0963].
- 33 Aaij R., Bobrov A., Bondar A., Eidelman S., Krokovny, Poluektov A., Shekhtman L., et al. (LHCb Collab.). Search for the lepton number violating decays $B^+ \rightarrow \pi^- \mu^+ \mu^+$ and $B^+ \rightarrow K^- \mu^+ \mu^+$. // [arXiv:1110.0730].
- 34 Aaij R., Bobrov A., Bondar A., Eidelman S., Krokovny, Poluektov A., Shekhtman L., et al. (LHCb Collab.). Absolute luminosity measurements with the LHCb detector at the LHC. // [arXiv:1110.2866].
- 35 R. Aaij., A. Bobrov, A. Bondar, S. Eidelman, P. Krokovny, A. Poluektov, L. Shekhtman, et al. (By LHCb Collab.). Measurement of the effective $B_s \rightarrow K^+ K^-$ lifetime. // [arXiv:1111.0521].
- 36 R. Aaij., A. Bobrov, A. Bondar, S. Eidelman, P. Krokovny, A. Poluektov, L. Shekhtman, et al. (By LHCb Collab.). Measurement of b hadron production fractions in 7 TeV pp collisions. // [arXiv:1111.2357].
- 37 R. Aaij., A. Bobrov, A. Bondar, S. Eidelman, P. Krokovny, A. Poluektov, L. Shekhtman, et al. (By LHCb Collab.). First observation of the decay $B_s^0 \rightarrow K^{*0} K^{*0}$. // [arXiv:1111.4183].
- 38 R. Aaij., A. Bobrov, A. Bondar, S. Eidelman, P. Krokovny, A. Poluektov, L. Shekhtman, et al. (By LHCb Collab.). Evidence for CP violation in time-integrated $D^0 \rightarrow h^- h^+$ decay rates. // [arXiv:1112.0938].
- 39 Aaij R., Bobrov A., Bondar A., Eidelman S., Krokovny, Poluektov A., Shekhtman L., et al. (LHCb Collab.). Measurement of the CP violating phase ϕ_s in $\bar{B}_s^0 \rightarrow J/\psi f_0(980)$. // [arXiv:1112.3056].
- 40 Aaij R., Bobrov A., Bondar A., Eidelman S., Krokovny, Poluektov A., Shekhtman L., et al. (LHCb Collab.). Measurement of the CP-violating phase ϕ_s in the decay $B_s \rightarrow J/\psi \phi$. // [arXiv:1112.3183].
- 41 Aaij R., Bobrov A., Bondar A., Eidelman S., Krokovny, Poluektov A., Shekhtman L., et al. (LHCb Collab.). Differential branching fraction and angular analysis of the decay $B^0 \rightarrow K^{*0} \mu^+ \mu^-$. // [arXiv:1112.3515].
- 42 Aaij R., Bobrov A., Bondar A., Eidelman S., Krokovny, Poluektov A., Shekhtman L., et al. (LHCb Collab.). Measurement of the $B_s^0 - \bar{B}_s^0$ oscillation frequency Δm_s in $B_s^0 \rightarrow D_s^- (3) \pi$ decays. // [arXiv:1112.4311].
- 43 Aaij R., Bobrov A., Bondar A., Eidelman S., Krokovny, Poluektov A., Shekhtman L., et al. (LHCb Collab.). Measurement of charged particle multiplicities in pp collisions at $\sqrt{s} = 7$ TeV. // [arXiv:1112.4592].
- 44 Aaij R., Bobrov A., Bondar A., Eidelman S., Krokovny, Poluektov A., Shekhtman L., et al. (LHCb Collab.). First observation of $B_s \rightarrow J/\psi f_2'(1525)$ in $J/\psi K^+ K^-$ final states. // [arXiv:1112.4695].
- 45 Aaij R., Bobrov A., Bondar A., Eidelman S., Krokovny, Poluektov A., Shekhtman L., et al. (LHCb Collab.). Measurement of mixing and CP violation parameters in two-body charm decays. // [arXiv:1112.4698].
- 46 Aaij R., Bobrov A., Bondar A., Eidelman S., Krokovny, Poluektov A., Shekhtman L., et al. (LHCb Collab.). Measurement of b-hadron masses. // [arXiv:1112.4896].
- 47 Aaij R., Bobrov A., Bondar A., Eidelman S., Krokovny, Poluektov A., Shekhtman L., et al. (LHCb Collab.). Observation of $X(3872)$ production in pp collisions at $\sqrt{s} = 7$ TeV. // [arXiv:1112.5310].
- 48 Bodenstern S., Eidelman S., et al. Confronting electron-positron annihilation into hadrons with QCD: an operator product expansion analysis. // [arXiv:1110.2026], accepted by JHEP.
- 49 Adachi I., Aulchenko V., Arinstein K., Bondar A., Eidelman S., Epifanov D., Gabyshev N., Garmash A., Krokovny P., Kuzmin A., Matvienko D., Poluektov A., Shebalin V., Shwartz B., Usov Yu., Vinokurova A., Zhilich V., Zhulanov V., Zyukova O., et al. (Belle Collab.). First observation of the P-wave spin-singlet bottomonium states $h_b(1P)$ and $h_b(2P)$. // [arXiv:1103.3419], accepted by Phys. Rev. Lett.
- 50 Staric M., Aulchenko V., Arinstein K., Bondar A., Eidelman S., Epifanov D., Gabyshev N., Garmash A., Krokovny P., Kuzmin A., Matvienko D., Poluektov A., Shebalin V., Shwartz B., Usov Yu., Vinokurova A., Zhilich V., Zhulanov V., Zyukova O., et al. (Belle Collab.). Search for CP violation in D meson decays to $\phi \pi^+$. [arXiv:1110.0694], accepted by Phys. Rev. Lett.
- 51 Hoi C.-T., Aulchenko V., Arinstein K., Bondar A., Eidelman S., Epifanov D., Gabyshev N., Garmash A., Krokovny P., Kuzmin A., Matvienko D., Poluektov A., Shebalin V., Shwartz B., Usov Yu., Vinokurova A., Zhilich V., Zhulanov V., Zyukova O., et al. (Belle Collab.). Evidence for direct CP violation in $B^\pm \rightarrow \eta h^\pm$ and observation of B^0

→ ηK^0 . // [arXiv:1110.2000], accepted by Phys. Rev. Lett.

- 52 Bondar A., Aulchenko V., Arinstein K., Eidelman S., Epifanov D., Gabyshev N, Garmash A., Krovovny P., Kuzmin A., Matvienko D., Poluektov A., Shebalin V., Shwartz B., Usov Yu., Vinokurova A., Zhilich V., Zhulanov V., Zyukova O., et al. (Belle Collab.). Observation of two charged bottomonium-like resonances in ($5S$) decays. // [arXiv:1110.2251], accepted by Phys. Rev. Lett.
- 53 Aad G., ..., Beloborodova O., Bobrovnikov V.S., Bogdanchikov A., Kazanin V.A., Kolachev G.M., Korol A., Malyshev V., Maslennikov A.L., Maximov D.A., Orlov I., Peleganchuk S.V., Skovpen K., Schamov A.G., Soukharev A., Talyshev A., Tikhonov Yu.A., Zaytsev A., et al. (ATLAS Collab.). Jet energy measurement with the ATLAS detector in proton-proton collisions at $\sqrt{s} = 7$ TeV. // arxiv.org 1201.5595v1 [hep-ex]. Submitted to Eur. Phys. J. C, 9 p.
- 54 Aad G., ..., Anisenkov A., Beloborodova O., Bobrovnikov V.S., Bogdanchikov A., Kazanin V.A., Kolachev G.M., Korol A., Malyshev V., Maslennikov A.L., Maximov D.A., Orlov I., Peleganchuk S.V., Skovpen K., Schamov A.G., Soukharev A., Talyshev A., Tikhonov Yu.A., Zaytsev A., et al. (ATLAS Collab.). Measurement of inclusive jet and dijet production in pp collisions at $\sqrt{s} = 7$ TeV using the ATLAS detector. // arxiv.org 1112.6297 [hep-ex]. Submitted to Phys. Lett. B, 41p.
- 55 Aad G., ..., Anisenkov A., Beloborodova O., Bobrovnikov V.S., Bogdanchikov A., Kazanin V.A., Kolachev G.M., Korol A., Malyshev V., Maslennikov A.L., Maximov D.A., Orlov I., Peleganchuk S.V., Skovpen K., Schamov A.G., Soukharev A., Talyshev A., Tikhonov Yu.A., Zaytsev A., et al. (ATLAS Collab.). Search for heavy vector-like quarks coupling to light generations in proton-proton collisions at $\sqrt{s} = 7$ TeV with the ATLAS detector. // arXiv:1112.5755 [hep-ex]. Submitted to Phys. Lett. B, 7p.
- 56 Aad G., ..., Anisenkov A., Beloborodova O., Bobrovnikov V.S., Bogdanchikov A., Kazanin V.A., Kolachev G.M., Korol A., Malyshev V., Maslennikov A.L., Maximov D.A., Orlov I., Peleganchuk S.V., Skovpen K., Schamov A.G., Soukharev A., Talyshev A., Tikhonov Yu.A., Zaytsev A., et al. (ATLAS Collab.). Observation of a new χ_b state in radiative transitions to $Y(1S)$ and $Y(2S)$ at ATLAS. // arXiv:1112.5154v4 [hep-ex]. ccepted by Phys. Rev. Lett, 4p.
- 57 Aad G., ..., Anisenkov A., Beloborodova O., Bobrovnikov V.S., Bogdanchikov A., Kazanin V.A., Kolachev G.M., Korol A., Malyshev V., Maslennikov A.L., Maximov D.A., Orlov I., Peleganchuk S.V., Skovpen K., Schamov A.G., Soukharev A., Talyshev A., Tikhonov Yu.A., Zaytsev A., et al. (ATLAS Collab.). Search for first generation scalar leptoquarks in pp collisions at $\sqrt{s} = 7$ TeV with the ATLAS detector. // arxiv.org 1112.4828 [hep-ex]; Phys. Lett. B, 709 (2012) 158-176, 8p.
- 58 Aad G., ..., Anisenkov A., Beloborodova O., Bobrovnikov V.S., Bogdanchikov A., Kazanin V.A., Kolachev G.M., Korol A., Malyshev V., Maslennikov A.L., Maximov D.A., Orlov I., Peleganchuk S.V., Skovpen K., Schamov A.G., Soukharev A., Talyshev A., Tikhonov Yu.A., Zaytsev A., et al. (ATLAS Collab.). **Measurement of D^* meson production in jets from pp Collisions at $\sqrt{s} = 7$ TeV with the ATLAS Detector.** // arxiv.org 1112.4432.
- 59 Aad G., ..., Anisenkov A., Beloborodova O., Bobrovnikov V.S., Bogdanchikov A., Kazanin V.A., Kolachev G.M., Korol A., Malyshev V., Maslennikov A.L., Maximov D.A., Orlov I., Peleganchuk S.V., Skovpen K., Schamov A.G., Soukharev A., Talyshev A., Tikhonov Yu.A., Zaytsev A., et al. (ATLAS Collab.). Search for Scalar Bottom Pair Production with the ATLAS Detector in pp Collisions at $\sqrt{s} = 7$ TeV. // arxiv.org 1112.3832.
- 60 Aad G., ..., Anisenkov A., Beloborodova O., Bobrovnikov V.S., Bogdanchikov A., Kazanin V.A., Kolachev G.M., Korol A., Malyshev V., Maslennikov A.L., Maximov D.A., Orlov I., Peleganchuk S.V., Skovpen K., Schamov A.G., Soukharev A., Talyshev A., Tikhonov Yu.A., Zaytsev A., et al. (ATLAS Collab.). **Search for Production of Resonant States in the Photon-Jet Mass Distribution using pp Collisions at $\sqrt{s} = 7$ TeV collected by the ATLAS Detector.** // arxiv.org 1112.3580.
- 61 Aad G., ..., Anisenkov A., Beloborodova O., Bobrovnikov V.S., Bogdanchikov A., Kazanin V.A., Kolachev G.M., Korol A., Malyshev V., Maslennikov A.L., Maximov D.A., Orlov I., Peleganchuk S.V., Skovpen K., Schamov A.G., Soukharev A., Talyshev A., Tikhonov Yu.A., Zaytsev A., et al. (ATLAS Collab.). Search for the Higgs boson in the $H \rightarrow WW^{(*)} \rightarrow l\nu l\nu$ decay channel in pp collisions at $\sqrt{s} = 7$ TeV with the ATLAS detector. // arxiv.org 1112.2577.
- 62 Aad G., ..., Anisenkov A., Beloborodova O., Bobrovnikov V.S., Bogdanchikov A., Kazanin V.A., Kolachev G.M., Korol A., Malyshev V., Maslennikov A.L., Maximov D.A., Orlov I., Peleganchuk S.V., Skovpen K., Schamov A.G., Soukharev A., Talyshev A., Tikhonov Yu.A., Zaytsev A., et al. (ATLAS Collab.). **Search for Extra Dimensions Using Diphoton Events in 7 TeV Proton-Proton Collisions with the ATLAS Detector.** // arxiv.org 1112.2194.

- 63 Aad G., ..., Anisenkov A., Beloborodova O., Bobrovnikov V.S., Bogdanchikov A., Kazanin V.A., Kolachev G.M., Korol A., Malyshev V., Maslennikov A.L., Maximov D.A., Orlov I., Peleganchuk S.V., Skovpen K., Schamov A.G., Soukharev A., Talyshev A., Tikhonov Yu.A., Zaytsev A., et al. (ATLAS Collab.). Measurement of the WZ Production Cross Section and Limits on Anomalous Triple Gauge Couplings in Proton-Proton Collisions at $\sqrt{s} = 7$ TeV with the ATLAS Detector. // arxiv.org 1111.5570. Accepted by Phys. Lett. B, 6p.
- 64 Aad G., ..., Anisenkov A., Beloborodova O., Bobrovnikov V.S., Bogdanchikov A., Kazanin V.A., Kolachev G.M., Korol A., Malyshev V., Maslennikov A.L., Maximov D.A., Orlov I., Peleganchuk S.V., Skovpen K., Schamov A.G., Soukharev A., Talyshev A., Tikhonov Yu.A., Zaytsev A., et al. (ATLAS Collab.). Search for Diphoton Events with Large Missing Transverse Energy with 1 fb⁻¹ of 7 TeV Proton-Proton Collision Data with the ATLAS Detector. // arxiv.org 1111.4116. Accepted by Phys. Lett. B, 8p.
- 65 Aad G., ..., Anisenkov A., Beloborodova O., Bobrovnikov V.S., Bogdanchikov A., Kazanin V.A., Kolachev G.M., Korol A., Malyshev V., Maslennikov A.L., Maximov D.A., Orlov I., Peleganchuk S.V., Skovpen K., Schamov A.G., Soukharev A., Talyshev A., Tikhonov Yu.A., Zaytsev A., et al. (ATLAS Collab.). Search for strong gravity signatures in same-sign dimuon final states using the ATLAS detector at the LHC. // arxiv.org 1111.0080. Accepted by Phys. Lett. B, 38p.
- 66 Aad G., ..., Anisenkov A., Beloborodova O., Bobrovnikov V.S., Bogdanchikov A., Kazanin V.A., Kolachev G.M., Korol A., Malyshev V., Maslennikov A.L., Maximov D.A., Orlov I., Peleganchuk S.V., Skovpen K., Schamov A.G., Soukharev A., Talyshev A., Tikhonov Yu.A., Zaytsev A., et al. (ATLAS Collab.). Measurement of the production cross section for Z/gamma* in association with jets in pp collisions at $\sqrt{s} = 7$ TeV with the ATLAS Detector. // arxiv.org 1111.2690. Phys. Rev. D, 85 (2012) 032009, 48p.
- 67 Aad G., ..., Anisenkov A., Beloborodova O., Bobrovnikov V.S., Bogdanchikov A., Kazanin V.A., Kolachev G.M., Korol A., Malyshev V., Maslennikov A.L., Maximov D.A., Orlov I., Peleganchuk S.V., Skovpen K., Schamov A.G., Soukharev A., Talyshev A., Tikhonov Yu.A., Zaytsev A., et al. (ATLAS Collab.). Kshort and Lambda production in pp interactions at $\sqrt{s} = 0.9$ and 7 TeV measured with the ATLAS detector at the LHC. // arxiv.org 1111.1297. Phys. Rev. D, 85 (2012) 012001, 16p.
- 68 Aad G., ..., Anisenkov A., Beloborodova O., Bobrovnikov V.S., Bogdanchikov A., Kazanin V.A., Kolachev G.M., Korol A., Malyshev V., Maslennikov A.L., Maximov D.A., Orlov I., Peleganchuk S.V., Skovpen K., Schamov A.G., Soukharev A., Talyshev A., Tikhonov Yu.A., Zaytsev A., et al. (ATLAS Collab.). Searches for supersymmetry with the ATLAS detector using final states with two leptons and missing transverse momentum in $\sqrt{s} = 7$ TeV proton-proton collisions. // Phys. Lett. B, 709 (2012) 137-157, 10p. [arxiv.org 1110.6189].
- 69 Aad G., ..., Anisenkov A., Beloborodova O., Bobrovnikov V.S., Bogdanchikov A., Kazanin V.A., Kolachev G.M., Korol A., Malyshev V., Maslennikov A.L., Maximov D.A., Orlov I., Peleganchuk S.V., Skovpen K., Schamov A.G., Soukharev A., Talyshev A., Tikhonov Yu.A., Zaytsev A., et al. (ATLAS Collab.). A measurement of the material in the ATLAS inner detector using secondary hadronic interactions. // arxiv.org 1110.6191. JINST 7 (2012) P01013, 22p.
- 70 Aad G., ..., Anisenkov A., Beloborodova O., Bobrovnikov V.S., Bogdanchikov A., Kazanin V.A., Kolachev G.M., Korol A., Malyshev V., Maslennikov A.L., Maximov D.A., Orlov I., Peleganchuk S.V., Skovpen K., Schamov A.G., Soukharev A., Talyshev A., Tikhonov Yu.A., Zaytsev A., et al. (ATLAS Collab.). Measurement of the ZZ production cross section and limits on anomalous neutral triple gauge couplings in proton-proton collisions at $\sqrt{s} = 7$ TeV with the ATLAS detector. // arxiv.org 1110.5016. Phys. Rev. Lett., 108 (2012) 041804, 5p.
- 71 Aad G., ..., Anisenkov A., Beloborodova O., Bobrovnikov V.S., Bogdanchikov A., Kazanin V.A., Kolachev G.M., Korol A., Malyshev V., Maslennikov A.L., Maximov D.A., Orlov I., Peleganchuk S.V., Skovpen K., Schamov A.G., Soukharev A., Talyshev A., Tikhonov Yu.A., Zaytsev A., et al. (ATLAS Collab.). Electron performance measurements with the ATLAS detector using the 2010 LHC proton-proton collision data. // arxiv.org 1110.3174. Accepted by Eur. Phys. J. C, 45p.
- 72 Aad G., ..., Anisenkov A., Beloborodova O., Bobrovnikov V.S., Bogdanchikov A., Kazanin V.A., Kolachev G.M., Korol A., Malyshev V., Maslennikov A.L., Maximov D.A., Orlov I., Peleganchuk S.V., Skovpen K., Schamov A.G., Soukharev A., Talyshev A., Tikhonov Yu.A., Zaytsev A., et al. (ATLAS Collab.). Performance of the ATLAS Trigger System in 2010. // arxiv.org 1110.1530. Eur. Phys. J. C, 72 (2012) 1849, 50p.
- 73 Aad G., ..., Anisenkov A., Beloborodova O., Bobrovnikov V.S., Bogdanchikov A., Kazanin V.A., Kolachev G.M.,

- Korol A., Malyshev V., Maslennikov A.L., Maximov D.A., Orlov I., Peleganchuk S.V., Skovpen K., Schamov A.G., Soukharev A., Talyshev A., Tikhonov Yu.A., Zaytsev A., et al. (ATLAS Collab.). Search for squarks and gluinos using final states with jets and missing transverse momentum with the ATLAS detector in $\sqrt{s} = 7$ TeV proton-proton collisions. // arxiv.org 1109.6572. Accepted by Phys. Lett. B, 9p.
- 74 Aad G., ..., Anisenkov A., Beloborodova O., Bobrovnikov V.S., Bogdanchikov A., Kazanin V.A., Kolachev G.M., Korol A., Malyshev V., Maslennikov A.L., Maximov D.A., Orlov I., Peleganchuk S.V., Skovpen K., Schamov A.G., Soukharev A., Talyshev A., Tikhonov Yu.A., Zaytsev A., et al. (ATLAS Collab.). Search for supersymmetry in final states with jets, missing transverse momentum and one isolated lepton in $\sqrt{s} = 7$ TeV pp collisions using 1 fb-1 of ATLAS data. // arxiv.org 1109.6606. Phys. Rev. D, 85 (2012) 012006, 31p.
- 75 Aad G., ATLAS Collab., Beloborodova O., Bobrovnikov V.S., Bogdanchikov A., Kazanin V.A., Kolachev G.M., Korol A., Malyshev V., Maslennikov A.L., Maximov D.A., Orlov I., Peleganchuk S.V., Shamov A.G., Skovpen K., Soukharev A., Talyshev A., Tikhonov Y.A., Zaytsev A., et al. Measurement of the inclusive W^{+-} and Z/γ cross sections in the electron and muon decay channels in pp collisions at $\sqrt{s} = 7$ TeV with the ATLAS detector. // arxiv.org 1109.5141. Accepted by Phys. Rev. D, 43p.
- 76 Aad G., ATLAS Collab., Beloborodova O., Bobrovnikov V.S., Bogdanchikov A., Kazanin V.A., Kolachev G.M., Korol A., Malyshev V., Maslennikov A.L., Maximov D.A., Orlov I., Peleganchuk S.V., Shamov A.G., Skovpen K., Soukharev A., Talyshev A., Tikhonov Y.A., Zaytsev A., et al. Search for new phenomena in $t\bar{t}$ events with large missing transverse momentum in proton-proton collisions at $\sqrt{s} = 7$ TeV with the ATLAS detector. // arxiv.org 1109.4725. Phys. Rev. Lett., 108 (2012) 041805, 5p.
- 77 Aad G., ATLAS Collab., Beloborodova O., Bobrovnikov V.S., Bogdanchikov A., Kazanin V.A., Kolachev G.M., Korol A., Malyshev V., Maslennikov A.L., Maximov D.A., Orlov I., Peleganchuk S.V., Shamov A.G., Skovpen K., Soukharev A., Talyshev A., Tikhonov Y.A., Zaytsev A., et al. Search for displaced vertices arising from decays of new heavy particles in 7 TeV pp collisions at ATLAS. // arxiv.org 1109.2242. Phys. Lett. B, 707 (2012) 478-496, 8p.
- 78 Aad G., ATLAS Collab., Beloborodova O., Bobrovnikov V.S., Bogdanchikov A., Kazanin V.A., Kolachev G.M., Korol A., Malyshev V., Maslennikov A.L., Maximov D.A., Orlov I., Peleganchuk S.V., Shamov A.G., Skovpen K., Soukharev A., Talyshev A., Tikhonov Y.A., Zaytsev A., et al. Measurement of the cross section for the production of a W boson in association with b-jets in pp collisions at $\sqrt{s} = 7$ TeV with the ATLAS detector. // arxiv.org 1109.1470. Phys. Lett. B, 707 (2012) 418-437, 10p.
- 79 Aad G., ATLAS Collab., Beloborodova O., Bobrovnikov V.S., Bogdanchikov A., Kazanin V.A., Kolachev G.M., Korol A., Malyshev V., Maslennikov A.L., Maximov D.A., Orlov I., Peleganchuk S.V., Shamov A.G., Skovpen K., Soukharev A., Talyshev A., Tikhonov Y.A., Zaytsev A., et al. Measurement of the cross-section for b-jets produced in association with a Z boson at $\sqrt{s} = 7$ TeV with the ATLAS detector. // arxiv.org 1109.1403. Phys. Lett. B, 706 (2012) 295-313, 8p.
- 80 Aad G., ATLAS Collab., Beloborodova O., Bobrovnikov V.S., Bogdanchikov A., Kazanin V.A., Kolachev G.M., Korol A., Malyshev V., Maslennikov A.L., Maximov D.A., Orlov I., Peleganchuk S.V., Shamov A.G., Skovpen K., Soukharev A., Talyshev A., Tikhonov Y.A., Zaytsev A., et al. Measurements of the electron and muon inclusive cross-sections in proton-proton collisions at $\sqrt{s} = 7$ TeV with the ATLAS detector. // arxiv.org 1109.0525. Phys. Lett. B, 707 (2012) 438-458, 25p.
- 81 Aad G., ATLAS Collab., Beloborodova O., Bobrovnikov V.S., Bogdanchikov A., Kazanin V.A., Kolachev G.M., Korol A., Malyshev V., Maslennikov A.L., Maximov D.A., Orlov I., Peleganchuk S.V., Shamov A.G., Skovpen K., Soukharev A., Talyshev A., Tikhonov Y.A., Zaytsev A., et al. Search for new physics in the dijet mass distribution using 1 fb-1 of pp Collision Data at $\sqrt{s} = 7$ TeV collected by the ATLAS Detector. // arxiv.org 1108.6311. Phys. Lett. B, 708 (2012) 37-54, 7p.
- 82 Aad G., ATLAS Collab., Beloborodova O., Bobrovnikov V.S., Bogdanchikov A., Kazanin V.A., Kolachev G.M., Korol A., Malyshev V., Maslennikov A.L., Maximov D.A., Orlov I., Peleganchuk S.V., Shamov A.G., Skovpen K., Soukharev A., Talyshev A., Tikhonov Y.A., Zaytsev A., et al. Measurement of the transverse momentum distribution of W Bosons in pp collisions at $\sqrt{s} = 7$ TeV with the ATLAS Detector. // arxiv.org 1108.6308. Phys. Rev. D, 85 (2012) 012005, 36p.
- 83 Aad G., ATLAS Collab., Beloborodova O., Bobrovnikov V.S., Bogdanchikov A., Kazanin V.A., Kolachev G.M., Korol A., Malyshev V., Maslennikov A.L., Maximov D.A., Orlov I., Peleganchuk S.V., Shamov A.G., Skovpen K., Soukharev A., Talyshev A., Tikhonov Y.A., Zaytsev A., et al. Measurement of the centrality dependence of the

- charged particle pseudorapidity distribution in lead-lead collisions at $\sqrt{s} = 2.76$ TeV with the ATLAS detector. // arxiv.org/1108.6027. Accepted by Phys. Lett. B, 17p.
- 84 Aad G., ATLAS Collab., Beloborodova O., Bobrovnikov V.S., Bogdanchikov A., Kazanin V.A., Kolachev G.M., Korol A., Malyshev V., Maslennikov A.L., Maximov D.A., Orlov I., Peleganchuk S.V., Shamov A.G., Skovpen K., Soukharev A., Talyshev A., Tikhonov Y.A., Zaytsev A., et al. Measurement of the pseudorapidity and transverse momentum dependence of the elliptic flow of charged particles in lead-lead collisions at $\sqrt{s_{NN}} = 2.76$ TeV with the ATLAS detector. // arxiv.org/1108.6018. Phys. Lett. B, 707 (2012) 330-348, 39p.
- 85 Aad G., ATLAS Collab., Beloborodova O., Bobrovnikov V.S., Bogdanchikov A., Kazanin V.A., Kolachev G.M., Korol A., Malyshev V., Maslennikov A.L., Maximov D.A., Orlov I., Peleganchuk S.V., Shamov A.G., Skovpen K., Soukharev A., Talyshev A., Tikhonov Y.A., Zaytsev A., et al. Performance of missing transverse momentum reconstruction in proton-proton collisions at 7 TeV with ATLAS. // arxiv.org/1108.5602. Eur. Phys. J. C, 72 (2012) 1844, 22p.
- 86 Aad G., ATLAS Collab., Beloborodova O., Bobrovnikov V.S., Bogdanchikov A., Kazanin V.A., Kolachev G.M., Korol A., Malyshev V., Maslennikov A.L., Maximov D.A., Orlov I., Peleganchuk S.V., Shamov A.G., Skovpen K., Soukharev A., Talyshev A., Tikhonov Y.A., Zaytsev A., et al. Search for a heavy Standard Model Higgs boson in the channel $H \rightarrow ZZ \rightarrow llqq$ using the ATLAS detector. // arxiv.org/1108.5064. Phys. Lett. B, 707 (2012) 27-45, 11p.
- 87 Aad G., ATLAS Collab., Beloborodova O., Bobrovnikov V.S., Bogdanchikov A., Kazanin V.A., Kolachev G.M., Korol A., Malyshev V., Maslennikov A.L., Maximov D.A., Orlov I., Peleganchuk S.V., Shamov A.G., Skovpen K., Soukharev A., Talyshev A., Tikhonov Y.A., Zaytsev A., et al. A measurement of the ratio of the W and Z cross sections with exactly one associated jet in pp collisions at $\sqrt{s} = 7$ TeV with ATLAS. // arxiv.org/1108.4908. Phys. Lett. B, 708 (2012) 221-240, 10p.
- 88 Aad G., ATLAS Collab., Beloborodova O., Bobrovnikov V.S., Bogdanchikov A., Kazanin V.A., Kolachev G.M., Korol A., Malyshev V., Maslennikov A.L., Maximov D.A., Orlov I., Peleganchuk S.V., Shamov A.G., Skovpen K., Soukharev A., Talyshev A., Tikhonov Y.A., Zaytsev A., et al. Measurement of the W to $\tau \nu$ cross section in pp collisions at $\sqrt{s} = 7$ TeV with the ATLAS experiment. // arxiv.org/1108.4101. Phys. Lett. B, 706 (2012) 276-294, 8p.
- 89 Aad G., ATLAS Collab., Beloborodova O., Bobrovnikov V.S., Bogdanchikov A., Kazanin V.A., Kolachev G.M., Korol A., Malyshev V., Maslennikov A.L., Maximov D.A., Orlov I., Peleganchuk S.V., Shamov A.G., Skovpen K., Soukharev A., Talyshev A., Tikhonov Y.A., Zaytsev A., et al. Measurement of the top quark pair production cross-section in the dilepton channel. // arxiv.org/1108.3699. Phys. Lett. B, 707 (2012) 459-477, 9p.
- 90 Aad G., ATLAS Collab., Beloborodova O., Bobrovnikov V.S., Bogdanchikov A., Kazanin V.A., Kolachev G.M., Korol A., Malyshev V., Maslennikov A.L., Maximov D.A., Orlov I., Peleganchuk S.V., Shamov A.G., Skovpen K., Soukharev A., Talyshev A., Tikhonov Y.A., Zaytsev A., et al. Measurement of isolated di-photon cross-section in pp collision at $\sqrt{s} = 7$ TeV with the ATLAS detector. // arxiv.org/1107.0581. Phys. Rev. D, 85 (2012) 012003, 15p.
- 91 A.V. Gramolin, J. Arrington, L.M. Barkov, V.F. Dmitriev, V.V. Gauzshtein, R.A. Golovin, R.J. Holt, V.V. Kaminsky, B.A. Lazarenko, S.I. Mishnev, N.Yu. Muchnoi, V.V. Neufelda, D.M. Nikolenko, I.A. Rachek, R.Sh. Sadykov, Yu.V. Shestakov, V.N. Stibunov, D.K. Toporkov, H. de Vries, S.A. Zevakov, V.N. Zhilich. Measurement of the two-photon exchange contribution in elastic ep scattering at VEPP-3. // arXiv: 1112.5369v1 [nucl-ex] 22 Dec 2011.
- 92 Brambilla N., Eidelman S., Levichev E., et al. Heavy quarkonium: progress, puzzles, and opportunities. // E-print: arXiv:1010.5827 [hep-ph].

Authorial papers 2011

1. BLINOV V.E. Measurement of mass of τ -lepton. // 01.04.16 - elementary particle physics, and atomic nuclear physics. Author. papers of thesis for the degree of doctor of phys.-math. science: Novosibirsk, 2011, BINP, SB RAS.
2. BATRAKOV A.M. Analog to digital electronics for control systems of experimental facilities. // 01.04.20 - physics of charged particle beams and accelerator techniques, Author. papers of thesis for the degree of doctor of technical science: Novosibirsk, 2011, BINP, SB RAS.
3. MUCHNOI N.Yu. Comptons scattering in the precise experiments on electron-positron colliders. // 01.04.20 - physics of charged particle beams and accelerator techniques, Author. papers of thesis for the degree of doctor of phys.-math. science: Novosibirsk, 2011, BINP, SB RAS.
4. NIKITIN S.A. Polarized beams in the precision experiments at the VEPP-4M collider with the KEDR detector. // 01.04.20 - physics of charged particle beams and accelerator techniques, Author. papers of thesis for the degree of doctor of phys.-math. science: Novosibirsk, 2011, BINP, SB RAS.
5. KUPER K.E. Development of the techniques of X-ray microscopy and tomography on the synchrotron radiation source of VEPP-3. // 01.04.01 – instruments and methods of experimental physics. Author. papers of thesis for the degree of candidate of phys.-math. science: Novosibirsk, 2011, BINP, SB RAS.
6. SHICHKOV D.S. The complex software for the production and control of accelerator magnetic elements. // 01.04.01 – instruments and methods of experimental physics. Author. papers of thesis for the degree of candidate of technical science: Novosibirsk, 2011, BINP, SB RAS.
7. GOLDENBERG B.G. Development of LIGA technology complex on VEPP-3 SR source. // 01.04.01 – instruments and methods of experimental physics. Author. papers of thesis for the degree of candidate of technical science: Novosibirsk, 2011, BINP, SB RAS.
8. ZHULANOV V.V. Registration hardware for study of detonation and shock wave processes using synchrotron radiation. 01.04.01 – instruments and methods of experimental physics. Author. papers of thesis for the degree of candidate of technical science: Novosibirsk, 2011, BINP, SB RAS.
9. NIKOLENKO A.D. Absolute calibration of detectors in the soft X-ray range using synchrotron radiation. // 01.04.01 – instruments and methods of experimental physics. Author. papers of thesis for the degree of candidate of phys.-math. science: Novosibirsk, 2011, BINP, SB RAS.
10. SHOSHIN A.A. Study of interaction of powerful hot-electron plasma stream with targets at the multimirror trap GOL-3. // 01.04.08 - physics of plasma, Author. papers of thesis for the degree of candidate of phys.-math. science: Novosibirsk, 2011, BINP, SB RAS
11. SHTOL L.A. Measurement of the cross section for the $e^+e^- \rightarrow \eta\pi^+\pi^-$ process in the energy range of $\sqrt{s}=1.04 - 1.38$ GeV with the detector SND on the VEPP-2M collider. // 01.04.16 - elementary particle physics, and atomic nuclear physics. Author. papers of thesis for the degree of candidate of phys.-math. science: Novosibirsk, 2011, BINP, SB RAS.
12. ROMANOV A.L. Tuning orbit and optics of VEPP-2000 storage ring using method of response matrixes. // 01.04.20 - physics of charged particle beams and accelerator techniques, Author. papers of thesis for the degree of candidate of phys.-math. science: Novosibirsk, 2011, BINP, SB RAS.
13. SHATUNOV P.Yu. Magnet structure of electron-positron storage ring VEPP-2000. // 01.04.20 - physics of charged particle beams and accelerator techniques, Author. papers of thesis for the degree of candidate of phys.-math. science: Novosibirsk, 2011, BINP, SB RAS.
14. LEVICHEV A.E. Parallel coupled accelerating structure with waveguide type exciting cavity. // 01.04.20 - physics of charged particle beams and accelerator techniques, Author. papers of thesis for the degree of candidate of phys.-math. science: Novosibirsk, 2011, BINP, SB RAS.
15. BUBLEI A.V. The electron coolers with variable beam profile of electron beam. // 01.04.20 - physics of charged particle beams and accelerator techniques, Author. papers of thesis for the degree of candidate of phys.-math. science: Novosibirsk, 2011, BINP, SB RAS.

Participation in conferences 2011

1. XXXVIII International Zvenigorod Conference on Plasma Physics and Controlled Fusion, Zvenigorod, 14 - 18 February, 2011.
2. VIII All-Russia Workshop on Radiophysics of Millimeter and Submillimeter Wavelengths, March 1 - 4, 2011, Nizhny Novgorod.
3. III Workshop on Nuclei and Mesoscopic Physics (WNMP11), March 5 - 9, East Lansing, USA.
4. 2011 Particle Accelerator Conference, March 28 - April 1, 2011, New York, USA.
5. Conference: Nuclear Physics in Astrophysics V, 3 - 8 April, 2011, Eilat, Israel.
6. V Russian Scientific-Technical Conference "Resource and Diagnostics of Materials and Structures" 25-29 April, 2011, Yekaterinburg, Russia.
7. IV Cherenkov Readings, 12 April, 2011, Moscow.
8. International Conference: XVI SuperB General Meeting, April, 2011, Frascati, Italy.
9. 20th IMEKO TS2 Symposium on Photonics in Measurement (20th ISPM), May 16 - 18, 2011, Linz, Austria.
10. 10th European Workshop on Beam Diagnostics and Instrumentation for Particle Accelerators (DIPAC 2011), May 16 - 18, Hamburg, Germany.
11. 7th International Scientific and Technical Conference «Ensuring the Safety of Nuclear Power Plants with WWR», 17 - 20 May, 2011, Podolsk, Russia.
12. 19th International Workshop on Photon-Photon Collisions (PHOTON2011), May 22 - 27, 2011, SPA, Belgium.
13. International Conference: XVII SuperB Workshop and Kick off Meeting, May - June, 2011, Elba, Italy.
14. International Workshop: Low x Meeting, June 3-7, 2011, Santiago de Compostela, Spain.
15. International Meeting on Radiation Processing (IMRP 2011), June 13 - 16, 2011, Montreal, Canada.
16. XIV International Conference on Hadron Spectroscopy (Hadron 2011), 13 - 17 June, 2011, Munich, Germany.
17. Ershov's Computer Science Conference «Science Intensive Applied Software», 27 June - 1 July, 2011, Academgorodok, Novosibirsk., Russia.
18. 38th EPS Conference on Plasma Physics, June 27 - July 1, 2011, Strasbourg, France.
19. Workshop «ALICE Upgrade Forum», June, 2011, CERN, Switzerland.
20. 8th International Workshop, July 9 - 16, 2011, Nizhny Novgorod - St.-Peterburg, Russia.
21. XXI Europhysics Conference on High Energy Physics (EPS-HEP2011), 21 - 27 July, 2011, Grenoble, Rhones Alpes, France.
22. PANIC 11, 24 - 29 July, 2011, MIT, USA.
23. VI Scientific Conference "Supercritical Fluids: Fundamentals, Technology and Innovation", July 2011, Listvyanka, Russia.
24. Workshop «Posipol 2011», August 28 - 30, 2011, IHEP, Beijing, China.
25. 2nd International Conference on Micro-Pattern Gaseous Detectors, 29 August - 1 September 2011, Kobe, Japan.
26. 8th RD51 Collaboration Meeting, 2 - 3 September 2011, Kobe, Japan.
27. 19th International Conference on Advanced Laser Technologies (ALT'11), 3 - 8 September, 2011, Golden Sands, Bulgaria.
28. 2nd International Particle Accelerators Conference (IPAC 2011), 4 - 9 September, 2011, Kursaal, San Sebastian, Spain.
29. 14th International Workshop on Advanced Computing and Analysis Techniques in Physics Research (ACAT2011), September 5 - 9, 2011, Uxbridge, London, UK.
30. GGI Workshop: High-Energy QCD after the Start of the LHC, September 11 - 30, 2011, Florence, Italy.
31. Workshop on Fusion for Neutrons and Sub-Critical Nuclear Fission, September 12 - 15, 2011, Villa Monastero Varenna (Lecco), Italy.

32. 14th International Conference on Ion Sources, 12 - 16 September, 2011, Giardini Naxos, Italy.
33. Workshop on Beam Cooling and Related Topics (COOL 11), September 12 - 16, 2011, Pansionat "Dubna", Alushta, Ukraine.
34. XIV International Workshop on Polarized Sources, Targets and Polarimetry, 12 - 16 September, 2011, St. Petersburg, Russia.
35. 2nd International Conference on the History of Computers and Informatics in the Soviet Union and Russian Federation (SORUCOM-2011), 12-16 September, Veliky Novgorod, Russia.
36. 22nd International Conference on Magnet Technology, 12 - 16 September, 2011, Marseille, France.
37. IX International Symposium (RREPS-11), September 12-16, 2011, Egham, United Kingdom.
38. IX International Seminar on the Problems of Charged Particles Accelerators in Memory of Prof. V.P. Sarantsev, 17 - 21 September, 2011, Alushta, Ukraine.
39. VII All-Russia. Conference on X-ray Analysis, 19-23 September, Novosibirsk, 2011, Russia.
40. X Russian Conference on Semiconductor Physics, 19 - 23 September, 2011, Nizhny Novgorod, Russia.
41. International Conference «From Phi to Psi», 19-24 September 2011, BINP SB RAS, Novosibirsk, Russia.
42. 2nd International School "Nanomaterials and Nanotechnology in Living Systems. Safety and Nanomedicine," 19 - 24 September, 2011, Moscow Region, Russia.
43. 2nd International Workshop on Plasma Material Interaction Facilities for Fusion Research (PMIF 2011), 19-21 September 2011, Jülich, Germany.
44. 8th International Conference "Nuclear and Radiation Physics", 20 -23 September, 2011, Almaty, Kazakhstan.
45. XXII International Seminar for Charged Particle Accelerator, 22-28 September, 2011, Alushta, Ukraine.
46. International Workshop on Future Linear Colliders (LCWS2011), 26 - 30 September, 2011, Granada, Spain.
47. International Conference "1st SuperB Collaboration Meeting", September, 2011, London, Great Britain.
48. 36th International Conference on Infrared Millimeter, and Terahertz Waves (IRMMW-THz 2011), October 2 - 7, 2011, Houston, Texas, USA.
49. 8th International Workshop of QWG, October 4-7, 2011, Darmstadt, Germany.
50. Humboldt-Kolleg "Cooperation and Networking of Universities and Research Institutes - study by doing research", 6-10 October 2011, Chieinru, Moldova.
51. 13th International Conference on Accelerator and Large Experimental Physics Control Systems (ICALEPCS 2011), 10 - 14 October, 2011, WTC Grenoble, France.
52. II All-Russian Conference "Deformation and fracture of heterogeneous media and structures", October 10-14, 2011, Novosibirsk, Russia.
53. XI National School-Conference of Young Scientists "Actual Problems of Thermophysics and Physical Hydrodynamics", 17-19 October, 2010, Novosibirsk, Russia.
54. XXII International Particle Accelerator Seminar. 27 - 28 October, 2011, BINP, Novosibirsk, Russia.
55. Experimental Seminar of BINP, October 2011, Novosibirsk, Russia.
56. VIII National Conference "X-ray, Synchrotron Radiation, Neutrons and Electrons for the Study of Nanosystems and Materials. Nano-Bio-Info-Cognitive Technology" (RSNE - NBIC 2011); All-Russia Workshop on the Application of X-rays for Materials Research, Moscow, November 14-18, 2011, Moscow:
57. Scientific Session-Conference of NP Section of DPN of RAS "Physics of Fundamental Interactions". 21 - 25 November, 2011, ITEP, Moscow.
58. 2nd International Conference: Frontiers in Diagnostic Technologies, 28 - 30 November 2011, Frascati, Italy.
59. 6th Young Researchers Boron Neutron Capture Therapy Meeting, December 4 - 8, 2011, Hsinchu, Taiwan.
60. XVIII Science-Technical Conference «Vacuum Technique and Technology», 2011, Sudak.
61. Laser and Plasma Accelerator Workshop 2011, Shanghai & Wuzhen, China, 2011.
62. 19th International Conference on Advanced Laser Technologies (ALT'11), Golden Sands, Bulgaria.

List of Collaboration Agreements between the Budker INP and Foreign Laboratories

№	1	2	3	4
Name of Laboratory	Title or Field of Collaboration	Dates	Principal Investigators	
1	<i>Daresbury (England)</i>	Generation and utilization of SR.	1977	<i>G. Kulipanov (INP); I. Munro (Daresbury)</i>
2	<i>BESSY (Germany)</i>	Development of the wigglers for BESSY-2.	1993	<i>A. Skrynsky, N. Mezentsev (INP); E. Jaeschke (BESSY)</i>
3	<i>Research Centre Rossendorf (Germany)</i>	Physical foundations of a plasma neutron source.	1994	<i>E. Kruglyakov, A. Ivanov (INP); K. Noack (Germany)</i>
4	<i>Nuclear Centre "Karlsruhe" (Germany)</i>	1. Development of conceptual project and data base for neutron source on the basis of GDT device. 2. Simulation of processes in diverter of ITER device.	1994	<i>E. Kruglyakov, A. Ivanov, A. Burdakov (INP); G. Kessler (Germany)</i>
5	<i>GSI (Germany)</i>	Collaboration in the field of accelerator physics: electron cooling; electron-ion colliders.	1995	<i>Yu. Shatunov, V. Parkhomchuk (INP); H. Eickhoff (GSI)</i>
6	<i>DESY (Germany)</i>	Elementary-particle physics, synchrotron radiation, accelerator physics and technology, electronics and experimental equipment.	1995	<i>A. Skrynsky, G. Kulipanov (INP); A. Vagner, K. Scherff (DESY)</i>
7	<i>CELLS (Spain)</i>	Collaboration in the field of application of new equipment for SR sources.	2008	<i>E. Levichev (INP); Joan Bordas and Orpinell (CELLS)</i>
8	<i>CIEMAT (Spain)</i>	Accelerator technology and plasma physics.	2007	<i>E. Levichev (INP), J. Rubio (CIEMAT)</i>
9	<i>INFN (Italy)</i>	Development of intense source for radioactive ion beams for experiments in nuclear physics	1984	<i>P. Logachev (INP); L. Techio (INFN)</i>
10	<i>University of Milan (Italy)</i>	Theoretical and numerical studies of dynamic chaos in classic and quantum mechanics.	1991	<i>A. Skrynsky, V. Sokolov (INP); T. Montegazza, J. Kasati (Italy)</i>
11	<i>INFN-LNF (Italy)</i>	Development of collider project DAFNE-II	2004	<i>E. Levichev (INP); S. Biscari (INFN-LNF)</i>
12	<i>University of Padua (Italy)</i>	Development of cryogenic detectors for experiments in neutrino physicist.	2008	<i>Yu. Tikhonov, A. Bondar (INP); A. Gudlielmi (Italy)</i>
13	<i>National Nuclear Center. Park of Nuclear Technology (Kazakhstan)</i>	Development and application of industrial accelerators, generation and utilization of neutron beams, development of SR sources, RF-generators.	2007	<i>G. Kulipanov (INP); K. Kadyrzhanov, A. Kusainov (Kazakhstan)</i>

List of Collaboration Agreements

<i>№</i>	<i>1</i>	<i>2</i>	<i>3</i>	<i>4</i>
14	<i>National Nuclear Center. Al-Farabi National University (Kazakhstan)</i>	Creation and development of a multi-purpose research complex of radiation technology and terahertz radiation.	2009	<i>G. Kulipanov (INP); K. Kadyrzhanov, B. Zhumagulov (Kazakhstan)</i>
15	<i>Institute of Morden Physics and Techniques, Lanchzou (China)</i>	Collaboration in the field of accelerator physics: electron cooling	2000	<i>V. Parkhomchuk (INP); S. Yang (PRC)</i>
16	<i>WOER Company, Shenzhen, (China)</i>	Using of electron accelerator ILU-10, exchanging of personal, information and experimental equipment.	2005	<i>A. Bryazgin (INP); Leo Li (WOER)</i>
17	<i>SINAP Shanghai, (China)</i>	Researching in field of industrial electron accelerators.	2006	<i>A. Bryazgin (INP); Hu Hounku (SINAP)</i>
18	<i>IHEP (China)</i>	Work of Chinese scientists on BINP installations, work of BINP scientists on IHEP installations.	2007	<i>A. Skrinsky (INP); H. Chen (IHEP)</i>
19	<i>Industrial and Technological Center of Cooperation with Russia and Belorussia of Heilongjiang Province (P.R.C) (China)</i>	Exchange of information about BINP-developed devices and the technology and product demand of the Chinese factories	2009	<i>D. Grigoriev (INP); Zhan Hun-Vei (PRC)</i>
20	<i>POSTECH (Korea)</i>	Creation of beam accelerators, add-on devices, SR experiments.	1992	<i>A. Skrinsky, N. Mezentsev (INP); H. Kim (POSTECH)</i>
21	<i>KAERI (Korea)</i>	Development of FEL and accelerator-recuperator.	1999	<i>N. Vinokurov (INP); B.Ch. Lee (KAERI)</i>
22	<i>BNL, Brookhaven (USA)</i>	1. Measurement of the magnetic muon anomaly. 2. Joint research of RHIC spin.	1991 1993	<i>L. Barkov (INP); J. Bunse (BNL) Yu. Shatunov (INP); S. Ozaki (BNL)</i>
23	<i>ANL, Argonn (USA)</i>	1. Experiments with polarized gas jet target at VEPP-3. 2. SR instrumentation.	1988 1993	<i>L. Barkov (INP); R. Holt (ANL) G. Kulipanov, A. Skrinsky (INP); G. Shenoy (USA)</i>
24	<i>University of Pittsburgh (USA)</i>	Experiments on VEPP-2M and ϕ -factory.	1989	<i>S. Eidelman, E. Solodov (INP); V. Savinov (USA)</i>
25	<i>University of Duke (CIIA)</i>	Free electron lasers.	1992	<i>N. Vinokurov (INP); J. Wu (Duke)</i>

List of Collaboration Agreements

<i>№</i>	<i>1</i>	<i>2</i>	<i>3</i>	<i>4</i>
26	<i>BNL, Brookhaven (USA)</i>	Collaboration on electron-ion colliders.	1993	<i>V. Parkhomchuk (INP); I. Benzvi (USA)</i>
27	<i>FERMILAB (USA)</i>	Collaboration in the field of accelerator physics: electron cooling; conversion system.	1995	<i>V. Parkhomchuk (INP); O. Finli (FERMILAB)</i>
28	<i>FERMILAB (USA)</i>	Exchange of scientists and engineers for scientific research.	2005	<i>A. Skrinsky (INP); P. Oddone (FERMILAB)</i>
29	<i>SLAC, Stanford (USA)</i>	Obtainment of submicron beams and intensive positron beams, development of B-factory elements, detectors, RF-generators based on magnicons.	1994	<i>A. Skrinsky (INP); Persis Drel (SLAC)</i>
30	<i>Institute of Plasma Physics ASCR (Czech Republic)</i>	Collaboration in the field of plasma physics and plasma diagnostics research.	2008	<i>A. Ivanov (INP); P. Hruška (Czech Republic)</i>
31	<i>CERN (Switzerland)</i>	1. Research and development of the detectors for LHC. 2. Development of the LHC elements.	1992 1996	<i>A. Bondar; Yu. Tikhonov (INP); T. Nakada, P. Yenni (CERN)</i> <i>V. Anashin (INP); L. Evans (CERN)</i>
32	<i>Paul Scherrer Institute (Switzerland)</i>	Collaboration in the field of particle physics.	2009	<i>D. Grigoriev (INP); D. Mecom (Paul Scherrer Institute)</i>
33	<i>CERN (Switzerland)</i>	Research and development of micro-pattern detector technology..	2009	<i>Yu. Tikhonov (INP); S. Bertolucci (CERN)</i>
34	<i>CERN (Switzerland)</i>	Collaboration in the development of the electron-positron colliders with super-high luminosity.	2009	<i>E. Levichev (INP); S. Myers (CERN)</i>
35	<i>RIKEN Spring-8 (Japan)</i>	Collaboration in the field of accelerator physics and synchrotron radiation	1996	<i>G. Kulipanov (INP); H. Kamitsubo (Japan)</i>
36	<i>KEK (Japan)</i>	Research in accelerator physics and allied fields, development of elementary particle detectors.	1995	<i>A. Skrinsky (INP); A. Suzuki (KEK)</i>
37	<i>Center of Plasma Research, Tsukuba (Japan)</i>	Collaboration on Open traps.	2007	<i>A. Ivanov (INP); T. Imai (Japan)</i>

Research Personnel

Members of Russian Academy of Science

Academicians:

Barkov Lev Mitrofanovich
Dikansky Nikolai Sergeevich
Kruglyakov Edward Pavlovich
Kulipanov Gennady Nikolaevich
Skrinsky Alexandr Nikolaevich

Corresponding members RAS:

Bondar Alexandr Evgenievich
Dimov Gennady Ivanovich
Khriplovich Iosif Bentsionovich
Logachev Pavel Vladimirovich
Parkhomchuk Vasily Vasilievich
Shatunov Yury Michailovich
Vinokurov Nikolai Alexandrovich

Director Board

Director:

Skrinsky Alexandr Nikolaevich

Adviser RAS:

Kruglyakov Edward Pavlovich

Deputy Director (scientific):

Ivanov Alexandr Alexandrovich
Kulipanov Gennady Nikolaevich
Levichev Evgeny Borisovich
Tikhonov Yury Anatolievich

Scientific Secretary:

Vasiljev Alexei Vladimirovich

Scientific Council

1. Academician, Chairman
2. Doctor of phys.-math. science, Co-Chairman
3. Academician, Co-Chairman
4. Doctor of phys.-math. science, Co-Chairman
5. Doctor of phys.-math. science, Co-Chairman
6. Candidate of phys.-math. science, Scientific Secretary
7. Candidate of techn. science
8. Doctor of phys.-math. science, Professor
9. Academician
10. Candidate of phys.-math. science
11. Corr. Member RAS
12. Doctor of phys.-math. science

Skrinsky A.N.
Ivanov A.A.
Kulipanov G.N.
Levichev E.B.
Tikhonov Yu.A.
Vasiljev A.V.
Anashin V.V.
Arzhannikov A.V.
Barkov L.M.
Blinov V.E.
Bondar A.E.
Burdakov A.V.

13. Corr. Member RAS	Vinokurov N.A.
14. Academician	Dikansky N.S.
15. Corr. Member RAS	Dimov G.I.
16. Doctor of phys.-math. science	Druzhinin V.P.
17. Doctor of phys.-math. science	Koop I.A.
18. Academician	Kruglyakov E.P.
19. Doctor of techn. science	Kuper E.A.
20. Corr. Member RAS	Logachev P.V.
21. Candidate of techn. science	Medvedko A.S.
22. Doctor of phys.-math. science	Mezentsev N.A.
23. Corr. Member RAS	Parkhomchuk V.V.
24. Doctor of techn. science, Professor	Salimov R.A.
25. Doctor of phys.-math. science, Professor	Serednyakov S.I.
26. Doctor of phys.-math. science, Professor	Fadin V.S.
27. Doctor of phys.-math. science	Khazin B.I.
28. Corr. Member RAS	Khriplovich I.B.
29. Corr. Member RAS	Shatunov Yu.M.
30. Candidate of techn. science	Shiaynkov S.V.
31. Candidate of phys.-math. science	Taskaev S.Yu. -- Representative of Trade Union
32. Candidate of phys.-math. science	Shoshin A.A. -- Representative of Council of Young scientists

Specialized Sections of Scientific Council

Accelerators for Applied Purposes

Kulipanov G.N. (Chrmn)	Knyazev B.A.	Pindyurin V.F.
Gorbunov V.A. (Secr.)	Kolmogorov V.V.	Pyata E.E.
Anashin V.V.	Korchagin A.I.	Rakshun Ya.V.
Antokhin E.I.	Kuksanov N.K.	Salimov R.A.
Batratkov A.M.	Kuper E.A.	Shatunov Yu.M.
Bryazgin A.A.	Kuper K.E.	Shevchenko O.A.
Chernyakin A.D.	Kurkin G. Ya.	Shkaruba V.A.
Cheskidov V.G.	Kuznetsov G.I.	Skrinsky A.N.
Churkin I.N.	Levichev E.B.	Sukhina B.N.
Dikansky N.S.	Medvedko A.S.	Tkachenko V.O.
Erokhin A.I.	Mezentsev N.A.	Tribendis A.G.
Fadeev S.N.	Nemytov P.I.	Tumaikin G.M.
Goldenberg B.G.	Nikolenko A.D.	Vinokurov N.A.
Gurov D.S.	Parkhomchuk V.V.	Vostrikov V.A.
Ivanov A.A.	Petrichenkov M.V.	Zolotarev K.V.
Karpov G.V.	Petrov V.M.	

Plasma Physics and Controlled Fusion Problems

Ivanov A.A. (Chrmn)	Khilchenko A.D.	Sanin A.L.
Kandaurov I.V. (Secr.)	Kulipanov G.N.	Shiyankov S.V.
Akhmetov T.D.	Kuznetsov A.S.	Sinitsky S.L.
Anikeev A.V.	Konstantinov S.G.	Skrinsky A.N.
Arzhannikov A.V.	Kotelnikov I.A.	Soldatkina E.I.
Astrelin V.T.	Kruglyakov E.P.	Solomakhin A.L.
Bagryansky P.A.	Lizunov A.A.	Sorokin A.V.
Beklemishev A.D.	Lotov K.V.	Sulyaev Yu.S.
Belchenko Yu.I.	Mekler K.I.	Taskaev S. Yu.
Burdakov A.V.	Murakhtin S.V.	Timofeev I.V.
Burmasov V.S.	Polosatkin S.V.	Vasiljev A.V.
Davydenko V.I.	Popov S.S.	Volosov V.I.
Dimov G.I.	Postupaev V.V.	Voskoboinikov R.V.
Ivanov I.A.	Prikhodko V.V.	Vyacheslavov L.N.
Kapitonov V.A.		

Colliding Beams

Parkhomchuk V.V. (Chrmn)	Koop I.A.	Petrov V.M.
Petrov V.V. (Secr.)	Krasnov A.A.	Reva V.B.
Anashin V.V.	Kruglyakov E.P.	Salimov R.A.
Barkov L.M.	Kulipanov G.N.	Shatilov D.N.
Batnikov A.M.	Kuksanov N.K.	Shatunov P.Yu.
Berkaev D.E.	Kuper E.A.	Shatunov Yu.M.
Blinov V.E.	Kurkin G.Ya.	Shwartz D.B.
Bondar A.E.	Levichev E.B.	Shiyankov S.V.
Bryazgin A.A.	Logachev P.V.	Simonov E.A.
Dikansky N.S.	Medvedko A.S.	Skrinsky A.N.
Erokhin A.I.	Meshkov O.I.	Solodov E.P.
Gorbunov V.A.	Mezentsev N.A.	Starostenko A.A.
Gorniker E.I.	Mishnev S.I.	Tikhonov Yu.A.
Gurov S.M.	Nesterenko I.N.	Tumaikin G.M.
Karpov G.V.	Nikitin S.A.	Vasiljev A.V.
Khazin B.I.	Onuchin A.P.	Vinokurov N.A.
Kiselev V.A.	Perevedentsev E.A.	Vobly P.D.
Kolmogorov V.V.	Pestrikov D.V.	Zolotarev K.V.

Physics of Elementary Particles

Bondar A.E. (Chrmn)	Khazin B.I.	Popov A.S.
Strakhovenko V.M. (Secr.)	Khriplovich I.B.	Rachek I.A.
Achasov M.N.	Kononov S.A.	Redin S.I.
Aulchenko V.M.	Koop I.A.	Ryskulov N.M.
Barkov L.M.	Kravchenko E.A.	Serednyakov S.I.
Baru S.E.	Krokovny P.P.	Shamov A.G.
Berkaev D.E.	Kuzmin A.S.	Shatunov Yu.M.
Blinov A.E.	Lee R.N.	Shekhtman L.I.
Blinov V.E.	Levichev E.B.	Shwartz B.A.
Buzulutskov A.F.	Logachev P.V.	Shwartz D.B.
Chernyak V.L.	Logashenko I.B.	Silagadze Z.K.
Eidelman S.I.	Lukin P.A.	Skovpen Yu.I.
Dimova T.V.	Malyshev V.M.	Skrinsky A.N.
Dmitriev V.F.	Maslennikov A.L.	Smalyuk V.V.
Druzhinin V.P.	Milshtein A.I.	Sokolov A.V.
Fadin V.S.	Muchnoi N.Yu.	Sokolov V.V.
Fedotov G.V.	Nikolaev I.B.	Solodov E.P.
Garmash A. Yu.	Nikolenko D.M.	Tayursky V.A.
Golubev V.B.	Obrazovsky A.E.	Telnov V.I.
Grebenyuk A.A.	Onuchin A.P.	Terekhov I.S.
Grigoriev D.N.	Pakhtusova E.V.	Todyshev K. Yu.
Groshev V.R.	Parkhomchuk V.V.	Tikhonov Yu.A.
Grozin A.G.	Peleganchuk S.V.	Toporkov D.K.
Ignatov F.V.	Pestov Yu.N.	Vasiljev A.V.
Katkov V.M.	Pivovarov S.G.	Vorob'ev A.I.
Kharlamov A.G.	Pomeransky A.A.	Zhilich V.N.

Automation

Tikhonov Yu.A. (Chrmn)	Faktorovich B.P.	Levichev E.B.
Kuper E.A. (Co-Chrmn)	Frolovskaya N.N.	Logashenko I.B.
Baldin E.M. (Secr.)	Grozin A.G.	Maximova S.V.
Dubrov S.V. (Secr.)	Kaplin V.I.	Medvedko A.S.
Aleshaev A.N.	Khilchenko A.D.	Nekhanevich E.L.
Amosov S.A.	Klimenko A.S.	Shatunov Yu.M.
Aulchenko V.M.	Koop I.A.	Shukaev A.N.
Banzarov V.Sh.	Korol A.A.	Shuvalov B.N.
Berdyugin A.V.	Kozak V.R.	Solodov E.P.
Belov S.D.	Kovalenko Yu.V.	Sukharev A.M.
Berkaev D.E.	Kuzin M.V.	Tararyshkin S.V.
Bogdanchikov A.G.	Kupchik V.I.	Tsukanov V.M.
Bolkhovityanov D. Yu.	Kurilin O. Yu.	Vasiljev A.V.
Buzykaev A.R.	Kvashnin A.N.	Zaitsev A.S.
Cheblakov P.B.		

Research Staff and Publications

Abakumova E.V.	138, 139, 140	Achasov M.N.	6, 28, 48, 49, 57, 70, 73, 77, 79, 85, 86, 90, 138, 218, 219, 220, 429, 430, 433, 11p
Abdrashitov A.G.	296, 488	***	***
Abdrashitov G.F.	296	Babichev E.A.	231, 344
Abdulmanov V.G.		Bagryansky P.A.	133, 135, 279, 288, 290, 291, 292, 294, 295, 299, 300, 490, 491, 492, 495, 498, 499, 507
Abramsky A. Yu.	120	Bak P.A.	267, 396, 464, 465
Averbukh I.I.	132, 4p	Baldin E.M.	222, 253, 254, 437, 438, 439, 440, 441, 442, 443, 444, 445, 25p, 26p, 27p, 28p
Avilov M.S.		Banzarov V.Sh.	31
Avrorov A.P.	304, 378, 508	Barkov L.M.	31, 167, 168, 232, 91p
Akberdin R.R.		Barladyan A.K.	222, 253, 254, 437, 438, 439, 440, 441, 442, 443, 444, 445, 25p, 26p, 27p, 28p
Akimov A.V.	405, 426, 464	Barnyakov A.M.	
Aleinik V.I.	282, 283, 485, 486, 9p	Barnyakov A. Yu	220, 222, 223, 224, 253, 254, 429, 430, 437, 438, 439, 440, 441, 442, 443, 444, 445, 446, 447, 448, 449, 450, 451, 452, 11p, 25p, 26p, 27p, 28p
Aleshaev A.N.	478, 10p	Barnyakov M. Yu.	222, 223, 224, 253, 254, 437, 438, 439, 440, 441, 442, 443, 444, 445, 446, 447, 448, 449, 450, 451, 452, 25p, 26p, 27p, 28p
Alinovsky N.I.	470	Baru S.E.	31, 222, 230, 231, 235, 236, 253, 254, 344, 437, 438, 439, 440, 441, 442, 443, 444, 445, 25p, 26p, 27p, 28p
Alyakrinsky O.N.	266	Baryshev V.B.	
Amirov V.X.	499	Basok I. Yu.	222, 223, 253, 254, 443, 444, 445, 446, 447, 448, 451, 452, 25p, 26p, 27p, 28p
Anashin V.V.	121, 140, 222, 253, 254, 394, 425, 437, 438, 439, 440, 441, 442, 443, 444, 445, 10p, 16p, 25p, 26p, 27p, 28p	Batazova M.A.	464
Anikeev A.V.	133, 288, 290, 293, 294, 300, 495, 497, 500, 501, 526	Batkin V.I.	134, 306
Anisenkov A.V.	112, 170, 171, 172, 54p, 55p, 56p, 57p, 58p, 59p, 60- 65p, 66p-70p, 71p-74p	Batrakov A.M.	116, 119, 267, 403, 405, 426, 464, 465, 470, 10p, 2A
Antokhin E.I.	321, 390	Bashtovoi N.S.	31
Anchugov O.V.	405, 426, 10p	Bayanov B.F.	283, 284, 486
Arakcheev A.S.	274, 23p	Bedareva T.V.	470
Arbuzov V.S.	106	Bezuglov V.V.	326, 555
Arzhannikov A.V.	24, 115, 302, 303, 305, 306, 311, 315, 316, 336, 346, 347, 375, 502, 514, 516, 519, 520, 521, 522, 523, 524, 525, 535, 536, 537	Beklemishev A.D.	16, 17, 128, 133, 135, 279, 292, 302, 373, 374, 383, 490, 515, 526
Arinstein K.E.	39, 42, 50, 60, 84, 87, 89, 91, 95, 260, 261, 262, 263, 49p, 50p, 51p, 52p		
Astigeevich P.M.	112, 11p		
Astrelin V.T.	129, 302, 304, 306, 317, 318, 378, 507, 508, 515, 522, 536		
Aulchenko V.M.	31, 39, 47, 60, 61, 84, 87, 89, 222, 233, 253, 254, 260, 261, 262, 263, 355, 356, 359, 365, 429, 437, 438, 439, 440, 441, 442, 443, 444, 445, 11p, 25p, 26p, 27p, 28p, 49p, 50p, 51p, 52p		
Akhmetov T.D.	289		
Akhmetshin R.R.	31		

Buzulutskov A.F.	27, 251, 252, 343, 453, 454, 29p, 30p, 31p	Gabyshev N.I.	31, 39, 42, 47, 50, 53, 60, 74, 87, 89, 91, 93, 95, 260, 261, 262, 263, 49p, 50p, 51p, 52p
Buzykaev A.R.	40, 41, 43, 44, 45, 51, 52, 54, 56, 59, 62, 63, 64, 65, 66, 67, 71, 72, 75, 76, 78, 80, 81, 83, 92, 96, 222, 223, 224, 253, 254, 437, 438, 439, 440, 441, 442, 443, 444, 445, 446, 447, 448, 449, 450, 451, 452, 25p, 26p, 27p, 28p	Galt A.A.	349, 395
Bukin D.A.	218, 219, 220, 429, 430, 11p	Garmash A.Yu.	39, 42, 50, 87, 89, 91, 93, 95, 144, 260, 261, 262, 263, 49p, 50p, 51p, 52p
Burdakov A.V.	134, 282, 283, 302, 303, 304, 305, 306, 307, 308, 311, 312, 313, 316, 317, 318, 346, 371, 375, 378, 485, 486, 502, 503, 504, 508, 510, 511, 514, 515, 516, 517, 519, 523, 526, 531, 532, 534, 539, 540	Gauzshtein V.V.	167, 168, 169, 387, 388, 389, 91p
Burenkov D.V.	426, 10p	Gayazov S.E.	112
Burmasov V.S.	306, 314, 512, 516	Gentselev A.N.	118, 363
Bykov E.V.	3p	Gerasimov V.V.	2, 3, 102, 113, 332, 333, 335, 337, 345, 349
Bykov P.V.	304, 378, 508	Getmanov Ya.V.	332, 349, 417
***	***	Glukhov S.A.	10p
Vasiljev A.V.	218, 219, 220, 429, 430, 11p	Glukhovchenko Yu.M.	222, 253, 254, 437, 438, 439, 440, 441, 442, 4p, 10p, 25p, 26p, 27p, 28p
Vasichev S.P.	10p	Golkovsky M.G.	114, 320, 321, 322, 323
Vasichev S.S.		Golovin R.A.	91p
Velikanov Yu.M.	395	Golubev V.B.	40, 41, 43, 44, 45, 51, 52, 54, 56, 59, 62, 63, 64, 65, 67, 71, 72, 75, 76, 78, 80, 81, 83, 92, 96, 218, 219, 220, 224, 429, 430, 432, 11p
Veremeenko V.F.	395, 10p	Golubenko Yu.I.	550, 551
Vesenev V.M.	429, 11p	Golubtsov S.K.	118
Vinokurov N.A.	97, 98, 101, 110, 332, 335, 349, 395, 409, 417	Goldenberg B.G.	118, 120, 328, 363, 7A
Vinokurova A.N.	39, 42, 47, 50, 60, 74, 87, 89, 91, 93, 95, 260, 261, 262, 263, 49p, 50p, 51p, 52p	Goncharov A.D.	415, 470, 471, 472, 476
Vlasenko M.G.	113, 332, 334, 335, 349	Goncharova N.F.	121
Vobly P.D.	116, 119, 127, 349, 377, 382, 403, 406, 416, 419, 422, 423, 541	Gorbovsky A.I.	310, 488
Volkov A.A.	414	Gorbunov V.A.	326
Volkov V.N.	271, 420, 421	Gordeev O.P.	10p
Volosov V.I.		Gorlovoi A.V.	361
Vorob'ev A.I.	222, 253, 254, 437, 438, 439, 440, 441, 442, 443, 444, 445, 25p, 26p, 27p, 28p	Gorniker E.I.	106, 477
Vorob'ev V.S.	17p	Gorchakov K.M.	112, 405, 426, 470
Voronin L.A.	326	Gosteev V.K.	466, 470
Voskoboinikov R.V.		Grabovsky A.V.	158, 159, 15p
Vostrikov V.A.		Gramolin A.V.	232, 388, 91p
Vyacheslavov L.N.	306, 313, 316, 346, 371, 503, 509, 514, 516, 519, 523, 534, 540	Grebenyuk A.A.	27, 31, 251, 252, 343, 29p, 30p
***	***	Grevtsov K.A.	429, 430, 11p
		Grigoriev D.N.	31, 225, 226, 227, 228, 231, 254, 344, 25p, 27p, 28p
		Grishnyaev E.S.	539
		Grozin A.G.	153, 154, 18p
		Groshev V.R.	231, 344
		Gubin K.V.	
		Gudkov B.A.	410
		Gulevich V.V.	222, 223, 224, 253, 254, 437, 438, 439, 440, 441, 442, 443, 444, 445, 446, 447, 448, 451, 452, 25p, 26p, 27p, 28p

Research staff and publications

Gurov D.S.	116, 426	Zhirov O.V.	152, 165, 166, 19p, 20p
Gurov S.M.	403, 405, 413, 426	Zhmaka A.I.	10p
Gusev G.A.	140	Zhmurikov E.I.	105, 362
Gusev D.V.	222, 253, 254, 437, 438, 439, 440, 441, 442, 25p, 26p, 27p, 28p	Zhukov A.A.	138, 139
Gusev E.A.		Zhulanov V.V.	39, 42, 47, 50, 53, 74, 84, 87, 89, 91, 93, 95, 222, 233, 234, 253, 254, 260, 261, 262, 263, 355, 437, 438, 439, 440, 441, 442, 443, 444, 445, 25p-28p, 49p, 50p, 51p, 52p, 8A
Gusev I.A.	467, 470	Zhuravlev A.N.	222, 253, 254, 393, 437, 438, 439, 440, 441, 442, 10p, 25p, 26p, 27p, 28p
***	***	***	***
Davidovsky V.G.		Zaigraeva N.S.	332, 349
Davydenko V.I.	126, 132, 134, 136, 282, 286, 287, 309, 310, 401, 487, 488, 489, 518, 527, 530, 538	Zaitsev A.S.	8, 9, 13, 25, 31, 32, 33, 35, 55, 58, 69, 82, 94, 170, 171, 172, 173, 174, 175, 176, 177, 178, 179, 180, 181, 182, 183, 184, 185, 186, 187, 188, 189, 190, 191, 192, 193, 194, 195, 196, 197, 198, 199, 200, 201, 202, 203, 204, 205, 206, 207, 208, 209, 210, 211, 212, 213, 214, 215, 216, 412, 53p, 54p, 55p-60p, 61p-70p, 71p-80p, 81p-90p
Devyataikina T.A. (Yaskina T.A.)	403	Zaitsev K.F.	133, 135, 279, 490
Deichuli P.P.	132, 136, 296, 310, 488, 518, 527, 529	Zapryagaev I.A.	
Dementjev E.N.	349, 409	Zapaytkin N.P.	470
Derevyankin G.E.	304, 378, 508	Zverev S.I.	
Dikansky N.S.	264	Zevakov S.A.	167, 168, 169, 232, 387, 388, 389, 91p
Dimov G.I.	14, 127, 377, 382	Zemlyansky I.M.	112, 220, 546, 11p
Dimova T.V.	218, 219, 220, 429, 11p	Zinin E.I.	122, 10p
Dmitriev V.F.	23, 141, 167, 168, 232, 463, 91p	Zolotarev K.V.	140, 350, 364, 366, 368, 16p
Dneprovsky L.V.	443, 444, 445	Zubarev P.V.	296
Dovzhenko B.A.	395, 470	Zubkov N.I.	116
Domarov E.V.	550	Zyukova O.	39, 42, 50, 74, 91, 95
Donin A.S.	133, 296, 301	***	***
Dorokhov D.V.		Ivanenko V.G.	308
Dranichnikov A.N.	488	Ivanenko S.V.	291, 314, 491, 509, 512
Druzhinin V.P.	40, 41, 43, 44, 45, 51, 52, 54, 56, 59, 62, 63, 64, 65, 66, 67, 71, 72, 75, 76, 78, 80, 81, 83, 92, 96, 218, 219, 220, 258, 429, 430, 11p	Ivanov A.A.	15, 126, 132, 133, 134, 136, 282, 286, 287, 289, 301, 302, 309, 310, 314, 386, 401, 485, 487, 488, 489, 493, 494, 496, 515, 517, 518, 526, 527, 530, 538, 9p
Dubrovin A.N.	405	Ivanov A.V.	108, 467, 468, 470
Dudnikov A.V.	324	Ivanov I.A.	303, 306, 307, 308, 311, 316, 371, 503, 511, 515, 516, 519, 526, 531, 532
***	***		
Eliseev A.A.	464		
Eliseev V.S.	320, 321, 390		
Emanov F.A.	403, 464		
Emelev I.S.	127, 377, 382		
Epifanov D.A.	20, 31, 39, 42, 47, 50, 260, 261, 262, 263, 49p,-52p		
Erokhin A.I.	405, 426, 470		
Erokhov V.N.	10p		
***	***		
Zhilich V.N.	39, 42, 47, 50, 68, 74, 84, 89, 91, 93, 95, 222, 233, 253, 254, 260, 261, 262, 263, 437, 438, 439, 440, 441, 442, 443, 444, 445, 10p, 25p, 26p-28p, 49p-52p, 91p		

Ivanova L.A.	509, 512	Kobets V.V.	127, 377, 382, 403, 405, 426
Ivantsivky M.V.	306, 313, 316, 371, 503, 514, 519, 540	Kovalenko N.V.	
Ivlyushkin D.V.	361	Kovalenko Yu.V.	133, 291, 491
Ignatov F.V.	31	Kovrizhin D.P.	112, 220, 429, 430, 11p
Iljin I.V.	116, 119	Kogut D.A.	550, 551
***	***	Kozak V.P.	395, 478, 3p, 10p
Kadyrov R.A.	267	Kozlov M.G.	160, 12p, 13p
Kazanin V.F.	31, 53p, 54p, 55p, 56p, 57p, 58p, 59p, 60p-70p, 71-80p, 81p-90p	Kozyrev A.N.	112
Kalinin P.V.	24, 346, 516, 520, 521, 522, 523, 525, 534, 535, 536, 537	Kozyrev E.V.	106
Kaminsky V.V.	138, 10p, 91p	Koisin Yu.I.	470
Kandaurov I.V.	304, 317, 376, 378, 506, 508	Kokin E.N.	326
Kapitonov V.A.	132, 134, 304, 309, 378, 508, 538	Kolesnikov E. Yu.	135, 279
Kaplin V.I.	412, 10p	Kolmogorov A.V.	286, 287
Kardapoltsev L.V.	112, 218, 220, 429, 430, 434, 494, 11p	Kolmogorov V.V.	254, 401, 405, 426, 488, 25p, 27p, 28p
Karmakulov K.G.		Kolobanov E.I.	332, 349
Karnaev S.E.	222, 253, 254, 397, 398, 405, 426, 437, 438, 439, 440, 441, 442, 10p, 25p, 26p, 27p, 28p	Kolokolnikov Yu.M.	416
Karpov G.V.	222, 253, 254, 391, 405, 426, 437, 438, 439, 440, 441, 442, 443, 444, 445, 470, 10p, 25p, 26p, 27p, 28p	Kondakov A.A.	488
Karpov I.E.	507	Kondaurov M.N.	467, 470
Karpov S.V.	31, 222, 253, 254, 437, 438, 439, 440, 441, 442, 443, 444, 445, 25p, 26p, 27p, 28p	Kondratiev V.I.	118, 120, 354
Kasaev A.S.	430	Kononov S.A.	222, 223, 224, 253, 254, 437, 438, 439, 440, 441, 442, 443, 444, 445, 446, 447, 448, 449, 450, 451, 452, 25p, 26p, 27p, 28p
Kasatov A.A.	313, 314, 371, 372, 503, 505, 512, 514, 540	Konstantinov V.M.	405, 426
Kasatov D.A.	314, 486, 512	Konstantinov E.S.	476
Katkov V.M.	156, 457	Konstantinov S.G.	
Kvashnin A.N.	291, 491, 492, 509, 510, 513, 539	Koop I.A.	21, 31, 112, 218, 219, 220, 319, 423, 430, 541, 542, 545, 546, 548, 549, 11p
Kenzhebulatov E.K.	477	Korepanov A.A.	405, 426, 464
Kirilin G.G.		Korzhavina M.S.	133, 290, 490
Kirpotin A.N.	112, 542, 546, 11p	Korobeinikov M.V.	124, 326, 552, 553, 554, 555
Kiselev V.A.	222, 253, 254, 393, 404, 405, 426, 437, 438, 439, 440, 441, 442, 10p, 25p, 26p, 27p, 28p	Korol A.A.	25, 32, 33, 35, 55, 58, 69, 82, 94, 170, 171, 172, 173, 174, 175, 176, 177, 178, 179, 180, 181, 182, 183, 184, 185, 186, 187, 188, 189, 190, 191, 192, 193, 194, 195, 196, 197, 198, 199, 200, 201, 202, 203, 204, 205, 206, 207, 208, 209, 210, 211, 212, 213, 214, 215, 216, 218, 219, 220, 429, 430, 11p, 53p, 54p, 55p-60p, 61p-70p, 71p-80p, 81p-90p
Klimenko A.S.	390	Korchagin A.I.	550
Klyuev V.F.	476	Kosov A.V.	117, 353, 354
Knyazev B.A.	2, 3, 102, 113, 327, 331, 332, 333, 334, 335, 337, 339, 340, 345, 349	Kotelnikov I.A.	135, 277, 278, 279, 302, 341, 483, 484

Research staff and publications

Kotov K. Yu.	8, 222, 253, 254, 437, 438, 439, 440, 441, 442, 443, 444, 445, 25p, 26p, 27p, 28p	Kurkuchekov V.V.	304, 376, 378, 506, 508
Koshuba S.V.	218, 219, 220, 429, 430, 11p	Kuskov R.E.	
Kravchenko E.A.	40, 41, 43, 44, 45, 52, 54, 56, 59, 62, 63, 64, 65, 66, 67, 71, 72, 80, 81, 83, 96, 222, 223, 224, 253, 254, 429, 437, 438, 439, 440, 441, 442, 443, 444, 445, 446, 447, 448, 449, 450, 451, 452, 11p, 25p, 26p, 27p, 28p	Kukhnov I.A.	223, 446, 447, 448, 451, 452
Krasnov A.A.	138, 139, 140, 394, 425	***	***
Krokovny P.P.	31, 237, 238, 239, 240, 241, 242, 244, 245, 246, 260, 261, 262, 263, 32p, 33p, 34p, 35p, 36p-40p, 41p-47p, 49p-52p	Lavrukhin A.V.	550
Kruglyakov E.P.	133, 302, 512, 517	Lazarenko B.A.	232, 91p
Krutikhin S.A.	477	Lapik R.M.	
Kryuchkov A.M.	468, 470	Lebedev N.N.	
Kubarev V.V.	332, 342, 347, 348, 349, 385	Lev V.H.	400, 414
Kudryavtsev V.N.	233, 254, 443, 444, 445, 25p, 27p, 28p	Levichev A.E.	109, 14A
Kuznetsov A.S.	282, 485, 9p	Levichev E.B.	137, 140, 222, 253, 254, 259, 365, 402, 405, 406, 422, 423, 426, 437, 438, 439, 440, 441, 442, 443, 444, 445, 541, 10p, 25p, 26p, 27p, 28p, 92p
Kuznetsov G.I.	124, 464, 555, 10p	Legkodymov A.A.	358, 361, 367
Kuznetsov S.A.	4, 5, 305, 306, 336, 346, 347, 375, 502, 514, 516, 519, 521, 522, 523, 524, 534, 535, 536,	Leonov V.V.	231, 344
Kuzmin A.S.	31, 39, 42, 47, 50, 53, 61, 68, 74, 84, 89, 95, 257, 260, 261, 262, 263, 443, 444, 445, 49p, 50p, 51p, 52p	Lee R.N.	143, 161, 162, 163, 164, 462
Kuzminykh V.S.	140, 391, 405, 426	Lizunov A.A.	133, 291, 296, 299, 301, 490, 491
Kuklin K.N.	303, 306, 311, 314, 316, 512, 519, 531	Lisitsin A.D.	470
Kuksanov N.K.	550, 551	Listopad A.A.	126, 487
Kulenko Ya.V.	464	Logachev P.V.	267, 319, 464, 465
Kulikov V.F.	222, 253, 254, 437, 438, 439, 440, 441, 442, 443, 444, 445, 25p, 26p, 27p, 28p	Logashenko I.B.	31
Kulipanov G.N.	97, 110, 332, 335, 338, 342, 349, 350, 352, 359, 365, 8p, 10p	Lopatkin I.A.	470
Kuper K.E.	100, 120, 5A	Lotov K.V.	103, 104, 272, 273, 274, 275, 276, 370, 381, 479, 480, 481, 482, 21p, 22p, 23p, 24p
Kuper E.A.	117, 222, 253, 254, 395, 405, 410, 426, 437, 438, 439, 440, 441, 442, 443, 444, 445, 10p, 25p, 26p, 27p, 28p	Lukin A.N.	326, 555
Kurkin G. Ya.	222, 253, 254, 418, 437, 438, 439, 440, 441, 442, 477, 10p, 25p, 26p, 27p, 28p	Lukin P.A.	31
		Lysenko A.P.	31, 112, 430, 546, 11p
		Lvovsky A.V.	492
		Lyakh V.V.	361
		***	***
		Makarov A.N.	282, 283, 485, 486
		Makarov I.G.	124, 326, 555
		Makarov M.A.	303, 305, 306, 307, 308, 312, 315, 316, 346, 371, 503, 504, 511, 514, 516, 519, 523, 532, 534
		Maximov V.V.	133, 135, 279, 295, 386, 490, 493
		Maximov D.A.	69, 94, 170, 171, 172, 173, 174, 175, 176, 177, 178, 179, 180, 181, 182, 183, 184, 185, 186, 187, 188, 189, 190, 191, 192, 193, 194, 195, 196, 197,

	198, 199, 200, 201, 202, 203, 204, 205, 206, 207, 209, 210, 211, 212, 222, 253, 254, 437, 438, 439, 440, 441, 442, 443, 444, 445, 25p, 26p, 27p, 28p, 53p-60p, 61p-70p, 71p-80p, 81p-90p			
Maximov S.A.	326		Mezentsev N.A.	350, 352, 353, 364, 365, 400, 414
Maximovskaya V.V.	357, 364		Mekler K.I.	134, 303, 305, 306, 307, 308, 311, 312, 316, 346, 371, 375, 502, 503, 504, 511, 514, 516, 519, 523, 532, 534
Malyshev V.M.	8, 9, 13, 25, 32, 33, 35, 55, 58, 69, 82, 94, 170, 171, 172, 173, 174, 175, 176, 177, 178, 179, 180, 181, 182, 183, 184, 185, 186, 187, 188, 189, 190, 191, 192, 193, 194, 195, 196, 197, 198, 199, 200, 201, 202, 203, 204, 205, 206, 207, 208, 209, 210, 211, 212, 213, 214, 215, 216, 222, 253, 254, 437, 438, 439, 440, 441, 442, 443, 444, 445, 25p, 26p, 27p, 28p, 53p-60p, 61p-70p, 71p-80p, 81p-90p		Meshkov O.I.	222, 253, 254, 391, 393, 405, 426, 437, 438, 439, 440, 441, 442, 10p, 25p, 26p, 27p, 28p
Mamkin V.R.	405, 426, 470, 10p		Miginskaya E.G.	414
Martin K.A.	112, 220, 224, 429, 430, 11p		Miginsky S.V.	18, 107, 332, 349, 14p
Martyshkin P.V.			Mikaiylov A.I.	10p
Maslennikov A.L.	8, 9, 13, 25, 32, 33, 35, 55, 58, 69, 82, 94, 170, 171, 172, 173, 174, 175, 176, 177, 178, 179, 180, 181, 182, 183, 184, 185, 186, 187, 188, 189, 190, 191, 192, 193, 194, 195, 196, 197, 198, 199, 200, 201, 202, 203, 204, 205, 206, 207, 208, 209, 210, 211, 212, 213, 214, 215, 216, 222, 253, 254, 437, 438, 439, 440, 441, 442, 443, 444, 445, 25p, 26p, 27p, 28p, 53p-60p, 61p-70p, 71p-80p, 81p-90p		Milstein A.I.	23, 141, 142, 143, 144, 145, 222, 26p
			Mironenko L.A.	349, 10p
			Mityanina N.V.	111
			Mikhailov K.Yu.	31
			Mishagin V.V.	309, 310, 487, 488, 538
			Mishnev S.I.	167, 168, 222, 232, 253, 254, 437, 438, 439, 440, 441, 442, 10p, 25p, 26p, 27p, 28p, 91p
			Moiseev D.V.	296, 513
			Morozov I.I.	222, 253, 254, 437, 438, 439, 440, 441, 442, 10p, 25p, 26p, 27p, 28p
			Murakhtin S.V.	99, 133, 296, 298, 490, 529
			Muchnoi N.Yu.	6, 28, 48, 49, 57, 70, 73, 79, 85, 90, 138, 222, 253, 254, 437, 438, 439, 440, 441, 442, 443, 444, 445, 10p, 25p, 26p, 27p, 28p, 91p, 3A
			***	***
			Neifeld V.V.	222, 253, 254, 405, 426, 437, 438, 439, 440, 441, 442, 10p
			Nemytov P.I.	550, 551
			Nesterenko I.N.	542, 543, 546, 11p
			Nefedov N.B.	405, 426
			Nekhaev V.E.	
			Nikitin S.A.	222, 253, 254, 404, 406, 422, 423, 437, 438, 439, 440, 441, 442, 443, 444, 445, 541, 10p, 25p, 26p, 27p, 28p, 4A
Matveenkov A.N.	97, 271, 421		Nikolaev I.V.	464
Matvienko D.V.	42, 47, 61, 68, 257, 260, 261, 262, 263, 49p, 50p, 51p, 52p		Nikolaev I.B.	49, 70, 73, 79, 86, 138, 222, 253, 254, 404, 437, 438, 439, 440, 441, 442, 443, 444, 445, 10p, 25p, 26p, 27p, 28p
Mashkovtsev M.R.	361		Nikolenko A.D.	363, 9A
Medvedev L.E.	332, 349, 395		Nikolenko D.M.	167, 168, 169, 232, 387, 388, 389, 427, 10p, 91p
Medvedko A.S.	222, 253, 254, 395, 405, 409, 426, 437, 438, 439, 440, 441, 442, 443, 444, 445, 470, 10p, 25p, 26p, 27p, 28p			

Research staff and publications

***	***		
Obrazovsky A.E.	112, 220, 428, 429, 430, 11p	Parkhomchuk V.V.	268, 269, 270, 319, 415, 466, 467, 468, 469, 470, 471, 472, 473, 474, 475, 476
Ovtin I.B.	223	Pakhtusova E.V.	218, 219, 220, 429, 430, 11p
Ovchar V.K.	349, 394, 10p	Pachkov A.A.	464
Ogurtsov A.B.	116, 119	Peleganchuk S.V.	8, 9, 13, 25, 32, 33, 35, 55, 58, 69, 82, 94, 170, 171, 172, 173, 174, 175, 176, 177, 178, 179, 180, 181, 182, 183, 184, 185, 186, 187, 188, 189, 190, 191, 192, 193, 194, 195, 196, 197, 198, 199, 200, 201, 202, 203, 204, 205, 206, 207, 208, 209, 210, 211, 212, 213, 214, 215, 216, 222, 253, 254, 437, 438, 439, 440, 441, 442, 443, 444, 445, 25p, 26p, 27p, 28p, 53p-60p, 61p-70p, 71p-80p, 81p-90p
Okunev I.N.	222, 253, 254, 405, 406, 422, 423, 426, 437, 438, 439, 440, 441, 442, 541, 10p, 25p, 26p, 27p, 28p	Perevedentsev E.A.	31, 112, 545, 546, 11p
Onuchin A.P.	40, 41, 43, 44, 45, 51, 52, 54, 56, 59, 62, 63, 64, 65, 66, 67, 71, 72, 75, 76, 78, 80, 81, 83, 92, 96, 222, 223, 224, 253, 254, 429, 437, 438, 439, 440, 441, 442, 443, 444, 445, 446, 447, 448, 449, 450, 451, 452, 10p, 11p, 25p, 26p, 27p, 28p	Persov B.Z.	332, 349
Oreshkin S.B.	222, 253, 254, 437, 438, 439, 440, 441, 442, 443, 444, 445, 25p, 26p, 27p, 28p	Pestov Yu.N.	11, 12, 34, 36, 37, 46, 88
Oreshonok V.V.	392, 10p	Pestrikov D.V.	264, 265
Orlov I.O.	8, 9, 13, 25, 32, 33, 35, 58, 69, 82, 94, 170, 171, 172, 173, 174, 175, 176, 177, 178, 179, 180, 181, 182, 183, 184, 185, 186, 187, 188, 189, 190, 191, 192, 193, 194, 195, 196, 197, 198, 199, 201, 202, 203, 204, 205, 206, 207, 208, 209, 210, 211, 212, 213, 214, 215, 216, 222, 253, 254, 437, 438, 439, 440, 441, 442, 443, 444, 445, 25p, 26p, 27p, 28p, 53p-60p, 61p-70p, 71p-80p, 81p-90p	Petrenko A.V.	26, 123
Osipov A.A.	222, 253, 254, 437, 438, 439, 440, 441, 442, 443, 444, 445, 25p, 26p, 27p, 28p	Petrichenkov M.V.	405, 407, 426
Osipov A.V.	167, 168, 232	Petrov V.V.	222, 253, 254, 426, 437, 438, 439, 440, 441, 442, 4p, 5p, 10p, 25p, 26p, 27p, 28p
Osipov V.N.	10p	Petrov V.M.	106, 111, 405, 418, 477, 10p
Ostreiko G.N.	124, 555	Petrova E.V.	120
Otboev A.V.	21, 319, 546	Petrozhitsky A.V.	476
Ottmar A.V.	464	Pivovarov I.L.	
Okhapkin V.S.	31	Pivovarov S.G.	222, 253, 254, 437, 438, 439, 440, 441, 442, 443, 444, 445, 25p, 26p, 27p, 28p
***	***	Pilan A.M.	106, 477
Pavlenko A.V.	267, 465	Pilipenko R.V.	
Pavlov V.M.	109	Piminov P.A.	222, 253, 254, 402, 406, 422, 423, 437, 438, 439, 440, 441, 442, 541, 10p, 25p, 26p, 27p, 28p
Pavlov O.A.	464	Pindyurin V.F.	118, 120, 361, 363
Panasyuk V.M.	415, 466, 467, 470, 471, 472	Pinzhenin E.I.	133, 295, 386, 490, 493
Panov A.N.	267, 396, 464, 465	Pirogov S.A.	
Panfilov A.D.	124, 326, 555	Plotnikova O.A.	10p
Panchenko V.E.	16p	Podobaev V.S.	326, 555
Papushev P.A.	231, 344, 355	Podyminogin A.A.	132
		Poletaev I.V.	363, 470
		Polosatkin S.V.	134, 302, 303, 306, 307, 308, 309, 311, 312, 313, 316, 346, 371, 375, 502, 503, 504, 511, 516, 518, 519, 523, 527, 528, 530, 531, 532, 538, 539, 540

Polukhin V.A.	403, 470	Rovenskih A.F.	134, 303, 304, 305, 306, 307, 308, 312, 314, 316, 346, 371, 375, 378, 502, 503, 504, 508, 510, 511, 512, 513, 516, 519, 523, 532, 534, 539
Poluektov A.O.	39, 42, 50, 60, 84, 87, 89, 95, 222, 237, 238, 239, 240, 241, 242, 244, 245, 246, 253, 254, 260, 261, 262, 263, 437, 438, 439, 440, 441, 442, 443, 444, 445, 17p, 25p, 26p, 27p, 28p, 32p-47p, 49p, 50p, 51p, 52p	Rogovsky Yu.A.	112, 220, 430, 542, 543, 544, 546, 11p
Polyansky A.V.	426, 10p	Rodionov D.G.	334
Pomeransky A.A.		Rodyakin V.A.	443, 444, 445
Popik V.M.	329, 330, 332, 349	Romanov A.L.	112, 220, 430, 542, 546, 11p, 12A
Popov A.S.	31, 225, 226, 306, 313, 314, 316, 371, 372	Rotov E.A.	10p
Popov S.S.	503, 505, 512, 514, 516, 519, 540	Ruban A.A.	31, 222, 253, 254, 437, 438, 439, 440, 441, 442, 443, 444, 445, 25p, 26p, 27p, 28p
Popova N.I.	455	Ruvinsky S.I.	405, 426
Porosev V.V.	224, 231, 344	Rudenko A.S.	29, 38, 146, 147, 148
Postupaev V.V.	134, 302, 303, 305, 306, 307, 308, 311, 312, 313, 316, 317, 346, 371, 375, 502, 503, 504, 511, 512, 513, 514, 515, 516, 519, 523, 526, 531, 532, 534, 540	Rybitskaya T.V.	405
Prisekin V.G.	222, 253, 254, 437, 438, 439, 440, 441, 442, 443, 444, 445, 1p, 25p, 26p, 27p, 28p	Ryzhenenkov A.E.	112
Prikhodko V.V.	133, 135, 279, 289, 290, 292, 295, 301, 490, 492, 494, 495, 496	Ryskulov N.M.	31
Prozorenko P.S.	320, 322	***	***
Protopopov A.Yu.	470	Savinov G.A.	222, 231, 253, 254, 344, 437, 438, 439, 440, 441, 442, 443, 444, 445, 25p, 26p, 27p, 28p
Pupkov Yu.A.	140, 5p, 6p, 10p	Savkin V.Ya.	99, 133, 291, 298, 487, 490, 491
Pureskin D.N.	405, 426, 467, 470	Sadykov R.Sh.	167, 168, 169, 232, 91p
Puryga E.A.	314, 509, 510, 512, 539	Sazansky V.Ya.	267, 465
Putmakov A.A.	467, 470	Саликова Т.В.	332, 349
Pyata E.E.	138	Salimov R.A.	550
***	***	Salnikov S.G.	23
Radchenko V.M.	124, 326	Sandyrev V.K.	222, 253, 254, 437, 438, 439, 440, 441, 442, 10p, 25p, 26p, 27p, 28p
Razorenov V.V.		Sanin A.L.	
Rakshun Ya.V.	351, 352, 353, 357, 364, 366, 368	Svischev V.V.	10p
Rastigeev S.A.	268, 269, 475, 476	Sedlyarov I.K.	10p
Rachek I.A.	167, 168, 169, 232, 387, 388, 389, 427, 91p	Selivanov A.N.	10p
Raschenko V.V.	415	Selivanov P.A.	410
Reva V.B.	270, 415, 466, 467, 468, 469, 470, 471, 472, 473	Semenov A.V.	405
Redin S.I.	31	Semenov A.M.	121, 140, 425, 426
Reznichenko A.V.	12p, 13p	Semenov E.P.	470
Repkov V.V.	10p	Semenov Yu.I.	
		Senchenko A.I.	112
		Senkov D.V.	405, 426, 467, 470
		Serdobintsev G.V.	124, 555
		Serednyakov S.I.	40, 41, 43, 44, 45, 51, 52, 54, 56, 59, 62, 63, 64, 65, 66, 67, 71, 72, 75, 76, 78, 80, 81, 83, 92, 96, 112, 218, 219, 220, 224, 258, 429, 430, 431, 11p

Research staff and publications

Serednyakov S.S.	332, 349, 395, 397, 409, 410, 426	Snopkov R.G.	443, 444, 445
Sidorov A.A.	169, 232, 387, 388, 389	Sokolov A.V.	27, 222, 251, 253, 254, 343, 437, 438, 439, 440, 441, 442, 443, 444, 445, 25p, 26p, 27p, 28p, 30p
Sidorov A.V.	124, 292, 325, 326, 555	Sokolov V.V.	152, 456
Silagadze Z.K.	1, 7, 218, 219, 220, 429, 430, 11p	Soldatkina E.I.	135, 279, 490
Simonov E.A.	137, 222, 253, 254, 437, 438, 439, 440, 441, 442, 10p, 25p, 26p, 27p, 28p	Solodov E.P.	31, 40, 41, 43, 44, 45, 51, 52, 54, 56, 59, 62, 63, 64, 65, 66, 67, 71, 72, 75, 76, 78, 80, 81, 83, 92, 96
Singatulin Sh.R.		Solomakhin A.L.	291, 297, 299, 490, 491, 492
Sinitsky S.L.	283, 302, 303, 304, 305, 306, 307, 308, 312, 315, 316, 317, 346, 371, 375, 378, 486, 502, 503, 504, 508, 511, 514, 515, 516, 519, 520, 521, 522, 523, 526, 532, 534, 535, 536, 537	Sorokin A.V.	132, 296, 310, 488
Sinyatkin S.V.	222, 253, 254, 350, 406, 422, 423, 426, 437, 438, 439, 440, 441, 442, 541, 10p, 25p, 26p, 27p, 28p	Sorokin I.N.	282, 485, 9p
Sklyarov V.F.	305, 306, 314, 346, 375, 502, 512, 514, 516, 519, 523, 534	Sorokina N.V.	134, 306, 312, 504, 511, 519
Skovorodin D.I.	128, 373, 374	Sorokoletov D.S.	352, 357
Skovpen K. Yu.	8, 9, 25, 32, 33, 35, 55, 58, 69, 82, 94, 170, 171, 172, 173, 174, 175, 176, 177, 178, 179, 180, 181, 182, 183, 184, 185, 186, 187, 188, 189, 190, 191, 192, 193, 194, 195, 196, 197, 198, 199, 200, 201, 202, 203, 204, 205, 206, 207, 208, 209, 210, 211, 212, 213, 214, 215, 216, 217, 220, 429, 430, 11p, 53p-60p, 61p-70p, 71p-80p, 81p-90p	Stankevich A.S.	112
Skovpen Yu.I.	40, 41, 43, 44, 45, 51, 52, 54, 56, 59, 62, 63, 64, 65, 66, 67, 71, 72, 75, 76, 78, 80, 81, 83, 92, 96, 222, 253, 437, 438, 439, 440, 441, 442, 443, 444, 445, 26p	Starostenko A.A.	
Skorobogatov D.N.	415, 467, 470, 471, 472	Starostenko D.A.	464
Skrinsky A.N.	110, 112, 218, 219, 220, 222, 253, 254, 319, 332, 349, 408, 429, 430, 437, 438, 439, 440, 441, 442, 443, 444, 445, 546, 10p, 11p, 25p, 26p, 27p, 28p	Starostina E.V.	222, 253, 254, 437, 438, 439, 440, 441, 442, 10p, 25p, 26p, 27p, 28p
Smalyuk V.V.	140, 222, 253, 254, 391, 392, 393, 394, 404, 10p, 25p, 26p, 27p, 28p	Stepanov V.D.	312, 315, 346, 504, 516, 522, 523, 534, 536
		Strakhovenko V.M.	141, 155, 458
		Stupishin N.V.	136, 310, 518, 527, 530
		Sudnikov A.V.	306, 307, 308, 316, 511, 519, 532
		Sulyaev Yu.S.	134, 306, 307, 316, 346, 510, 511, 516, 523, 534, 539
		Surin I.K.	112, 220, 429, 430, 11p
		Sukhanov A.V.	426
		Sukhanov D.P.	392, 393, 394, 10p
		Sukharev A.M.	8, 9, 25, 32, 33, 35, 55, 58, 69, 82, 94, 170, 171, 172, 173, 174, 175, 176, 177, 178, 179, 180, 181, 182, 183, 184, 185, 186, 187, 188, 189, 190, 191, 192, 193, 194, 195, 196, 197, 198, 199, 200, 201, 202, 203, 204, 205, 206, 207, 208, 209, 210, 211, 212, 213, 214, 215, 216, 222, 253, 254, 412, 437, 438, 439, 440, 441, 442, 443, 444, 445, 25p, 26p, 27p, 28p, 53p-60p, 61p-70p, 71p-80p, 81p-90p
		Sukhina B.N.	
		Syrovatina V.M.	414
		***	***

Talyshev A.A.	8, 9, 25, 32, 33, 35, 55, 58, 69, 82, 94, 170, 171, 172, 173, 174, 175, 176, 177, 178, 179, 180, 181, 182, 183, 184, 185, 186, 187, 188, 189, 190, 191, 192, 193, 194, 195, 196, 197, 198, 199, 200, 201, 202, 203, 204, 205, 206, 207, 208, 209, 210, 211, 212, 213, 214, 215, 216, 222, 230, 253, 254, 411, 437, 438, 439, 440, 441, 442, 443, 444, 445, 446, 447, 448, 449, 450, 451, 452, 25p, 26p, 27p, 28p, 53p-60p, 61p-70p, 71p-80p, 81p-90p	Toporkov D.K.	167, 168, 169, 232, 387, 388, 389, 427, 10p, 91p
Tarayshkin S.V.	410, 478, 3p, 10p	Tribendis A.G.	
Tarnetsky V.V.	124, 326, 555	Trunev Yu.A.	134, 304, 376, 378, 506, 507, 508
Taskaev S.Yu.	282, 283, 284, 285, 485, 486, 7p	Tumaikin G.M.	222, 253, 254, 437, 438, 439, 440, 441, 442, 10p, 25p, 26p, 27p, 28p
Tayursky V.A.	222, 253, 254, 437, 438, 439, 440, 441, 442, 443, 444, 445, 25p, 26p, 27p, 28p	***	***
Tekutiev A.I.	11p	Ukrainsev Yu.G.	227, 228, 229, 230, 231, 344
Telnov V.I.	222, 230, 253, 254, 435, 436, 437, 438, 439, 440, 441, 442, 443, 444, 445, 25p, 26p, 27p, 28p	Usov Yu.V.	39, 68, 74, 87, 89, 91, 220, 222, 230, 253, 254, 260, 261, 262, 263, 429, 437, 438, 439, 440, 441, 442, 443, 444, 445, 11p, 25p, 26p, 27p, 28p, 49p, 50p, 51p, 52p
Terekhov I.S.	142, 143	Utkin A.V.	116, 119, 426
Timofeev I.V.	131, 302, 317	Utyupin N.F.	10p
Titov V.M.	234, 355	***	***
Tiunov M.A.	124, 127, 309, 326, 377, 382, 538, 555	Fadeev S.N.	550
Tikhonov Yu.A.	8, 9, 13, 25, 32, 33, 35, 55, 58, 69, 82, 94, 170, 171, 172, 173, 174, 175, 176, 177, 178, 179, 180, 181, 182, 183, 184, 185, 186, 187, 188, 189, 190, 191, 192, 193, 194, 195, 196, 197, 198, 199, 200, 201, 202, 203, 204, 205, 206, 207, 208, 209, 210, 211, 212, 213, 214, 215, 216, 217, 220, 222, 231, 253, 254, 344, 429, 430, 437, 438, 439, 440, 441, 442, 443, 444, 445, 10п, 11п, 25п, 26п, 27п, 28п, 53п, 54п, 55п-60п, 61п-70п, 71п-80п, 81п-90п	Fadin V.S.	157, 158, 159, 160, 459, 460, 461, 12p, 13p, 15p
Tkachenko V.O.	326, 555	Faktorovich B.L.	124, 326, 555
Todyshev K.Yu.	40, 41, 43, 44, 45, 51, 52, 54, 56, 59, 62, 63, 64, 65, 66, 67, 71, 72, 75, 76, 78, 80, 81, 83, 92, 96, 138, 222, 253, 437, 438, 439, 440, 441, 442, 443, 444, 445, 25p, 26p, 27p, 28p	Fatkin G.A.	267, 464, 465, 470
Tokarev Yu.F.		Fedotov M.G.	469, 470, 10p
Tolochko B.P.	234, 321, 354, 355, 356, 359, 365, 390, 8p	Fedotov G.V.	10, 31
		Filipchenko A.V.	121, 350, 426
		Frolov A.R.	11, 476
		***	***
		Khavin N.G.	116
		Khazin B.I.	31, 112, 225, 226
		Kharlamov A.G.	218, 220, 429, 430, 11p
		Kharlamova T.A.	222, 253, 254, 437, 438, 439, 440, 441, 442, 443, 444, 445, 25p, 26p, 27p, 28p
		Khatsimovsky V.M.	149, 150, 151
		Khilchenko A.D.	291, 296, 309, 491, 492, 509, 510, 513, 539, 10p
		Khilchenko V.A.	309, 513
		Kholopov M.A.	116, 352, 357, 419
		Khriplovich I.B.	29, 147, 148
		Khrushchev S.V.	414, 16p
		***	***
		Tsidulko Yu.A.	125, 130, 135, 279, 280, 281, 290, 294, 369, 379, 380, 384
		Tsukanov V.M.	400, 414, 10p
		Tsyganov A.S.	403
		***	***
		Chakin I.K.	320, 322
		Cheblakov P.B.	397, 398, 399, 405, 426
		Chekavinsky B.P.	467, 470
		Cherepanov V.P.	256, 391, 392, 405, 426, 10p
		Cherepkov V.G.	

Research staff and publications

Chernov V.A.	352, 353, 364	Sheromov M.A.	117, 360
Chernov K.N.	124, 326, 555	Shestakov Yu.V.	167, 168, 169, 232, 387, 388, 389, 427, 91p
Chernoshtanov I.S.	290, 369, 379, 380, 384	Shekhtman L.I.	231, 232, 233, 234, 237, 238, 239, 240, 241, 242, 244, 245, 246, 344, 355, 443, 444, 445, 32p, 33, 34p, 35p, 36p, 37p, 38p, 39p, 40p, 41p, 42p, 43p, 44p, 45p, 46p, 47p
Chernyak V.L.		Shikhovtsev I.V.	132, 310
Chernyakin A.D.	405, 426	Shichkov D.S.	116, 119, 426, 6A
Cheskidov V.G.	98, 106, 124, 349, 405, 409, 426, 469, 470, 555, 4p	Shiyankov S.V.	319, 426, 10p
Choporova Yu. Yu.	113, 331, 332, 335, 340, 349	Shkaruba V.A.	414
Chudaev V. Ya.	407	Shoshin a.A.	303, 306, 308, 311, 531, 10A
Chupyra A.G.		Shtarklev E.A.	326, 552, 553, 554, 555
Churkin I.N.	405, 426, 10p	Shtol D.A.	220, 429, 430, 11p, 11A
***	***	Shubin E.I.	409, 10p
Shamanaeva L.I.	230	Shukaev A.N.	429, 11p
Shamov A.G.	8, 9, 25, 32, 33, 35, 58, 69, 82, 94, 138, 170, 171, 172, 173, 174, 175, 176, 177, 178, 179, 180, 181, 182, 183, 184, 185, 186, 187, 188, 189, 190, 191, 192, 193, 194, 195, 196, 197, 198, 199, 200, 201, 202, 203, 204, 205, 206, 207, 208, 209, 210, 211, 212, 213, 214, 215, 216, 222, 230, 233, 253, 254, 437, 438, 439, 440, 441, 442, 443, 444, 445, 10p, 25p, 26p, 27p, 28p, 53p-60p, 61p-70p, 71p-80p, 81p-90p	Shulzhenko G.I.	310, 487
Shatilov D.N.	137, 222, 253, 254, 406, 422, 423, 437, 438, 439, 440, 441, 442, 541, 10p, 25p, 26p, 27p, 28p	Shusharo A.I.	443, 444, 445
Shatunov P. Yu.	112, 220, 319, 430, 546, 11p, 13A	***	***
Shatunov Yu.M.	22, 31, 112, 218, 219, 220, 319, 429, 430, 542, 546, 547, 11p	Scheglov M.A.	332, 349
Shwartz B.A.	30, 31, 39, 47, 50, 61, 68, 89, 95, 222, 247, 248, 249, 250, 253, 254, 260, 261, 262, 263, 437, 438, 439, 440, 441, 442, 443, 444, 445, 25p, 26p, 27p, 28p, 49p, 50p, 51p, 52p	Schegolev L.M.	121, 405, 426
Shwartz D.B.	112, 220, 319, 430, 542, 546, 11p	Schudlo I.M.	308, 486
Shvedov D.A.	426, 10p	***	***
Shebalin V.E.	39, 42, 47, 50, 87, 89, 93, 95, 260, 261, 262, 263, 49p, 50p, 51p, 52p	Eidelman S.I.	10, 31, 39, 42, 47, 50, 53, 60, 61, 68, 74, 84, 87, 89, 91, 93, 95, 222, 237, 238, 239, 240, 241, 242, 243, 244, 245, 246, 253, 254, 255, 256, 257, 258, 259, 260, 261, 262, 263, 437, 438, 439, 440, 441, 442, 25p, 26p, 27p, 28p, 32p, 33p-40p, 41p-52p, 92p
Shevchenko O.A.	97, 98, 332, 342, 349, 417, 419	Eidelman Yu.I.	
Shemyakin D.N.	112	Epstein L.B.	112
Shemyakina E.O.	251, 30p	***	***
		Yudin Yu.V.	31, 225, 226
		Yurov D.V.	494, 495, 496
		Yurchenko Yu.B.	231, 344
		Yushkov A.N.	40, 41, 43, 44, 45, 51, 52, 54, 56, 59, 62, 63, 64, 65, 66, 67, 71, 72, 75, 76, 78, 80, 81, 83, 92, 96, 222, 253, 254, 437, 438, 439, 440, 441, 442, 443, 444, 445, 25p, 26p, 27p, 28p
		***	****
		Yaminov K.R.	405, 426
		Yarovoi V.A.	304, 378, 508

SIBIRIAN BRANCH OF RUSSIAN ACADEMY OF SCIENCES
BUDKER INSTITUTE OF NUCLEAR PHYSICS

ANNUAL REPORT
2011

Cover E.D. Bender

Ответственный за выпуск А.В. Васильев
Работа поступила 12.05. 2012 г.

Сдано в набор 14.05. 2012 г.
Подписано в печать 15.10. 2012 г.
Формат 60x90 1/16 Объем 14,6 печ.л., 11,7 уч.-изд.л.
Тираж 100 экз. Бесплатно. Заказ № 22

Обработано на РС и отпечатано
на ротапринте «ИЯФ им. Г.И. Будкера» СО РАН,
Новосибирск, 630090, пр. Академика Лаврентьева, 11